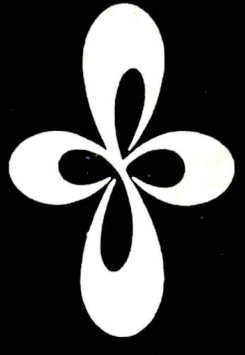
ANNUAL REVIEW

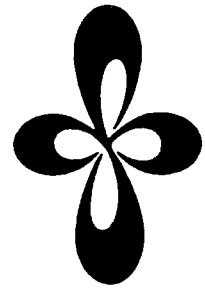
INSTITUTE FOR MOLECULAR SCIENCE



1996

ANNUAL REVIEW

INSTITUTE FOR MOLECULAR SCIENCE



1996

Published by
Institute for Molecular Science
Okazaki National Research Institutes
Myodaiji, Okazaki 444, Japan
Phone 0564-55-7418 (Secretary room)
Telex 4537-475 KOKKEN J
Fax 0564-54-2254

Editorial Committee 1996 : Kazushi KANODA (Chairman),
Yasuhiro NAKAZAWA, Ko OKUMURA,
Hiroyuki OZEKI, Nobuaki TANAKA,
Yukito NAITOH, Yuko HOSOKOSHI,
Satoshi TAKEUCHI, Hideaki MONJUSHIRO,
Kiyoshi TSUGE, Shinkoh NANBU,
Koichiro MITSUKE, Kyoko ONO
and Kayoko SUGIYAMA

IMS 1996



Institute for Molecular Science (IMS) is now recognized as an important institute for basic research in molecular science. We are proud of the achievements of all the IMS staff. World-leading research programs are being developed by the groups at IMS, and their scientific level is very high, when measured by international standards. Nevertheless, it is now necessary for IMS to reach for even higher achievements that will have a great impact on the scientific community. I believe that such accomplishments really promotes science. To do so, IMS should be courageous in exploring new fields, more tolerant in accepting new ideas, and more open in its discussions. Every effort must be made with this goal in mind.

A new laboratory - Molecular Cluster Science- has been added this year to the Department of Applied Molecular Science. This laboratory is operated by faculty members who transferred from other universities. Based on the plan made last year, we are working towards an early realization of the plan to remodel and build new research facilities. Two research development centers (laser and materials) will be established by reorganization of the present three research facilities.

The turnover of personal has been very high in the last year. A newly added laboratory - Theoretical Studies IV- was started by appointing Professor F. Hirata from Kyoto University and Associate Professor K. Yonemitsu from Tohoku University. Associate Professor K. Fuke of the Instrument Center moved to Kobe University as a full professor and his successor is Associate Professor N. Sarukura from Physical and Chemical Research Institute. Associate Professor T. Takahashi of the Coordination Chemistry Laboratory moved to Hokkaido University as a full professor. Dr. K. Inoue of Kitazato University was appointed as an associate professor of the Department of Applied Molecular Science. Professor M. Haga and Associate Professor T. Sakurai took positions in the Synthetic Coordination Chemistry Laboratory by transferring from Mie University and Kanazawa University, respectively. Professor N. Nishi and Associate Professor T. Nagata were assigned as staff of the newly created Molecular Cluster Science Laboratory by transferring from Kyushu University and Tokyo University. Mr. A. Uchida, who was a head of the Technical Division for a long time, retired from IMS and was succeeded by Mr. K. Sakai. We also had a high turnover of research associates and technical associates.

The last year was a year of honors and awards for many people associated with IMS. The Chemical Society of Japan Award was given to Professor K. Yoshihara and the Spectroscopical Society of Japan Award to Professor T. Kitagawa. Associate Professor H. Hosono and Dr. Mizutani, a research associate of the Molecular Dynamic Laboratory, received the W. H. Zachariasen Award and the Inoue Research Award for Young Scientists. Professor K. Isobe of Osaka City University, Professor Y. Udagawa of Tohoku University and Professor H. Kawazoe of Tokyo Institute of Technology, who were previously member of the IMS faculty, received the Divisional Award of the Chemical Society of Japan in respective field. I would like to congratulate these distinguished persons for their achievements.

September, 1996

Mitsuo Ito

Mitsuo Ito
Director-General

CONTENTS

IMS 1996 ..... Mitsuo Ito iii

CONTENTS v

ORGANIZATION AND STAFF 1

COUNCIL 11

BUILDINGS AND CANPUS 12

RESEARCH ACTIVITIES I

Department of Theoretical Studies 15

A. Development of New Theoretical and Numerical Techniques in the Study of Molecular Structures 15

1. On Approximating Electron Repulsion Integrals with Linear Combination of Atomic-Electron Distributions 15
2. Multi-Exponential Approaches to Electronic Structure Calculations with Chemical Accuracy: Importance of Orbital Relaxation Effects 15
3. Theoretical Studies of the Photoionization and Photodetachment Cross Section Using the L^2 Basis Set 15

B. Structures, Spectra and Dynamics of Water Cluster Complexes with Atoms, Atomic Ions, and Organic Molecules 15

1. Theoretical Studies of Geometric Structures of Phenol-water Clusters and Their Infrared Absorption Spectra in the O-H Stretching Region 16
2. Does the Proton Transfer reaction Take Place in the Ground State of Phenol-$(H_2O)_4$ Clusters ? 16
3. Hybrid Procedure of Ab Initio Molecular Orbital Calculation and Monte Carlo Simulation for Studying the Intracluster Reaction: Application to $Mg^+(H_2O)_n$ (n=1-4) 16
4. High-Resolution Laser-Induced Fluorescence Spectra of 7-Azaindole-Water Complexes and its Dimer 16
5. Molecular Orbital Studies of the Structures and Reactions of a Singly Charged Calcium Ion with Water Clusters, $Ca^+(H_2O)_n$ 16
6. Theoretical Prediction of Intracluster Reactions of $B^+(H_2O)_2$ and $B^+(H_2O)_3$ Clusters; Hybrid Calculations of Ab Initio MO and Monte Carlo Samplings 17

C. Structures of Binary Element Molecules and Clusters 17

1. Ab Initio Studies of Silicon and Nitrogen Clusters: Cyclic or Linear Si_2N ? 17
2. Structures and Energetics of New Nitrogen and Silicon Molecules: An Ab Initio Studies of Si_2N_2 17
3. Diazasilene (SiNN) : Is There a Conflict Between Experiment and Theory ? 17
4. Ab Initio Studies on the Structures, vertical Electron Detachment Energies and Fragmentation Energies of C_nB^- Clusters 18
5. Ab Initio Studies on the Structures, Vertical Electron Detachment Energies and Fragmentation Energies of C_nN^- Clusters 18
6. Ab Initio Studies on the Structures, Vertical Electron Detachment Energies and Stabilities of C_nP^- Clusters 18
7. Theoretical Study of Carbon Doped Small Silicon Clusters: Electron Affinities of Si_nC (n=2-5) 19
8. Photoelectron Spectroscopy of Silicon-Fluorine Binary Cluster Anions ($Si_nF_m^-$) 19
9. Ab Initio MO Studies of Neutral and Anionic SiC_n Clusters 19
10. Ab Initio MO Studies of Si_4H_2 and Si_4NO^+ 19

D. Structures of Unstable Molecules and Clusters, and of Reaction Intermediates 20

1. Theoretical Studies of the Chemical Processes of Producing Methylamine and Methanol in the Intersteller Space 20
2. Theoretical Study of Cyclic Isomers of HNO_x (x=2-6) 20
3. Ab Initio Studies on Structures of the Hexa-Coordinate Phosphorus Intermediate for the Phosphoryl Ester Exchange and N→ O Migration Reactions of Dimethyloxyphosphoryl-threonine 20
4. Theoretical Predicion of the ^{31}P NMR Chemical Shift of the Hexa-Coordinate Phosphorus Intermediate for the Phosphoryl Ester Exchange and NO Migration Reactions of Dimethyloxyphos-phoryl-threonine 20
5. Unprotonated Ammonia Cluster Cations: How Does or Does Not the Proton Transfer Reaction Takes place? 21
6. Geometrical and Electronic Structures of $[(CO_2)_nROH]^-$(R = H, CH_3) 21
7. Theoretical Studies on the Reaction of $(CO_2)_{N^-}$ with CH_3 21

E. Potential Energy Surfaces of Low-Lying States of Simple Molecules 22

1. The Electronic Structures of HCCS and NCS 22

2. Theoretical Characterization of the Low-Lying Electronic States of the SiB, SiB^+, SiAl, and $SiAl^+$ Molecular Species 22
3. Ab Initio Investigation of the Photodissociation of HOCl 22
4. Ab Initio Studies of the Isomers: HSiNN, HNSiN, and HNNSi 23
F. Electronic Structure of Some Basic Molecules Containing the Transition Metal Atoms 23
1. Theoretical Studies of the Ground and Low-lying Excited Electronic States of the Early Transition Metal Dihydrides with State Averaged MC SCF Method 23
2. Quadratic Configuration Interaction Versus Coupled Cluster Theory : Importance of Drbital Relaxation Phenomena in CuH and CuF 23
3. The Structures of FeNO 23
G. Structures, Spectra and Dynamics of Rare Gas Atomic Clusters 24
1. Size Dependence of the Photoabsorption Spectra of Ar_n^+, n = 4 - 25 24
H. Novel Molecular Systems with Symmetry Breaking 24
1. Theoretical Study of the Vibrational Spectrum of $H_2O_2^{+\bullet}$ Radical Cation: An Illustration of HF Symmetry Breaking 24
I. Prediction of Protein Tertiary Structures from the First Principles 25
1. Molecular Dynamics, Langevin, and Hybrid Monte Carlo Simulations in Multicanonical Ensemble 25
2. Numerical Comparisons of Three Recently Proposed Algorithms in the Protein Folding Problem 25
3. Monte Carlo Simulations in Generalized Ensemble: Multicanonical Algorithm Versus Simulated Tempering 25
4. Global Minimum Configuration of a Small Peptide for the ECEPP/2 and ECEPP/3 Force Field 25
J. Three-Dimensional Shape Analysis and Visualization of Protein Molecules 25
1. Visualization of the Electrostatic Energy of Protein Binding Site 25
K. Developing a New Method for Diagonalization of Large Hermitian Matrices 25
1. A Method for Calculating the Eigenvalues of Large Hermitian Matrices by Second-Order Recursion Formulae 25
L. Semiclassical Theory of Chaotic Systems 26
1. Stokes Phenomenon in Chaotic Systems: Pruning Trees of Complex Paths with Principle of Exponential Dominance 26
2. Chaotic Tunneling I: A Remarkable Manifestation of Complex Classical Dynamics in Non-integrable Quantum Phenomena 26
3. Euler-type Product of the Fredholm Determinant Appearing in Boundary Element Method for Two-dimensional Quantum Billiards 26
M. Theoretical Studies of Chemical Reaction Dynamics 26
1. Quantum Dynamics $O(^3P)+HCl \rightarrow OH+Cl$ 26
2. Quantum Dynamics of the Tetra-atomic Reaction Systems: H_2+OH and NH+NO 27
3. Multidimensional Tunneling in Terms of Complex Classical Mechanics: Wave Functions, Energy Splitting, and Decay Rates in Nonintegrable Systems 27
N. Theory of Nonadiabatic Transitions 27
1. Semiclassical Analysis of Resonance States Induced by a Conical Intersection 27
2. Two-by-two Diabatic Approach for Multi-Channel Curve Crossing Problems 27
3. Quantum Mechanically Exact Analytical Solutions of a Two-State Exponential Model 27
4. Semiclassical Theory for Two-State Exponential Potential Models 28
5. Semiclassical Theory of Time-Dependent Curve Crossing Problems 28
6. Exact Analytical Solution for Coupled Time-Independent Schrödinger Equations with Certain Model Potentials 28
7. Unified Semiclassical Theory for the Two-State System: Analytical Solutions for Scattering Matrices 28
O. Theoretical Studies of Characteristics and Dynamics of Superexcited States of Molecules 28
1. Superexcited States of CO near the First Ionization Threshold 28
2. A General Theoretical Procedure to Reveal Characteristics and Dynamics of Superexcited States of Diatomic Molecules 28
P. New Molecular Switching Elements 29
Q. Laser Assisted Surface Ion Neutralization 29
R. Theoretical Studies of Nonlinear Optical Spectroscopy of Molecules in the Condensed Phase 29
1. Unified Time-Path approach to the Effect of Anharmonicity on the Molecular Vibrational Spectroscopy in Solution 29
2. Femtosecond Two-Dimensional Spectroscopy from Anharmonic Vibrational Modes of Molecules in the Condensed Phase 29
3. The $(2n+1)$th-order Off-Resonant Spectroscopy from the $(n+1)$th-order Anharmonicities of Molecular Vibrational Modes in the Condensed Phase 29
4. First-, Third-, and Fifth-Order Resonant Spectroscopy of an Anharmonic Displaced Oscillators System in the Condensed Phase 30

S. Theoretical Studies of a Strongly Correlated Electron System 30
1. *Ab Initio* Molecular Orbital Calculations by the Resonating Hartree-Fock Approach: Superposition of Non-Orthogonal Slater Determinants 30
2. The SDW-CDW Phase Transition in the One Dimensional Extended Hubbard Model 30
T. Structures and Dynamics of Condensed Molecular Systems 30
1. Growth and Collapse of Structural Patterns in the Hydrogen Bond Network in Liquid Water 30
2. Mechanism of Fast folding and Kinetic Branching Process of the Model Protein 31
3. Evolution of Foldability and Local Structural Ordering 31
U. Electronic Structure of a Molecule in Solution 31
1. Irregular Order in Basicities of Methylamines in Aqueous Solution: A RISM-SCF Study 31
2. The Solvent Effect on the Acidities of Haloacetic Acids in Aqueous Solution. A RISM-SCF Study 32
3. Solvent Effect on Acidity: A Hybrid Approach Based on the RISM and the Hartree-Fock Equations 32
4. Theoretical Study for the Basicities of Methylamines in Aqueous Solution: A RISM-SCF Calculation of Solvation Thermodynamics 32
5. Analytical Energy Gradient for the Reference Interaction Site Model Multiconfigurational Self-consistent-field Method: Application to 1,2-Difluoroethylene in Aqueous Solution 32
V. Solvation Thermodynamics of Protein and Related Molecules 33
1. Application of the Reference Interaction Site Model Theory to Analysis on Surface-induced Structure of Water 33
2. Analysis on Salting-out Phenomena for Noble Gases Using the Reference Interaction Site Model Theory 33
3. Calculation of Hydration Free Energy for a Solute with Many Atomic Sites Using the RISM Theory: Robust and Efficient Algorithm 34
4. Ion Hydration: Revisiting with an Integral Equation Theory of Liquids 34
5. Solvation Free Energies of Non-polar and Polar Solutes Reproduced by the Combination of the Extended Scaled Particle Theory and the Poisson-Boltzmann Equation 34
6. Solvation Free Energy of Protein Reproduced by The Combination of The Extended Scaled Particle Theory and The Poisson-Boltzmann Equation 34
7. The Cold Denaturation of Protein is Predicted by the Extended Scaled Particle Theory 34
W. Spatial and Temporal Density Fluctuation in Molecular Liquids 35
1. Surrogate Hamiltonian Description of Solvation Dynamics. Site Number Density and Polarization Charge Density Formulations 35
2. An Interaction-Site Representation of the Dynamic Structure Factor of Liquid and Solvation Dynamics 36
3. Molecular Theory for the Nonequilibrium Free Energy Profile in Electron Transfer Reaction 36
4. Non-Linear Effects in the Free Energy Profile of Electron Transfer Reaction: An Integral Equation Approach 36
5. The Free Energy Profiles for the Electron Transfer Reactions Calculated from the Integral Equation Method of Liquids 36
6. Nonlinear Electrical Potential Fluctuations of Solvent around Solutes: an Integral Equation Study 36
7. Shear-Induced Distortion of Intra- and Intermolecular Correlations in Liquids –Time Dependent Density-Functional Theory– 36
8. Statistical Mechanics of Deformable Molecular Liquids – Thermal Expansion and Isomerization of Diatomic Molecul– 37
X. Theoretical Studies of Low-Dimensional Correlated Electron Systems 37
1. Electron-Phonon Interaction and Spin Gap in Nearly-Half-Filled Correlated Electron Systems 37
2. Spin-Gap Phase in Nearly-Half-Filled One-Dimensional Conductors Coupled with Phonons 37
3. Spin Gap in One-Dimensional Electron-Phonon Systems 37
4. Mott Transition in Quasi-One-Dimensional Electron Systems at Quarter Filling 37
Y. Theoretical Studies of Superconductors under Magnetic Field 38
1. Bands of In-Gap States in *s*- and *d*-Wave Superconductors under High Magnetic Field 38

RESEARCH ACTIVITIES II

Department of Molecular Structure 39

A. Laboratory and Astronomical Spectroscopy of Transient Molecules 39
1. Microwave Spectroscopy of the HCCS and DCCS Radicals($X^2\Pi_i$) in Excited Vibronic States: A Study of the Renner-Teller Effect 39
2. Microwave Spectrum and Molecular Structure of the Dihydrophosphoryl Radical H_2PO in the X^2A' Ground Electronic State 39
3. Microwave Spectrum of a New Phosphorus Containing Carbene: HCCP($X^3\Sigma^-$) 40
4. Microwave Spectrum of the CHF_2 Radical in the X^2A' Electronic State: Hyperfine Structure Alternation in Inversion Doubling 40
5. The Microwave Spectrum of NCl in the Second Electronically Excited State($b^1\Sigma^+$) 40

6. Microwave Spectra of 3d Transition Metal Oxide Radicals:MnO($^6\Sigma^+$), CoO($^4\Delta_i$), CuO($^2\Pi_i$), and TiO($^3\Delta_r$) 41
7. Microwave Spectrum of the AsH($^3\Sigma^-$) Radical 41
8. Isotopic NS Rotational Spectra: $^{14}N^{33}S$ and $^{15}N^{32}S$ 42
9. Microwave Measurement of Spectral Lines of $Si^{18}O$ for Astronomical Use 42
B. Development of a Mt. Fuji Submillimeter-Wave Telescope 42
1. Measurement of 220 GHz Atmospheric Opacity on Mt. Fuji with a Radiometer/Radome System 42
2. Development of Wide-Band Acousto Optical Spectrometer(AOS) for the Mt. Fuji Telescope 43
C. Laser Investigation of Antiproton-Helium Compounds 43
1. Isotope Effects on Delayed Annihilation Time Spectra of Antiprotonic Helium Atoms in a Low-Temperature Gas 43
2. Laser-Induced Resonant Transitions in the $\upsilon=n\text{-}l\text{-}1=2$ and 3 Metastable Cascades of Antiprotonic ^{3}He Atoms 43
3. Observation of Double Resonant Laser Induced Transitions in the $\upsilon=n\text{-}l\text{-}1=2$ Metastable Cascade of Antiprotonic Helium-4 Atoms 44
4. Laser Resonance Studies of the Interactions of Metastable Antiprotonic Helium Atomcules $\bar{p}^4He^+$ with Surrounding H_2 Molecules 44
5. High-Precision Structural Studies of the Antiprotonic Helium Atom $\bar{p}^4He^+$ by Observing Laser Resonances with $\Delta\upsilon=\Delta(n\text{-}l\text{-}1)=2$ 44
6. Observation of a Line-Splitting in a $\Delta\upsilon=\Delta(n\text{-}l\text{-}1)=2$ Transition in Metastable Antiprotonic ^{4}He Atoms 44
D. Laser Cooling and Trapping of Neutral Atoms 44
1. Number Enhancement in Laser-Trapped He* Atoms through Collision-Control with an Additional Laser 45
E. Laser Spectroscopic Studies of Ions in Liquid Helium 45
1. Laser Spectroscopy of Barium Ions in Liquid Helium 45
F. Molecular Science of Biomolecules 46
1. The Proximal Residue Largely Determines the CO Distortion in Carbonmonoxy Globin Proteins An *ab Initio* Study of a Heme Prosthetic Unit 46
2. Distal Residue-CO Interaction in Carbonmonoxy Myoglobins: A Molecular Dynamics Study of Three Distal Mutants 46
3. Time-Resolved Resonance Raman Evidence for Tight Coupling between Electron Transfer and Proton Pumping of Cytochrome c Oxidase upon the Change from the Fe^V Oxidation Level to the Fe^{IV} Oxidation Level 46
4. Two Amine Oxidases from Aspergillus Niger AKU 3302 Contain Topa Quinone as the Cofactor: Unusual Cofactor Link to the Glutamyl Residue Occurs Only at One of the Enzymes 47
5. Perturbation of the Fe-O_2 Bond by Near-by Residues in Heme Pocket: Observation of $\nu_{Fe\text{-}O2}$ Raman Bands for Oxymyoglobin Mutants 47
6. Resonance Raman Studies of Compounds I and II of *Arthromyces ramosus* Peroxidase : Close Similarities in Their Raman Spectra but Distinct Oxygen Exchangeability of the Fe=O Heme 47
7. Ultraviolet Resonance Raman Spectra and Ab initio Vibrational Analyses of 1,4-Benzoquinone: Reassignments of the ν_2 and ν_3 Bands 48
8. Resonance Raman and FTIR Spectra of Isotope-Labeled Reduced 1,4-Benzoquinone and Their Protonated Forms in Solutions 48
9. Effects of Concerted Hydrogen Bonding of Distal Histidine on Active Site Structures of Horseradish Peroxidase; Resonance Raman Studies with Asn-70 Mutants 48
10. Red-Excited Time-Resolved Resonance Raman Study of the Oxoiron Intermediates of Fully Reduced Cytochrome *c* Oxidase 49
11. Selective Observation of Resonance Raman Spectra of Q_A^- and Q_B^- in *Rb.* Sphaeroides R26 Photosynthetic Reaction Centers 49
12. Effects of GTP Binding to Soluble Guanylate Cyclase on Its Heme Vicinity as Probed by Resonance Raman Spectroscopy 49
G. Fast Dynamics of Photoproducts in Solution Phases 49
1. Developments of Widely Tunable Light Sources for Picosecond Time-Resolved Resonance Raman Spectroscopy 50
2. Direct Observation of Vibrational Energy Relaxation for Photodissociated Heme of Carbonmonoxy Myoglobin 50
3. Vibrational Energy Relaxation in the (*d, d*) Excited State of Nickel Octaethylporphyrin 50
4. Picosecond Time-resolved Resonance Raman Study on Photo-induced Ligation of Pyridine to Nickel Octaethylporphyrin 50
5. Time-Resolved Resonance Raman Spectra of Octaethylporphinato Copper(II) in the Lowest Excited Triplet State 50
H. Molecular and Electronic Structures of Metallofullerenes and the Fullerene Radical Anions 51
1. ESR Measurements of C_{60}^- Anion Crystals 51
2. ESR Study on Electronic Structure and Chemical Reactivity of Metallofullerenes 51
I. Site Selective Spectroscopy in Solid Crystals 51
1. Heterodyne Detection of Optical Magnetic Double-Resonance 51

2. Measurements on the Zero Phonon Line of the Luminescence of the NV Center in Synthetic Ib Diamonds 51
J. State Correlated Raman Spectroscopy 52
1. Two Dimensional Raman Spectroscopic Study on the N-I Phase Transition of Liquid Crystal 52
2. FT-IR and FT-Raman Spectroscopies on Structural Characterization of 'Command Surfaces' LB Films and Photo-Regulation of Reorientation for Liquid Crystal Molecules 52

RESEARCH ACTIVITIES III

Department of Electronic Structure 53
A. Ultrafast Intermolecular Electron Transfer 53
1. Dynamics in Intermolecular Electron Transfer 53
2. Deuterium Isotope Effect on Ultrafast Intermolecular Electron Transfer 53
3. Deuterium Isotope Effect on the Solvation Dynamics of Methanol: CH_3OH, CH_3OD, CD_3OH, and CD_3OD 55
B. Liquid Dynamics Studied by Higher Order Nonlinear Spectroscopy 55
1. Fifth-Order Nonlinear Spectroscopy on the Low-Frequency Modes of Liquid CS_2 55
2. Temporally Two-Dimensional Femtosecond Spectroscopy of Binary Mixture of CS_2 56
3. Overtone Vibrational Dephasing in Liquids Studied by Femtosecond Fifth-Order Nonlinear Spectroscopy 56
4. Temporally Two-Dimensional Overtone Vibrational Dephasing Spectroscopy in Liquids 56
C. Development of Ultrafast Fluorescence Up-Conversion Technique 57
1. Femtosecond Fluorescence Up-Conversion System with Time Resolution Better Than 80 fs (FWHM) 57
D. Ultrafast Dynamics of UV-Photoexcited Simple Molecules in Solution by Femtosecond Transient Absorption Spectroscopy 58
1. Photoinduced Chemical Reaction in Neat CH_3I 58
2. Photoinduced Reactions of CH_2I_2 in Solution Studied by the Ultrafast Transient Absorption Spectroscopy 59
3. Ultrafast Dynamics of Photoexcited trans-1,3,5-Hexatriene in Solution 59
E. Primary Energy and Electron Transfers in Photosystem I Reaction Center Complex 60
1. Excitation and Electron Transfer from Selectively Excited Primary Donor Chlorophyll (P700) in Photosystem I Reaction Center 60
2. ΔG^0 Dependence of the Electron Transfer Rate in Photosynthetic Reaction Center of Plant Photosystem I: Natural Optimization of Reaction between Chlorophyll a (A_0) and Quinone 61
F. Dynamic Behavior of Electronic Excited States 62
1. Temperature Dependent Radiative Lifetime of J-Aggregates 62
2. Femtosecond Electron-Transfer Dynamics at a Sensitizing Dye-Semiconductor (TiO_2) 62
G. Photochemistry on Well-Defined Surfaces 63
1. Adsorbate-Localized Excitation in Surface Photochemistry: Methane on Pt(111) 63
2. Adsorption State of Methane and Laser-Induced Photochemistry on Pt(111) 64
H. Reaction Dynamics on Well-Defined Surfaces 64
1. Mechanism for the Desorption of Molecularly and Dissociatively Adsorbed Methane on Pt(111) Probed by Pulse-Laser Heating 64
I. Hot Atom Surface Reactions 65
1. Adsorbed States and Thermal Reactions of N_2O on Si(100) below Room Temperature: Desorption Induced by Dissociation 65
J. Multiphoton Photoelectron Spectroscopy of Electronic States at Metal Surfaces 66
1. Surface and Image-Potential States on Pt(111) Probed by Two- and Three-Photon Photoemission 66
K. Dynamic Processes in Electronically-and/or Vibrationally-Excited Molecules 66
1. Nascent Rotational and Vibrational Distributions in ^{16}OH and ^{18}OH Produced in the Reaction of $O(^1D)$ with $H_2{}^{18}O$ 66
2. Photochemical Reaction Dynamics of the $N_2O{\cdot}H_2{}^{18}O$ van der Waals Complex 67
3. Hole-Burning Spectroscopy of *m*-Cresol Rare-Gas Complexes 68
4. Torsional Potential of the Methyl Group in Toluene Derivatives Forming 1:1 Complexes with a Rare Gas Atom 68
5. The N_2 Rotational State Dependence of Anisotropy in the Angular Distribution of Photofragment from N_2O 69
6. Photodissociation Study of CH_3CHO: The rate of Formation of Photofragment 69
L. Self-Organization in Chemical Reactions 70
1. Origin of Chemical Instability in the Bromate-Sulfite Flow System. 70
2. Mechanism of the Oscillatory Bromate Oxidation of Sulfite and Ferrocyanide in a CSTR 71
3. pH Oscillations in the Bromate-Sulfite-Marble Semibatch and Flow System 72
4. Chaotic pH Oscillations in the Sulfur(IV)-Hydrogen Peroxide-Marble Flow System 72
5. Chaotic pH Oscillations in the Hydrogen Peroxide-Sulfite-Ferrocyanide-Hydrogen Carbonate Flow System 72

6. Light-Induced Period Doubling Route from Simple pH Oscillations to Chaos in the Hydrogen Peroxide-Sulfite-Ferrocyanide-Hydrogen Carbonate Flow System 73
7. Photo-Response of the Ferrocyanide-Bromate-Sulfite Chemical Oscillator under Flow Conditions 73
8. The Primary Process of Photoinduction of Chemical Oscillations in the Ferrocyanide-Bromate-Sulfite System 74
9. Pulse Light Irradiation for B-Z Reaction - Photoresponse Near the Bifurcation Point 74
10. The Effect of Light on the Belousov-Zhabotinsky Reaction in Water-in-Oil Microemulsion of AOT in Octane. 75
11. Photoinduced Bifurcation and Multistability in the Oscillatory Briggs-Rauscher Reaction 75

M. Dynamical Stereochemistry in Molecular Photodissociation 76
1. Simultaneous Measurement of Recoil Velocity and Alignment of $S(^1D_2)$ Atoms in Photodissociation of OCS 76
2. Multiple Dissociation Channels and Orbital Alignment in Ultraviolet Photodissociation of N_2O 77
3. Wavelength Dependence in Photodissociation of OCS 77
4. Semiclassical Analysis of Vector Correlation in Photodissociation and its Application to Photofragment Imaging 78
5. C-Cl Bond Rupture in Ultraviolet Photodissociation of Vinylchloride 78

N. Electronic Relaxation and Predissociation Dynamics of Acetylene 78
1. Energy and State Dependence in the Quenching and Predissociation of C_2H_2 78
2. State Dependence and Absolute Value of Fluorescence Quantum Yield from $\tilde{A}^1A_u$ State of C_2H_2 78
3. Anomalous Line Intensities and Lifetime Variations within the V^2K^1 Manifold of C_2H_2 79
4. State Dependent Fluorescence Decay Dynamics of $C_2D_2(\tilde{A})$ 79

O. Femtosecond Real Time-Clocked Photofragment Imaging 79
1. Photofragment Imaging with Femtosecond Laser Pulses 79

P. Crossed Beam Studies of Bimolecular Reaction Dynamics 80
1. Construction of a Crossed Molecular Beam Machine with a Photolytic Atomic/Radical Beam Source 80

Q. One Atom Cage Effect and a Search for Dynamical Resonance 81
1. Measurement of Absorption Spectra of Size-Selected Clusters by Population Labeling Spectroscopy 81

R. Jet Spectroscopy of Benzyl and Substituted Benzyl Radicals 82
1. Laser Induced Fluorescence Spectra of Jet Cooled *p*-Chlorobenzyl Radical 82

S. Photochemical Processes Studied by Time-Resolved ESR 82
1. Time-Resolved ESR Studies on Ketyl Type Radical-Amine Complexes 82
2. Absolute Magnitude of Spin Polarization in the Radical-Triplet Pair Mechanism: CIDEP Generation by Level Crossings in a Triplet-Doublet Interaction 82

T. Laser Ablation-Molecular Beam Method. Competitive Solvation of Monopositive Metal Ions in the Gas Phase 82
1 Laser Ablation-Molecular Beam Method: A Simple and Versatile Diagnosis to Study Chemistry of Monopositive Metal Ions in the Gas Phase 83

U. Laser Chemistry of Polymers and Solids. Reconstruction of Polymer Films from Laser-Ablated Fragments, Surface Treatment of Polymers with Pulsed Lasers, and Raman Probe of Laser Deterioration of Solids 83
1. Preparation of Polymer Films by Laser Ablation of Polyacrylonitrile: Significant Dependence on Ablation Wavelengths 83
2. Preparation of Polyacenic Semiconductive Thin Films by Excimer Laser Ablation of a Bulk Phenol-Folmaldehyde Resin or Pyrolyzed Polyacenic Semiconductive Materials 83
3. Preparation of Low-dimensional Conducting Polymer Films by UV Light-induced Deposition with Excimer Laser Beams 83
4. Raman Spectroscopy as a Useful Probe of Mechanisms of Deterioration of Metal Oxide Materials due to Laser Irradiation 84

V. Raman Spectroscopy of Photochromic Merocyanine Dye Aggregates 84
1. A Raman Spectroscopic Study of Merocyanine Aggregates of a ^{15}N-Isotopomer of 6-Nitro-1',3',3'-trimethylspiro[2H-1-benzopyran-2,2'-indoline]. A Direct Evidence for the Association through the NO_2-Bridges 84

W. Magnetic Behavior of Stable Radical Crystals and Electronic Structures of Organic High-Spin Molecules 84
(i). Magnetic Behavior of Stable Radical Crystals 84
1. Ferro- and Antiferromagnetic Behaviors of Stable Free Radical Crystals of *N*-(Arylthio)-2,4,6-triarylphenylaminyls 84
2. Magnetic Properties of Purely Organic Radical Magnets, *N*-(Arylthio)-2,4,6-triarylphenyl-aminyls: Susceptibility and Heat Capacity Measurements 84
3. Exceptionally Persistent Nitrogen-Centered Free Radicals. Syntheses, ESR Spectra, Isolation, and X-ray Crystallographic Structures of *N*-(Arylthio)-2-*tert*-butyl-4,6-diarylphenylaminyl and N-(Arylthio)-4-tert-butyl-2,6-diarylphenyl-aminyl Radicals 85

4. A Single-Crystal ESR Study of Magnetism and Spin Dynamics in *N*-[(2,4-Dichlorophenyl)thio]-2,4,6-triphenylphenylaminyl Radical Crystal 85
(ii). Electronic Structures of Organic High-Spin Molecules 85
1. Direct Evidence of the Spin Contraction in the Limited-Size Ferrimagnetic Organic Spin System: Determination of the Spin Densities at the Divalent Carbon and Theoretical Calculation of the Spin Contraction 85

RESEARCH ACTIVITIES IV

Department of Molecular Assemblies 87
A. Solid State Properties of Phthalocyanine Salts and Related Compounds 87
1. π-d Interaction in Phthalocyanine Conductors 87
2. Compressibility and High-Pressure Electrical Resistivity of One-Dimensional Phthalocyanine Conductors: the Relationship with d-π Charge Transfer. 87
3. Anisotropic Magnetic Susceptibility Measurement of $CoPc(AsF_6)_{0.5}$. 87
B. Structure and Properties of Organic Conductors 88
1. Characterization of the Half-Filled DMTSA-BF_4 by Optical and Magnetic Measurements 88
2. Electron-Electron Correlations with Articular Attention to m-BDNT-PF_6: Spin Susceptibility 89
3. Preparation of New Organic Magnetic Conductors, $[M(mnt)_2]_n$-BDNT (M=Au, Pt, Pd, Ni, n=1 and 2) 89
4. Synthesis and Properties of a New Ferromagnetic 2,2'-bipyridine-$MnPS_3$ Intercalation Compound 89
5. A Key to the Understanding of Electron-Molecular Vibration Coupling in Organic Charge-Transfer Salts: Application of the Two-Site Hubbard Model 89
C. Development of a Spiro-Conjugated Donor System: a New Type Donor Able to form Charge-Transfer Salts with a 2-D or 3-D Electronic Conduction Band 90
1. Design of a New Organic Donor having Two Equivalent π-Electronic Systems Perpendicular to Each Other by a Spiro-Conjugation 90
2. Synthesis, Redox Property and Spin-Spin Interaction in Bis(Tetrathiafulvalenyldithio)Germane 90
D. NMR Study of Organic Conductors 91
1. Nesting Instability in a Family of α-$(BEDT\text{-}TTF)_2MHg(SCN)_4$ Studied by ^{13}C-NMR 91
2. ^{13}C-NMR and Susceptibility Studies on β-$(BEDT\text{-}TTF)_2I_3$ 91
3. ^{13}C-NMR Study of Mott Insulating Phase in κ-$(BEDT\text{-}TTF)_2X$ Family 92
4 Recent Progress in NMR Studies on Organic Conductors 92
E. Electron Transport and Magnetic Study of Anisotropic Superconductors 93
1. Highly Anisotropic Superconductivity in the Organic Conductor α-$(BEDT\text{-}TTF)_2NH_4Hg(SCN)_4$ 93
2. Vortex State in a Highly Anisotropic Superconductor, α-$(BEDT\text{-}TTF)_2NH_4Hg(SCN)_4$ 93
F. Thermodynamic Study of Organic Conductors 94
1. Electronic Structure of Insulating Salts of the κ-$(BEDT\text{-}TTF)_2X$ Family Studied by Low-Temperature Specific Heat Measurements 94
2. Specific Heat around the Magnetic Phase Transition of κ-$(BEDT\text{-}TTF)_2Cu[N(CN)_2]Cl$ 94
3. Low-Energy Excitations in the Superconducting State of κ-$(BEDT\text{-}TTF)_2Cu[N(CN)_2]Br$ Salt 95
G. Novel Electronic States of d-π System of $(DCNQI)_2M$ 95
1. Electronic State of the Organic Salt, $(DI\text{-}DCNQI)_2Ag$ 95
2. Carrier Doping to $(DCNQI)_2Li$ 95
H. Development and Physical Properties of New Molecular Superconductors and Related Systems 96
1. Phase Diagram of λ-type BETS Organic Superconductors 96
2. Meissner and Diamagnetic Shielding Effect of α-EDT-TTF$[Ni(dmit)_2]$ 97
3. Shubnikov-de Haas Effect and Angular Dependent Magnetoresistance Oscillation of κ-$BETS_2GaCl_4$ 97
I. Development and Physical Properties of Magnetic Molecular Metals 97
1. New BETS Conductors with Magnetic Anions (BETS=bis(ethylenedithio) tetraselenafulvalene) 98
2. Coupled Magnetic and Electrical Phase Transition of λ-$BETS_2FeCl_4$—Molecular Metal with Field Restored Highly Conducting State 98
3. Phase Diagram of λ-$BETS_2(Ga_xFe_{1-x})Cl_4$—A Clue to Magnetic Molecular Superconductor 99
4. Structural, Electrical and Magnetic Properties of Molecular Metal with Binuclear $Cu_2Cl_6^{2-}$ Anions 99
5. Phase Diagram of DCNQI-Cu System-Origin of Reentrant Metal-Insulator-Metal Transition 99
J. Development of New Molecular Conductors 100
1. New Molecular Conductors Based on Transition Metal Complexes 100
2. New Synthetic Metals Based on a Thiadiazole Network 100
3. Crystal Structures and Electrical Properties of New $Ni(dmise)_2$ Conductors —A Precursor of Three-Dimensional π Metals 101
4. κ- and Modified κ-Type Molecular Arrangement and Electrical Resistivities of $BETS_2InCl_4$, $BETS_2ClO_4(TCE)_{0.5}$ and $BETS_2[(C_2H_5)_4N]_{0.7}InCl_5$ (TCE=1,1,2-trichloroethane) 101
5. Crystal Growth and Physical Properties of Alkali Metal Fullerides—$M_xC_{60}(THF)_y$ (M=Li, Na) 102

K. X-Ray Diffraction Studies at Low Temperature 102
1. Low-Temperature Crystal and Band Electronic Structures of Two-Dimensional $Ni(dmit)_2$ Conductors 102
2. Origin of the Resistivity Anomalies of (EDT-TTF)[$M(dmit)_2$] (M=Ni, Pd) 103
L. Development of Pulsed Field Gradient NMR Spectroscopy 103
1. New PFG-NMR Spectrometer with a Rotatable Quadrupole Coil for the Measurement of Anisotropic Self-Diffusion Coefficient Tensor 103
2. Inversion of Self-Diffusion Anisotropy by Chemical Substitution in Smectic A Liquid Crystalline CBOOA and TFBOOA 103
3. Difference in Self-Diffusion Anisotropy in Two Smectic A Phases of a Doubly Reentrant Liquid Crystal CBOBP 104
M. Phase Transitions and Dynamical Ordering in Liquid Crystals 104
1. Combined Two-Dimensional ^{13}C NMR Spectroscopies for Complete Analysis of the Molecular and Internal Order Parameters in Antiferroelectric Liquid Crystal 104
2. Microscopic Origin of Antiferroelectricity in Liquid Crystal Studied by High Resolution ^{13}C NMR 106
3. Orientational Change of the Trifluorometh-yl Group at the Ferroelectric-Antiferroelectric Transition Observed by NMR Spectroscopy 106
N. Hydrogen Dynamics in Dielectric Solids with Ferroelectric vs. Antiferroelectric Competing Interactions 107
1. Dimensionality Crossover and Nonlinear Dielectric Response in Betaine Phosphate/Arsenate Mixed Crystals 107
2. Anisotropic Dipole-Glass Freezing in Rubidium/Ammonium Dihydrogen Phosphate Mixed Crystal and its Perdeuterated Analogue 107
O. Electronic Properties of Alkali-Hydrogen-Carbon Systems 107
1. ^{1}H and ^{23}Na NMR Studies of Sodium-Hydrogen-Graphite Ternary Intercalation Compound 107
2. NMR Study in $Na_xH_yC_{60}$ 108
P. Search for Novel Electronic Systems Based on Organic Charge Transfer Complexes 108
1. Construction of an Organic Spin-Ladder System Based on BEDT-TTF Charge Transfer Complex 109
2. Organic Antiferromagnets Based on BEDT-TTF and Difluoro-TCNQs with Various Polarity 109
3. Structures and Solid State Properties of (BEDT-TTF)(TCNQ derivatives) : Correlation between the Structure of the Acceptor and the Resultant Complexes 109
Q. Strong Correlation Effects in Organic Conductors 110
1. Phase Diagram of Two-Dimensional Organic Conductors : $(BEDT\text{-}TTF)_2X$ 110
R. Spin Gap and Disorder 110
1. Antiferromagnetic Long Range Order in Disordered Spin-Peierls Systems 110
2. Impurity Induced Antiferromagnetism in Spin-1/2 Heisenberg Two-Leg Ladder Systems 111
3. Non-Magnetic Impurities in Spin Gap Systems 111
S. Many-Body Effects and Superconductivity in Organics 111
1. Integrable Chain of Electrons Coupled with Phonons 111
2. Integrable Chain of Electrons Coupled with Squeezed Phonons 112
3. Strong Electron Correlations in κ- $(BEDT\text{-}TTF)_2X$ Salts 112
4. Superconducting κ-BEDT-TTF Salts as Layered Correlated Electron Systems 112
5. κ-$(BEDT\text{-}TTF)_2CuX$ Salts: Electronic Structure, Insulator-Metal Transition, Superconductivity 112
6. Insulator-Metal Transition in the κ-ET_2X Salts, where "ET" is the bis(ethylenedithio) tetrathiafulvalane (BEDT-TTF) Molecule 112
7. κ- BEDT-TTF Organics as It Is Seen for Hubbardist 112
8. Electronic Structure and Origin of κ-ET_2X Insulators, where "ET" is the bis(ethylenedithio) tetrathiafulvalane (BEDT-TTF) Molecule 112
9. Electron Molecular Vibration Coupling in Organic Charge-Transfer Salts: Application of Spectroscopic and Hubbard Models 113
10. Electronic Structure, Insulator-Metal Transition and Superconductivity in κ- BEDT-TTF Salts 113
11. The Order of the Band Filling in the Periodical Anderson Model 113
12. Path-Integral Treatment for Localized Electrons in the Periodic Anderson Model 113
T. Electronic Structures and Physical Properties of Quasi-One-Dimensional Halogen-Bridged Mixed-Valence Metal Complexes (MX-Chains) 114
1. Photoexcitations in MX Chains: Dynamics of Solitons and Polarons in $[Pt(en)_2]$ $[Pt(en)_2I_2](ClO_4)_4$ 114
2. Subgap Optical Absorption Induced by Quantum Lattice Fluctuations at the Peierls Edge in PtCl-Chain Complexes 114
3. Determination of the Electronic Structure in the Strongly Correlated 1-D Electron Systems: X-Ray Photoelectron and Auger Spectroscopy of Halogen-Bridged Nickel Complexes 114
4. Mixed-Valence State in MMX-Chains Complexes, $Pt_2(dta)_4I$ 114

U. Organic-Inorganic Hybrid-Type Charge Transfer Complexes 115
1. Physical Properties of Quasi-One-Dimensional Charge Transfer Metal Complexes; [M(HBQD)$_2$]TCNQ (M=Ni, Pd; H_2BQD=1,2-Benzoquinonedioxime) 115
V. Low-Dimensional Magnetic Systems 115
1. Crystal Structure and Magnetic Properties of the S=1 Quasi-One-Dimensional Compound Ni([15]aneN_4)N_3(PF_6) 115
2. Inducing a Magnetic Ordering in the Haldane Materials Ni($C_5H_{14}N_2$)$_2N_3$(ClO_4) by Magnetic Field 115
W. Photoelectron Spectroscopy of Organic Solids in Vacuum Ultraviolet Region 115
1. Photoelectron Angular Distribution of Thin Films of Copper Phthalocyanine on MoS_2 Surfaces: Quantitative Determination of Molecular Orientation 115
2. Angle-resolved Photoemission from Oriented Thin Films of Naphthacene: Comparison with Theoretical Spectra 116
3. Angle-resolved UPS of Ultrathin Films of Functional Organic Molecules with Synchrotron Radiation: Determination of Molecular Orientation by Quantitative Analysis of Photoelectron Angular Distribution 116
X. Electrical Conduction and its Related Properties of Organic Solids 116
1. Novel Organic Semiconductor BTQBT with High Conductivity and High Mobility 116
2. Molecular Metals Based on Nonplanar Donor BEDT-ATD: Appearance of Metal-Insulator Transition by Anion or Solvent Replacement 116
3. Superconductivity in NaH Intercalated C_{60} 117

RESEARCH ACTIVITIES V

Department of Applied Molecular Science 118
A. Highly Oxidized Iron Porphyrin and Nonheme Model Complexes 118
1. Preparation, Characterization, and Reactivities of O=Fe^V Porphyrin Complexes 118
2. New Oxidation Reaction of Iron Porphyrin Complex Related to Heme Catabolism 118
3. New Carbon-Carbon Bond Cleavage Reactions of Aldehydes by Peroxo(porphinato) iron(III) Complexes 119
4. A Novel Hydroperoxo-Iron (III) Complex: Synthetic Model for Mono-Nuclear Nonheme Enzymes 119
B. Molecular Mechanisms of Oxygen Activation by Heme Enzymes 119
1. Preparation and Reactions of Myoglobin Mutants Bearing Both Proximal Cysteine Ligand and Hydrophobic Distal Cavity 119
2. The Catalytic Roles of the Distal Site Asparagine-Histidine Couple in Peroxidases 119
3. Conversion of Myoglobin into a Highly Stereospecific Peroxygenase by the L29H/H64L Mutation 120
C. Transition Metal Sulfide Clusters 120
1. Structures, Bonding, and Reactivity of M-S-M' (M and M' = Rh, W, and Cu) Groups in Higher-Nuclearity Heterometallic Sulfide Clusters 120
D. New High T_C Molecular Magnets 121
1. Assemblage of the Electron Spins of the Organic Trinitroxide Radical with a Quartet Ground State by Means of Complexation with Paramagnetic Transition Metal Complexes. A Molecule-Based Magnet with Three-Dimensional Structure and High T_C of 46 K 121
2. Magnetic Characterization of One-Dimensional Molecule-Based Metamagnet Made of Mn(hfac)$_2$ and 1,3-Bis-*N*-oxy-tert-butylamino)benzene 121
E. Synthesis of New High Spin Hydrocarbons 122
1. Toward Dendritic Two-Dimensional Polycarbenes: Synthesis of 'Starburst'-Type Nona- and Dodecadiazo Compounds and Magnetic Study of Their Phtoproducts 122
F. Pressure Effect on Molecular Magnetism 123
1. Pressure Effect on Organic Radicals 123
G. Study of Low-temperature Magnetism of Organic Radicals 123
1. Low-temperature Magnetic Properties of Nitronyl Nitroxides 123
H. New Charge-Transfer Complexes Exhibiting Novel Magnetic Properties 124
1. Synthesis and Redox Property of Bis(tetrathiafulvalenyldithio)germane 124
2. Ferromagnetic Behavior of a Tetra-fluorotetracyanoquinodimethanide Salt at Room Temperature 125
3. Crystal Structures and Magnetic Properties of Tetrafluorotetracyanoquinodimethanide Salts 125
4. Remarkably Strong Antiferromagnetic Interaction through an Intervening Hydrogen Atom in *N*-(*n*-Propyl)pyridinium-substituted Imidazolin-1-oxyl Iodide 125
I. Syntheses, Crystal Structures, and Solid State Properties of Halogen-Bridged Metal Complexes with Linear Chain Structures 126
1. X-ray Structural Study of the Phase Transition of Iodo-Bridged One-Dimensional Pt Dimer, $Pt_2(dta)_4I$ 126
J. Spectroscopic Studies on Charge Delocalization and Charge Transfer in Molecular Cluster Ions and Pure Liquid. 127
1. Pump-Probe Photodepletion Spectroscopy of Mass-Selected $(C_6H_6)_2^+$ 127

2. Construction of a Soft Landing Ion Fixation / Matrix Isolation System of Size-selected Molecular Cluster Ions for Direct Absorption Measurements of IR, VIS, and UV Spectra 127
K. Infrared Laser Spectroscopy of Negatively-Charged Molecular Clusters 128
1. Construction of Apparatus for Infrared Spectroscopy of Cluster Anions 128
2. *Ab Initio* Calculations on Geometrical Structures of $[(CO_2)_nH_2O]^-$ 129

RESEARCH ACTIVITIES VI

Department of Vacuum UV Photoscience 130
A. Electronic Structure and Decay Mechanism of Inner-shell Excited Molecules 130
1. Angular Distribution of Fragment Ions following the S 1s Photoexcitation of H_2S 130
2. Jahn-Teller Effect in the S 1s $\rightarrow 6t_{1u}$ excited state of SF_6 130
3. Angular Correlation between Fragment Ions from the Nitrogen *K*-shell Excited and Ionized N_2O 130
4. Rydberg and Valence States in the C 1s Photoabsorption and Resonance Auger Spectra of CH_3F 131
5. Inner-Shell Excitation Spectroscopy of Closo-Carboranes 131
6. (LS) versus (jj) Coupling in P 2p Inner-Shell Excited States of PF_3 131
B. Soft X-ray Photoelectron-Photoabsorption Spectroscopy and Electronic Structure of Transition Metal Compounds 131
1. Polarization Dependence of Ni 2p Photoexcitation of Nickel Dimethylglyoxime 131
2. Resonant Auger Spectra of Nickel Dimethylglyoxime Following the Ni 2p Excitation 132
3. Photon Energy Dependence of Ni 2p Resonant Auger Spectra of $K_2Ni(CN)_4$ 132
C. Studies on Photochemical Reactions using Ultrafast Laser and Synchrotron Radiation 133
1. Construction of Femtosecond Fluorescence Up-conversion Spectrometer 133
2. Ultrafast Fluorescence Study on the Excited Singlet State Dynamics of all-*trans* Retinal 134
3. Development of an Optical Heterodyne Detected Impulsive Stimulated Raman Scattering Spectrometer with a "phase-stabilizing" Mechanism 134
4. Polarization Dependence of Optical Heterodyne Detected Impulsive Stimulated Raman Scattering of Liquids 135
5. Synchronization Between Picosecond Mode-Locked Laser and Synchrotron Radiation 136
6. A Proposal of Picosecond Time-resolved Far-Infrared Spectroscopy using Synchrotron Radiation 136
D. Synchrotron Radiation Stimulated Surface Reactions 137
1. *In Situ* Observation of Silicon Hydrides on Si(100) Surfaces during Synchrotron-Radiation-Stimulated Si_2H_6 Gas Source Molecular Beam Epitaxy 137
2. Synchrotron Radiation Irradiation Effects for SiH_n on Si(100) Surface in the Synchrotron Radiation Stimulated Si Gas Source Molecular Beam Epitaxy 137
3. IRAS and TDS Study on the Photolytic Decarbonylation of Iron Pentacarbonyl Adsorbed on a SiO_2 Film with a Buried Metal Layer 137
4. Metallization on Piezoelectric Ceramics Surfaces by Synchrotron Radiation Irradiation 138
5. Synchrotron Radiation-Stimulated Semiconductor Process and New Prospects of Core Electron Excitation Photochemistry 138
6. Synchrotron Radiation Irradiation Effects on Low-Temperature Condensed Layer of Dimethyl Aluminum Hydride on SiO_2 Surface 138
7. Development of Electron-Ion Coincidence Spectroscopy for the Study of Surface Dynamics Combined with Synchrotron Radiation 138
8. Auger-Final-State Selected Ion Desorption Study of Condensed NH_3 and ND_3 by Using Auger Electron-Photoion Coincidence Spectroscopy 139
E. Photoionization Dynamics Studied by Electron Spectroscopy Combined with a Continuous Synchrotron Radiation Source 139
1. Observation of the $(3\sigma_g)^{-1}(3p\sigma_u)^1$ Rydberg State of Acetylene 139
2. Formation of Autoionizing Atomic Nitrogen from Superexcited States of Nitric Oxide 140
3. Autoionization of Sulfur Atom Produced by Dissociation of Superexcited OCS 140
4. Autoionization of Superexcited Sulfur Atoms Produced from Doubly Excited Rydberg States of SO_2 141
F. Vacuum UV Spectroscopy Making Use of the Combination of Synchrotron Radiation and Mode-Locked UV Laser 141
1. Detector of the Laser and SR Photon Pulses 141
2. Time-Resolved Experiment of $He^*(1s2p\ ^1P)$ by Using the Laser-SR Combination 142
G Rebuilding the Monochromator on the Beamline BL2B2 in UVSOR 143
1. Main Parameters of the Renewed Beamline 143
H. Absolute Photoabsorption Cross Section and Radiative Dissociation of Polyatomic Molecule Excited at Valence Shell 143
1. Photoabsorption Cross Section and Radiative Processes of $GeCl_4$ in the Valence Region of 6-31eV 143
2. Photoabsorption and Fluorescence Excitation Spectra of CF_3CN in the Region of 6-41 eV 144

3. Photoabsorption and Emission Cross Sections of $SnCl_4$ and $Sn(CH_3)_4$ in the 6-31 eV Region 144
4. Hydrogen Isotope Effect in the Photodissociative Excitation of CH_3CN, CD_3CN, C_2H_5CN and C_2D_5CN 144
5. Photoabsorption Cross Section of C_6F_5X (X=H, F, Cl, Br, I) and Fluorescence Excitation Spectra of $C_6F_5X^{\bullet+}$ Radical Cation in the 30-160 nm Region 144
6. Photodissociation Spectroscopy of BrCN in the Vacuum Ultraviolet Region 145
7. Photoexcited States of Malononitrile in the VUV Energy Region 145

I. Angle-Resolved Photofragmentation of Polyatomic Molecule Excited at *K*-Shell 145
1. Reaction Processes of CF_3CN Excited at the *K*-Edge of C, N, and F Atoms 145

J. Elucidation of Ion-Solid Chemistry in Ion-Implanted Amorphous SiO_2 and Creation of Novel Materials by Implantation 146
1. Proton-Implantation-Induced Nanosized Ge Crystal Formation in SiO_2:GeO_2 Glasses 146
2. Probing Interface Properties of Nanocomposites by Third-Order Nonlinear Optics 146

K. Electronic Structure Design of Wide Gap Conductors and Control of Their Conduction Behavior 146
1. Working Hypothesis to Explore Novel Wide Band Gap Electrically Conducting Amorphous Oxides and Examples 146
2. Amorphous Transparent Electroconductor $2CdO \cdot GeO_2$: Conversion of Amorphous Insulating Cadmium Germanate by Ion Implantation 146
3. New Amorphous Semiconductor: $2CdO \cdot PbO_x$ 147
4. Features of Valence Band Structure of $TlAlF_4$ 147

L. UV Photoelectron Spectroscopic Study of Functional Organic Materials and their Interfaces with Metals 147
1. Electronic Structures of Porphyrins and Their Interfaces with Metals Studies by UV Photoemission 147
2. Electronic Structures of Organic Carrier Transporting Material/Metal Interfaces as a Model Interface of Electroluminescent Devices Studied by UV Photomission 148
3. Angle-Resolved Ultraviolet Photoelectron Spectroscopy of Oriented Film of Model Compound of Poly(p-Phenylene): Wave Number(*k*)-Conservation and *k*-Blurring in a System with Small Number of Repeating Units 148

M. Ultraviolet Photoelectron Spectroscopy of Organic and Inorganic Solids 148
1. Determination of Two-Dimensional Structures of Ultrathin Films of H_2- and Cu-phthalocyanine on MoS_2 by Angle-Resolved Ultraviolet Photoemissn and Low Energy Electron Diffraction 148
2. Strucure of Ultrathin Films of Chloro-alminium Phthalocyanine on MoS_2 Studied by Means of Penning Ionization Electron Spectroscopy, Angle-Resolved UPS and LEED 149
3. Photoemission Study on Poly(pyridine-2,5-diyl), Poly(2,2'-bipyridine-5,5'-diyl), and their K-doped States 149
4. Photoemission Spectroscopy of Bi_2CuO_4 149
5. Physical Properties and Electronic Structure of Potassium-Oxygen-Graphite Intercalation Compounds 149
6. Ultraviolet Photoelectron Spectra of C_{86} and C_{90} 149
7. Photoelectron Spectra of Metal Fullerenes: Are Metal Fullerenes Molecular Crystals or Not? 150

RESEARCH ACTIVITIES VII

Coordination Chemistry Laboratories 151

A. Proton-induced Molecular Switches Using Supramolecular Metal Complexes 151
1. Proton-induced Switching of Electron Transfer Pathways in Dendrimer-Type Tetranuclear $RuOs_3$ Complexes 151
2. Proton-induced Tuning of Electrochemical and Photophysical Properties in Mononuclear and Dinuclear Ruthenium Complexes Containing 2,2'-Bis(benzimidazol-2-yl)-4,4'-bipyridine: Synthesis, Molecular Structure, and Mixed-Valence State and Excited-State Properties 152
3. Electrospray and Collision-induced Dissociation Mass Analysis of Star-burst Type Tetranuclear Complexes 152
4. Analysis of Multiply Charged Ions of Ruthenium(II) Tetranuclear Complexes by Electrospray Ionization Mass Spectrometry. 153

B. Synthesis and Characterization of Self-Assembled Organic Ligands and Metal Complexes on Surface Towards Solution-Phase Molecular Epitaxy 153
1. Synthesis and Properties of Surfactant Ruthenium Complexes Containing 6,6'-Bis(benzimidazolyl)-2,2'-bipyridine with Long Alkyl Chains 153
2. Characterization of Surface Electronic Structures of Silicon Wafers under Air Atmosphere by Ultraviolet Photoelectron Yield Spectroscopy 154
3. Structure of Self-Assembled Layers of Terminally Functionalized Organosilyl Compounds on Silicon Substrates 154
4. Probing Depth of Ultraviolet Photoelectron Yield Spectroscopy in Hydro-Carbon Films 154
5. Charge-up Phenomena of Insulated Metals in X-ray Photoelectron Spectroscopy 154

C. Metal Ions in Biological Systems 155
1. Restrained Reduction of Type 3 Copper in Laccase and Ascorbate Oxidase by Azide 155
2. EPR Spectra of Type 3 Copper Centers in *Rhus vernicifera* Laccase and *Cucumis sativus* Ascorbate Oxidase 155
3. Room Temperature ESR Spectra of *Rhus vernicifera* Laccase and Derivatives 155
4. Direct Electrochemistry of Blue Copper Proteins at Au Electrodes Modified with Promoters 156
5. Cyclic Voltammetry of Cucumber Ascorbate Oxidase 156
6. FT-IR Spectra of the Azide-Type 3 Copper in Laccase and Ascorbate Oxidase 156
7. Dinuclear Nickel Complexes Containing a Dinucleating Ligand N,N,N',N'-Tetrakis-[(1-ethyl-2-benzimidazolyl)methyl]-2-hyrdoxy-1,3-diaminopropane and an Acetate Ion 156
8. Crystal Structures and Hydrogen Bonding in One-Dimensional Chains of 4,5-Dicyanoimidazole and 4,5-Dichloroimidazole 156
9. EPR Study on the Charge Transfer Complexes of N-salicylideneanilines Containing NHO Hydrogen Bond as a Dynamic Function 156
10. Characterization of Poly-CuPc Sheet Polymers Synthesized under High Pressure 157
11. New Cation-Diffusing Phase of $(CH_3NH_3)Bi_2Cl_{11}$ 157
12. Charge-Transfer Effects in a Strongly Hydrogen-Bonded System: Potassium Salt of Acetylenedicarboxylic Acid 157

D. Stereochemical and Kinetic Studies of Coordination Compounds 157
1. New Triamine-type Platinum(II) Complexes of Phenyl-subsituted Ethylenedi-amine : Reactivity with 5'-GMP 157
2. Thermodynamic and Kinetic Studies of Zinc(II)-Triamine Complexes as Models of CA and AP 157
3. Photochemical Desulfurization of a Sulfinato-*S*-Cobalt(III) Complex. Formation of an Organic Peroxide Complex 158
4. Syntheses, Characterization, and Molecular Mechanics Calculations of Optically Active Silatrane Derivatives 158
5. Preparation of a Stable Sulfonato-Cobalt(III) Complex by Oxidation of a Sulfinato-*O* Complex 158
6. Stereochemistry of (*R*)-2-Methyllaziridine Complexes of Cobalt(III) and Dimerization of the Ligand 159
7. Photolysis of Cobalt(III) Complexes Containing Sulfinate-*S* Ligands. Formation of Organic Peroxide Complexes through Desulfurization 159
8. Photochemistry of Cobalt(III) Complexes Containing a Sulfinate-*S* Ligand. Linkage and Geometrical Isomerization 159

E. Creation of Complexes Containing New Types of Bonds between a Transition Metal and a Phosphorus 159
1. Conversion of Transition-Metal Complexes with Stannyl and Phosphenium Ligands into Those with Stannylene and Phosphine Ligands by Alkyl Migration from Sn to P 160
2. Cationic Phosphenium Complexes of Group 6 Transition Metals. Systematic Approach to Elucidation of Influence of Substituents of the Phosphenium Phosphorus on the Stability of the Complexes 160
3. ^{95}Mo NMR Studies on Cationic Phos-phenium Complexes of Molybdenum 160
4. Migratory Insertion Reaction of a Phosphenium Ligand into Mo- and W-alkyl Bonds 161
5. Palladium (II) and Platinum(II) Complexes of Tetraphosphamacrocycle. X-Ray Crystal Structures of Phosphorus Analogs of a (Tetramethylcyclam)metal Complex 161
6. Migration Reactions of a Phosphorane Fragment to the Cyclopentadienyl Ring in Ru-Phosphorane Complexes 161

F. Targeting of Nucleic Acids and Related Biomolecules by Metal Complexes 162
1. Design and Synthesis of a Novel Zn(II) Complex for the Structural and Functional Conversion of AT-Rich Sequences in the Transcriptional Regulatory Domain of DNA 162
2. Catalytic DNA with a Metallic Reaction Center 162
3. Novel Redox-Active Metallopeptides for Structural Control of DNA 163
4. Macrocyclic Metal Complexes for Selective Recognition of Nucleic Acid Bases and Manipulation of Gene Expression 163
5. Recognition and Transformation of Biomolecules by Macrocyclic Polyamine Rare Earth Complexes 163
6. DNA Cleavage by a Novel Nickel(II) Complex of Pyridyl-pendant Dioxocyclam 164
7. Molecular Recognition of Terephthalic Acid by Supramolecular Self-Assembly of an Acridine-pendant Cyclen-Zn^{II} Complex 164
8. A Zinc(II)-Cyclen Complex Attached to an Anthraquinone Moiety that Acts as a Redox-Active Nucleobase Receptor in Aqueous Solution 165
9. Differential Contribution of Metal Complexation and Dimerization to the Chemotherapeutic Potential of Bicyclen-Zn^{II}_2 Complex against Human Immunodeficiency Virus 165

G. Activation of Carbon Dioxide on Metal Complexes 165
1. Ruthenium Formyl Complexes as the Branch Point in Two- and Multi-Electron Reduction of CO_2 165

2. Multi-Step CO_2 Reduction Catalyzed by $[Ru(bpy)_2(qu)(CO)]^{2+}$ (bpy = 2,2'-bipyridine, qu = quinoline). Double Methylation of Carbonyl Moiety Resulting from Reductive Dispropor-tionation of CO_2 166
3. Comparison of Ru-C Bond Characters Involved in Successive Reduction of Ru-CO_2 to Ru-CH_2OH 166
4. Crystal Structure of $[Ru(bpy)_2(CO)(\eta^1\text{-}C(O)OH)]^+$ as a Key Intermediate in CO_2/CO Conversion 166
5. Catalytic Generation of Oxalate through Activation of Two CO_2 Molecules on $[(IrC_p^*)_2(Ir\text{-}\eta^4\text{-}C_p^*CH_2CN)(\mu_3\text{-}S)_2]$ 166
6. Structural and Electrochemical Comparison of Copper(II) Complexes with Tripodal Ligands 167
7. Control of Coordination Mode of η^1- and η^2-1,8-Naphthyridine Ligated to Ru(II)-bis(bipyridine) Complexes 167
8. Synthesis and Characterization of Ruthenium-dioxolene-terpyridine Complexes 168
9. Interconversion among CO, CO_2 and CO_3^{2-} using Ruthenium Complex in Aprotic Media 168

H. Multidimensional Crystal Engineering of Supramolecular Metal Complexes 169
1. Construction of Three-dimensional Supramolecular Coordination Copper(I) Compounds with Channel Structures Hosting a Variety of Anions by Changing the Hydrogen-Bonding Mode and Distances 169
2. Self-assembly of Copper(I) Complexes into Three-Dimensional Coordination Polymers with Channel Networks by Hydrogen Bonding or Tridentate Ligands 169
3. One-, Two- and Three-Dimensional Copper(I), and Silver(I) Complexes of 2,11-Dithia[3,3]paracyclophane 169
4. Synthesis, Structures and Polymeric Silver(I) Complex of Tetrakis- (methylthio)tetrathiafulvalene: The First Example of the Silver(I) Ion Coordinated Directly to TTF-Derivatives 170
5. Three-fold Interpenetrating Diamond Frameworks with π-π Stacking of Alternate Coordinated and Uncoordinated Ligands: Crystal Structures of Copper(I) Coordination Compounds, $[Cu(DMTPN)_2]_2X(DMTPN)(thf)$ (DMTPN=2,5-Dimethylterephthalonitrile; X=BF_4, ClO_4) 170
6. Synthesis and Characterization and X-Ray Crystal Structures of Tetrakis(ethylthio)-tetrathiafulvalenium Hexachlorodicopper(II) and Hexabromodicopper(II) 171
7. A Unique Coordination Polymer Consisting of Two Parallel $C_5H_4S_5$ Molecules Bridging Two Silver(I) Ions ($C_5H_4S_5$=4,5-ethylenedithio-1,3-dithiole-2-thione) 171
8. Reversible Photochromism of a Crystalline Dithienylethene Copper(I) Polymer 171
9. Synthesis, Structures and Properties of Palladium(II) Complexes with Photochromic 4-Methoxyazobenzene 172
10. An Unusual Tetranuclear Copper(I) Acetate Structure with an Open Cubane Cu_4O_4 Framework 172

I. Metal-Complex Based Magnetic Materials Constructed by Building Block Method 173
1. Synthesis, Crystal Structure, and Magnetic Property of a One-Dimensional Ferromagnet with a Mn(III)-NC-Fe(III) Linkage $[NEt_4]_2[Mn(acen)]$ $[Fe(CN)_6]$ (NEt_4 = Tetraethylammonium, acen = N, N'-Ethylenebis(acetylacetonylideneiminato)) 173
2. Synthesis, Crystal Structure, and Magnetic Property of a Ferrimagnetic Layer Compound, $[NEt_4][Mn(5\text{-}Clsalen)]_2[Fe(CN)_6]$ (NEt_4 = Tetraethylammonium, 5-Clsalen = N, N'-Ethylenebis(5-chlorosalicylideneiminato)) 173
3. Syntheses, Structures, and Magnetic Properties of Discrete Bi-, Tri-, and Penta-nuclear Complexes derived from Manganese(III) Salen-like Schiff Base Complexes and Tetraethyl-ammonium Hexacyanoferrate and Spontaneous Magnetization Behavior of their DesolvatedCompounds 174

RESEARCH ACTIVITIES VIII

Computer Center 176

A. Theoretical Studies of Highly Excited Vibrational States in Polyatomic Molecules 176
1. Semiclassical Study of Nonintegrable Systems 176
2. Theoretical Study of the Potential Energy Surfaces and Dynamics of CaNC/CaCN 176
3. Theoretical Calculation of Reaction Rate Constant of Hydrofluorocarbon 176
4. Theoretical Analysis of the Jahn-Teller Distortions of C_{60}^- 177

Chemical Materials Center 178

B. Preparation and Properties of Novel Heterocyclic Compounds for Advanced Materials 178
1. Oxidative Intramolecular Cyclization of 2,2'-Bis(1,4-dithiafulven-6-yl) 3,3'-bithienyls Affording Bis(1,3-dithiole) Electron Donors 178
2. Metallic Cation Radical Salts of BEDT-ATD Incorporating Solvent Molecules 178
3. Synthesis and Properties of Dication Salts of TTF Analogues Containing Quinoid Structures 179
4. New Narrow-Bandgap Polymers Composed of [1,2,5]Thiadiaolo[3,4-g]quinoxaline and Aromatic Heterocycles 179
5. Design of Narrow-Bandgap Polymers. Syntheses and Properties of Monomers and Polymers Containing Aromatic-Donor and *o*-Quinoid-Acceptor Units 179
6. Synthesis and Properties of N-Silylated Diaminothiophene Derivatives: A Novel Building Block for Precisely Defined Conjugated Macromolecules 180
7. Crystal Structure and Physical Properties of (EDTTDA-TTF)SbF_6 Salt 181

Instrument Center 182
C. Developments and Researches of New Laser Materials 182
1. Broad-Band Tunable, Compact, Low-Threshold, Ti:Sapphire Laser Using a Single Time-Resolved Resonance Raman Spectra of Octaethylporphinato Copper(II) in the Lowest Excited Triplet State Set of Extremely Broad-Band Optics 182
2. 1-GHz Repetition-Rate Mode-Locked Ti:Sapphire Laser Using a Saturable Bragg Reflector 182
3. Ultraviolet Picosecond Pulses from an All-Solid-State Ce:LiSAF/Ce:LiCAF Master Oscillator and Power Amplifier System 183
4. Lithium Tetraborate ($Li_2B_4O_7$) Crystals for the High-Energy Fifth Harmonic Generation of Nd:YAG Lasers 183
5. Characterization of Far Infrared Radiation from InAs and GaAs Excited by Femtosecond Optical Pulses 184
6. All-Solid-State, Short Pulse, Far-Infrared Source Using a Saturable Bragg Reflector in a Femtosecond Mode-Locked Laser 184
D. Studies of Nanoscale Carbons 185
1. Removal of sp^2 Carbon Nanospheres from Single-Wall Carbon Nanotubes by using Microfiltration Method 185
2. Tube Diameter Analysis of Triangular Packed Single-Wall Nanotubes by Electron Diffraction 186
3. Infrared and Raman Spectroscopic Studies of Single-Wall Carbon Nanotubes 187
4. Magnetic Properties of Nested Carbon Nanostructures Studied by Electron Spin Resonance and Magnetic Susceptibility Measurements 187
E. The Applications of a Magic-Angle Turning Technique for Half-Integer Quadrupolar Nuclei 188
1. Spinning Sideband Summation for Quadrupole MAS NMR Spectra Using a Magic-Angle Turning Technique 188
2. Spinning-Sideband Suppression in DOR NMR Spectra Using a Magic-Angle Turning Technique 189
Equipment Development Center 189
F. Activities of Division of "IMS Machines" 189
1. ESDIAD Detector with Time-of-Flight Type Mass Separator 189
G. Development of Experimental Devices 189
1. Design and Construction of SGM-TRAIN* Monochromator 189
Ultraviolet Synchrotron Orbital Radiation Facility 191
H. Development of the UVSOR Light Source 191
1. A Helical Optical Klystron for UV Storage Ring Free Electron Lasers 191
I. Development of Beam Lines and Equipment for UVSOR 191
1. Construction of New Monochromator (SGM-TRAIN) at BL5A 191
2. Construction of Spin- and Angle-resolved Photoelectron Spectrometer 192
3. Design of a Helical Undulator for UVSOR 192
4. Reconstruction of BL7B for UV, VIS and IR Spectroscopy with a 3m Normal Incidence Monochromator 193
5. Performance of YB66 Soft X-ray Monochromator Crystal at the Wiggler Beamline 193
J. Researches by the USE of UVSOR 194
1. Photoelectron and Luminescence Spectra of BaFCl, BaFBr, and $CsTaF_6$ 194
2. Photon-Stimulated Desorption of Excited-State Sodium Atom from NaF and NaCl under Valence-Band and Core-Level Excitations 194
3. Surface Core Exciton of Alkali Chloride Film on Si(100) 194
4. Magnetic Circular Dichroism at $M_{2,3}$ edges of Ni(110) Surface 195
5. Photoelectron Spectro-Microscopy Studies at the UVSOR 195
RESEARCH FACILITIES 197
Computer Center 197
Chemical Material Center 197
Instrument Center 197
Low-Temperature Center 197
Equipment Devalopment Center 197
Division of IMS Machines 197
Ultraviolet Synchrotron Orbital Radiation Facility 197
SPECIAL RESEARCH PROJECTS 199
(1) Development of Microscopic Environments with Functionality and Quantum Steering for Reactions 199
Structures, Reactions and Spectroscopies of Molecules and Molecular Clusters 199
Prediction of Protein Tertiary Structures by Multicanonical Algorithms 199
Quantum Mechanical and Semiclassical Studies of Chemical Reaction Dynamics 199
Gaussian-Markovian Multi-State Quantum Fokker-Planck Equation Approach to Nonlinear Spectroscopy of Displaced Morse Oscillators System 200
Constructing Molecular Theory of Chemical Processes in Solution 200

Development of High-Sensitivity Submillimeter-wave to Far Infrared Spectrometer Systems for the Study of Transient Molecules 200
Studies on Laser Cooling and Trapping of Neutral Atoms 201
Laser Spectroscopic Studies of Ions in Liquid Helium 201
Mechanism of Oxygen Activation by Heme-Copper Terminal Oxidase Superfamily 201
Laser Raman Beat Detection of Magnetic Resonance 201
Liquid Dynamics Studied by New Ultrafast Higher-Order Nonlinear Spectroscopy 201
Ultrafast Chemical Reactions in Condensed Phase 202
Studies of Laser-Induced Photochemistry on Solid Surfaces 202
Light Sensitivity of the Self-Organizing Chemical Systems 202
Laser Investigation of Elementary Reactions in the Gas Phase 203
Spectroscopic Studies of Intermolecular Interaction in Molecular Dimer Cations 203
Reactions of Gas-Phase Cluster Anions Studied by Photoelectron Spectroscopy 203
Time-resolved Spectroscopic Studies on Chemical Reactions using Ultrafast Laser and Synchrotron Radiation 203
Study of Ion Desorption Induced by Core-Level Excitations of Condensed $Si(CH_3)_4$ by Using Photoelectron-Photoion Coincidence Spectroscopy (PEPICO) Combined with Synchrotron Radiation 204
Pump-Probe Spectroscopy of Atoms and Molecules with a Combination of Ultraviolet Laser and Synchrotron Radiation 204
New Apparatus for Studying Reaction Dynamics of the Inner Core Excited Polyatomic Molecule 204
Rotation Induced Vibrational Mixing in Highly Excited Vibrational States of Formaldehyde II 205
Development of the New Lasers for Molecular Science 205
Ultra-High-Vacuum Friction Test Apparatus 205
Investigation of Electronic Structures of New Materials by Using Synchrotron Radiation 205
Study for High Brilliant Radiation Using the UVSOR Electron Storage Ring 206
Studies of Solid Surfaces by Photoelectron Spectroscopy 206
(2) Study of Molecular Solid toward Molecular Electronics 206
Theory of Electronic Phases in Molecular Conductors and Insulators: Electron Correlation and Electron-Phonon Effects in Quasi-One-Dimensional Systems 206
Materials Science on Molecular Devices π-d Interaction in Molecular Metals 207
Search for Negative-*U* Materials in Molecular Solid 207
Toward Comprehensive Understanding of Various Electronic Phases in Molecular Conductors; Superconductivity in $(BEDT\text{-}TTF)_2X$ Family 207
Development and General Phase Diagram of Two-Dimensional Organic Superconductors 207
Development of Magnetic Molecular Metals 208
NMR Studies on the Dynamical Properties of Condensed Matter Systems 208
Pressure Effect on Molecule-Based Magnetism 208
Construction of the Ultraviolet Inverse Photoemission Spectrometer 209
Photoelectron Spectroscopic Study of Organic / Metal Interfaces 209
Organic Conductors Based on Novel Heterocyclic Compounds 209
(3) Material Control in Multi-Reaction Centers 210
Catalytic Intermediates of Polyethylene Glycoled Horseradish Peroxidase (PEG-HRP) in Benzene 210
Coordination Chemistry on Surface Towards Solution-phase Molecular Epitaxy 210
Assembled Metal Centers in Enzymes 210
Construction of Metal Complexes for Artificial Gene Control 211
Stereochemistry and Electrochemistry of Cobalt(II) and Cobalt(III) Complexes Containing Optically Active Tetradentate Schiff Base Ligands 211
1,3-Migration of a Substituent on a Phosphorus in a Transition Metal Coordination Sphere 211
Activation of Carbon Dioxide on Metal Complexes Directed Toward Carbon-Carbon Bond Formation 212

OKAZAKI CONFERENCES 213

JOINT STUDIES PROGRAM 216
1) Special Projects 216
2) Research Symposia 218
3) Cooperative Research 218
4) Use of Facilities 218
5) UVSOR 218

FOREIGN SCHOLARS 220

AWARDS 223

LIST OF PABLICATIONS 224

REVIEW ARTICLES AND TEXTBOOKS 236

AUTHOR INDEX -RESEARCH ACTIVITIES AND SPECIAL RESEARCH PROJECTS 239

ORGANIZATION AND STAFF

Organization

The Institute for Molecular Science compromises twenty three research laboratories each staffed by a professor, an associate professor, two research associates and several technical associates, two research laboratories with foreign visiting professors, and six research facilities. The laboratories are grouped into six departments and one facility for coordination chemistry:

Department of Theoretical Studies	Theoretical Studies I
	Theoretical Studies II
	Theoretical Studies III[1)]
	Theoretical Studies IV
Department of Molecular Structure	Molecular Structure I
	Molecular Structure II[1)]
	Molecular Dynamics
Department of Electronic Structure	Excited State Chemistry
	Excited State Dynamics
	Electronic Structure[1)]
	Molecular Energy Conversion[2)]
Department of Molecular Assemblies	Solid State Chemistry
	Molecular Assemblies Dynamics
	Molecular Assemblies[1)]
Department of Applied Molecular Science	Applied Molecular Science I
	Applied Molecular Science II[1)]
	Molecular Clusters (April '96-)[3)]
Department of Vacuum UV Photoscience	Photochemistry
	Chemical Dynamics
	Interface Molecular Science[3)]
	Synchrotron Radiation Research[2)]
Coordination Chemistry Laboratories	Synthetic Coordination Chemistry[3)]
	Complex Catalysis
	Fundamental Coordination Chemistry
	Coordination Bond[1)]
Research Facilities are:	Computer Center
	Chemical Materials Center
	Instrument Center
	Low-Temperature Center
	Equipment Development Center
	UVSOR (Ultraviolet Synchrotron Orbital Radiation) Facility

1)Professors and associate professors are visiting professors from other universities.
2)Research laboratories with foreign visiting professors.
3)Professors, associate professors, and research associates, along with their positions, are transferred from other universities.

Scientific Staff

Mitsuo ITO	**Professor, Director-General**

Emeritus Professors

Saburo NAGAKURA	President, The Kanagawa Academy of Science and Technology
Eiji HIROTA	President, The Graduate University for Advanced Studies
Katsumi KIMURA	Professor, Japan Advanced Institute of Science and Technology
Keiji MOROKUMA	Professor, Emory University, U.S.A.
Hiroo INOKUCHI	Distinguished Research Consultant, Institute for Molecular Science
Yusei MARUYAMA	Professor, Hosei University

Department of Theoretical Studies

Theoretical Studies I

Suehiro IWATA	Professor
Yuko OKAMOTO	Associate Professor
Tsutomu IKEGAMI	Research Associate
Akira SHUDO	Research Associate (-March '96)[1]
Ulrich HANSMANN	Research Associate (May '96-)
Takeshi TSURUSAWA	Technical Associate
Toshio ASADA	IMS Fellow (-June '96)[2]
Masato MASUYA	IMS Fellow (April '96-)
Toshiaki FUJII	Graduate Student
Hidekazu WATANABE	Graduate Student
Pradipta BANDYOPADHYAY	Graduate Student (January '96-)
Ayori MITSUTAKE	Graduate Student (from Nara Women's University*) (April '96-)
Tadayoshi SUZUKI	Graduate Student (from Waseda University*) (April '96-)
Chang-Guo ZHAN	Visiting Scientist (from Central China Normal University, China); JSPS Ronpaku Fellow (June '96- August '96)[3]
Jong Keun PARK	Visiting Scientist; KOSEF Fellow (May '95- April '96)[4]
Yumin LI	Visiting Scientist; JSPS Post-Doctoral Fellow (June '95-)
Dukhwan LEE	Visiting Scientist (from Sogang University, Korea); MONBUSHO Invited Fellow (December '95- February '96)[5]
Simon MATHIEU	Visiting Scientist (from Universite Paul Sabatier, France) (August '95-February '96)[6]
Fernando R. ORNELLAS	Visiting Professor (from Institute of Chemistry, University of São Paulo, Brazil) (August '95-June '96)[7]
Jan HRUSAK	Visiting Scientist (from J. Heyrousky Institute of Physical Chemistry Academy of Sciences of the Czech Republic, Czech); MONBUSHO Invited Fellow (March '96-)
Surjit SINGH	Visiting Scientist (from Indian Institute of Technology, Madras, India); MONBUSHO Invited Fellow (October '95- October '95)[8]
Wenning WANG	Visiting Scientist (from Fudan Univ.); JSPS Sangaku Project Fellow (December '95- February '96)[9]
Melly NAPHCHA	Visiting Scientist; MONBUSHO Invited Fellow (January '96- May '96)[10]
Patrizio SEVERINO	Visiting Scientist; EC Fellow (May '96-)
Andreas FIEDLER	Visiting Scientist; JSPS Post-Doctoral Fellow (May '96-)

Theoretical Studies II

Hiroki NAKAMURA	Professor
Yoshitaka TANIMURA	Associate Professor
Chaoyuan ZHU	Research Associate
Ko OKUMURA	Research Associate
Youko SUZUKI	Technical Associate (January '96-)
Norikazu TOMITA	IMS Fellow (-November '95)[11]
Akira OKADA	IMS Fellow (-March '96)[12]
Isaakovich Oleg TOLSTIKHIN	IMS Fellow (July '96-)
Miyabi HIYAMA	Graduate Student
Yutaka MARUYAMA	Graduate Student
Yutaka IMAMURA	Graduate Student (April '96-)

Yoshiaki TERANISHI	Graduate Student (April '96-)
Frank O. GOODMAN	Visiting Professor (from University of Waterloo, Canada) (November '94-September '95)[13]
Abraham BEN-REUVEN	Visiting Scientist (from Tel Aviv University, Israel); MONBUSHO Invited Fellow (August '95- October '95)[14]
Henrik SZICHMAN	Visiting Professor (from Soreq Nuclear Research Institute, Israel) (October '95-)
Vladimir I. OSHEROV	VisitiNG SCIEntist (from Institute of Chemical Physics, Russia); MONBUSHO Invited Fellow (December '95- June '96)[15]
Devorakonda A. PADMAVATHI	Visiting Scientist; JSPS Sangaku Project Fellow (January '96- March '96) Visiting Scientist; (April '96- May '96)[16]

Theoretical Studies III

Eisaku MIYOSHI	Visiting Professor (from Kyushu University) (-March '96) [17]
Shigeki MITAKU	Visiting Professor (from Tokyo University of Agriculture and Technology) (April '96-)
Masaki SASAI	Visiting Associate Professor (from Nagoya University) (-March'96) [18]
Atsunari HIRAYA	Visiting Associate Professor (from Hiroshima University) (April '96-)
Seiichiro TEN-NO	Research Associate
Katsuyuki NOBUSADA	Research Associate (October '95-)

Theoretical Studies IV

Fumio HIRATA	Professor (October '95-)
Kenji YONEMITSU	Associate Professor (February '96-)
Hirofumi SATO	Research Associate (August '96-)
Sarah A. MAW	Visiting Graduate Student (from Manchester University, the United Kingdom); MONBUSHO Invited Fellow (July '96- August '96)[19]

Department of Molecular Structure

Molecular Structure I

Shuji SAITO	Professor
Norio MORITA	Associate Professor
Shuro TAKANO	Research Associate (-September '96)[20]
Yoshiki MORIWAKI	Research Associate
Mitsutaka KUMAKURA	Technical Associate
Kaori KOBAYASHI	Technical Associate
Hideo FUJIWARA	IMS Fellow
Imtiaz K. AHMAD	Visiting Scientist; JSPS Post-Doctoral Fellow (April '96-)
Jian TANG	Graduate Student (-March '96); Research Fellow (April '96 - June '96) [21]
Tsuyoshi HIRAO	Graduate Student
Kei-ichi NAMIKI	Graduate Student
Naomi INADA	Graduate Student (from Hiroshima University)*
Mitsunori ARAKI	Graduate Student (April '96-)

Molecular Structure II

Isao MORISHIMA	Visiting Professor (from Kyoto University)
Masao KITANO	Visiting Associate Professor (from Kyoto University) (-March '96)
Hideto KANAMORI	Visiting Associate Professor (from Tokyo Institute of Technology) (April '96-)
Takashi OGURA	Research Associate
Hiroyuki OZEKI	Research Associate

Molecular Dynamics

Teizo KITAGAWA	Professor
Tatsuhisa KATO	Associate Professor
Michio MATSUSHITA	Research Associate
Yasuhisa MIZUTANI	Research Associate
Masahiro MUKAI	Research Associate
Naoki HAYASHI	Technical Associate
Shigeki NAGATOMO	Technical Associate (October '95-)
Yong-Rok KIM	Visiting Scientist (June '96 - August '96); MONBUSHO Invited Fellow[22]

Jörg MATYSIK	Visiting Scientist; JSPS Post-Doctoral Fellow
Shun HIROTA	JSPS Post-Doctoral Fellow (-March '96)[23]
Xiaojie ZHAO	Research Fellow
Denis A.PROSHLYAKOV	Graduate Student (-September '95)[24]
Takeshi KODAMA	Graduate Student (-March '96)[25]
Tadashi IWASE	Graduate Student
Takeshi TOMITA	Graduate Student
Yuki UESUGI	Graduate Student
Michihiko AKI	Graduate Student (April '96-)
Yasuko KOBAYASHI	Graduate Student (April '96-)
Koji YAMAMOTO	Graduate Student (April '96-)

Department of Electronic Structure

Excited State Chemistry

Keitaro YOSHIHARA	Professor
Yoshiyasu MATSUMOTO	Associate Professor
Kyoichi SAWABE	Research Associate (-March '96)[26]
Keisuke TOMINAGA	Research Associate
Shigeichi KUMAZAKI	Technical Associate
Kazuo WATANABE	Technical Associate
Toshihisa ANAZAWA	IMS Fellow
Ikuo KINOSITA	Visiting Scientist[27]
Hiroyuki KATO	Graduate Student
Ken-ichi SAITOW	Graduate Student
Hideaki SHIROTA	Graduate Student
Kaoru OHTA	Graduate Student (from Kyoto University)*
Haridas PAL	Visiting Scientist (from Bhabha Atomic Research Centre, India); JSPS Invited Fellow (-March '96)
Jangseok MA	Visiting Scientist (-December '95)[28]
Igor V. RUBTSOV	IMS Fellow (April '96-)
Narayanan GAYATHRI	Visiting Scientist (from Indian Institute of Science, India); JSPS Invited Fellow (August '96-)
Tae J. KANG	Visiting Scientist (from Taegu University, Korea) (June '96-)
Nilmoni SARKAR	Visiting Scientist (from Indian Association of Cultivation of Science, India); JSPS Invited Fellow (March-May '96)
Stephen R. MEECH	Visiting Scientist (from University of East Anglia, UK) (March-April '96)

Excited State Dynamics

Ichiro HANAZAKI	Professor
Toshinori SUZUKI	Associate Professor
Kenichi TONOKURA	Research Associate
Suketu R. GANDHI	Research Associate
Hideki KATAYANAGI	Technical Associate
Akiko KAMINAGA	Technical Associate
Nobuaki YONEKURA	IMS Fellow (-March '96)[29]
Yuxiang MO	Visiting Scientist (-October '95)[30]
Yang SHI	Visiting Scientist (from Institute of Chemistry, Chinese Academy of Sciences, China); JSPS Invited Fellow (January '96-)
Noriaki OKAZAKI	JSPS Post-Doctoral Fellow (-October '95); IMS Fellow (November '95-)
Tatuo GEJO	Visiting Scientist (October '95); IMS Fellow (November '95-March '96)[31]
Gyula RÁBAI	Visiting Scientist (from Kossuth Lajos University, Hungary); JSPS Fellow (February '96-)
Hiroshi KOGUCHI	Visiting Scientist (April '96-)
Nobuhisa HASHIMOTO	Graduate Student
Takeshi SHIBATA	Graduate Student

Electronic Structure

Kinichi OBI	Visiting Professor (from Tokyo Institute of Technology) (April '96-)
Hiroyasu SATO	Visiting Professor (from Mie University) (-March '96)
Yoshio TEKI	Visiting Associate Professor (from Osaka City University)
Nobuaki TANAKA	Research Associate
Yukito NAITOH	Research Associate

Molecular Energy Conversion

Michael C. HEAVEN	Visiting Professor (from Emory University, USA) (January-August '96)

Department of Molecular Assemblies

Solid State Chemistry

Kyuya YAKUSHI	Professor
Kazushi KANODA	Associate Professor
Akito UGAWA	Research Associate
Yasuhiro NAKAZAWA	Research Associate
Ken-ichi IMAEDA	Technical Associate
Kazuya MIYAGAWA	Technical Associate
Mikio URUICHI	Technical Associate
Takafumi MIYAZAKI	JSPS Post-Doctoral Fellow (-September '95)[32]
Makoto INOKUCHI	JSPS Post-Doctoral Fellow
Toshihiro HIEJIMA	Graduate Student (-March '96)[33]
Jian DONG	Graduate Student (-March '96), Visiting Scientist; Toyota Scientific Research Fellow (April '96-)
Yukako YONEHARA	Graduate Student (April '96-)
Hiromi TANIGUCHI	Graduate Student
Ko-ichi HIRAKI	Graduate Student
Jingui QIN	Visiting Scientist (from Wuhan University, China); MONBUSHO Invited Fellow (-October '95)[34]
Valery A. IVANOV	Visiting Scientist (from Kurnakov Institute of General and Inorganic Chemistry of Russian Academy of Science, Russia); MONBUSHO Invited Fellow (November '95-)
Wang PING	Visiting Scientist (from University of Alabama, U.S.A.) (October '95-February '96)
Mkhitar V. SIMONYAN	Visiting Scientist (from Institute for Physical Research of Armenian National Academy of Science, Armenia); JSPS Post-Doctoral Fellow (January '96-August '96)
Chikako NAKANO	Visiting Scientist

Molecular Assemblies Dynamics

Hayao KOBAYASHI	Professor
Seiichi MIYAJIMA	Associate Professor
Hironori OGATA	Research Associate
Hideki FUJIWARA	Research Associate (April '96-)
Osamu OISHI	Technical Associate
Toshihito NAKAI	IMS Fellow (-February '96)[35]
Hiroki AKUTSU	IMS Fellow (April '96-)
Jonas V. KRÖBER	JSPS Post-Doctoral Fellow (-March '95), Visiting Scientist (April '96-July '96)
Jong-Jean KIM	Visiting Scientist (from Korean Advanced Institute of Science and Technology, Korea); MONBUSHO Invited Fellow (-September '95, December '95- February '96)[36]
Akane SATO	Graduate Student (April '96-)
Emiko ARAI	Graduate Student (from Toho University)*(April '96-)

Molecular Assemblies

Kousuke SHOBATAKE	Visiting Professor (from Nagoya University)(-March'96)
Hidetoshi FUKUYAMA	Visiting Professor (from University of Tokyo)(April '96-)
Masahiro YAMASHITA	Visiting Associate Professor (from Nagoya University)
Shinji HASEGAWA	Research Associate
Tomoyuki MOCHIDA	Research Associate

Department of Applied Molecular Science

Applied Molecular Science I

Yoshihito WATANABE	Professor
Katsuya INOUE	Associate Professor (January '96-)
Kwang-Hyun AHN	Visiting Associate Professor (from Kyung Hee University, Korea); MONBUSHO Invited Scientist (June-August '96)
Masaaki ABE	Research Associate (-March '96)[37]
Shin-ichi OZAKI	Research Associate
Yuko HOSOKOSHI	Research Associate (June '96-)

Senji WADA	IMS Fellow
Abdel Wahed ElZaizi	Visiting Scientist (from CNRS (Toulouse), France); JSPS Post-Doctoral Fellow (March-June '96)[38]
Toshitaka MATSUI	Graduate Student
Yoshio GOTO	Graduate Student
Kunio HATANAKA	Graduate Student (-March '96)[39]
Tetsuji ITO	Graduate Student (-March '96)[40]
Minoru MITSUMI	Graduate Student
Koichi TAMAKI	Graduate Student
Md.Badruz ZAMAN	Graduate Student (-March '96)[41]

Applied Molecular Science II

Toyonari SUGIMOTO	Visiting Professor (from Research Inst. for adv. Sci. and Tech., Osaka Prefecture University) (April '96-)
Koshiro TORIUMI	Visiting Associate Professor (from Himeji Inst.Tech.)
Seiji OGO	Research Associate (June '96-)

Molecular Clusters

Nobuyuki NISHI	Professor (May '96-)
Takashi NAGATA	Associate Professor (May '96-)
Kazuhiko OHASHI	Research Associate (May '96-)
Lei ZHU	Research Associate (May '96-)
Yoshiya INOKUCHI	Graduate Student (from Kyushu University) (May '96-)*
Morihisa SAEKI	Graduate Student (from Tokyo University) (August '96-)*

Department of Vacuum UV Photoscience

Photochemistry

Nobuhiro KOSUGI	Professor
Tahei TAHARA	Associate Professor
Yasutaka TAKATA	Research Associate
Satoshi TAKEUCHI	Research Associate
Haruhiko OHASHI	Technical Associate
Jun-ichi ADACHI	Technical Associate
Motohiko NAKAMURA	IMS Fellow (- March '96)[42]
Shigeki MATSUO	IMS Fellow
Atsuhiko SHIMOJIMA	IMS Fellow (April '96 -)
Misa KAYAMA	Graduate Student
Takaki HATSUI	Graduate Student (April '96 -)

Chemical Dynamics

Tsuneo URISU	Professor
Koichiro MITSUKE	Associate Professor
Kazuhiko MASE	Research Associate
Hiroaki YOSHIDA	Research Associate
Yoshiyuki TSUSAKA	Research Associate
Hideo HATTORI	Technical Associate
Mitsuru NAGASONO	Technical Associate
Masakazu MIZUTANI	IMS Fellow
Akitaka YOSHIGOE	Graduate Student (- March '96)[43]
Shinya HIRANO	Graduate Student
Yoshiaki IMAIZUMI	Graduate Student
Yasumasa HIKOSAKA	Graduate Student (from Tokyo Institute of Technology)
Gheyas Syed IRFAN	Graduate Student (from Saga University) (- March '96); JSPS Post-Doctoral Fellow (April '96 - June'96); Visiting Scientist (July '96 -)
Harutaka MEKARU	Graduate Student (April '96 -)

Interface Molecular Science

Norio IBUKI	Professor
Hideo HOSONO	Associate Professor
Naoyuki UEDA	Research Associate
Hisao ISHII	Research Associate
Kazumasa OKADA	IMS Fellow (April '96 -)
Mitsuhiko KONO	JSPS Post-Doctoral Fellow (School of Chemistry,University of Bristol)
Takayuki MIYAMAE	Visiting Scientist

Naoto KIKUCHI	Graduate Student (from Tokyo Institute of Technology) (-March '96)[44]
Ryuta WASEDA	Graduate Student (from Tokyo Institute of Technology) (-March '96)[45]
Kazushige UEDA	Graduate Student (from Tokyo Institute of Technology) (April '96-)
Masafumi MIZUGUCHI	Graduate Student (from Tokyo Institute of Technology) (April '96-)

Synchrotron Radiation Research

Frank O. GOODMAN	Visiting Professor (from University of Waterloo, Canada) (November '94 - September '95)
Enrique J. SZICHMAN	Visiting Professor (from Soreq Nuclear Research Institute, Israel) (October '95 -)
Fernando R. ORNELLAS	Visiting Professor (from Institute of Chemistry, University of SaoPaulo, Brazil) (August '95- June '96)

Coordination Chemistry Laboratories

Koji TANAKA	Director

Synthetic Coordination Chemistry

Yuzo YOSHIKAWA	Professor (-March '96)[46]
Masa-aki HAGA	Professor (April '96-)
Hiroshi NAKAZAWA	Associate Professor (-March '96)[47]
Takeshi SAKURAI	Associate Professor (April '96-)
Yasushige KURODA	Research Associate (-March '96)[46]
Tsutomu MIZUTA	Research Associate (-March '96)[47]
Sadamu TAKEDA	Research Associate (April '96-)
Hideaki MONJUSHIRO	Research Associate (April '96-)
Takashi FUJIHARA	IMS Fellow (-October '95)[48]
Kazumasa HARADA	IMS Fellow (November '95-)
Yasuharu OMORI	Graduate Student (from Okayama University)* (-March '96)
Yoshitaka YAMAGUCHI	Graduate Student (from Hiroshima University)* (-March '96)
Koji YUTOH	Visiting Scientist (from Okayama University)* (-March '96)
Yuri MIZUNO	Graduate Student (from Nara Women's University)* (-March '96)
Kazuhiko ITOH	Graduate Student (from Hiroshima University)* (-March '96)
Kazumori KAWAMURA	Graduate Student (from Hiroshima University)* (-March '96)
Toshinori MORI	Graduate Student (from Okayama University)* (-March '96)
Mitsuru KISHISHITA	Graduate Student (from Hiroshima University)* (-March '96)
Katsuya YAMAMOTO	Graduate Student (from Hiroshima University)* (-March '96)
Nobuhiko SAKURAI	Graduate Student (from Kanazawa University)* (April '96-)
Huang HONG-WEI	Graduate Student (from Kanazawa University)* (April '96-)
Isao HARA	Graduate Student (from Kanazawa University)* (April '96-)
Ituko MURATA	Graduate Student (from Mie University)* (April '96-)
Delower Md. HOSSAIN	Graduate Student (from Mie University)* (April '96-)

Complex Catalysis

Mitsuhiko SHIONOYA	Professor
Yutaka FUKUDA	Visiting Professor (from Ochanomizu Women's University) (-March '96)[49]
Yuzo YOSHIKAWA	Visiting Professor (from Okayama University) (April '96-)
Junichiro SETSUNE	Visiting Associate Professor (from Kobe University) (-March '96)[50]
Hiroshi NAKAZAWA	Visiting Associate Professor (from Hiroshima University) (April '96-)
Kentaro TANAKA	Research Associate (December '95-)
Akio OJIDA	IMS Fellow (October '95-)
Michito SHIOTSUKA	IMS Fellow (April '96-)
Motoyuki TASAKA	Graduate Student (April '96-)

Functional Coordination Chemistry

Koji TANAKA	Professor
Noriyuki SUZUKI	Research Associate (-April '96)[29]
Kiyoshi TSUGE	Research Associate
Ryuichiro HARA	Technical Associate (-March '96)[51]
Tetsunori MIZUKAWA	Technical Associate
Masato KURIHARA	IMS Fellow
Tadahiro NAKAMOTO	IMS Fellow (November '95-)

Hiroshi NAKAJIMA	Graduate Student (-March '96)[52]
Kiyotsuna TOYOHARA	Graduate Student (-March '96)[53]
Kayoko KASAI	Graduate Student (-March '96)[54]
Zhenfeng XI	Graduate Student (-November '95)[51]
Yasushi NISHIHARA	Graduate Student (-February '96)[51]
Md. Meser ALI	Graduate Student (April '96-)
Reinald FISCHER	Visiting Associate Professor (from Friedrich-Schiller University Jena, Germany) (-September '95)[55]
Yong Kwang PARK	Visiting Scientist (from Kangwon National University, Korea); MONBUSHO Invited Fellow (December '95-February '96)[56]
Philippe DROGNAT ANDRE	Visiting Scientist (from Hokkaido University) (-October '95)[51]
Shou-Quan HUO	Visiting Scientist (from Hokkaido University) (-February '96)[51]
Daniele STEPHANE	Visiting Scientist (from Nice-Sophia-Antipolis University, France); JSPS Post-Doctoral Fellow (March'96-June'96)[57]

Coordination Bond

Megumu MUNAKATA	Visiting Professor (from Kinki University)
Naohide MATSUMOTO	Visiting Professor (from Kyushu University)

Research Facilities

Computer Center

Suehiro IWATA	Director
Mutsumi AOYAGI	Associate Professor
Shinkoh NANBU	Research Associate
Toshiya TAKAMI	Research Associate
Satoshi MINAMINO	Techinical Associate
Kouichi MOGI	IMS Fellow

Chemical Materials Center

Yoshito WATANABE	Director
Yoshiro YAMASHITA	Associate Professor
Shoji TANAKA	Research Associate
Masaaki TOMURA	Technical Associate
Chitoshi KITAMURA	Guraduate Sutudent (-March '96); JSPS Post-Doctoral Fellow (April '96-)
Akira OHTA	Guraduate Sutudent (-March '96); JSPS Post-Doctoral Fellow (May '96-)

Instrument Center

Shuji SAITO	Director
Nobuhiko SARUKURA	Associate Professor (February '96-)
Shunji BANDOW	Research Associate
Daisuke KUWAHARA	Research Associate
Hideyuki OHTAKE	Research Associate (April '96-)
Ryozo TAKASU	Graduate Student (-March '96)
Shinji IZUMIDA	Graduate Student
Zhenlin LIU	Graduate Student
Keith A WILLIAMS	Visiting Scientist (April '96 - May '96)

Low-Temperature Center

Kyuya YAKUSHI	Director

Equipment Development Center

Teizo KITAGAWA	Director
Michio WATANABE	Associate Professor
Shuji ASAKA	Research Associate

Ultraviolet Synchrotron Orbital Radiation Facility

Nobuhiro KOSUGI	Director
Masao KAMADA	Associate Professor
Toyohiko KINOSHITA	Associate Professor
Hiroyuki HAMA	Associate Professor
Kazutoshi FUKUI	Visiting Associate Professor (from Fukui Univ.)
Aleksandr LUSHCHICK	Visiting Associate Professor (from Estonian Academy) (October '96-)

Atsunari HIRAYA	Research Associate (-September '95)[58]
Shin-ichiro TANAKA	Research Associate
Shin-ichi KIMURA	Research Associate
Masahito HOSAKA	Research Associate (October '95-)
Tatsuo GEJO	Research Associate (April '96-)
Yong Q. CAI	Visiting Scientist; JSPS Foreign Research Fellow (-January '96)[59]
Sayumi HIROSE	JSPS Post-Doctral Fellow
Shinya YAGI	IMS Fellow (-March '96)[58]
Masamitsu WATANABE	IMS Fellow (April '96-)
Naoshi TAKAHASHI	Graduate Student
Kazuhiko KIMURA	Graduate Student
Krishna G. NATH	Graduate Student (January '96-)
Masatake ICHIKAWA	Graduate Student (October '95-)

Technical Staff

Akira UCHIDA	Technical Division Head (-September '95)
Kusuo SAKAI	Technical Division Head (October '95-)
Osamu MATSUDO	Technical Section Chief
Kiyonori KATO	Technical Section Chief
Fumio NISHIMOTO	Technical Section Chief
Fumitsuna TESHIMA	Computer Center
Fumiyasu MIZUTANI	Computer Center
Shigeki NAITO	Computer Center
Masaaki NAGATA	Chemical Materials Center (Unit Chief)
Sachiyo NOMURA	Chemical Materials Center
Takaya YAMANAKA	Instrument Center (Unit Chief)
Masahiro SAKAI	Instrument Center
Hisashi YOSHIDA	Low-Temperature Center (Unit Chief)
Takashi TAKAYAMA	Low-Temperature Center
Hideo SHIBAYAMA	Low-Temperature Center** (September '96-)
Toshio KINOSHITA	Electronic Structure (Unit Chief)
Toshio HORIGOME	Equipment Development Center (Unit Chief)
Mitsukazu SUZUI	Vacuum UV Photoscience (Unit Chief) (-September '95)[60]
Tatsuharu TORII	Equipment Development Center (October '95-)
Shinji KATO	Equipment Development Center (-March '96)[61]
Nobuo MIZUTANI	Equipment Development Center
Kouichi UCHIYAMA	Equipment Development Center
Tomonori TOYODA	Equipment Development Center
Takayuki YANO	Equipment Development Center
Masami HASUMOTO	UVSOR Facility (Unit Chief)
Jun-ichiro YAMAZAKI	UVSOR Facility
Eiken NAKAMURA	UVSOR Facility

* Carries out graduate research of IMS on Cooperative Education Program of IMS with other graduate schools.
** Technical supporting staff for scientific research.

1) Present Address:	Department of Physics, Kwansei Gakuin University, 1-1-155 Uegahara Nishinomiya 662
2) Present Address:	College of Integrated Arts and Sciences, University of Osaka Prefecture, 1-4 Gakuen-cho, Sakai-city, Osaka 593
3) Present Address:	Department of Chemistry, Central China Normal University, Wuhan 430070, P.R.China
4) Present Address:	Department of Chemistry, Pusan National University, Kumjeong-ku, Pusan 609-735, Korea
5) Present Address:	Department of Chemistry, Sogang University, Seoul, Korea
6) Present Address:	Labatoire de Physique Quantique-URA 505 IRSAMC, Universite Paul Savatier, 118 Route de Narborne, 31062 Toulouse Cedex, France
7) Present Address:	Instituto de Quimica Universidade de Saö Paulo, Caixa Postal 26077, SP.,05599-970, Brazil
8) Present Address:	Indian Inst. of Technology, Madras, Madras 600036, India
9) Present Address:	Department of Chemistry, Fudan University, 220 Handan Rd., 200433, P.R.China
10) Present Address:	Fritz Haber Institute for Molecular Dynamics, The Hebrew Univ. of Jerusalem, Givat Ram, Jerusalem, Israel
11) Present Address:	National Research Institute for High Energy Physics, Oho 1-1 Tsukuba 305

12) Present Address: College of Arts and Science, Department of Chemistry, University of Rochester, Rochester, NY 14627-0216, U.S.A.
13) Present Address: Department of Applied Mathematics and Department of Physics, University of Waterloo, Waterloo, Ontario, Canada N2L 3G
14) Present Address: School of Chemistry, Tel Aviv University, 69978 Tel Aviv, Israel
15) Present Address: Russian Academy of Sciences, Institute of Chemical Physics, 12432 Chernogolovka, Russia
16) Present Address: Chemistry Deprtment, IIT Powai, Bombay-76, India
17) Present Address: Department of Chemistry, Faculty of Engineering, Kyushu University, Ropponmatsu, Chuo-ku, Fukuoka 810
18) Present Address: Division of Informatics for Science, Graduate School of Human Informatics, Nagoya University, Chikusa-ku,Nagoya 464-01
19) Present Address: Department of Chemistry, Manchester University, Oxford Road, Manchester M13 9PL, England, UK
20) Present Address: Physikalisches Institut, Universität zu Köln, D-50937 Cologne Germany.
21) Present Address: Department of Chemistry, University of Chicago, 5735 South Ellis Avenue, Chicago, Illinois 60637, U.S.A.
22) Present Address: Department of Chemistry, Yonsei University 134, Seodaemoon-Gu, Shinchon-Dong Seoul, 120-749, Korea.
23) Present Address: Department of Chemistry, Nagoya University, 464-01, Japan.
24) Present Address: Department of Chemistry, College of Natural Science, Michigan State University, East Lansing, MI 48824-1322, U.S.A.
25) Present Address: Department of Chemistry, Tokyo Metropolitan University, Minami Osawa 1-1, Hachioji 192-03
26) Present Address: Department of Molecular Design and Engineering, Nagoya University, Graduate School, Furocho, Chikusa-ku, Nagoya, Aichi 464-01
27) Permanent Address: Yokohama City University, 22-2 Seto, Kanazawa-ku, Yokohama 236
28) Present Address: Siyoung Apt. 124-302, Shincheon-dong, Songpa-gu, Seoul 138-240, Korea
29) Present Address: The Institute of Physical and Chemical Research (RIKEN), 2-1 Hirosawa, Wako, Saitama 351-01
30) Present Address: Max-Planck-Institut für Strömungsforschung, Bunsenstrasse 10, D-37073 Göttingen, Germany
31) Present Address: UVSOR, IMS
32) Present Address: Dept. of Chemistry, Toyama Univ., Gofuku 3190, Toyama 930.
33) Present Address: Dept. of Industrial Chemistry, Tokyo Inst. of Polytechnics, Iiyama 1583, Atsugi, Kanagawa 243-02.
34) Present Address: Dept. of Chemistry, Wuhan University, Wuhan 430072, China.
35) Present Address: Tsukuba Advanced Research Alliance, Univ. of Tsukuba, Tennodai 1-1-1, Tsukuba, Ibaraki 305.
36) Present Address: Korean Advanced Institute of Science and Technology, 373-1 Kusong-Dong, Yusong-Gu, Taejon, 305-701, Korea.
37) Present Address: Div. of Chemistry, Graduate School of Science, Hokkaido Univ., Kita-ku, Sapporo 060
38) Present Address: Laboratoire de Chemie de Coordination (CNRS), 205 Route de Narbonne 31077, Toulouse, France
39) Present Address: Teijin Chemicals Ltd., Kitayoshida-cho, Matsuyama, Ehime 791
40) Present Address: Institute for Fundamental Research of Organic Chemistry, Kyushu Univ., Hakosaki, Higashi-ku, Fukuoka 812-81
41) Present Address: Dept. of Applied Chemistry, Dhaka Univ., Dhaka-1000
42) Present Address: Department of Physics, Nara University of Education, Takabatake-cho, Nara 630
43) Present Address: Department of Electrical and Electronic Engineering, Toyohashi University of Technology, Tempaku-cho, Toyohashi 441
44) Present Address: Tokyo Institute of Technology, Higashirinkan 6-8-23-203, Sagamihara, 228
45) Present Address: Central Glass Co. Ltd., Kusael-2-13 Ube, 755
46) Present Address: Department of Chemistry, Faculty of Science, Okayama University, 3-1-1 Tushima-naka, Okayama 700
47) Present Address: Department of Chemistry, Faculty of Science, Hiroshima University, 1-3-1 Kagamiyama, Higashi-Hiroshima Hiroshima 739
48) Present Address: Department of Chemistry, Faculty of Science, Saitama University, 255 Shimo-Okubo, Urawa Saitama 338
49) Present Address: Department of Chemistry, Faculty of Science, Ochanomizu Women's University, 2-1-1 Otuka, Bunkyou-ku, Tokyo 112
50) Present Address: Department of Chemistry, Faculty of Science, Kobe University, 1-1 Rokkodai, Nada-ku, Kobe, Hyogo 657
51) Present Address: Catalysis Research Center, Hokkaido University, Kita-ku, Sapporo 060
52) Present Address: School of Materials Science, Japan Advanced Institute of Science and Technology (JAIST), Asahidai, Tatsunokuchi-machi, Ishikawa 923-12
53) Present Address: Teijin Limited, Polymer & Materials Research Laboratories, 2-1 Hinode-cho, Iwakuni, Yamaguchi 740
54) Present Address: Miyagi University of Education, Aoba, Aoba-ku, Sendai 980
55) Present Address: Institute fur Anorganische und Analytische Chemie, Friedrich-Schiller University, Am Steiger 3, D-07743 Jena, Germany
56) Present Address: Department of Chemistry, College of Natural Science, Kangwong National University, Chuncheon 200-701, Kangwon-do, Korea
57) Present Address: Nice-Sophia-Antipolis University, 06108 Nice Cedex 2, France
58) Present Address: Department of Materials Science, Fuculty of Science, Hiroshima University, Kagamiyama 1-3, Higashi-Hiroshima, 724
59) Present Address: Fritz-Haber-Institut der Max-Planck-Gesellschaft Faradayweg 4-6, D-14195, Berlin-Dahlem, Germany.
60) Present Address: School of Science, Nagoya University, Furo-cho, Chikusa-ku, Nagoya 464-01
61) Present Address: National Institute for Fusion Science, Oroshi-cho 322-6, Toki, Gifu 509-5

COUNCIL

Mitsuo ITO **Director-General**

Councilors

Chairman	Yukio HORI	Vice President, Kanazawa Institute of Technology
Vice-Chairman	Mitsuo TASUMI	Professor, Saitama University
	Schunichi AKIMOTO	Professor Emeritus, The University of Tokyo
	Yoshikazu ITO	Chairman of the Board, Toray Industries, Inc.
	Hiizu IWAMURA	Professor, Kyusyu University
	Nobuo KATO	President, Nagoya University
	Haruo KURODA	Professor, Science University of Tokyo
	Kazuhiro MARUYAMA	President, Kyoto Institute of Technology
	Noboru MATAGA	Division Head, Institute for Laser Technology Professor Emeritus, Osaka University
	Yoshio MATSUNAGA	Professor, Kanagawa University
	Hidetake MORIMOTO	Adviser, Toyota Centeral Research & Development Laboratories, Inc.
	Toru MORIYA	Professor, Science University of Tokyo
	Hitoshi OHTAKI	Professor, Ritsumeikan University
	Shinichi SASAKI	President, Toyohashi University of Technology
	Ryoichi SHIMIZU	Director, The Institute of Statistical Mathematics
	Hiroshi SHIONO	Professor, Seikei University
	Hisashi TANAKA	Professor Emeritus, Kyoto University
	Soji TSUCHIYA	Professor, Japan Women's University
	Edward William SCHLAG	Director, Institute for Physical Chemistry, Technical University of Munchen
	Mostafa A. EL-SAYED	Professor, Georgia Institute of Technology

The Council is the advisory board for the Director-General. Two of the councilors are selected among distinguished foreign scientists.

Distinguished Research Consultants

Hiroaki BABA	Professor Emeritus, Hokkaido University
Kenichi FUKUI	President, Institute for Fundamental Chemistry
Hiroo INOKUCHI	Professor Emeritus, Institute for Molecular Science
Saburo NAGAKURA	President, The Kanagawa Academy of Science and Technology
Ikuzo TANAKA	President, National Institute for Academic Degrees

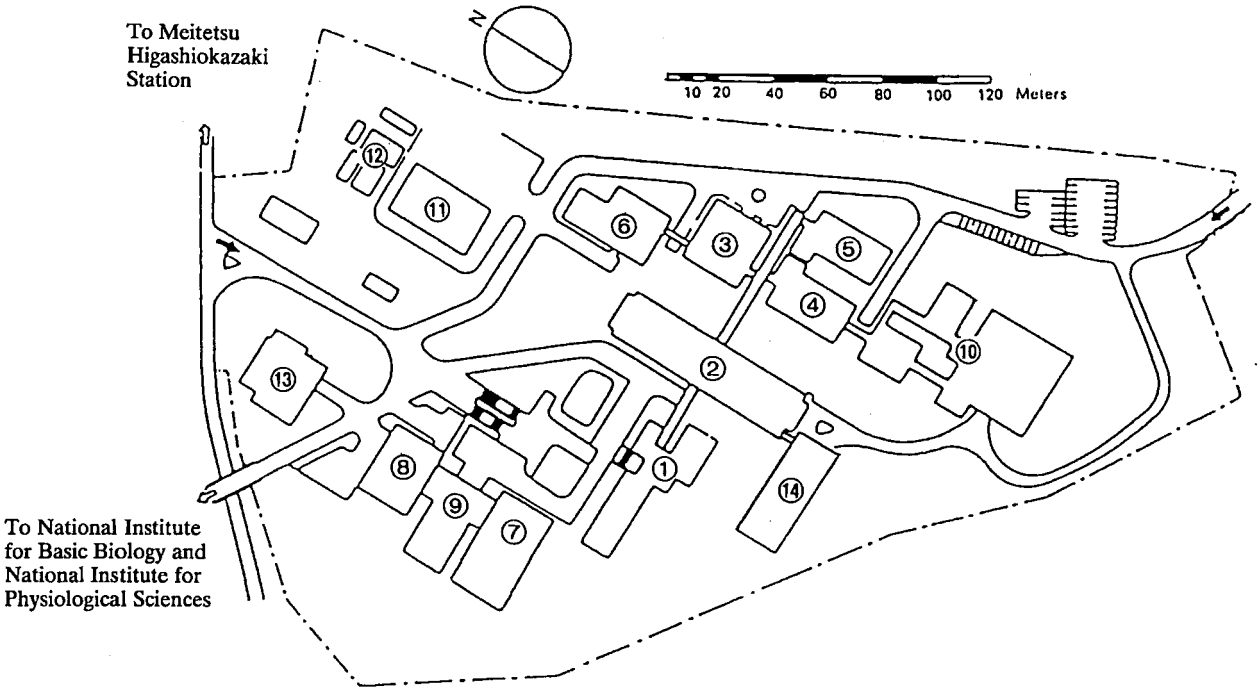
Administration Bureau

Mikio HASHIMOTO	Director-General, Administration Bureau
Akihiro SHIBASAKI	Director, General Affairs Department
Kenji KANDA	Director, Finance and Facilities Department
Isao FUJII	Head, Personnel Division (-March '96)
Masaki YOKOYAMA	Head, Personnel Division (April '96-)
Ryouichi KUWABARA	Head, Personnel Division (-March '96)
Youji IWAI	Head, Personnel Division (April '96-)
Shigeaki AIHARA	Head, Research Cooperation and International Affairs Division (-March '96)
Yousuke HASHIMOTO	Head, Research Cooperation Division (April '96-)
Kouji TAKAHARA	Head, International Affairs Division (April '96-)
Takashi KODAMA	Head, Budget Division (-March '96)
Norimichi IMAZU	Head, Budget Division (April '96-)
Kenzo KOZEKI	Head, Accounts Division
Takashi SUZUKI	Head, Construction Division (-March '96)
Takeshi KITATANI	Head, Construction Division (April '96-)
Yoshiaki KAMACHI	Head, Equipment Division (-March '96)
Yoshitaka MOCHIZUKI	Head, Equipment Division (April '96-)

BUILDINGS AND CAMPUS

The IMS campus covering 62343 m^2 is located on a low hill in the middle of Okazaki City. The inequality in the surface of the hill and growing trees are preserved as much as possible, and low-storied buildings are adopted for conservation of the environment. The buildings of IMS are separated according to their functions as shown in the map. The Research Office Building and all Research Facilities except for the Computer Center are linked organically to the Main Laboratory Building by corridors. Computer Center, Library and Administration Buildings are situated between IMS and the neighboring National Institute for Basic Biology and National Institute for Physiological Sciences, because the latter two facilities are common to these three institutes.

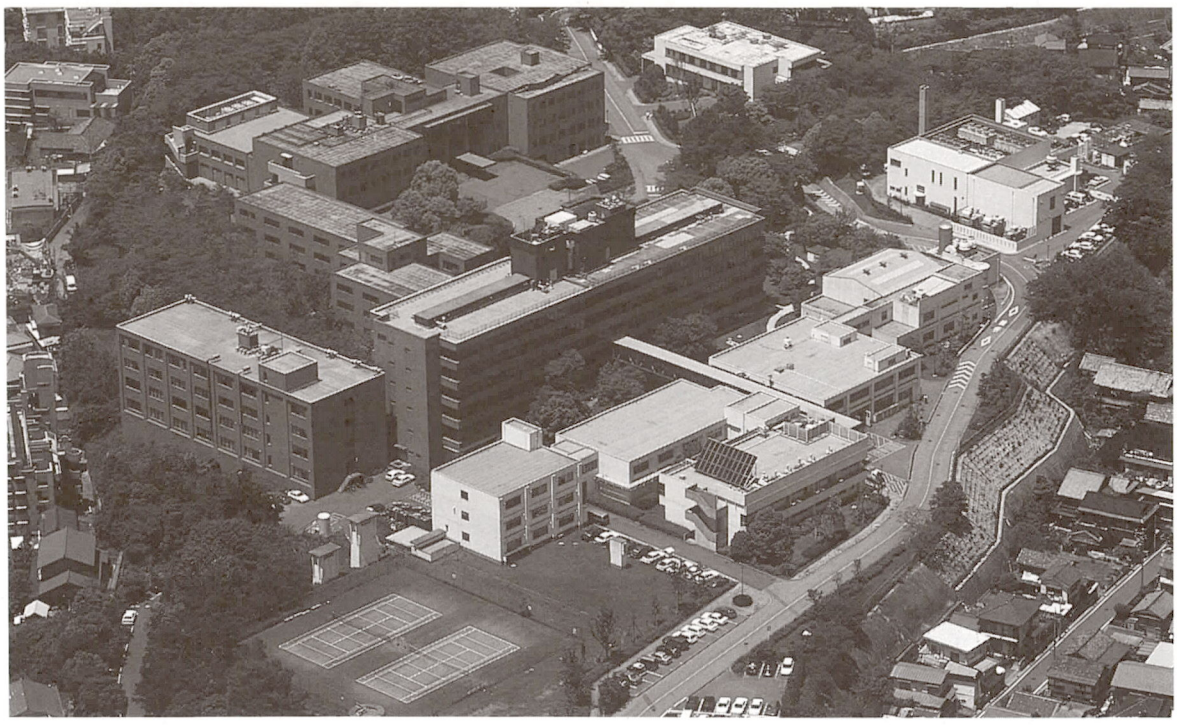
The lodging facility of IMS called Yamate Lodge, located within ten minutes' walk, has sleeping accommodations for 15 guests and two families. Mishima Lodge, located within four minutes' walk east of IMS can accommodate 74 guests and 20 families. Scientists who visit IMS as well as two other institutes can make use of these facilities. Foreign visiting scientists can also live at these lodgings with their families during their stays. The Okazaki Conference Hall for scientific meetings is now under construction in Mishima area.



1. Research Office Building
2. Main Laboratory Building
3. Equipment Development Center
4. Instrument Center
5. Chemical Materials Center
6. Low-Temperature Center
7. Computer Center
8. Library
9. Central Administration
10. UVSOR Facility
11. Power Station
12. Waste-Water Disposition Facilities
13. Faculty Club
14. South Laboratory Building



Okazaki (population 300,000) is 260 km west of Tokyo, and can be reached by train in about 3 hours from Tokyo via New Tokaido Line (Shinkansen) and Meitetsu Line.
The nearest large city is Nagoya, about 40 km northwest of Okazaki.



RESEARCH ACTIVITIES I
Department of Theoretical Studies

I-A Development of New Theoretical and Numerical Techniques in the Study of Molecular Structures

I-A-1 On Approximating Electron Repulsion Integrals with Linear Combination of Atomic-Electron Distributions

Seiichiro TEN-NO and Suehiro IWATA

[*J. Chem. Phys.* **105**, 3604 (1996); *Int. J. Quantum Chem. Symp.*, in press (1996)]

(1) We present a multiconfiguration self-consistent field (MCSCF) procedure employing recently developed approximations for electron repulsion integrals called the RI-LCAD method. Molecular charge distributions in the two-electron interaction part are expanded into atomic-electron distributions without linear dependencies, and the four-center quantities of electron repulsion integrals are reduced to two- and three-center quantities. The method is plugged into the approximate second-order MCSCF procedure and applied to calculations of the HNO molecule. This procedure enables us to reduce the CPU time of the integral transformation step which is usually the most time-consuming. It is also shown that the present approximation is very accurate not only for the ground state but also for the low-lying excited states, even after a substantial reduction of the number of required integrals. (2) The MCSCF procedure without explicitly setting up Hessian and the Slater-determinant-based direct configuration interaction (CI) methods incorporating the RI-LCAD method are discussed. In both of the methods, new ideas are proposed to avoid explicitly setting up four-indexed integrals and the fundamental scaling properties of the methods are improved. They therefore enable us to handle smaller size of data and lead to new aspects in the ab initio methods for large molecular systems.

I-A-2 Multi-Exponential Approaches to Electronic Structure Calculations with Chemical Accuracy: Importance of Orbital Relaxation Effects

Seiichiro TEN-NO

The author proposes several methods based on the spin-adapted superposition of nonorthogonal Slater determinants. The conventional MCSCF method cannot reproduce important correlation effects, the orbital relaxation effects (ORE), due to the strong orbital partitioning of active and inactive levels. Since the ORE consists of cooperative motion of electrons, it is long-range and includes many (at least more than two) electron excitations in nature. This means that the pair-electron correlation picture breaks down in the multireference (MR) methods based on the MCSCF reference functions. By extending the idea of the resonating Hartree-Fock method which was recently applied to *ab initio* calculations , a nonorthogonal multi-determinant SCF method is developed. In the method, the nonorthogonal determinants are represented by multi-exponential transformations of unitary group generator such that the ORE as well as near-degeneracy correlation effects can be reproduced. Double excitation CI (DCI) from the two-exponential function is always more accurate than the single reference CCSD and the MRSDCI methods; it recovers almost 99% of correlation energies of the ground state hydrogen fluoride molecule at any geometry. This implies that the present method is much more efficient than the conventional MR methods. Furthermore it is shown that the extension to the full cluster expansion is more straightforward. In this case, the resulting equations are regarded as a nonorthogonal generalization of the Jeziorski-Monkhrost-type MR coupled cluster theory.

Reference

N. Tomita, S. Ten-no and Y. Tanimura, *Chem. Phys. Lett.*, in press

I-A-3 Theoretical Studies of the Photoionization and Photodetachment Cross Section Using the L^2 Basis Set

Takeshi TSURUSAWA and Suehiro IWATA

We develop the method for calculating the photo-detachment cross section using L^2 basis set and conventional ab initio MO CI wave functions. This method is based on the Stieltjes Imaging (Lanczos Recursive) method. By using this method, we can avoid the explicit construction of the continuum electronic wave function. We applied the method to evaluating the photodetachment cross section of $[Cl(H_2O)_n]^- \; Cl(H_2O)_n + e^-$. As a preliminary calculation, we have obtained the optimized geometry of anion clusters by using 6-311+G** basis set and MP2 gradient calculation, and the vertical detachment energies(VDE) were calculated by MP4(STDQ) energy calculation for n=1 to 4. All the structure we have obtained are hydrogen-bonded type ones. We cannot get the linear structure for n=2, which was previously reported with smaller basis sets as an optimized structure. The VDE increases linearly from n=1 to 3. The rate of increase of VDE diminishes slightly at n=4.

I-B Structures, Spectra and Dynamics of Water Cluster Complexes with Atoms, Atomic Ions, and Organic Molecules

I-B-1 Theoretical Studies of Geometric Structures of Phenol-water Clusters and Their Infrared Absorption Spectra in the O-H Stretching Region

Hidekazu WATANABE *(GUAS and IMS)* and Suehiro IWATA

[*J. Chem. Phys.* **105**, 420 (1996)]

The structures of the phenol-$(H_2O)_n$ clusters ($n \leqq 4$) ≤are determined with ab initio molecular orbital methods, and their infrared spectra are calculated to analyze the experimental spectra reported in the preceding paper. The experimental infrared spectra of phenol-$(H_2O)_n$ clusters for have "window regions", which are intervals of two types of OH stretching modes of the water molecules. The calculated IR spectra of isomers with a ring structure will reproduce these window regions. The ring is formed by a network of the hydrogen bonds of the -OH group of the phenol and water molecules. For n=4, two kinds of spectra are reported in the experiments. One spectrum has a window region similar to that of $n \leqq 3$. It is, therefore, identified to the isomers of a ring structure. The other one has several bands in the window region. The calculations for several isomers and large clusters suggest that this spectra might be attributed either (i) to the mixture of several branched isomers, (ii) to the products of evaporation of larger clusters, or (iii) to the product of the proton transfer reaction in phenol-$(H_2O)_n$ cluster.

I-B-2 Does the Proton Transfer Reaction Take Place in the Ground State of Phenol-$(H_2O)_4$ Clusters ?

Hidekazu WATANABE *(GUAS and IMS)* **and Suehiro IWATA**

[*Int. J. Quantum Chem.* , in press (1996)]

In recent experimental studies of infrared (IR) spectra of hydrated phenol clusters, the Mikami and Ebata group at Tohoku University attributed apparently two very different spectra to phenol-$(H_2O)_4$. The first spectrum has a wide transparent region between 3500 and 3700 cm^{-1}, which they names a window region. The second spectrum has several absorption bands in this window region. Our previous study revealed that the first spectrum was assigned to the isomers which have a single-ring structure of a hydrogen-bonding network of OH's of phenol and waters. The experimentalists suggested that the second spectrum might be identified to a proton-transferred phenol-water cluster. In the present article, the geometrical structures of proton-transferred hydrated phenol clusters were determined with the ab initio molecular orbital method and their IR spectra were calculated. The proton-transferred phenol-water cluster is at a stable local minimum, but the energy is much higher than that of the most stable nontransferred clusters. The calculated IR spectrum has a still wider window region and is far different from the experimental spectrum of the second type.

I-B-3 Hybrid Procedure of Ab Initio Molecular Orbital Calculation and Monte Carlo Simulation for Studying the Intracluster Reaction: Application to $Mg^+(H_2O)_n$ (n=1-4)

Toshio ASADA and Suehiro IWATA

[*Chem. Phys. Letters*, **260**, 1 (1996)]

A procedure is developed to investigate the intracluster reaction. At each step of Monte Carlo simulation ab initio molecular orbital calculation is carried out. To allow the reaction take place, at a half of the total steps an atom is a unit of the move and at the other half one of the molecules defined in the cluster is moved. The procedure is applied to study the $Mg^+(H_2O)_n$ clusters (n=1-4). For n=1,2 and 3, during the simulation the geometric structures of the clusters do not deviate much from that of the most stable conformer, but for n=4 in most of the time a six-membered ring found in the most stable conformer is broken. As the cluster size increases, the charge fluctuation on the Mg^+ ion becomes significant. In the present simulation for $n \leqq 4$ at T=300K the intracluster hydrogen elimination reactions are not found; the reaction is expected to take place thermochemically for $n \geqq 5$.

I-B-4 High-Resolution Laser-Induced Fluorescence Spectra of 7-Azaindole-Water Complexes and its Dimer

Atsushi NAKAJIMA*(Keio Univ.)*, **M. HIRANO***(Keio Univ.)*, **Ryouji HASUMI***(Keio Univ.)*, **Koji KAYA***(Keio Univ.)*, **Hidekazu WATANABE***(GUAS and IMS)*, **C. C. CARTER***(Ohaio State Univ.)*, **J. M. WILLIAMSON** *(Ohaio State Univ.)* **and Terry A. MILLER***(Ohaio State Univ.)*

[*J. Phys. Chem.* , in press (1996)]

The geometric structures of 7-azaindole-water complexes, (7-AzI)-$(H_2O)_n$, and 7-AzI dimer were investigated by laser-induced fluorescence (LIF) spectroscopy with high resolution (-0.01 cm^{-1}). For the 7-AzI-$(H_2O)_n$ complexes (n=1-3), the LIF spectra show partially resolved rotational structure, which has been analyzed in combination with theoretical calculations. This analysis yields the rotational constants and characterizes the structures. In 7-AzI-$(H_2O)_1$, the H_2O molecule is located in the molecular plane, forming a six-membered ring with two hydrogen bonds. Analysis for 7-AzI-$(H_2O)_2$ and -$(H_2O)_3$ show, furthermore, that both the second and the third H_2O are located in the molecular plane of 7-AzI, forming a network ring of hydrogen bonds. For the 7-AzI dimer, the LIF spectrum shows an unresolved rotational envelope. The rotational contour has been analyzed and the possible structures of the dimer are proposed.

I-B-5 Molecular Orbital Studies of the Structures and Reactions of a Singly Charged Calcium Ion with Water Clusters, $Ca^+(H_2O)_n$

Hidekazu WATANABE *(GUAS and IMS)* **and Suehiro IWATA**

[*J. Phys. Chem.* , submitted (1996)]

Structure of hydrated singly positive charged calcium-water clusters $Ca^+(H_2O)_n$ and their hydrogen eliminated products $(CaOH)^+(H_2O)_{n-1}$ were optimized using the ab initio molecular orbital methods, and are compared with cationic magnesium-water clusters which was investigated previously. For $n \leqq 2$, the structures of $Ca^+(H_2O)_n$ are different from those of $Mg^+(H_2O)_n$. In the $Mg^+(H_2O)_n$ clusters, a pyramidal $Mg^+(H_2O)_3$ forms the first shell. In contrast, a quasi-square planar $Ca^+(H_2O)_4$ is the first shell. The structures of $(CaOH)^+(H_2O)_{n-1}$ are also different from structures $(MgOH)^+(H_2O)_{n-1}$. The structural difference is attributed to the participation of the d orbitals of Ca atom to the bonding. In spite of these structural differences, the core molecular ion $(CaOH)^+$ in the hydrogen eliminated products $(CaOH)^+(H_2O)_{n-1}$ is very similar to the

corresponding core ion $(MgOH)^+$. Both ions, $CaOH^+$ and $MgOH^+$, are strongly polarized to $Ca^{2+}\ O^-\ H$ and $Mg^{2+}\ O^-\ H$. Consequently, the hydrogen energies of the $(CaOH)^+(H_2O)_n$ is much larger than those of the corresponding $Ca^+(H_2O)_n$. The internal energy change of the hydrogen elimination reactions of the $Ca^+(H_2O)_n$ is positive for n=1-4, but becomes negative for $n \geqq 5$, which is consistent with the experimentaly observed isotope effects and metal dependency.

I-B-6 Theoretical Prediction of Intracluster Reactions of $B^+(H_2O)_2$ and $B^+(H_2O)_3$ Clusters; Hybrid Calculations of Ab Initio MO and Monte Carlo Samplings

Hidekazu WATANABE *(GUAS and IMS)*, **Toshio ASADA and Suehiro IWATA**

[*Bull. Chem. Soc. Jpn.*, submitted]

For investigation of the intracluster reactions of $B^+(H_2O)_n$ (n=2 and 3), we used the recently developed hybrid procedure of ab initio molecular orbital (MO) method and Monte Carlo (MC) samplings. In this method, we do not assume the potential energy function in the MC samplings. For energy evaluation at each sampling, the ab initio MO calculation is carried out. A simple device for the nuclear motions in the samplings makes it possible to deal with the intracluster reaction such as cis-trans isomerization and proton transfer reactions. In the cluster $B^+(H_2O)_2$, a series of intracluster reactions takes place at the room temperature. A hydrated boron ion$B^+(H_2O)_2$ is transformed to the sp^2 type of $HBOH^+(H_2O)$ under thermal equilibrium at the room temperature. The isomerization reaction proceeds via $BOH(H_3O^+)$ and the sp type of $HBOH^+(H_2O)$, which are all possible intermediate structures. But even in the thermal equilibrium structure the sp^2 type of $HBOH^+(H_2O)$, several symptoms of the further reactions are seen in the structural and charge fluctuations. For $B^+(H_2O)_3$, the Monte Carlo samplings have started from several isomers, and more complicated isomerization and dissociation reactions are found.

I-C Structures of Binary Element Molecules and Clusters

I-C-1 Ab Initio Studies of Silicon and Nitrogen Clusters: Cyclic or Linear Si_2N ?

Fernando R. ORNELLAS *(Univ. São Paulo and IMS)* **and Suehiro IWATA**

[*J. .Phys. Chem.* **100**, 10919 (1996)]

Theoretical studies are carried out on the doublet and quartet states of three isomeric forms of the species Si_2N. Correlation effects on the structural parameters, harmonic frequencies, and relative energies are investigated at increasingly higher levels of theory (MP2, MP4, and CCSD(T)), and basis sets (DZP, cc-pVTZ-f, and cc-pVTZ). At the highest level of theory (CCSD(T)/cc-pVTZ) all three isomers are found to be thermochemically stable species with the symmetric linear structure (SiNSi) as the global minimum; a symmetric cyclic structure (93.1°) lies only 4.90 kcal/mol higher in energy, while the asymmetric linear isomer (SiSiN) is located much higher (85.2 kcal/mol). Dissociation of the most stable isomer into the channels SiN + Si and Si_2 + N would require 123 and 148 kcal/mol, respectively, including the zero-point vibration correction. Chemical bonding as reflected in bond distances indicates a SiN bond character intermediate that of a single and a double bonds in the linear SiNSi isomer (1.644A), changing then to a single bond in the cyclic structure (1.695A), and a double bond in SiSiN (1.608A). The energetics involved in various dissociation channels is also analyzed, as well as the strength of the vibronic interaction in the linear isomer estimated by the Renner parameter. A comparison with the molecules C_2N, Si2C, Si_2C^- and Si_2O clearly shows structural and stability trends among these triatomics.

I-C-2 Structures and Energetics of New Nitrogen and Silicon Molecules: An Ab Initio Studies of Si_2N_2

Fernando R. ORNELLAS *(Univ. São Apauloa and IMS)* **and Suehiro IWATA**

[*J.Phys.Chem.* **100**, 16155 (1996)]

New species with molecular formula Si_2N_2, not yet observed experimentally, are described theoretically for the first time. Nine different stationary points have been examined and the effects of electronic correlation on the structural parameters, harmonic frequencies, and relative energies are described at increasingly higher levels of correlation treatment (MP2, MP4 and CCSD(T)). The global minimum corresponds to a linear singlet state ($1S^+_g$) SiNNSi. At the CCSD(T) level, the next stable species (at 15.1 kcal/mol) has a non-classical tetrahedral-like structure similar to the global minimum of Si_2H_2. This is followed by another local minimum with a linear structure SiNSiN (at 20.3 kcal/mol) and by a rhomboidal-type structures (at 21.3 kcal/mol), which is in fact a transition state connecting two equivalent tetrahedral-like structures. Another non-classical structure similar to the monobridged one in the case of Si_2H_2 was also found to be a local minimum (at 28.2 kcal/mol). An interconversion path from this latter structure to the linear SiNNSi one is likely to occur via another transition state located at about 38 kcal/mol. With the exception of the linear isomer SiNNSi, the triplet states were found to lie very high energetically and to correspond to unstable structures. None of these species exhibit any appreciable amount of silicon-silicon bonding, and the analog of cyanogen (NCCN) NSiSiN is unstable. The nature of the bonding in the most relevant species is also discussed, as well as the energetics of the dissociation. An analysis of the energetics and structural similarities and differences between Si_2N_2, C_2N_2, Si_2H_2, and Si_2C_2 is also carried out. Caution must be exercised in generalizing at a low level of theory since they have not been confirmed by the CCSD(T) calculations.

I-C-3 Diazasilene (SiNN) : Is There a Conflict Between Experiment and Theory ?

Fernando R. ORNELLAS *(Univ. São Paulo and IMS)*, **Leonardo T. UENO** *(Univ. São Paulo)* **and Suehiro IWATA**

[*J.Chem.Phys.*, submitted.]

The molecular SiNN was investigated with the highly correlated coupled cluster method with single and double excitations and corrections for connected triples (CCSD(T)), and with the multi-reference single and double excitation configuration interaction approach (MRCI). A series of basis sets ranging from the simple 6-31G*, 6-311G*, and Dunning's double-zeta (DZ) plus polarization basis sets to the more extended correlated consistent cc-pVTZ and cc-pVQZ ones were employed to check the dependence of the geometry optimization and of the frequency evaluation on the basis sets . Our highest level result of 1859 cm^{-1} for the harmonic stretching frequency of the NN bond differs considerably from a previous CCSD(T)/DZ prediction of 1726 cm^{-1}. In fact, most of the results analyzed in this study point to a frequency value greater than 1810 cm^{-1}. Reexamining the scarce experimental evidence, we estimate the harmonic frequency to be very close to 1830 cm^{-1}. Surprisingly, an extended internally contracted MRCI calculation with the cc-pVTZ basis set predicts a frequency 144 cm^{-1} higher than the corresponding CCSD(T)/cc-pVTZ result. Comparisons with existing density functional studies and with a previous MRCI calculation are also carried out. At the CCSD(T)/cc-pVTZ level, other isomers of SiN_2 are further investigated for the first time. One symmetric linear ($^3S_g^-$), and one symmetric bent ($^1A_1$) structures are found to lie relatively high in energy: 84.6 and 102.2 kcal/mol, respectively, relative to SiNN($^3S^-$) However, one cyclic $^1A_1$ and the singlet asymmetric isomer SiNN ($^1S^+$) are only 6.1 and 15.8 kcal/mol above the global minimum. Although the higher frequencies of the former isomers do not fall in the region of relevance to the experimental assignment discussed in this work, that of the lowest lying $^1A_1$ state (1850cm^{-1}) is indeed practically identical to CCSD(T)/cc-pVTZ frequency computed for the $^3S^-$ state.

I-C-4 Ab Initio Studies on the Structures, vertical Electron Detachment Energies and Fragmentation Energies of C_nB^- Clusters

Chang-Guo ZHAN *(Central China Normal Univ. and IMS)* **and Suehiro IWATA**

[*J. Phys. Chem.*, in press (1996)]

Recently, Wang, Huang, Liu and Zhang reported the experimental and theoretical studies on C_nB^- as well as the C_nN^- clusters (n= 1 to 13). They claimed that both clusters should be linear chains, based on the HF/3-21G ab initio MO geometry optimizations. In the present paper, we re-examine the geometries of C_nB^- at higher levels of ab initio MO approximations. In the MP2/6-31G* level of the geometry optimization, up to n=4, the linear structures of C_nB^- are indeed stable, but larger n of C_nB^- are very floppy quasi-linear. The vertical electron detachment energy and fragmentation energies of C_nB^- in the ground state are evaluated with the MP4SDTQ approximation using 6-31G* augmented with a set of diffuse sp functions. The fragmentation energies are also evaluated with the QCISD(T) method to confirm the convergence of the perturbational results. The calculated fragmentation energies show that the C_nB^- clusters with even n are more stable than those with odd n, which is consistent with the odd-even alternatation of TOF signal intensities. In terms of the MO diagram, the odd-even alternation in C_nB^- and C_nN^- is discussed.

I-C-5 Ab Initio Studies on the Structures, Vertical Electron Detachment Energies and Fragmentation Energies of C_nN^- Clusters

Chang-Guo ZHAN *(Central China Normal Univ. and IMS)* **and Suehiro IWATA**

[*J.Phys. Chem.*, in press (1996)]

In a recently published paper on the time-of-flight mass spectroscopy studies and ab initio RHF/3-21G calculatioins of the C_nN- clusters (n=1 to 13), Wang, Huang, Liu, and Zhang claimed that the C_nN^- clusters should be the singlet state of a linear conformation. In this report we examine the C_nN^- anion clusters with higher levels of ab initio MO methods. Various levels of basis sets are examined for the geometries and the vertical electron detachment energies. It turns out that the polarization functions are indispensable to determine the geometries of the anions. Diffuse functions are necessary to evaluate the electron detachment energy, but they do not make any effects on the geometries of the anion. To reduce the number of basis sets and to avoid the over-completeness, the diffuse functions are added only on the two end atoms; the approximation is carefully examined for C_2N^-. For a series of cluster anions $C_{2m+1}N^-$, the ground state is the singlet state of the electron configuration $(s)^2(p)^4$ and has a linear or quasi-linear conformation. For m>2, the molecules are very floppy against the bending motion. On the other hand, the electron configuration of the ground state of the series of $C_{2m}N^-$ is $(p)^4(s)^0$ at a linear conformation, and the HOMO (p) and LUMO (s) gap is very small. Hence, the linear triplet state $(p)^2(s)^2$ is the ground state of C_2N^-. It is also true that at a linear conformation the triplet state is the lowest state for C_4N^- and C_6N^-, but for $C_{2m}N^-$ (m>1) the bent singlet state is the ground state. The vertical detachment energy and fragmentation energy are evaluated, and both of them clearly show the even-odd alternation, which is consitent with the observed TOF mass spectrum.

I-C-6 Ab Initio Studies on the Structures, Vertical Electron Detachment Energies and Stabilities of C_nP^- Clusters

Chang-Guo ZHAN *(Central China Normal Univ. and IMS)* **and Suehiro IWATA**

[*Z.Phys D*, submitted]

The geometric structures, vertical electron detachment energies and fragmentation energies of C_nP^- clusters (n=1 to 7) are studied with the MP2/6-31G+(d) level of the approximation. The relative energies are further evaluated with the higher level of correlated wave functions. The ground state of the molecules with odd n is the singlet state of the electron configuration $(p)^4(s)^2$, and is linear or quasi-linear. On the other hand, the ground state of C_2P^- is the triplet state of $(s)^2(p)^2$, and for larger even n, the ground state becomes the singlet state of $(p)^4(s)^0$ In C_4P^-, the singlet and triplet states are quasi degenerate, both having a linear conformation. The geometric structures of odd n are very similar to the corresponding C_nN^- but for even n>4, C_nN^- becomes bent at the second next

carbon to the N atom. This difference is explained by the relative energy of carbon 2p and phosphorus 3p. The calculated vertical electron detachment energy and fragmentation energy of C_nP^- in the ground state reveal that the C_nP^- clusters with odd n are more stable than those with even n, which is consistent with the observed odd-even alternation in the TOF signal intensities. But, the calculated even - odd alternation in the fragmentation is not as large as in C_nN^- clusters. This is also consistent with the results reported recently.

I-C-7 Theoretical Study of Carbon Doped Small Silicon Clusters: Electron Affinities of Si_nC (n=2-5)

Reiko KISHI *(Keio Univ.)*, **Motoki GOMEI** *(Keio Univ.)*, **Atsushi NAKAJIMA** *(Keio Univ.)*, **Suehiro IWATA and Koji KAYA** *(Keio Univ.)*

[*J.Chem.Phys.* **104**, 8593 (1996)]

The geometries and energies of Si_nC and Si_nC^- (n=2-5) were investigated with *ab initio* MO calculations including electron correlation. The Møller-Plesset perturbation theory was used for n=3-5. The configuration interaction (CI) calculations were carried out for n=2 and 3. The most stable isomers of the neutral Si_nC clusters have the structure in which a Si atom having the largest *sp* hybridization in the corresponding Si_{n+1} cluster is replaced by a C atom. For their anions, the structures in which an excess electron is distributed avoiding a C atom become stable. Moreover, the adiabatic electron affinities of Si_nC and vertical detachment energies of anionic Si_nC^- were computed. They reproduced the trends of photoelectron spectra of Si_nC^- reported previously.

I-C-8 Photoelectron Spectroscopy of Silicon-Fluorine Binary Cluster Anions ($Si_nF_m^-$)

Hiroshi KAWAMATA *(Keio Univ.)*, **Yuichi NEGISHI** (Keio Univ.), **Reiko KISHI** *(Keio Univ)*, **Suehiro IWATA**(*IMS*) , **Atsushi NAKAJIMA** *(Keio Univ. and RIKEN)* **and Koji KAYA** *(Keio Univ. and RIKEN)*

[*J.Chem. Phys.*, in press(1996)]

Electronic properties of silicon-fluorine cluster anions ($Si_nF_m^-$; n=1-11, m=1-3) were investigated by photoelectron spectroscopy using a magnetic-bottle type electron spectrometer. The binary cluster anions were generated by a laser vaporization of a silicon rod in He carrier gas mixed with a small amount of SiF_4 or F_2 gas. The highly abundant clusters are SiF_m^- (m=3, 5) and Si_nF^- (n=6, 7, 10) in their mass spectra. In the photoelectron spectra of SiF_m^- (m=1-5), the clusters having odd m have higher electron affinity (EA) than those having even m, indicating that the even/odd alternation in EA is attributed to their electronic structures of a closed/open valence shell. Comparison between photoelectron spectra of Si_nF^- and Si_n^- (n=4-11) gives the insight that the doped F atom can remove one electron from the corresponding Si_n^- cluster without any serious rearrangement of Si_n framework, because only the first peak of Si_n^-, corresponding singly occupied molecular orbital (SOMO), disappears and other successive spectral features are unchanged with the F atom doping. In some clusters, furthermore, the vibrational structures could be resolved to determine a vibrational frequency and to presume the geometry with ab initio molecular orbital calculations.

I-C-9 Ab Initio MO Studies of Neutral and Anionic SiC_n Clusters

Motoki GOMEI(*Keio Univ*), **Reiko KISHI**(*Keio Univ*), **Atsushi NAKAJIMA**(*RIKEN and Keio Univ*), **Suehiro IWATA and Koji KAYA**(*RIKEN and Keio Univ.*)

The geometric structures of SiC_n and SiC_n^- (n=2 - 5) were investigated with ab initio MO calculations. The geometries were optimized with the second order Moller-Plesset perturbation MP2 method, and the relative energies of the isomers are evaluated with the MP4 and CCSD(T) levels of approximation. The adiabatic electron affinity as well as the vertical electron detachment energy (VDE) were also evaluated, and the recently reported photoelectron spectra of SiC_n^- were analyzed. For the neutral odd n series the linear triplet state is the most stable isomer, but the singlet state having a deformed rhomboidal structure with a silicon atom at one of the corners lies closely in energy. In the anions of odd n, the energy separation of the two isomers, both doublet state, is also small. The observed photoelectron spectra and the calculated VDE suggest that the detected clusters of odd series are the linear ones. Among even n clusters, SiC_2 and SiC_2^- are very special. The neutral SiC_2 molecule is definitely the singlet state, but a very floppy molecule; the barrier height of the rotation of a silicon atom around C_2 is less than 2000 cm^{-1}. In the anion SiC_2^- the doublet P state is very close to the T shape doublet A' state in energy, but two states are separated with a high barrier (about 4000 cm^{-1}). The calculated VDE supports the linear configuration for the anion, but the detection of the T shape structure cannot be excluded. For both anion and neutral SiC_4, the linear conformer is the most stable, although ring isomers are also found to be at local minima on the potential energy surfaces.

I-C-10 Ab Initio MO Studies of Si_4H_2 and Si_4NO^+

Wenning WANG *(Fudan Univ. and IMS)* **and Suehiro IWATA**

Tetramer Si_4 is a minimum unit of a series of silicon clusters and is expected to be rich in reactivity. We examine the reaction products of Si_4 with H_2 and Si_4^+ with NO using the ab initio MO method. The structure of the most stable isomers of Si_4 is rhomboidal, which was first determined with the high levels of ab initio MO calculations and later confirmed by the photoelectron spectra of anion Si_4^-. There are tremendous amount of experimental and theoretical studies on Si_n clusters. But not many works are reported for the reactions of the size-controlled silicon clusters. In few years ago Kaya and his collaborators examined the reaction of Si_n^+ (n>6) with NO molecules. In the present work, we study the reaction products of Si_4 with H_2 and Si_4^+ with NO. Since both systems have an even number of electrons, we can start with the closed shell SCF wavefunction. With the MP2/6-31G** level of approximation six isomers are found. The most stable isomer is a rhomboidal Si_4 frame and one of silicon atoms forms a silylene unit SiH_2, and the exothermal energy from $Si_4 + H_2$ is as large as 28.3kcal/mol. There are two isomers in which two diagonal silicon atoms bond with a hydrogen atom. In these systems the rhomboidal

form of Si_4 frame does deform slightly from pure Si_4. On the other hand, the most stable isomers of chemical formula $[Si_4NO]^+$ is the product of the insertion reaction, $(Si_3N)^+OSi$, in which $(Si_3N)^+$ forms a nearly planar ring and the oxygen atom of OSi is bound to one of silicon atoms of the ring. This isomer is a precursor of the product clusters $(Si_nN)^+$ observed in the experiments of Kaya's group.

I-D Structures of Unstable Molecules and Clusters, and of Reaction Intermediates

I-D-1 Theoretical Studies of the Chemical Processes of Producing Methylamine and Methanol in the Intersteller Space

Yoko SONODA *(Keio Univ.)* **and Suehiro IWATA**

[*Bull.Chem.Soc. Jpn.* **69**, 575 (1996)]

A hypothesis for the mechanism forming CH_3NH_2 and CH_3OH in intersteller space is examined with the ab initio MO calculations. In the hypothesis, both of CH_3NH_2 and CH_3OH are assumed to be formed via two steps, radiative association reaction followed by dissociative recombination reaction as

$$CH_3^+ + NH_3 \quad CH_3NH_3^+ + hn,$$
$$CH_3NH_3^+ + e \quad CH_3NH_2 + H\,.$$

The correlated level of the MO calculations support the plausibility of the two-step mechanism for CH_3OH. On the other hand, the first step radiative association reaction for the CH_3NH_2 forming reaction is found to be energetically unfavorable, because the direct hydrogen stripping reaction

$$CH_3^+ + NH_3 \quad CH_3NH_2^+ + H$$

prevents the association reaction to form the molecular ion $CH_3NH_3^+$. The alternative mechanism to form the ion is proposed and examined with the MO calculations. The proposed reaction is hydrogen stripping reaction from a hydrogen molecule

$$CH_3NH_2^+ + H_2 \quad CH_3NH_3^+ + H\,,$$

which is a direct reaction without any barrier.

I-D-2 Theoretical Study of Cyclic Isomers of HNO_x (x=2-6)

Yumin LI and Suehiro IWATA

[*Bull. Chem. Soc. Jpn.,* in press]

A series of cyclic isomers of HNO_x (x=2-6) are examined with ab initio MO methods. All of these cyclic isomers have a ring comprised of one nitrogen atom and two to five oxygen atoms. They are classified under the following three types. Type A: NO_x ring with an exo hydrogen bonded to a nitrogen; type B: NOx ring with an exo OH bonded to a nitrogen, and type C: NOx ring with an exo OOH bonded to a nitrogen. The geometry optimizations are carried out at the HF and MP2 levels of approximation with 6-31G** basis set, and the energies are evaluated at the MP4SDTQ approximation. We have failed to locate a five-membered ring HNO_x at the MP2 level. The geometries and vibrational frequencies are discussed by comparing them with the data of the related known stable molecules. The conformational preferences among the isomers are interpreted in terms of an intramolecular long range hydrogen-oxygen interaction.

I-D-3 Ab Initio Studies on Structures of the Hexa-Coordinate Phosphorus Intermediate for the Phosphoryl Ester Exchange and N → O Migration Reactions of Dimethyloxyphosphoryl-threonine

Chang-Guo ZHAN *(Central China Normal Univ. and IMS)* **and Suehiro IWATA**

[*Chem.Phys.Letters.* **247**, 401 (1995)]

Recently observed unusual chemical reactivities of the N-phosphoryl amino acids reveal a special hexa-coordinate phosphorus intermediate may exist in the reaction process. It looks unstable and has not been observed directly. We study the geometric structures and stability of the reactant and product as well as the assumed intermediate of the reaction at the HF/6-31G* level of approximation. The model compound is dimethyoxyphosphoryl-threonine, which consists of a phosphorus atom, thirteen second-period atoms and fourteen hydrogen atoms. The geometries of three species are fully optimized. To confirm the true stability, the harmonic vibrational frequencies are evaluated. The reaction intermediate has a hexa-coordinated phosphorus atom as the experimental group has assumed, though the energy is rather high without solvation. At the intermediate, while the N—P bond still retains, new N—O bonds are formed, and thus, the phosphorus atom is hexa-coordinated. Then, the N—P bond and one of N—O bonds are broken, and the N → O migration completes. By replacing O-CH_3 with S-CH_3, we have tried to locate the intermediate in vain, which is consistent with the experimental substitution effects.

I-D-4 Theoretical Predicion of the ^{31}P NMR Chemical Shift of the Hexa-Coordinate Phosphorus Intermediate for the Phosphoryl Ester Exchange and NO Migration Reactions of Dimethyloxyphosphoryl-threonine

Chang-Guo ZHAN *(Central China Normal Univ. and IMS)* **and Suehiro IWATA**

[*Chem.Letters*, submitted]

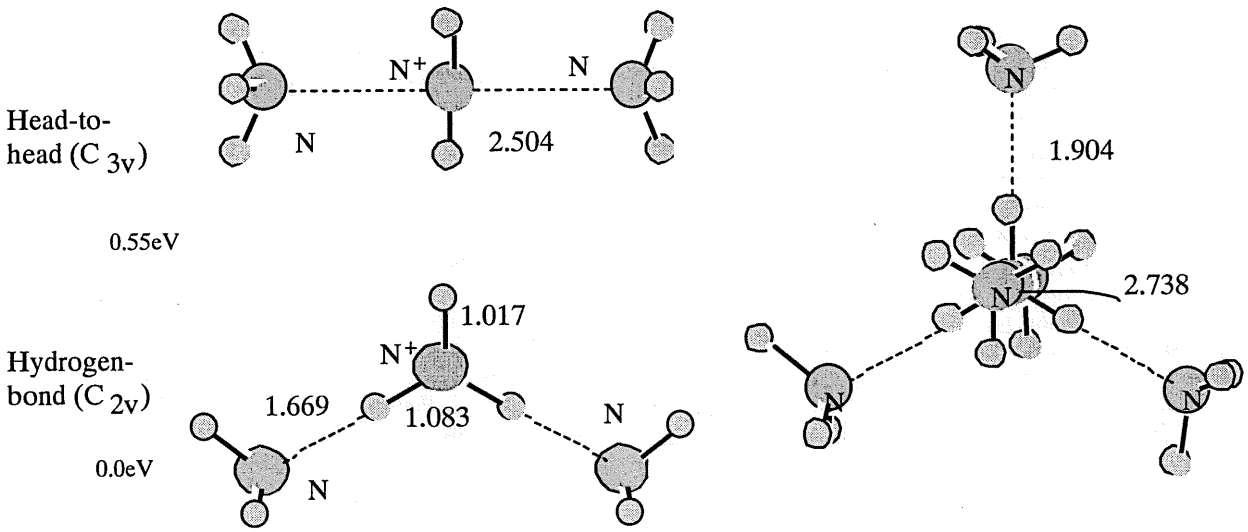
Ab initio GIAO(Gauge Independent Atmic Orbital) magnetic shielding calculations have been carried out on the hexa-coordinated phosphorus intermediate and the corresponding reactant and product for the N → O migration reaction of dimethyloxyphosphoryl-threonine. After several trials, the basis set selected is 6-311+G**, which requires more than 400 contracted Gaussian type basis functions. The electron correlation effect on the chemical shift of ^{31}P is examined and it turns out to be very small. The chemical shift of phosphoric acid is used as a standard. The ^{31}P chemical shift of hexa-coordinate intermediate shows a very large down-field shift up to -138 ppm, while the corresponding shifts of the tetra-coordinated reactant and product are 4.9 and -6.6 ppm, respectively. The calculated shifts of the reactant and product are in good agreement with observed ones for the

molecules with a longer alkyl group. Thus, we may safely propose where the experimenters look for the signals of ^{31}P of the intermediates of low concentration.
This series of the computations is only possible with a large memory and working disk storage of the supercomputer SX-3/34R at the computer center of IMS.

I-D-5 Unprotonated Ammonia Cluster Cations: How Does or Does Not the Proton Transfer Reaction Takes place?

Jong K. PARK and Suehiro IWATA

Ammonia clusters are one of the most well studied molecular clusters. But, when they are ionized either by electron impact or by photoionization for detection in the mass spectrospectra, they are mostly observed as chemical forms of $(NH_4)^+(NH_3)_n$, often called protonated ammonia clusters, which are the products of the proton transfer reactions and evaporation processes in the clusters.. Depending on the ionization condition, however, the mass spectra corresponding to the unprotonated ammonia clusters $(NH_3)_n^+$ are detected, though they are often weak. Even in the theoretical studies only the protonated ammonia clusters are mostly examined, and the studies for the unprotonated ammonia clusters are very scarce except for the dimer cation $(NH_3)_2^+$. The most stable isomers of the chemical form $N_2H_6^+$ is, as easily guessed by a chemical instinct, the proton transferred protonated product $(NH_4)^+NH_2$. Besides, there are two possible structures for the head-to-head type conformation, in which two nitrogen atoms face to each other. One is symmetric and the positive charge is delocalized over two molecules. In the other structure the positive charge is almost localized on one ammonia molecule, which becomes planar. The relative energy of the two structures is very small and depends on the approximation levels, though the delocalized structure seems slightly favored. The experimental study of the vibrational spectroscopy may resolve the question on the structure of the dimer cation. In figure 1, two isomers of trimer cations are shown. In both isomers the positive charge is localized on a planar ammonia at the center. Interestingly, when two hydrogen atoms of the ammonia cation are hydrogen-bonded to neutral molecules, the proton transfer does not proceed to form an ammonium ion. As shown below, in hexamer cation $(NH_3)^{6+}$, three of neutral ammonia molecules are hydrogen-bonding to the core cation, and two other molecules form a head-to-head type complex. Five molecules form the first shell of the cation clusters $(NH_3)_n^+$.



I-D-6 Geometrical and Electronic Structures of $[(CO_2)_nROH]^-$(R = H, CH_3)

Morihisa SAEKI *(Univ. of Tokyo.)*, **Tatsuya TSUKUDA***(Univ. of Tokyo.)*, **Takashi NAGATA** *(Univ. of Tokyo. and IMS)* **and Suehiro IWATA**

Structures and stabilities of $[(CO_2)_nROH]^-$(R = H, CH_3) with n = 1 and 2 were investigated by ab initio calculations at MP2 level. The calculations predict several stable conformations for $[(CO_2)ROH]^-$, where the solvation of ROH stabilizes the CO_2^- core through the formation of hydrogen bonds. It is also demonstrated that two types of isomers having different electronic structures ("electronomers") coexist in $[(CO_2)_2ROH]^-$; one has a structure described as $[C_2O_4^-ROH]$ where the excess electron is delocalized over two CO_2 constituents to form a $C_2O_4^-$ molecular anion, and the other involves a monomer anionic core as $[CO_2^-$ ROH $CO_2]$. These results will explain the photoelectron spectral features of $[(CO_2)_nROH]^-$.

I-D-7 Theoretical Studies on the Reaction of $(CO_2)_N^-$ with CH_3

Morihisa SAEKI *(Univ. of Tokyo.)*, **Tatsuya TSUKUDA***(Univ. of Tokyo.)*, **Takashi NAGATA** *(Univ. of Tokyo. and IMS)* **and Suehiro IWATA**

Reactions of negatively-charged clusters of CO_2 and CH_3I results in the formation of $[(CO_2)_NCH_3I]^-$. The smallest member of these product anions, $[CO_2CH_3I]^-$, possesses a large vertical detachment energy (VDE) of 3.55 eV, which is

greater by 2 eV than the VDE value of CO_2^-. Ab initio calculations were performed to provide an decisive answer to the fundamental question regarding its electronic properties; namely, what is the extent of charge delocalization in $[CO_2CH_3I]^-$. The calculations provide an acetate-iodine charge-resonance complex $[CH_3CO_2^-I]$ as a possible structure of $[CO_2CH_3I]^-$ and reveal that an O-I bond is formed in the most stable structure. Based on these calculations, it is concluded that $(CO_2)_N^-$ acts as a nucleophilic reagent in the gas-phase cluster ion-molecule reactions and that the reactions of $(CO_2)_N^-$ with CH_3I leads to the formation of novel charge resonance complex $[CH_3CO_2I]^-$.

I-E Potential Energy Surfaces of Low-Lying States of Simple Molecules

I-E-1 The Electronic Structures of HCCS and NCS

Yumin LI and Suehiro IWATA

To obtain the accurate spectroscopic data of astronomically interesting molecules HCCS and its iso-valence molecule NCS, the potential energy surfaces and equilibrium geometries of three states (X^2P, A^2P and B^2S^+) are studied using complete active space SCF (CASSCF) and multireference configuration interaction (MRCI) methods of MOLPRO 94, and coupled cluster (CCSD(T)) method of Gaussian 94 program for each molecule. Furthermore, the Renner-Teller effect in both ^2P states are also investigated. The basis set used is cc-pVTZ.
The main electronic configurations of three states (X^2P, A^2P and B^2S^+) for both HCCS and NCS are $(1\text{-}5)s^21p^4(6\text{-}8)s^29s^22p^43p^34p^0$ for X^2P, $(1\text{-}5)s^21p^4(6\text{-}8)s^29s^22p^33p^44p^0$ or A^2P and $(1\text{-}5)s^21p^4(6\text{-}8)s^29s^12p^43p^44p^0$ for B^2S^+. In the CASSCF and MRCI calculations for PES's and equilibrium geometries, the active space includes all valence pp orbitals and the highest occupied s orbital. For HCCS, the ground state (X^2P) and second excited state (B^2S^+) are linear, but the first excited state (A^2P) is bent. An odd electron is mainly on the S atom in X^2P P. The first vertical excitation energy is 23700cm^{-1}, which is close to the experimental energy (24307, 24102cm^{-1}, which correspond to the 3/2 and 1/2 multiplets, respectively.) For NCS, the three states, X^2P, A^2P and B^2S^+, are all linear, and the energy gap between the A^2P and B^2S^+ states is small, which is consistent with the experimental results. In the CASSCF and MRCI studies for Renner-Teller splitting, the active space consists of all valence p orbitals, but for HCC bent mode of HCCS, the full valence CASSCF calculation is also done. The Renner-Teller effect in HCCS is much more complicated than that in NCS, because two bent modes, HCC and CCS, have an opposite effect and are coupled to each other, the Renner-Teller effect in excited state (A^2P) of HCCS is quite different from that in its ground state (X^2P).

I-E-2 Theoretical Characterization of the Low-Lying Electronic States of the SiB, SiB$^+$, SiAl, and SiAl$^+$ Molecular Species

Fernando R. ORNELLAS *(Univ. of São Paulo and IMS)* **and Suehiro IWATA**

Our main concern in this study is to present a global, reliable, and accurate characterization of the low-lying electronic states of the diatomics SiB, SiB$^+$, SiAl, and SiAl$^+$. This characterization includes a detailed description of the potential energy curves, vibrational states, spectroscopic constants, dissociation energies, and dipole moment functions. For the most relevant states, transition moment functions are also evaluated as well as radiative transition probabilities and lifetimes. For each ion/neutral pair a theoretical prediction of the photoelectron spectrum is also presented. Electronic wave functions and energies have been computed within the internally contracted multireference configuration interaction (CMRCI) formalism as implemented in the MOLPRO-94 suite of programs. Natural orbitals generated from a full valence complete active space self-consistent field (CASSCF) calculation were used in the CMRCI wave function. Atomic basis sets of the cc-pVQZ quality were employed. We note that existing studies in the literature besides being very incomplete, also report incorrect results for some of states.

I-E-3 Ab Initio Investigation of the Photodissociation of HOCl

Fernando R. ORNELLAS *(Univ. of São Paulo and IMS)* **and Suehiro IWATA**

The possibility of acting as a chlorine reservoir and thus contribute to a decrease in the depletion of ozone in the stratosphere has motivated several experimental and theoretical studies on the molecule HOCl. This molecule is known to have a strong absorption peak at about 240 nm but a second absorption peak at about 310 nm has been the subject of controversy among experimentalists, and also among theoreticians. If HOCl can absorb at wavelengths greater than 300 nm, then it will readily dissociate yielding two very reactive radicals and thus have a destructive role rather than serving as temporary reservoir for chlorine species. Recently, contrary to previous theoretical studies, we have reported results which predict the existence of two absorption peaks. However, the relatively small size of the basis set employed and also the amount of correlation effect incorporated in the configuration interaction wave function has resulted in a shift of the absorption peaks towards longer wavelengths. Also the intensity of the peak at 310 nm turned out to be much weaker than experimentally observed. Since, experimentally, the nature of this peak has also been a reason for controversy, we have undertook a reinvestigation of this system at a much higher level of correlation treatment with a major goal of accounting for both the proper location and the intensities of both peaks. The electronic wave functions and energies were computed within the Internally Contracted Multi-reference Configuration Interaction (CMRCI) formalism using the MOLPRO-94 suite of programs. The molecular orbitals (MOs) used in the CMRCI calculation were the natural orbitals obtained by diagonalizing the density matrix obtained in a previous valence shell complete active space self-consistent field (CASSCF) calculation. By distributing nine electrons in fourteen MOs, CASSCF reference spaces of dimensions

184 (A') and 152 (A") were constructed on top of which single and double excitations were generated in the CI expansions (549866 (A') and 322585 (A") CSFs) The aug-cc-pVTZ basis set was used in the expansion of the MOs. The absorption cross section was computed by treating (HO)Cl as a pseudo diatomic molecule with a fixed OH internuclear distance and with explicit inclusion of the continuum wave function. The calculations so far have shown good agreement with experiment for both peak locations and also for the intensity of the smaller wavelength peak. The cross section has shown to be sensitive to bond angle changes. Increasing the bond angle by about 10% has increased the intensity of the less energetic band bringing a further agreement with experiment. Studies are now in progress to treat this problem taking into account the wave function of the two-dimensional Schroedinger equation.

I-E-4 Ab Initio Studies of the Isomers: HSiNN, HNSiN, and HNNSi

Fernando R. ORNELLAS *(Univ. of São Paulo and IMS)* **and Suehiro IWATA**

The difficulty of properly describing the triatomics SiNN with the conventional SCF, MCSCF, and SDCI methodologies, all predicting a very weakly bound complex Si--NN, and the success of the CCSD(T) in predicting a reasonable stable structure for SiNN has motivated us to reexamine the [H,Si,N,N] potential energy surface with this latter methodology and the 6-311G(2d) basis set. In this study, we present new structural, energetics, and vibrational frequencies data which we hope can help in the search of the yet unknown species, and can also contribute to a better understanding of the silicon-nitrogen gas phase chemistry. Three local minima were found on the potential energy surface. That of the structure HSiNN (II) is the most stable, in contrast with a previous study which predicted a weakly bound complex HSi--NN. Next follows the isomer HNNSi (I) 13.6 kcal/mol higher in energy, and the species HNSiN (III) 47.6 kcal/mol above the global minimum. All three structures have C_s symmetry (^{2}A") with the heavy atoms nearly linear (173.9ß (I), 171.1ß (II), and 180.0ß (III)); the bond angle between the hydrogen and the heavy atom moiety takes the values 108.1ß (I), 86.2ß (II), and 121.1ß (III). A discussion of the nature of the bonds is also presented.

I-F Electronic Structure of Some Basic Molecules Containing the Transition Metal Atoms

I-F-1 Theoretical Studies of the Ground and Low-lying Excited Electronic States of the Early Transition Metal Dihydrides with State Averaged MC SCF Method

T. Shunmei FUJII and Suehiro IWATA

[*Chem.Phys. Letters* **251**, 150 (1996)]

The ground and low-lying excited electronic states, which are quasi-degenerated, of a series of dihydrides of the third-row metals, MH_2 (M= Ca, Sc, Ti, V, Cr, and Mn) are examined with the state averaged(SA) CAS SCF calculations for the qualitative discussions of valency of metal - hydrogen bonds. The molecular states, correlated with the electron configuration s^2d^n of the metal atom, are equally treated with the SA CAS SCF method. The shape and the depth of the potential energy surfaces of these states are similar to each others they are relatively indifferent to the occupation in the d orbitals. The state splittings in the series of MH_2 are explained by the slight difference in the stability of 3d originated orbitals; the orbital ordering is dd < dp < ds .

I-F-2 Quadratic Configuration Interaction Versus Coupled Cluster Theory : Importance of Drbital Relaxation Phenomena in CuH and CuF

Jan HRUŠÁK, Seiichiro TEN-NO and Suehiro IWATA

[*J. Chem. Phys.*, submitted]

The potential energy surface, the dipole moment and the spectroscopic constants of the ground states CuH and CuF are calculated by using single reference (SR) many electron theories. Since these molecules have large amplitudes, the comparisons offer critical examinations of the SR theories. The methods used in the calculations are the coupled cluster doubles (CCD), singles and doubles (CCSD), Brueckner doubles (BD) and quadratic configuration interaction singles and doubles (QCISD); all these methods are supposed to give the same results when the Hartree-Fock orbitals coincide with the approximate Brueckner orbitals. Furthermore we examine the perturbative treatment of triples to these methods, CCD(T), CCSD(T), BD(T), QCISD(T). For CuH, all the strict SR theories, the CCD, CCSD, BD, CCD(T), CCSD(T) and BD(T), result in parallel potential energy curves. The QCISD energy is however too low in comparison with the others. Furthermore the inclusion of triples gives an obviously wrong potential energy curve. The calculated dipole moment based on the finite field method and the diagnostic of amplitudes clearly demonstrate that the single electron excitations are over-estimated in the QCISD at the bonding region. This is mainly due to the absence of disconnected products. Such effects are even more pronounced in the CuF case. The results indicate that the systems become more multireference at the bonding region and the QCI results consequently become less reliable within the SR many electron theories.

I-F-3 The Structures of FeNO

Andreas FIEDLER and Suehiro IWATA

We are using an economic density functional/Hartree-Fock hybrid method for the examination of the qualitative aspects of the [Fe,N,O] potential energy hypersurfaces from doublet up to sextet spin multiplicity. Additionally, the recently developed averaged quadratic coupled cluster approach a size consistent extension of the well known multireference configuration interaction method, is than applied for a more sophisticated description. Using this approach we characterized numerous isomers of [Fe,N,O], namely nitrosyl iron FeNO, inserted nitro iron oxid NFeO,

having different bond types, oxygen bound isomers FeON, and even cyclic forms. All interconnecting transition structures also have been examined. Interestingly, the calculations indicate that the global minimum, FeNO, has a low-spin ^{2}D ground state which is not originated from the ground state asymptote of the fragments, Fe (^{5}D) and NO$^\cdot$ (^{2}P). Thus, this molecule cannot be the result of a simple single covalent s bond between Fe $4s^23d^6$ and the NO$^\cdot$ radical, which is expected to have a bent structure and quartet multiplicity. This is pointing to a remarkable alternative binding mechanism, in which charge transfer plays an essential role. The calculated stabilization energy relative to the lowest exit channel, ground state Fe and NO$^\cdot$, amounts to 14 kcal/mol. The bent quartet isomers are 2. and 2.5 kcal/mol less stable, ^{4}A" and ^{4}A' respectively. Even the lowest sextet isomer, FeNO ^{6}A", is energetically located slightly below the dissociation products (1 kcal/mol) and also may be observed experimentally. The geometry optimizations result also in oxygen bound and alternatively cyclic minima However, these isomers are slightly higher in energy than the exit cannel, and have only very small barriers in the order of 2 kcal/mol for rotation to the more stable FeNO structures. Contrary, the most stable inserted OFeN ^{4}A" species is 27 kcal/mol more energy demanding than the global minimum. It is, however, separated from rearrangement reaction to the more stable isomers by a significantly high barrier (33 kcal/mol). Actually, while preparing this paper the experimental evidence for such an isomer has been reported.

I-G Structures, Spectra and Dynamics of Rare Gas Atomic Clusters

I-G-1 Size Dependence of the Photoabsorption Spectra of Ar_n^+, n = 4 - 25

Tsutomu IKEGAMI and Suehiro IWATA

[*J. Chem. Phys.*, submitted]

The photoabsorption spectra of argon cluster ions, Ar_n^+, are calculated for n = 4 to 25. The internal motion of the cluster is accounted for by the molecular dynamics method. The diatomics-in-molecules (DIM) potential energy surface is used for the calculation. There are basically two peaks in the spectra. At a low internal energy, the primary peak shifts from 510 nm to 550 nm at $n\approx10$, and then shifts abruptly to 600 nm at $n\approx14$. As the internal energy increases, the spectra become broad and the clear transition disappears. The spectral shift is explained by the solvation of the ion core in the cluster, with the rest of the constituent atoms acting as solvent atoms. The first red shift is due to the crossover of the energy levels between the ion core and the solvent shell. The second one takes place because the solvation energy is increased abruptly, which is explained in terms of the structural change in the solvation shell.

I-H Novel Molecular Systems with Symmetry Breaking

I-H-1 Theoretical Study of the Vibrational Spectrum of $H_2O_2^{+\cdot}$ Radical Cation: An Illustration of HF Symmetry Breaking

Jan HRUŠÁK *(J. Heyrovsky Institute of Physical Chemistry and IMS)* **and Suehiro IWATA**

Experimental results for the $[H_2,O_2]^{+\cdot}$ system are very scarce and concern basically only photoelectron studies. Based on theoretical calculations the first broad (10.5-14 eV) structured band in the photoelectron spectrum was rationalized in terms of superposition of ionization processes to the ^2B_g (*trans*) and $^2A_2$ (*cis*) electronic states. The ionization energies of 11.69 eV (^{2}B) and 12.69 eV (^{2}A) are in agreement with the results of previous ab initio CISD studies, while the OO stretching vibration was calculated significantly higher (1568 cm^{-1}) than the proposed 1050 cm^{-1} estimated from the experiment.
The results of correlated methods based on RHF, UHF, and CASSCF wave functions are presented and the effect of the choice of the reference wave function on the shape of the correlated potential energy surface is studied. In addition to the standard ab initio MO methods two different density functional methods were employed.
The MPn calculated force constants for the assymmetrical vibration are very large and consequently the corresponding n_5 (b_u or b_2) calculated frequency approaches unphysical numbers, which are two orders of magnitude larger as expected. In addition the n_2 (b_u) frequency, which is for the *trans*- conformer in the proper range around 1350 cm^{-1} , possesses huge IR intensities. For the *cis*-structure even the first asymmetrical frequency n_4 (b_2) is too high (2216 - 2444 cm^{-1}) accompanied with unreasonable IR intensities. It is shown that the symmetry breaking is fully responsible for this unphysical behavior and lead to unreliable predictions of the whole vibrational spectrum at any single determinant based MP(n) levels. Similarly, the CISD single determinant based method fails to calculate the vibration spectrum properly. On the other hand, the more complete QCISD(T), CCSD(T), and BD(T) methods do not suffer so much from the symmetry breaking since they are less sensitive to the reference function. Surprisingly, also the both DFT methods used predict a spectrum very close to the more sophisticated ab initio results.

I-I Prediction of Protein Tertiary Structures from the First Principles

I-I-1 Molecular Dynamics, Langevin, and Hybrid Monte Carlo Simulations in Multicanonical Ensemble

Ulrich H.E. HANSMANN, Yuko OKAMOTO and Frank EISENMENGER *(Humbolt Univ.)*

[*Chem. Phys. Lett.* **259**, 321(1996)]

We demonstrate that the multicanonical approach is not restricted to Monte Carlo simulations, but can also be applied to simulation techniques such as molecular dynamics, Langevin, and hybrid Monte Carlo algorithms. The effectiveness of the methods are tested with an energy function for the protein folding problem. Simulations in the multicanonical ensemble by the three methods are performed for a penta peptide, Met-enkephalin. For each algorithm, it is shown that from only one simulation run one can not only find the global-minimum-energy conformation but also obtain probability distributions in canonical ensemble at any temperature, which allows the calculation of any thermodynamic quantity as a function of temperature.

I-I-2 Numerical Comparisons of Three Recently Proposed Algorithms in the Protein Folding Problem

Ulrich H.E. HANSMANN and Yuko OKAMOTO

[*J. Comp. Chem.,* in press]

We compare numerically the effectiveness of three recently proposed algorithms, multicanonical simulations, simulations in a 1/k-ensemble, and simulated tempering, for the protein folding problem. For this we perform simulations with high statistics for one of the simplest peptides, Met-enkephalin. While the performances of all three approaches is much better than traditional methods, we find that the differences among the three are only marginal.

I-I-3 Monte Carlo Simulations in Generalized Ensemble: Multicanonical Algorithm versus Simulated Tempering

Ulrich H.E. HANSMANN and Yuko OKAMOTO

[*Phys. Rev. E,* in press]

It is shown that two Monte Carlo methods in generalized ensemble, multicanonical algorithm and simulated tempering, are closely related. The equivalence and effectiveness of the two methods are illustrated by taking an energy function for the protein folding problem as an example.

I-I-4 Global Minimum Configuration of a Small Peptide for the ECEPP/2 and ECEPP/3 Force Field

Frank EISENMENGER *(Humbolt Univ.)* and Ulrich H.E. HANSMANN

We use the multicanonical ansatz to search for low energy configurations of a small peptide, Met-Enkephalin. We found that the global minimum configuration of ECEPP/3 differs from that of the ECEPP/2 force field. The distribution and relative weight for various temperatures of the two configurations are calculated and compared for both force-fields. We show that expectation values of physical quantities are robust under changes from ECEPP/2 to ECEPP/3.

I-J Three-Dimensional Shape Analysis and Visualization of Protein Molecules

I-J-1 Visualization of the Electrostatic Energy of Protein Binding Site

Masato MASUYA and Junta DOI *(Univ. of Tokyo)*

[*J. Mol. Graphics,* in press]

The electrostatic energy contributes most to the stability of porteins among binding energies, such as, van der Waals energy, hydrogen bond energy, and solvation energy. Therefore, the energy stabilization of whole protein and/or complex is mostly dependent on the electrostatic energy. We visualized the electrostatic energy of protein binding site for understanding the protein binding mechanism. The binding site of receptor protein as cavities and of ligand protein as portions in contact with cavities are extracted using the discrete mathematical morphology. They are obtained as the sets of lattice points which are included in each binding sites. The electrostatic potential and electoric charge at each lattice points are calculated and the electrostatic energy is derived from them. We discuss the electrostatic property of binding site on the basis of energy values and visualized figures.

I-K Developing a New Method for Diagonalization of Large Hermitian Matrices

I-K-1 A Method for Calculating the Eigenvalues of Large Hermitian Matrices by Second-Order Recursion Formulae

Ayori MITSUTAKE *(Nara Women's Univ.)* , Toshiaki IITAKA *(Inst. Phys. Chem. Res.)* and Yuko OKAMOTO

[*Comp. Phys. Comm.* **96**, 217 (1996)]

A general discussion of a method for solving the eigenvalue problem of large N × N Hermitian matrices by using second-order recursion formulae is given. In principle, the method is suitable for finding not only the extreme eigenvalues and the corresponding eigenvectors but also any other eigenvalues in the range of one's specification. The effectiveness of the algorithm is illustrated by calculation of a few low-lying eigenvalues of the Heisenberg model for an antiferromagnetic chain with N up to 1048576.

I-L Semiclassical Theory of Chaotic Systems

I-L-1 Stokes Phenomenon in Chaotic Systems: Pruning Trees of Complex Paths with Principle of Exponential Dominance

Akira SHUDO and Kensuke S. IKEDA *(Ritsumeikan Univ.)*

[*Phys. Rev. Lett.* **76**, 4151 (1996)]

Stokes phenomenon is investigated in the complex semiclassical theory of chaotic tunneling, and a rule for locating contributing tunneling paths out of a complicated set of candidates is proposed. The proposal is based on discovery of a tree structure hidden in entangled tunneling paths: The candidates are ordered along the tree, and the *Principle of Exponential Dominance(PED)* is extended to prune noncontributing paths. This rule enables construction of semiclassical tunneling wave functions systematically. A phenomenon for which PED plays a crucial role in also demonstrated.

I-L-2 Chaotic Tunneling I: A Remarkable Manifestation of Complex Classical Dynamics in Nonintegrable Quantum Phenomena

Akira SHUDO and Kensuke S. IKEDA *(Ritsumeikan Univ.)*

[submitted to Nonlinearity]

The tunneling phenomenon in chaotic systems is analyzed in terms of the complex semiclassical method in the time domain. In contrast to the tunneling paths in integrable systems, it is discovered that there exist a tremendous number of candidate complex branches (*Laputa branches*) which may contribute to the semiclassical propagator. The origin of a lot of characteristic structures observed in the tunneling tail in chaotic systems, which are completely absent in case of integrable systems, can fully be interpreted using such complex paths. In particular, we found a remarkable object forming chain-like structures(*Laputa chains*), which are hidden in the set of initial values displayed on the complex plane and they just generate a variety of structures in tunneling tails. The relationship between the tunneling tail and the structure of the Laputa chain is analyzed in detail. The candidate trajectories, however, contain unphysical noncontributing part as a manifestation of *Stokes Phenomenon*, and empirical rules how to remove such noncontributing parts is also discussed. On the basis of the whole story constructed here, *chaotic tunneling* is proposed as a universal tunneling mechanism originating in the complicated structure of classical chaotic manifolds in the complex regime. Several questions arose in the present study, but not clarified yet, are also list up in relation to the theories of complex semiclassical method and complex dynamical systems.

I-L-3 Euler-type Product of the Fredholm Determinant Appearing in Boundary Element Method for Two-dimensional Quantum Billiards

Shuichi TASAKI*(Inst. for Fundamental Chemistry)*, **Takahisa HARAYAMA***(ATR)* **and Akira SHUDO**

[submitted to *Comm. Math. Phys.*]

Euler-type infinite product expansion of the Fredholm determinant appearing the boundary element method for two-dimensional quantum billiards is rigorously derived under the assumptions that the boundary of the billiard domain is piecewise twice continuously differentiable. The Fredholm determinant can be expressed as a product of the Fredholm determinant of interior Dirichlet problem and that of exterior Neumann Problem, and each one also has an explicit expression using the Green function on each domain. This result suggests that Kac's famous inverse problem, 'Can one hear the shape of a drum?' should be modified as 'Can one hear the shape of a drum through the spectrum of the interior Dirichlet problem and the cross sections of the exterior Neumann scattering?'.

I-M Theoretical Studies of Chemical Reaction Dynamics

With use of the hyperspherical coordinate approach the accurate quantum dynamics studies of triatomic chemical reactions have been continued with an emphasis on the heavy-light-heavy systems. Some intriguing features have been found. Tetra-atomic systems are also challenged.

I-M-1 Quantum Dynamics $O(^3P)+HCl \rightarrow OH+Cl$

Katsuyuki NOBUSADA, Kengo MORIBAYASHI and Hiroki NAKAMURA

Extending the previous studies of the title reaction system[1], we have been studing effects of the reagent rotational excitation. Preliminary calculations show that the rotational excitation ($j_i \sim 10$) strongly enhances the reaction, and that a peak around $j_f \sim 10$ appears in the product rotational state distribution in the energy range studied ($E_{tot} \cong 0.4 \sim 1.0$eV). These features may be ascribed to the topography of the potential energy surface and the bent structure of the transition state.

Reference

1) Moribayashi and Nakamura, *J.Phys.Chem.* **99**, 15410 (1995)

I-M-2 Quantum Dynamics of the Tetra-atomic Reaction Systems: H_2+OH and NH+NO

Henrik SZICHMAN, Michael BAER *(Soreq Nuclear Research Center, Israel and IMS)* **and Hiroki NAKAMURA**

Time-independent quantum dynamics studies of the reaction $H_2+OH \rightarrow H_2O+H$ have been carried out at low energies mainly to reveal the final internal state distribution. The 3 ~ 5D calculations were performed to compare with each other. The OH bond freezing approximation is, for instance, confirmed to work well. The same method is being applied to the NH+NO reaction.

I-M-3 Multidimensional Tunneling in Terms of Complex Classical Mechanics: Wave Functions, Energy Splitting, and Decay Rates in Nonintegrable Systems

Shoji TAKADA

[*J. Chem. Phys.* **104**, 3742 (1996)]

A semiclassical theory of multidimensional tunneling is formulated to calculate the tunneling wave function, energy splitting in a double well and decay rate constant from a metastable state. First, the tunneling wave function is calculated by analytic continuation of a quantized torus prepared in analytic forms using either the Chapman-Garrett-Miller method or the Birkhoff-Gustavson normal form method. For a weakly nonintegrable system, tunnelings are confirmed to be classified into two qualitatively different domains; pure tunneling in the I region and mixed tunneling in the C region. Semiclassical wave functions agree with quantum mechanical ones within a few percent both in classically allowed and tunneling regions. Breakdown of this simple picture is exemplified for cases of relatively strong couplings. Second, expressions of the tunneling energy splitting in a double well potential and the decay from a metastable state are derived. The wave function near a well formulated above is connected with the semiclassical Green's function in the deep tunneling region. The latter is expressed by complex trajectories which start from the complex quantized torus. A preliminary numerical comparison with the quantum mechanical value is also done for the energy splitting.

I-N Theory of Nonadiabatic Transitions

The semiclassical theory of nonadiabatic transitions due to curve crossing, pioneered by Landau, Zener, and Stueckelberg, has been recently completed in a form very convenient for various applications. All the shortcomings of the LZS theory are practically removed. Now, the theory has been extended into various directions.

I-N-1 Semiclassical Analysis of Resonance States Induced by a Conical Intersection

Chaoyuan ZHU, Evgueni E. NIKITIN *(Technion, Israel and IMS)* **and Hiroki NAKAMURA**

[*J.Chem.Phys.* **104**, 7059 (1996)]

The resonance states induced by nonadiabatic coupling in the conical intersection problem are analyzed semiclassically. Not only the general framework but also the explicit analytical expressions of resonance positions and widths are presented. Interestingly, the nonadiabatic transition schemes are found to be quite different in the two representations employed, i.e., the adiabatic and generalized adiabatic(or dynamical state, or post-adiabatic) representations. In the former case the transition is assigned to be of the Landau-Zener (LZ) type, and the latter case is analyzed by a mixture of LZ- and Rosen-Zener (RZ) -type in the case of $m \geqq 3/2$ and by the nonadiabatic tunneling (NT) type in the case of $m = 1/2$, where m is the angular momentum quantum number. Both of these semiclassical results agree well not only with each other in spite of the very different schemes, but also with the exact numerical results in a wide range of energy and angular momentum.

I-N-2 Two-by-two Diabatic Approach for Multi-Channel Curve Crossing Problems

Chaoyuan ZHU and Hiroki NAKAMURA

[*Chem.Phys.Lett.* **258**, 342 (1996)]

A practically useful method is proposed to deal with multi-channel curve crossing problems. This method deals with each crossing based on the relevant two coupled diabatic states and provides a corresponding transition matrix (*I*-matrix). The total reduced scattering matrix can be expressed by a product of these *I*-matrices. In this way, the present method can make full use of the advantages of the newly completed semiclassical theory for two-state curve crossing problems, and can treat the multi-state curve crossing problems as simply as the two-state case. Some numerical demonstrations within a three-state model are presented.

I-N-3 Quantum Mechanically Exact Analytical Solutions of a Two-State Exponential Model

Vladimir I. OSHEROV *(Inst. Chem. Phys., Russia and IMS)* **and Hiroki NAKAMURA**

[*J.Chem.Phys.* **105**, 2770 (1996)]

A certain two-state exponential potential model is solved quantum mechanically exactly. Compact expressions for nonadiabatic transition matrices are obtained. Interesting quantum mechanical threshold effects are found. Simple very accurate expressions are found from a semiclassical viewpoint for the nonadiabatic transition probabilities, indicating that the exponential model may present a third important basic model in addition to the Landau-Zener-Stueckelberg and the Rosen-Zener-Demkov models. Extension to general cases is also briefly discussed.

I-N-4 Semiclassical Theory for Two-State Exponential Potential Models

Vladimir I. OSHEROV *(Inst. Chem. Phys., Russia and IMS)* **and Hiroki NAKAMURA**

A two-state exponential potential model (with the same exponents but different pre-exponential factors) is solved semiclassically in terms of the confluent hypergeometric functions. This is more general than the Nikitin model, and the solutions can be compared with the quantum mechanically exact one in the special case. The basic semiclassical parameters can be expressed in terms of phase integrals, which enables us to generalize the theory so as to be applicable to general exponential models.

I-N-5 Semiclassical Theory of Time-Dependent Curve Crossing Problems

Yoshiaki TERANISHI *(Graduated Univ. for Advanced Studies)* **and Hiroki NAKAMURA**

The recently completed semiclassical theory of the Landau-Zener-Stueckelberg type curve crossing problems in coordinate space can be applied to time-dependent problems. The quadratic potential case can be solved exactly, and general crossing and non-crossing problems can be treated accurately by the generalized semiclassical theory. These are confirmed by numerical solutions of some examples.

I-N-6 Exact Analytical Solution for Coupled Time-Independent Schrödinger Equations with Certain Model Potentials

Chaoyuan ZHU

[*J.Phys.A:Math.Gen.***29**, 1293 (1996)]

Exact analytical solution is obtained for coupled time-independent Schrödinger equations with model potentials:

$$V_{11}(x)=V_1+\beta V_0 e^{-\alpha x}, V_{22}(x)=V_2+\frac{1}{\beta}V_0 e^{-\alpha x}, \text{and } V_{12}(x)=V_{21}(x)=V_0 e^{-\alpha x}$$

This is made possible by solving a single fourth-order ordinary differential equation derived from the original coupled equations. Exact closed-form solutions for the nonadiabatic transition matrices (or scattering matrices) are found for scattering boundary conditions with three, two and one open channels, respectively. How to apply the present results to deal with general potentials is also briefly analyzed.

I-N-7 Unified Semiclassical Theory for the Two-State System: Analytical Solutions for Scattering Matrices

Chaoyuan ZHU

[*J.Chem.Phys.* **105**, 4159 (1996)]

Unified semiclassical theory is established for general two-state system by employing an exactly analytical quantum solution[1] for the Nikitin exponential-potential model which contains the two-state curve crossing and noncrossing cases as a whole. Analytical solutions for scattering matrices are found for both three- and two-channel cases within the time-independent treatment. This is made possible by introducing a very important parameter

$$d(R_0)=\sqrt{1+\frac{4V_{12}^2(R_0)}{[V_{22}(R_0)-V_{11}(R_0)]^2}}$$ ($V_{11}(R)$, $V_{22}(R)$ and $V_{12}(R)$ are diabatic potentials and coupling, R_0 is real part of complex crossing point betweentwo adiabatic potentials) which represents a type of nonadiabatic transition for the two-state system. For instance, $d=\infty$ represents the Landau-Zener type and $d=\sqrt{2}$ represents Rosen-Zener type. Since $d(R_0)$ runs from unity to infinity, this parameter provides a quantitative description of nonadiabatic transition. The idea used here is the parameter comparison method which makes an unique link between the model and general potential system at the complex crossing point. This method is testified by not only numerical examples, but also agreement of the present semiclassical formulas with all existing semiclassical formulas.

Reference

1) Zhu, *J. Phys.* **A29**, 1293(1996)

I-O Theoretical Studies of Characteristics and Dynamics of Superexcited States of Molecules

The characteristics and dynamics of superexcited states of molecules are studied with use of the quantum chemical methods and the multichannel quantum defect theory. A general theoretical procedure applicable to diatomic molecules has been developed.

I-O-1 Superexcited States of CO near the First Ionization Threshold

Miyabi HIYAMA *(Graduated Univ. for Advanced Studies)* **and Hiroki NAKAMURA**

[*Chem. Phys. Lett.* **248**, 316 (1996)]

Characteristics of the superexcited states of CO which dominate the various dynamic processes near the first ionization potential are determined by using quantum chemical calculations and multi-channel quantum defect theoretical analyses. Quantum defects are obtained as functions of the internuclear distance for the sσ, pσ, pπ, dσ, dπ and dδ symmetries. Two dissociative states ($^1\Sigma^+$ and $^1\Pi$) which cross the ionic potential curve near the equilibrium internuclear distance of CO^+ are also determined.

I-O-2 A General Theoretical Procedure to Reveal Characteristics and Dynamics of Superexcited States of Diatomic Molecules

Miyabi HIYAMA *(Graduated Univ. for Advanced Studies)* **and Hiroki NAKAMURA**

The general procedure is composed of (1) SCF calculations of quantum defect functions to characterize the second kind of superexcited states (SES), (2) restricted CI calculations of the first kind of SES to evaluate the potential

curves and electronic wave functions, (3) MQDT analysis of spectroscopic data to improve the results of (1) and (2), (4) expansions of two center coulombic functions is terms of gaussian functions to represent the ionization continuum, (5) evaluation of the electronic couplings as functions of the electron energy and the internuclear distance with use of the electronic wave functions obtained in (2) and (4), (6) non-perturbative solution of the K-matrix integral equation associated with the electronic coupling, and (7) MQDT studies of various dynamic processes.

I-P New Molecular Switching Elements

Shinkoh NANBU, Hiroki NAKAMURA and Frank O. GOODMAN *(Univ. of Waterloo and IMS)*

A new idea of molecular switching and its basic theory are presented. The idea based on the intriguing phenomenon of complete reflection in a two-state nonadiabatic tunneling type transition. Complete switching of transmission is theoretically possible in finite dimensional periodic systems. An idea of energy filter is also introduced. This can be designed so as to switch off the transmission in a desirable energy range. All the interesting features can be numerically well demonstrated.

I-Q Laser Assisted Surface Ion Neutralization

Frank O. GOODMAN *(Univ. of Waterloo and IMS)*, **Zoran L. MISKOVIC** *(Univ. of Waterloo)* **and Hiroki NAKAMURA**

We consider three approximation schemes for the theory of laser-assisted surface ion neutralization (LASIN), labeling them Z1 (appropriate for relatively small laser frequencies h), Z2 (for relatively large h), and H (for intermediate h); exact results are labeled E. It is shown how a single approximation (A) may be built from a suitable combination of Z1 and Z2 for the case of a relatively weak laser field. Comparisons of Z1, Z2, H, A and E are made over wide regions of the system parameter-space. At the same time, several aspects of LASIN are considered, and it is concluded that experiments, based on our suggestions of parameter-values, are now possible, and we call on experimentalists to test the predictions made herein and elsewhere.

I-R Theoretical Studies of Nonlinear Optical Spectroscopy of Molecules in the Condensed Phase

The nonlinear optical response of molecules in the condensed phase subjected to femtosecond laser pulses is studied using various techniques developed in statistical physics and field theory.

I-R-1 Unified Time-Path approach to the Effect of Anharmonicity on the Molecular Vibrational Spectroscopy in Solution

Ko OKUMURA and Yoshitaka TANIMURA

[*J. Chem. Phys.* **105**, 7294 1996]

We obtain a closed expression for the response function for damped anharmonic vibrational modes using the Feynman rule obtained through the nonequilibrium generating functional derived in our previous paper[1]. The linear absorption spectra are explicitly calculated through the Feynman diagrams for molecules with anharmonic potential in solution. The dependence of the spectra both on the temperature and on the solvent nature can be taken into account in our theory. The result is examined numerically for various dampings, anharmonicities, and temperatures.

Reference

1) K. Okumura and Y. Tanimura, *Phys. Rev. E* **53**, 214 (1996).

I-R-2 Femtosecond Two-Dimensional Spectroscopy from Anharmonic Vibrational Modes of Molecules in the Condensed Phase

Ko OKUMURA and Yoshitaka TANIMURA

[*J. Chem. Phys.*, submitted]

We developed a theory of the fifth-order off-resonant spectroscopy from anharmonic vibrational modes. The fifth-order signal arises from anharmonicity of adiabatic potentials as well as nonlinear dependence of polarizability on nuclear coordinates. A profile of the signal varies depending on the relative importance of the two effects — the anharmonicity and the nonlinearity. This makes it possible to distinguish anharmonicity of a potential from the other effects such as the nonlinearity or the inhomogeneity of vibrational modes. In order to carry out calculations analytically, we employed the multi-mode Brownian oscillator model and treated anharmonicity as perturbation to the harmonic vibrational modes. A simple analytical expression for the fifth-order polarization was obtained from the nonequilibrium generating functions with use of the Feynman rule. Using the spectral distribution obtained from the third-order experiments, we calculated the fifth order signal for $CHCl_3$ and CS_2 in the anharmonic case and the nonlinear case. Our results were compared with the corresponding experimental data from CS_2, which indicates a possibility that anharmonicity may contribute to the fifth-order signal.

I-R-3 The (2n+1)th-order Off-Resonant Spectroscopy from the (n+1)th-order Anharmonicities of Molecular Vibrational Modes in the Condensed Phase

Ko OKUMURA and Yoshitaka TANIMURA

[*J. Chem. Phys.* 01 Feb. 1997 (in press)]

Feynman diagram technique for the nonequilibrium multi-time correlation functions is presented to calculate response functions relevant to the higher-order off-resonant spectroscopy. Assuming that the polarization is a linear function of the nuclear coordinate, i.e. $\alpha(q)=\alpha_0+\alpha_1 q$, we obtain analytical expressions of the $(2n+1)$th-order signals and show that the leading order of the signals ($n>1$) are proportional to g_{n+1} where g_{n+1} is the coefficient of the anharmonic potential $V(q)= g_3 q^3/3!+ g_4 q^4/4!+\cdots$. In other words, detection of the $(2n+1)$th-order signal implies the direct observation of the $(n+1)$th-order anharmonicity within the approximation. Based on this fact we discuss a possibility to detect the $(n+1)$th-order anharmonicity directly from the $(2n+1)$th-order experiment. With help of the double-sided Feynman diagram, we draw physical pictures of higher-order off-resonant optical processes. Representative calculations for $CHCl_3$ of the fifth-, seventh-, and ninth-order optical processes are presented and discussed.

I-R-4 First-, Third-, and Fifth-Order Resonant Spectroscopy of an Anharmonic Displaced Oscillators System in the Condensed Phase

Yoshitaka TANIMURA and Ko OKUMURA

[*J. Chem. Phys.*, Feb. 1997 (in press)]

We have obtained Nth-order response functions for a two-level system described by displaced anharmonic potential surfaces coupled to a heat bath. The anharmonicity of the potentials has been taken into account as a perturbation of harmonic potentials. The heat-bath was assumed to be an ensemble of harmonic oscillators: Coupling between the two-level system and the bath was assumed to be bilinear. The calculations were done analytically using the Liouville-space generating functional, which had been obtained by way of the path-integral approach. The response functions has been defined in terms of line-shape functions with these line-shape functions being expressed in terms of the bath spectral density and the temperature. We have carried out model calculations of the first-, third- and fifth-order optical processes for various parameters of anharmonicity to show that anharmonicity plays a minor role in linear absorption, impulsive pump-probe, and photon echo experiments, but plays a major role, in some cases, in fifth-order two-dimensional resonant spectroscopy which is proposed in this study.

I-S Theoretical Studies of a Strongly Correlated Electron System

We study macroscopic and microscopic electronic structures of strongly correlated electron systems. The purpose of this study is to understand the mechanism of conductivity, superconductivity and magnetization of low dimensional electron systems.

I-S-1 *Ab Initio* Molecular Orbital Calculations by the Resonating Hartree-Fock Approach: Superposition of Non-Orthogonal Slater Determinants

Norikazu TOMITA, Seiichiro TEN-NO and Yoshitaka TANIMURA

[*Chem. Phys. Lett.*, in press]

The resonating Hartree-Fock (ResHF) method is applied to *ab initio* molecular orbital calculations of the carbon mono-oxide molecule around the equilibrium bond distance. This method approximates correlated wave functions by superposition of non-orthogonal Slater determinants, where both the CI coefficients and the orbitals in the determinants are variationally determined. The ResHF wave function, with two or three generating Slater determinants, explains the correlation energy to the same extent as the full valence CASSCF wave function with 328 configuration state functions. This is because the ResHF method is free from the partitioning of orbitals and it makes the wave function flexible enough to explain the orbital relaxation effects among configuration state functions. Furthermore, it turns out that the present method reproduces the dipole moment more accurately than the MCSCF method, reflecting the better long range behavior of the wave function. This implies that the ResHF wave function may be a more suitable reference in multi-reference methods.

I-S-2 The SDW-CDW Phase Transition in the One Dimensional Extended Hubbard Model

Norikazu TOMITA, Akira IKAWA *(Kyoto Univ.)* **and Hideo FUKUTOME** *(Kyoto Univ.)*

[*J.Phys. Soc. Jpn.* **65**, 195(1996)]

We study phase transition in the one dimensional extended Hubbard model at a half-filling. A scaling analysis using the resonating Hartree-Fock method with the numbers of electrons from 8 to 20 strongly suggests that the ground state is many-fold degenerate ($^1A_1^+$, $^1B_1^+$, $^3A_2^-$, and $^3B_2^-$ states) in the SDW region while it is doubly degenerate ($^1A_1^+$ and $^1B_2^-$ states) in the CDW region. Only the $^1A_1^+$ state makes a continuous phase transition from the SDW state to the CDW one. The $^1B_1^+$, $^3A_2^-$, and $^3B_2^-$ states cross the $^1B_2^-$ state around the phase boundary. We show that the continuous phase transition in the $^1A_1^+$ state is brought about by defects connecting the SDW-CDW domains called halfons. The correlation structures of these states are shown to clarify the origin of the degeneracies of the ground states.

I-T Structures and Dynamics of Condensed Molecular Systems

I-T-1 Growth and Collapse of Structural Patterns in the Hydrogen Bond Network in Liquid Water

Eli SHIRATANI *(Nagoya Univ.)* **and Masaki SASAI** *(Nagoya Univ. and IMS)*

[*J. Chem. Phys.* **104**, 7671 (1996)]

Intermittent and chaotic motions of the hydrogen bond network are studied with the molecular dynamics simulation. By analyzing the fluctuation in the radial distribution function, it is shown that individual water molecule alternately goes through two different periods; the structured period and the destructured period. At room temperature the lifetime of each period is hierarchically distributed from a few hundreds fsecs to several psecs. This intermittent structural fluctuation is quantitatively analyzed by defining a new quantity, local structure index (LSI). Molecules which have the large LSI value have tendency to be close to each other to form clusters. Temporal and spatial correlations of LSI are studied by analyzing the information flow in the network. Dynamics of clusters of structured molecules should give a hint to understand the transition between low density phase and high density phase in the supercooled region.

I-T-2 Mechanism of Fast folding and Kinetic Branching Process of the Model Protein

Seiji SAITO *(Nagoya Univ.)* **and Masaki SASAI** *(Nagoya Univ. and IMS)*

By using a newly developed knowledge-based Hamiltonian, molecular dynamics simulation of protein folding is performed and trajectories are analyzed in detail. Trajectories are classified into the fast folding ones and the slow folding ones. Fast folding trajectories should explain the recent experimental data of folding in micro-sec scale observed with the technique of laser chemistry. Kinetic branching between fast and slow folding trajectories takes place in the early stage of folding after the chain collapses into the globule. Mechanism of branching is studied by developing a spin-glass model of folding. Consistent growth of various structural orders, secondary structure, motives, and tertiary structure, is a necessary condition for trajectories to reach the fast folding funnel.

I-T-3 Evolution of Foldability and Local Structural Ordering

Seiji SAITO *(Nagoya Univ.)* **, Tetsuya YOMO** *(Osaka Univ.)* **and Masaki SASAI** *(Nagoya Univ. and IMS)*

Sequences are selected with computer by using the criterion whether the chain can fold to the conformation with several residues located in expected positions. This criterion mimics the situation that sequences of enzymes are selected not by their whole conformation but by their functionality : If we assume that the functionality is mostly determined by the local structure in the active site region, then such local structure should be a criterion to select sequences. By using the knowledge-based Hamiltonian, folding simulations are performed and sequences are selected by examining the generated local conformations. A spin-glass model for this selection is also developed and results are compared. Possibility of evolution to the unique conformation is discussed and evolution of features in folding kinetics are analyzed.

I-U Electronic Structure of a Molecule in Solution

Chemical reaction is undoubtedly the most important issue in the theoretical chemistry, and the electronic structure is a key to solve the problem. As long as molecules in the gas phase are concerned, the theory for the electronic structure has been enjoying its great success. However, when it comes to molecules in solution, the stage of the theory is still an infant. We have recently proposed a new method refered to as RISM-SCF based on the integral equation theory of molecular liquids (RISM) and the ab initio electronic structure theory (SCF).[1] The integral equation approach replaces the reaction field in the continuum models by a microscopic expression in terms of the site-site radial distribution functions between solute and solvent.

$$V_\lambda = \rho \sum_j \int_0^\infty \frac{q_j}{r} g_{\lambda j}(r) 4\pi r^2 dr$$

where j and λ specify solvent and solute sites, respectively, and ρ denotes the solvent density. The site-site radial distribution functions $g_{\lambda j}(r)$ can be calculated from the extended RISM equation. Using V_λ the solvated Fock operator is defined as,

$$F^s = F^g - \sum_\lambda V_\lambda b_\lambda$$

where b_λ is a population operator of solute atoms. The statistical solvent distribution around solute is determined by the electronic structure or the partial charges of solute, while the electronic structure of solute is influenced by the solvent distribution. Therefore, the Hartree-Fock equation and the RISM equation should be solved in a self-consistent manner. It is this self-consistent determination of the solute electronic structure and the solvent distribution around the solute that features the RISM-SCF procedure.

The latest development along this line includes some applications of the RISM-SCF method to the coupled solvent and substitution effects upon the proton afinity of a molecule in water. Those studies are reported below along with the generalization of the method of the electronic structure theory (SCF) to the multiconfigurational self-consisitent-field (MCSCF) method which can be used for exploring the excited state of a molecule in solution.

References

1) S. Ten-no, F. Hirata, S. Kato, *Chem. Phys. Lett.*, **214**, 391 (1993): *J. Chem. Phys.*, **100**, 7443 (1994)

I-U-1 Irregular Order in Basicities of Methylamines in Aqueous Solution: A RISM-SCF Study

Masaaki KAWATA*(Kyoto Univ.)*, **Seiichiro TEN-NO, Shigeki KATO***(Kyoto Univ.)* **and Fumio HIRATA**

[*J. Am. Chem. Soc.*, **117**, 1638 (1995)]

The irregular order in basicities of a series of methylamines in aqueous solution is studied by means of an ab initio quantum chemical calculation combined with the extended reference interaction site method in statistical mechanics of molecular liquids (RISM-SCF method). By using the restricted Hartree-Fock level approximation in the theoretical treatment for solute electronic structure, the irregular order in basicities is reproduced in qualitative agreement with well-established experimental results. The method does not require a priori cavity assumption in solution, which introduces ambiguous parameters into the theories and enables us to explain the physical origin of the basicity entirely from a microscopic point of view. Solvation structures around methylamines are also examined in terms of radial distribution functions. The result is an encouraging indication of the potential usefulness of the RISM-SCF approach to investigate a variety of quantum processes in solution.

I-U-2 The Solvent Effect on the Acidities of Haloacetic Acids in Aqueous Solution. A RISM-SCF Study

Masaaki KAWATA(*Kyoto Univ.*), **Seiichiro TEN-NO, Shigeki KATO**(*Kyoto Univ.*) **and Fumio HIRATA**

[*Chem. Phys. Letter*, **240**, 199 (1995)]

The acidities of acetic, fluoroacetic and chloroacetic acids in aqueous solution are calculated by means of the ab initio method combined with the reference interaction site method in the statistical mechanics of molecular liquids(the RISM-SCF method). The inversion in the order of acidities experimentally observed when a series of haloacetic acids is immersed into aqueous solution is reproduced. It is shown that the inversion is caused by competition between substitution and solvation effects. The solvation effect is discussed in molecular detail in terms of the charge distribution of the solute and the solute-solvent radial distribution functions.

I-U-3 Solvent Effect on Acidity: A Hybrid Approach Based on the RISM and the Hartree-Fock Equations

Masaaki KAWATA(*Kyoto Univ.*), **Seiichiro TEN-NO, Shigeki KATO**(*Kyoto Univ.*) **and Fumio HIRATA**

[*J. Phys. Chem.*, **100**, 1111 (1996)]

The reference interaction site model-self-consistent field (RISM-SCF) method, which has been proposed a while ago to calculate the electronic structure of a solvated molecule, is applied to a classical problem of the acidity of halo-substituted acetic acids in aqueous solution. The well-established experimental result, *i.e.*,the inversion of the acidity from (fluoroacetic acid > chloroacetic acid) in the gas phase to (fluoroacetic acid < chloroacetic acid) in the aqueous phase is reproduced qualitatively. Detailed analyses are presented with respect to the solvent effect on the electronic structure of solute, the solvent structure around the solute, and the energetics associated with the solvation as well as the substitution.

I-U-4 Theoretical Study for the Basicities of Methylamines in Aqueous Solution: A RISM-SCF Calculation of Solvation Thermodynamics

Masaaki KAWATA(*Kyoto Univ.*), **Seiichiro TEN-NO, Shigeki KATO**(*Kyoto Univ.*), **Fumio HIRATA**

[*Chem. Phys.*, **203**, 53 (1996)]

An ab initio quantum chemical calculation combined with the extended reference interaction site method in statistical mechanics of molecular liquids (the RISM-SCF method) is used to examine the basicities of methylamines in aqueous solution. Free energy changes upon protonation are calculated for a series of methylamines in the gas phase and in aqueous solution, respectively. The gas phase results show a monotonical increase in the basicity with successive methyl substitutions in accord with experiment and earlier theoretical studies. In aqueous solution, however, the results show an irregular order in basicity, which is in qualitative agreement with well established experimental data. Several contributions to free energy changes such as those resulting from solvation and from substitutions are analyzed entirely from a microscopic point of view. It is shown that solvation free energies play an essential role in the determination of the basicity in the solution. Further, it is shown that the solvation structures and the solute electronic structures are altered by the self-consistent treatment in the determination of solute-solvent interactions and that such alterations cause substantial effects on the basicity.

I-U-5 Analytical Energy Gradient for the Reference Interaction Site Model Multiconfigurational Self-consistent-field Method: Application to 1,2-Difluoroethylene in Aqueous Solution

Hirofumi SATO, Fumio HIRATA and Shigeki KATO
(Kyoto Univ.)

[*J. Chem. Phys.*, **105**, 1546 (1996)]

We have reformulated the reference interaction site model self-consistent-field (RISM-SCF) method to calculate the molecular properties of solute insolutions. The key feature is to introduce the Helmholtz free energy given as a sum of the solute electronic energy estimated by ab initio molecular orbital (MO) methods and the hypernetted-chain (HNC) excess chemical potential of solvation for the extended reference interaction site (XRISM) method. The variational conditions for the multiconfigurational self-consistent-field (MCSCF) wave functions were derived. It was also shown that, in the case of the Hartree-Fock (HF) method, the present expression gives the same Fock matrix defined previously. Moreover the expression for the first derivatives of the free energy with respect to the solute nuclear coordinates were obtained. Sample calculations for the chemical equilibrium of *cis*- and *trans*-isomers if 1,2-difluoroethylene are presented.
With the use of analytical energy gradients for the MCSCF and HF methods, the solute molecular geometries were determined in an aqueous solution.

I-V Solvation Thermodynamics of Protein and Related Molecules

Concerning biomolecules such as protein, it is a final goal for the biochemistry and biophysics to explore the relation between conformations and biological functions. The first essential step toward the goal would be to explain the confomational stability of biomolecules in terms of the microscopic structure of the molecules in solvent. It is an extremely difficult probelm by any means due to the overwhelmingly large degrees of freedom to be handled, including protein and solvent. As long as small and/or short-time fluctuations of protein around the native structure is concerned, a variety of molecular simumaltion techniques is a quite powerful tool to explore the microscopic structure of protein and solvent. However, the techniques are are not so effective to characterize stability of the macromolecules, to which the thermodynamic limit is concerned. The semi-microscopic approach based on the Poisson-Boltzmann equation and the scaled particle theory deserves to draw attention from such a view point.[1] Inspite of the oversimplification employed for the model of solvent, the method could have succeeded to reproduce fundamental characteristics of the solvation thermodynamics of a protein, including the cold denaturation.[2] A well-addressed weakness of the treatment is the less sophisticated representation of the microscopic structure of solvent water. The extended RISM theory has potential capability of overcoming the problem at least in the level of microscopic description based on the pair correlation functions. Obvious technical difficulties which one may face in applying the theory to such a large system are not only the computation time but also the stability of the numerical solution.[3]

Here, we present our recent effort to tackle the problem based on the two theoretical tools: extnded RISM and the scaled particle theory (SPT). The studies for the solvation thermodynamics of small molecules such as ions are also included because it is regarded as elementary processes for the solvation of biomolecules, and because it is prerequisite for studying the more complicated molecules.

References

1) M. Irisa, K. Nagayama, F. Hirata, *Chem. Phys. Lett.*, **207**, 430 (1993); M. Irisa, T. Takahashi, K. Nagayama, F. Hirata, *Mol. Phys.*, **85**, 1227(1995).
2) Irisa, F. Hirata, A.Kidera, H. Nakamura, T. Yanagida, in preparation
3) A. Kitao, F. Hirata, N. Go, *J. Phys. Chem.*, **97**, 10231 (1993)

I-V-1 Application of the Reference Interaction Site Model Theory to Analysis on Surface-induced Structure of Water

Masahiro KINOSHITA*(Kyoto Univ.)* **and Fumio HIRATA**

[*J. Chem. Phys.*, **104**, 8807 (1966)]

We consider the extended simple point charge (SPC/E) model water near uncharged and charged macroparticles. It is shown that the size of the macroparticle tested is sufficiently large and it acts in effect as a planar wall. The reference interaction site model (RISM) theory is employed, and a robust and very efficient algorithm has been developed for solving the basic equations. The algorithm is a hybrid of the Picard and Newton-Raphson methods. The Jacobian matrix is just part of the input data and need not be recalculated at all. Sufficiently accurate solutions are obtained in only 7 to 16 iterations. The reduced density profile of oxygen atoms near an uncharged macroparticle indicates significant dewetting and a clear contribution of the icelike structure. The surface potential calculated is positive but very small. When the macroparticle is charged, the number of water molecules in the close vicinity of the surface increases regardless of sign of the charge. The interaction between uncharged macroparticles with sufficiently large sizes immersed in pure water is attractive and very strong at small separations. The interaction between negatively charged macroparticles is "more repulsive" than between positively charged macroparticles. On the whole, however, the asymmetry of the SPC/E water in responding to positively and negatively charged surfaces is not high. It has been shown that the results obtained from the RISM theory combined with the SPC/E water are in qualitative accord with those calculated by the reference hypernetted-chain (RHNC) theory for hard spheres with embedded dipoles and tetrahedral quadrupoles, in terms of reduced density profiles, surface potential, and macroparticle interactions.

I-V-2 Analysis on Salting-out Phenomena for Noble Gases Using the Reference Interaction Site Model Theory

Masahiro KINOSHITA*(Kyoto Univ.)* **and Fumio HIRATA**

[*J. Chem. Phys.*, submitted]

We have developed robust and very efficient algorithms for solving the reference interaction site model (RISM) equations for salt solutions in the bulk and near a solute atom of noble gases. The theory of dielectric consistency recently developed for solutions at finite salt concentrations is employed in the formalism. The change in water structure in the bulk caused by addition of salts have been examined for model 1-1 salt solutions (LiCl, NaCl, KCl, KF, KBr, KI and CsI). The density and orientational structures of each salt solution near a solute atom have been analyzed. Ions characterized by positive hydration (F^-, Li^+ and Na^+) are strongly hydrated in the bulk and stay sufficiently far from the atom. Those of negative hydration (Cl^- and Br^-) or hydrophobic hydration (Cs^+ and I^-) are excluded from the bulk to the atom. Due to a specific orientational order of water molecules adjacent to the solute atom, there is a trend that cations stay less closer to the atom than anions. The relation between these structures and the salting coefficient is discussed in detail. The agreement between the calculated and experimental values for the salting coefficient is excellent for He. However, the discrepancy becomes larger as the number of electrons of the solute atom increases (the calculated value is always larger), which implies that the ion-induced dipole interaction neglected has significantly large effects.

I-V-3 Calculation of Hydration Free Energy for a Solute with Many Atomic Sites Using the RISM Theory: Robust and Efficient Algorithm

Masahiro KINOSHITA(*Kyoto Univ.*), **Yuko OKAMOTO and Fumio HIRATA**

[*J. Comp. Chem.*, submitted]

We have developed a rebust and very efficient algorithm for solving the reference interaction site model (RISM) equations for water near a solute molecule with many atomic sites (interaction sites). It is a hybrid of the Newton-Raphson and Picard methods. Various considerations are given so that the computer time can be saved as greatly as possible. It has been demonstrated for calculating hydration free energies of metenkephalin (a peptide with 73 sites) with different conformations. Its stability is quite insensitive to the initial guess. The Jacobian matrix is treated as part of the input data, and even the same matrix can be used for another conformation unless the conformation is considerably different from the last one.

I-V-4 Ion Hydration: Revisiting with an Integral Equation Theory of Liquids

Song-Ho CHONG(*Kyoto Univ.*) **and Fumio HIRATA**

[*J. Phys. Chem.* submitted]

We present a theoretical study for the ion hydration based on an integral equation method referred to as the extended reference interaction site method (ex-RISM). We analyze the thermodynamic functions of solvation, especially the partial molar volumes of individual ions at infinite dilution. A special attention is paid to information contained in the partial molar volumes, and to the problem if the partial molar volumes of individual ions reflect the true nature of ion-water interactions. Our results suggest, on the contrary to the previous work given by Kusalik and Patey, that the partial molar volumes do reflect the nature of ion-water interactions. Concerning the microscopic description of the ion hydration, the earlier model proposed by Samoilov is revisited based on ex-RISM. Characterization due to the integral equation method is found to be in an accord with that proposed by Samoilov. We also discuss the structural changes of water due to the presence of an ion utilizing the density derivatives of the solvent distribution functions. Qualitative difference of the density derivatives between the so-called 'positively hydrated' and 'negatively hydrated' ions was observed.

I-V-5 Solvation Free Energies of Non-polar and Polar Solutes Reproduced by the Combination of the Extended Scaled Particle Theory and the Poisson-Boltzmann Equation

Masayuki IRISA(*Yanagida bio- motron project ERATO JRDC*), **Takuya TAKAHASHI**(*Nagayama protein array project ERATO JRDC*), **Kuniaki NAGAYAMA** (*Nagayama protein array project ERATO JRDC*) **and Fumio HIRATA**

[*Mol. Phys.*, **85** , 1227 (1995)]

A hybrd approach using extended scaled particle theory and the Poisson-Boltzmann (PB) equation is proposed for calculating the solvation free energy of a solute with partial charges indilute aqueous solution. The applicability of this method is demonstrated by taking a series of the normal alcohols and normal alkanes. The solavtion free energy of normal alkanes, which has been studied previously based on a rather crude model, is recalculated using a more elaborate model. The electrostatic contribution to the free energy for the polar solute is calculated by the PB equation. In order to take into account the complicated boundary condition associated with the shape of molecular surface, the PB equation is solved numerically using a finite difference method. A superposition of hydrophobic and electrostatic contributions to the solvation free energy gives reasonable agreement with corresponding experimental data for the polar solute. The possibility of further applications of the method is discussed.

I-V-6 Solvation Free Energy of Protein Reproduced by The Combination of The Extended Scaled Particle Theory and The Poisson-Boltzmann Equation

Masayuki IRISA(*Yanagida bio- motron project ERATO JRDC*), **Takuya TAKAHASHI**(*Nagayama protein array project ERATO JRDC*), **Fumio HIRATA and Toshio YANAGIDA**(*Yanagida bio- motron project ERATO JRDC*)

[*J. Mol. Liquids*, **65/66**, 381 (1995)]

A hybrid approach of the extended scaled particle theory (SPT) and the Poisson- Boltzmann (PB) equation for the solvation free energy of non-polar and polar solutes has been proposed by us. This new method is applied for the hydration free energy of the protein, avian pancreatic polypeptide (36 residues). The contributions form the cavity formulation and the attractive interaction between the solute and the solvent to the solvation free energy compensate each other. The electrostatic contribution is much larger than other terms in this hydration free energy, because hydrophilic residues are ionized in water. This work is the first step toward further applications of our new method to free energy difference calculation appeared in the stability analysis of protein.

I-V-7 The Cold Denaturation of Protein is Predicted by the Extended Scaled Particle Theory

Masayuki IRISA(*Kysshu Institute of Technology*), **Fumio HIRATA, Akinori KIDERA** (*Kyoto Univ.*), **Haruki NAKAMURA** (*Biomol. Engineering Research Institute*) **and Toshio YANAGIDA**(*Yanagida bio- motron project ERATO JRDC*)

The cold denaturation of protein is an outstanding phenomenon which rejects any naive consideration concerning the stability of macromolecules. A naive consideration based on the chain statistics for a macromolecule inevitably leads to the 'thermal denaturation' due to the entropic preference for the denatured conformation over the native state. It is the solvent that makes the denatured state preferable upon decreasing temperature, and it is the solvent that has made the problem remained unsolved for long time. Increasing attention has been paid to

the theoretical determination of the solvation free energy from a variety of fields including the stability analysis of protien. The solvation free energies of molecules, especially, large ones are very difficult to calculate by any standard due to the overwhelmingly large configurational space to be smapled.

Recently, we have developed a new method to determine the hydrophobic contribution of the solvation free energy by extending the scaled particle theory to a system including a solute molecule with an aribitrary geometry. As has been well documentred, the SPT is a rigorous statistical mechanical theory for a system of hard-spheres and yet gives a reasonable account to the solvation of a hydrophobic solute in aqueous systems. The method was applied for calculating the hydration free energy of alkanes, alcohols, and the avian pancreatic polypeptide (APP), with the help of the Poisson-Boltzmann equation which is used to calculate the elecrostatic contribution to the solvation free energy. In this work, we apply the new method to study general aspects of the cold denaturationof protein by using APP as a model, because APP is considered to be the smallest protein that forms a regular tertiary structure in the monomer state.

Temperature dependence of the hydrophobic part of the hydration free energies of APP is calculated both in the native and denatured conformations. A simple model was employed as the extended conformation in order to calculate the free energy of the denatured state of protein. The difference of the hydrophobic hydration free energies between the extended and the native conformations exhibits the maximum at 110 C and decreases at low temperature. The fact demonstrates that the native conformation is destabilized at low temperature due to the hydrophobic effects. Our results coincide with the experimental observation for the cold denaturation based on the micro-calorimetry.

I-W Spatial and Temporal Density Fluctuation in Molecular Liquids

The latest development in the experimental techniques including the high resolution NMR and a variety of techniques in the time-resolved laser-spectroscopies have revealed the molecular nature of the solvent dynamics around solute, or the solvation dynamics, which refuse any naive interpretation based on the continuum models. A microscopic or statistical-mechanical description for the solvation dynamics requires formulation of the temporal as well as spatial fluctuations of solvent density around solute. A general recipe to such a problem is to use the generalized Langenvin equation (GLE). The GLE in principle gives the dynamics of a system in any resolution in space and time depending on the level of projection. However, its actual usefulness for a problem is largely determined by a choice of dynamic variables onto which other degrees of freedom are projected. It is the pair correlation functions which researves the microscopic nature of the system and yet tractable within the current development in the statistical-mechanical theory of liquids. A natural choice of the dynamic variables which lead to the density-density pair correlation function as an important ingredient in the dynamical equations is a set of the collective density field and its conjugate momentum density field. Such a choice leads to a Smoluchowsky-Vlasov type diffusion equation in the overdamped limit. As to the model for molecular diffusion in polar liquids, there are two quite different point of view. One is the traditinal rot-translational model[1] and the other the interaction-site description which sees the diffusion of a molecule as a correlated motion of each atoms (sites).[2] The interaction-site description employes the site-site Ornstein-Zernike (SSOZ) equation (or RISM equation) in order to represent the site-site direct correlation functions, which proves to be successful in a variety of application to molecualr liquid including water.[3]

In what follows, the latest progress which we have made in the theory of the structure and dynamics of molecular liquids is reviewed. We also report our effort to formulate the non-equlibrium free energy profile along a solvent coordinate based on the extended RISM theory, which has played an essential role in the Marcus theory of the electron transfer reaction.

References

1) D. F. Calef and P. G. Wolynes, *J. Chem. Phys.*, **78**, 4145 (1983).

2) F. O. Raineri, Y. Zhou, H. L. Friedman, and G. Stell, *Chem. Phys.*, **152**, 202 (1991): F. Hirata, *J. Chem. Phys.*, **96**, 4619 (1992).

I-W-1 Surrogate Hamiltonian Description of Solvation Dynamics. Site Number Density and Polarization Charge Density Formulations

Harold L. FRIEDMAN*(State Univ.of New York)*, **Fernando O. RAINERI***(State Univ.of New York)*, **Fumio HIRATA and Baw-Ching PERNG***(State Univ.of New York)*

[*J. Stat. Mech.*, **78**, 239 (1995)]

We explore a recently developed theory of solvation dynamics that analyzes the molecular response of the solvent to a sudden change of the charge distribution of a solute particle immersed in it. We derive an approximate nonequilibrium distribution function $f^h_x(\Gamma;t)$ for a "surrogate" Hamiltonian description of the solvation dynamics process. The surrogate Hamiltonian is expressed in terms of renormalized solute-solvent interactions, a feature that allows us to introduce a simple reduction scheme in the many-body dynamics problem without losing essential solute-solvent static correlations that rule the equilibrium solvation. With $f^h_x(\Gamma;t)$ in hand we calculate the solvation time correlation function in two ways. The first one, previously reported, is basically a "dielectric formulation" in which the local polarization charge density of the solvent is the primary dynamical variable that couples to the field of the solute. In the new development reported here, the "site number density formulation," the primary dynamical variables comprise the set of local solvent site number densities. We find that the dielectric formulation is embedded in the solvent site number density formulation as shown, for example, by comparing the respective time correlation functions of the solvation dynamics. An im-

portant feature of our approach is that at every stage the coupling between the solute and solvent is formulated in terms of the solute-solvent intermolecular interactions, rather than some sort of cavity construction. Furthermore, both the solute and the solvent molecules are represented by interaction site models. Applications of the dielectric theory are illustrated with calculations of the solvation dynamics of a cation in water and an exploration of the effect of the details of the charge distribution on the solvation dynamics of a benzenelike solute in acetonitrile.

I-W-2 An Interaction-Site Representation of the Dynamic Structure Factor of Liquid and Solvation Dynamics

Fumio HIRATA, Toyonori MUNAKATA(*kyoto Univ.*), **Fernando O. RAINERI**(*State Univ.of New York*) **and Harold L FRIEDMAN**(*State Univ.of New York*)

[*J. Mol. Liquids*, **65/66**, 15 (1995)]

A recent development in the theory for the dynamics structure factor of molecular liquids, which employs the interaction-site model, is outlined. The theory is applied for a description of the solvation dynamics associated with a photo-excitation of a molecule in polar liquid. Preliminary results of the solvation time correlation functions for an atomic molecule in a variety of solvents are presented.

I-W-3 Molecular Theory for the Nonequilibrium Free Energy Profile in Electron Transfer Reaction

Song-Ho CHONG(*Kyoto Univ.*), **Shin-ichi MIURA**(*Kyoto Univ.*), **Gautam BASU**(*Kyoto Univ.*) **and Fumio HIRATA**

[*J. Phys. Chem.*, **99**, 10526 (1995)]

We present a new method for obtaining the free energy profile for electron transfer reaction in a polar solvent based on the extended reference interaction site method (ex-RISM) in the statistical mechanical theory of molecular liquids. The method, applied to a simple model of an exchange reaction, yields quantitatively good results in terms of agreement with simulation results. We also discuss the parabolicity of the free energy profile and potential applicability of our method.

I-W-4 Non-Linear Effects in the Free Energy Profile of Electron Transfer Reaction: An Integral Equation Approach

Song-Ho CHONG(*Kyoto Univ.*) **and Fumio HIRATA**

[*J. Mol. Liquids*, **65/66**, 345 (1995)]

The free energy profile for the electron transfer reaction in a polar solvent is examined based on the extended reference interaction site method (ex-RISM) applying it to a simple model of a charge separation reaction which was previously studied by Carter and Hynes with molecular dynamics simulations. Due to the nonlinear nature of the hypernetted chain (HNC) closure to solve the RISM equation, our method can shed light on the non-linearity of the free energy profiles, and we discuss these problems based on the obtained free energy profile.

I-W-5 The Free Energy Profiles for the Electron Transfer Reactions Calculated from the Integral Equation Method of Liquids

Song-Ho CHONG(*Kyoto Univ.*) **and Fumio HIRATA**

[*Molecular Simulation*, **16**, 3 (1996)]

A microscopic description of the free energy profile for the electron transfer reaction is presented based on the extended reference interaction site method (ex-RISM) in the statistical mechanical theory of molecular liquids. We employed the scheme proposed by Marcus to characterize the non-equilibrium solvent polarizations at the intermediate states of the reaction. The method is applied to two models of electron exchange reactions where the redox pairs have valence charges of 1/2+/1/2- and 2+/3+, and to a model of a charge separation reaction. Due to the non-linear nature of the hypernetted chain (HNC) closure to solve the RISM equation, our method can shed light on the non-linearity of the free energy profiles.

I-W-6 Nonlinear Electrical Potential Fluctuations of Solvent around Solutes: an Integral Equation Study

Song-Ho CHONG(*Kyoto Univ.*) **and Fumio HIRATA**

[*J. Chem. Phys.*, submitted]

We present s theoretical formulation for the solvent force constant and the asymmetry parameter which characterize the free energy profile governing the electrical potential fluctuations of the solvent molecules around solutes. This formulation allows us the calculation of these parameters via the extended reference interaction site method (ex-RISM), an integral equation theory developed for molecular liquids and solutions. Since ex-RISM is inherently a nonlinear theory, we can shed some light on the possible nonlinear effects in the electrical potential fluctuations. The nonlinear effects in the solvent force constants and the validity of the linear approximation will be examined by a series of calculations for monatomic and diatomic solutes immersed in various solvents. The origin of the solute-dependent solvent force constants is briefly discussed.

I-W-7 Shear-Induced Distortion of Intra- and Intermolecular Correlations in Liquids –Time Dependent Density-Functional Theory–

Shuhei YOSHIDA(*Kyoto Univ.*), **Fumio HIRATA and Toyonori MUNAKATA**(*Kyoto Univ.*)

[*Phys. Rev. E.* **52**, No.2 (1996), in press]

Shear viscosity of molecular liquids is formulated and calculated with use of a time-dependent density-functional theory. Allowing for non-rigidity of each molecule, we obtain shear-induced distortion of both intra- and intermolecular correlations self-consistently, which makes it possible to calculate the shear viscosity. As a byproduct we derived and solved a new HNC closure for equilibrium correlations in deformable molecular liquids.

I-W-8 Statistical Mechanics of Deformable Molecular Liquids –Thermal Expansion and Isomerization of Diatomic Molecul–

Toyonori MUNAKATA(*Kyoto Univ.*), **Shuhei YOSHIDA**(*Univ. of Tennessee*) **and Fumio HIRATA**

[*Phys. Rev.*, submitted]

Equilibrium two-body correlations in liquids composed of deformable molecules are formulated with use of the density functional theory and the interaction site formalism. As applications, we study two model systems, liquid nitrogen and simplified liquid n-butane in which each molecule has two stable bond lengths. The latter may be considered as a toy model to study conformational equilibrium.

I-X Theoretical Studies of Low-Dimensional Correlated Electron Systems

Long-distance correlation functions in one- and quasi-one-dimensional electron systems are studied by a renormalization-group method. Our goal is to clarify the interplay between Umklapp processes and electron-phonon interactions at different electron fillings.

I-X-1 Electron-Phonon Interaction and Spin Gap in Nearly-Half-Filled Correlated Electron Systems

Kenji YONEMITSU and Masatoshi IMADA (*Univ. of Tokyo*)

[*Physica C* **263**, 82 (1995)]

Renormalization-group equations are solved to study phase diagrams of nearly-half-filled one-dimensional conductors interacting with phonons. A spin-gap charge density wave phase exists between a gapless density wave phase and a spin-gap superconductor phase. On-site and inter-site electron-phonon couplings show large differences near half filling in the presence of on-site electron repulsion.

I-X-2 Spin-Gap Phase in Nearly-Half-Filled One-Dimensional Conductors Coupled with Phonons

Kenji YONEMITSU and Masatoshi IMADA (*Univ. of Tokyo*)

[*Phys. Rev. B* **54**, 2410 (1996)]

Asymptotic properties of nearly-half-filled one-dimensional conductors coupled with phonons are studied through a renormalization group method. Due to spin-charge coupling via electron-phonon interaction, the spin correlation varies with filling as well as the charge correlation. Depending on the relation between cut-off energy scales of the Umklapp process and of the electron-phonon interaction, various phases appear. We found a metallic phase with a spin gap and a dominant charge-density-wave correlation near half filling between a gapless density-wave phase (like in the doped repulsive Hubbard model) and a superconductor phase with a spin gap. The spin gap is produced by phonon-assisted backward scatterings which are interfered with the Umklapp process constructively or destructively depending on the character of electron-phonon coupling.

I-X-3 Spin Gap in One-Dimensional Electron-Phonon Systems

Kenji YONEMITSU and Masatoshi IMADA (*Univ. of Tokyo*)

[*Mol. Cryst. Liq. Cryst.*, in press]

The exponents of spin and charge correlations of one-dimensional electron systems are calculated by a renormalization-group method. We study combined effects of electron-phonon interaction and the Umklapp process on renormalization flows. As scattering processes are successively integrated out, these two processes are interfered with each other depending on the type of electron-phonon coupling, phonon frequency and filling. We demonstrate how these factors control a spin gap formation and density-wave/superconductor correlations.

I-X-4 Mott Transition in Quasi-One-Dimensional Electron Systems at Quarter Filling

Kenji YONEMITSU

[*Synth. Met.*, in press]

Renormalization-group equations are derived and numerically solved for one-dimensional, quarter-filled electron systems with a backward scattering, the Umklapp process, and couplings with 0, $2k_F$, $4k_F$ phonons. A charge gap opens when the Umklapp process becomes relevant through constructive interference with the coupling with $4k_F$ phonons, though the Umklapp process itself is weak. Meanwhile, a spin gap opens when the coupling with $2k_F$ phonons is strong enough. We consider three-dimensionality by cutting off the logarithmic divergence in the Cooper or $2k_F$ electron-hole channel. The former case may explain a qualitative difference between the resistivity of $(DMe\text{-}DCNQI)_2Ag$ and that of $(DI\text{-}DCNQI)_2Ag$.

I-Y Theoretical Studies of Superconductors under Magnetic Field

Pairing order parameter, density and current in *s*- and *d*-wave superconductors are calculated self-consistently. Our goal is to clarify the role of bound states in a core of magnetic flux on the local density of states and magnetization.

I-Y-1 Bands of In-Gap States in *s*- and *d*-Wave Superconductors under High Magnetic Field

Takayuki NISHIO *(Tohoku Univ.)*, **Kenji YONEMITSU and Hiromichi EBISAWA** *(Tohoku Univ.)*

Spatial variations of order parameters and in-gap states are studied for *s*- and *d*-wave superconductors under a high magnetic field, by using the two-dimensional extended Hubbard model with an attractive interaction. Bogoliubov-de Gennes equations are numerically solved, assuming periodic configurations for vortices. We found the amplitudes of the wave functions of the low-energy states bound in a magnetic flux have a four-fold symmetry reflecting the shape of the Fermi surface in the *s*-wave case. In the *d*-wave case, they are less anisotropic reflecting both the Fermi surface and the pairing potential. These states are overlapped with each other, forming quasi-particle energy bands. Thus the density of states is finite at the chemical potential not only near but also much bellow H_{c2} we can numerically adopt.

RESEARCH ACTIVITIES II
Department of Molecular Structure

II-A Laboratory and Astronomical Spectroscopy of Transient Molecules

Vast, cold, and low-density space environment is a unique laboratory, whose physical and chemical conditions are rarely attained in the laboratory on Earth. The unique space laboratory is favorable to the existence of transient molecules such as molecular ions, free radicals, and unstable molecules, most of which are very exotic and nonterrestrial. These exotic transient molecules are generally difficult and challenging problems for laboratory spectroscopy. Laboratory spectroscopy may be enriched by astronomical studies on non-terrestrial transient species which represent new developments in high-resolution molecular spectroscopy. On the other hand, detailed knowledge about new transient molecules obtained by laboratory spectroscopy is essential to a deeper understanding of physical and chemical processes in space. We developed a high-sensitivity submillimeter-wave and far-infrared spectrometers suitable for high-resolution spectroscopy of transient molecules of astronomical interest. We expect that our laboratory spectroscopy may accelerate the mutually beneficial aspect between laboratory spectroscopy, and astrochemistry and astrophysics.

II-A-1 Microwave Spectroscopy of the HCCS and DCCS Radicals($X^2\Pi_i$) in Excited Vibronic States: A Study of the Renner-Teller Effect

Jiang TANG(*Graduate Univ. for Advanced Studies*) **and Shuji SAITO**

[*J. Chem. Phys.* **105**, 8020 (1996)]

We reported the microwave spectrum of linear carbon-chain radicals, HCCS and DCCS, in the excited states of two bending modes, ν_4 and ν_5.[1] The anomalously large γ_{eff} constants obtained for the vibronic μ/κ $^2\Sigma$ states can not be understood by the current Renner-Teller theory. We developed a formulation of the Renner-Teller effect in a linear molecule with two bending vibrations so as to explain the anomalous features observed. We included a cross vibronic interaction between two vibronic $^2\Sigma(v_i=1)$ states in different bending modes.[2] Since the difference of the vibrational quantum numbers for these states is $\Delta(v_4+v_5)=0$, the interaction has a much larger effect than the one considered by a previously proposed theory for the vibronic states with $\Delta(v_4+v_5)=\pm 2$.[3] The anomalously large γ_{eff} constants for the vibronic μ/κ $^2\Sigma$ states are successfully explained by the newly developed theory with the Renner-Teller parameters of ε_4=-0.37, ε_5=+0.10, and $|\varepsilon_{45}|$=0.4 for the cross vibronic interaction. The cross interaction term ε_{45} is obtained for the first time. The relative sign of the above ε_4 and ε_5 values is explicitly judged to be correct. In addition, the B_{eff} and the P-doubling constants in the $^2\Pi_i$ and $^2\Delta_i$ states are found to be affected by a higher-order perturbation of the cross vibronic interaction. The relative energis obtained for the vibronic levels studied are schematically shown in Figure 1.

References

1) J. Tang and S. Saito, *Ann. Rev.* II-A-6(1994).
2) J. Tang and S. Saito, *Ann. Rev.* II-A-5(1995).
3) A. N. Petelin and A. A. Kiselev, *Int. J. Quantum Chem.* **6**, 701(1972).

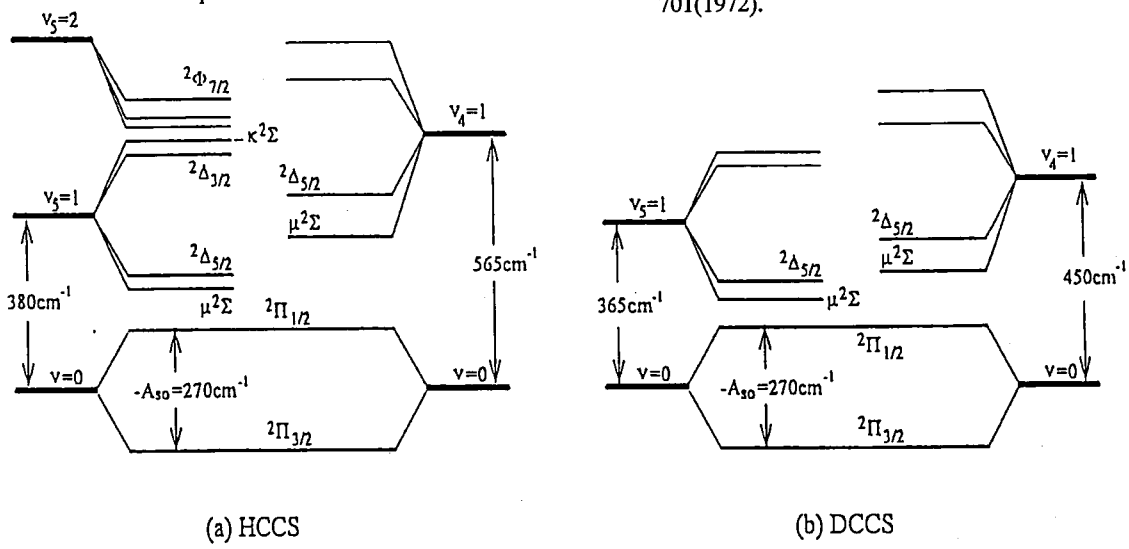


Figure 1. Energy level diagram for the vibronic structures of (a)HCCS and (b) DCCS.

II-A-2 Microwave Spectrum and Molecular Structure of the Dihydrophosphoryl Radical H_2PO in the X^2A' Ground Electronic State

Tsuyoshi HIRAO(*Graduate Univ. for Advanced Studies*), **Shuji SAITO and Hiroyuki OZEKI**

[*J. Chem. Phys.* **105**, 3450 (1996)]

We have reported the microwave spectrum of a new phosphorus containing free radical $H_2PO(X\,^2A')$.[1] The observed spectral pattern including hyperfine structure

suggests that the radical has a pyramidal structure with C_s symmetry. Subsequently we measured the spectral lines of $H_2P^{18}O$ and determined its molecular constants. The precise molecular structure of H_2PO was derived from the rotational constants for the main and ^{18}O species: r(PO) = 1.4875(10) Å, r(PH) = 1.4287(14) Å, ∠HPO = 115.52(10)°, and ∠HPH=102.56(4)°, as shown in Figure 1. This result clearly indicates that H_2PO has a PO bond intermediate between the normal single and double PO bonds. The spin density of unpaired electrons for H_2PO was ascertained from the hyperfine coupling constants for the P and H atoms. The p-character and s-charcter spin density for the P atom electrons is 45.5% and 7.7%, respectively, and the s-character spin density for each H atom is 7.7%, resulting in the spin density of 31.5% for the O atom. The spin density obtained is consistent with the molecular structure determined above. The present results resolve the different artifacts discussed in the ab initio calculations using different levels.[2)]

References

1) T. Hirao, S. Saito and H. Ozeki, *Ann. Rev.* II-A-7(1995).
2) C. J. Cramer and M. H. Lim, *J. Phys. Chem.* **98**, 5024(1994) and references cited therein.

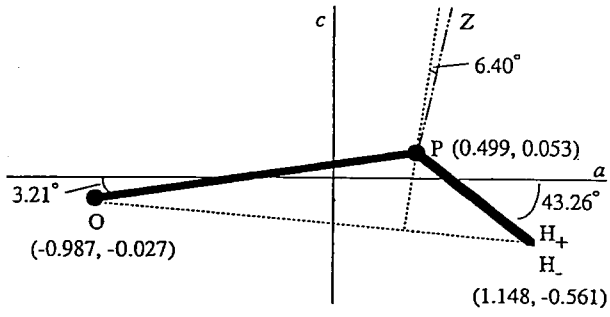


Figure 1. Molecular structure of H_2PO given in the unit of angstrom: a projection on the ac plane.

II-A-3 Microwave Spectrum of a New Phosphorus Containing Carbene: HCCP($X^3\Sigma^-$)

Imtiaz AHMAD *(Univ. of London and IMS)*, **Hiroyuki OZEKI, Tsuyoshi HIRAO** *(Graduate Univ. for Advanced Studies)* **and Shuji SAITO**

Carbon-chain molecules C_nX(or HC_nX) are unique molecular species among the interstellar molecules reported so far, and several series of carbon-chain molecules have been detected in space: X=CN, H, O, S, N, and Si. We have detected for the first time by the microwave spectroscopic method a new phosphorus containing carbene, HCCP, whose existence even in the laboratory has not been reported to date. Microwave spectral lines of the HCCP radical and its isotopomers, DCCP and $H^{13}C^{13}CP$, were measured using a source-modulated spectrometer. HCCP was produced by dc glow discharge in a mixture of PH_3 and C_2H_2. A C_2D_2 or $^{13}C_2H_2$ sample was used instead of C_2H_2 for the production of DCCP or $H^{13}C^{13}CP$, respectively. Hyperfine structure pertaining to the phosphorus and hydrogen nuclei was observed for several low-N transitions. The corresponding hyperfine coupling constants were ascertained in addition to the rotational and centrifugal distortion constants by a least-squares analysis of the measured frequencies. The r_o structure was established from the observed rotational constants for the main species and isotopomers, and the spin density of the unpaired electrons were calculated on comparison of the hyperfine coupling constants with the atomic values. Thus molecular structural characterization of a new phosphorus bearing carbene was accomplished for the first time.

II-A-4 Microwave Spectrum of the CHF_2 Radical in the X^2A' Electronic State: Hyperfine Structure Alternation in Inversion Doubling

Naomi INADA *(Hiroshima Univ. and IMS)* **Hiroyuki OZEKI, Shuji SAITO, Ko SAITO** *(Hiroshima Univ.)* **and Michiro HAYASHI** *(Hiroshima Univ.)*

We have reported the detection of microwave spectral lines of CHF_2 in the ground electronic state.[1)] However, we found that it was rather difficult to obtain a set of generally applicable molecular parameters for all rotational transitions observed. A preliminary analysis of the rotational transitions with I_F=0 or 1 where I_F=I(F_1)+I(F_2) resulted in the finding that I_F=0 or I_F=1 components of a particular rotational level correspond to the plus or minus inversion state depending on the parity of the rotational level. For the ground inversion state, the *ee* or *oo* symmetric rotational level combines with the symmetric spin function, whereas the *eo* or *oe* antisymmetric rotational level with the antisymmetric function. For the first excited inversion state, combination between rotational symmetry and spin symmetry is inverted. Such hyperfine structure alternation in the inversion doubling of a free radical usually appears as statistical weight in a singlet diamagnetic molecule with appropriate symmetry. This is the first case where hyperfine structure alternation was observed for inversion doubling. A further analysis based on the correct assignment of inversion parity for hyperfine structures suggested that $\Delta K = \pm 1$ Coriolis-type interaction exists between the different inversion states. A computer program has been developed to calculate the detailed rotational levels with fine and hyperfine structure affected by inversion interaction.

References

1) N. Inada, H. Ozeki, S. Saito, K. Saito and M. Hayashi, *Ann. Rev.* II-A-6(1995).

II-A-5 The Microwave Spectrum of NCl in the Second Electronically Excited State($b^1\Sigma^+$)

Kaori KOBAYASHI and Shuji SAITO

[*J. Phys. Chem.* accepted]

The difficulty in producing metastable molecules has prevented the observation of pure rotational spectra of such species. Concerning the second electronically excited state there are only two such examples of microwave spectra, CO($b\,^3\Sigma^+$)[1)] and SO($b\,^1\Sigma^+$).[2)] Other than these examples, some reports on molecules in the first electronically excited state, that is, SO($a\,^1\Delta$), O_2($a\,^1\Delta_g$), CO($a\,^3\Pi$), NF($a\,^1\Delta$), and NCl($a\,^1\Delta$)[3)] are known. These electronic systems clearly reflect that a $b\,^1\Sigma^+$-$X\,^3\Sigma^-$ transition is weakly allowed via the magnetic dipole selection rule whereas the $a\,^1\Delta$-$X\,^3\Sigma^-$ transition is spin and orbital forbidden. The

pure rotational transitions of $N^{35}Cl$ and $N^{37}Cl$ in the second electronically excited state, $b\ ^1\Sigma^+$ were detected for the first time by microwave spectroscopy. The NCl radical in the $b\ ^1\Sigma^+$ state was generated sufficiently by dc-glow discharge of a N_2 and Cl_2 mixture. One of the measured spectral lines is shown in Figure 1. The rotational constant, centrifugal distortion constant, and quadrupole coupling constant of the Cl nucleus were determined. The observation of rotational transitions in the vibrational excited state made it possible to derive equilibrium structural parameters. A discussion on the internuclear potential of the three low-lying states of NCl was made.

References

1) S. Yamamoto and S. Saito, *J. Chem. Phys.* **89**, 1936(1988).
2) S. Yamamoto, *Chem. Phys. Lett.* **212**, 113(1993).
3) K. Kobayashi, M. Goto, S. Yamamoto and S. Saito, *J. Chem. Phys.* **104**, 8865(1996).

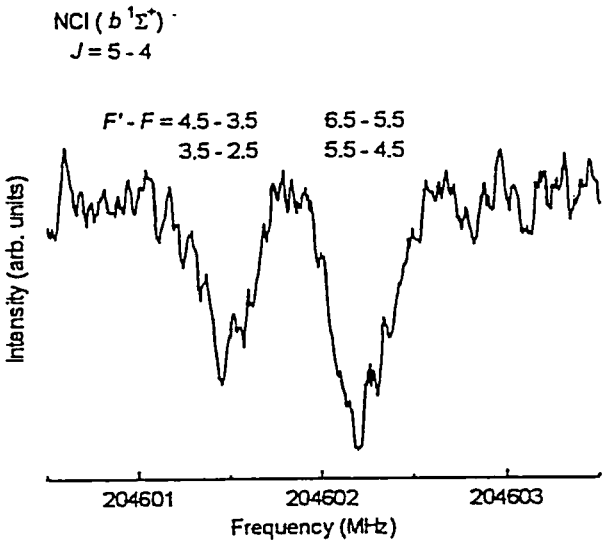


Figure 1. J=5-4 transition of NCl($b^1\Sigma^+$, v=0). The quadrupole hyperfine structure due to the chlorine nucleus is resolved.

II-A-6 Microwave Spectra of 3d Transition Metal Oxide Radicals:MnO($^6\Sigma^+$), CoO($^4\Delta_i$), CuO($^2\Pi_i$), and TiO($^3\Delta_r$)

Kei-ichi NAMIKI*(Graduate Univ. for Advanced Studies)*, **Timothy C. STEIMLE***(Arizona State Univ. and IMS)* **and Shuji SAITO**

As a continuing interest to the diatomic oxides of the 3d transition metals,[1] we studied four examples, MnO($^6\Sigma^+$), CoO($^4\Delta_i$), CuO($^2\Pi_i$), and TiO($^3\Delta_r$) by microwave spectroscopy aiming to obtain a good systematic example of the chemical bonds dependent on the 3d orbital of the metal and the 2p orbital of oxygen. All the four oxides were generated by dc-sputtering(a few hundred mA) of metal in flakes or metal bearing cluster compound which was placed in the inner bottom of the cathode, or of a metal cathode in the atmosphere of a mixture of oxygen and helium. The cell is usually maintained below -180 °C. Several rotational transitions of each species, accompanied by fine and hyperfine structures with appropriate electron and nuclear spins, were measured in the frequency region up to 400 to 450 GHz. An example of observed spectral lines showing the hyperfine structure of the manganese nucleus in MnO is given in Figure 1. The measured frequencies of spectral lines for each species were least-squares analyzed and its molecular constants are precisely determined. So as to obtain a small standard deviation of the fit, comparable to measurement errors, we took into account higher-order spin-orbit interaction(γ_s and Θ terms), spin-orbit and Fermi contact interaction(b_s), which are characteristic of the high-spin electronic state, and furthermore, the centrifugal distortion term of the Fermi contact term(b_{FD}) for MnO($^6\Sigma^+$). The new and precise molecular constants were compared with those reported, if available, and were discussed on the basis of the known electronic staructure for each free radical.

References

1) K. Namiki and S. Saito, *Chem. Phys. Lett.* **252**, 343(1996).

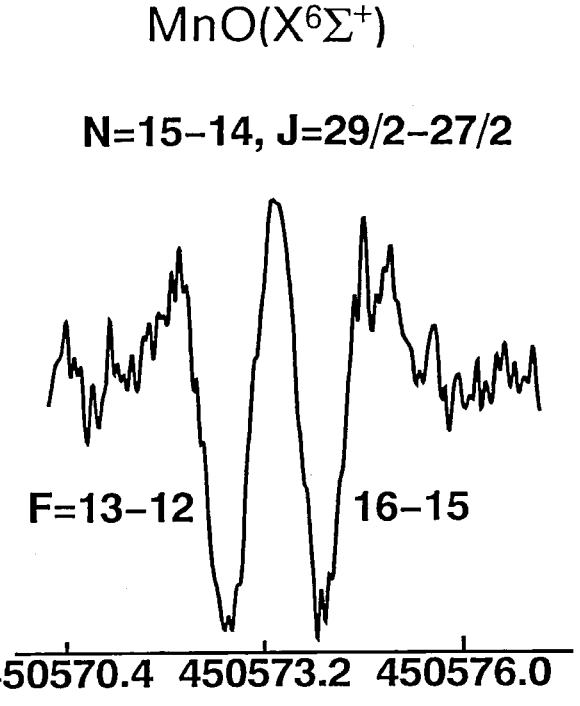


Figure 1. Portion of the observed hyperfine structure for the N=15-14, F_4 transition of MnO($^6\Sigma^+$).

II-A-7 Microwave Spectrum of the AsH($^3\Sigma^-$) Radical

Hideo FUJIWARA, Kaori KOBAYASHI, Hiroyuki OZEKI, Shuji SAITO and A. JAMAN*(Saha Institute of Nuclear Physics)*

[*Trans. Faraday Soc.* submitted]

Simple hydride molecules have relatively small number of rotational transitions in the submillimeter-wave region. Recently we showed that microwave spectroscopic measurements even for a small number of rotational transitions made it possible to determine their particular hyperfine structure with high precision.[1,2] We extended such a spectroscopic study to another hydride AsH in its $^3\Sigma^-$ ground electronic state. The rotational lines of AsH and AsD radicals were observed for the first time in the submillimeter-wave region. The AsH radical was generated by a dc glow discharge in pure AsH_3 gas, and the AsD radical by the reaction of arsenic powder with dc glow

discharge in a D_2 and O_2 mixture. The rotational transitions split by hyperfine structure of AsH, N,J=(0,1-1,0), (2,1-1,1) and (3,2-2,2) were measured in the 120-338 GHz region, and five transitions of AsD, N,J=(0,1-1,0), (2,1-1,0), (2,2-1,1), (4,3-3,3) and (5,4-4,4), in the 173-440 GHz range. The molecular constants, including the hyperfine coupling constants associated with the arsenic, hydrogen and deuterium nuclei were precisely determined by least-squares fitting to the observed spectral lines. Using the results of both AsH and AsD, the equilibrium structure was derived, where the adiabatic correction was taken into account: r_e^{BO}=1.522368(27) Å.

References

1) S. Saito and M. Goto, *Astrophys. J.* **410**, L53(1993).
2) M. Goto and S. Saito, *Chem. Phys. Lett.* **211**, 443(1993).

II-A-8 Isotopic NS Rotational Spectra: $^{14}N^{33}S$ and $^{15}N^{32}S$

Axel H. SALECK*(Univ. of Koeln and IMS)*, **Hiroyuki OZEKI and Shuji SAITO**

[*Chem. Phys. Lett.* **244**,199(1995)]

Since the NS radical is one of the main sulfur bearing interstellar molecules, precise rest frequencies of spectral lines and precise molecular constants for its isotopic species as well as for the main species are essential to radio astronomical studies using their interstellar spectral lines. The mm-wave spectra of the NS radical isotopomers $^{14}N^{33}S$ and $^{15}N^{32}S$ were measured. Furthermore, new lines of the $^{14}N^{34}S$ species were recorded. The radicals were generated in a dc glow discharge of a mixture of N_2 and H_2S. All new lines belong to the $^2\Pi_{1/2}$ substates and were observed in natural abundance. The new data were fitted simultaneously together with previously reported $^{14}N^{32}S$ and $^{14}N^{34}S$ lines to yield molecular constants, including the Born-Oppenheimer corrections Δ_{01}^S and Δ_{01}^N and the ^{33}S hyperfine constants d and a-(b+c)/2.

II-A-9 Microwave Measurement of Spectral Lines of $Si^{18}O$ for Astronomical Use

S-H. CHO*(Korean Astronomical Observatory)* **and Shuji SAITO**

Silicon monoxide has been known to exist in the relatively energetic regions of molecular clouds and circumstellar envelopes and is the most fundamental and important silicon bearing interstellar molecule. Since there have been no reports on one of its isotopic species, $Si^{18}O$, we measured its millimeter- and submillimeter-wave lines to facilitate the identification of $Si^{18}O$ in space. Silicon O-18 oxide was generated by dc-glow discharge(100mA) in a mixture of oxygen(10 mTorr), tetramethylsilane(30 mTorr), and He(30 mTorr) in the free-space absorption cell kept at about -90 °C. Ten rotational transitions from J=1-0 to 11-10 were precisely measured with one standard measurement error of less than 20 kHz in the 40-450 GHz range. The rotational constant and centrifugal distortion constant were accordingly determined with high precision.

II-B Development of a Mt. Fuji Submillimeter-Wave Telescope

Shuji SAITO, Hiroyuki OZEKI, Hideo FUJIWARA, Satoshi YAMAMOTO*(Univ. of TOKYO)*, **Yutaro SEKIMOTO***(Univ. of Tokyo)*, **Junji INATANI***(National Astronomical Observatory)*, **Masatoshi OHISHI***(National Astronomical Observatory)* **and Norio KAIFU***(National Astronomical Observatory)*

In recent years the submillimeter-wave to far infrared region has attracted much attention in the field of astronomy because the initial stage of star forming activity or in other words, the final stage of molecular cloud contraction shows various physical and chemical phenomena in the energy region of this wavelength. Several submillimeter-wave telescopes have now been developed to study astrophysics and astrochemistry of the star-forming regions through atomic and molecular spectral lines. Since atmospheric attenuation, mainly due to water vapor, becomes high in the submillimeter-wave to far infrared region, astronomical observations should be made at a high-altitude site with a cold environment.

We plan to build a submillimeter-wave telescope at the summit of Mt. Fuji. The main scientific purpose of our project is (1) a survey of the neutral carbon line at 492 GHz, and (2) a search for new simple and fundamental molecules, especially related to interstellar dust chemistry, which will help us to understand evolutionary physical and chemical processes of molecular clouds as a whole.

II-B-1 Measurement of 220 GHz Atmospheric Opacity on Mt. Fuji with a Radiometer/Radome System

Yutaro SEKIMOTO*(Univ. of Tokyo)*, **Hiroshige YOSHIDA***(Univ. of Tokyo)*, **Tomoya HIROTA***(Univ. of Tokyo)*, **Yasushi TAKANO***(Univ. of Tokyo)*, **Eri FURUYAMA***(Univ. of Tokyo)*, **Satoshi YAMAMOTO** *(Univ. of Tokyo)*, **Shuji SAITO, Hiroyuki OZEKI, Junji INATANI***(National Astronomical Observatory)*, **Masatoshi OHISHI***(National Astronomical Observatory)*, **Apostle G. CARDIASMENOS***(ESSCO)* **and Samuel L. HENSEL***(ESSCO)*

[*Internat. J. Infrared and MM waves*, **17**, 1263(1996)]

Atmospheric opacity at 220 GHz was measured at the summit of Mt. Fuji in order to explore a feasibility of submillimeter-wave astronomical observations. A 220 GHz radiometer system enclosed in a radome has been developed for this purpose as described before.[1-2] The 220 GHz opacity was lower than 0.06 for a significant fraction of time(45 %) from November 1994 to March 1995. Diurnal variation of the opacity at the summit of Mt. Fuji is so small that continuous observation at submillimeter-wave is possible through day and night. Yearly variation of the opacity is studied from water vapor pressure data measured at the weather station for the past 3

years. To prevent accumulation of ice and snow on the Gore-Tex membrane of the radome, the outer membrane was kept at a higher temperature with a thermal flux of 0.63 kWm^{-2} and the adjacent metal radome surfaces were supplied with a flux 0.9kWm^{-2}. We evaluate from the 220 GHz transmission data that this heat flux is sufficient to keep the membrane of the radome free of ice and snow during 83 % of the time in 5 winter months. The summit of Mt. Fuji appears to be one of the best sites for submillimeter-wave astronomical observations.

References

1) S. Saito et al. *Ann. Rev.* II-B(1993).

2) S. Saito et al. *Ann. Rev.* II-B(1994).

II-B-2 Development of Wide-Band Acousto Optical Spectrometer(AOS) for the Mt. Fuji Telescope

Hiroyuki OZEKI, Hideo FUJIWARA, Hisashi YOSHIDA, Toshio HORIGOME and Shuji SAITO

The acousto optical spectrometer(AOS) constitutes a central part of the back end system of the radio telescope, which converts RF signals of a receiver system to a spectral image. Construction of an AOS system is one of the main developments in the Mt. Fuji submillimeter-wave telescope project because a wide band AOS operating in such a severe environment at the summit of Mt. Fuji requires additional efforts to realize high stability and reliability over a long period.

The spectrometer covers the IF frequency of 1.74-2.61 GHz with 1024 channel photo diode array(PDA). The frequency band width per one channel is calculated to be 0.85 MHz. However, due to collimating optics that we employed, the diffraction beam is focused on the PDA with a spot size of around 35 microns which is larger than that of the element of the PDA so that resolution band width is obtained to be about 1.2 MHz. The PDA signal is saturated with the input IF power of -20dBm/MHz. This fact means that the total power of 8.5dBm is sufficient to operate the spectrometer when we chose the IF band width to be 700 MHz. The typical band character of our AOS system is shown in Figure 1. The variation of the PDA signal over 700 MHz IF band width is about 2.0 dB, which enables us to operate the spectrometer without any band character correction. The size of our AOS spectrometer is 20×20×60 cm^3 with a weight of approximately 15 kg. The thickness of base, side and top plates are 15 mm and all the optical components are screw-fixed to the base plate in order to attain sufficient stability against shocks or vibrations to the specrometer during its transportation and mounting. We are now in the phase of environmental testing to ensure the stability of the spectrometer against temperature changes.

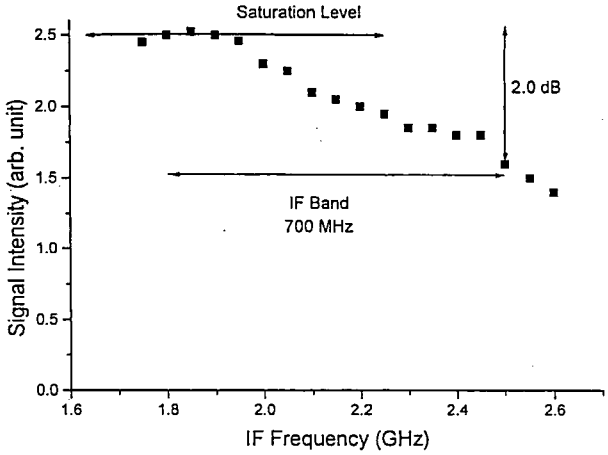


Figure 1. The band character of the AOS system constructed for the Mt. Fuji submillimeter-wave telescope.

II-C Laser Investigation of Antiproton-Helium Compounds

A recent discovery of anomalous survival of antiprotons in dense helium media suggested the creation of an antiproton-helium compound. If the creation of such an unusual compound is true, it is the first long-lived exotic atom containing hadrons other than the normal protons and neutrons. Moreover, from the viewpoint of atomic and molecular spectroscopy, this new compound is a very attractive object of study, because it has characters of both atoms and molecules; in other words, it is neither an atom nor a molecule, but a completely new entity. Therefore, we started the laser spectroscopic investigation of this compound in order, first, to get a definite evidence of the creation, second, to study its properties and dynamics, and finally to explore the possibility of its applications.

II-C-1 Isotope Effects on Delayed Annihilation Time Spectra of Antiprotonic Helium Atoms in a Low-Temperature Gas

B. KETZER*, F. J. HARTMANN*, H. DANIEL*, T. von EGIDY*, A. NIESTROJ*, S. SCHMID*, W. SCHMID* *(*Munchen Tech. Univ.)*, **T. YAMAZAKI**, I. SUGAI**, K. NAKAYOSHI**** *(**INS, Tokyo Univ.)*, **R.S. HAYANO†, F. E. MAAS†, H. A. TORII†, T. ISHIKAWA†, H. TAMURA†** *(†Tokyo Univ.)*, **N. MORITA, D. HORVATH** *(KFKI Inst.)*, **J. EADES†† and E. WIDMANN††** *(††CERN)*

[*Phys. Rev. A* **53**, 2108 (1996)]

The delayed annihilation time spectra (DATS) of antiprotonic helium atoms have been studied in isotopically pure low-temperature ^{3}He and ^{4}He gas at various densities. The DATS taken at 5.8K and 400 mbar are very similar in shape except for (i) a small difference in the time scale and (ii) the presence of a distinct fast decay component in the case of ^{3}He. The ratio of overall trapping times (mean lifetimes against annihilation), $R = T_{trap}(^4\mathrm{He}) / T_{trap}(^3\mathrm{He})$, has been determined to be 1.144 ± 0.009, which is in good agreement with a theoretical estimate yielding $R=[M^*(\bar{p}^4\mathrm{He})/M^*(\bar{p}^3\mathrm{He})]^2=1.14$, where M^* denotes the reduced mass of the $\bar{p}$-He^{2+} system. The presence of a short-lived component with a lifetime of 0.154 ± 0.007 μs in the case of ^{3}He suggests that the $\bar{p}^3He^+$ atom has a state of intermediate life.

II-C-2 Laser-Induced Resonant Transitions in the v=n-l-1=2 and 3 Metastable Cascades of Antiprotonic ^{3}He Atoms

H. A. TORII*, M. HORI*, T. ISHIKAWA*, F. E. MAAS*, R. S. HAYANO* (*Tokyo Univ.), N. MORITA, M. KUMAKURA, I. SUGAI(INS, Tokyo Univ.), B. KETZER**, H. DANIEL**, F. J. HARTMANN**, R. POHL**, R. SCHMIDT** , T. von EGIDY** (**Munchen Tech. Univ.), D. HORVATH(KFKI Inst.), E. WIDMANN†, J. EADES† and T. YAMAZAKI† (†CERN)

[*Phys. Rev. A* **53**, R1931 (1996)]

Laser-induced resonant transitions in metastable antiprotonic ^{3}He atoms have been found. The observed transitions at wavelengths 593.388 ± 0.001 nm and at 463.947 ± 0.002 nm have been respectively ascribed to the $(n, l)=(38, 34) \rightarrow (37, 33)$ and the $(36, 33) \rightarrow (35, 32)$ transitions, showing excellent agreements to 50 ppm with recent predictions of Korobov.

II-C-3 Observation of Double Resonant Laser Induced Transitions in the v=n-l-1=2 Metastable Cascade of Antiprotonic Helium-4 Atoms

R. S. HAYANO*, T. ISHIKAWA*, H. A. TORII*, M. HORI*, F. E. MAAS* (*Tokyo Univ.), N. MORITA, M. KUMAKURA, I. SUGAI(INS, Tokyo Univ.), F. J. HARTMANN†, H. DANIEL†, T. von EGIDY†, B. KETZER†, R. POHL† (†Munchen Tech. Univ.), D. HORVATH(KFKI Inst.), J. EADES††, E. WIDMANN†† and T. YAMAZAKI†† (††CERN)

A new laser-induced resonant transition in the v=n-l-1=2 metastable cascade of antiprotonic ^{4}He atoms has been found by using a double resonance technique. This was done by setting the first laser to the already known 470.724 nm resonance $(n, l) = (37, 34) \rightarrow (36, 33)$, while the $(38, 35) \rightarrow (37, 34)$ transition was searched for with the second laser. The resonant transition was found at wavelength of 529.622 ± 0.002 nm, showing excellent agreement with a recent prediction of Korobov.

II-C-4 Laser Resonance Studies of the Interactions of Metastable Antiprotonic Helium Atomcules $\bar{p}^4He^+$ with Surrounding H_2 Molecules

T. YAMAZAKI*, E. WIDMANN*, J. EADES* (*CERN), B. KETZER**, H. DANIEL**, F. J. HARTMANN**, M. HASINOFF**, R. POHL**, R. SCHMIDT**, T. von EGIDY** (**Munchen Tech. Univ.), D. HORVATH(KFKI Inst.), M. KUMAKURA, N. MORITA, I. SUGAI, Y. FUJITA (INS, Tokyo Univ.), H. A. TORII†, M. HORI†, T. ISHIKAWA†, F. E, MAAS†, H. TAMURA† and R. S. HAYANO† (†Tokyo Univ.)

We have employed a laser resonance method to studies of the interactions of individual states of metastable antiprotonic atomcules pHe^+ with surrounding H_2 molecules. We have found that the lifetimes of the $(n, l) = (37, 34)$ and the $(39, 35)$ states are influenced by small admixtures of H_2 molecules in quite different ways.

II-C-5 High-Precision Structural Studies of the Antiprotonic Helium Atom $\bar{p}^4He^+$ by Observing Laser Resonances with Δv=$\Delta(n$-l-1)=2

T. YAMAZAKI*, E. WIDMANN*, J. EADES* (*CERN), M. KUMAKURA, N. MORITA, H. A. TORII**, M. HORI**, T. ISHIKAWA**, F. E, MAAS**, H. TAMURA**, R. S. HAYANO** (**Tokyo Univ.), I. SUGAI†, Y. FUJITA† (†INS, Tokyo Univ.), B. KETZER††, H. DANIEL††, F.J. HARTMANN††, M. HASINOFF††, R. POHL††, R. SCHMIDT††, T. von EGIDY†† (††Munchen Tech. Univ.) and D. HORVATH(KFKI Inst.)

Very weak laser resonances of unfavoured transitions $(n, l) \rightarrow (n+1, l-1)$ have been observed in metastable $\bar{p}^4He^+$ atoms by using a pulsed antiproton beam. The observed wavelengths (713.578 ± 0.006 nm for $l = 34$ and 726.095 ± 0.004 nm for $l = 35$), as well as those of the known favoured transitions, are to a few ppm accounted for by a recent variational calculation of Korobov, which includes the relativistic correction.

II-C-6 Observation of a Line-Splitting in a Δv=$\Delta(n$-l-1)=2 Transition in Metastable Antiprotonic ^{4}He Atoms

E. WIDMANN*, J. EADES*, T. YAMAZAKI* (*CERN), N. MORITA, M. KUMAKURA, R. S. HAYANO**, T. ISHIKAWA**, H. A. TORII**, M. HORI** (**Tokyo Univ.), I. SUGAI(INS, Tokyo Univ.), F. J. HARTMANN†, H. DANIEL†, T. von EGIDY†, B. KETZER†, C. MARIEL†, R. POHL† (†Munchen Tech. Univ.) and D. HORVATH(KFKI Inst.)

A precise measurement of the previously discovered laser-induced transition $(n, l) = (37, 35) \rightarrow (38, 34)$ in antiprotonic ^{4}He revealed a doublet structure with a separation of the two sublines of $\Delta\nu$=1.73 ± 0.05 GHz. This hyperfine splitting is due to the interaction of the antiproton orbital angular momentum and the electron spin.

II-D Laser Cooling and Trapping of Neutral Atoms

When an atom absorbs or emits a photon, the atom is accelerated or decelerated because a photon has momentum. On the other hand, a strong radiation field modifies the internal energy of an atom, so that an atom in an inhomogeneous radiation field receives a force from the field. The former mechanism allows us to cool the translational temperature of neutral atoms to an extremely low temperature by laser radiation, and the latter enables the spatial control of neutral atoms with lasers. As the translational temperature goes down to nano kelvin region, the atomic de Broglie wavelength becomes a macroscopic size, and macroscopic quantum-mechanical collective motion of atoms can then be expected to occur. The long de Broglie wavelength also enables us to realize an atomic interferometry. On the other hand, the easy control of atomic spatial position and velocity with lasers is expected to open the possibility of various applications. For these reasons, we have been studying the laser cooling and trapping of neutral atoms.

II-D-1 Number Enhancement in Laser-Trapped He* Atoms through Collision-Control with an Additional Laser

Mitsutaka KUMAKURA and Norio MORITA

By means of an additional laser to control ultracold collisions of laser-trapped He* atoms, enhancement of the number of trapped atoms has been realized. For a He* trap, ionizing collisions between the trapped atoms are considered to be the main loss mechanism in the trap. Therefore, to increase the number of He* atoms in a trap, it is quite important to suppress those ionizing collisions. One of the useful methods for this purpose is to use a laser to control the collisions. For ultracold atoms, it is possible to control collisions through laser radiation, because kinetic energies of colliding atoms at an extremely low temperature are so small that they have enough time to absorb laser photons during a collision. When a colliding pair of atoms is excited to the upper repulsive potential, the atoms feel force to push away each other and so the collision rate should be decreased. Therefore, to suppress ionizing ultracold collisions and increase the number of the trapped He* atoms, the trap needs to be irradiated by a laser positively detuned from the resonant frequency of an unperturbed atom.

The experiment has been performed under the condition that the trap temperature is about 700μK and the number of the trapped atoms is about 10^5. He* atoms have been loaded continuously into the trap, and the number of the atoms has been measured by monitoring the fluorescence image of the trap with a video camera. Figure 1 shows the dependence of the ratio N_c / N_{nc} on the detuning of the collision-control laser, where N_c and N_{nc} are the number of the trapped atoms with and without the collision-control laser, respectively. In positive detuning, it is seen that the ultracold collision is considerably suppressed and the number of the trapped atoms is increased, and that the enhancement is maximum (about four times) when the detuning is 100MHz.

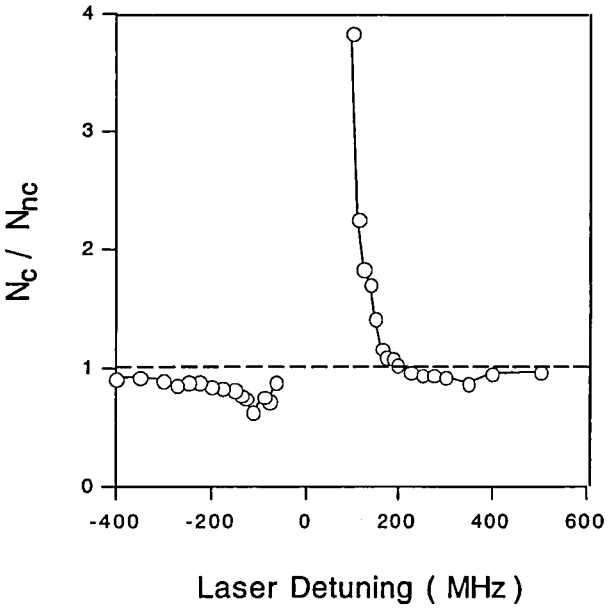


Figure 1. The dependence of the number of trapped He* atoms on the detuning of the collision-control laser. N_c and N_{nc} are the number of trapped atoms with and without the collision-control laser, respectively.

II-E Laser Spectroscopic Studies of Ions in Liquid Helium

An ion in liquid helium attracts helium atoms surrounding the ion by the polarization force, and forms a snow ball. But, in the innermost space, helium atoms are expelled by the Pauli repulsive force between electrons, then the ion resides in a bubble-like cavity. Physical properties in these exotic surroundings are determined by the potential energy of the ion-He_n system, the surface tension energy of liquid helium, and the pressure-volume work. Spectroscopic studies on such ions in liquid helium are expected not only to give important information on the structure and dynamics of the snow balls and bubbles, but also to contribute to the study on the low temperature plasma and on the property of liquid helium (superfluid helium).

II-E-1 Laser Spectroscopy of Barium Ions in Liquid Helium

Yoshiki MORIWAKI and Norio MORITA

Through laser ablation of a barium tip in liquid helium with the second harmonic wave of a YAG laser pulse, small barium clusters have been produced in the liquid helium, then these clusters have been dissociated into atoms and ions with the third harmonic wave of another YAG laser pulse, and finally a dye laser pulse has been introduced to excite the bubbles. With this method, we have observed many emission spectra with small shifts (<1nm) compared with gas phase spectra of barium atoms, and also an excitation spectrum of barium atom transition $6s6p\,^1P_1 \rightarrow 6s6s\,^1S_0$ with a large blue shift (-7nm) and a large width (15nm in FWHM). These spectral properties are considered to be typical to the bubbles, and their analysis is now in progress.

In this study, we have also observed some strange spectra: sharp excitation and emission spectra have been observed at the same wavelength as barium ion transitions in the gas phase. The excitation spectra have asymmetric shapes tailing in the blue side. Tuning the dye laser wavelength to each of these ion transitions, we have found that many emission lines corresponding to atomic bubble transitions near the ion transition appear. Each of these emission spectra has been found to take its maximum when the excitation laser is tuned to each ion transition. These spectra might be due to the dissociation of barium clusters or charged clusters, but this still does not explain the reason why the dissociation occurs at the laser wavelength resonant to the ion transitions.

In general, laser ablation produces many species of particles, such as atoms, ions and clusters, and these are apt to complicate the observation. Therefore, we are now preparing to construct a linear radio-frequency quadrupole trap (linear RF trap) to confine a specific ion species within a small region in superfluid helium for a long time. This method is expected to have the following merits: (1) ions can be selected due to the mass, (2) ions can be selected due to the sign of charge, (3) observation is not disturbed by turbulent flow in liquid helium after the ion production procedure, and (4) detection efficiency can be enhanced by the long observation time.

II-F Molecular Science of Biomolecules

Elucidation of structure-function relationship of proteins is a current subject of this group. The primary technique used for this project is the stationary and time-resolved resonance Raman and absorption spectroscopies. The main themes that we want to explore are (1) mechanisms of oxygen activation by enzymes, (2) mechanisms of electron- and proton-transfers through proteins and their coupling in energy transducing membranes, (3) coupling mechanism of proton- and electron-transfers by quinones in photosynthetic reaction centers, and (4) higher order protein structures and their dynamics. In category (1), we have examined stationary complexes of a variety of cytochrome oxidases, cytochrome P-450's, and peroxidases, and also treated their enzymatic reaction intermediates by using the mixed flow transient Raman apparatus and the Raman/absorption simultaneous measurement device. We recently demonstrated that the so-called "peroxy" and "ferryl" intermediates of cytochrome oxidase in dioxygen reduction are also generated in the reaction of oxidized cytochrome oxidase with H_2O_2. For (2) we are investigating cytochrome *c* oxidase. (3) we have succeeded in identifing UV resonance Raman spectra of quinones A and B in bacterial photosynthetic reaction centers for the first time and in analysing Raman spectra of electrochemically reduced isotope-labeled quinones to characterize the spectra of reaction center. For (4), we developed a novel technique for UV Raman measurements based on the combined use of the first/second order dispersions of two gratings in an ordinary double monochromator and applied it successfully to 235-nm-excited RR spectra of several proteins including viruses and site-directically mutated hemoglobin. It is noted that a new spinning cell system developed for UV Raman experiments requires only a small amount of samples and therefore, it became possible to determine the UVRR spectra of mutant proteins. We applied this system to β37 and α42 mutants of Hb A and established the Raman spectra of β37-Trp and α42-Tyr of Hb A in the T and R quaternary structures. From this year we started studies of NO and succeeded in isolating soluble guanylate cyclase from bovine lung and observing its resonance Raman spectra. We are going to extend the study of NO by constructing new ultra-sensitive IR spectrometer.

II-F-1 The Proximal Residue Largely Determines the CO Distortion in Carbonmonoxy Globin Proteins. An *ab Initio* Study of a Heme Prosthetic Unit

Philip JEWSBURY *(PERI and IMS)*, **Shigeyoshi YAMAMOTO** *(Chukyo Univ.)*, **Tsutomu MINATO** *(Nara Univ.)*, **Minoru SAITO** *(PERI)* **and Teizo KITAGAWA**

[*J. Phys. Chem.* **99**, 12677(1995)]

An *ab initio* investigation of a model heme prosthetic group based on the carbon monoxy myoglobin (MbCO) 1MBC X-ray structure reproduces the large off-perpendicular distortions of the Fe-C-O unit reported for the protein. The distortion is mainly caused by the nonequilibrium orientation of the proximal residue and not by the distal residue: inclusion of the distal residue in a supermolecule calculation has a smaller effect on the Fe-C-O geometry. If such a mechanism primarily determines the Fe-C-O distortion in the protein itself, then the large strain energies implied by the Fe-C-O geometries in the X-ray structures are delivered by the protein tertiary structure, via the proximal residue, and not by the mobile distal side chain as had been previously proposed. The structure-function relationship, as revealed by the X-ray structure, would thus be clarified. Distortion of the Fe-C-O geometry is largely determined by the proximal desidue, and so Fe-C-O is nonperpendicular even in the His64Gly mutant. The distal residue is *not* subject to a large repulsive interaction with the carbonyl ligand; thus, its orientation in the solvate protein can be determined by weaker attractive electrostatic interactions, as inferred from recent experimental studies of distal residue mutant myoglobins. This result removes the need to invoke a large stabilization of the distal side chain orientation by a rigid hydrogen-bonding network, an interpretation of the physiological structure-function relationship that was at odds with the X-ray B factors and the mobility of surface residue side chains expected under physiological conditions.

II-F-2 Distal Residue-CO Interaction in Carbonmonoxy Myoglobins: A Molecular Dynamics Study of Three Distal Mutants

Philip JEWSBURY *(PERI)* **and Teizo KITAGAWA**

[*Biophysical J.* **68**, 1283(1995)]

Six 90-ps molecular dynamics trajectories, two for each of three distal mutants of sperm whale carbonmonoxy myoglobin, are reported; solvent waters within 16Å of the active site have been included. In both His64Gln trajectories, the distal side chain remains part of the heme pocket, forming a "closed" conformation similar to that of the wild type $64N_\delta H$ tautomer. Despite a connectivity more closely resembling the $N_\varepsilon H$ histidine tautomer, close interactions with the carbonyl ligand similar to those observed for the wild type $64N_\varepsilon H$ tautomer are prevented in this mutant by repulsive interactions between the carbonyl O and the $64O_\varepsilon$. The aliphatic distal side chain of the His64Leu mutant shows little interaction with the carbonyl ligand in either His64Leu trajectory. Solvent water molecules move into and out of the active site in the His64Gly mutant trajectories; during all the other carbonmonoxy myoglobin trajectories, including the wild type distal tautomers considered in an earlier work, solvent molecules rarely encroach close than 6Å of the active site. These results are consistent with a recent structural interpretation of the wild type infrared spectrum, and the current reinterpretation that the distal-ligand interaction in carbonmonoxy myoglobin is largely electrostatic, not steric, in nature.

II-F-3 Time-Resolved Resonance Raman Evidence for Tight Coupling between Electron Transfer and Proton Pumping of Cytochrome c Oxidase upon the Change from the Fe^{V} Oxidation Level to the Fe^{IV} Oxidation Level

Takashi OGURA, Shun Hirota, Denis A. PROSHLYAKOV *(Graduate Univ. for Advanced Studies)*, **Kyoko SHINZAWA-ITOH** *(Himeji Inst. of Tech.)*, **Shinya YOSHIKAWA** *(Himeji Inst. of Tech.)* **and Teizo KITAGAWA**

[*J. Am. Chem. Soc.* **118**, 5443(1996)]

The mechanism of dioxygen reduction catalyzed by cytochrome c oxidase, the terminal enzyme of the respiration chain of aerobic organisms, has been investigated with time-resolved resonance Raman spectroscopy. Five oxygen isotope sensitive Raman bands have been identified for $^{16}O_2/^{18}O_2$ intermediates at 571/544, 804/764, 356/342, 785/750, and 450/425 cm^{-1} in the order of appearance. The first and last ones, which have been assigned to the Fe^{III}-O_2^- and Fe^{III}-OH^- stretching modes, respectively, are in general consensus, but the remaining three band are currently under debate. This study establishes that the 804/764 cm^{-1} species is generated prior to the 785/750 cm^{-1} species, and the latter is not observed when we start from the mixed valence enzyme. Therefore, the enzyme oxidation state of the 804/764 cm^{-1} species is higher by one oxidative equivalent than that of the 785/750 cm^{-1} species, although both bands have been assigned to the Fe=O stretching mode. The excitation wavelength dependences of these two sets of Raman bands are distinctly different, suggesting that the electronic properties of the two hemes are quite different. We found that the conversion from the 804/764 cm^{-1} species to the 785/750 cm^{-1} species was significantly slower in D_2O than in H_2O, suggesting strong coupling between electron and vector proton transfers at this stage. Presumably, Cu_B at the binuclear site causes heterolytic cleavage of the O-O bond, givig rise to an oxoiron in the Fe^V oxidation level of the enzyme with the 804/764 cm^{-1} bands, and the electron transfer to this oxoiron is accompanied by some protein conformational changes, which cause distortion of the oxoheme and thus appearance of the His-Fe=O bending Raman bands at 356/342 cm^{-1} and simultaneously active transport of protons.

II-F-4 Two Amine Oxidases from Aspergillus Niger AKU 3302 Contain Topa Quinone as the Cofactor: Unusual Cofactor Link to the Glutamyl Residue Occurs Only at One of the Enzymes

Ivo FREBORT *(Yamaguchi Univ.)*, **Pavel PEC** *(Palacky Univ.)*, **Lenka LUHOVA** *(Palacky Univ.)*, **Hirohide TOYAMA** *(Yamaguchi Univ.)*, **Kazunobu MATSUSHITA** *(Yamaguchi Univ.)*, **Shun HIROTA, Teizo KITAGAWA, Tamio UENO** *(Kyoto Univ.)*, **Yasuhisa ASANO** *(Toyama Prefectural Univ.)*, **Yasuo KATO** *(Toyama Prefectural Univ.)* **and Osao ADACHI** *(Yamaguchi Univ.)*

[*Biochim. Biophys. Acta* **1295**, 59(1996)]

Amine oxidases (EC 1.4.3.6) from Aspergillus niger, AO-I (2´75 kDa) and AO-II (80 kDa), were examined to determine the cofactor structure. Inactivated with *p* -nitrophenylhydrazine, they showed absorption and fluorescence spectra similar to those published for other copper amine oxidases and to topa hydantoin *p* -nitrophenylphydrazone. After digestion by thermolysin and pronase, cofactor peptides were purified by HPLC and sequenced. For thermolytic peptides, a typical topa consensus sequence, Asn-X-Glu-Tyr, was obtained for AO-II, although in case of AO-I it overlapped with Val-Val-Ile-Glu-Pro-Tyr-Gly. For pronase peptides of AO-I, only the latter sequence was obtained. NMR and mass spectroscopy confirmed the residue X as topa *p*-nitrophenylhydrazone in AO-II and revealed the presence of a residue Z attached to the Glu in the peptide Val-Val-Ile-Glue(Z)-Pro of AO-I. This residue was separated from the peptide by hydrolysis and identified as a product derived from topa quinone. The data, together with amino-acid sequence of AO-I, confer strog evidence for topa quinone as the cofactor, bound in the typical consensus sequence. Raman spectra of the *p* -nitrophenyl-hydrazone derivative of AO-I and its pronase peptide showed essentially the same peaks matching to a model compound for topa *p* -nitrophenylhydrazone. However, there may exist an unusual ester link between the topa-404 and Glu-145 in the native enzyme.

II-F-5 Perturbation of the Fe-O_2 Bond by Near-by Residues in Heme Pocket: Observation of $\nu_{Fe\text{-}O_2}$ Raman Bands for Oxymyoglobin Mutants

Shun HIROTA, Tiansheng LI *(Rice Univ.)*, **George N. PHILLIPS, JR.** *(Rice Univ.)*, **John S. OLSON** *(Rice Univ.)*, **Masahiro MUKAI and Teizo KITAGAWA**

[*J. Am. Chem. Soc.* **118**, 7845 (1996)]

Replacement of amino acids in the heme pocket often causes large changes in the Fe-CO stretching frequency of CO-myoglobin (COMb) which have been ascribed to changes in the electrostatic field adjacent to the bound ligand. The effects of these mutations on O_2 adducts have not been examined due to rapid autoxidation of some of the mutants. We have succeeded in observing the $\nu_{Fe\text{-}O_2}$ Raman band for three key mutants (H64L, L29F and L29W) of sperm whale Mb by modifying our flow system which was originally developed for studies of cytochrome *c* oxidase. Wild-type and H64L oxyMb have almost identical $\nu_{Fe\text{-}O_2}$ bands at 570-571 cm^{-1}, whereas H64L COMb has a $\nu_{Fe\text{-}CO}$ band which is ~20 cm^{-1} lower than that for the wild-type protein. Although little affected by electrostatic fields, $\nu_{Fe\text{-}O_2}$ does depend on the Fe-O-O bond angle, shifting to higher frequency as the angle decreases. Thus, the effects of near-by protein residues on the vibrational properties of the bound ligand differ markedly between the Fe-O_2 and Fe-CO adducts.

II-F-6 Resonance Raman Studies of Compounds I and II of *Arthromyces ramosus* Peroxidase : Close Similarities in Their Raman Spectra but Distinct Oxygen Exchangeability of the Fe=O Heme

Denis A. PROSHLYAKOV*(Graduate Univ. for Advanced Studies)*, **Insook R. PAENG** *(Seoul Women's Univ.)*, **Ki-Jung PAENG** *(Yonsei Univ.)* **and Teizo KITAGAWA**

[*Biospectroscopy*. 2,317(1996)]

Simultaneous measurements of resonance Raman and absorption spectra were performed for intermediates generated upon addition of hydrogen peroxide to ferric *Arthromyces ramosus* peroxidase (ARP) using the microcirculating system constructed in this laboratory, which enables generation of desirable intermediates under steady state conditions. Compound I of ARP generated at neutral pH was stable over tens of minutes in the absence of laser illumination with this circulation system, but was gradually degraded under laser illumination, giving rise to a new irreversible species with an iron-oxo

heme. Such photosensitivity was not observed for compound II in the steady state at alkaline pH. Surprisingly, the Raman spectrum of compound I of ARP in the high-frequency region, where characteristic frequency shifts are expected upon oxidation of the macrocycle, was quite close to that of compound II, despite the fact that the reduced Soret absorption indicated the formation of a π-cation radical. The Fe=O stretching ($\nu_{Fe=O}$) frequency of compound I was observed at 781 cm^{-1} for the ^{16}O-derivative but appeared as a doublet at 744 and 731 cm^{-1} for the ^{18}O-derivative. The isotope sensitivity of the $\nu_{Fe=O}$ mode of compound I was seen upon $H_2{}^{16}O/H_2{}^{18}O$ solvent substitution but not upon $H_2{}^{16}O_2/H_2{}^{18}O_2$ peroxide substitution in $H_2{}^{16}O$ at neutral pH. This directly indicates the occurrence of an oxygen atom exchange between the oxo-heme and bulk water, providing the first example of such exchange in compound I of peroxidases. The oxygen exchange was abolished for compound II at alkaline pH, for which the $\nu_{Fe=O}$ mode was seen at 787/749 cm^{-1} only upon $H_2{}^{16}O_2/H_2{}^{18}O_2$ peroxide substitution. The oxygen exchangeability seems to depend on protonation of a nearby residue with pK_a~9 and to correlate with stability of compound I

II-F-7 Ultraviolet Resonance Raman Spectra and *Ab initio* Vibrational Analyses of 1,4-Benzoquinone: Reassignments of the ν_2 and ν_3 Bands

Xiaojie ZHAO, Hiroshi IMAHORI *(Osaka Univ.)*, **Chang-Guo ZHAN** *(Central China Normal Univ.)*, **Yasuhisa MIZUTANI, Yoshiteru SAKATA** *(Osaka Univ.)* **and Teizo KITAGAWA**

[*Chem. Phys. Lett.* in press]

Ultraviolet Resonance Raman (UVRR) spectra excited at 245 and 325 nm are reported for 1,4-benzoquinone (BQ) and its $^{18}O_2$ and d_4 isotopomers. Depolarization ratios were determined for nonresonance Raman spectra excited at 647 and 441.6 nm and solvent effects were examined for UVRR spectra. The UVRR bands at 1665 and 1639 cm^{-1}, the latter of which exhibited much larger $^{18}O_2$ isotopic frequency shift than the former, are conclusively reassigned to ν_2 (in-phase C=O/C=C stretches) and ν_3 (out-of-phase C=O/C=C stretches), respectively, on the basis of the observed $^{18}O_2$- and d_4-isotope frequency shifts and unscaled *ab initio* vibrational analyses with MP2 method using an extended basis set.

II-F-8 Resonance Raman and FTIR Spectra of Isotope-Labeled Reduced 1,4-Benzoquinone and Their Protonated Forms in Solutions

Xiaojie ZHAO, Hiroshi IMAHORI *(Osaka Univ.)*, **Chang-Guo ZHAN** *(Central China Normal Univ.)*, **Yoshiteru SAKATA** *(Osaka Univ.)*, **Suehiro IWATA and Teizo KITAGAWA**

[*J. Phys. Chem.* in press]

Resonance Raman (RR) and FTIR spectra were observed for 1,4-benzoquinone (BQ) and its $^{18}O_2$- and d_4-isotopomers in the reduced states and their protonated forms including anion radical ($BQ^{\cdot-}$), semiquinone radical ($BQH^{\cdot}$), dianion (BQ^{2-}), and protonated anion (BQH^-) in water and acetonitrile. The reduced species were generated electrochemically and RR spectra were excited *in situ* at 441.6, 363.8, 351.1, 325, and 235 nm in resonance with three lowest electronic transitions. The observed bands were assigned empirically on the basis of the observed $^{18}O_2$- and d_4-isotopic frequency shifts and depolarization ratios and further with *ab initio* MO calculations at MP2 level. In contrast with neutral BQ, the ^{18}O atoms of $BQ^{\cdot-}$ and BQ^{2-} were rapidly exchanged with bulk water during the RR measurements for aqueous solutions. Upon reduction from BQ to $BQ^{\cdot-}$ and BQ^{2-}, the C=O stretching mode (ν_{7a} in Wilson's notation) shifts from 1639 to 1452 and 1275 cm^{-1}, respectively, while the ν_{8a} mode exhibits smaller shifts from 1666 to 1609 and 1596 cm^{-1}, respectively. The ν_{8a} and ν_{8b} separation was 293, 149, and 81 cm^{-1} for BQ, $BQ^{\cdot-}$,and BQ^{2-}, respectively, indicating that the six-membered ring increasingly approaches to a benzenoid ring as reduction proceeds. These frequency changes are in qualitative agreement with those expected from the optimized bond-lengths of the MO calculations. The RR spectra of BQH^- was close to that of BQ^{2-}, suggesting that the extra charges of BQ^{2-} are mainly localized on the two oxygen atoms. Three b_{3g} vibrations were resonance enhanced for $BQ^{\cdot-}$ via vibronic coupling and this determines the symmetry of the first allowed electronic excited state to be $^2B_{3u}$ in D_{2h} group. Assumption of D_{2h} symmetry to $BQ^{\cdot-}$ predicts the presence of five polarized RR bands in the region below 1700 cm^{-1} but nine fundamentals were observed in addition to several overtones and combinations. In addition, one band appears both in IR and RR spectra. Therefore, practical molecular symmetry is reduced to C_s owing to solvation.

II-F-9 Effects of Concerted Hydrogen Bonding of Distal Histidine on Active Site Structures of Horseradish Peroxidase; Resonance Raman Studies with Asn-70 Mutants

Masahiro MUKAI, Shingo NAGANO *(Kyoto Univ. and Keio Univ.)*, **Motomasa TANAKA** *(Kyoto Univ.)*, **Koichiro ISHIMORI** *(Kyoto Univ.)*, **Isao MORISHIMA** *(Kyoto Univ.)*, **Takashi OGURA, Yoshihito WATANABE and Teizo KITAGAWA**

[*J. Am. Chem. Soc.* in press]

Effects of a highly conserved hydrogen-bond between the distal histidine (His) and a nearby asparagine residue (Asn) of peroxidases upon the active site structures were investigated using resonance Raman (RR) and EPR spectroscopy. Although there is no crystallographic data for horseradish peroxidase (HRP), Asn70 is deduced to be the hydrogen-bond acceptor for HRP. Accordingly, site-directed mutagenesis of Asn 70 to Val (N70V) and to Asp (N70D) was carried out with HRP and their RR spectra were compared with those of native and wild type (WT) enzymes in the resting, reduced, CN-bound ferric and compound II states. In the resting state, the six-coordinate high-spin structure is the main component for N70V and N70D mutants, while the five-coordinate high-spin structure is dominant for the native and WT HRPs. This was confirmed with EPR spectra. The Fe^{III}-CN stretching frequency was lower for the mutants than for native enzyme and the spectral patterns of the mutants at pH 7.0 resemble that of the basic form of native HRP. The Fe-histidine stretching bands of reduced HRPs exhibit pH dependent frequency shifts and the midpoint pH were 7.2, 5.9, and 5.5 for native, N70V, and N70D, respectively. This change is ascribed to the acid-base transition of the distal His. While the Fe^{IV}=O stretching ($\nu_{Fe=O}$) fre-

quency of compound II at pD 7.0 is lower than that at pD 10.0 for native enzyme, the $\nu_{Fe=O}$ band of the mutants show no pH dependent frequency shifts between pD 7.0 and 10.0. However, the H_2O/D_2O frequency change of $\nu_{Fe=O}$ and the oxygen atom exchange with bulk water suggested the presence of the hydrogen bond between the oxygen ligand of the ferryloxo heme and distal His for these mutants at pD. 10.0. On the basis of these observations, it is proposed that the hydrogen bond between the N_δ-proton of distal His and Asn70 regulates the pK_a of N_ε-proton and thus a reactivity of compound II in the distal side and also affects the Fe-His bond in the proximal side via tertiary structure changes.

II-F-10 Red-Excited Time-Resolved Resonance Raman Study of the Oxoiron Intermediates of Fully Reduced Cytochrome *c* Oxidase

Jörg MATYSIK, Takashi OGURA, Kyoko SHINZAWA-ITOH *(Himeji Inst. Tech.)*, **Shinya YOSHIKAWA** *(Himeji Inst. Tech.)* **and Teizo KITAGAWA**

The reaction of bovine fully reduced cytochrome *c* oxidase with dioxygen has been pursued with red-yellow excited time-resolved resonance Raman (RR) spectroscopy using a flow cell. The 607-nm probed RR spectra gave rise to the oxygen isotope sensitive bands at 804/764 cm^{-1} for the $^{16}O_2/^{18}O_2$ derivatives, but not the 780/750 cm^{-1} bands. In contrast, the 580-nm probed RR spectra revealed the presence of the 780/750-cm^{-1} bands but not the 804/764 cm^{-1} bands. Thus, the RR enhancements for the 607 nm and 580 nm intermediates are very selective. The time course of the intermedaites were analysed in terms of a consecutive reaction kinetics. It has been confirmed that the 607-nm intermediate precedes the 580-nm intermediate. The 356/342 cm^{-1} bands, which have been identified in blue excitation, were not resonance enahnced in red. Similar experiments in D_2O indicated that the life times of both the 607 nm and 580 nm intermediates became longer than those in H_2O.

II-F-11 Selective Observation of Resonance Raman Spectra of $Q_A^{\cdot-}$ and $Q_B^{\cdot-}$ in *Rb. Sphaeroides* R26 Photosynthetic Reaction Centers

Xiaojie ZHAO, Takashi OGURA, Melvin OKAMURA *(Univ. of California, San Diego)* **and Teizo KITAGAWA**

Resonance Raman (RR) spectra of two reduced quinones, $Q_A^{\cdot-}$ and $Q_B^{\cdot-}$ in photosynthetic reaction centers of *Rhodobacter Sphaeroides* R26 were observed for the first time and are compared with those of ubiquinone-10 anion radical in organic solvents. Three prominent bands were observed at 1486, 1523, 1605 cm^{-1} for $Q_A^{\cdot-}$ and at 1489, 1532, 1613 cm^{-1} for $Q_B^{\cdot-}$ in 1400-1700 cm^{-1} region, which were assigned to ν_{7a}, ν_{19b}, and ν_{8a}, respectively, on the basis of the observed ^{13}C isotopic frequency shifts *in vivo* and separate model compound studies. The frequency differences between $Q_A^{\cdot-}$ and $Q_B^{\cdot-}$ are ascribed to differential hydrogen bonding effects on C=O groups and π electrons of quinones.

II-F-12 Effects of GTP Binding to Soluble Guanylate Cyclase on Its Heme Vicinity as Probed by Resonance Raman Spectroscopy

Takeshi TOMITA *(Graduate Univ. for Advanced Studies)*, **Takashi OGURA, Shingo TSUYAMA** *(Osaka Prefecture Univ.)*, **Yoshio IMAI** *(Oska Prefecture Univ.)* **and Teizo KITAGAWA**

Soluble guanylate cyclase (sGC) was purified from bovine lung and its resonance Raman (RR) spectra were investigated with a focus on its nitrosyl adduct. Nitrosyl sGC gave NO-isotope sensitive RR bands at 1682 and 520 cm^{-1}. The former and the latter were downshfited to 1650 and 512 cm^{-1} with ^{15}NO, respectively, and accordingly assigned to N-O stretch (ν_{N-O}) and Fe-NO stretch (ν_{Fe-NO}). Upon addition of guanosine triphosphate (GTP) which is a substrate of this enzyme, nitrosyl sGC gave a new ν_{NO} Raman band at 1699 cm^{-1}, which exhibited a downshift to 1667 cm^{-1} upon ^{15}NO substitution, while there was no new feature in the ν_{Fe-NO} region. Relative intensities and frequencies of all porphyrin Raman bands were scarcely influenced by binding of GTP. The RR spectra of sGC without NO exhibited no change upon addition of GTP with the same concentration. This observation suggests that the binding of GTP alters direct interactions between bound NO and the protein in the distal side and conversely that the binding of NO is communicated to the catalytic site through conformation change of the protein.

II-G Fast Dynamics of Photoproducts in Solution Phases

Picosecond time-resolved resonance Raman (ps-TR^3) spectroscopy is a promising technique to investigate ultrafast structural changes of molecules. However, this technique has not been as widely used to study interesting chemical and biological reactions as nanosecond TR^3 spectroscopy owing to practical limitations. The most crucial factor in ps-TR^3 spectroscopy is the light source which should have suitable repetition rates of pulses and wavelength tunability. We have challenged to overcome this problem. In the pump and probe TR^3 experiments, we need two sets of pulses, the pump and probe pulses. The pump pulse is used to photoexcite the molecules of interest and the probe pulse monitors Raman spectra of the excited molecules to pursue the subsequent changes. In order to obtain TR^3 spectra with high S/N ratio, first it is indispensable to provide two independently tunable light sources for pump and probe pulses. Second, the repetition rate should be higher than kilohertz to keep a moderate average laser power without allowing the photon density of probe pulses too high. Unfortunately, no authentic method which meets these requirements for ps-TR^3 measurements, has been established so far. Therefore, we started from developing the light sources for ps-TR^3 spectroscopy with wide tunability and kHz repetition, and applied them successfully to TR^3 studies on fast dynamics of photoproducts in solution phases. Since we have already completed to set up ns-TR^3 apparatus, the system was applied to metalloporphyrins in solutions.

II-G-1 Developments of Widely Tunable Light Sources for Picosecond Time-Resolved Resonance Raman Spectroscopy

Yuki UESUGI *(Graduate Univ. for Advanced Studies)*, **Yasuhisa MIZUTANI and Teizo KITAGAWA**

Two widely tunable light sources for picosecond time-resolved resonance Raman spectroscopy have been developed using a 1 kHz ps-Ti:sapphire laser/regenerative amplifier system and their performances were examined in terms of pulse duration, spectral width, pulse energy and shot-to-shot stability. One system consists of a white light continuum generation using water followed by an optical parametric amplification using β-barium borate. Tunability in the 500-660-nm range has been demonstrated with 1.3-2.1-ps pulse duration and 15-μJ pulse energy. The other system consists of a lithium triborate optical parametric generator in a type II noncritical phase matching configuration followed by β-barium borate optical parametric amplification Visible pulses with a pulse duration of 1.5-2.4 ps and pulse energy of as high as 18 μJ have been achieved in 520-630 nm. The shot-to-shot stability of the generated pulses was found to be less than 10% for both systems.

II-G-2 Direct Observation of Vibrational Energy Relaxation for Photodissociated Heme of Carbonmonoxy Myoglobin

Yasuhisa MIZUTANI and Teizo KITAGAWA

The formation of vibrationally excited heme upon photodissociation of CO from carbonmonoxy myoglobin and its subsequent vibrational energy relaxation have been monitored by picosecond pump-probe anti-Stokes resonance Raman spectroscopy. Hot heme in the ground electronic state appeared immediately after photodissociation (within 1.5-ps experimental time resolution), and the anti-Stokes Raman intensity decayed with a time constant of 1.8±1 ps. The decay of the anti-Stokes intensity of ν_4 is synchronous to narrowing of its Stokes counterpart. The time constant of heme cooling is compared to femtosecond time-resolved IR study by Hochstrasser and coworkers. The anti-Stokes/Stokes intensity ratio of ν_4 indicates a vibrational temperature of heme to be ~500 K above room temperature shortly after the photodissociation.

II-G-3 Vibrational Energy Relaxation in the *(d, d)* Excited State of Nickel Octaethylporphyrin

Yasuhisa MIZUTANI, Yuki UESUGI *(Graduate Univ. for Advanced Studies)* **and Teizo KITAGAWA**

The formation of hot photoproducts of nickel octaethylporphyrin (NiOEP) and its subsequent vibrational energy relaxation were monitored by picosecond time-resolved resonance Raman spectroscopy. Anti-Stokes ν_4 band of hot *(d, d)* excited state of NiOEP appeared immediately after ($\pi\pi^*$) excitation and its intensity decayed with time constants of ~10 and ~300 ps. However, the rise of anti-Stokes ν_7 intensity was not instantaneous, but was delayed by ~2 ps. This observation suggests that IVR is not completed in subpicosecond time regime. The peak positions of ν_4 and ν_7 bands were shifted by nearly 10 cm^{-1} between 0 and 20 ps. This can be attributed to vibrational relaxation from higher excited states ($\upsilon \geqq 2$).

II-G-4 Picosecond Time-resolved Resonance Raman Study on Photo-induced Ligation of Pyridine to Nickel Octaethylporphyrin

Yuki UESUGI *(Graduate Univ. for Advanced Studies)*, **Yasuhisa MIZUTANI and Teizo KITAGAWA**

Picosecond time-resolved resonance Raman (ps-TR^3) spectra of nickel octaethylporphyrin (NiOEP) in pyridine were measured with pump/probe technique using 1 kHz picosecond pulses with pulse duration of 3 ps. Most of NiOEP in pyridine adopts four-coordinated structure (A_{1g}) in the electronic ground state. Transient absorption studies suggested that , upon photoexcitation, the four-coordinated NiOEP is converted into six-coordinated complex ($B_{1g}(L)_2$), ligated by two pyridine molecules at two axial positions of the (d, d) electronic excited Ni^{II} ion (B_{1g}). We successfully pursued the structural changes of NiOEP in the process of photo-induced ligation of pyridine to it by ps-TR^3 measurements. Shortly after photoexcitation to ($\pi\pi^*$) state, Raman bands assignable to the B_{1g} state appeared. This phenomenon is the same as the case of NiOEP in non-coordinating solvents. Around a few hundreds of picosecond after the photoexcitation new Raman bands appeared. We assigned these bands to a six-coordinated complex of NiOEP with two pyridine molecules at axial positions by comparing the spectrum with that of NiOEP in piperidine which is strongly coordinating solvent. The time constant of ligation was found to be 630 ps. We also measured anti-Stokes TR^3 spectra to study the vibrational relaxation processes which compete with the photo-induced ligation.

II-G-5 Time-Resolved Resonance Raman Spectra of Octaethylporphinato Copper(II) in the Lowest Excited Triplet State

Motoko ASANO-SOMEDA *(Tokyo Inst. of Tech.)*, **Katsuhiro AOYAGI** *(Fukushima Natl. College of Tech.)* **and Teizo KITAGAWA**

[*Chem. Phys. Lett.* **257**, 492(1996)]

Time-resolved resonance Raman spectra were observed with the pump/probe technique using two 7 ns pulsed lasers for octaethylporphinato Cu(II) [(OEP)Cu] and its isotopomers (OEP-meso-d_4 and OEP-^{15}N) in the lowest excited triplet state. Raman bands were assigned on the basis of depolarization ratios and isotope shifts. The ν_2, ν_3 and ν_4 modes of the macrocycle in the T_1 state were shifted to lower frequencies by 7, 37 and 57 cm^{-1}, respectively compared with those of the ground state, but the peripheral ethyl internal modes were shifted little. The porphyrin skeletal modes exhibited significant broadening in the T_1 state but the ethyl modes did not.

II-H Molecular and Electronic Structures of Metallofullerenes and the Fullerene Radical Anions

The continued interest in radical ions of fullerenes and metallofullerenes has resulted from the discovery of superconductivity in the CT complexes of alkali metals with fullerenes. Spectroscopic information concerning the electronic structure of C_{60}^- isolated in a single crystal salt has been obtained by EPR, absorption and fluorescence measurements at low temperature. The metallofullerenes are of great interest because they could give rise to new chemical entities with novel properties, such as the superconductivity or the ferromagnetism. However, little is known about the chemical reactivities.

II-H-1 ESR Measurements of C_{60}^- Anion Crystals

Takeshi KODAMA, Tatsuhisa KATO and Masako KATO
(Nara Women's Univ.)

The anisotropic components of the g factor of C_{60}^- were determined with accuracy from the analysis of angular dependent ESR spectra of single crystal C_{60}^- salts. The evaluation of the g factor was performed according to the classification of symmetry of the C_{60}^- geometry. It was found out from the evaluation that the molecular structure of C_{60}^- should be distorted to the lower symmetry of C_{2h} or C_i. This conclusion was well explained theoretically by the ab initio MO calculations.

II-H-2 ESR Study on Electronic Structure and Chemical Reactivity of Metallofullerenes

Tatsuhisa KATO, Takeshi AKASAKA *(Niigata Univ.)*, **Kaoru KOBAYASHI** *(Tokyo Metropol. Univ.)*, **Shigeru NAGASE** *(Tokyo Metropol. Univ.)* **and Kazunori YAMAMOTO** *(Power Reactor & Nucle. Fuel Development Corp.)*

Since the discovery of C_{60} in carbon soot by Kroto, Smalley and coworkers in 1985, metallofullerenes have interested people because of their posibilities of the free tune of "outside chemistry". However, little is known yet about the physical property and there are no reports concerning the chemical property of these species. During the course of our studies on the chemical derivatization of fullerenes, we have found a new photochemical exohedral derivatization of typical empty fullerenes such as C_{60} and C_{70} with disilirane while the corresponding derivatization does not occur thermally. Moreover, we have very recently found for the first time the chemical derivatization of endohedral metallofullerenes, $La@C_{82}$ and $Gd@C_{82}$ with disilirane. An important finding is that the metallofullerenes can be exohedrally derivatized with the organosilicon compound in both thermal and photochemical ways.

II-I Site Selective Spectroscopy in Solid Crystals

The line broadening due to the variation of the environment over the some sites in the crystal structure prevents from determining small energy splitting between pair of closely spaced levels with high accuracy. However the broadening effects give a nice probe to investigate the intermolecular interaction in the crystal structure. On the other hand some techniques of the site selective spectroscopy to eliminate the disturbance were proposed. We are applying the technique of the heterodyne detection of optical magnetic double-resonance to some systems of crystal.

II-I-1 Heterodyne Detection of Optical Magnetic Double-Resonance

Michio MATSUSHITA and Tatsuhisa KATO

Pr^{3+} ion doped into LaF_3 crystal has two long-lived electronic excited states in visible, $^1D_2$ at 592 nm and $^3P_0$ at 477nm. Since the fluorescence life time at liquid helium temperatures is in the range of 100μsec, many spectroscopic studies have been made to reveal hyperfine interaction. For the $^3P_0$ state, however, techniques were limited to those utilizing pulsed lasers, partly due to inconvenience of cw lasers at the excitation wavelength. Recently we have built up the system of Raman heterodyne detection of optical-RF double resonance. As a first cw study of $^3P_0$ state, we applied this technique to $^3H_4$ - $^3P_0$ transition. Two transitions of nuclear quadrupole resonance (NQR) of the excited $^3P_0$ were observed at 3.45 and 3.49 MHz. The linewidth of the excited state NQR is about 10kHz, which is one order of magnitude narrower than the ground $^3H_4$ state.

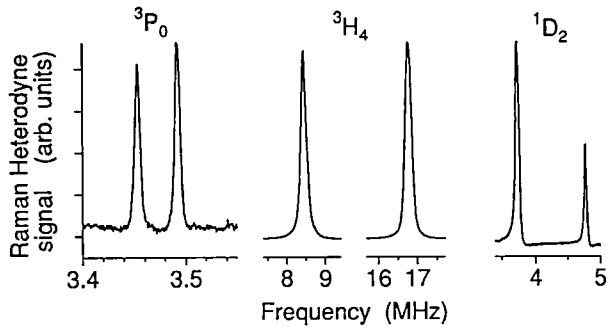


Figure1.

II-I-2 Measurements on the Zero Phonon Line of the Luminescence of the NV Center in Synthetic Ib Diamonds

Tatsuhisa KATO, Michio MATSUSHITA, Hiromasa HANZAWA *(Osaka University)* **and Yoshio NISHIDA** *(Osaka University)*

The NV center in synthetic Ib diamonds exhibits the characteristic zero-phonon line of luminescence at 637.5nm, which is attributed to a ^3A - ^3E transition. Some spectro-

scopic measurements, however, indicates that the other electronic states become involved in the optical cycle and effect the interpretation of the data. Then the luminescence decay time of the NV center was measured by using the picosecond excitation system at room temperature and around 5K. The decay profile with two expo
nential components of 2.0 ± 0.1nsec and 8.0 ± 0.2nsec has been obtained at room temperature. Around 5K, the long decay component becomes slightly long. The decay times observed at 637.5nm of the zero-phonon line and at 670nm in the phonon-side band are independent of wavelength. This value is compared with the previous value observed by the other workers.

II-J State Correlated Raman Spectroscopy

The vibrational Raman polarizability tensor responds to molecular reorientation, vibrational relaxation process, and the structural environment in condensed media. The measurement of Raman scattering is a powerful technique for the study of molecular motion and of the mechanism of phase transition. We've built up the system of multichannel type detection of Raman scattering conbined with the temperature-controlled cell.

II-J-1 Two Dimensional Raman Spectroscopic Study on the N-I Phase Transition of Liquid Crystal

Naoki HAYASHI and Tatsuhisa KATO

Microcanonical features of a liquid crystal molecule reflect on their macrocanonical properties. The critical temperature of the liquid crystal largely depends on its exact size and character of the substructure of a liquid crystal molecule. The series of liquid crystal molecules which have the same skeleton are investigated by the vibrational Raman spectroscopy. The change of the polarizabilities of the each vibrational line are recorded as the function of temperature in the process of the phase transition. The function of the polarizability for the each vibrational line exhibits the charateristic change in the process of the phase transition. The lines which are due to the normal coordinate having the specific vector against the molecular axis shows the irregular dependence on the inceasing of temperature in the process of the phase transition.

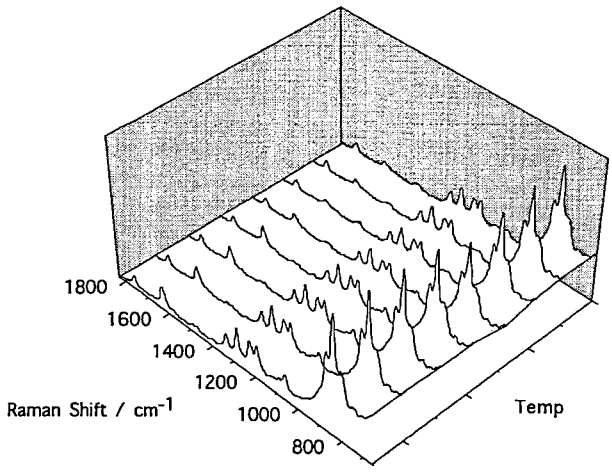


Figure 1.

II-J-2 FT-IR and FT-Raman Spectroscopies on Structural Characterization of 'Command Surfaces' LB Films and Photo-Regulation of Reorientation for Liquid Crystal Molecules

Naoki HAYASHI, Tatsuhisa KATO, Norihisa KATAYAMA *(Kitasato University)*, **Makio IWAHASHI***(Kitasato University)* **and Takahiro SEKI***(Tokyo Institute of Technology)*

Structural characterization and orientation of liquid crystals (LC) photo-regulated by azobenzene derivative Langmuir-Blodgett (LB) film has been studied by FT-IR and polarized Raman spectroscopy. The obtained Raman spectra of the LC cell suggest that the LC molecule reorients with conformational change of the LB film. It is also indicated that Raman spectroscopy is useful for the study of anisotropy and orientational order parameter of the LC. The intensity change of each band in FT-IR spectra is reflected by homeotropic-planer reorientation and orientational order of the LC molecule.

RESEARCH ACTIVITIES III
Department of Electronic Structure

III-A Ultrafast Intermolecular Electron Transfer

Ultrafast fluorescence quenching of excited dye molecules in neat electron-donating solvents is attributed to intermolecular electron transfer (ET). Accurate measurements of fluorescence decay are made with xanthenes and coumarins in anilines (aniline, N-alkylanilines and N,N-dialkylanilines) and some of deuterated homologues. It was found that there are significant effects of deuterium isotope effects in some solvents. To understand the role of solvent dynamics and intramolecular motion in ET, it is important to study the time dependence of the reaction in detail. We further studied deuterium isotope effects of deuterated methanol and found that the isotope effect of the hydroxyl group and methyl group was simply additive.

III-A-1 Dynamics in Intermolecular Electron Transfer

Keitaro YOSHIHARA, Haridas PAL, Hideaki SHIROTA *(Graduate Univ. for Advanced Studies)*, **Yutaka NAGASAWA** *(Graduate Univ. for Advanced Studies)* **and Keisuke TOMINAGA**

[*Ultrafast Phenomena X*, in press]

Ultrafast intermolecular electron transfer (ET) from electron donating solvents such as aniline, N-monoalkylanilines and N,N-dialkylanilines to a number of excited (S_1) coumarin dyes have been investigated using femtosecond fluorescence up-conversion technique. It has been observed that in many of these systems the ET processes occur with rates much greater than the inverse of the solvation times of the electron donating solvents. The effect of the substituents of the acceptor dyes and also of the donor solvents has been thoroughly investigated to understand the joint role of the solvent dynamical motions and the vibrational motions to govern the dynamics of these ET reactions. The effect of the deuterium isotopic substitution of both donor solvents and acceptor dyes has also been investigated to get more insight into the mechanistic details of these ultrafast ET dynamics. The results are analyzed within the frame work of two-dimensional ET model with the classical solvent and nuclear coordinates (Figure 1).

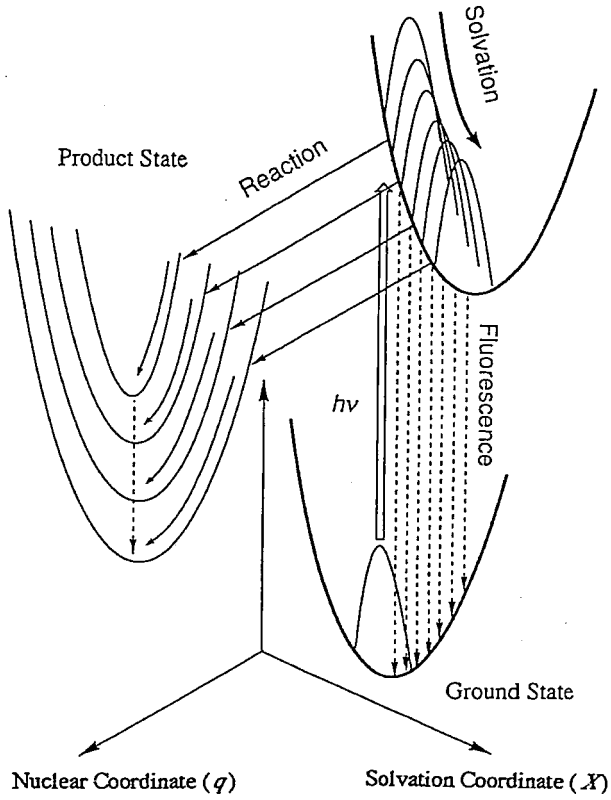


Figure 1. A conceptual picture of the two-dimensional model. Solvation occurs on the solvation coordinate (X) and ET occurs on the nuclear coordinate (q) with the participation of the high frequency vibrational mode as the accepting channels.

III-A-2 Deuterium Isotope Effect on Ultrafast Intermolecular Electron Transfer

Haridas PAL, Yutaka NAGASAWA *(Graduate Univ. for Advanced Studies)*, **Keisuke TOMINAGA and Keitaro YOSHIHARA**

[*J. Phys. Chem.* **100**,11964 (1996)]

Deuterium isotope effects on ultrafast intermolecular electron transfer (ET) from electron donating solvents such as aniline (AN) and N,N-dimethylaniline (DMA) to a number of excited (S_1) coumarin dyes have been investigated by femtosecond fluorescence up-conversion technique. We carry out investigations using both normal and deuterated solvents and the normal and deuterated coumarin dyes. With perdeuterated AN (AN-d7) or aminodeuterated AN (AN-d2) we observe almost the same extent of reduction in the ET rate constants in comparison

to those in normal AN as shown in Figure 1. In the case of DMA we do not observe any isotope effect on substituting all the N-methyl group hydrogens by deuterium (DMA-d6). Using deuterated coumarins, where the 7-amino group hydrogens are substituted by deuterium, we do not observe any change in the ET dynamics. The effect of isotopic substitution of AN on the ET dynamics has been discussed in terms of the several ET parameters. From cyclic voltammetric measurements it is indicated that the isotopic substitution of the solvent AN causes a reduction in the driving force for the ET processes. It is inferred that the differences in the driving force for the normal and the deuterated AN as the donor solvents mainly arise from the solvent structural effects, caused by the intermolecular hydrogen bondings in this solvent. The present results have also been correlated well with the theoretical predictions by the two-dimensional ET model.

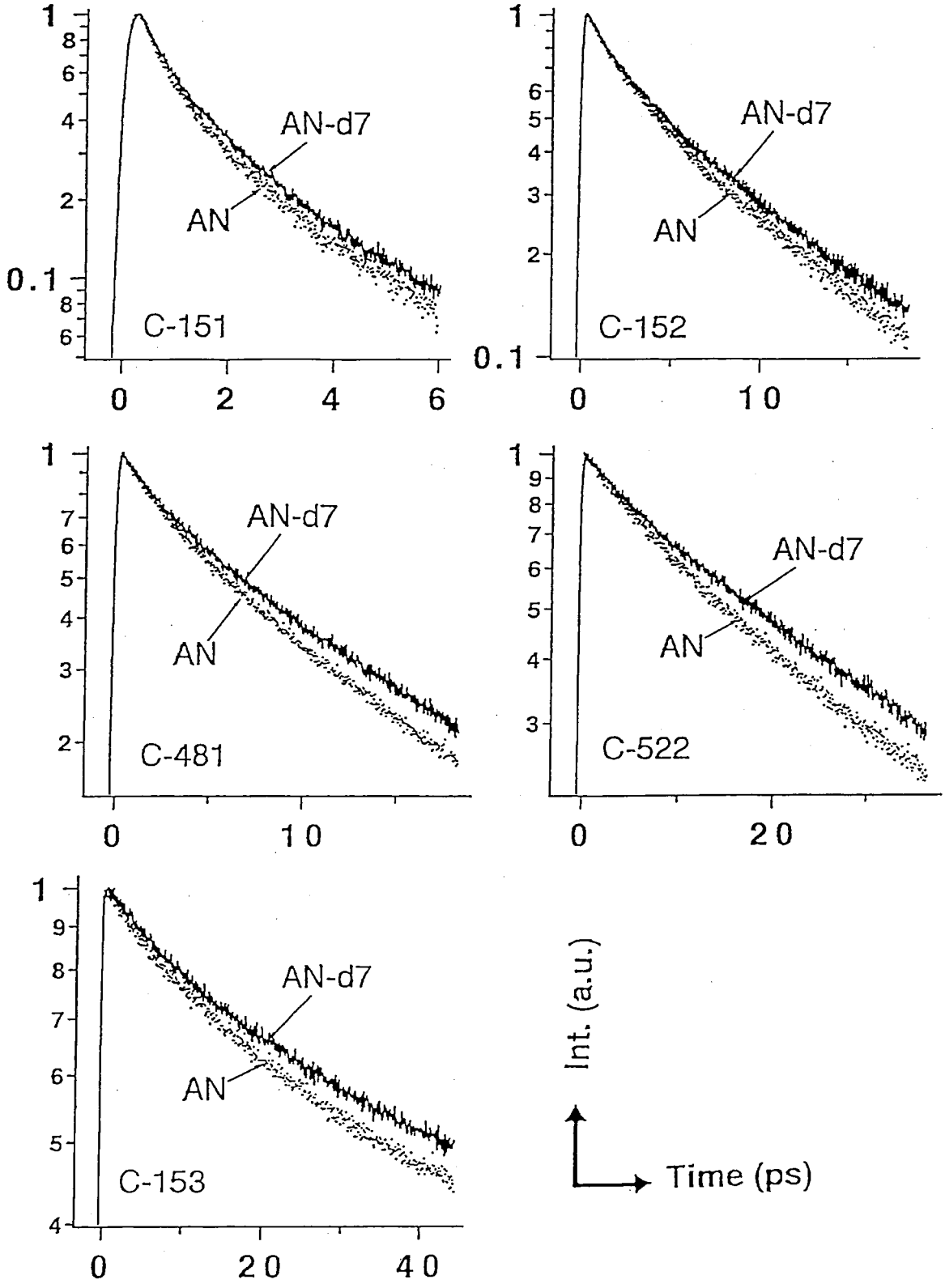


Figure 1. Comparison of the fluorescence decays of coumarines in aniline (AN) (dotted lines) and AN-d_7 (solid lines). For all coumarins the decays are slower in AN-d_7 than AN.

III-A-3 Deuterium Isotope Effect on the Solvation Dynamics of Methanol: CH_3OH, CH_3OD, CD_3OH, and CD_3OD

Hideaki SHIROTA *(Graduate Univ. for Advanced Studies)*, **Haridas PAL, Keisuke TOMINAGA and Keitaro YOSHIHARA**

[*J. Phys. Chem.* **100**, 14575 (1996)]

We have investigated the deuterium isotope effects on the solvation dynamics of methanol by using the femtosecond fluorescence up-conversion technique. Deuterated methanols (CH_3OD, CD_3OH and CD_3OD) show slower solvation dynamics than normal methanol. The obtained solvation parameters are listed in Table 1. The important points to be noted from Table 1 are: (i) The average solvation time is increased by about 10% on deuterium substitution of the hydroxyl hydrogen. (ii) The average solvation time is increased by about 5% on deuterium substitution of the methyl hydrogens. (iii) The isotope effects arising from the hydroxyl group and methyl group behave independently and do not interfere each other; the two effects appear to be simply additive. We suggest that the isotope effect of the OH group on the solvation dynamics is arising from the effect of hydrogen-bonding effect and that of the CH_3 group on the solvation dynamics is arising from the frictional effect.

solvent	a_{s1}	τ_{s1} (ps)	a_{s2}	τ_{s2} (ps)	a_{s3}	τ_{s3} (ps)	$\langle\tau_s\rangle^b$ (ps)	$\langle\tau_s\rangle$(D)/$\langle\tau_s\rangle$(H) total	OD/OH	CD_3/CH_3
CH_3OH	0.29	0.18	0.31	1.96	0.40	15.36	6.80			
CH_3OD	0.30	0.17	0.31	2.12	0.39	17.31	7.46	1.10	1.10	
CD_3OH	0.27	0.17	0.33	2.01	0.40	15.99	7.11	1.05		1.05
CD_3OD	0.29	0.20	0.32	2.12	0.39	18.03	7.77	1.14	1.09	1.04

a Error limit in τ is ± 0.05 ps.

b $\langle\tau_s\rangle = a_{s1}\tau_{s1} + a_{s2}\tau_{s2} + a_{s3}\tau_{s3}$; $a_{s1} + a_{s2} + a_{s3} = 1$.

III-B Liquid Dynamics Studied by Higher Order Nonlinear Spectroscopy

We have developed techniques to observe higher order (fifth and seventh order) nonlinear optical response from liquids to investigate microscopic dynamics and structures of liquids. The experiments include vibrational echo-type experiments for high- and low-frequency modes and overtone dephasing experiments for high-frequency modes. The vibrational echo-type experiments are temporally two-dimensional spectroscopy and can determine the relative importance of inhomogeneity of the spectral broadening. The overtone dephasing experiments allow us to investigate the vibrational quantum number dependencies of the dephasing mechanisms.

III-B-1 Fifth-Order Nonlinear Spectroscopy on the Low-Frequency Modes of Liquid CS_2

Keisuke TOMINAGA and Keitaro YOSHIHARA

[*J. Chem. Phys.* **104**, 4419 (1996)]

We have observed fifth order optical response from liquid CS_2 by six-wave mixing with five different short pulses and investigated the inhomogeneity in the spectral broadening of the low-frequency intermolecular vibrational modes. There are a couple of distinct differences in the time profile of the fifth order signal from that of the third order signal. The fifth and third order signals obtained experimentally are compared with the prediction by the theory of Tanimura and Mukamel. We simulate the third and fifth order signals in the two cases, the homogeneous limit case and the partially inhomogeneously broadened case with a Gaussian distribution function. The experimental results can be reproduced well in terms of two vibrational modes, one overdamped mode in the homogeneous limit and one underdamped mode with an inhomogeneous width of 2.5 ps^{-1}.

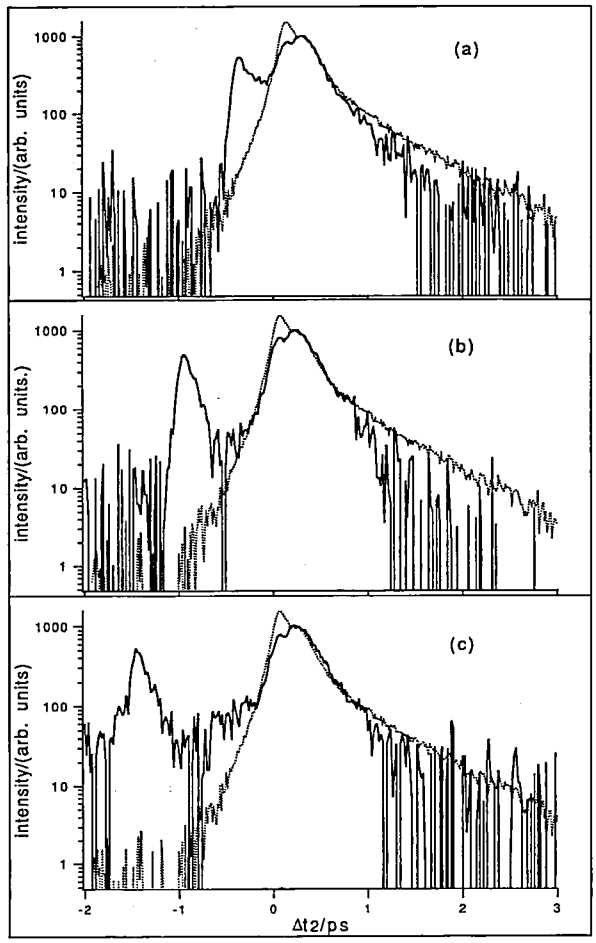


Figure 1. Solid lines: fifth order response signal from CS_2 as a function of Δt_2 with different Δt_1. Values of Δt_1 are shown in the figure. Broken lines: The impulsive stimulated light scattering signal from CS_2. The signal intensities are shown in a log scale.

III-B-2 Temporally Two-Dimensional Femtosecond Spectroscopy of Binary Mixture of CS_2

Keisuke TOMINAGA and Keitaro YOSHIHARA

[*J. Chem. Phys.* **104**, 1159 (1996)]

We have studied the inhomogeneity of the low-frequency modes of binary mixtures of CS_2 with various cosolvents by the temporally two-dimensional spectroscopy with femtosecond pulses. The inhomogeneity in the underdamped mode is found to be decreased upon dilution for all the solvents investigated.

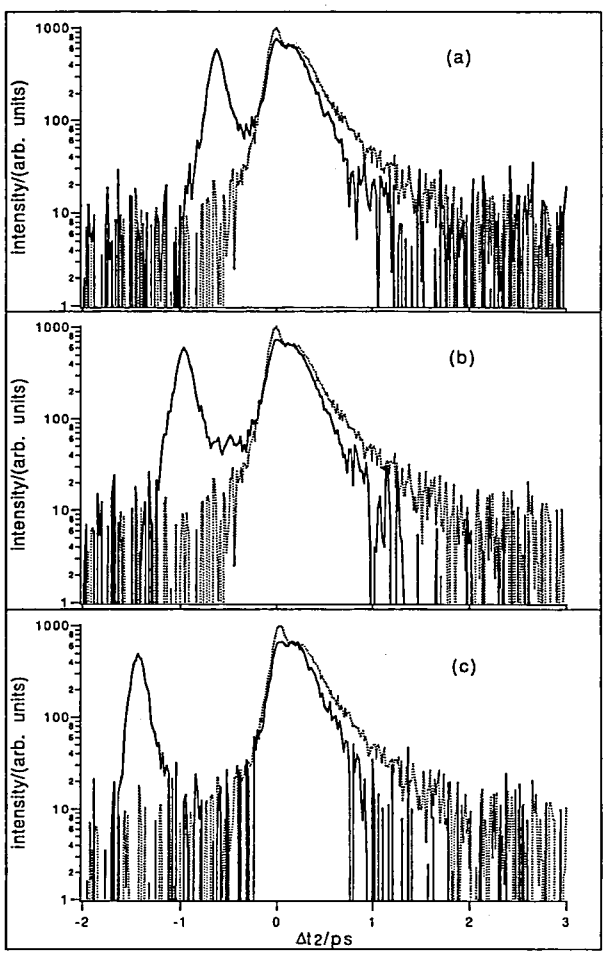


Figure 1. Solid lines: Fifth order signal from a binary mixture of CS_2 with methanol-d_4 (1:2 mol/mol) as a function of Δt_2 with different Δt_1. Δt_1 is (a) 0.50, (b) 1.00, and (c) 1.50 ps. Dotted lines: The ISS signal from the same binary mixture.

III-B-3 Overtone Vibrational Dephasing in Liquids Studied by Femtosecond Fifth-Order Nonlinear Spectroscopy

Keisuke TOMINAGA and Keitaro YOSHIHARA

[*Phys. Rev. Lett.* **76**, 987 (1996)]

We have directly observed vibrational dephasing of the first overtone bands in liquids by the femtosecond fifth-order nonlinear spectroscopy for the first time to our knowledge. The overtone and fundamental dephasing processes have been studied for the C-D stretching of $CDCl_3$ and the *sym*-methyl stretching of CD_3I in neat liquid and in its binary mixture with $CHCl_3$. Simulations based on the simple stochastic theory or the perturbation theory for a harmonic oscillator do not explain both of the overtone and fundamental dephasing simultaneously.

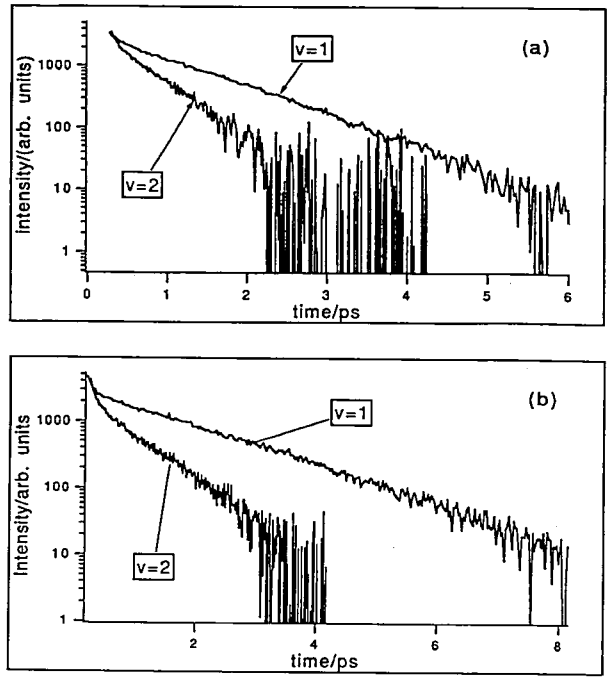


Figure 1. Time-profiles of the vibrational dephasing of the first overtone and fundamental bands of (a) the C-D stretching of $CDCl_3$ and (b) the *sym*-methyl stretching of CD_3I in neat liquids.

III-B-4 Temporally Two-Dimensional Overtone Vibrational Dephasing Spectroscopy in Liquids

Keisuke TOMINAGA and Keitaro YOSHIHARA

[*Phys. Rev. A.* in press]

A temporally two-dimensional overtone vibrational dephasing spectroscopy, which is based on the fifth order nonlinearity, is proposed to investigate correlation between fluctuations of different vibrational frequencies in liquids. The experiment is done for the C-D stretching of neat $CDCl_3$ liquid. We found that a signal decay as a function of the second pulse interval gets faster as the first pulse interval increases.

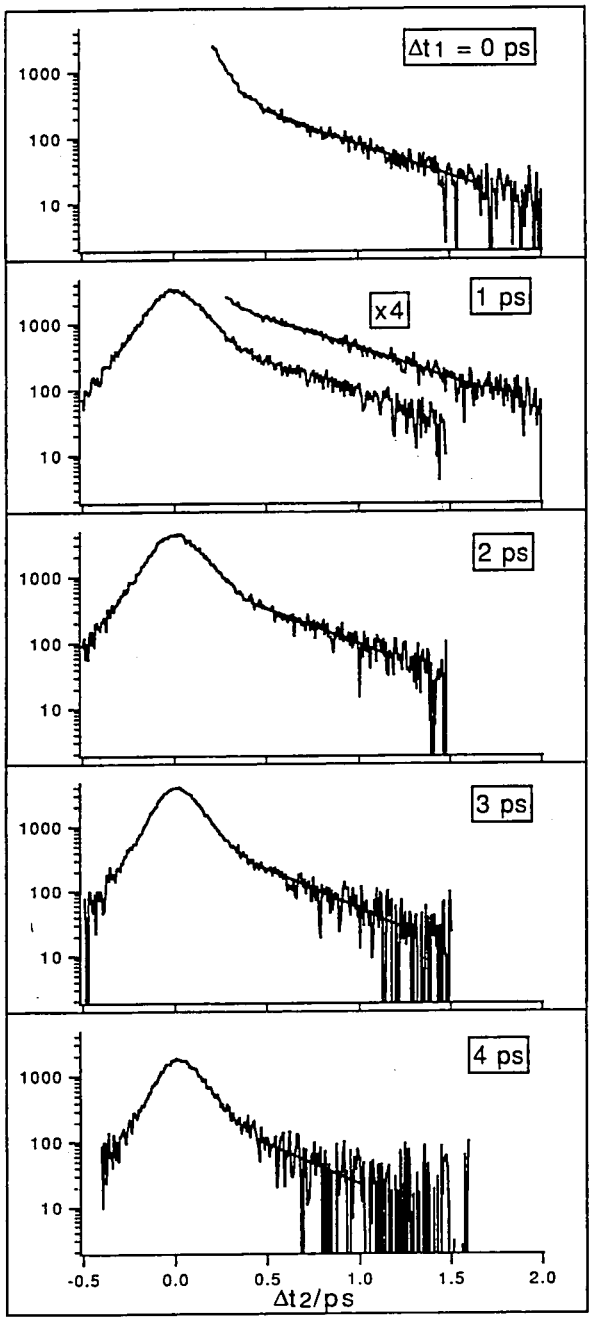


Figure 1. Time profiles of the two-dimensional overtone vibrational dephasing signal for the C-D stretching of $CDCl_3$ as a function of Δt_2 with fixed Δt_1. The Dt_1 values are shown in the figure. The best fits to the vibrational part of the signal by an exponential function is shown.

III-C Development of Ultrafast Fluorescence Up-Conversion Technique

The development of lasers with ultra-short pulses permits, in principle, to study chemical processes with time resolution same as laser pulse duration. Nevertheless, up to now the best time resolution (FWHM) of fluorescent up-conversion technique, achieved in the world, is not better than 100 fs, despite of the fact that many laboratories have lasers with pulses shorter than 50 fs. The main problems are pulse broadening in harmonic generation and signal broadening in up-conversion crystal.

We have developed the fluorescence up-conversion system with record time resolution of 70 fs - FWHM of cross-correlation function. For this setup we used chromium-doped forsterite (Cr^{4+}:Mg_2SiO_4) laser which has been developed in our group. Using this setup it is now possible to study ultrafast molecular dynamics with measuring the fluorescence of excited molecules. The initial stages of very fast electron transfer processes is investigated.

III-C-1 Femtosecond Fluorescence Up-Conversion System with Time Resolution Better Than 80 fs (FWHM)

Igor V. RUBTSOV *(Inst. Chem. Phys. in Chernogolovka, Russian Acad. and IMS)*, **Jangseok MA, Haridas PAL, Hideaki SHIROTA** *(Graduate Univ.for Advanced Studies)* **and Keitaro YOSHIHARA**

We construct the fluorescence up-conversion system with an apparatus function reached 70 fs with the full width at half-maximum (FWHM). The solid-state chromium-forsterite femtosecond laser working in cavity dumped operation was used. We use second harmonic

(λ = 635 nm,τ_{FWHM} = 43 fs, E = 3 nJ) for excitation of molecules and fundamental (λ = 1270 nm, τ_{FWHM} = 55 fs, E = 30 nJ) as a gate pulse. The sum frequency were generated in type-I BBO crystal of 0.3 or 0.5 mm thickness. We use two additional prism pair compression stages: one for fundamental and theother for second harmonic. The broadening of the cross-correlation function at the up-conversion crystal cannot be compensated and determined by the type of the crystal and its thickness. For a BBO crystal (0.3 mm) and wavelength region around 700 nm this broadening is not larger than 20 fs.

As an example, we present here the fluorescence decay signal of oxazine-1 (OX-1) in electron donating solvent N,N-dimethylaniline (DMA). As has been shown previously[1], the electron transfer in this system is very fast, and obtained values were determined by instrument function (~250 fs). Now we observed two exponential fluorescence decay (Figure 1) with the main component of 80 fs (~95%) and small slow part of ~500 fs.

Reference

1) Y. Nagasawa, A. P. Yartsev, K. Tominaga, A. E. Johnson, and K. Yoshihara, *J. Chem. Phys.* **101**, 90 (1994).

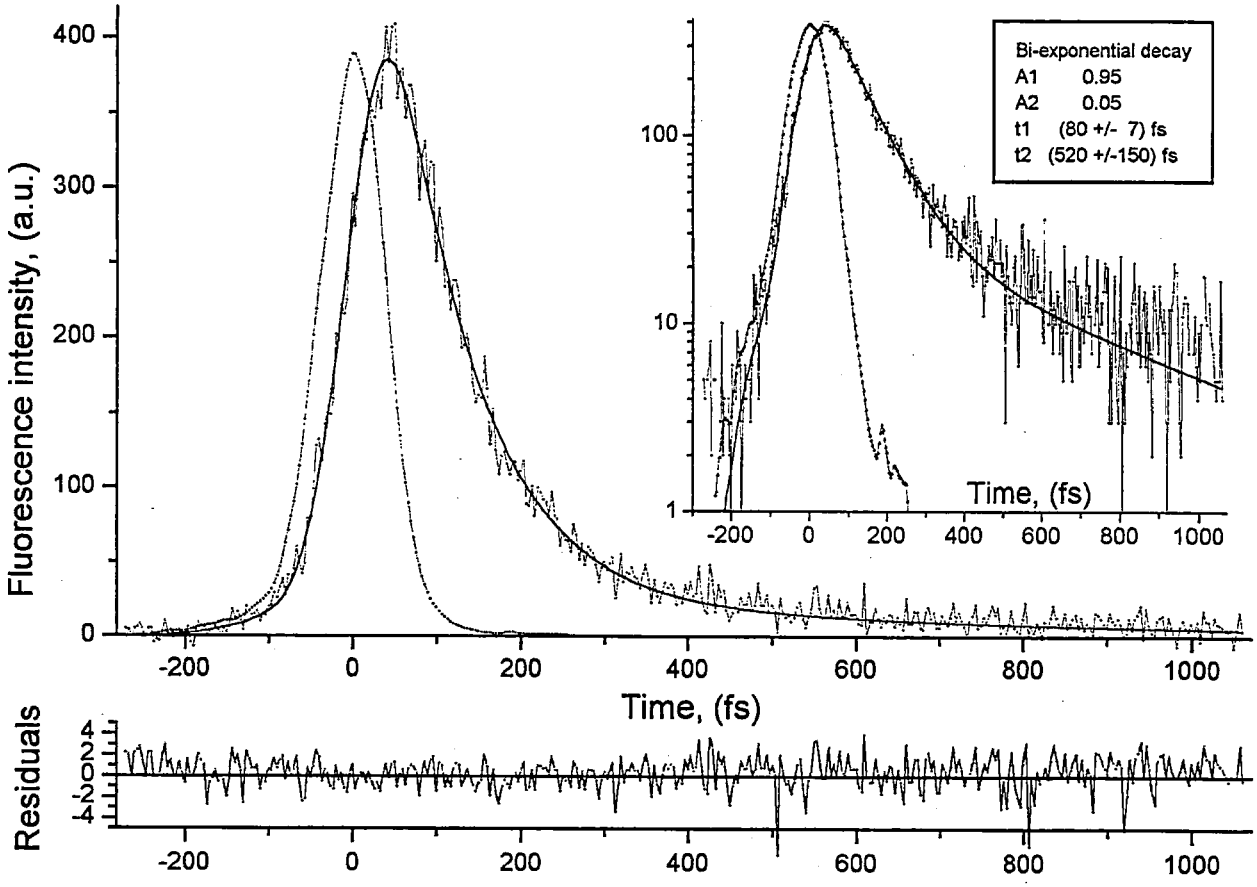


Figure 1. Fluorescence up-conversion data of OX-1 in DMA, measured at 450 nm (corresponds to the 695 nm of fluorescence). Cross-correlation function is also shown. Solid line is the best fitted two exponential curve. In the inset - same signal in a logarithmic scale.

III-D Ultrafast Dynamics of UV-Photoexcited Simple Molecules in Solution by Femtosecond Transient Absorption Spectroscopy

We have studied photoinduced primary processes of molecules in solution such as photodissociation, isomerization, and so on. In order to understand these processes suffering continuous interactions from solvent, the time-resolved observation of photoproducts is very useful. Simple molecules have been chosen as samples, whose first absorption bands are in the UV region. The comparative studies of dynamics of such simple molecules well studied on the isolated condition can help to make clear the characteristic feature in solution. On the following three systems, we have used the common apparatus measuring the transient absorption based on the femtosecond regeneratively amplified Ti:Sapphire laser. The third harmonic of fundamental output is used as the pump pulse and the white light continuum, which is generated by focusing the fundamental or second harmonic pulse into D_2O flow cell, is used as the probe pulse. We can get absorption change of transients at a given wavelength using interference filters and/or as a spectrum using a monochromator with a multichannel diode array.

III-D-1 Photoinduced Chemical Reaction in Neat CH_3I

Yukito NAITOH and Keitaro YOSHIHARA

In order to study the chemical reaction dynamics in solution, we need to control the encounter of reactants. However, under usual conditions, it is difficult because the translational diffusion of solute controls the rate of

chemical reactions and it takes longer time than the actual reaction time. If we can prepare such a condition of photoexcitation of a solute molecule as one reactant and a solvent molecule as the other reactant, the transition state of chemical reaction in solution could be studied in principle in bimolecular reations in solution. Such condition could be fulfilled for the photochemical reaction in neat liquid.

We have studied I_2 formation in neat CH_3I by UV excitation. This starts from photodissociation of CH_3I followed by the reaction between the photofragment $I^*(^2P_{1/2})$ and solvent CH_3I. We have probed the transient absorption of product I_2 corresponding to the B-X transition at several wavelengths in the visible region. These consist of rapid rise and slow decay. Recently, we also have observed the transient absorption spectrum and ascertained a time-dependent shift from red to blue occured in the ultrafast time region. It appears that, as the reaction goes on, the ground state potential of I_2 gets more stable than the B state in the neat CH_3I. On the other hand, the slow decay has a similar time constant (10~20 ps) at all observed wavelengths. We can regard this decay as the disappearance of I_2 due to the reverse reaction. The cluster spectroscopic study claims that this reaction is not a stepwise one, but a concerted one in the CH_3I dimer. To examine whether the scheme is true in solution phase, the experiment in the dilute solution of CH_3I is in progress.

III-D-2 Photoinduced Reactions of CH_2I_2 in Solution Studied by the Ultrafast Transient Absorption Spectroscopy

Ken-ichi SAITOW *(Graduate Univ. for Advanced Studies)*, **Yukito NAITOH, Keisuke TOMINAGA and Keitaro YOSHIHARA**

[*Chem. Phys. Lett.*, **262**, 621 (1996)]

We have studied the photoinduced reaction of CH_2I_2 upon excitation at 268 nm in solution by the femtosecond transient absorption spectroscopy. As shown in Figure 1, the time profile of transients observed at 400 nm consists of three components; fast rise (200 fs), fast decay (500 fs), and slow rise (7-13 ps). The first two components are independent of the solute concentrations and are assigned to generation of CH_2I radical by direct photodissociation of CH_2I_2 and disappearance due to the geminate recombination in the solvent cage. The slow rise becomes faster by increasing concentrations, and we have assigned it to formation of charge transfer complex (CT-complex) between the photofragment I and CH_2I_2. This is followed by full electron transfer from CH_2I_2 to I to cause $CH_2I_2^+$, which has an absorption band around 400 nm. If formation of the CT-complex were due to the translational diffusion, it would have taken 5-100 ns in the present concentration range. We consider CH_2I_2 aggregates is formed in solution and this introduces CT-complex in the picosecond time scale.

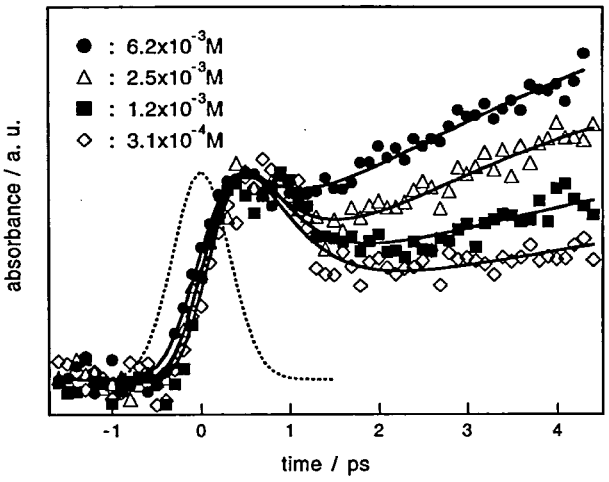


Figure 1. Transient absorption of photoproducts upon photoexcitation of CH_2I_2 at 268 nm in CH_3CN probed at 400 nm. Concentrations are from $3.1x10^{-4}$ to $6.2x10^{-3}$M. Solid lines are the fits of experimental data with a convolution of the instrumental response function and a three-exponential function. Absorbance is normalized at the peak of the fast rise. Dashed line represents the instrument response function constructed by the rise of rhodamine 6G in ethanol.

III-D-3 Ultrafast Dynamics of Photoexcited trans-1,3,5-Hexatriene in Solution

Kaoru OHTA *(Kyoto Univ. and IMS)*, **Yukito NAITOH, Ken-ichi SAITOW** *(Graduate Univ. for Advanced Studies)*, **Keisuke TOMINAGA, Noboru HIROTA** *(Kyoto Univ.)* **and Keitaro YOSHIHARA**

[*Chem. Phys. Lett.* **256**, 629 (1996)]

We have investigated the ultrafast dynamics of trans-1,3,5-hexatriene in cyclohexane and acetonitrile solutions by femtosecond transient absorption spectroscopy. After the photoexcitation to the S_2 state (1^1B_u), we observed the transient absorptions in the visible region as displayed in Figure 1. They consist of the instantaneous rise (<150 fs) and subpicosecond decay at each wavelength. The observed signal at 400 nm decays at about 400 fs. At longer wavelengths, the decay becomes faster and reaches the instrumental response function at the probe wavelengths longer than 450 nm. The instantaneous rise of the signal corresponds to the internal conversion from the S_2 to S_1 state and the dependence of the decay on the probe wavelength is attributed to the vibrational energy redistribution process in the S_1 state. We also measured the bleach recovery processes by one-color pump-probe experiment. The transient shows an instrument-limited appearance of a bleach followed by the recovery which occurs in three time scales. The first two recovery times are around 1 ps and 15-20 ps. The first one indicates that it takes 1 ps to observe the population of the vibrationally excited S_0 state at 268 nm. The second one comes from the vibrational relaxation in the S_0 state. The time constant of the third component is around 150-300 ps. One possible origin is a conformation change around the C-C single bond. After photoexcitation, s-cis isomer is produced in the excited state or in the vibrationally excited ground state and returns back to the original s-trans one in a 150-300 ps.

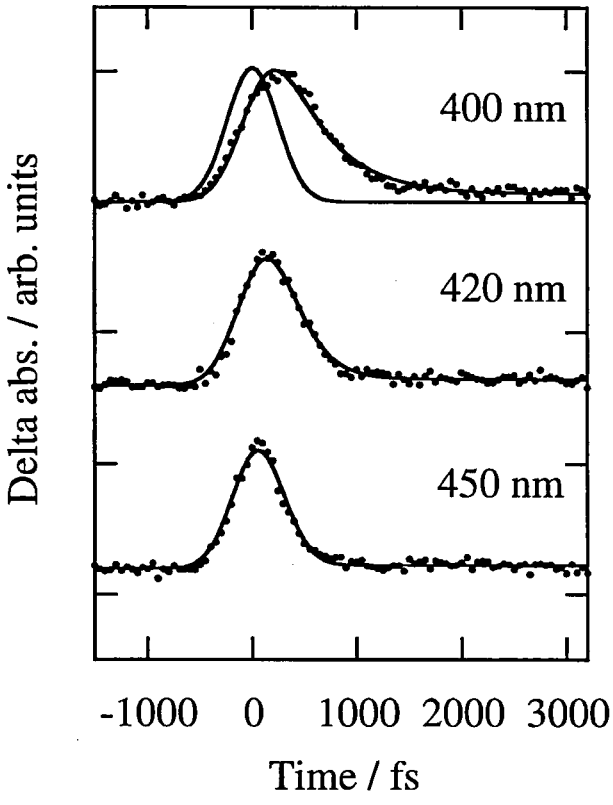


Figure 1. Transient absorption signals probed at three different wavelengths for trans-1,3,5-hexatriene in cyclohexane. The instrumental response function is shown in the top decay curve. The solid lines represent the best fits to the data by the convolution of the instrumental response function with an exponential function.

III-E Primary Energy and Electron Transfers in Photosystem I Reaction Center Complex

The primary processes of photosynthesis involve light energy absorption, electronic excitation energy transfer (excitation transfer), and charge separation across the photosynthetic membrane. In photosystem I (PS I) reaction center (RC) pigment-protein complex of plants and cyanobacteria, the charge separation is a series of electron transfers starting from the lowest excited singlet state of the primary electron donor chlorophyll (P700*). The time constants of electron transfers have been proposed as:

$$\text{P700}^* \xrightarrow{< 6.5\ \text{ps}} A_0 \xrightarrow{20\text{ - }32\ \text{ps}} \text{phylloquinone} \xrightarrow{20\text{ - }260\ \text{ns}} F_X \rightarrow F_B/F_A ,$$

where A_0 is the electron acceptor chlorophyll *a* and F_X, F_A and F_B are iron-sulfur centers. The most recent X-ray analysis on the crystal structure of PS I RC has shown similar arrangements of the electron carriers to those of purple bacterial RC. P700 seems to be a pair of chlorophyll *a* molecules (Chl). Four chlorophyll *a* molecules are located at analogous positions to those of two bacteriochlorophylls (B_L and B_M) and two bacteriopheophytins (H_L and H_M) in the RCs of purple bacteria. A_0 may occupy the position equivalent to that of the electron carrier bacteriopheophytin (H_L) in the purple bacterial RC.

The excitation transfer and charge separation from and to P700 are most crucial in modeling of excitation equilibration and charge separation. However, due to the spectral congestion of more than 100 Chl, it has been difficult to trace the excitation transfer and the subsequent electron transfer on specific Chl form in PS I RC retaining many antenna Chls. Enrichment of P700 in PS I RC would enable one to selectively excite P700 and observe the subsequent primary processes.

It is also interesting to study the free-energy-gap-dependence of the electron transfer reaction in RC. The results will be interpreted by electron transfer theories. Reconstitutions of various artificial quinones in place of phylloquinone have enabled us to observe the so-called inverted region in the highly negative ΔG^0 reaction.

III-E-1 Excitation and Electron Transfer from Selectively Excited Primary Donor Chlorophyll (P700) in Photosystem I Reaction Center

Shigeichi KUMAZAKI, Isamu IKEGAMI *(Teikyo Univ.)* **and Keitaro YOSHIHARA**

[*J. Phys. Chem.*, in press]

The primary processes in photosystem I reaction center were studied by fluorescence up-conversion with a subpicosecond time resolution at room temperature. The sample was P700 (primary donor chlorophyll)-enriched particles which contained 14 chlorophylls per P700. Upon selective excitation of P700 at 701 nm, anisotropy of the fluorescence at 749 nm decayed from 0.3 to 0.15 with a time constant of 1 ps (Figure 1(a) and (b)). The dynamic depolarization is attributed to electronic excitation equilibration between P700 and surrounding chlorophylls. In the isotropic fluorescence kinetics, at least two decaying

components of 2.2 ps (≈ 35 %) and 15 ps (≈ 55 %) were found (Figure 1(c)). Compared with the rise of $P700^+A_0^-$ with a time constant of 6.5 ps,[1] the fast and slow components indicate the charge separation before and after full equilibration of excitation energy, respectively. A kinetic model calculation based on the above results supports the following kinetic features: (1) excitation transfer from P700 to shorter-wavelength-absorbing chlorophylls is as fast as the primary charge separation even after the selective excitation of P700, (2) a lower limit for the intrinsic rate constant of the primary charge separation from P700* is estimated to be $(4\ ps)^{-1}$.

Reference

1) S. Kumazaki, H. Kandori, H. Petek, K. Yoshihara and I. Ikegami, *J. Phys. Chem.* **98**, 10335, (1994).

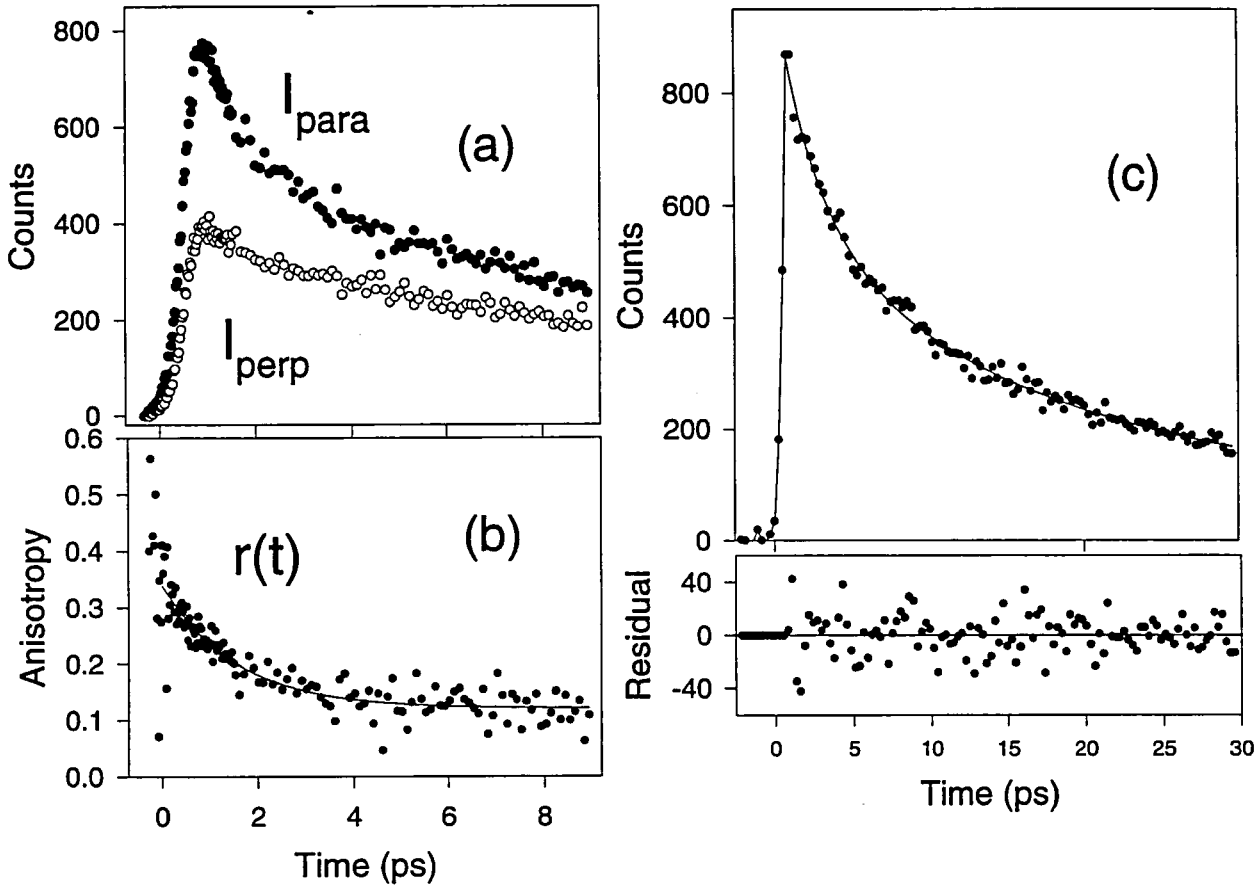


Figure 1. (a) Polarization-dependent fluorescence decays of P700-enriched reaction center upon selective excitation of P700. The sample was excited at 701 nm and the fluorescence was detected at 749 nm. Fluorescence polarized parallel (closed circles) or perpendicular (open circles) to the excitation polarization. (b) Raw experimental anisotropy (dots: $r(t)=(I_{para}-I_{perp})/(I_{para}+2*I_{perp})$) calculated from the data in (a), and a single exponential fit. (c) Isotropic fluorescence decay detected at 749 nm upon excitation at 701 nm. Data (dots) are compared with a convoluted curve of a double-exponential function with the instrumental response function (line).

III-E-2 ΔG^0 Dependence of the Electron Transfer Rate in Photosynthetic Reaction Center of Plant Photosystem I: Natural Optimization of Reaction between Chlorophyll *a* (A_0) and Quinone

Masayo IWAKI *(NIBB)*, **Shigeichi KUMAZAKI, Keitaro YOSHIHARA, Tatsuo ERABI** *(Tottori Univ.)* **and Shigeru ITOH** *(NIBB)*

[*J. Phys. Chem.* **100**, 10802 (1996)]

The rate of the electron transfer reaction from the reduced primary electron acceptor chlorophyll *a* (A_0^-) to the secondary acceptor quinone (Q) was measured by ps-ns laser spectroscopy at 280 K in the photosynthetic reaction center (RC) complex of plant photosystem I (PS I). The free energy change (ΔG^0) of the reaction was varied between -1.1 and +0.2 eV by the reconstitution of thirteen different quinone/quinoid compounds after the extraction of the intrinsic phylloquinone. Phylloquinone and its natural analog menaquinone, both of which show the ΔG^0 value of -0.34 eV, gave the highest rate constant (k) of $(23\ ps)^{-1}$. Analysis of log k versus ΔG^0 plot according to the quantum mechanical electron transfer theory gave the total reorganization energy (λ_{total}) of 0.30 eV and the electronic coupling (V) of 14 cm^{-1} (Figure 1). The natural system is shown to be highly optimized to give a $\Delta G^0 = -\lambda_{total}$. The λ_{total} value is smaller and the V value is larger than those estimated in the corresponding reaction between the reduced primary acceptor bacteriopheophytin (H^-) and the secondary acceptor ubiquinone (Q_A) in the purple bacterial RC complex.[1] It is concluded that the $A_0^-Q \rightarrow A_0Q^-$ reaction in PS I RC occurs in the protein environments, which give a low dielectric property, with a shorter electron transfer distance compared to the reaction between H^- and Q_A.

Reference

1) M.R. Gunner and P.L. Dutton, *J. Am. Chem. Soc.* **111**, 3400 (1989).

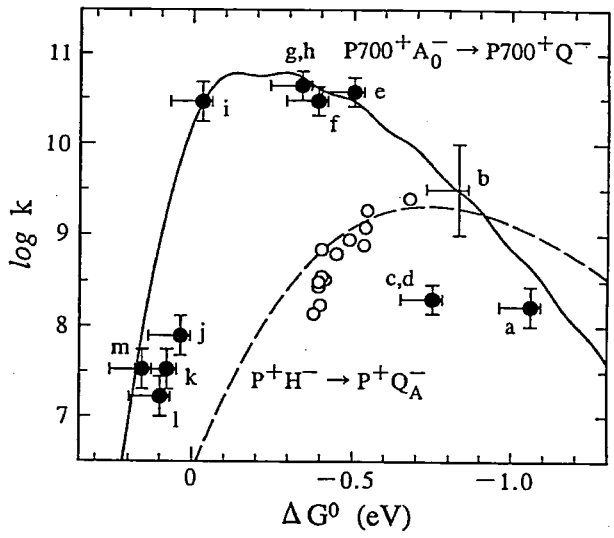


Figure 1. Logarithmic plot of the rate constant (●) vs. free energy difference for $P700^+A_0^- \rightarrow P700^+Q^-$ reaction in the PS I RCs with reconstituted quinones. The same plot (○) for the $P^+H^- \rightarrow P^+Q_A^-$ reaction in purple bacterium *Rb. sphaeroides* RCs, with different reconstituted quinones, is also shown.[1] The solid and dashed lines are the fits obtained by using a quantum mechanical electron transfer theory.

III-F Dynamic Behavior of Electronic Excited States

Optical excitation of molecules to electronically excited states causes a variety of dynamical behavior, depending upon the nature of electronic structures of molecules and their and environments, such as energy transfer, proton transfer, chemical reaction, radiationless transition, ionization, and others. Most of these processes fall into the nanosecond, picosecond and femtosecond times scales. In this chapter we firstly discuss our observation of exciton dynamics of dye aggregates and their relations to dimensionality of aggregation. Secondly we report electron transfer dynamics from excited dye to the substrate TiO_2.

III-F-1 Temperature Dependent Radiative Lifetime of J-Aggregates

Valey K. KAMALOV *(Inst. Chem. Phys. Russian Academy of Sciences and IMS)*, **Irina A. STRUGANOVA** *(Laser for Photochemistry Ltd.)* **and Keitaro YOSHIHARA**

[*J. Phys. Chem.* **100**, 8640 (1996)]

The emission quantum yield of carbocyanine dye J-aggregates decreased 4-fold when temperature increased from 20K to 80K. Independent measurements of emission quantum yield and decay were used to elucidate both radiative and nonradiative rate constants in the temperature range of 4-140K. The radiative lifetime is found linearly increases as temperature rises as shown in Figure 1. This is explained by the two-dimensional structure of J-aggregates assuming thermal distribution of excitons with the requirement that only excitons with a small value of the center-of-mass wave can recombine radiatively. Nonradiative relaxation becomes efficient with a rise of temperature and is explained by exciton self-trapping.

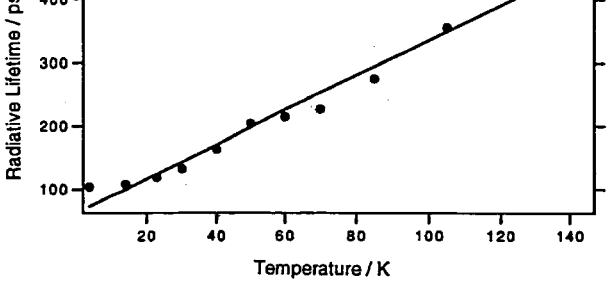


Figure 1. Temperature dependence of the radiative lifetime of BIC J-aggregates in the PVA film.

III-F-2 Femtosecond Electron-Transfer Dynamics at a Sensitizing Dye-Semiconductor (TiO_2)

Julie M. REHM *(Univ. of Rochester)*, **George L. MCLENDON** *(Univ. of Rochester)*, **Yutaka NAGASAWA** *(Graduate Univ. for Advanced Studies)*, **Keitaro YOSHIHARA, Jacques MOSER***(Ecole Polytechnique Federale, Lausanne)* **and Michael GRAETZEL***(Ecole Polytechnique Federale, Lausanne)*

[*J. Phys. Chem.* **100**, 9577 (1996)]

The charge injection dynamics of dye sensitization from a surface-bound dye (coumarin 343 (C343)) to the conduction band (CB) of the TiO_2 is reported here for the first time. Ultrafast fluorescence dynamics demonstrate that the charge separation from C343 to the CB of TiO_2 occurs on a time scale of ca. 180 fs measured by fluorescence up-conversion method as shown in Figure 1. The charge injection efficiency is attributed to strong electronic coupling between the dye and TiO_2 energy level. The results yield a rate of injection of 5×10^{12} s^{-1}.

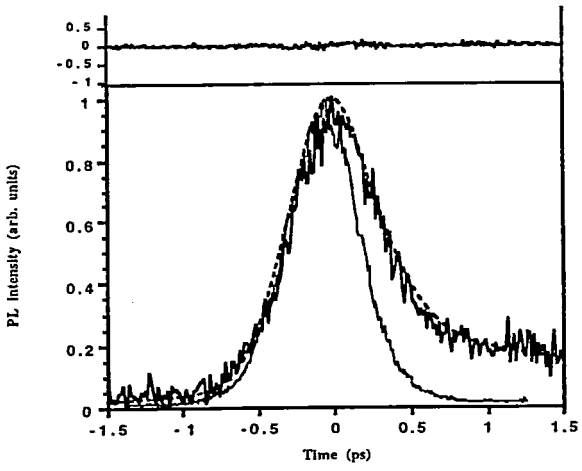


Figure 1. Fitted ultrafast fluorescence up-conversion signal of a sensitized TiO_2 solution. The sample is $1x10^{-4}$ M C343, 1 g/L TiO_2 in 95:5 H_2O:aceton monitored at 480 nm. The excitation wavelength was 400 nm. The two component fit, ca. 180 fs (95%) and >5 ps, is shown as well.

III-G Photochemistry on Well-Defined Surfaces

Upon the irradiation of light in the wavelength range from visible to ultraviolet, a number of adsorbed molecules on metal surfaces reveal variety of photochemical processes, including photo-stimulated desorption, rearrangement of adsorbed states, photodissociation, and photo-initiated reactions with coadsorbates. A central and fundamental question in the surface photochemistry is to clarify how adsorbate-substrate systems are excited by photon irradiation. In addition, since photo-initiated reactions can be induced without any thermal activation of reactants, they may provide good opportunities for studying a new class of surface reactions which may not be induced thermally. We have studied photochemistry of various adsorption systems on well-defined metal and semiconductor surfaces mainly by temperature-programmed desorption (TPD), X-ray photoelectron spectroscopy (XPS), work function measurements, Near edge x-ray absorption fine structure (NEXAFS) and angular-resolved time-of-flight (TOF) spectroscopy of photodesorbed species associated with pulsed laser irradiation. In this year, we have focused on the excitation mechanism in uv-photochemistry of methane by measuring polarization dependent cross sections.

III-G-1 Adsorbate-Localized Excitation in Surface Photochemistry: Methane on Pt(111)

Kazuo WATANABE, Kyoichi SAWABE and Yoshiyasu MATSUMOTO

[*Phys. Rev. Lett.* **76,** 1751 (1996)]

Methane on Pt(111) dissociates or desorbs under irradiation by 193-nm photons. The polarization-dependent cross sections of the photochemical processes have been measured as a function of the incident angle by using post-irradiation temperature-programmed desorption. Figure 1 shows that the incident-angle dependence of the cross sections obtained with *p* polarization substantially deviates from that of the substrate absorbance. This clearly indicates that an adsorbate-localized excitation plays an important role in the photochemistry of methane.

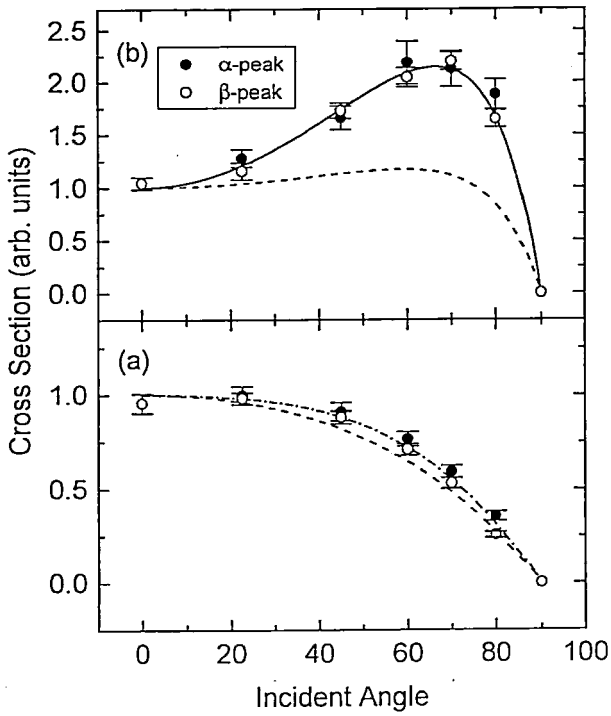


Figure 1. Incident-angle(γ) dependence of photochemical cross sections determined by using the α(solid circles) and the β (open circles) desorption peaks in post-irradiation TPD with various numbers of photons incident on the surface. The impinging light was polarized (a) perpendicular (*s*-polarization) and (b) parallel (*p*-polarization) to the plane of incidence. The dashed curves are calculated absorbance of the platinum substrate. The dash-dotted curve in the lower panels is $\langle E_y^2 \rangle / \cos\gamma$. The solid curve in the upper panel represents the best fitting result to Eq. (1), resulting $\theta = 66°$ at $|\varepsilon_{eff}| = 1$.

III-G-2 Adsorption State of Methane and Laser-Induced Photochemistry on Pt(111)

Yoshiyasu MATSUMOTO, Yuri A. GRUZDKOV, Kazuo WATANABE and Kyoichi SAWABE

[*J.Chem.Phys.* **105**, 4775 (1996)]

Adsorption states and photochemistry of methane and deuterated methane on a Pt(111) surface have been investigated by measuring temperature-programmed desorption spectra, X-ray photoelectron spectra, work function changes, and angle-resolved time-of-flight distributions of desorbed species. Methane weakly adsorbed on the Pt(111) surface at 40 K is dissociated to methyl and hydrogen fragments with laser irradiation at 193 nm. This is remarkably different from the photochemistry of methane in the gas phase where photodissociation takes place only at $\lambda < 145$ nm. While the photofragments mostly remain on the surface, some fraction of methyl desorbs with average translational energy of 0.27 eV. Photodesorption of methane is a minor channel. Desorbed methane is sharply collimated along the surface normal and shows two hyperthermal velocity components. Among the two, the faster component is attributed to associative recombination between a methyl adsorbate and a hydrogen atom produced by the photodissociation of adsorbed methane. The photochemical processes are substantially suppressed when the surface is covered with methyl adsorbate of 0.14 ML achieved by an extensive irradiation of 193-nm photons. In contrast, no photochemical reactions result from the 193-nm irradiation of methane adsorbed on a Xe/Pt(111) overlayer or from the 248-nm irradiation of methane on the bare Pt surface. These results indicate that the photochemical processes occur only for methane in close contact with substrate atoms under the irradiation of 193-nm photons. The incident angle dependence of cross sections of the photochemistry obtained with linearly polarized light indicates that direct electronic excitation of methane adsorbate plays an important role in the photochemistry of methane. The photochemistry of methane on Pt(111) at the wavelength substantially longer than that in the gas phase implies that the electronic excited state of methane is significantly mixed with substrate electronic states.

III-H Reaction Dynamics on Well-Defined Surfaces

Vast majority of surface reactions studied so far has been interpreted in terms of a Langmuir-Hinshelwood mechanism; reactants are first adsorbed on a surface and a reaction takes place between two chemisorbed species. Although reactants are in equilibrium with surface atoms, the energetics of desorbed products are determined by potential energy surfaces along reaction coordinates. In particular, associative desorption, which is often a reversed process of activated dissociative chemisorption, shows interesting features manifested by a potential barrier near the exit channel. In this project, we focus on the energetics and angular distributions of desorbed species via thermal associative recombination.

III-H-1 Mechanism for the Desorption of Molecularly and Dissociatively Adsorbed Methane on Pt(111) Probed by Pulse-Laser Heating

Kazuo WATANABE, M. C. LIN*(Emory University and IMS)*, Yuri A. GRUZDKOV and Yoshiyasu MATSUMOTO

[*J.Chem.Phys.* **104**, 5974 (1996)]

Dynamics of the thermal desorption of CD_4 molecularly and dissociatively adsorbed on Pt(111) has been studied by laser-induced thermal desorption (LITD). CD_4 adsorbates were prepared at the surface temperature of 55 K and the coadsorbates of CD_3 and D were prepared by UV photolysis of CD_4 adsorbates. The thermal desorption was induced by irradiating the surface with pulses of a frequency-doubled Nd:YAG laser and time-of-flight distributions of CD_4 in each desorption channel were measured as a functions of the desorption angle (θ). The desorption of molecularly adsorbed CD_4 shows a broad angular distribution ($\cos^{2.5}\theta$) and its translational energy distribution can be approximately described by the Maxwell-Boltzmann distribution with the temperature close to the estimated maximum surface temperature. In contrast, associatively formed CD_4 desorbs sharply along the surface normal ($\cos^{31}\theta$) and its average translational energy is almost constant at 0.43 eV in the range of θ=0°~ 25°. The experimental results are compared with the calculated ones obtained from the statistical model developed by Ukraintsev and Harrison [J. Chem. Phys. **101**, 1564 (1994)]. Although the statistical model apparently succeeds in describing some of adsorption/desorption features by fitting the data of sticking coefficient measurements with molecular beams, it fails to predict the LITD data for the reverse process when their fitted data are applied in total.

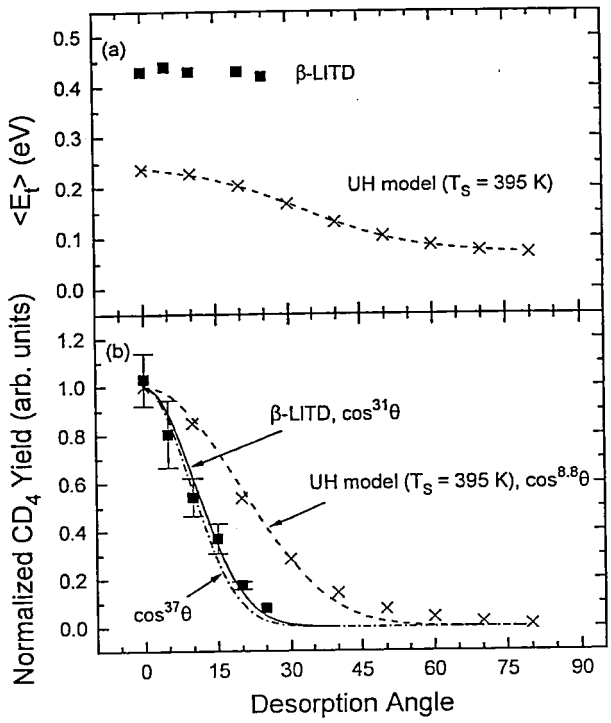


Figure 1. Desorption-angle (θ) dependence of (a) the average translational energy and (b) the desorption yield of CD_4 associatively desorbed from Pt(111) covered with CD_3 and D (β-LITD). The laser fluence was 130 mJ/cm^2. The solid curve of cos^{31}θ is the best fit to the experimental data of β-LITD. The dashed-and-dotted curve of cos^{37}θ is the best fit to the conventional TPD results. The dashed curves represent the calculated results based on the UH model by using direct count method for sum of states at T_S=395 K.

III-I Hot Atom Surface Reactions

In contrast to the Langmuir-Hinshelwood mechanism, reactions can also occur directly between an adsorbed species and a reagent incident from the gas phase, by way of a so-called Eley-Rideal mechanism. Reactions initiated by hot atoms or radicals on surfaces can be regarded as an intermediate case between the two mechanisms. Hot atoms are produced by photo- and thermal dissociation of precursor adsorbates. In this project, the dynamics of reactions where hot atoms play an important role are investigated.

III-I-1 Adsorbed States and Thermal Reactions of N_2O on Si(100) below Room Temperature: Desorption Induced by Dissociation

Hiroyuki KATO *(Graduate Univ. for Advanced Studies)*, **Kyoichi SAWABE and Yoshiyasu MATSUMOTO**

[*Surf. Sci.* **351**, 43 (1996)]

The adsorption states of N_2O on Si(100) and its thermal reactions occurring below room temperature have been studied by X-ray photoelectron spectroscopy, temperature-programmed desorption, and low energy electron diffraction. N_2O physisorbs on clean Si(100) at less than 60 K. When the surface is annealed to 80 K, physisorbed N_2O is either desorbed or dissociated to produce silicon oxide at the top-most layer and N_2 desorbing from the surface. Above 120 K, a small fraction of N_2O chemisorbs molecularly on the partially oxidized surface. The chemisorbed N_2O is mostly dissociated with further annealing. The kinetics of desorption from the first layer is very similar to that of dissociation. We propose a desorption model to explain the desorption kinetics; the desorption of the first-layer N_2O is induced by dissociation of neighboring N_2O following the formation of new Si-O bonds.

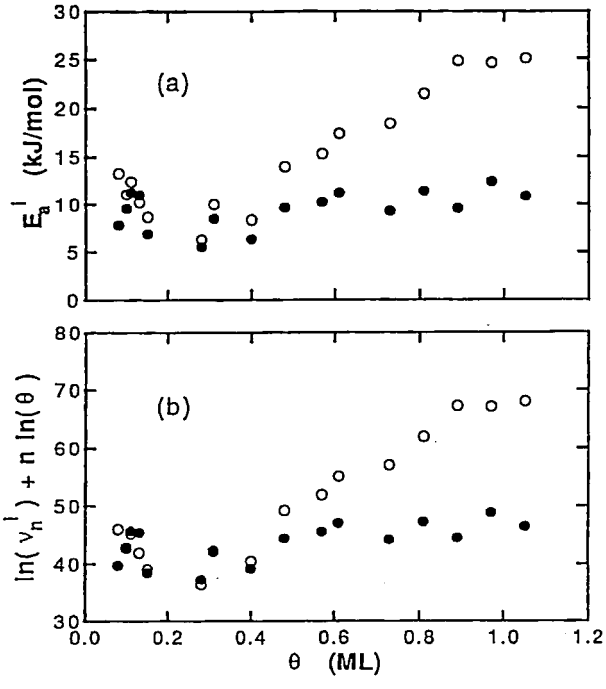


Figure 1. Coverage dependence of (a) the activation energy and (b) the intercept for desorption (open circles) and dissociation (solid circles) obtained from isosteric Arrhenius plots.

III-J Multiphoton Photoelectron Spectroscopy of Electronic States at Metal Surfaces

A central and fundamental question in surface photochemistry is to clarify how adsorbate-substrate systems are excited with photon irradiation. Two different excitation mechanisms have been frequently discussed : (1) indirect excitation via substrate-mediated charge transfer and (2) direct excitation within adsorbate. In the former mechanism electrons or holes created by photon absorption of metal and semiconductor substrates are attached resonantly to adsorbates. In any case, it is crucial to obtain information on electronic excited states of adsorbate-substrate systems. One of the best methods, and most relevant to surface photochemical measurements, is multiphoton photoelectron spectroscopy. We have newly developed an experimental setup for the spectroscopy in this year.

III-J-1 Surface and Image-Potential States on Pt(111) Probed by Two- and Three-Photon Photoemission

Ikuo KINOSHITA *(Yokohama City Univ.)*, **Toshihisa ANAZAWA, Yoshiyasu MATSUMOTO**

[*Chem. Phys. Lett.* **259**, 445 (1996)]

The surface state and image-potential state (IPS) on Pt(111) have been studied by multi-photon photoemission spectroscopy. The intensity of two-photon photoemission by ns laser pulses shows a resonant transition from the sp-derived surface state to the n=1 IPS at 5.39 ± 0.03 eV. The three-photon photoelectron spectrum by fs pulses shows two peaks: photoemission from the n=1 IPS populated by nonresonant transitions and that from the surface state. The surface state is located at 0.19 ± 0.05 eV below the Fermi level and the n=1 IPS at 0.78 ± 0.05 eV below the vacuum level.

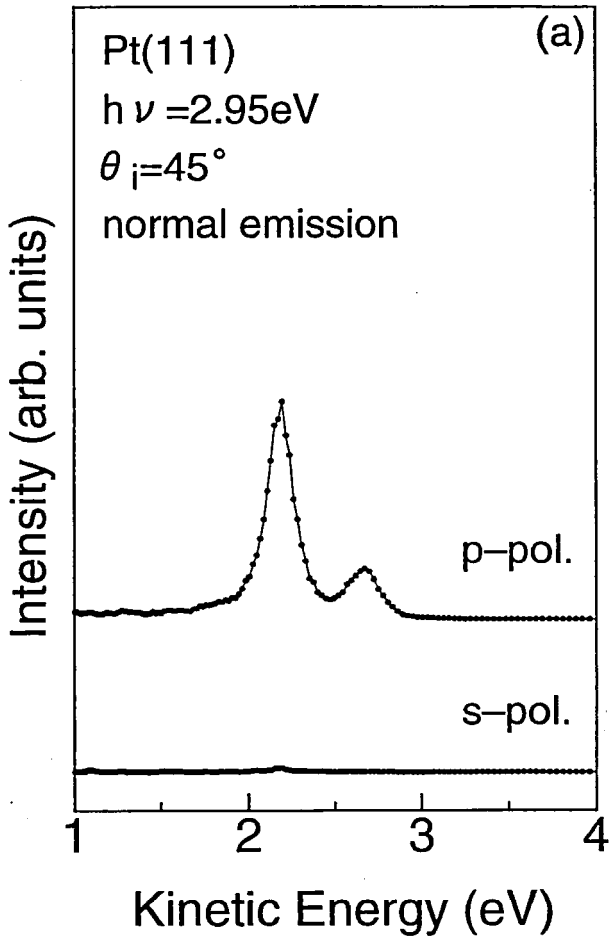


Figure 1. Three-photon photoelectron spectra from Pt(111) with fs laser pulses. The spectra were recorded at $h\nu$=2.95 eV with p- (upper) and s- (lower) polarization.

III-K Dynamic Processes in Electronically-and/or Vibrationally-Excited Molecules

Fundamental molecular aspects of chemical reactions and energy transfer processes in the electronically or vibrationally excited states have been studied. Particular interests have been directed to the study of the dynamics of vibrationally-excited van der Waals complexes using the stimulated-emission-pumping-laser-induced-fluorescence (SEPLIF) spectroscopy and the hole-burning spectroscopy, and to the photochemical reaction dynamics of the weakly-coupled complexes such as van der Waals and hydrogen-bonded complexes. The SEPLIF and hole-burning spectroscopy have also been applied to the determination of the molecular geometries and potential surfaces for the internal rotation of molecules.

III-K-1 Nascent Rotational and Vibrational Distributions in ^{16}OH and ^{18}OH Produced in the Reaction of $O(^1D)$ with $H_2{}^{18}O$

Nobuaki TANAKA, Masao TAKAYANAGI *(Tokyo Univ. of Agric. and Tech.)* **and Ichiro HANAZAKI**

[*Chem. Phys. Lett.*, **254**, 40 (1996)]

Rotational and vibrational state distributions of the OH radicals produced in the reaction, $^{16}O(^1D) + H_2{}^{18}O \rightarrow {}^{16}OH + {}^{18}OH$, have been determined using a laser-induced fluorescence technique. $^{16}O(^1D)$ was prepared by the 193 nm photodissociation of N_2O. The rotational distribu-

tions for ^{16}OH and ^{18}OH in the v = 0 level are characterized by the Boltzmann temperatures of 6000 and 2600 K, respectively. A considerable amount of ^{16}OH exists in the v = 1 state while ^{18}OH was produced predominantly in the v = 0 state. The difference in the rotational distribution between two OH radicals can be explained as the result of a spectator-stripping type reaction of $^{16}O(^1D)$ with $H_2{}^{18}O$, where the activation barrier locates at an earlier stage of the reaction coordinate, $^{16}O\cdots H\cdots{}^{18}O$. The higher rotational excitation of ^{16}OH should occur through the torque imparted by the movement of attacking ^{16}O or the torque imparted on the exit surface after the reaction barrier.

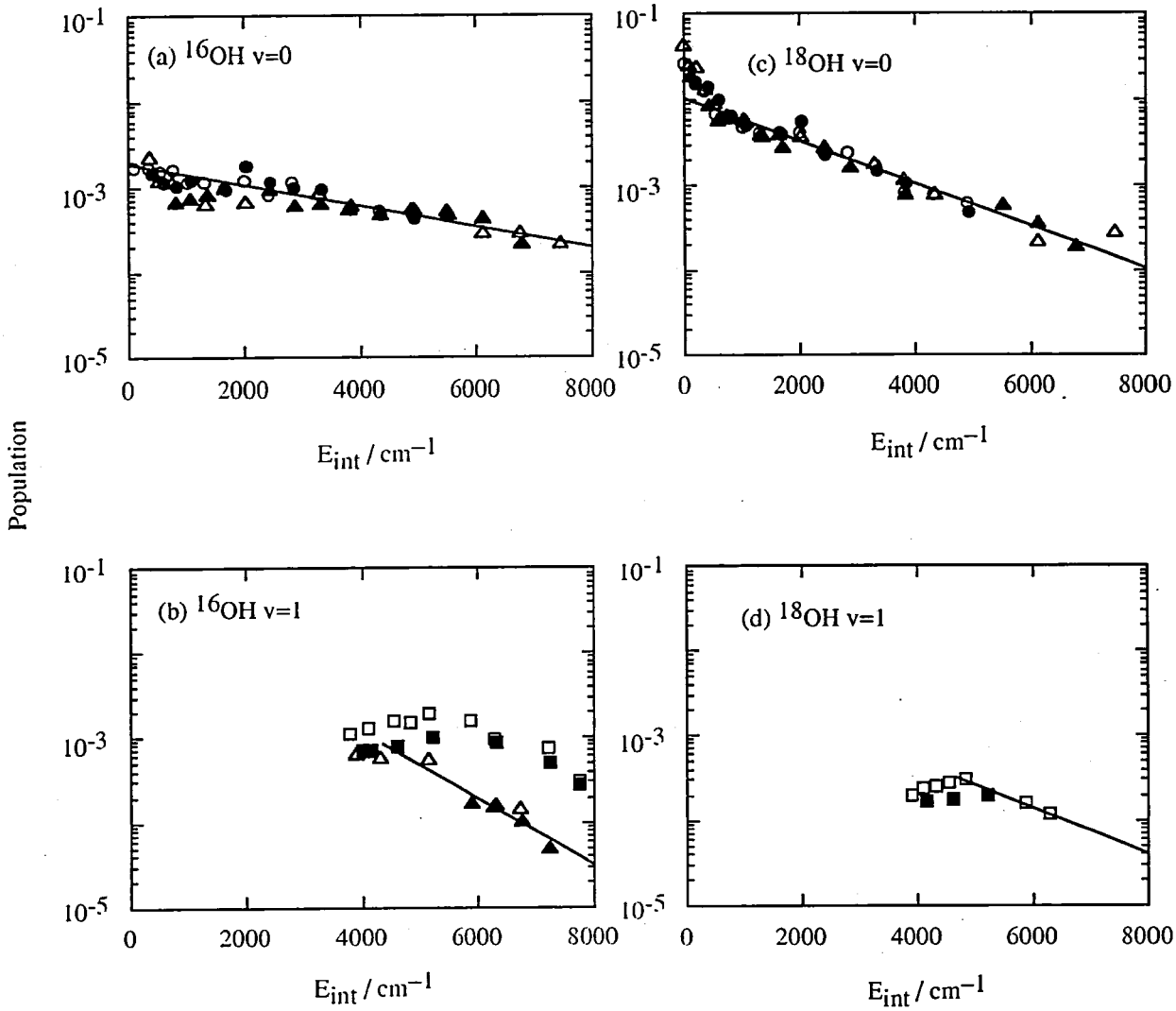


Figure 1. Rotational distributions in ^{16}OH and ^{18}OH plotted against the internal energy $E_{int} = E_R + E_V$. (a) v = 0 and (b) v = 1 for ^{16}OH and (c) v = 0 and (b) v = 1 (d) for ^{18}OH. Symbols denote the rotational branches as: P_{11} (○), P_{22} (●), Q_{11} (△), Q_{22} (▲), R_{11} (□) and R_{22} (■).

III-K-2 Photochemical Reaction Dynamics of the $N_2O{\cdot}H_2{}^{18}O$ van der Waals Complex

Nobuaki TANAKA, Umpei NAGASHIMA *(Ochanomizu Univ.)*, **Masao TAKAYANAGI** *(Tokyo Univ. of Agric. and Tech.)*, **Hong Lae KIM** *(Kangweon Natl. Univ.)* **and Ichiro HANAZAKI**

[*J. Phys. Chem.*, in press]

The rotational and vibrational energy distributions have been determined for the OH radicals resulting from the 193 nm photolysis of the van der Waals complex $N_2O{\cdot}H_2O$. Laser-induced fluorescence was used to probe the OH radicals. The rotational distributions of OH are characterized by the Boltzmann temperatures of 1700 K for ^{16}OH v"=0 and v"=1, and of 1600 K for ^{18}OH v"=0. 29 % of ^{16}OH exists in the v=1 state while ^{18}OH is produced almost exclusively in the v=0 state.

		$N_2O{\cdot}H_2O$	$O_3{\cdot}H_2O$[1)]
^{16}OH	T_R(v=0)/K	1700	1300
	T_R(v=1)/K	1700	1300
	P(v=1)/P(v=0)	0.41	0.23
^{18}OH	T_R(v=0)/K	1600	1100
	E_R/E_{avail}	0.0708	0.0714
	E_V/E_{avail}	0.0320	0.0342

The remarkable resemblance of E_R/E_{avail} and E_V/E_{avail} between $N_2O{\cdot}H_2O$ and $O_3{\cdot}H_2O$ suggests that both system react commonly through an intermediate of the type of $^{16}O\cdots H\cdots{}^{18}OH$.

Reference
1) D. S. King, D. G. Sauder and M. P. Casassa, *J. Chem. Phys.* **100**, 4200 (1994).

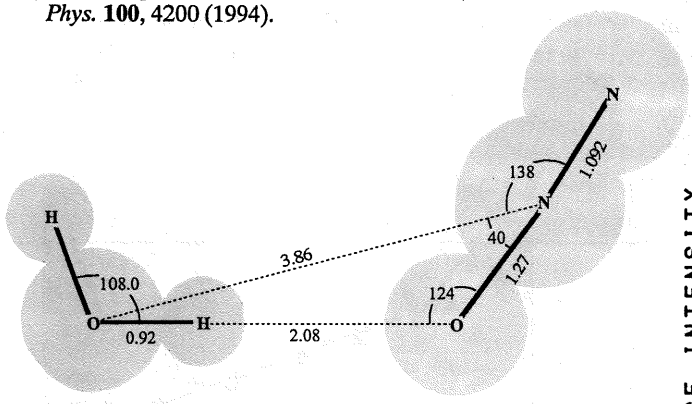


Figure 1. Structure of the N_2O•H_2O complex determined by an *ab initio* calculation. Bond distances and angles are given in units of and degree, respectively. The shaded circles represent the covalent-bond radius.

III-K-3 Hole-Burning Spectroscopy of *m*-Cresol Rare-Gas Complexes

Masao TAKAYANAGI *(Tokyo University of Agriculture and Technology)* **and Ichiro HANAZAKI**

The $S_1 \leftarrow S_0$ excitation spectra of *m*-cresol and its 1:1 complexes with rare gas atom were measured under the supersonic jet condition by the LIF (laser-induced fluorescence) and hole-burning techniques. Both of two possible conformers of *m*-cresol, *cis* and *trans*, concerning the direction of the OH group with respect to the methyl group, were studied. Bands due to the complex are so weak in the LIF excitation spectra that they are often hidden under the intense bands due to the monomer. Moreover, it is sometimes difficult to assign a band observed in the LIF excitation spectra to a specific species. Excitation spectra of specific species can be measured by the hole-burning technique. We measured hole-burning spectra of *cis-m*-cresol monomer, *trnas-m*-cresol monomer, *cis-m*-cresol-Ar, *trnas-m*-cresol-Ar and *cis-m*-cresol-Kr. Spectra for the Ar complexes are shown in Figure 1. For each species, transitions from the ground vibrational state and from the low-lying torsional vibrational excited state were observed in different hole-burning spectra. Torsional levels of the methyl group of *m*-cresol and intermolecular vibrations in the S_1 states are observed in the hole-burning spectra. Torsional potential of the methyl group of *m*-cresol in the complexes can be investigated on the basis of observed frequencies.

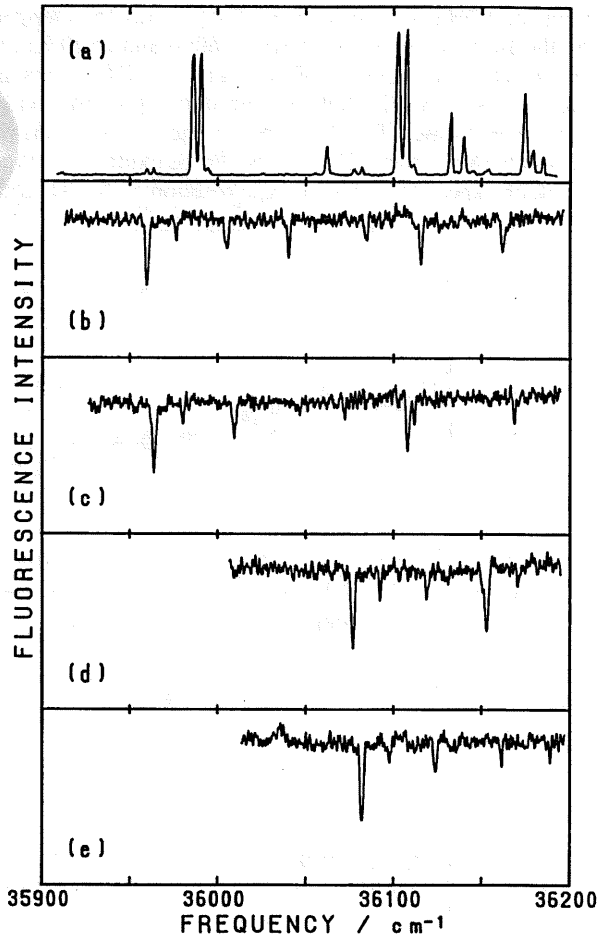


Figure 1. **(a)** LIF-excitation spectrum of *m*-cresol seeded in He containing 3 % Ar in a supersonic jet. **(b)** and **(c)** Hole-burning spectra of the *cis-m*-cresol-Ar complex measured with the probe frequency set at the 0' ← 0" and 1' ← 1" transitions, respectively. **(d)** and **(e)** Hole-burning spectra of the *trans-m*-cresol-Ar complex measured with the probe frequency set at the 0' ← 0" and 1' ← 1" transitions, respectively.

III-K-4 Torsional Potential of the Methyl Group in Toluene Derivatives Forming 1:1 Complexes with a Rare Gas Atom

Masao TAKAYANAGI *(Tokyo University of Agriculture and Technology)* **and Ichiro HANAZAKI**

Torsional potential of the methyl group was determined for the S_1 states of the *m*-tolunitrile-rare gas and *m*-cresol-rare gas complexes by adjusting calculated torsional frequencies with those observed in the LIF (laser-induced fluorescence)-excitation and hole-burning spectra. In the calculations, torsional potential with the form of $V(\phi) = (1/2)\{V_3[1-\cos(3\phi)] + V_6[1-\cos(6\phi)]\}$ were assumed, where ϕ is the torsional angle, and V_3 and V_6 are the parameters determining potential heights. Figure 1 shows the potential change upon the complex formation. A big difference is observed in the height of the torsional potential for *m*-tolunitrile monomer and *m*-cresol monomer, since *m*-tolunitrile has an electron withdrawing CN group, while *m*-cresol has an electron donating OH group. Nevertheless, the changes upon the complex formation are similar for *m*-tolunitrile and *m*-cresol; Magnitudes of V_3 and V_6 tend to increase and decrease, respectively, upon complex formation with heavier rare gas atom. In Figure 1, the potential change for *m*-cresol

complexes is not so obvious as that for the *m*-tolunitrile complexes. This is because the potential height for the *m*-cresol is originally much higher than that for *m*-tolunitrile. The difference between *cis*- and *trans*-*m*-cresol was found not to be significant.

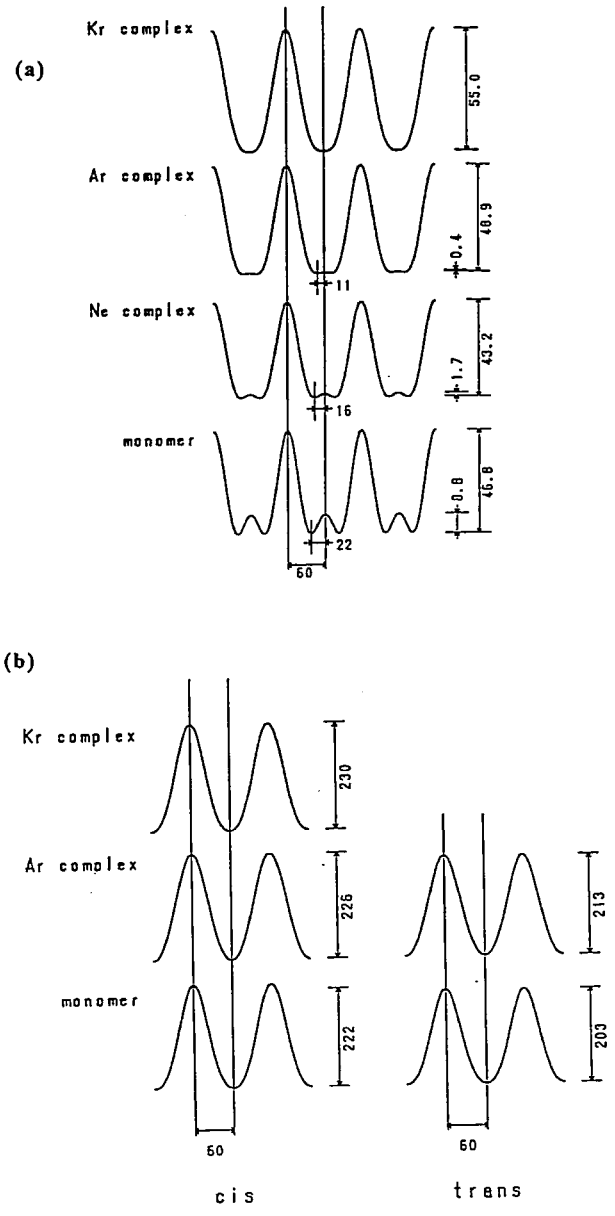


Figure 1. (a) Methyl torsional potential of the *m*-tolunitrile monomer, *m*-tolunitrile-Ne, *m*-tolunitrile-Ar and *m*-tolunitrile-Kr. (b) Methyl torsional potential of the *m*-cresol monomer (*cis* and *trans*), *m*-cresol-Ar (*cis* and *trans*) and *m*-cresol-Kr (*cis* only). Torsional angles are shown in units of degree, while potential heights are shown in units of cm^{-1}.

III-K-5 The N_2 Rotational State Dependence of Anisotropy in the Angular Distribution of Photofragment from N_2O

Suketu R. GANDHI and Ichiro HANAZAKI

N_2O dissociates into rotationally excited N_2 and $O(^1D)$ upon absorption of 170 - 210 nm photons. In previous studies[1-3], anisotropy β in the angular distribution of photofragmens has been characterized by monitoring $O(^1D)$ as; $\beta = 0.5$ at the 193 nm dissociation,[1,2] and $\beta = 0.6$ at the 205.5 nm dissociation.[3] They represent the averaged values over all rotational states of N_2.

In our experiments, N_2O is dissociated at ~ 203 nm, and the resulting photofragment N_2 is detected at the same wavelength through the 2+1 REMPI in a time-of-flight mass spectrometer (TOFMS). By operating the TOFMS in a low mass resolution, it is possible to obtain the translational energy E_{tr} and the angular distribution. Figure 1 shows the TOF spectra of N_2 dissociated by a parallel-polarized light at 203 nm. E_{tr} and β for the N_2 photofragment are as follows: $E_{tr} = 62$ kJ/mole and $\beta = 1.5$ at $\lambda = 202.87$ nm (N_2, J = 60), $E_{tr} = 55$ kJ/mole and $\beta = 1.4$ at 202.99 nm (N_2, J = 66), and $E_{tr} = 37$ kJ/mole and $\beta = 0.8$ at 203.30 nm (N_2, J = 79). The trend clearly shows that β decreases as J increases. The reduction of β indicates the more torque gets exerted into N_2 during the dissociation process, which is in accordance with the increase of J.

References

1) P. Felder, B.-M. Haas and J. R. Huber, Chem. Phys. Lett. **186**, 177 (1991).
2) L. L. Springsteen, S. Satyapal, Y. Matsumi, L. M. Dobeck and P. L. Houston, J. Phys. Chem. **97**, 7239 (1993).
3) T. Susuki, H. Katayanagi, Y. Mo and K. Tonokura, Chem. Phys. Lett. **256**, 90 (1996).

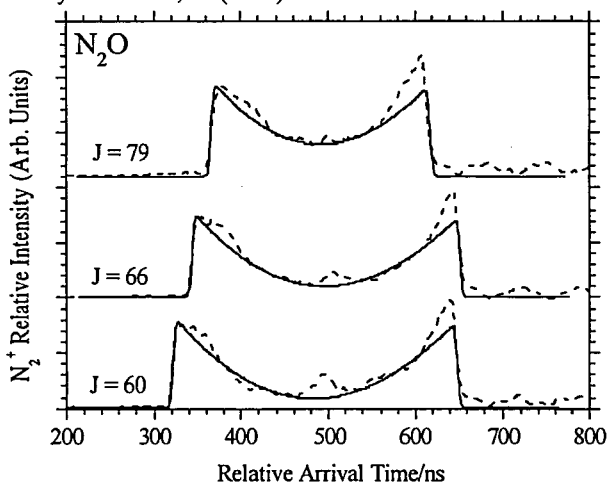


Figure 1. Plot of the N_2^+ intensity at selected J states of N_2 upon photodissociation of N_2O. The dashed lines (---) are the experimentally observed values, and the solid lines (——) are the computer simulation of the TOF spectra.

III-K-6 Photodissociation Study of CH_3CHO: The rate of Formation of Photofragment

Suketu R. GANDHI and Ichiro HANAZAKI

Absorption of UV photons by CH_3CHO at $\lambda \leqq 320$ nm results in the photodissociation into $\bullet CH_3$ and $\bullet CHO$. We have measured the rate of $\bullet CH_3$ formation by detecting the fragment with the 2+1 REMPI. In the range of excitation of 280 - 320 nm, CH_3 gets formed primarily in the ground vibrational state. Figure 1 shows the rate of $\bullet CH_3$ formation upon photodissociation of CH_3CHO at a few different wavelengths. At 315 nm, the rate constant for the formation of CH_3 is determined to be ~ 1.1×10^8 s^{-1} after convoluting both the dissociation and detection laser pulse widths. At 295 and 280 nm, the molecule dissociates within the pulse duration of 5 ns. This indicates that the $\bullet CH_3$ is formed in ~10 ns at the photon energy close to the dissociation threshold, while the rate of formation increases with the available energy.

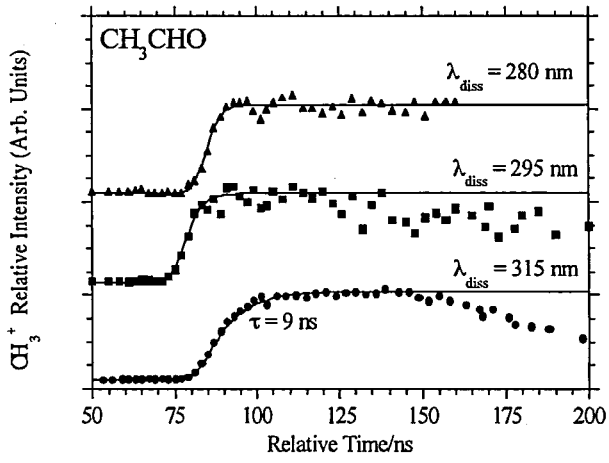


Figure 1. Plot of CH_3 formation vs. relative delay time between the dissociation and detection laser pulses.

III-L Self-Organization in Chemical Reactions

The self-organizing process in chemical systems is known to occur as a result of nonlinear chemical processses. This kind of chemical systems exhibit sustained temporal chemical oscillations and spatial pattern formation. Moreover, they sometimes exhibit more complicated nonlinear phenomena such as bistability, excitability, multi-frequency oscillations, and the chaotic behavior. They have received attention for thier close relation to the activity of living systems in the spontaneously-organized dynamic behavior. Possible applications of such phenomena to the sensing- and image storage devices have also been interested in. We have paid a special attention to the response of chemical oscillator systems to photo-illumination, which is very important in view of the above-mentioned interests but have not been studied so far in any systematic manner. The topics among our results in this year include the finding of photo-induced multistability in the Briggs-Rauscher system, as well as a proposition of a new photo-regulated autocatalysis in this system, and the finding of the chemical chaos in the BrO_3^--H_2O_2-marble system, for which a new realistic reaction scheme has been established.

III-L-1 Origin of Chemical Instability in the Bromate-Sulfite Flow System.

Ichiro HANAZAKI and Gyula RÁBAI(*Kossuth Lajos Univ., Hungary)*

[*J. Chem. Phys.*, in press]

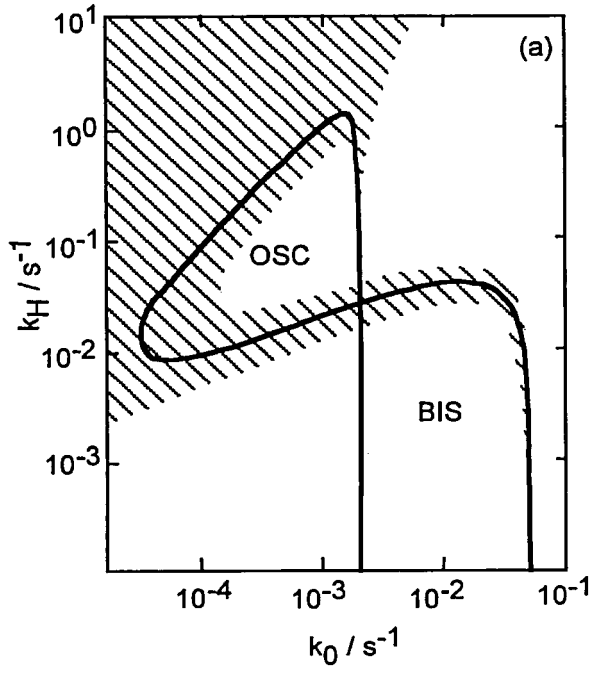
Origin of the instability observed in the bromate-sulfite-proton system is discussed. This is known as a subsystem of the pH oscillators which provides the positive feedback channel for H^+. It is composed of the following two fast equilibria

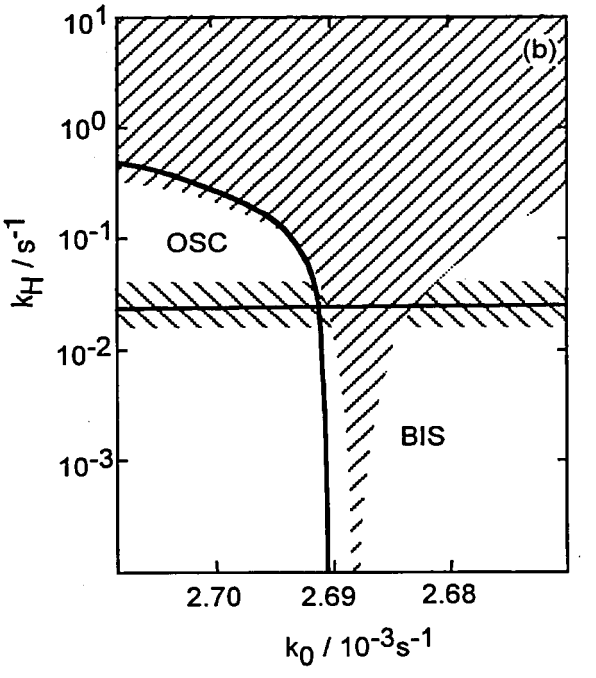
$$H^+ + SO_3^{2-} \Leftrightarrow HSO_3^-$$
$$H^+ + HSO_3^{2-} \Leftrightarrow H_2SO_3$$

and the oxidation of HSO_3^- and H_2SO_3 by BrO_3^- to recover the initially supplied proton as:

$$3HSO_3^- + BrO_3^- \rightarrow 3SO_4^{2-} + Br^- + 3H^+$$
$$3H_2SO_3 + BrO_3^- \rightarrow 3SO_4^{2-} + Br^- + 6H^+$$

This scheme exhibits bistability under flow conditions. It gives rise to chemical oscillations if it is coupled with a simple linear decay of H^+ as a negative feedback channel. It is also capable of exhibiting chaotic behavior in the presence of HCO_3^-. We analyze the nature of the strong nonlinearity provided by the above scheme in detail and show that it arises essentially from the fast reaction of H_2SO_3 with bromate. The simplicity of the scheme enables us to describe the system dynamics with three variables without any approximation. A state diagram, spanned by the flow rate and the decay rate of H^+, is illustrated in Figure 1. As a result, we now have a model in hand in which we can compare the theoretical results directly and quantitatively with the corresponding experiments. This situation may open a way to understand the complexity in nonlinear chemical systems in a more quantitative manner. Some recent experimental findings of the complex oscillatory behaviors including chaos for the system with more realistic negative feedback channels, or for the system in which BrO_3^- is replaced with H_2O_2, are discussed on the basis of the present analysis.





Fifure 1. (a) State diagram spanned by the flow rate (k_0) and the decay rate of H^+ (k_H). Parameters used in the calculation are $[H^+]_0$ = 15 mM, $[SO_3^{2-}]_0$ = 90 mM, $[BrO_3^-]_0$ = 75 mM, K_S = $9.9'10^6$ M^{-1}, K_D = 50 M^{-1}, k_S = $6.53'10^{-2}$ $M^{-1}s^{-1}$, and k_D = 18.0 $M^{-1}s^{-1}$. The hatched part inside the OSC region denotes that the system leaves the stationary point in an oscillating manner, while those outside of the region show that the point converges with damped oscillations. The hatched part in the BIS region means that one of the branches (with higher X values) converges to itself in an oscillating manner, while the other branch converges monotonously.
(b) An expanded view of (a) near the crossing point.

III-L-2 Mechanism of the Oscillatory Bromate Oxidation of Sulfite and Ferrocyanide in a CSTR

Gyula RÁBAI *(Kossuth Lajos Univ., Hungary)*, **Akiko KAMINAGA and Ichiro HANAZAKI**

[*J. Phys. Chem.*, **100**, 16441 (1996)]

pH oscillations and related phenomena in the BrO_3^- - SO_3^{2-}-$Fe(CN)_6^{4-}$ flow system can be simulated with an old mechanism proposed for the bromate-sulfite subsystem[1] if it is combined with a rate law of the bromate-ferrocyanide reaction.

$$HSO_3^- + BrO_3^- \rightarrow \{HSO_3^-.BrO_3^-.H_2O\} \rightarrow SO_4^{2-} + BrO_2^- + H^+ \quad (1)$$
$$H_2SO_3 + BrO_3^- \rightarrow \{SO_2.BrO_3^-.H_2O\} \rightarrow SO_4^{2-} + BrO_2^- + 2H^+ \quad (2)$$

It is the first step in the six-equivalent reduction of bromate that is rate determining one. The bromine intermediates further react with S(IV) rapidly. Since step (2) is faster than step (1) and H^+ is produced when H_2SO_3 or HSO_3^- get oxidized to sulfate, the reaction accelerates in an unbuffered solution due to the protonation of an increasing fraction of HSO_3^-. A slow removal of H^+ by bromate-ferrocyanide reaction provides a negative feedback.

References

1) Williamson, F. S.; King, E. L. *J. Am. Chem. Soc.* **79**, 5397 (1957).
2) Edblom, E. C.; Luo, Y.; Orbán, M.; Kustin, K.; Epstein, I.R. *J. Phys. Chem.* **93**, 2722 (1989).

III-L-3 pH Oscillations in the Bromate-Sulfite-Marble Semibatch and Flow System

Gyula RÁBAI *(Kossuth Lajos Univ., Hungary)* **and Ichiro HANAZAKI**

[*J. Phys. Chem.* **100**, 10615 (1996)]

A self-accelerating oxidation of an unbuffered aqueous sodium sulfite-hydrogen sulfite solution by sodium bromate and a selective removal of the hydrogen ion by solid marble chips from the reaction mixture have been used to construct an oscillatory system. The system exhibits large amplitude oscillations between pH 3.5 and 7.5 at 25.0 °C in a continuous-flow stirred tank reactor and in a semibatch configuration. The shape, the periodic time and the region of oscillations can be controlled by using different amounts and grade size of marble chips. The mechanism of the self-accelerating part (positive feedback) should obviously be the same as that of the bromate-sulfite-ferrocyanide reaction (see above). The removal of the hydrogen ion (negative feedback) can be described by a first order rate equation. There is no "crosstalk" between the positive and the negative feedbacks. This oscillator may be applicable for the pH-controlled periodic drug delivery. In this context its advantage is that the length of the low pH state relative to that of the high pH state within a cycle can be varied by using different amount of marble.

III-L-4 Chaotic pH Oscillations in the Sulfur(IV)-Hydrogen Peroxide-Marble Flow System

Gyula RÁBAI *(Kossuth Lajos Univ., Hungary)* **and Ichiro HANAZAKI**

[*J. Phys. Chem.*, **100**, 15454 (1996)]

We constructed a chaotic chemical system by combining the H_2O_2 oxidation of sulfur(IV) with dissolution of marble chips in a diluted acidic aqueous solution in a CSTR. The mechanism is simple, because the composite reactions can interact only via the hydrogen ion concentration. The following reaction scheme describes the dynamical behavior:

$$H_2O_2 + HSO_3^- \rightarrow H^+ + SO4^{2-} + H_2O \quad (1)$$
$$CaCO_3 + H^+ \rightarrow Ca^{2+} + HCO_3^- \quad (2)$$
$$HSO_3^- \rightarrow H^+ + SO_3^{2-} \quad (3)$$
$$CO_2(aq) + H_2O \rightarrow H^+ + HCO_3^- \quad (4)$$
$$CO_2(aq) \rightarrow CO_2(gas) \quad (5)$$

Reaction (1) has a two-term rate law: $v_1=(k_1+k_1'[H^+])[HSO_3^-][H_2O_2]$, reactions (2-5) have first or second order kinetics equations. Simulations based on reactions 1-5 predicted regular pH oscillations, bursting, and chaotic responses. Most of the simulated phenomena were found experimentally in the vicinity of the predicted conditions. The parameters of the experimental oscillations also agree well with their calculated counterparts.

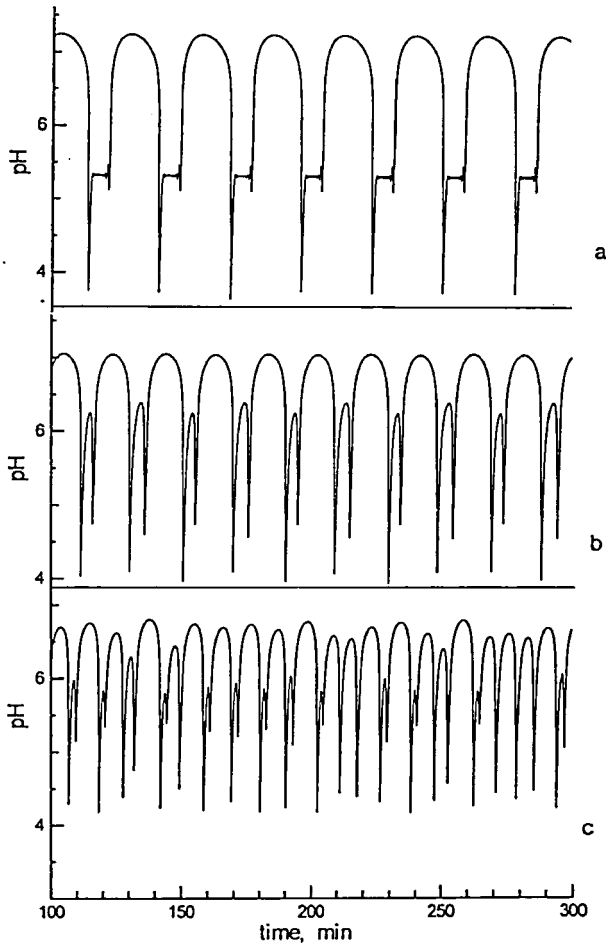


Figure 1. Calculated bursting (a) double period oscillations (b) and chaotic responses (c). $k_5 = 1.0\cdot10^{-3}$ s^{-1} and k_0(flow rate) = $6.0\cdot10^{-4}$ s^{-1} for bursting; $k_5 = 1.5\cdot10^{-3}$ s^{-1} and $k_0 = 3.0\cdot10^{-4}$ s^{-1} for double periods; and $k_5 = 1.0\cdot10^{-3}$ s^{-1} and $k_0 = 3\ .0\cdot10^{-4}$ s^{-1} for chaos. Other rate constant values at 4.0 °C are $k_1 = 1.5$ M^{-1} s^{-1}, $k_1' = 6.5\cdot10^{6}$ M^{-2} s^{-1}, $k_2 = 0.03$ s^{-1}, $k_3 = 1\cdot10^{3}$ s^{-1}, $k_{-3} = 1\cdot10^{10}$ M^{-1} s^{-1}, $k_4 = 1.1\cdot10^{-2}$ s^{-1}, and $k_{-4} = 2.5\cdot10^{4}$ M^{-1} s^{-1}. Input concentrations $[H_2O_2]_0 = 0.010$, $[SO_3^{2-}]_0 = 0.0050$, $[H^+] = 5.0\cdot10^{-4}$ M.

III-L-5 Chaotic pH Oscillations in the Hydrogen Peroxide-Sulfite-Ferrocyanide-Hydrogen Carbonate Flow System

Gyula RÁBAI *(Kossuth Lajos Univ., Hungary)*, **Akiko KAMINAGA and Ichiro HANAZAKI**

[*Chem. Commun.*, 2181 (1996)]

Combining the $CO_2(aq) + H_2O \rightarrow H^+ + HCO_3^-$ equilibrium with an oscillatory H_2O_2-HSO_3^-- $Fe(CN)_6^{4-}$ system gives rise to chaotic temporal pH changes in a continuous flow stirred tank reactor. A slow removal of CO_2 by nitrogen stream from the solution plays a critical role in the negative feedback. This system may be regarded as a combination of two oscillatory reactions characterized with very different frequencies because the H_2O_2-HSO_3^- -HCO_3^- subsystem itself is an oscillatory one. A period doubling route from simple oscillations to chaos can be measured as a result of the interactions of the two frequencies (20 periods/hour and 2 periods/hour, respectively). The chaos could be simulated with a reaction scheme consisting of the rate laws of the composite reactions. Chaotic behavior exists in a surprisingly wide range of flow rate both in the experiments and in the calcula-

tions. Windows of stabile period three oscillations are also found in the chaotic region. Such windows are a universal feature of the period doubling route to chaos.

This mode of chaos is light sensitive that offers an opportunity for regulation by light.

III-L-6 Light-Induced Period Doubling Route from Simple pH Oscillations to Chaos in the Hydrogen Peroxide-Sulfite-Ferrocyanide-Hydrogen Carbonate Flow System

Gyula RÁBAI *(Kossuth Lajos Univ., Hungary)* **and Ichiro HANAZAKI**

Dynamical behavior of the title system is light sensitive as the H^+ consuming reaction between ferrocyanide and hydrogen peroxide is accelerated by illumination. Under appropriate initial conditions high frequency regular oscillations can be measured in darkness. Under continuous illumination with visible light a period doubling route from simple oscillations through period 2, period 4 traces to chaotic pH responses can be measured when the light power is increased step by step (Figure 1a). The chaos can be transferred through a reverse period doubling route to low frequency regular oscillations by increasing further the light power (Figure 1b). Windows of stable period 3 oscillations are also found in the chaotic region under illumination. At even higher light intensity, oscillations are completely inhibited.

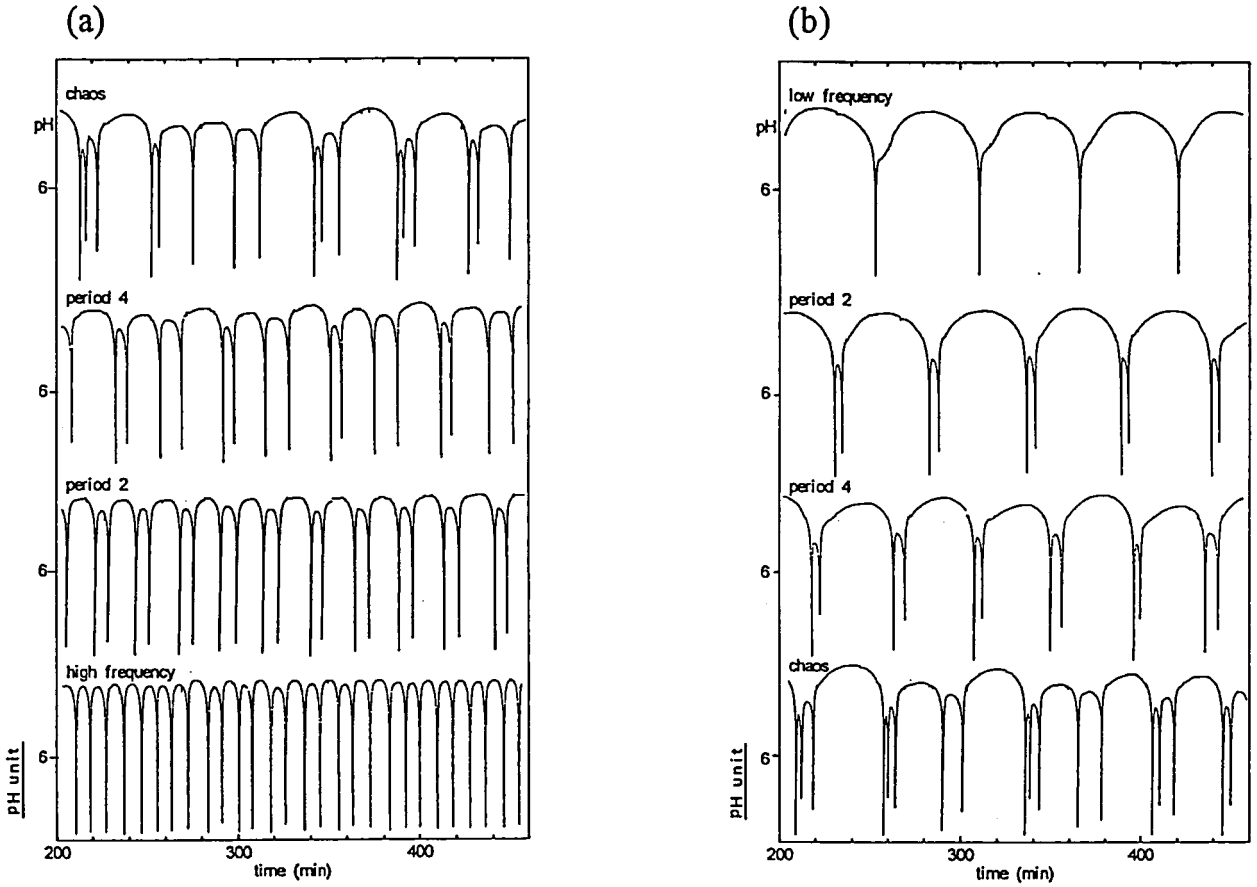


Figure 1. (a) Light induced period doubling route from simple oscillations to chaos in the hydrogen peroxide-sulfite-ferrocyanide-hydrogen carbonate system. Input concentrations in the combined feed: $[H_2O_2]_0 = 0.010$; $[SO_3^{2-}]_0 = 0.0050$, $[Fe(CN)_6^{4-}]_0 = 0.0010$, $[H^+]_0 = 5.0 \cdot 10^{-4}$, $[HCO_3^-]_0 = 5.0 \cdot 10^{-4}$ M. T = 5.0°C; N_2-flow rate 7.0 mL/min; liquid flow rate $k_0 = 2.07 \cdot 10^{-4}$ s^{-1}; diameter of the light beam: 1.0 cm; optical pathlength in the reaction mixture: 2.6 cm; light power for high frequency: 0.0, for period 2: 0.7, for period 4: 1.15, for chaos: 1.55 mW.
(b) Conditions are the same as in (a) but the light power from the bottom: 1.70, 2.05, 3.1, 5.15 mW.

III-L-7 Photo-Response of the Ferrocyanide-Bromate-Sulfite Chemical Oscillator under Flow Conditions

Akiko KAMINAGA, Gyula RÁBAI *(Kossuth Lajos Univ., Hungary)*, **Yoshihito MORI** *(Nagoya Inst. Tech.)* **and Ichiro HANAZAKI**

[*J. Phys. Chem.*, **100**, 9389 (1996)]

The photoresponse of the ferrocyanide-bromate-sulfite system, known as the pH oscillator in a continuous-flow stirred tank reactor (CSTR), has been studied in the visible region. Photoinduced oscillations are observed for the system in the low-pH steady state in the dark, while the photoinhibition of oscillations are observed for the system oscillating in the dark. We have conducted the pre-irradiation experiments for the subsystem, $Fe(CN)_6^{4-}$-BrO_3^--H^+, where the acidic aqueous solution of ferrocyanide is irradiated for some time before the reaction is started by adding bromate. Solid curves in Figure 1A show the time profiles of pH for the acidic ferrocyanide solution in a batch reactor pre-irradiated at 436 nm. The broken curve shows the result of continuous irradiation throughout the measurement. The pre-irradiation effect is determined simply by the total light energy injected into the solution before the reaction starts (Figure 1B). We have confirmed that the enhanced formation of $Fe(CN)_5(H_2O)_3^-$ from

photoexcited $HFe(CN)_6^{3-}$, which is the major species in the acidic solution, is responsible for the photoacceleration of the negative feedback process.

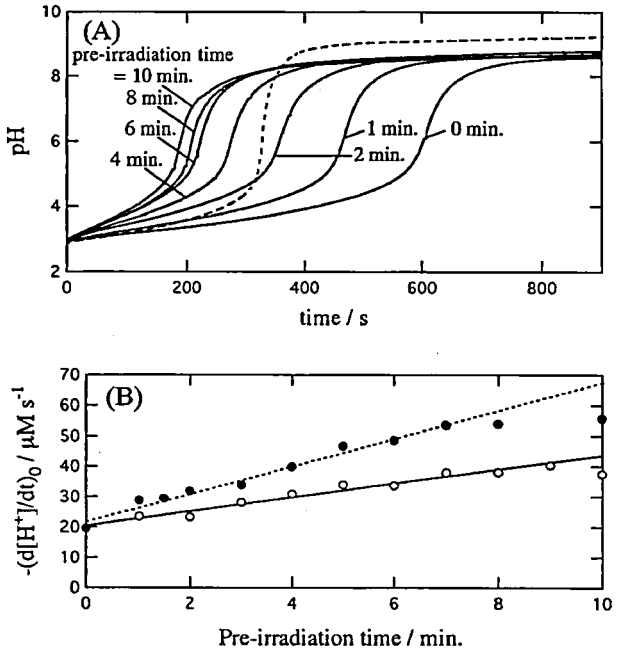


Figure 1. Panel (A): Time profile of pH for the batch BrO_3^--$Fe(CN)_6^{4-}$ reaction. Solid curves: the dark reaction pre-irradiated at 436 nm with P/P_{max} = 0.25, where P_{max} = 1.3 W. Broken curves: without pre-irradiation, but irradiated throughout the reaction at 436 nm with P/P_{max} = 0.25. Panel (B): the initial rate of $[H^+]$ consumption plotted against the pre-irradiation time. P/P_{max} = 0.25 (○) and P/P_{max} = 0.50 (●). The initial concentrations are $[BrO_3^-]_0$ = 75 mM, $[Fe(CN)_6^{4-}]_0$ = 15 mM and $[H_2SO_4]_0$ = 6.0 mM. T = 35 °C.

III-L-8 The Primary Process of Photoinduction of Chemical Oscillations in the Ferrocyanide-Bromate-Sulfite System

Akiko KAMINAGA, Yoshihito MORI *(Nagoya Inst. Tech.)*, **Gyula RÁBAI** *(Kossuth Lajos Univ., Hungary)* **and Ichiro HANAZAKI**

We have recently studied the photoresponse of the bomate-sulfite-ferrocyanide system, which is known as one of the flow-controlled pH oscillators. To determine the primary light absorber in this system, we have tried to determine wavelength dependence of the relative cross section (s_R, action spectrum) for the photoinduction of oscillations. Figure 1 shows the wavelength dependence of s_R and the absorption spectrum of the reaction mixture. High absorbance of the reaction mixture observed in the 400 nm region is due to $Fe(CN)_5(H_2O)^{3-}$ and/or $Fe(CN)_6^{3-}$. On the other hand, s_R has no significant peak in this region and its shape is similar to the absorption spectrum of $HFe(CN)_6^{3-}$, which is the major species in the acidic solution of $Fe(CN)_6^{4-}$. The result has confirmed directly our previous proposal that the primary light absorber is $HFe(CN)_6^{3-}$, the protonated ferrocyanide, which causes the photoinduction of oscillations by enhancing the formation of $Fe(CN)_5(H_2O)^{3-}$.

This work was carried out under the National Institute of Basic Biology Cooperative Research Program for the Okazaki Large Spectrograph.

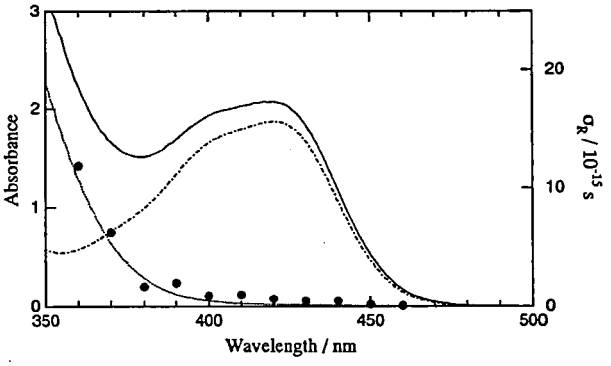


Figure 1. Relative cross section (s_R) of photoinduction of oscillations (closed circle) and absorption spectrum (———) of the $Fe(CN)_6^{4-}$-BrO_3^--SO_3^{2-} solution measured with the optical pathlength of 5 mm. Absorption spectra of the 15 mM $Fe(CN)_6^{4-}$ aqueous solution containing 6 mM H_2SO_4 (·····) and of the 2 mM $Fe(CN)_6^{3-}$ aqueous solution (—•—•) measured in a 1 cm cell are also shown.

III-L-9 Pulse Light Irradiation for B-Z Reaction - Photoresponse Near the Bifurcation Point

Akiko KAMINAGA and Ichiro HANAZAKI

The B-Z reaction system in the reduced steady states in a continuous flow-stirred tank reactor was irradiated with a pulse of visible light. The system in the reduced steady state under the dark condition exhibits a pulse response near the subcritical bifurcation point to a pulse light illuminatuion above a certain critical light power. The critical light power (ΔP_c) increases as the initial concentration of Br^-, which serves as an inhibitor of chemical oscillations, increased (Figure 1A), while it decreases as the initial concentration of the bromate ion is increased (Figure 1B).

This pulse response can be thought as an "excitability", since, a single pulse response with a constant amplitude is observed independently of the power P of the externally applied light pulse, while no response is observed when P is lower than a threshhold value (ΔP_c). No response is observed when the system in the oxidized steady states under the dark condition iss irradiated with a pulse light.

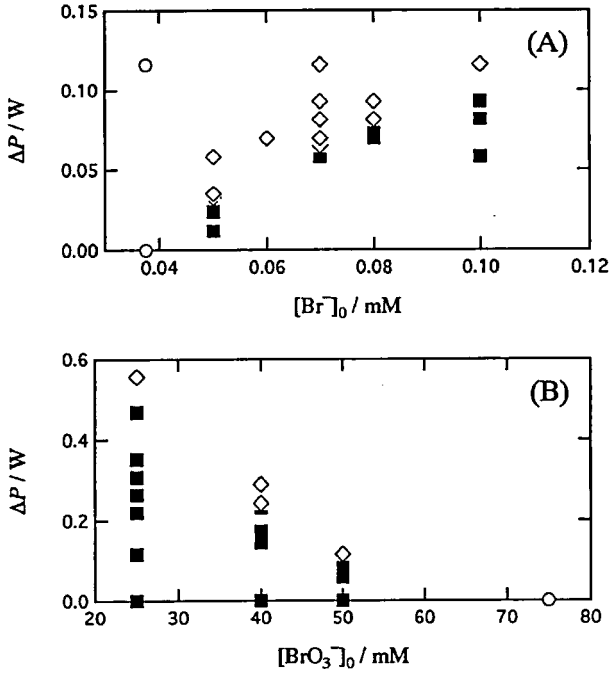


Figure 1 Photoresponse of the B-Z system for pulse light irradiation. Symbols: (○) oscillatory, (■) steady, (◇) pulse response. The initial concentrations are $[Ru(bpy)_3^{2+}]_0 = 0.1$ mM, $[malonic\ acid]_0 = 7.5$ mM, $[H_2SO_4]_0 = 800$ mM, $[BrO_3^-]_0 = 50$ mM (A), and $[Br^-]_0 = 0.1$ mM (B).

III-L-10 The Effect of Light on the Belousov-Zhabotinsky Reaction in Water-in-Oil Microemulsion of AOT in Octane

Vladimir K. VANAG *(N. N. Semenov Institute of Chemical Physics, Russian Academy of Sciences)* **and Ichiro HANAZAKI**

A ferroin-catalyzed Belousov-Zhabotinsky reaction running in water-in-oil microemulsion of anionic surfactant Aerosol OT (AOT) is found to be sensitive to visible and ultraviolet light, while the corresponding homogeneous aqueous solution with the same initial concentrations is insensitive to illumination. Depending on the experimental conditions, the photoillumination initiates or damps oscillations, changes the oscillation waveform and increases the frequency. In the micelle BZ sytem without malonic acid, we found that the primary photochemical step is the photoexcitation of ferriin, $Fe(phen)_3^{3+}$, which is then reduced to ferroin through the reaction with the negative ion of AOT existent in the micelles. A more complicated photoreduction mechanism is suggested for the full BZ system in the AOT microemulsion.

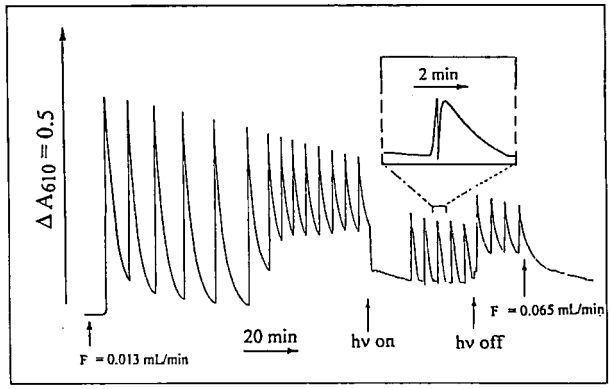


Figure 1. The effect of light on the AOT-BZ reaction after the frequency-multiplying bifurcation. Conditions: $[H_2SO_4]_0 = 0.3$ M, $[MA]_0 = 0.25$ M, $[NaBrO_3]_0 = 0.1$ M, $[ferroin]_0 = 2.24$ mM, $w = 18$, $\phi_w = 0.11$, $k_0 = 0.013$ mL/min, $V_0 = 20$ mL. Arrows "hn on" and "hn off" denote the moments of switching on and switching off the white light with power P = 28 W. A section of oscillations enclosed in a dotted square frame is presented in the insert on an enlarged scale. All 5 oscillations occurred when the AOT-BZ reaction was illuminated have similar "recoil" peaks, the same as the one presented in the insert.

III-L-11 Photoinduced Bifurcation and Multistability in the Oscillatory Briggs-Rauscher Reaction

Noriaki OKAZAKI, Yoshihito MORI *(Nagoya Inst. Tech.)* **and Ichiro HANAZAKI**

[*J. Phys. Chem.*, **100**, 14941 (1996)]

The effect of continuous light irradiation on the Briggs-Rauscher (BR) system was studied by the light intensity scanning method. A cross-shaped phase diagram was established in the control parameter plane spanned by the initial concentration of I^- ($[I^-]_0$) and the light intensity (P). It exhits the oscillatory state (OS), the reduced steady state (SSI) and the oxidized steady state (SSII), the transitions between them being accompanied by hysteresis. A tristability is observed in the overlapped part of the two hysteresis regions. The transition between OS and SSI is explained by the switching of the autocatalysis in HIO_2 (AC), which is controlled by $[I^-]$ with respect to its threshold $[I^-]_{th}$. However, there exist several difficulties in explaining the transition between OS and SSII based on this scheme. First, in SSII, $[I^-]$ decreases monotonously with decreasing P. In spite of this, the system finally bifurcates into OS on further decreasing P. Second, the concentration of I_2, which was confirmed to undergo photodissociation, was observed to increase with P both in OS and SSII. In order to totally explain these observations, we proposed an additional photoautocatalysis

$$(1/2)I_2 + IO_3^- + HIO_2 + 2Mn^{2+} + (1/2)H_2O_2 + H_2O \rightarrow 2HIO_2 + I^- + 2MnOH^{2+} + (1/2)O_2 \qquad (AC')$$

The switching of AC' is primarily controlled by $[I^-]$ similarly to the case of AC, however, the value of $[I^-]_{th}$ depends now on P. The increase of $[I_2]$ with P can be understood as due to the contribution of a positive feedback loop composed of AC' and the dark reaction

$$HOI + I^- + H^+ \rightarrow I_2 + H_2O$$

Although the mechanism proposed here is still at the primitive stage, it has been shown to predict most of the complex photoresponse of the BR system qualitatively very well.

III-M Dynamical Stereochemistry in Molecular Photodissociation

Scalar and vector quantities of reaction products provide detailed insights into the dynamics of atomic/molecular collisions and molecular photodissociation. In particular, knowledge of vector quantities and their correlation is essential for the elucidation of stereochemical properties. In recent years, much attention has been paid to the correlation between the angular momentum (J) and recoil velocity (v) in photofragments. The v-J correlation for a molecular fragment is mainly created by the repulsive force and torque at the bond cleavage. Therefore, it reflects the topography of the potential energy surface (PES), but it is not sensitive to electronic symmetry. On the other hand, the v-J correlation in an atomic fragment is due to electronic orbital alignment, so that it will reflect the electronic character of the PES. So far, investigations of the alignment of atomic fragments were primarily concerned with overall alignment in the laboratory frame detected by polarized emission from atoms. Instead of observing emission, atomic fragments can be detected by resonance-enhanced multi-photon ionization (REMPI). REMPI allows us to examine not only the alignment from the polarization analysis, but also the velocity of atoms from ion imaging techniques. Multi-photon excitation is also more advantageous than a one-photon process for extracting higher order terms in angular momentum polarization. Two-dimensional (2D) photofragment ion imaging and quantum-mechanical analysis were performed to determine the alignment and the recoil velocity of atomic fragments simultaneously.

III-M-1 Simultaneous Measurement of Recoil Velocity and Alignment of S($^1D_2$) Atoms in Photodissociation of OCS

Yuxiang MO, Hideki KATAYANAGI, Michael C. HEAVEN and Toshinori SUZUKI

[*Phys. Rev. Lett.*, 77, 830 (1996)]

The recoil velocity and alignment of S($^1D_2$) atoms produced by 223 nm photodissociation of OCS have been measured by a 2D ion imaging method. The polarization dependence of the 2D images has been analyzed quantum mechanically, and helicity distributions have been determined for different velocity components of S($^1D_2$) atoms. Good agreement has been obtained between the images experimentally observed and those simulated. Although OCS is linear in the ground electronic state, it can be bent in excited states by Renner-Teller interactions. The major component in the 223 nm photoabsorption of OCS is the transition to the Renner-Teller A' component of a $^1\Delta$ state. For the lower symmetry of the bent states (C_s point group), states can be classified as either A' or A" according to whether they are symmetric or antisymmetric with respect to reflection through the molecular plane. Since the electronic state of the diatomic fragment CO X($^1\Sigma^+$) is symmetric, the overall symmetry of the asymptotic state is determined by the symmetry of the S($^1D_2$) atom. Our result indicates that 20% of the asymptotic states were of A' symmetry, even though the optical transition is A' $\leftarrow$ A'. The appearance of products with A" symmetry is ascribed to Coriolis coupling in the dissociation process.

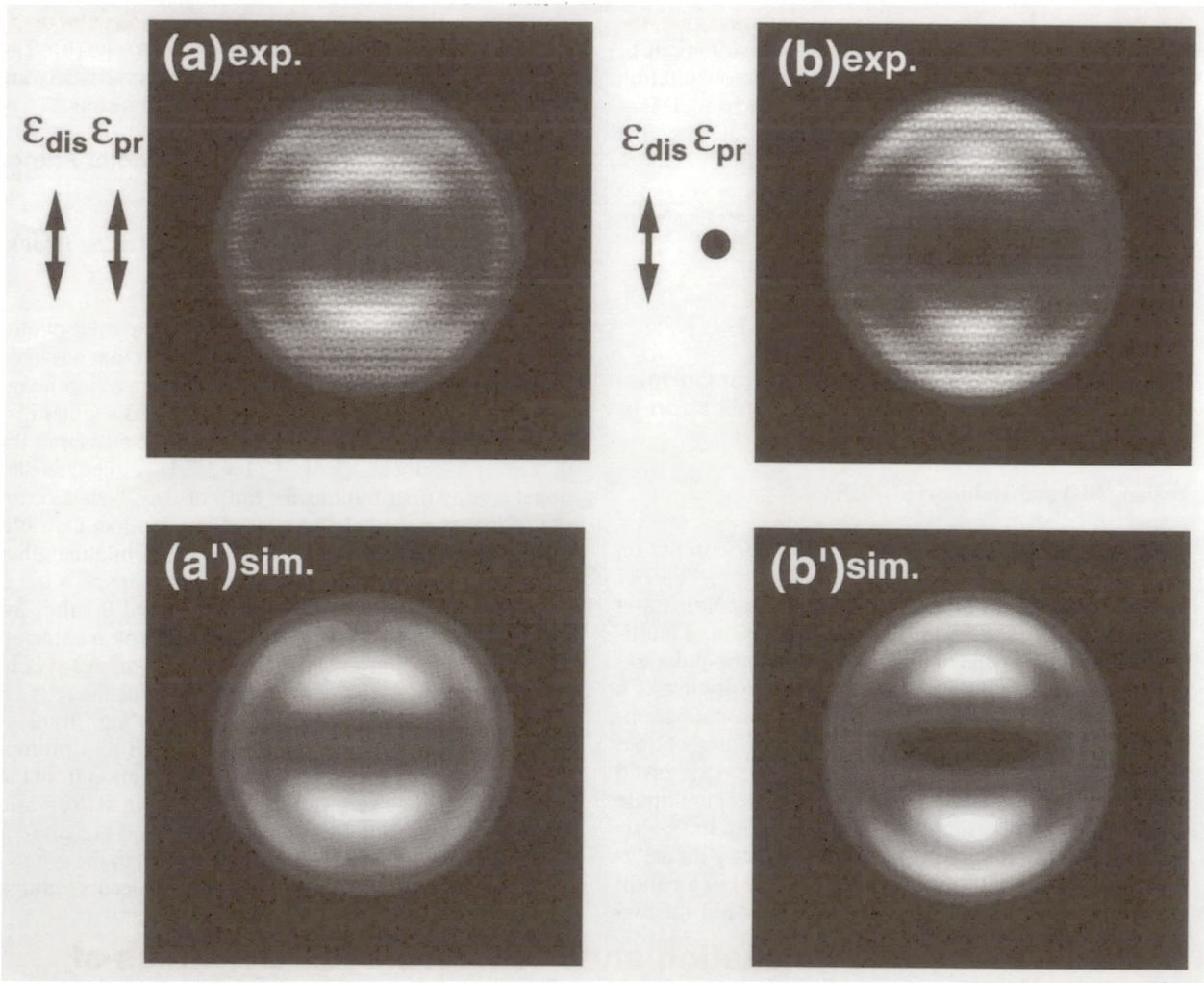


Figure 1. 2D ion image of $S(^1D_2)$ produced by 223 nm photodissociation of OCS. (a) and (b) are the experimental data. (a') and (b') are the simulated images. The polarization direction of photolysis and probe laser beams are shown in the figure as ε_{dis} and ε_{pr}. The experimental data have been symmetrized for ease of comparison with the calculated images.

III-M-2 Multiple Dissociation Channels and Orbital Alignment in Ultraviolet Photodissociation of N_2O

Tatsuo GEJO and Toshinori SUZUKI

Despite the small photoabsorption cross section (σ_{abs} = 9.0 x 10^{-20} cm^2 at 193 nm at 301 K), ultraviolet photodissociation of N_2O near 200 nm has been often employed as a source of $O(^1D_2)$ atoms in reaction dynamics and kinetics experiments. Although the photodissociation of N_2O has been considered to be well characterized, there exists potential complication in the photodissociation dynamics due to Renner-Teller interaction in the excited states. In our previous work,[1] the recoil velocity distribution of $O(^1D_2)$ atoms produced by 205 nm photodissociation of N_2O has been measured by one-color photofragment imaging. It was found that the velocity distribution consists of at least two components, and that the electronic orbitals of $O(^1D_2)$ atoms are aligned in the molecular frame. In order to confirm these results and obtain further information about dissociation dynamics, a two-color imaging experiment has been performed. N_2O in a molecular beam has been photodissociated at 203.3 nm and $O(^1D_2)$ fragments were observed by [2+1] REMPI via the $^1P_1$ state at 205.47 nm. The dependence of the image on pump and probe laser polarization was clearly seen, confirming that the electronic orbitals of $O(^1D_2)$ photofragments were aligned.

Reference
T. Suzuki *et al.*, Chem. Phys. Lett., **256**, 90 (1996).

III-M-3 Wavelength Dependence in Photodissociation of OCS

Hideki KATAYANAGI, Shinkoh NANOBU, Tatsuo GEJO, Mutsumi AOYAGI and Toshinori SUZUKI

The photodissociation dynamics of isovalent molecules such as CO_2, N_2O, OCS are complicated because the Renner-Teller interaction results in overlapping optical transitions and/or non-adiabatic transitions between excited states. It has been shown that the speed and angular distributions of $S(^1D_2)$ atoms produced by ultraviolet photodissociation of OCS consist of two components, one with high anisotropy and slow speed and the other with small anisotropy and fast speed. In our previous work,[1] we have suggested that these two components are due to the overlapping transitions to the A' Renner-Teller component of the $^1\Delta$ state and the A"($^1\Sigma^-$) state. Owing to the difference in the $^1\Delta \leftarrow \tilde{X}$ and $^1\Sigma^- \leftarrow \tilde{X}$ absorption spectra, a wavelength dependence is expected for the dissocia-

tion dynamics. In order to examine our interpretation, the variation of speed, angular, and alignment distributions of $S(^1D_2)$ were measured as a function of photoexcitation wavelength. It was found that A" component increases for the longer photoexcitation wavelength, indicating that the A" component is not due to A" Renner-Teller component of the $^1\Delta$ state but due to the A"($^1\Sigma^-$) state. *Ab initio* calculations of the exited potential energy surfaces were also performed.

Reference
1) H. Katayanagi *et al.*, Chem. Phys. Lett., **247**, 571 (1995).

III-M-4 Semiclassical Analysis of Vector Correlation in Photodissociation and its Application to Photofragment Imaging

Yuxiang MO and Toshinori SUZUKI

A semiclassical theory to treat vector correlation in diatomic photofragments has been developed. Theory for optical detection of angular momentum polarization contains two key factors. One is the expression of multipole moments that specify angular momentum polarization, and the other is optical transition intensity that is a function of multipole moments and experimental parameters. When the rotational angular momentum is large, angular momentum polarization can be expressed semiclassically. We have derived semiclassical multipole moments in two coordinate systems; one with the z-axis fixed along the velocity vector, and the other with the z-axis fixed along the transition dipole moment of a parent molecule. We have also derived an expression for two photon transition intensities for diatomic molecules in the intermediate coupling case of Hund's case (a) and (b). The theory has been applied to the 355 nm photodissociation of NO_2 and tested against the experimental results.

III-M-5 C-Cl Bond Rupture in Ultraviolet Photodissociation of Vinylchloride

Kenichi TONOKURA, Lizla B. DANIELS, Hideki KATAYANAGI and Toshinori SUZUKI

Cl atomic elimination through ultraviolet photodissociation of vinylchloride at 193 and 210 nm has been studied by a state-resolved 2D photofragment ion imaging technique. The translational energy and angular distributions of the Cl atomic fragments were measured for the two spin-orbit states of ^2P_J (J = 3/2,1/2). The translational energy distributions for both of the ^2P_J states consist of two components; one is a Gaussian-like distribution with high anisotropy, $\beta = 1.0 \pm 0.2$, while the other is a statistical distribution with low anisotropy, $\beta = 0.3 \pm 0.2$. These features were almost identical for the two photoexcitation wavelengths. The anisotropy parameter, β, of the Gaussian translational energy component is in good agreement with the value predicted for the $\pi^* \leftarrow \pi$ transition by *ab initio* calculations. The high translational energy component of Cl is assigned to a prompt dissociation induced by the electronic relaxation from the (π,π^*) bound state to a $(\pi(Cl),\sigma^*)$ repulsive state, while the low translational energy component is assigned to a slow dissociation by relaxation from (π,π^*) to the ground electronic state. The Cl atomic elimination occurs through single C-Cl bond rupture.

III-N Electronic Relaxation and Predissociation Dynamics of Acetylene

Although acetylene is one of the smallest hydrocarbon molecules and is of great importance in combustion chemistry, its photophysical and photochemical properties are still poorly understood. In 193.3 nm photoexcitation, it has been found that C_2H_2 undergoes dissociation into C_2H ($\tilde{X}^2\Sigma$ and $\tilde{A}^2\Pi$) + $H(^2S)$. Nevertheless, it has not been established at which energy the dissociation starts and which electronic state is the doorway for dissociation. This project aims at obtaining comprehensive picture of the electronic relaxation and predissociation dynamics from the $\tilde{A}$ state of acetylene.

III-N-1 Energy and State Dependence in the Quenching and Predissociation of C_2H_2

Nobuhisa HASHIMOTO *(Graduate Univ. for Advanced Studies)* **and Toshinori SUZUKI**

[*J. Chem. Phys.*, **104**, 6070 (1996)]

The energy and state dependence in quenching and predissociation of acetylene from the $\tilde{A}^1A_u$ state has been investigated by direct absorption, laser induced fluorescence, and H-atom action spectroscopies. It has been found that (a) H photofragment starts to be produced from a level 221 cm^{-1} above the dissociation energy, (b) the predissociation rate increases with the excitation of rotation around the a-axis, (c) the quenching and predissociation have different J-dependence, and (d) J-dependent quenching occurs at V^3K^1 level which lies below the dissociation threshold. From the translational energy release calculated from Doppler line widths of H atoms, it has also been found that there exists an exit energy barrier of about 560 cm^{-1}. The result indicates that the doorway state for dissociation is a triplet state.

III-N-2 State Dependence and Absolute Value of Fluorescence Quantum Yield from $\tilde{A}^1A_u$ State of C_2H_2

Nobuhisa HASHIMOTO *(Graduate Univ. for Advanced Studies)* **and Toshinori SUZUKI**

Absolute values for the fluorescence quantum yields of selected levels of the $\tilde{A}^1A_u$ state of C_2H_2 have been measured. Fluorescence from the A state of nitric oxide was used as a reference. The values determined were as low as 0.13, 0.021, 0.016, and 3.5×10^{-4} for J'=1 levels of V^2K^1, V^3K^1, V^4K^1, and V^5K^1, respectively. The results indicate that acetylene is quenched up to 90% at energies 2000 cm^{-1} below the dissociation threshold. The major part of this efficient quenching was assigned to be intersystem crossing to T_1. The state-dependence of the quenching has been modeled by assuming that spin-orbit coupling mediates interactions with the triplet state (T_1) and that Coriolis coupling causes mixing with the ground state.

III-N-3 Anomalous Line Intensities and Lifetime Variations within the V^2K^1 Manifold of C_2H_2

Yang SHI, Michael C. HEAVEN and Toshinori SUZUKI

Several vibronic levels of $C_2H_2(\tilde{A})$ exhibit anomalous rotational line intensity distributions when they are examined by LIF techniques. These anomalies do not appear in the absorption spectrum, even when it is measured by observing the transmitted intensity of the beam used to excite LIF. It was found that the effective quantum yield for $C_2H_2(\tilde{A})$, defined by dividing the LIF spectrum by the absorption spectrum, exhibited an alternation for even and odd J in some vibronic levels. This behavior was particularly unusual because the effective fluorescence quantum yields appeared to be anticorrelated with the collision free fluorescence decay rates. We have studied this phenomenon in some detail for the V^2K^1 rotational manifold. Through new measurements of the fluorescence decay lifetimes, self-quenching rate constants, and LIF spectra recorded under extreme quenching conditions, we have shown that the anomalous line intensity patterns do not originate from variations in the fluorescence quantum yield. Experiments using filters to isolated regions of the fluorescence spectrum do not support the notion that state dependent changes in the fluorescence spectrum, resulting from localized perturbations, are the cause of the anomalies. Further work using jet cooling of C_2H_2 is in progress to determine the cause of the LIF intensity anomalies.

III-N-4 State Dependent Fluorescence Decay Dynamics of $C_2D_2(\tilde{A})$

Yang SHI, Michael C. HEAVEN and Toshinori SUZUKI

To obtain additional insights concerning non-radiative decay processes in the $\tilde{A}$ state of acetylene, we have initiated studies of C_2D_2. On deuteration, it is expected that the absolute and relative efficiencies of internal conversion and intersystem crossing will be modified due to changes in the Franck-Condon overlap between the $\tilde{A}$ state and the ground and triplet states. Processes mediated by nuclear spin will also be influenced when protons (I=1/2) are replaced by deuterons (I=1). Among other issues, it is of interest to see how the effective fluorescence quantum yield is affected by deuteration. Does the alternation with even and odd J persist in C_2D_2, and, if so, how does the modulation amplitude compare with that observed for C_2H_2?

At room temperature the C_2D_2 spectrum is congested by the presence of many hot bands, and the partitioning of population into many ro-vibrational levels greatly diminishes the absorptions produced by individual rotational lines. Consequently, we are probing the fluorescence quantum yield through measurements of the collision-free fluorescence decay rates. Cooling in a free-jet expansion was used to reduce the spectral congestion and problems associated with partitioning of the population.

III-O Femtosecond Real Time-Clocked Photofragment Imaging

Molecular photodissociation dynamics has been extensively studied by measuring speed and angular distributions of photofragments (PTS; photofragment translational spectroscopy). Nevertheless, PTS has hardly ever been coupled with direct observation of the time evolution of a photodissociation event. Reaction time scales have often been estimated from the reduction of angular anisotropy due to molecular rotation of a photoexcited molecule. Recent advances in femtosecond laser technology now provide an external time clocking faster than molecular rotation. By combining the femtosecond pump-probe technique and product mass analysis, the formation and decay of photoexcited parent molecules and of fragments can be monitored in real time. In addition, the speed and angular distributions of photofragments can be measured as a function of pump-probe time delay by 1D time-of-flight (TOF) measurement or 2D ion imaging technique. With femtosecond time-clocked imaging, the real time evolution of photofragment scattering distributions can be visualized frame by frame. The first femtosecond time-clocked photofragment imaging has been performed.

III-O-1 Photofragment Imaging with Femtosecond Laser Pulses

Takeshi SHIBATA *(Graduate Univ. for Advanced Studies)* **and Toshinori SUZUKI**

[*Chem. Phys. Lett.*, **262**, 115 (1996)]

Photofragment ion imaging with femtosecond real time clocking has been applied to α-bond cleavage from $^1(n,\pi^*)$ states of acetylchloride and acetone. Figure 1 shows a 2D ion image of CH_3CO produced by 253 nm photodissociation of acetylchloride. The image was measured with a *pump-probe* time delay of 1 ps. The result indicates that the dissociation occurred in less than a picosecond and that CH_3CO radicals were predominantly scattered along the pump laser polarization at high speed. An analysis of the Abel-transformed image has provided the center-of-mass translational energy release, $P(E_t)$, which was peaked at 17 ± 3 kcal/mol, and the anisotropy parameter of 0.9 ± 0.3 at the peak of $P(E_t)$. Since molecular rotation in such a short period of time can be neglected, the anisotropy observed is directly related to the transition dipole moment direction. The anisotropy observed in the present experiment indicates that the transition dipole moment is tilted by 37 ± 6° from the C-Cl bond axis, which is consistent with the assignement of an initial photoexcitation to a $\pi^* \leftarrow n$ transition. We have found that the reaction time for a-bond cleavage in acetone is longer than 15 ps. Although CH_3CO^+ fragments were seen within 15 ps, the ion image showed that they originate from dissociation of $(CH_3)_2CO^+$.

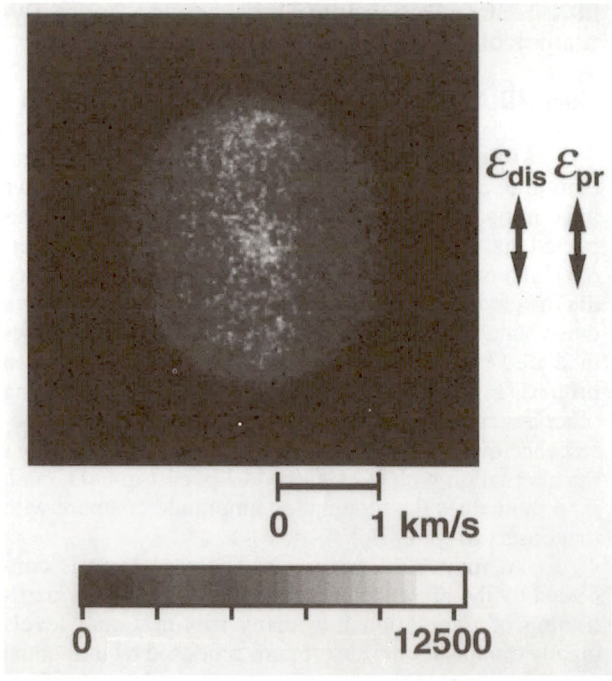


Figure 1. Two-dimensional ion image (384 x 384 pixels) of CH_3CO produced by 253 nm photodissociation of acetylchloride. The pump-probe time delay is 1 ps. The pump and probe laser polarizations are vertically aligned in the figure. The image was integrated over 6,000 laser shots. The numbers shown in the color map are the intensities in the image data.

III-P Crossed Beam Studies of Bimolecular Reaction Dynamics

In order to understand chemical reactions, a detailed knowledge of the dynamics of atomic and molecular collisions is needed. Crossed molecular beams provide a powerful and versatile approach for the study of reactive and inelastic encounters. However, with the conventional detection technique using electron impact ionization, differential cross sections were hardly measured with rotational resolution. This project aims at the measurement of fully state-resolved differential cross sections for reactive scattering processes via two-dimensional ion imaging. The reaction of $O(^1D_2)$ atoms will be investigated because of their importance and relevance in atmospheric chemistry.

III-P-1 Construction of a Crossed Molecular Beam Machine with a Photolytic Atomic/Radical Beam Source

Nobuaki YONEKURA, Hiroshi KOHGUCHI and Toshinori SUZUKI

A crossed molecular beam machine with 2D ion imaging apparatus and a photolytic atomic/radical beam source has been constructed. Each of the beam sources are pumped by two diffusion pumps (2×2000 l/s) backed by roots blowers (250 and 500 m^3/hour), while the main chamber is pumped by tandem turbo molecular pumps. An atomic (radical) beam is produced by the photolysis of precursor molecules at the throat of pulsed nozzle during the adiabatic expansion of the gas. Atomic and target beams are crossed in the main chamber and the quantum-state-resolved differential cross sections are measured by two-dimensional ion imaging method. The imaging apparatus consists of a microsphere plate (70 mm ϕ) with P47 phosphor screen and a gated camera.

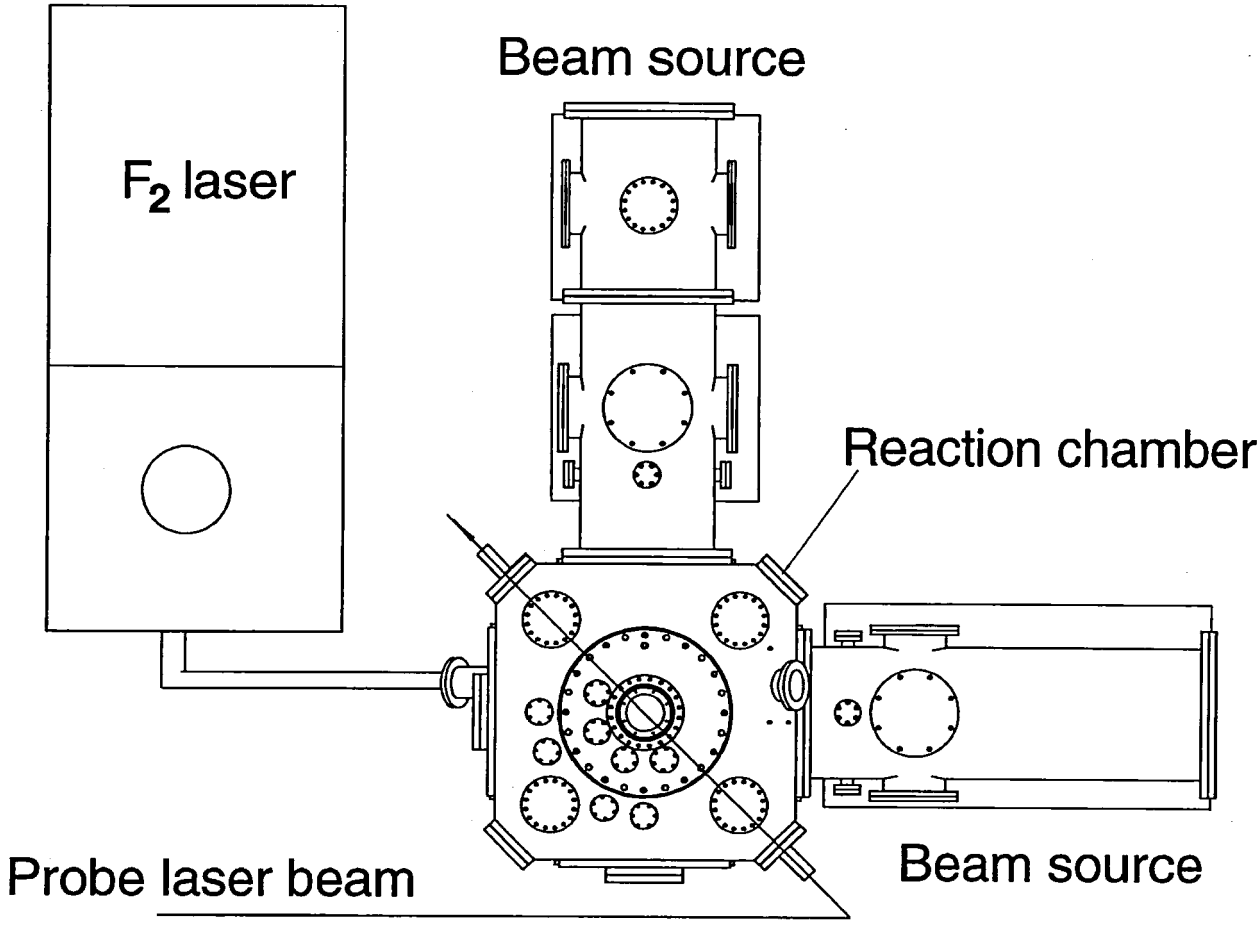


Figure 1. Schematic view of the crossed beam apparatus.

III-Q One Atom Cage Effect and a Search for Dynamical Resonance

The modification of dissociation dynamics caused by the presence of a rare gas atom in a binary complex (often referred to as the one atom cage effect) has attracted the attention of both experimentalists and theorists for many years. This problem is of interest because it may ultimately yield insights concerning the role of solvent effects in condensed phase chemistry. Theoretical analyses conclude that the rare gas atom - hydrogen halide (Rg-HX) complexes provide good model systems for exploration of the cage effect. Through photolysis of the HX bond, the signatures of trapped H-atom trajectories should be evident in the H atom scattering distributions and the absorption spectra.

III-Q-1 Measurement of Absorption Spectra of Size-Selected Clusters by Population Labeling Spectroscopy

Michael C. HEAVEN, Hideki KATAYANAGI and Toshinori SUZUKI

Ultrafast dynamics in an excited state can be seen in an absorption spectrum, since it provides the Fourier-transform of an autocorrelation function. In order to search for an evidence of dynamical resonances in absorption spectra, a sensitive method for observing the spectra of size-selected clusters is needed. Population labeling (hole-burning) spectroscopy allows us to measure an absorption spectrum as a depletion of the ground state population. By using REMPI via the Rydberg states, state- and size-selected detection of the ground state population of clusters is feasible. However, there has been no report of the electronic spectra of Rg-HX clusters. Consequently, we have endeavored to observe electronic spectra of the complexes using REMPI techniques. Preliminary work has yielded the first spectroscopic observation of Ar-HI. Five bands associated with the monomer $g^3\Sigma^-(0^+)$-$X^1\Sigma^+$ transition were observed. Analysis of these data show that the Ar is bound by 420 cm^{-1} in the excited state, and 200 cm^{-1} in the ground state. A progression of the van der Waals stretching mode was seen for the excited state, which yielded vibrational constants of ω_e=48.9 and $\omega_e x_e$=1.41 cm^{-1}. Studies of the photodissociation dynamics of Ar-HI, and the spectroscopy and dynamics of other Rg-HX complexes, are in progress.

III-R Jet Spectroscopy of Benzyl and Substituted Benzyl Radicals

Benzyl radical has two low-lying proximate doublet electronic states, 1^2A_2 and 2^2B_1, and other multiple state does not exist in the energy region of these excited states. These two states are mixed with each other through an asymmetric b_2 mode, which makes very complex vibronic structures in visible spectra. We have studied the effects of substitution on the electronic energy levels and analyzed the vibronic interaction between two states by using the jet spectroscopy.

III-R-1 Laser Induced Fluorescence Spectra of Jet Cooled *p*-Chlorobenzyl Radical

Masaru FUKUSHIMA *(Mitsubishi Heavy Industries Ltd.)* **and Kinichi OBI** *(Tokyo Inst. of Tech. and IMS)*

[*Chem. Phys. Lett.* **248**, 264 (1996)]

We have generated the p-chlorobenzyl radical in supersonic free expansion, and measured the laser-induced fluorescence excitation and dispersed spectra from single vibronic levels. Based on an analysis of the dispersed spectra, we find the two band origins, spaced only 94 cm^{-1} apart, of the D_1 1^2A_2 - and D_2 2^2B_1 - D_0 1^2D_1 transitions in the excitation spectrum. We also observed interstate level mixing between the 6b and 12 vibronic levels of the D_2 and D_1 states, respectively, and the vibronic coupling is analyzed using a simple model within the Born-Oppenheimer approximation

III-S Photochemical Processes Studied by Time-Resolved ESR

Photochemical processes generate abnormal electron spin polarization on excited molecules and free radicals, which is called as chemically induced dynamic electron spin polarization (CIDEP). We have studied photochemical reactions by probing CIDEP. Special subjects interested in are the photochemistry of benzophenone and the quenching of excited singlet and triplet states by free radicals.

III-S-1 Time-Resolved ESR Studies on Ketyl Type Radical-Amine Complexes

Akio KAWAI, Atsushi AOKI *(Tokyo Inst. of Tech.)*, **Yasuhiro KOBORI** *(Tohoku Univ.)* **and Kinichi OBI** *(Tokyo Inst. of Tech. and IMS)*

[*J. Phys. Chem.* **100**, 10021 (1996)]

Time-resolved (TR) ESR spectra were measured for α-hydroxybenzyl-amine (α-HB) and α-hydroxydiphenylmethyl-amine complexes. Hyperfine coupling constants (hfcc) of the complexes were determined, and considerable increase in hfcc was recognized on the hydrogen of hydroxy group of both radical complexes, which suggests that the complexes are produced through the hydrogen bond formation between hydroxy group of the radical and amino group of amines. Complex formation constants were determined for various α-HB-amine complexes by monitoring TR-ESR signals of the complexes against amine concentrations. It has been noticed that the degree of hydrogen substitution on nitrogen atom of aliphatic amine roughly determines the complex formation constant : Complexes with primary amines show the largest value of the complex formation constant while tertiary amines do the smallest one. This result is interpreted by introducing a new concept of radical-amine complex bond formation.

III-S-2 Absolute Magnitude of Spin Polarization in the Radical-Triplet Pair Mechanism: CIDEP Generation by Level Crossings in a Triplet-Doublet Interaction

Yasuhiro KOBORI *(Tohoku Univ.)*, **Masaaki MITSUI, Akio KAWAI** *(Tokyo Inst. of Tech.)* **and Kinichi OBI** *(Tokyo Inst. of Tech. and IMS)*

[*Chem. Phys. Lett.* **252**, 355 (1996)]

CIDEP generated through the interaction of the excited triplet state of benzophenone with TEMPO radical was investigated by time-resolved ESR spectroscopy in benzene. We carefully examined what factors control the CIDEP intensities. By comparing the CIDEP intensity of TEMPO obtained in the triplet benzophenone-TEMPO system with the intensity in the C_{60}-TEMPO system, the absolute magnitude of net emissive polarization was determined to be -6.9 in the unit of Boltzmann polarization. The emissive polarization is attributed to state mixing between a quartet and a doublet in the radical-triplet pair induced by the zero-field splitting interaction of the counter triplet molecule. Our result is quantitatively explained by the theory that the net CIDEP is generated predominantly in regions where the quartet and doublet levels cross. This indicates that the quenching of the excited triplet benzophenone by TEMPO in benzene can proceed via an electron-exchange interaction.

III-T Laser Ablation-Molecular Beam Method. Competitive Solvation of Monopositive Metal Ions in the Gas Phase

We have developed the laser ablation-molecular beam (LAMB) method, in which monopositive metal ions obtained by focusing pulsed laser light on a metal substrate in vacuum are allowed to react with molecules or clusters in a molecular beam injected near by. Product ions obtained on the ion-molecular reaction are probed by a quadrupole mass spectrometer. This method is a very simple and versatile diagnosis to study reactions of monopositive metal ions in the gas phase. Because any metal can be obtained as monopositive atomic ions, we can study novel chemistry of coordination (solvation) of monopositive metal ions in the gas phase. This year, competitive coordination (solvation) of monopositive metal ions has been studied by using binary clusters $(NH_3)_m(C_2H_6CO)_n$.

III-T-1 Laser Ablation-Molecular Beam Method: A Simple and Versatile Diagnosis to Study Chemistry of Monopositive Metal Ions in the Gas Phase

Osamu ITO, Koji FURUKAWA, Yasuhiro HORIKI, Satoru NISHIO, Akiyoshi MATSUZAKI and Hiroyasu SATO* *(Mi'e Univ., Mi'e Univ. and IMS*)*

[*Appl. Surf. Sci.*, in press]

Chemistry of monopositive metal ions in the gas phase has been studied with the laser ablation-molecular beam (LAMB) method developed by the authors' group. In this method, monopositive metal ions (M^+'s) are prepared in the gas phase by laser ablation of metal substrates in vacuum and they are allowed to react with molecules or clusters in a molecular beam injected nearby. The product ions are probed by a quadrupole mass spectrometry. This method has been proved to be a very simple and versatile diagnosis for the study of coordination (solvation) chemistry and organometallic chemistry of monopositive metal ions in the gas phase. Very interesting aspects of competitive coordination (solvation) have been revealed using ammonia-acetone binary clusters in the molecular beam, and they have been studied in comparison with ammonia-water, ammonia-methanol and methanol-water systems previously reported.

III-U Laser Chemistry of Polymers and Solids. Reconstruction of Polymer Films from Laser-Ablated Fragments, Surface Treatment of Polymers with Pulsed Lasers, and Raman Probe of Laser Deterioration of Solids

Laser chemistry of polymer materials and solids are studied. Research directions are threefold. (1) Ablated fragments are deposited on a solid substrate, and reconstructed polymer films are prepared. Taking polyacrylonitrile (PAN) as an example, remarkable wavelength dependence was observed for 308, 248 and 193 nm ablation. In addition, a very interesting intensity dependence was observed at 248 nm. (2) Polyacenic Semiconductive thin films are prepared by excimer laser ablation at 308 nm of a bulk phenol-formaldehyde (PF) resin and heat-treated PF resin. (3) Deterioration mechanisms of metal oxide materials due to excimer laser (308 nm) irradiation have been probed by Raman spectroscopy. A thermal deterioration mechanism is revealed by Raman/SEM measurements.

III-U-1 Preparation of Polymer Films by Laser Ablation of Polyacrylonitrile: Significant Dependence on Ablation Wavelengths

Satoru NISHIO, Tomonori CHIBA, Akiyoshi MATSUZAKI and Hiroyasu SATO* *(Mi'e Univ., Mi'e Univ. and IMS*)*

[*Appl. Surf. Sci.*, in press]

Preparation of reorganized polymer films has been made by deposition of laser-ablated fragments of polyacrylonitrile (PAN), using XeCl (308 nm), KrF (248 nm), and ArF (193 nm) excimer lasers. Morphologies, chemical compositions and molecular structures of reorganized films were probed by scanning electron microscopy (SEM), IR spectroscopy and X-ray photo-electron spectroscopy (XPS). Significant dependence on ablation wavelengths was observed for structural variation as compared to the original PAN: the original structure was essentially preserved by ablation at 308 nm, while extensive cyclization of the nitrile group to yield condensed-ring formation was observed by ablation at 248 nm. Ablation at 193 nm caused elimination of the nitrile group.

III-U-2 Preparation of Polyacenic Semiconductive Thin Films by Excimer Laser Ablation of a Bulk Phenol-Folmaldehyde Resin or Pyrolyzed Polyacenic Semiconductive Materials

Satoru NISHIO, Shinobu KATO, Akiyoshi MATSUZAKI, Hiroyasu SATO,* Hajime KINOSHITA, Shizukuni YATA,** Kazuyoshi TANAKA*** and Tokio YAMABE*** *(Mi'e Univ., Mi'e Univ. and IMS*, Kanebo, Co.**, Kyoto Univ.***)*

[*Synthetic Metals*, submitted]

Polyacenic semiconductive thin films (PAS-TF) were prepared onto a quartz substrate at room temperature by excimer laser ablation at 308 nm of a bulk phenol-formaldehyde (PF) resin and the bulk of PAS material which was obtained by heat treatment of the PF resin at 535°C (pyrolytic PAS(535°C)). Homogeneous brown and/or dark brown thin films consisting of fine particles were obtained. The electric conductivities of the films thus prepared from PF resin and pyrolytic PAS(535°C) were about 10^{-8} S cm^{-1} and 10^{-5} S cm^{-1} at room temperature, respectively. Remarkable increase of electric conductivities was achieved on increasing the substrate temperature during the deposition process. In particular, the conductivity of the film from pyrolytic PAS(535°C) reached more than 10^{-2} S cm^{-1}, which is comparable to that of bulk PAS material prepared by pyrolytic treatment at 775°C, when deposited on a substrate at 300°C.

III-U-3 Preparation of Low-dimensional Conducting Polymer Films by UV Light-induced Deposition with Excimer Laser Beams

Satoru NISHIO, Akiyoshi MATSUZAKI and Hiroyasu SATO* *(Mi'e Univ., Mi'e Univ. and IMS*)*

[*Synthetic Metals*, submitted]

Studies on preparation of low-dimensional conducting polymer films by two kinds of UV light-induced deposition methods with excimer laser beams are presented. Polythiophene thin films are prepared from several thiophene derivatives by excimer laser chemical vapor deposition (ELCVD) with 193 nm (ArF), 248 nm (KrF) and 308 nm (XeCl) beams. A film with highly oriented fibrous

structure is obtained from 2,5-dichlorothiophene (2,5-DCT) by ELCVD with a 193 nm beam. Excimer laser ablation (ELA) of 3,4,9,10-perylene tetracarboxylic dianhydride (PTCDA) with a 308 nm (XeCl) beam results in formation of semiconductive organic thin films consisting of polyperinaphthalene (PPN) structure on a substrate at 300°C.

III-U-4 Raman Spectroscopy as a Useful Probe of Mechanisms of Deterioration of Metal Oxide Materials due to Laser Irradiation

Hiroyasu SATO,* Satoru NISHIO, Shinobu KATO, Kenji MARUMO, Akiyoshi MATZUZAKI and Ryo YOSHIDA** *(Mi'e Univ. and IMS*, Mi'e Univ., Ise Vacuum Optics, Co.**)*

[*Bull. Chem. Soc. Jpn.*, **69**, 3381 (1996)]

Raman spectroscopy provides a very useful means to study mechanisms of deterioration of metal oxide materials due to laser irradiation. Excimer laser irradiation (308 nm) induced transition of anatase of TiO_2 to rutile, while it did not cause substantial changes for rutile or HfO_2. The deterioration mechanism is essentially a thermal one, as supported by the morphological changes monitored by SEM measurements.

III-V Raman Spectroscopy of Photochromic Merocyanine Dye Aggregates

We have found formation of large aggregates (10-100 μm) which precipitate out of solutions, when we UV-irradiated 6-nitro-1',3',3'-trimethylspiro[2H-1-benzopyran-2,2'-indoline] (6-nitro BIPS) in nonpolar solution. The colored aggregates are remarkably long-lived. Aggregate formation through the NO_2 bridges has been expected. A strong supporting evidence for the structure has been obtained by a ^{15}N-isotopomer study.

III-V-1 A Raman Spectroscopic Study of Merocyanine Aggregates of a ^{15}N-Isotopomer of 6-Nitro-1',3',3'-trimethylspiro[2H-1-benzopyran-2,2'-indoline]. A Direct Evidence for the Association through the NO_2-Bridges

Hiroyasu SATO,* Akiyoshi MATZUZAKI, Satoru NISHIO, Motohiro YOSHIMI, Katsutoshi YAMAMOTO and Hideo TOMIOKA *(Mi'e Univ. and IMS*, Mi'e Univ.)*

[*Chem. Lett.*, 715 (1996)]

A Raman spectroscopic study on large-sized merocyanine aggregates prepared by the irradiating a $^{15}NO_2$-isotopomer of 6-nitro-1',3',3'-trimethylspiro[2H-1-benzopyran-2,2'-indoline] (6-nitro BIPS) with UV light in a cyclohexane solution strongly indicates the association of merocyanine monomers through the NO_2-bridges.

III-W Magnetic Behavior of Stable Radical Crystals and Electronic Structures of Organic High-Spin Molecules

As promising candidates for purely organic molecule-based magnets, new types of stable radicals crystals having thioaminyl groups have been investigated. Three thioaminyl radical crystals showing one-dimensional ferromagnetic behaviors with large intermolecular exchange interactions were found. We examined their low-temperature magnetic behavior, heat capacity and magnetic phase transitions. In addition, the spin dynamics of the antiferromagnetic thioaminyls have been studied by single-crystal ESR experiments. We also investigated the spin density distribution of an organic high-spin polycarbene using single-crystal ^1H- and ^{13}C-ENDOR spectroscopies. The spin density distributions give the key information of the intramolecular spin alignment. A spin contraction as the quantum size-effect in the limited-size spin system has been clarified in this polycarbene.

(i) *Magnetic Behavior of Stable Radical Crystals*

III-W-(i)-1 Ferro- and Antiferromagnetic Behaviors of Stable Free Radical Crystals of *N*-(Arylthio)-2,4,6-triarylphenylaminyls

Yoshio TEKI *(IMS and Osaka City Univ.)*, **Yuko TAJIMA, Koichi ITOH, Sadaharu UENO, Yuichi KITAGISHI and Yozo MIURA** *(Osaka City Univ.)*

[*Mol. Cryst. Liq. Cryst.*, **278**, 301-308 (1996).]

As promising candidates for organic molecule-based ferromagnets, we have investigated several stable thioaminyl radicals in the solid states. In addition to *N*-[(2,4-dichlorophenyl)thio]-2,4,6-tris(3-chlorophenyl)-phenylaminyl (**2**) which we have already reported (Mol. Cryst. Liq. Cryst., in press (1995)), other thioaminyl radical crystal showing ferromagnetic behaviors have been found. Thus, *N*-[(2,4-dichlorophenyl)thio]-2,4,6-tris(4-chlorophenyl)phenylaminyl (**1**) radical shows one-dimensional ferromagnetic behavior. The magnetic behavior has been well interpreted in terms of the one-dimensional Heisenberg model with ferromagnetic intermolecular interactions of J/k = 14.0 K. In contrast, *N*-[(2,4-dichlorophenyl)thio]-2,4,6-triphenylphenylaminyl (**4**) shows antiferromagnetic behavior described by an alternating linear chain model with J/k = -8.4 K and a=0.55.

III-W-(i)-2 Magnetic Properties of Purely Organic Radical Magnets, *N*-(Arylthio)-2,4,6-triarylphenylaminyls: Susceptibility and Heat Capacity Measurements

Yoshio TEKI *(IMS and Osaka City Univ.)*, **Koichi ITOH, Yozo MIURA, Sinya KUROKAWA, Sadaharu UENO** *(Osaka City Univ.)* **Atsuhiko OKADA, Hirokazu YAMAKAGE, Tatsuo KOBAYASHI and Kiichi AMAYA** *(Osaka Univ.)*

[*Mol. Cryst. Liq. Cryst.*, in press.]

The magnetic properties of *N*-[(dichlorophenyl)thio]-2,4,6-tris(chlorophenyl)phenylaminyl radical crystals are reported. The stable radical crystals of *N*-[(2,4-dichlorophenyl)thio]-2,4,6-tris(4-chlorophenyl)phenyl-aminyl (**1**) and *N*-[(2,4-dichlorophenyl)thio]-2,4,6-tris(3-chlorophenyl)phenylaminyl (**2**) have shown one-dimensional ferromagnetic behavior which have described using the Bonner-Fisher model with the large ferromagnetic exchange interaction of J/k_B = 14.0 K and J/k_B = 5.7 K, respectively. In addition to these ferromagnetic compounds, *N*-[(3,5-dichlorophenyl)thio]-2,4,6-tris(4-chlorophenyl)phenyl-aminyl (**3**) has also shown the ferromagnetic intermolecular exchange interaction of J/k_B = 1.8 K. For these crystals, we have carried out low-temperature susceptibility and heat capacity measurements below 2 K. Radical **1** has shown a magnetic phase transition at 0.4 K. The susceptibility in the ordered state, however, shows spin-flop transition, indicating antiferromagnetic long range ordering. For the ordered state, the interchain interactions are also estimated to be J'/k_B = 0.02 K and J''/k_B = -0.01 K. In order to clarify the electronic structures, ab-initio molecular orbital calculations of their substituted radicals are carried out. The correlation between the magnetic interactions and the electronic structures is discussed

III-W-(i)-3 Exceptionally Persistent Nitrogen-Centered Free Radicals. Syntheses, ESR Spectra, Isolation, and X-ray Crystallographic Structures of *N*-(Arylthio)-2-*tert*-butyl-4,6-diarylphenylaminyl and *N*-(Arylthio)-4-*tert*-butyl-2,6-diarylphenylaminyl Radicals

Yozo MIURA, Masayoshi MOMOKI, Tomohiro FUCHIKAMI, *(Osaka City Univ.)*, **Yoshio TEKI** *(IMS and Osaka City Univ.)*, **Koichi ITOH and Hisashi MIZUTANI** *(Osaka City Univ.)*

[*J. Org. Chem.*, **61**, 4300-4308 (1996).]

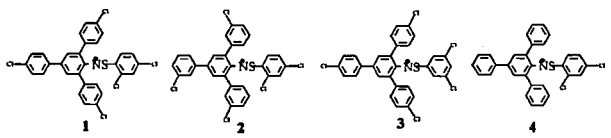
The preparation, ESR spectra, isolation, and X-ray crystallographic structure of *N*-(arylthio)-2-*tert*-butyl-4,6-diarylphenylaminyls and *N*-(arylthio)-4-*tert*-butyl-2,6-diarylphenyl-aminyls are described. The aminyls are generated by PbO2 oxidation. The kinetic ESR study shows that the aminyls are quite persistent, even in the presence of oxygen, and exist in individual radical forms. Among the seventeen aminyls prepared, five aminyls are isolated as radical crystals. The crystallographic structures for two of them are determined by the X-ray analysis. Their aminyls give similar ESR spectra consisting of 1:1:1 triplets with the a_N values of 0.921 - 0.948 mT. One of the purely deuterated aminyls gives satellite line due to ^{33}S isotopes at natural abundance from which a^{33}_S is determined to be 0.51 mT.

III-W-(i)-4 A Single-Crystal ESR Study of Magnetism and Spin Dynamics in *N*-[(2,4-Dichlorophenyl)thio]-2,4,6-triphenylphenylaminyl Radical Crystal

Yoshio TEKI *(IMS and Osaka City Univ.)*, **Yoshimasa OHMURA, Koichi ITOH and Yozo MIURA** *(Osaka City Univ.)*

[*Mol. Cryst. Liq. Cryst.*, in press.]

A single-crystal ESR study of the magnetic properties of *N*-[(2,4-dichlorophenyl)thio]-2,4,6-triphenylphenylaminyl radical crystals (**4**) is reported. The stable radical crystal shows a one-dimensional antiferromagnetic behavior which has described in terms of an alternating linear chain model with J/k_B = -7.5 K and an alternating parameter α=0.55. A detailed analysis of the angular and temperature dependence of the ESR linewidth and g-value has been carried out. The angular dependence of the line-width and line shape observed at 5 K has shown characteristic features expected for a one-dimensional magnetic system: $(3\cos^2\theta-1)^{4/3}$ angular dependence of line width and Lorentzian line shape at θ= 55°. Nagata's theory has applied for the analysis of the temperature dependence of the g-shift. However, the temperature dependence has been only qualitatively reproduced by the theory which is proposed for the one-dimensional regular Heisenberg model. We discuss on the origin of this unsatisfactory agreement. The magneto-structural correlation is also discussed based on the X-ray crystallographic and single-crystal ESR data.



(ii) *Electronic Structures of Organic High-Spin Molecules*

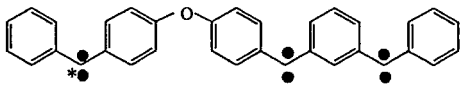
III-W-(ii)-1 Direct Evidence of the Spin Contraction in the Limited-Size Ferrimagnetic Organic Spin System: Determination of the Spin Densities at the Divalent Carbon and Theoretical Calculation of the Spin Contraction

Yoshio TEKI *(IMS and Osaka City Univ.)*, **Takamasa KINOSHITA, Takeji TAKUI and Koichi ITOH** *(Osaka City Univ.)*

[*Mol. Cryst. Liq. Cryst.*, in press.]

In order to clarify the quantum spin contraction in the limited-size organic spin systems, we have directly determined the s and p spin densities on the ^{13}C-isotope labeled divalent carbon site of an organic high-spin molecule, 4-(diphenylmethylene)-4'-[*m*-phenylenebis (phenylmethylene)] ether **1**. This is the most simple model compound for topologically controlled ferrimagnetic spin ordering. The magnitude of the spin density on the divalent carbon site in the diphenylmethylene moiety of **1** is almost one-half of that of diphenylmethylene molecule. This finding gives a direct evidence of the spin contraction expected as a quantum effect on the limited-size ferri-

magnetic spin system. We have also carried out the theoretical calculation of the spin-densities, spin-energies, and spin functions for the ferrimagnetic spin chain systems (-S^A-S^B-S^A-S^B-•••, $S^A \neq S^B$) with different chain lengths by the exact numerical calculation. With increasing number of the repeating unit -S^A-S^B-, the spin contraction has been recovered. The size dependency of the quantum spin contraction is discussed based on the theoretical calculation.



1

* : Carbon 13 labeled

RESEARCH ACTIVITIES IV
Department of Molecular Assemblies

IV-A Solid State Properties of Phthalocyanine Salts and Related Compounds

Some phthalocyanine molecules contain unpaired d-electrons in the conjugated π-electron system. Owing to this special nature, the itinerant π-electrons and localized unpaired d-electrons coexist in solid phthalocyanine salts, in which a one-dimensional double-chain system (metal and ligand chain) is formed. The exchange interaction of itinerant π-electrons with localized magnetic moments is a new aspect in the field of organic metals. For the basic understanding of these materials and to search for a new phenomenon, where a magnetic interaction takes an important role, we prepare and characterize solid phthalocyanine salts and related compounds.

IV-A-1 π-d Interaction in Phthalocyanine Conductors

Kyuya YAKUSHI, Toshihiro HIEJIMA* and Hideo YAMAKADO* *(*Grad. Univ. Adv. Studies)*

[*Proceedings of MMME'96, Tsukuba,* in press]

Partially oxidized phthalocyanine conductors such as $CoPc(AsF_6)_{0.5}$ and $NiPc(AsF_6)_{0.5}$ consist of one-dimensional double chain comprising a transition-metal and organic macrocycle chains. Each of these chains generates a narrow d-band and a wide π-band. The d-band is located near the Fermi level of the π-conduction-band. The interplay between these π- and d-bands will be introduced. The first examples of the interplay is the influence of the magnetic moments of unpaired d-electrons at the Co site to the itinerant π-holes on Pc chain. The exchange coupling with these magnetic moments suppresses the coherent motion of π-holes in $CoPc(AsF_6)_{0.5}$. This conclusion was derived from the comparative study of the isostructural conductors, non-magnetic $NiPc(AsF_6)_{0.5}$ and magnetic $CoPc(AsF_6)_{0.5}$. Another example is the transfer of holes from π- to d-band which is induced by high pressure. This *charge transfer* occurs at 0.5 GPa and continues up to 6 GPa in $NiPc(AsF_6)_{0.5}$. The same phenomenon was observed in $CoPc(AsF_6)_{0.5}$ as well. A metal-nonmetal transition is induced by the pressure at which the charge transfer begins in $NiPc(AsF_6)_{0.5}$.

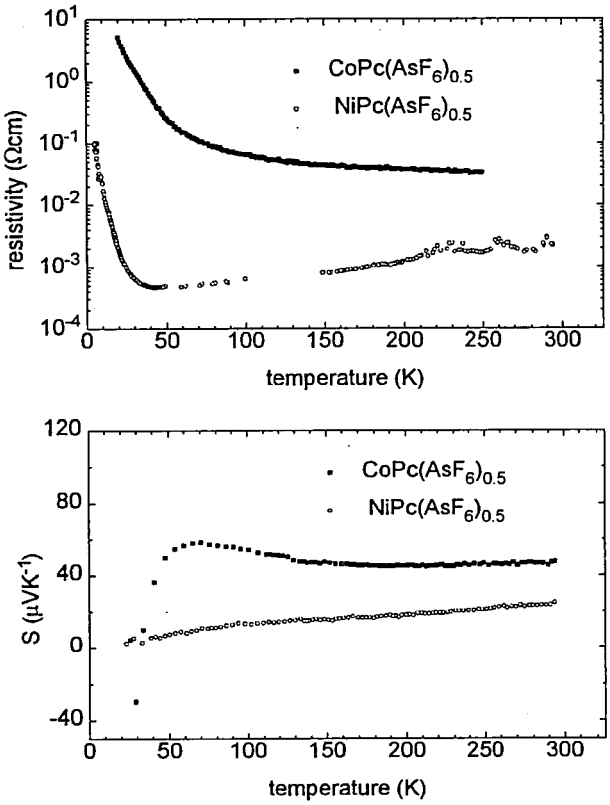


Figure 1. Comparison of the microwave (9.4 GHz) resistivity and thermopower of nearly isostructural $CoPc(AsF_6)_{0.5}$ and $NiPc(AsF_6)_{0.5}$

IV-A-2 Compressibility and High-Pressure Electrical Resistivity of One-Dimensional Phthalocyanine Conductors: the Relationship with d-π Charge Transfer.

Toshihiro HIEJIMA*, Kyuya YAKUSHI, Takafumi ADACHI *(*Grad. Univ. Adv. Studies)*, **Osamu SHIMOMURA** *(PF, KEK)*, **Ichimin SHROTANI** *(Muroran Inst.Tech.)*, **Ken-ichi IMAEDA and Hiroo INOKUCHI**

[*Mol. Cryst. Liq. Cryst.,* submitted]

Powder X-ray diffraction patterns of one-dimensional phthalocyanine conductors (phthalocyaninato)-nickel hexafluoroarsenate, $NiPc(AsF_6)_{0.5}$ and (phthalocyaninato) cobalt hexafluoroarsenate, $CoPc(AsF_6)_{0.5}$, were measured under high pressure. The crystal symmetries of the both compounds were maintained in the pressure range of 0-3.5 GPa. In both compounds, the compressibility along the chain axis is larger than that along the interchain axis. The compressibility of $NiPc(AsF_6)_{0.5}$ below 0.5 GPa is unusually larger than that of $CoPc(AsF_6)_{0.5}$. The relation between the lattice contraction along the chain axis and the pressure-induced d-π charge transfer (metal-ligand charge transfer) is discussed based on a simple ligand field theory. The enhancement of the electrical resistivity was observed at about 0.5 GPa in $NiPc(AsF_6)_{0.5}$. The temperature dependence of the resistivity below 0.5 GPa shows a metallic behavior, while that above 0.5 GPa shows a nonmetallic behavior. This enhancement and temperature dependence are consistent with the suggestion by the analysis of the pressure-dependent plasmon absorption. This resistivity change is attributed to the Anderson localization by the randomly distributed local charges on Ni ion which are produced by the metal-ligand charge transfer.

IV-A-3 Anisotropic Magnetic Susceptibility Measurement of $CoPc(AsF_6)_{0.5}$.

Mkhitar SIMONYAN and Kyuya YAKUSHI

Due to the additional magnetic moment at Co^{2+} site (d-electron), $CoPc(AsF_6)_{0.5}$ shows a much larger paramagnetism than $NiPc(AsF_6)_{0.5}$ in which π-electrons on Pc exhibit the Pauli paramagnetism of 5×10^{-5} emu/mol. The magnetic susceptibility was measured along the parallel and perpendicular directions to the one-dimensional stacking axis using more than 100 single crystals aligned on a quartz plate. Due to the large spin-orbit coupling on Co^{2+}, the magnetic susceptibility shows a large anisotropy. This anisotropy is larger than the anisotropy of the g-value ($g_{//} = 2.00$, $g_{\perp} = 3.20$) of CoPc. Taking account of the strong coupling between d- and π-electrons, the anisotropy of g-value seems to be smaller than that of pure CoPc. This means that $CoPc(AsF_6)_{0.5}$ has a big anisotropy in the antiferromagnetic exchange interaction. The system can be interperted by a XXZ model with $J_{\perp} > J_{//}$. These J are much larger than the room temperature energy, which is consistent with the estimation of J from the analysis of the polarized optical absorption of $CoPc(AsF_6)_{0.5}$.

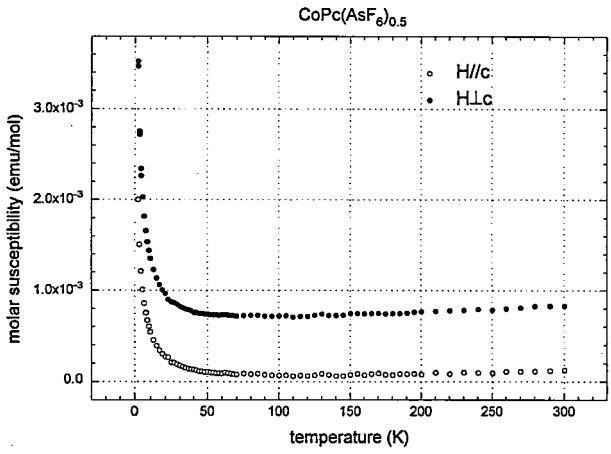


Figure 1. Magnetic susceptibilities of the aligned polycrystals of $CoPc(AsF_6)_{0.5}$.

IV-B Structure and Properties of Organic Conductors

The study of organic metals rapidly developed when the dimensionality of an intermolecular charge-transfer interaction is expanded. This expansion of dimensionality has been brought about by the discovery of new molecules such as BEDT-TTF or C_{60}. In this project we treat one-, two-, and three-dimensional organic metals and superconductors to know what is most important for stabilizing a metallic state and for designing new superconducting materials. We are interested in new organic compounds which may expand the frontier of organic conductors.

IV-B-1 Characterization of the Half-Filled DMTSA-BF_4 by Optical and Magnetic Measurements

Jian DONG, Kyuya YAKUSHI, K. TAKIMIYA* and Tetsuo OTSIBO* *(*Hiroshima Univ.)*

[*Synthetic Metals*, in press]

A quasi-one-dimensional charge-transfer salt with a half-filled band usually shows a insulating property and thus has been regarded as a Mott insulator. In contrast to this general property, DMTSA-BF_4 having a half-filled band shows a high conductivity (σ_{RT}=450 Scm^{-1}) and a metal-like temperature dependence down to *ca.* 180 K and gradually changes into a semiconductor-like behavior with the activation energy of 30 meV. The enhancement of the vibornic modes was observed below 100 K in the //c polarized reflection spectrum, which suggests the lattice distortion such as a dimerization of the DMTSA molecule. The magnetic susceptiblity, ESR intensity, and thermopower also shows the opening of the gap below 100 K. From all these results, we concluded that this metallic material undergoes Peierls transition about 150 K. This metallic property comes from the large transfer integral (t=0.36 eV) compared with the on-site Coulomb energy (U=1.1-1.4 eV) which are estimated from the analysis of the reflection spectrum.

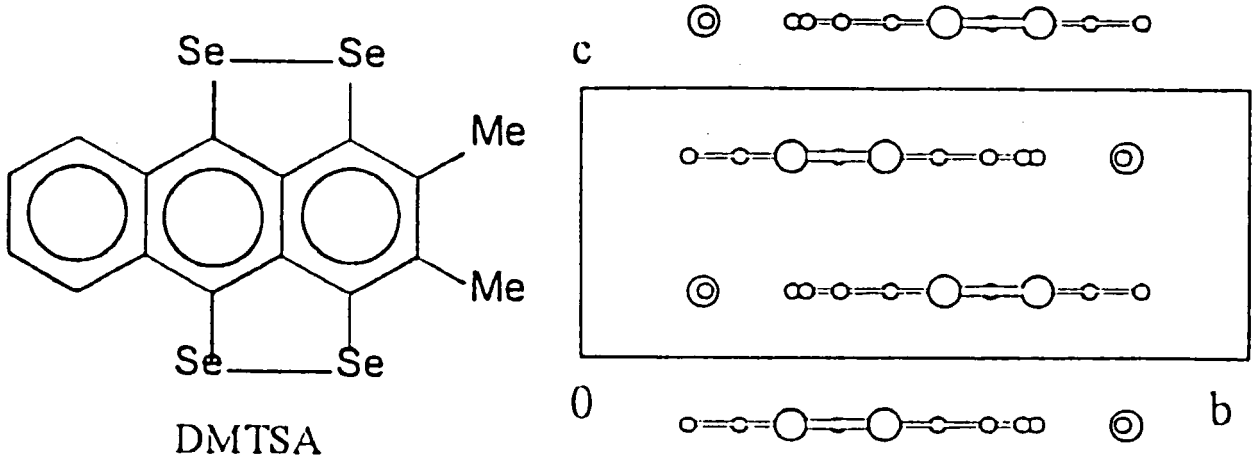


Figure 1. Structural formula of DMTSA and the sideview of the molecular column.

IV-B-2 Electron-Electron Correlations with Articular Attention to *m*-BDNT-PF_6: Spin Susceptibility

Valery A. IVANOV, Kyuya YAKUSHI and Jian DONG

[*Synthetic Metals*, in press]

The formulation of the magnetic susceptiblity of a one-dimensional half-filled correlated system was derrived from the perturbation technique for atomic X-operators and generalized ones [1] considering the Hamiltonian tunnel part as a perturbation. The magnetic susceptibility of a one-dimensional system with a recutangular density of state is

$$\chi(T) = \frac{\frac{1}{w}\left[\tanh\left(\frac{\xi_-(w)}{2T}\right) - \tanh\left(\frac{\xi_-(-w)}{2T}\right)\right]}{1+\frac{U}{\sqrt{w^2+U^2}}\left[\tanh\left(\frac{\xi_-(w)}{2T}\right) + \tanh\left(\frac{\xi_-(-w)}{2T}\right)\right]} + \chi_c$$

This fomula was applied to the high-temperature phase above the spin-Peierls transition temperature (T>150 K) of *m*-BDNT-PF_6, and qualitatively explained the linearly decreasing magnetic susceptiblity.

[1] V. A. Ivanov in *Studies on High-Tc Sperconductors*, vol. 11 (ed. by A. Narlikar) Nova Science, N.Y. (1993); J. Phys.:Condensed Matter **6** (1994) 2065.

IV-B-3 Preparation of New Organic Magnetic Conductors, $[M(mnt)_2]_n$-BDNT (M=Au, Pt, Pd, Ni, n=1 and 2)

Mikio URUICHI, Kyuya YAKUSHI, Yoshiro YAMASHITA and Jingui QIN* *(*Wuhan Univ.)*

Charge-transfer salts of BDNT were prepared by the direct reaction between BDNT-$(SbCl_6)_2$ and $(TBA)_2$-$M(mnt)_2$. All of these salts shows a high conductivity (σ_{RT}=0.1-1 Scm^{-1} for powder samples) at room temperature except $[Au(mnt)_2]_2$-BDNT, in which $BDNT^{2+}$ is not planar and $[Au(mnt)_2]^{1+}$ forms a dimer which is stacked like a crisscross. Naturally this compounds is an insulator ($\sigma_{RT}=10^{-6}$ Scm^{-1}). $Au(mnt)_2$ gives a three different charge-transfer salts: an insulating $[Au(mnt)_2]_2$-BDNT single crystal, conductive $[Au(mnt)_2]_2$-BDNT powder, and conductive $Au(mnt)_2$-BDNT. Among these $M(mnt)_2$-BDNT compounds, the most interesting one is $Ni(mnt)_2$-BDNT, the conductivity of which is 2 Scm^{-1} and shows a ferromagnetic interaction. The Curie temperature has not been determined yet. Lower temperature experiment (T<2 K) is necessary to confirm the ferromagnetism. From the ESR experiment this ferromagnetic behavior seems to be attributed to BDNT. Coexistence of a metallic conductivity and ferromagnetic property is very interesting. However, the low-temperature electrical property is not clear at the moment, since the single crystal has not been obtained.

IV-B-4 Synthesis and Properties of a New Ferromagnetic 2,2'-bipyridine-$MnPS_3$ Intercalation Compound

Jingui QIN, Chuluo YANG* *(*Wuhan Univ.)*, **Kyuya YAKUSHI, Yasuhiro NAKAZAWA and Kenji ICHIMURA**** *(**Kumamoto Univ.)*

[*Solid State Commun.*, in press]

Transition metal hexathiohypodiphosphates MPS_3 (M=Mn, Fe, Co, Ni, etc) have a layered structure made up of two-dimensional arrays of units coordinated to the Mn^{2+} ions. The M^{2+} ions are in the high spin state, and the compounds order antiferromagntically below a critical temperature (78 K for $MnPS_3$ and 120 K for $FePS_3$). We tried to intercalate several organic molecules into these layered compounds, and found a new intercalation compound $Mn_{0.86}PS_3(bipy)_{0.56}$ which was synthesized by a direct reaction of $MnPS_3$ with 2,2'-bipyridine. It was characterized by elemental analyses, thermogravimetry analysis, infrared spectroscopy, and X-ray powder diffraction. The X-ray diffraction shows that only the *c*-axis is expanded without changing the crystal system, which is clear evidence that 2,2-bipyridine is intercalated between the layers of $(MnPS_3)_2$ unit. This material shows a ferromagnetic phase transition at *ca.* 40 K. Characterizations of other intercalation compounds are going on.

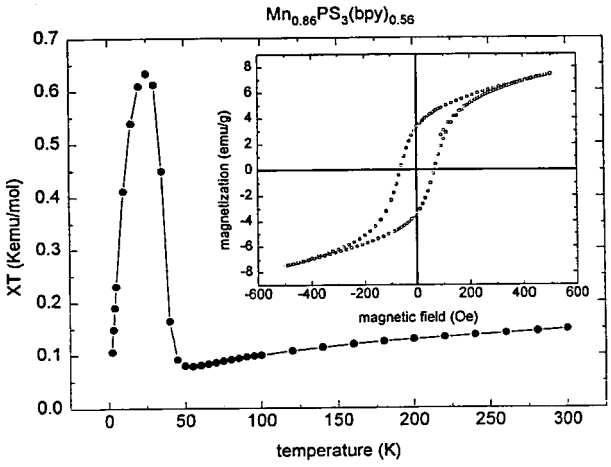


Figure 1. χT curve and hysteresis curve of magnetization at 5 K of $Mn_{0.86}PS_3(bipy)_{0.56}$.

IV-B-5 A Key to the Understanding of Electron-Molecular Vibration Coupling in Organic Charge-Transfer Salts: Application of the Two-Site Hubbard Model

Mikhail E. KOZLOV *(ETL and IMS)*, **Valery A. IVANOV and Kyuya YAKUSHI**

[*J. Phys. Condens. Matter* **8**, 1011 (1996)]

A two-site Hubbard model has been utilized for description of the electron-molecular vibration coupling (EMVC) in organic charge-transfer (CT) salts with dimerized structures. It was shown that the intermolecular charge oscillations in the anti-phase totally symmetric vibrations are accompanied by a decrease of energy of the occupied electronic state in the dimer. This effect is responsible for the frequency shift of i.r.-active electron-vibrational bands compared with relevant Raman modes, and can be described in terms of dimensionless coupling constants. The absorption coefficients for the bands were found to be proportional to the frequency shifts. The calculated values are in good quantitative agreement with experimental data for BEDT-TTF-based and TTF-based monovalent CT complexes.

IV-C Development of a Spiro-Conjugated Donor System: a New Type Donor able to form Charge-Transfer Salts with a 2-D or 3-D Electronic Conduction Band

The study of organic conductors has been rapidly developed after the finding of TTF-TCNQ, and is still progressing mainly on TMTSF, BEDT-TTF, DCNQI, and $M(dmit)_2$ systems. The basic concepts for how to design organic donor or acceptor to get metallic compound were presented already in early periods of this field, all of which concepts request a plane-conjugated molecular structure. The seek for new material is considered to be continued within this old framework as yet. We here mention the possibility of non-planner donor having a spiro-conjugated molecular structure, to yield charge-transfer salts with a multi-dimensional conduction band under less dependence of donor packing motif. The model molecule having a D_{2d} symmetry, its highest occupied molecular orbitals (HOMOs) are degenerated, and hence, we expect ferromagnetic interaction as well as metallic behavior in its radical salt.

IV-C-1 Design of a New Organic Donor having Two Equivalent π-Electronic Systems Perpendicular to Each Other by a Spiro-Conjugation

Akito UGAWA

Most of organic donors and acceptors ever known have been designed to take a planner structure to ensure π-conjugation overall the molecule, and also to have a fulvalene or a quinodimethane skeleton according to successful results. The seek for new materials within this framework seems to have reached the top for last several years, the necessity for breakthrough in this field becoming larger nowadays. We have systematically investigated the electronic structures of various $(BEDT\text{-}TTF)_2X$ salts, being one of very successful systems, by polarized reflectance technique and found that the most characteristic point of this system is a strong two-dimentionality of conduction band owing to loosing an intrastack interaction and simultaneously to closing an interstack interaction by unique packing motifs in its crystalline state, resulting in an increase of a relative two-dimensionality. This character suppresses not only a Peierls instability when it becomes very strong in a 1-D electronic system, but an electron correlation between conduction electrons. The two-dimensionality in BEDT-TTF salts, however, depends on its packing motif and then it can hardly be expected in almost all of other systems because we cannot control how the salt crystallizes. We therefore should consider to design the molecule having a structure able to interact two- or three-dimensionally without a tricky packing. We here present a model donor molecule, which consists of two equivalent π-electron systems perpendicular to each other by a spiro-conjugation. Figure 1 shows the molecular structure of a proposed donor, bis (tetrathiafulvalenyldithio) methane. We performed MO calculations using MINDO method followed by the structure optimization, the results given in Fig. 2, together with those of MDT-TTF for the purpose of comparison. The two TTF units are perfectly perpendicular to each other with a D_{2d} symmetry, and the HOMOs are then doubly-degenerated. There is any report about neither synthesis nor physical properties of this spiro-donors. Nobody knows whether our attempt will be successful or not, but there is no doubt that this is the one that should be tried.

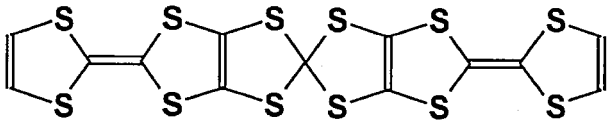


Figure 1. Molecular structure of bis(tetrathiafulvalenyldithio)methane.

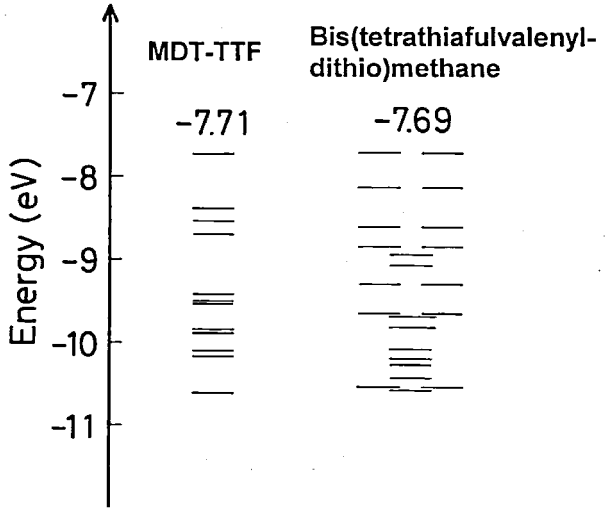


Figure 2. Energy levels of MDT-TTF (left) and Bis(tetrathiafulvalenyldithio)methane (right)

IV-C-2 Synthesis, Redox Property and Spin-Spin Interaction in Bis(Tetrathiafulvalenyldithio)Germane

Kazumasa UEDA, Toyonari SUGIMOTO *(Osaka Pref. Univ.)*, **Hideo FUJITA** *(Kyoto Univ.)*, **Akito UGAWA and Kyuya YAKUSHI**

[*Proceedings of the 17th International Symposium on the Organic Chemistry of Sulfur (ISOCS-17)*, in press]

New tetrathiafulvalene (TTF) derivatives continue to play an important role as donor molecules in the development of organic conductors and superconductors. We are rather interested in donor molecules such as bis(tetrathiafulvalenyldithio)-methane, silane, and germane, where two TTF moieties are arranged perpendicularly by a spiro-bond. In crystals of these donor molecules, it is possible that the two perpendicular TTF moieties are as a matter of course stacked two-dimensionally and furthermore ferromagnetic interaction occurs between the perpendicular stacks, giving an unprecedented organic ferromagnetic metal. For several years we attempted to synthesize this compound using a variety of methods, but there was no successful result. Now, we succeeded in the synthesis of a germanium compound (**1**) by the reaction of bis (tetramethylammonium)bis (tetrathiafulvalenydithiolate) zinc complex with an equimolar amount of germanium tetrachloride in DMF at -40°C. The (**1**) is a black solid (mp. 126-127°C) and very stable in air. The single crystals suitable for x-ray structure analysis is still not obtained. The redox exhibited two pairs of reversible waves at +0.51 and +0.77 V vs. SCE in benzonitrile at 0°C. These potentials are

shifted to a more positive region as compared with those of tetramethylthio-substituted TTF (+0.36 and +0.61 V). The delocalization of an unpaired electron in the radical cation as well as the spin-spin interaction in the dication of (1) will be discussed based on the ESR results.

The electrical conducting property is strongly related to arrangement of donor molecules in the solid. An increasing dimensionality in arrangement can bring a stable metallic state to lower temperatures. This requirement has so far been accomplished by introducing a substituent being capable of an intermolecular interaction into the TTF skeleton. Another approach is the use of donor molecule such as bis(tetrathiafulvalenyldithio)-methane, silane, and germane (1), where the two perpendicular TTF moieties could stack in a two-dimension. In addition, ferromagnetic interaction might be realize between neighboring columns, resulting in an unprecedented organic ferromagnetic metal.

IV-D NMR Study of Organic Conductors

The nuclear magnetic resonance (NMR) is a powerful method to examine electronic state of condensed matters. With this microscopic method, one can get further insight into nature of the metallic, superconducting and magnetic states of materials. In this research project, we aim at getting a comprehensive understanding of a variety of electronic phases in BEDT-TTF compounds by the NMR experiments.

IV-D-1 Nesting Instability in a Family of α-(BEDT-TTF)$_2$MHg(SCN)$_4$ Studied by ^{13}C-NMR

Kazuya MIYAGAWA, Atsushi KAWAMOTO (*Ochanomizu Univ.*) **and Kazushi KANODA**

[*Synth. Met.*, in press]

We have investigated low-temperature electronic states of the organic conductors, α-(BEDT-TTF)$_2$MHg(SCN)$_4$ [M=K, Rb, and NH$_4$] by means of ^{13}C-NMR and dc susceptibility measurements. In a higher temperature range above the nesting transitions, the salts of M=K and Rb show similar temperature dependence in relaxation rate and spin susceptibility while the NH$_4$ salt exhibits an exceptional behavior as seen in Figure 1. This may be related to the fact that the latter alone is free from the nesting instability. For all the compounds, however, the overall temperature dependence of $1/(T_1T)$ scales to that of χ_s^2 except below the nesting instability. This means that the effect of the electron correlation is not crucial in this family. For M=Rb and K salts, the $1/(T_1T)$ decreases below the transition temperature without line-broadening nor relaxation enhancement. All of the NMR data are successfully explained by reduction of the electronic density-of-states below the transition but do not have any sign of magnetic order.

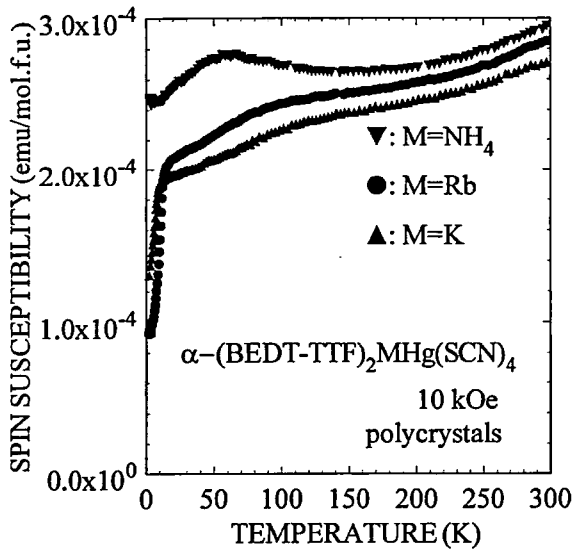


Figure 1. Temperature dependence of spin susceptibility of α-(BEDT-TTF)$_2$MHg(SCN)$_4$ [M=K, Rb, and NH$_4$].

IV-D-2 ^{13}C-NMR and Susceptibility Studies on β-(BEDT-TTF)$_2$I$_3$

Kazuya MIYAGAWA, Atsushi KAWAMOTO (*Ochanomizu Univ.*) **and Kazushi KANODA**

[*Synth. Met.*, in press]

The ^{13}C-NMR and spin susceptibility measurements were performed to investigate the electronic state of β-(BEDT-TTF)$_2$I$_3$ before and after annealing. Interrelation between incommensurate superlattice, low temperature electronic anomaly, superconducting transition temperature and electronic density of states in this salt was found as follows.

The system before annealing has a low-temperature anomaly, which is manifested in kinks in temperature dependence of χ_{spin} and NMR relaxation rate.

In an early stage of annealing less than 50 hours, the anomaly vanishes and an 2.3K superconducting phase with nearly full volume fraction appears.

A further annealing leads to appreciable increase in spin susceptibility (Figure 1) and NMR relaxation rate, suggesting increase of electronic density of states. This change of electronic state is associated with disappearance of the superlattice and appearance of the 7.5K superconducting phase.

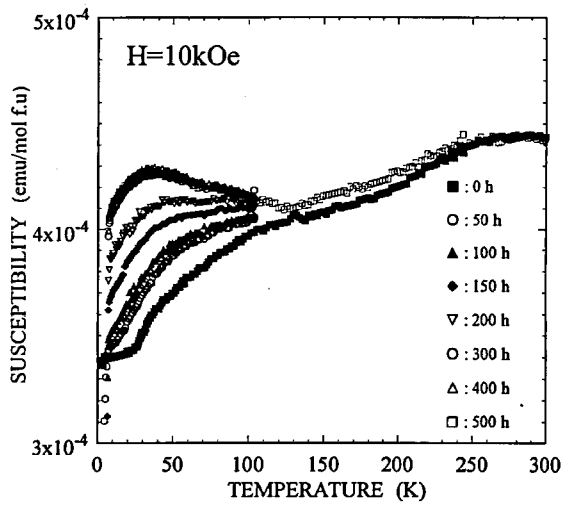


Figure 1. Temperature dependence of spin susceptibility before and during annealing of β-(BEDT-TTF)$_2$I$_3$.

IV-D-3 ^{13}C-NMR Study of Mott Insulating Phase in κ-(BEDT-TTF)$_2$X Family

Atsushi KAWAMOTO *(Ochanomizu Univ.)*, **Kazuya MIYAGAWA and Kazushi KANODA**

[*Synth. Met.*, in press]

The κ-(BEDT-TTF)$_2$X family are quite attractive in the study of metal-insulator transitions and competition between superconductivity and magnetic ordering. We previously reported ^{13}C-NMR study of X=Cu[N(CN)$_2$]Cl salt and discussed the electronic structure in comparison with the results of superconducting salts of X=Cu(NCS)$_2$ and Cu[N(CN)$_2$]Br. In the present work, we have found that the deuterated Cu[N(CN)$_2$]Br salt, when cooled rapidly, shows an antiferromagnetic ordering like the Cu[N(CN)$_2$]Cl salt with only minor fraction of superconducting phase. Figure 1 shows ^{13}C-NMR relaxation rate of κ-(d$_8$-^{13}C,BEDT-TTF)$_2$Cu[N(CN)$_2$]Br along with the results of the superconducting salts. The $(T_1T)^{-1}$ shows a divergent peak around 15 K. This result suggests that the deuterated salt contains a phase with the same properties as in the Cu[N(CN)$_2$]Cl salt. In case of slow cooling, however, $(T_1T)^{-1}$ shows a small hump around 30 K. The ac susceptibility measurements showed that there exists a comparable fraction of the superconducting phase in case of slow cooling while it is diminished to negligible fraction in case of rapid cooling. The hump of around 30 K is considered to reflect the superconducting (metallic) phase.

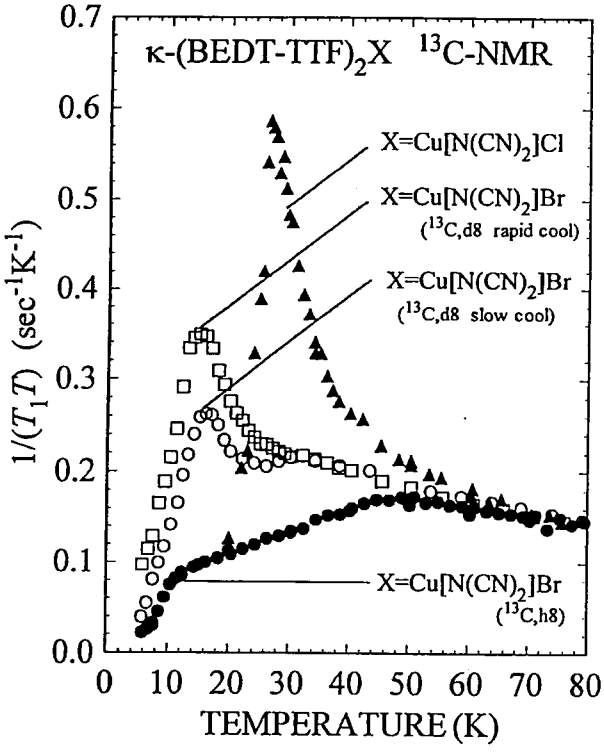


Figure 1. $(T_1T)^{-1}$ of κ-(BEDT-TTF)$_2$X

IV-D-4 Recent Progress in NMR Studies on Organic Conductors

Kazushi KANODA

[*Hyperfine Interactions*, in press]

Recent ^{13}C-NMR studies on a family of quasi-two-dimensional organic conductors based on BEDT-TTF molecules are reviewed in the light of the role of electron-electron correlation in a variety of electronic states and of the symmetry of electron pairing in the superconducting state. Comparison of the nuclear spin-lattice relaxation rate, conducting property and molecular arrangement indicates a close relationship between the molecular arrangement and manifestation of electron correlation. The metal/non-metal phases in the isostructural κ-(BEDT-TTF)$_2$X systems, which are in the strong dimeric regime, are understood as highly correlated metals and insulators crossing the Mott transition. For the 10-K superconducting phase situated near the Mott transition, the absence of Hebel-Slichter coherence peak and a low-temperature T^3-dependence of the nuclear spin-lattice relaxation rate suggest unconventional superconductivity with line nodes in gap parameter or highly anisotropic one. It is noteworthy that the transition temperatures of the BEDT-TTF superconductors do not correlate with the electronic specific heat coefficient, γ, namely the thermodynamic density of states, but with $(T_1T)^{-1}$, which is a measure of the antiferromagnetic spin fluctuations

IV-E Electron Transport and Magnetic Study of Anisotropic Superconductors

There are increasing interests in anisotropic transport and magnetic properties of layered superconductors, because their low-dimensional fluctuations around the transition temperature and dynamic properties of vortex motion are center of unsolved problems in physics of superconductors. In addition to this, such layered superconductors have some possibilities to be used as electronic devices. BEDT-TTF based organic charge transfer salts are typical systems for inquiry of such problems and possibilities, because of their structural peculiarity that the conducting donor layers are separated by thick anion layers. In some BEDT-TTF salts more highly two-dimensional characters than that of Bi-based high-T_c oxide have so far been reported.

IV-E-1 Highly Anisotropic Superconductivity in the Organic Conductor α-(BEDT-TTF)$_2$NH$_4$Hg (SCN)$_4$

Hiromi TANIGUCHI, Hirohiko SATO *(Tokyo Institute for Technology)* **Yasuhiro NAKAZAWA and Kazushi KANODA**

[*Phys Rev.* B **53** (1996) R8879]

A family of organic conductors, α-(BEDT-TTF)$_2$MHg(SCN)$_4$ are quasi-two-dimensional layered metals, where conducting layers composed of BEDT-TTF molecules are separated by thick insulating anion layers. The M=NH$_4$ salt shows superconductivity around 1K. Although the critical temperature is lower than other BEDT-TTF superconductors and high-T_c oxides, this material serves as a model system for comprehensive understanding of phenomenological aspects of two- dimensional nature of superconductivity. In this study, we performed resistivity and ac susceptibility measurements in the in-plane and out-of-plane configurations at a zero magnetic field for more than fifty samples. In Figure1, we show temperature dependence of in-plane and out-of-plane resistivities, which clearly shows an anisotropic nature of superconductive transition. The out-of-plane penetration depth determined from ac susceptibility measurement amounts to about 1.65mm (at 0.4K), which is comparable with the sample size, while the in-plane one is considered to be of an order of 1μm.

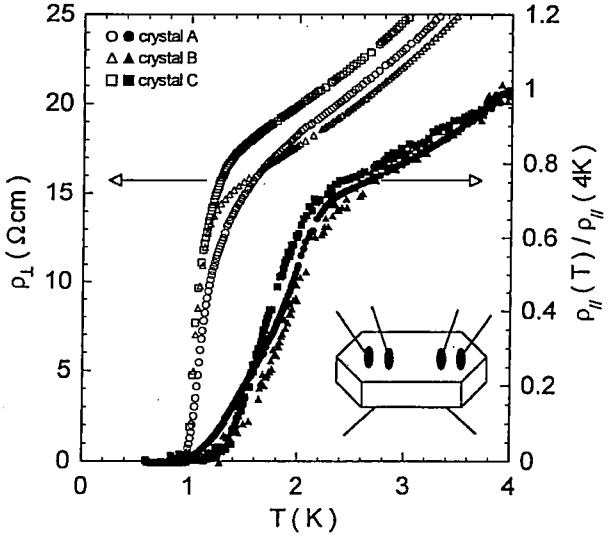


Figure 1. Temperature dependence of in-plane and out-of-plane resistivity of α-(BEDT-TTF)$_2$NH$_4$Hg(SCN)$_4$ samples.

IV-E-2 Vortex State in a Highly Anisotropic Superconductor, α-(BEDT-TTF)$_2$NH$_4$Hg(SCN)$_4$

Hiromi TANIGUCHI, Yasuhiro NAKAZAWA and Kazushi KANODA

[*Synth. Met.*, in press]

In order to characterize peculiar character of vortex state in quasi-two-dimensional superconductor, the H-T phase diagram of α-(BEDT-TTF)$_2$NH$_4$Hg(SCN)$_4$ were studied by specific heat, ac susceptibility and resistivity measurements under magnetic fields applied perpendicular to the plane. The onset temperature of ac susceptibilty in several dc fields gives peculiar lines in the mixed-state of superconducting phase, which is distinctly different from the H_{c2} line determined by the specific heat data. Although in-plane susceptibility which probes compression mode of vortex dynamics has appreciable frequency dependence, its low-frequency limit coincides well with that of out-of-plane ac susceptibility. This characteristic line in H-T phase diagram shown in Figure 1 means that the drastic change of vortex mobility occurs around here, suggesting an existence of vortex liquid state in superconducting state in this material.

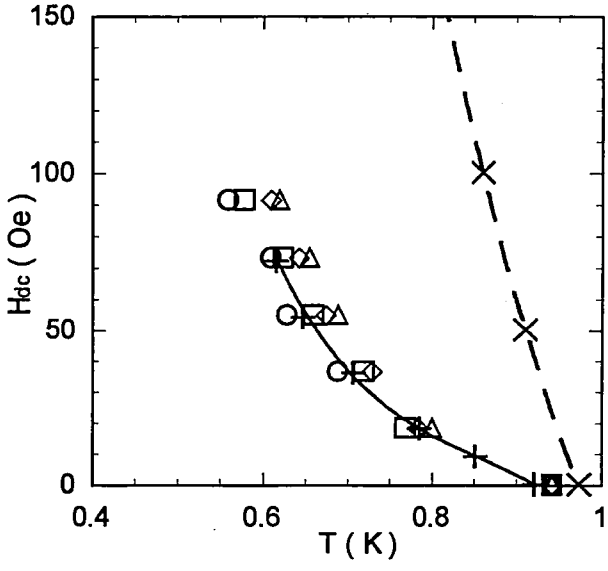


Figure 1. H-T phase diagram of α-(BEDT-TTF)$_2$NH$_4$Hg-(SCN)$_4$. The dashed line represents the mean field H_{c2} line and solid line is the onset of the out-of-plane ac susceptibility.

IV-F Thermodynamic Study of Organic Conductors

In order to get reliable information on the absolute value of electron density of states and on the entropy distribution around the phase transition, specific heat studies are inevitable. In this project, we constructed several calorimeters available at low-temperature region and also in magnetic fields and performed a systematic investigation on organic materials from a thermodynamic viewpoint.

IV-F-1 Electronic Structure of Insulating Salts of the κ-(BEDT-TTF)$_2$X Family Studied by Low-Temperature Specific Heat Measurements

Yasuhiro NAKAZAWA and Kazushi KANODA

[*Phys. Rev.* B **53** (1996) R8875]

The insulating salts of κ-(BEDT-TTF)$_2$Cu[N(CN)$_2$]Cl and κ-(d$_8$;BEDT-TTF)$_2$Cu[N(CN)$_2$]Br are interesting, because the band calculation predicts a similar kind of metallic states for these salts just as for the superconducting X=Cu(NCS)$_2$ and Cu[N(CN)$_2$]Br salts. The insulating nature was tentatively explained in terms of localization effects, where possible conformational disorder of the ethylene groups were supposed to give orientational disorder in the two-dimensional lattice. Recently, it was suggested that the magnetic nature of this material is Mott insulating state rather than disorder-induced localization. It is very important to characterize the ground state of the insulating phase from a thermodynamic point of view by evaluating the magnitude of electronic specific heat coefficient. The low-temperature specific heat was measured by the thermal relaxation method in a zero magnetic field and under magnetic fields up to 8T. In Figure 1, we show the case of d$_8$ X=Cu[N(CN)$_2$]Br salt. The γ value is exactly 0mJ/molK^2 and this value does not change at all in a strong field of 8T. This is also the case of X=Cu[N(CN)$_2$]Cl salt. These results suggest that the ground sate of these materials is an insulating state which has a distinct charge gap.

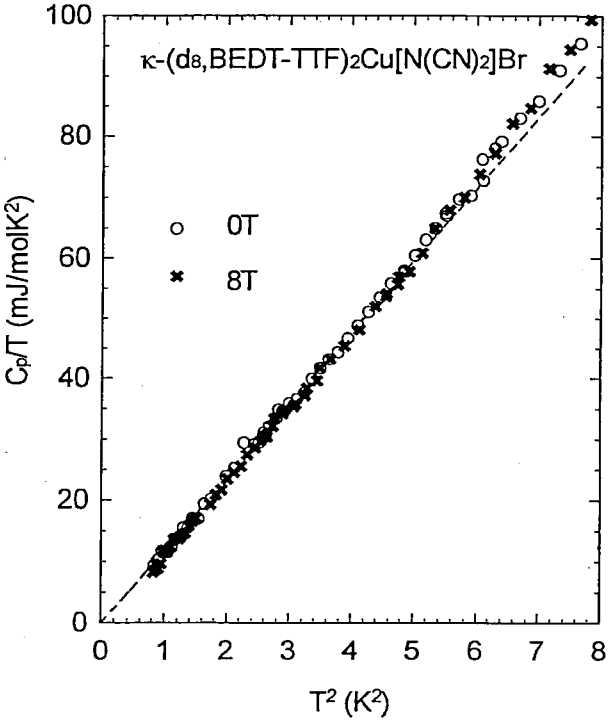


Figure 1. C_p/T vs T^2 plot of κ-(d$_8$; BEDT-TTF)$_2$Cu[N(CN)$_2$]Br.

IV-F-2 Specific Heat around the Magnetic Phase Transition of κ-(BEDT-TTF)$_2$Cu[N(CN)$_2$]Cl

Yasuhiro NAKAZAWA and Kazushi KANODA

[*Synth. Met.*, in press]

The ground state of κ-(BEDT-TTF)$_2$Cu[N(CN)$_2$]Cl salt is considered to be a Mott insulating state which has a magnetic ground state. This material undergoes an antiferromagnetic phase transition around 27K, which was confirmed as a three dimensional long-range order of localized moments by NMR experiment. In usual Mott insulators which have localized moments, the magnetic entropy of S=Rln2(=5.76mJ/molK) should distribute around the Néel temperature and a magnetic peak can be detected by specific heat. The temperature dependence of specific heat of κ-(BEDT-TTF)$_2$Cu[N(CN)$_2$]Cl obtained by adiabatic heat pulse method are compared with non-magnetic κ-(BEDT-TTF)$_2$Cu[N(CN)$_2$]Br salt in Figure1. There is no distinct peak around 27K. The magnetic interaction of neighboring two-dimers can be evaluated as $J=2t^2/U_{dimer}$, where t is inter-dimer transfer energy and U_{dimer} is on-dimer Coulomb interaction. Using the value of molecular parameters, J is estimated at 0.04eV. The two-dimensional short-range ordering dominated by this interaction possibly starts around room temperature, and almost all entropy of Rln2 may distribute in a wide and high-temperature range. In this sense, the situation is very similar to the case of antiferromagntic phase of high-T_c cuprates such as La_2CuO_4 and $YBa_2Cu_3O_6$.

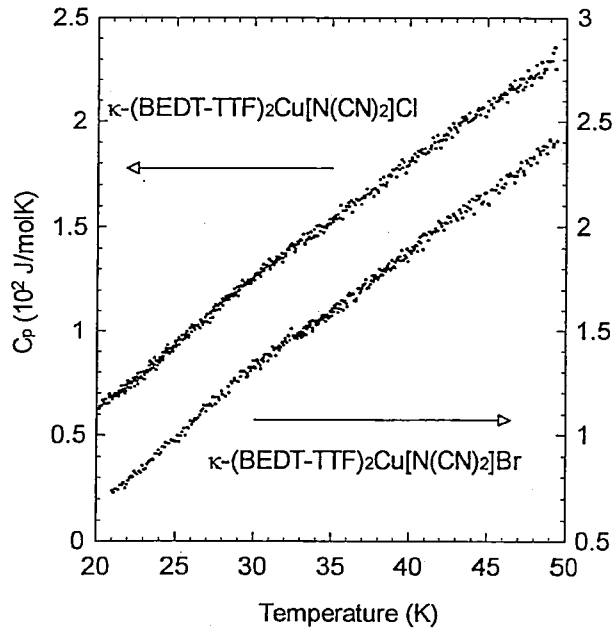


Figure 1. Temperature dependence of specific heat between 20K and 50K for κ-(BEDT-TTF)$_2$X (X=Cu[N(CN)$_2$]Br and Cu[N(CN)$_2$]Cl).

IV-F-3 Low-Energy Excitations in the Superconducting State of κ-(BEDT-TTF)$_2$Cu[N(CN)$_2$]Br Salt

Yasuhiro NAKAZAWA and Kazushi KANODA

The low-temperature specific heat of single crystals of κ-(BEDT-TTF)$_2$Cu[N(CN)$_2$]Br, which is known as a high-T_c salt among BEDT-TTF based organic superconductors, was studied in a temperature range between 0.11K and 4.5K. In order to obtain temperature dependence of electronic specific heat in the superconducting state, we improved resolution of our calorimeter mounted on the dilution refrigerator (Oxford Instruments KELVINOX 25 at Low-Temperature Center,). Assuming that the deuterated salt is a proper reference material to get information on lattice contribution at low-temperatures below 2K, we got temperature dependence of electronic part, which is shown in Figure 1. It is apparent from the figure that quasi-particle excitation over the superconductive gap has a power-law dependence and cannot be explained by the BCS theory which has an activation type dependence. The existence of a finite γ term of about 1-2mJ/molK^2 even in the superconducting state and very sensitive field-dependence of this term were also observed. These results are consistent with a picture of unconventional type of pairing in the superconductivity.

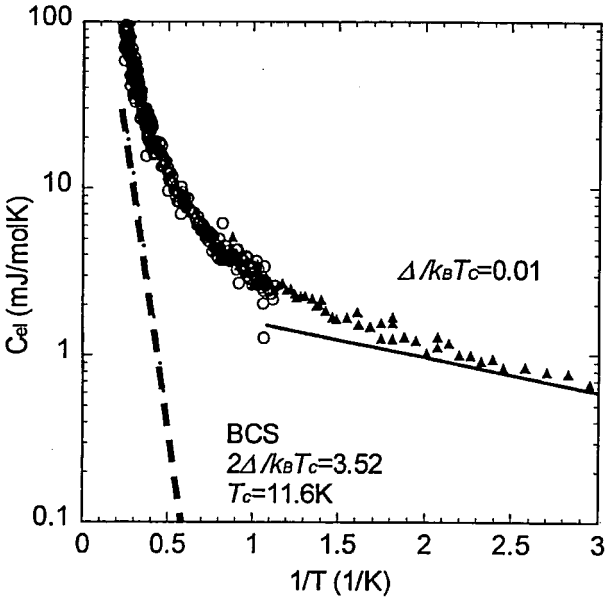


Figure 1. Temperature dependence of electronic specific heat.

IV-G Novel Electronic States of d-π System of (DCNQI)$_2$M

The hybrid electronic systems composed of itinerant and nearly localized electrons are new frontiers of materials. The DCNQI-metal complexes are one promising family of materials along this line. The members of this family can be nearly pure π electron systems or π-d interacting electronic systems, depending on the metal ions. In this research project, we aim at developing a new member of DCNQI-metal complexes with novel electronic properties and getting a comprehensive understanding of a rich variation of the electronic phases in this family.

IV-G-1 Electronic State of the Organic Salt, (DI-DCNQI)$_2$Ag

Ko-ichi HIRAKI and Kazushi KANODA

[*Phys. Rev.* B54 (1996) 17276]

(DI-DCNQI)$_2$Ag , a new member in the DCNQI-Metal complexs, has been investigated by electrical resistance, magnetic susceptibility and ^{1}H-NMR measurements. An activation type of temperature dependence in the resistivity curve suggests an existence of charge gap of about 490K. The magntic susceptibility shows a broad peak around 35K, reminiscent of the Bonner-Fisher type typically observable in low-dimensional system with localized moments. To probe the magnetic property in more detail, ^{1}H-NMR experiments were performed. A drastic change in both line-width and relaxation rate, as shown in Figure 1, occurred at 5.5K due to the antiferromagnetic phase transition. This is the first case, among the DCNQI-Metal family, that the π-electrons on the DCNQI colums have an antiferromagnetic ordered state. The magnetism revealed here indicates nature of the Mott insulator and demonstrates importance of electron correlation in the π-electron system in DCNQI-Metal complexes. The electronic states of (DI-DCNQI)$_2$M and (DMe-DCNQI)$_2$M (M=Cu,Ag) were discussed comparatively.

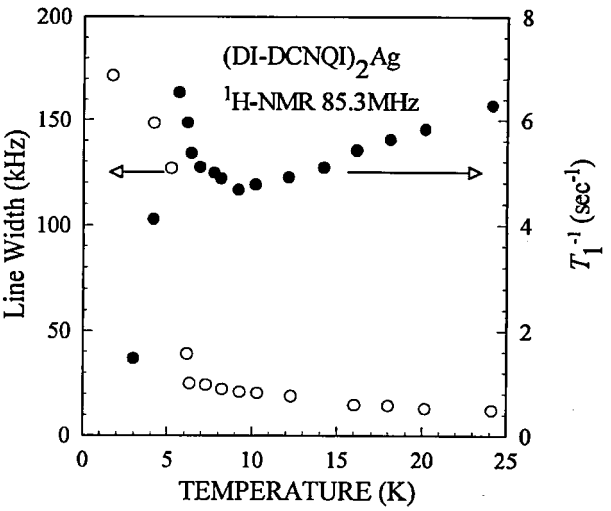


Figure 1. Line-width and relaxation rate of ^{1}H-NMR for (DI-DCNQI)$_2$Ag.

IV-G-2 Carrier Doping to (DCNQI)$_2$Li

Ko-ichi HIRAKI and Kazushi KANODA

[*Mol. Cryst. Liq. Cryst.*, **285** (1996) 157]

The alloy systems, (DMe-DCNQI)$_2$Li$_{1-x}$Cu$_x$, have been investigated with an aim at controlling the electronic state by doping of Cu ions into the (spin-) Peierls insulator, (DMe-DCNQI)$_2$Li. From the resistivity measurements, it

was found that the systems up to x~30% undergo the metal-insulator transition while the systems with x>50% are metallic in the whole temperature range investigated. The ^{13}C (in the cyano group) nuclear spin-lattice relaxation rate, $^{13}T_1^{-1}$, is shown in Figure 1. For x<30%, one can see abrupt decrease of $(^{13}T_1T)^{-1}$, which is associated with the spin-Peierls transition. The transition temperature slightly shifts with increasing x. For the Cu-rich systems of x>50%, $(^{13}T_1T)^{-1}$ does not exhibit any anomaly but converges into about 0.03 $sec^{-1}K^{-1}$ in the low-temperature limit. They show positive temperature dependence, which have a clear correlation with the doping content. This is an indication that the doping causes some change in the electronic states, particularly in excitation spectrum visualized in a higher temperature region.

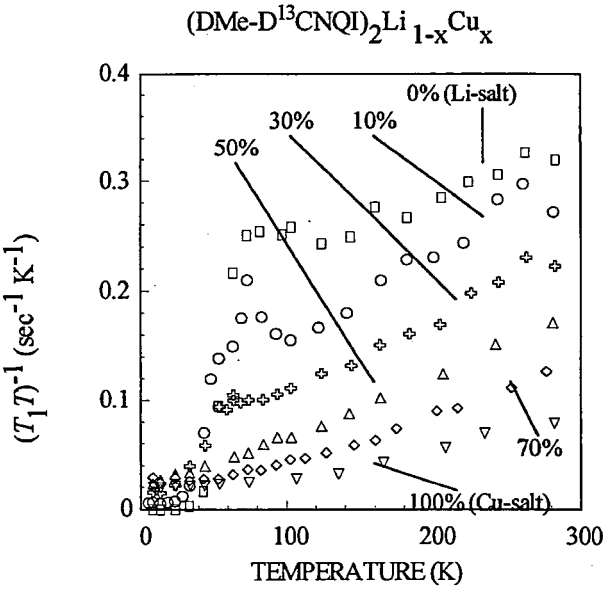
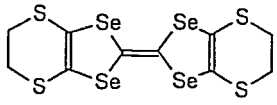


Figure 1. Temperature dependence of $(^{13}T_1T)^{-1}$of (DMe-DCNQI)$_2$Li$_{1-x}$Cu$_x$.

IV-H Development and Physical Properties of New Molecular Superconductors and Related Systems

The number of molecular superconductors is increasing year by year. However there is no commonly accepted theory on the Superconducting (SC) mechanism of molecular conductors. If the mechanism is clarified, the designability of the molecular systems will become of great advantage to develop new systems. One of the chemical approach to contribute to elucidate the SC mechanism is to develop new series of molecular superconductors, whose structural, electrical and magnetic properties can be changed continuously by chemical modification of the system. The κ-type BEDT-TTF (ET) superconductors are the most intensively studied molecular superconductors, where the physical properties can be controlled to some extent by anion exchange and/or isotope substitution. Recently we have found a new series of BETS superconductors whose electronic properties are tunable by the replacement of halogen atoms of counter anions.



BETS (=bis(ethylenedithio)tetraselenafulvalene)

IV-H-1 Phase Diagram of λ-type BETS Organic Superconductors

Hayao KOBAYASHI, Emiko ARAI, Hiroki AKUTSU, Toshio Naito *(Hokkaido University)*, **Hisashi TANAKA** *(The University of Tokyo)*, **Akiko KOBAYASHI** *(The University of Tokyo)* **and Taro SAITO** *(The University of Tokyo)*

We have reported the first BETS superconductor λ-$BETS_2GaCl_4$ in 1993 and recently prepared the crystals of λ-$BETS_2GaBr_xCl_{4-x}$. The superconducting behavior depended on the cooling rate, which may be attributable to the lattice disorder induced by halogen exchange. But fortunately, the disorder effect is relatively small, which permits the systematic studies of the phase diagram of λ-$BETS_2GaBr_xCl_{4-x}$. We have examined resistivities, magnetic susceptibilities and crystal structures of λ-$BETS_2GaCl_3F$, λ-$BETS_2GaBr_xCl_{4-x}$ ($0<x<4$) and λ'-$BETS_2GaBr_4$ with modified λ-type structure. The results are summarized as the form of the T-V phase diagram (V=unit cell volume, see Figure 1): (1) when V is small (e.g. λ-$BETS_2Cl_3F$), the system shows normal metallic behavior and T_c is less than 4 K. (2) In the case of the intermediate V, the small round resistivity maximum appears at 50-100 K, below which the system transforms to metallic phase. The superconducting transition appears at 4-8 K. (3) The system with large V is semiconducting and exhibits a magnetic transition at low temperature (< 50 K). It was confirmed that λ-$BETS_2GaBr_xCl_{4-x}$ (x~1.5) becomes a superconductor at 1 kbar. This phase diagram reminds us the T-P phase diagram of κ-type ET superconductors. The systematic studies of λ-$BETS_2GaBr_xCl_{4-x}$ will provide a clue to the universal phase diagram of the 2D π metal systems.

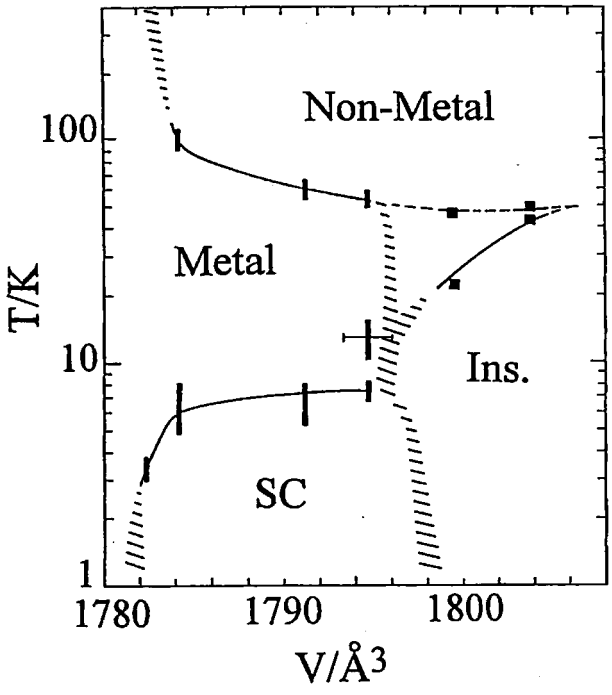


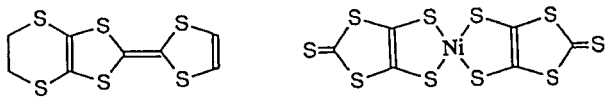
Figure 1. Phase diagram of λ-$BETS_2GaBr_xCl_{4-x}$.

IV-H-2 Meissner and Diamagnetic Shielding Effect of α-EDT-TTF[Ni(dmit)$_2$]

Hiroyuki TAJIMA *(Institute for Solid State Physics)*, **Akiko KOBAYASHI** *(The University of Tokyo)*, **Y. OOTUKA** *(The University of Tokyo)*, **Toshio NAITO** *(Hokkaido University)*, **Akane SATO** *(Graduate Univ. for Advanced Studies)* **and Hayao KOBAYASHI**

[*Synthetic Metals*, **79**, 141 (1996)]

α-EDT-TTF[Ni(dmit)$_2$] (dmit=4,5-dimercapto-1,3-dithiole-2-thione, EDT-TTF=ethylenedithiotetrathiafulvalene) is a donor-acceptor type molecular superconductor. In contrast with a typical organic conductor having only one kind of conduction sheet, α-EDT-TTF[Ni(dmit)$_2$] has two kinds of conduction sheets: one composed of EDT-TTF molecules and the other composed of Ni(dmit)$_2$ molecules. In this work, Meissner and diamagnetic shielding effects were investigated. The onset of the diamagnetic transition occurred at 1.39 K. From the measurements of the Meissner effect, the volume fraction of superconducting phase was estimated to be more than 62 %. From the measurements of diamagnetic shielding effect, this fraction was estimated to be about 93 %. This high level of volume fraction shows that the superconducting phase is the main phase in α-EDT-TTF[Ni(dmit)$_2$].



EDT-TTF Ni(dmit)2

IV-H-3 Shubnikov-de Haas Effect and Angular Dependent Magnetoresistance Oscillation of κ-$BETS_2GaCl_4$

Hiroyuki TAJIMA *(Institute for Solid State Physics)*, **Akiko KOBAYASHI** *(The University of Tokyo)*, **Toshio NAITO** *(Hokkaido University)* **and Hayao KOBAYASHI**

[*Solid State Commun.*, **48**, 755 (1996)]

The crystals of $BETS_2GaCl_4$ are polymorphic: λ-$BETS_2GaCl_4$ is a superconductor, whereas κ-$BETS_2GaCl_4$ retains metallic state down to at least 0.5 K. Recently, the Shubnikov-de Haas (SdH) effect and angular-dependent magnetoresistance (ADMRO) were observed in magnetoresistance measurements at 0.5 K (Figure 1). From a frequency of a SdH oscillation, a Fermi surface cross-section perpendicular to the crystallographic *b*-axis is estimated to be 4.20×10^{15} cm^{-2}, which corresponds to 105 % of the first Brillouin zone. From the results of ADMRO, a Fermi wave number along the crystallographic c-axis is evaluated to be 0.35 Å^{-1}. Both results are consistent with a band structure calculated on the basis of the extended Huckel method.

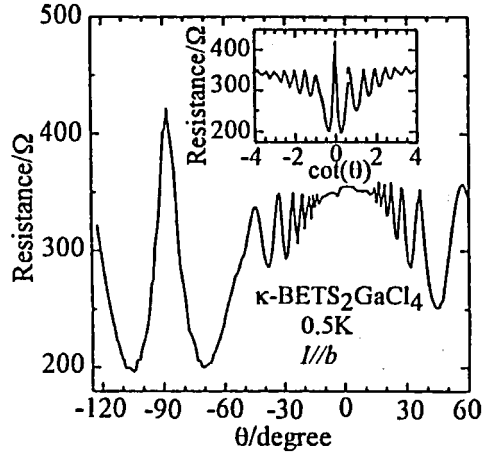


Figure 1. Angular-dependent magnetoresistance of κ-$BETS_2GaCl_4$.

IV-I Development and Physical Properties of Magnetic Molecular Metals

Recently, the π-d interaction has attracted a considerable interest in the field of molecular metals. In 1987, we have first pointed out the existence of pπ-d metal band in $DCNQI_2Cu$ (DCNQI=dicyanoquinonediimine), where mixed-valent Cu atom is coordinated tetrahedrally by the terminal N atoms of planar DCNQI molecules. With the aim of developing new molecular metals with π-d mixing bands, many trials were made to synthesize analogous conductors composed of modified DCNQI molecules. However these trials were not so successful because the unique electronic properties of $DCNQI_2Cu$ is lost by the small modification of the structure. In order to study systematically the role of π-d interaction in molecular crystals, the development of molecular metals, which permit the chemical modification, will be needed.

As the first step of the systematic studies on the π-d systems, we have tried to develop BETS compounds with transition metal complex anions having magnetic moments. Although the π-d interaction of such systems is considered to be weak, we have recently discovered the strongly coupled electrical and magnetic phase transitions.

IV-I-1 New BETS Conductors with Magnetic Anions (BETS=bis(ethylenedithio) tetraselenafulvalene)

Hayao KOBAYASHI, Hideto TOMITA *(Toho University)*, **Toshio NAITO** *(Hokkaido University)*, **Akiko KOBAYASHI** *(The University of Tokyo)*, **F. SAKAI** *(Institute for Solid State Physics)*, **Tokuko WATANABE** *(Tokyo University of Marine Science)* **and P. CASSOUX** *(CNRS)*

[J. Am. Chem Soc., **118**, 368 (1996)]

The preparation, crystal structures, and electric and magnetic properties of $(BETS)_2MX_4$ (BETS=bis(ethylenedithio)tetraselenafulvalene; M = Mn^{2+}, Fe^{3+}, Co^{2+}, Ni^{2+}, Cu^{2+}; X = Cl, Br, CN) were examined. Resistivity measurements down to 2 K revealed the coexistence of the BETS π conduction electrons and the localized magnetic moments of the anions in the κ-$(BETS)_2FeCl_4$ and κ-$(BETS)_4(CoCl_4)(C_2H_3Cl_3)$ salts. Another $FeCl_4$ phase, λ-$(BETS)_2FeCl_4$ undergoes a metal-insulator (MI) transition coupled with magnetic transition at 8.5 K (Figure 1). A superconducting transition is observed at 4.6 K in λ-$(BETS)_2(FeCl_4)_{0.5}(GaCl_4)_{0.5}$, where a half of the anion sites are occupied by magnetic ions. The salts with the $NiCl_4^{2-}$ and $MnCl_4^{2-}$ anions exhibit the behavior of a semi-metal down to 100K. The $(BETS)_4(Cu_2Cl_6)$ salt remains metallic down to 4.2 K. ESR studies show that the Fe^{3+} ions in κ- and λ-$(BETS)_2FeCl_4$ are in a high-spin state. The temperature dependencies of the spin susceptibilities of κ- and λ-$(BETS)_2FeCl_4$ indicate antiferromagnetic interactions between the Fe^{3+} ions. The crystal structure analyses of κ- and λ-$(BETS)_2FeCl_4$ at 298 K and 10 K showed closer BETS-$FeCl_4$ contacts in λ-$(BETS)_2FeCl_4$, which is consistent with the larger Weiss temperature of this compound.

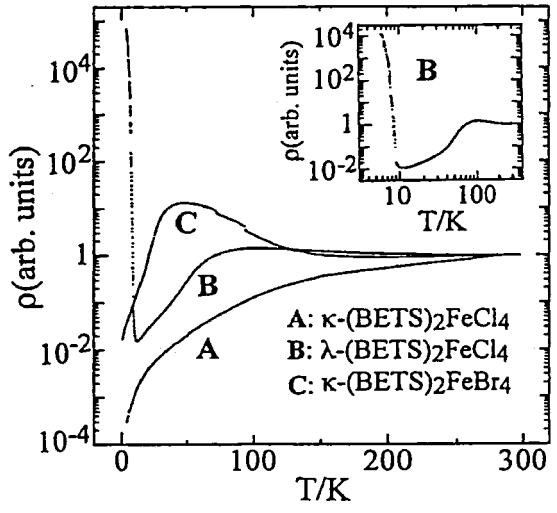


Figure 1. Resistivities of λ- and κ-$BETS_2FeX_4$ (X=Cl, Br).

IV-I-2 Coupled Magnetic and Electrical Phase Transition of λ-$BETS_2FeCl_4$—Molecular Metal with Field Restored Highly Conducting State

Hiroki AKUTSU, Emiko ARAI, Hayao KOBAYASHI, Akiko KOBAYASHI *(The University of Tokyo)*, **Madoka TOKUMOTO** *(Electrotechnical Laboratory)*, **L. BROSSARD** *(CNRS)* **and P. CASSOUX** *(CNRS)*

Brossard et al. have recently discovered a new metallic state of molecular crystal, that is field restored highly conducting state (FRHCS). λ-$BETS_2FeCl_4$ undergoes a metal-insulator (MI) transition at 8.5 K, where the antiferromagnetic spin ordering takes place in $FeCl_4$ sites. This unique transition suggesting a fairly strong interaction between localized spins and metal electron systems is suppressed by applying pressure and/or magnetic field. Since the Fe^{3+} ions is in high-spin state, the magnetization of $FeCl_4$ will tend to be saturated at high magnetic field. In fact, Tokumoto et al. have recently found that the magnetization of κ-$BETS_2FeCl_4$ having stable metallic state is saturated according to Brillouin function. Therefore at high magnetic field, the π conduction electrons and ferromagnetically aligned Fe^{3+} moments will coexist at low temperature. In the insulating low-magnetic field state, the Fe^{3+} spins are antiferromagnetically ordered with the easy axis being parallel to the crystallographic *c*-axis (needle axis of the crystal). The spin-flop transition occurs at 1-2 T. In order to make clear the natures of MI transition and π-d interaction, we are now examining the field and pressure dependencies of T_{MI} (Figure 1).

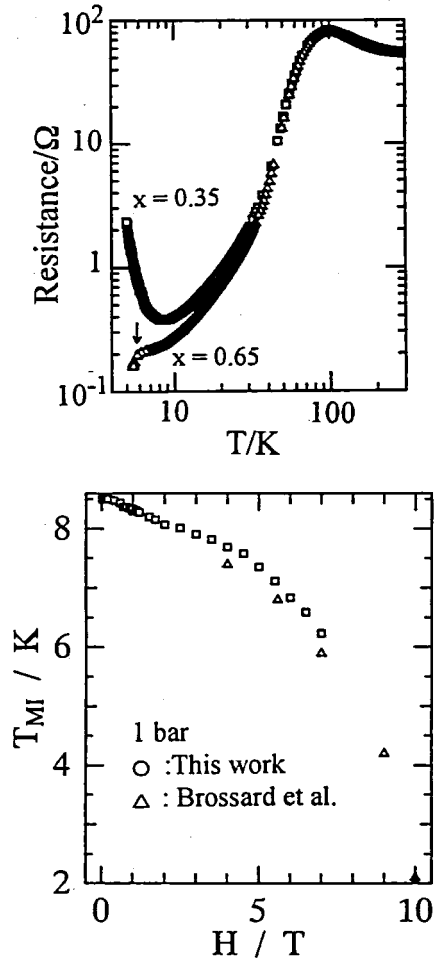


Figure 1. Magnetic field dependence of T_{MI} of λ-$BETS_2FeCl_4$.

IV-I-3 Phase Diagram of λ-$BETS_2(Ga_xFe_{1-x})Cl_4$—A Clue to Magnetic Molecular Superconductor

Hayao KOBAYASHI, Hiroki AKUTSU, Akane SATO *(Graduate Univ. for Advanced Studies)*, **Toshio NAITO** *(Hokkaido UNiversity)*, **Akiko KOBAYASHI** *(The University of Tokyo)* **and P. CASSOUX** *(CNRS)*

Contrary to λ-$BETS_2GaCl_4$ with superconducting (SC) ground state, an isomorphic salt of λ-$BETS_2FeCl_4$ undergoes a coupled metal-insulator(MI) and antifferomagnetic (AF) transition. The Curie-Weiss dependence of ESR intensity (θ=-23 K) of the metallic phase of λ-$BETS_2FeCl_4$ revealed the AF interaction between Fe^{3+}···Fe^{3+} ions. We have prepared crystals of λ-$BETS_2(Ga_xFe_{1-x})Cl_4$ (0<x<1) and examined their resistivities down to 4.2 K. As shown in Figure 1, there is no metallic ground state.. The MI transition temperature decreases with increasing x but T_{MI} is higher than 4 K even at x=0.5. Quite unexpectedly, SC state could be observed even in the crystals with 50% of Fe. Moreover T_c did not show clear x-dependence. We have found that even in the metallic state of the crystals with x ~ 0.65 and T_c ~ 4.5 K, AF interaction still exists between Fe^{3+} ions (θ=-3.1 K). It may be of special interest to see how AF interaction is changed at T_c. Around x=0.5, it might be possible that the AF transition takes place below T_c. Is it possible that similar to well-known Chevrel compounds, the SC phase and magnetic phase coexist? In order to clarify these problems, much systematic and careful studies will be needed. Anyway, λ-$BETS_2(Ga_xFe_{1-x})Cl_4$ is a unique system indicating a new possibility of the development of magnetic molecular superconductors.

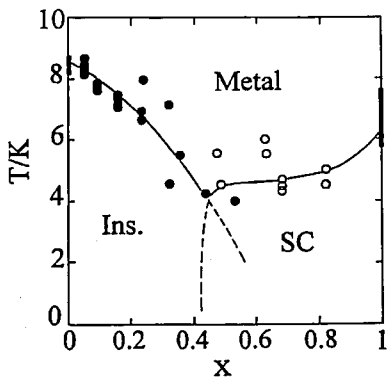


Figure 1. An example of resistivy behavior and phase diagram of λ-$BETS_2(Ga_xFe_{1-x})Cl_4$.

IV-I-4 Structural, Electrical and Magnetic Properties of Molecular Metal with Binuclear $Cu_2Cl_6^{2-}$ Anions

Akiko KOBAYASHI *(The University of Tokyo)*, **Akane SATO** *(Graduate Univ. for Advanced Studies)*, **Hayao KOBAYASHI, N. D. KUSHCH** *(CNSR)*, **P. CASSOUX** *(CNRS)*, **R. B. LUBOVSKII** *(Institute Chemical Physics, Chernogolovka)* **and M. V. KARTSOVNIK** *(Institute of Solid State Physics, Chernogolovka)*

In the course of the studies on the development of new BETS metals with magnetic anions, we have found a new complex θ-$BETS_4Cu_2Cl_6$ with metallic state down to 2 K. The tight-binding band calculation based on the room-temperature structure gave two-dimensional(2D) Fermi surface (FS). The magnetoresistance oscillation (MO) indicates the closed 2D FS with 38% area of the 1st brillouin zone (BZ), which is inconsistent with the calculated FS (22% of BZ). The preliminary results of the low-temperature crystal structure analysis indicates the change of the lattice symmetry. The temperature dependence of the static magnetic susceptibility measured by SQUID magnetometer is explained by the singlet-triplet model of $Cu_2Cl_6^{2-}$ (Figure 1). The paramagnetic contribution of π metal electrons of BETS was estimated as 2.3 × 10^{-4} emu/($BETS_2CuCl_3$). The angle dependent magnetoresistance oscillation (ADMRO) indicates the superposition of two kinds of ADMRO. Precise examination of low-temperature structure is now in progress.

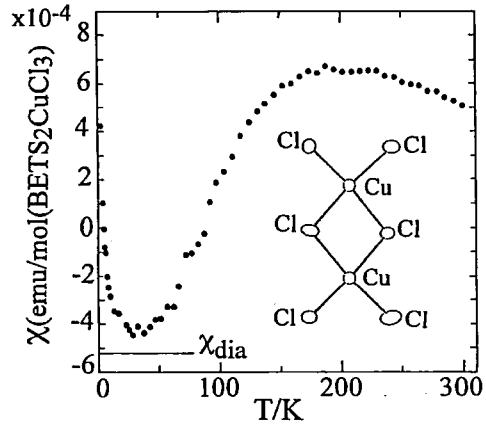
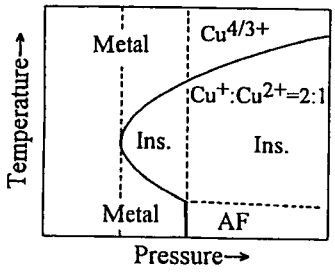


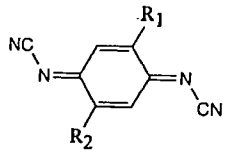
Figure 1. Magnetic susceptibility of θ-$BETS_4Cu_2Cl_6$.

IV-I-5 Phase Diagram of DCNQI-Cu System–Origin of Reentrant Metal-Insulator-Metal Transition

Yutaka NISHIO *(Toho University)*, **Masafumi TAMURA** *(Toho University)*, **Koji KAJITA** *(Toho University)*, **Shuji AONUMA** *(Institute for Solid State Physics)*, **Hiroshi SAWA** *(Chiba University)*, **Reizo KATO** *(Institute for Solid State Physics)* **and Hayao KOBAYASHI**

Almost a decade ago, we (A. Kobayashi, R. K. and H. K.) have pointed out that the unique properties of $DCNQI_2Cu$ is originated from the mixed-valency of Cu ($Cu^{+1.3}$). In the metallic state, the highest occupied 3d orbital of Cu is mixed with LUMO of DCNQI to produce pπ-d metal band. In the insulating phase, Cu^+ and Cu^{2+} are arranged regularly (Cu^+,Cu^+,Cu^{2+},....) and the magnetic moments of Cu^{2+} are ordered antiferromagnetically at low temperature (see Figure 1). In the special condition, the system shows a unique reentrant (metal → insulator → metal) transition. Recently Nishio et al. have examined specific heat of selectively deuterated $(DMe\text{-}DCNQI)_2Cu$ using thermal relaxation method in the temperature region between 0.5<T<20 K. The latent heat at the "high-temperature-metal—insulator transition" was precisely determined. It has been clarified that Cu^{2+} spin system plays the crucial role. The competition between the metal electron entropy (γT) and freedom of Cu^{2+} spins in insulator phase drives the reentrant MIM transition.





R_1,R_2-DCNQI

Fugure 1. Molecule of R_1,R_2-DCNQI and phase diagram of $DCNQI_2Cu$ System.

IV-J Development of New Molecular Conductors

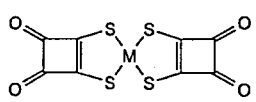
The development of new materials is the most important driving force for the field of solid state chemistry. The recent progress of the concept of the molecular design enriched greatly the physics and chemistry of crystalline molecular solids. The appearance of various types of molecular metals, superconductors and molecular ferromagnets have attracted an increasing interest of chemists and physicists. New physics is frequently provided by new material. For example, the development of two dimensional π metals enabled us to study the Fermiology of molecular crystals, from which new finding such as angular dependent magnetoresistance oscillation (ADMRO) was obtained.

As for the development of new molecular conducting systems, organic ferromagnetic metals and single component molecular metals (or superconductors) will be possible candidates of future targets. Although such systems seem to be within the scope of the present molecular design, many trivial traditional systems should be sufficiently examined before we embark on such challenging works.

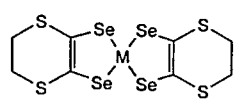
IV-J-1 New Molecular Conductors Based on Transition Metal Complexes

Hideki FUJIWARA, Emiko ARAI, Hayao KOBAYASHI, Hisashi TANAKA *(The University of Tokyo),* **Akiko KOBAYASHI***(The University of Tokyo)* **and Taro SAITO** *(The University of Tokyo)*

We have prepared new conducting systems based on dithiolene (or diselenolene) complexes such as $M(dts)_2$ and $M(ddds)_2$ (M=Ni, Pd, Pt, Au; dts= dithiosquarate; ddds=5,6-dihydro-1,4-dithiin-2,3-diselenolate). Crystal structures and electrical properties of several ET and BETS complexes with $M(dts)_2^{2-}$ were examined. In the semiconducting crystals of $BETS_2Pd(dts)_2$ and $BETS_2Pd(dts)_2$ (1,1,2,2-tetrachloroethane), every $Pd(dts)^{2-}$ anion is surrounded by six BETS molecules. Another complex $BETS_xPd(dts)_2$ (x~5) is metallic down to 4 K. The 1:1 salt of $BETSAu(dts)_2$ has mixed stacking columns of BETS and $Au(dmit)_2$. Nevertheless the system exhibits a fairly high conductivity (σ(RT)=0.4 Scm^{-1}). We have recently synthesized a new diselenolene complex $M(ddds)_2$. Since fairly good metals based on $M(dddt)_2$ have been already reported by Yagubskii et al., the analogous $M(ddds)_2$ complexes will be hopeful systems with enhanced metallic natures, which will be examined in near future.



$M(dts)_2$



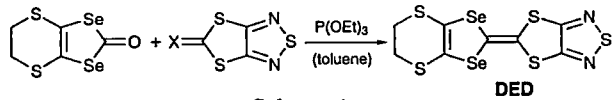
$M(ddds)_2$

IV-J-2 New Synthetic Metals Based on a Thiadiazole Network

Toshio NAITO *(Hokkaido University),* **Tamotsu INABE***(Hokkaido University),* **Masafumi TAMURA** *(Toho University),* **Yutaka NISHIO** *(Toho University),* **Koji KAJITA** *(Toho University),* **Akiko KOBAYASHI** *(The University of Tokyo),* **Emiko ARAI, Hayao KOBAYASHI and A. E. UNDERHILL** *(University of Wales)*

[*J. C. S. Chem. Commun.*, **1996**, 521]

The key point of designning a new molecular conductors is how to achieve intermolecular interaction. Although there are many atoms that can expected to enhance intermolecular interactions when incorporated into molecules, most of the known synthetic metals depend solely on a chalcogen network for metallic conduction. Hetrocycles including sulfur and nitrogen atoms and their isomers are known to form a close S-N network. We have synthesized a new asymmetrical donor molecule, thiadiazoleethylenedisulfunyldiselenadithiafulvalene (DED) (Scheme 1). Single crystals of $(DED)_2X(THF)_2$ ($X=PF_6$, AsF_6) were obtained electrochemically. The resistivity measurements showed the metallic nature down to 20-35 K, below which resistivities increased. The magnetic susceptibility exhibits Curie-like behavior down to ca. 20 K. and χT suddenly goes towards zero at low temperatures. Such behavior indicates that this salt could be a rare example of "pure organic" system whose electrical behavior at low temperature might be best explained as a results of Kondo effect.

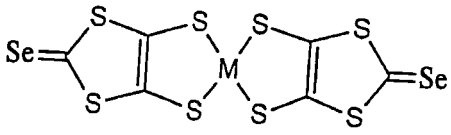


Scheme 1

IV-J-3 Crystal Structures and Electrical Properties of New Ni(dmise)$_2$ Conductors —A Precursor of Three-Dimensional π Metals

Akane SATO *(Graduate Univ. for Advanced Studies)*, **Hayao KOBAYASHI, Toshio NAITO** *(Hokkaido University)* **and Akiko KOBAYASHI** *(The University of Tokyo)*

Since the pioneer works by Cassoux et al., molecular conductors based on M(dmit)$_2$ (M=Ni, Pd, Pt,..) have been extensively studied, from which seven superconductors have been found out. Besides dmit ligand, dmise (=4,5-dimercapto-1,3-dithiole-2-selenone) including both sulfur and selenium atom is a potentially useful ligand which extended an intermolecular interaction towards "the third direction" through its outstreched part of the conjugated system, i.e. the selone. Cornerissen et al. have reported the semiconductive behavior of the first Ni(dmise)$_2$ complex in 1993. We have examined the crystal structures and electrical resistivities of several Ni(dmise)$_2$ conductors with ammonium and alkali-metal cations and TTF-like π donors. The tight-binding band calculation based on the room-temperature structure of $[(CH_3)_{4-n}H_nN]$ $[Ni(dmise)_2]_2$ gave three-dimensional (3D) Fermi surfaces (FS) due to fairly large intermolecular Se···Se interaction along the "third direction" (Figure 1). $Cs_xPd(dmise)_2$ is the first M(dmise)$_2$ conductors with stable metallic state down to 4K. It seems highly possible that except C_{60} complexes, this system is the first molecular metal with 3D closed FS at low temperature. However the preparation of good single crystal is a serious bottleneck for future development of new M(dmise)$_2$ conductors.



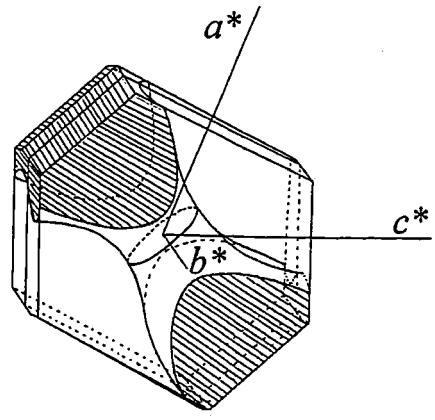


Figure 1. M(dmise)$_2$ molecule and Fermi surface of $[(CH_3)_2H_2N][Ni(dmise)_2]_2$.

IV-J-4 κ- and Modified κ-Type Molecular Arrangement and Electrical Resistivities of $BETS_2InCl_4$, $BETS_2ClO_4(TCE)_{0.5}$ and $BETS_2[(C_2H_5)_4N]_{0.7}InCl_5$ (TCE=1,1,2-trichloroethane)

Akiko KOBAYASHI *(The University of Tokyo)*, **Toshio NAITO** *(Hokkaido University)*, **Reizo KATO** *(Institute for Solid State Physics)* **and Hayao KOBAYASHI**

BETS (= bis(ethlenedithio)tetraselenafulvalene) has a strong tendency to produce two-dimensional (2D) molecular metals. Crystal structure analyses of $BETS_2ClO_4(TCE)_{0.5}$ and $BETS_2BF_4(TCE)_{0.5}$ revealed new type of 2D molecular arrangements based on BETS tetrad, named κ(4x4) molecular arrangements. $BETS_2(TEA)_{0.7}InCl_5$ (TEA=tetraethylammonium) has a distorted tetrad structure containing five-coordinated $InCl_5^{2-}$ anions (Figure 1). On the other hand, $BETS_2InCl_4$ has usual κ-type structure composed of BETS dimers. Except $BETS_2(TEA)_{0.7}InCl_5$ exhibiting a weakly metallic behavior down to about 100 K, the other BETS salts are metallic down to low temperatures. The weak metallic nature of $BETS_2(TEA)_{0.7}InCl_5$ is due to the inclusion of TEA cations.

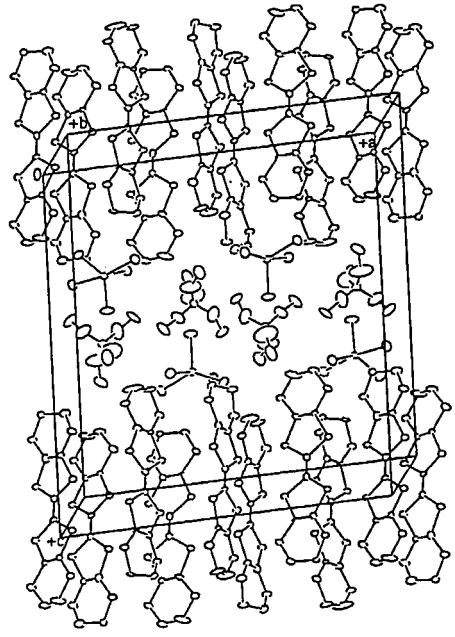
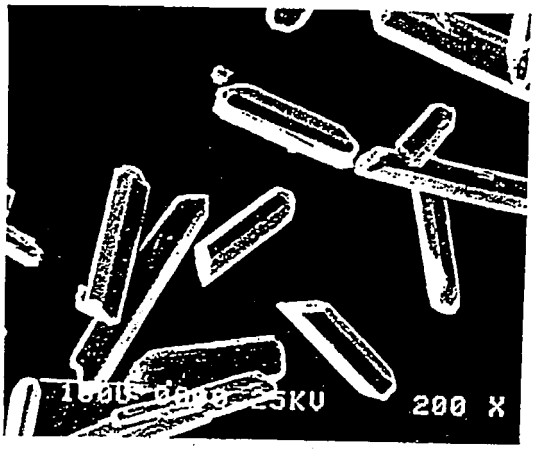


Figure 1. Crystal structure of $BETS_2(TEA)_{0.7}InCl_5$.

IV-J-5 Crystal Growth and Physical Properties of Alkali Metal Fullerides—$M_xC_{60}(THF)_y$ (M=Li, Na)

Hiroshi MORIYAMA *(Toho University),* **Tokuko WATANABE** *(Tokyo University of Marine Science)* **and Hayao KOBAYASHI**

The facile and simple wet-chemical synthesis of single crystals of alkali metal doped fullerenes was developed by means of diffusion in organic solvents of C_{60} and alkali metal tetraphenylborate. In 1994, we have reported the new metallic C_{60} compound $Na_xC_{60}(THF)_y$ (σ(RT) = 50 Scm^{-1}). $Na_xC_{60}(THF)_y$ exhibits a novel metal-metal transition accompanied by the structural phase transition around 170 K, where the hexagonal lattice constants are abruptly decreased. It might be imagined that alkaki metal cations are surrounded by THF molecules and the 170 K transition is related to the freezing of the molecular motion of THF. We have recently prepared fairy good crystals of $Li_xC_{60}(THF)_y$ (see Figure 1). The resistivity is almost constant between 300—160 K. Similar to $Na_xC_{60}(THF)_y$, a sharp metal-metal transition takes place around 150 K.



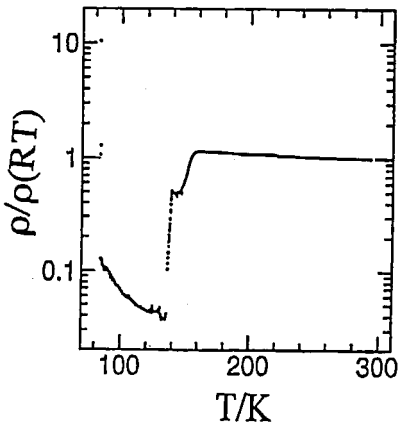


Figure 1. Single crystal of $Li_xC_{60}(THF)_y$ and its temperature dependence of resistivity.

IV-K X-Ray Diffraction Studies at Low Temperature

Crystal structure studies have played an essential role in the history of the development of molecular metals. More than two decades ago, X-ray photographs of $K_2[Pt(CN)_4]Br_{0.3}\cdot 3H_2O$ (KCP) and (TTF)(TCNQ) indicating giant Kohn anomalies convinced us clearly the existence of one-dimensional(1D) metal electrons in molecular crystals. And at that time the new age of 1D metals was opened. At the beginning of 1980s, a guiding principle to design stable π metal bands was noticed by the systematic structure-chemical examinations of molecular conductors based on multi-chalcogen π molecules. Recent development of molecular metals and superconductors has attracted much interest to the low-temperature properties of molecular crystals. Needless to say, the molecular crystal is rich in the structural freedom and the physical properties of molecular crystals are very sensitive to the structural changes. However, the low-temperature X-ray techniques was not improved for a long time and the lack of the information of low-temperature structure became serious. Recently we have develop X-ray imaging plate low-temperature system equipped with He refrigerator. The lowest temperature of the new system recently set up in this institute is 4.5 K. We are now examining the crystal structures of organic superconductors and structural phase transitions of molecular crystals.

IV-K-1 Low-Temperature Crystal and Band Electronic Structures of Two-Dimensional $Ni(dmit)_2$ Conductors

Akiko KOBAYASHI*(The University of Tokyo)*, **Akane SATO***(Graduate Univ. for Advanced Studies)* **and Hayao KOBAYASHI**

Contrast to the conductors composed of TTF-like π donor molecules, only a few π acceptor conductors can retain metallic states down to low temperatures. Almost a decade ago we have found the first $Ni(dmit)_2$ conductor with stable two-dimensional metallic state down to 1.5 K. Up to now three analogous systems have been found out. At first we expected these systems to be possible candidates of the first ambient-pressure pure π acceptor superconductors. However no sign of superconducting (SC) transition has not been detected so far. Recently we have examined the low-temperature crystal and band structures of these systems. In the cases of α-$[(CH_3)_2(C_2H_5)_2N][Ni(dmit)_2]_2$ and $[(CH_3)_2C_5H_{10}N][Ni(dmit)_2]_2$, we discovered the change of the lattice periodicity. Consequently, the Fermi surface at room temperature will be divided into small pieces. The magnatic susceptibilities also suggested the diminishing of the Fermi surfaces at low temperatures, which is disadvantageous to realize SC phase. Recently the crystal structure of the third candidate γ-$[(CH_3)_2(C_2H_5)_2N][Ni(dmit)_2]_2$ was determined at 4.5 K. The space group Pmna is changed into $P2_12_12$ and the heavily disordered atomic positions of $CH_3)_2(C_2H_5)_2N$ cation becomes ordered at low temperature (Figure 1). But the band structure remains almost unchanged. Thus this system seems to retain the high possibility of the superconducting transition at low temperatures. We are now trying to prepare high quality fresh crystals to examine the resistivity below 2K.

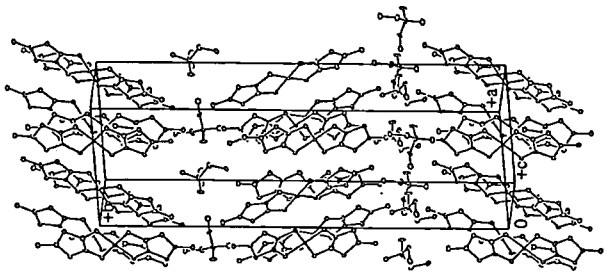


Figure 1. The crystal structure of γ-$[(CH_3)_2(C_2H_5)_2N][Ni(dmit)_2]_2$ at 4.5 K.

IV-K-2 Origin of the Resistivity Anomalies of (EDT-TTF)[M(dmit)$_2$] (M=Ni, Pd)

Akiko KOBAYASHI *(The University of Tokyo)*, **Akane SATO***(Graduate Univ. for Advanced Studies)*, **Hayao KOBAYASHI, Koichi KAWANO***(Toho University)*, **Toshio NAITO** *(Hokkaido University)* **and Tokuko WATANABE** *(Tokyo University of Marine Science)*

[*J. Mater. Chem.* **5**, 1671 (1995)]

α-(EDT-TTF)[Ni(dmit)$_2$] (EDT-TTF =ethylenedithiotetrathiafulvalene) is the first ambient pressure superconductor based on transition metal complex molecules. It comprises crossing colums of EDT-TTF and Ni(dmit)$_2$ and exhibits unique metallic behavior with a characteristic resistivity peak at around 14 K. The possibility of the development of superstructure was examined down to 9K but no extra X-ray reflections could be found below 14 K. This suggests that the 14 K anomaly is not originated from charge density wave (CDW) instability. New phases of γ-(EDT-TTF)[Pd(dmit)$_2$] and γ-(EDT-TTF)[Ni(dmit)$_2$] were found. γ-(EDT-TTF)[Pd(dmit)$_2$] has parallel columns of EDT-TTF and Pd(dmit)$_2$ and shows resistivity anomaly around 80K. Below 80 K, X-ray satellite reflections indicating $2k_F$-CDW formation were observed (Figure 1). γ-(EDT-TTF) [Ni(dmit)$_2$] undergoes a metal-insulator transition around 100 K.

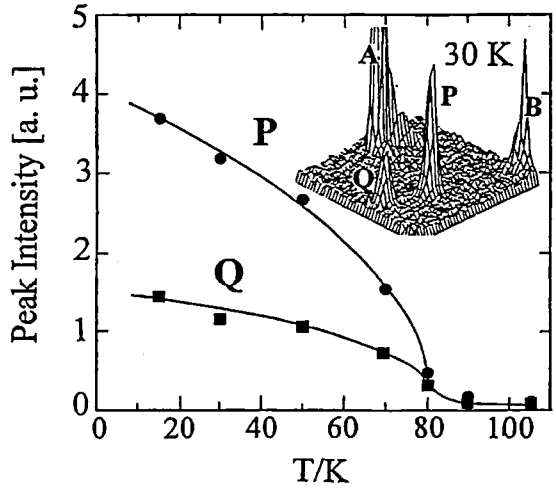


Figure 1. Temperature dependence of the $2k_F$-reflections of γ-(EDT-TTF)[Pd(dmit)$_2$].

IV-L Development of Pulsed Field Gradient NMR Spectroscopy

Pulsed field gradient (PFG) spin echo (SE) nuclear magnetic resonance (NMR) is a powerful method for the study of dynamics in condensed matter because it probes transitional motion of molecules selectively, without being affected by vibrational or rotational motions. Advantage of the method lies also in that incorporation of impurity probe is not necessary. However, applications of this technique to strongly dipole-coupled spin systems with short T_2 or to the study of slow and anisotropic self-diffusion are challenging problems for modern NMR spectroscopy because combined techniques of line-narrowing, pulsing of sharp and intense field gradients, and two-dimensional field-gradient generation are necessary. In the present study we developed PFG NMR spectroscopy to the study of slow and anisotropic self-diffusion dynamics in strongly dipole-coupled spin systems.

IV-L-1 New PFG-NMR Spectrometer with a Rotatable Quadrupole Coil for the Measurement of Anisotropic Self-Diffusion Coefficient Tensor

Osamu OISHI and Seiichi MIYAJIMA

[*J. Magn. Reson. A*, **123**, 64 (1996)]

A new pulsed field gradient (PFG) spin echo NMR spectrometer has been constructed which was specially designed for the measurement of slow and anisotropic self-diffusion by realizing intense and homogeneous field gradient of 12 T m^{-1} by a quadrupole coil and a high quality current stabilizer, and also realizing a mechanism that each of the sample cell and the quadrupole coil is rotated from the axis of the external field. Diffusion anisotropy is measured by combination of coil rotation and magic angle orientation of the sample. Theoretical basis for the method of measuring diffusion anisotropy, instrumentation details, and a couple of test data are given. Experimental result is reported for the rotation pattern of the diffusion coefficient of a smectic Ad liquid crystal of 4-Octyloxy-*N*-(4-cyanobenzylidene)aniline (CBOOA). The component parallel to the layer normal is revealed to be 2.1 times larger than the component within the layer.

IV-L-2 Inversion of Self-Diffusion Anisotropy by Chemical Substitution in Smectic A Liquid Crystalline CBOOA and TFBOOA

Osamu OISHI and Seiichi MIYAJIMA

PFG NMR method was applied to the study of anisotropic self-diffusion in smectic A liquid crystals. Diffusion anisotropy was found to be inverted by chemical substitution of the terminal group in homologous compounds. Rotation pattern of the diffusion coefficient tensor D was measured as a function of the angle ϕ between the coil axis and the main field, while the alignment axis of the sample (which is parallel to the director) was fixed at magic angle Θ_M from the main field to reduce homonuclear magnetic dipole-dipole interaction. The observed component is expressed by

$$D(\phi) = \frac{1}{2}(D_{//} + D_{\perp}) - \frac{1}{2}(D_{//} - D_{\perp})\cos(4\phi - 2\Theta_M),$$

where $D_{//}$ and $D_{\perp}$ represent the tensor components parallel and perpendicular to the director, respectively. Taking the layer structure in mind, they represent the dif-

fusion across and within the layer, respectively. Figure 1 shows the rotation pattern of the two liquid crystalline compounds, 4-Octyloxy-*N*-(4-substituted benzylidene)aniline (XBOOA), where X is -CN (CBOOA) or -OCF_3 (TFBOOA), in their smectic A phases. The experimental data exhibit sinusoidal oscillation with a period of $\pi/2$ in good agreement with the above equation, and the observed values at 72.4° and 27.4° correspond, respectively, to $D_{//}$ and $D_{\perp}$. A most striking fact is that the phases of the angular oscillation are inverted between the two compounds. For CBOOA the observed anisotropy, $D_{//}/D_{\perp}$=2.1, means that diffusion across the layer is faster than that within the layer, while for TFBOOA the fact, $D_{//}/D_{\perp}$=0.70, means that diffusion within the layer is faster.

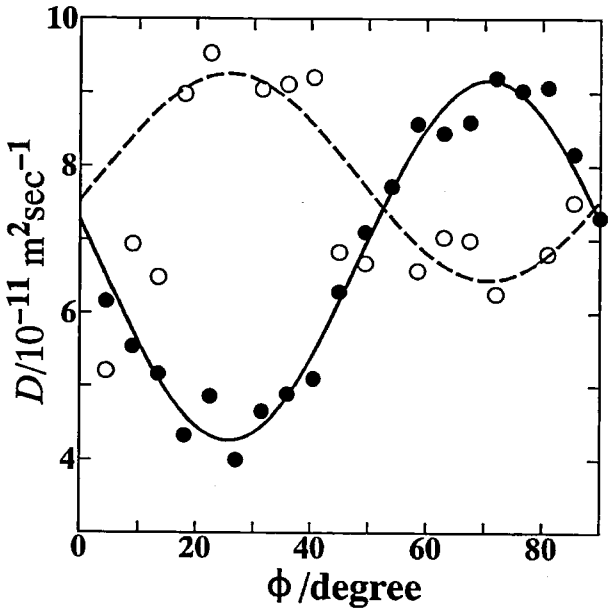


Figure 1. Angular rotation pattern of the anisotropic self-diffusion coefficient components for CBOOA (●) and TFBOOA (○) in smectic A phases.

IV-L-3 Difference in Self-Diffusion Anisotropy in Two Smectic A Phases of a Doubly Reentrant Liquid Crystal CBOBP

Osamu OISHI and Seiichi MIYAJIMA

Difference in translational dynamics in the two smectic A (S_{Ad} and S_{A1}) phases of a doubly reentrant liquid crystal[1] 4-cyanobenzoyloxy-[4-octylbenzoyloxy]-*p*-phenylene (CBOBP) was studied by means of angle-resolved PFG NMR spectroscopy. Figure 1 shows the result. In the high temperature S_{Ad} phase, the diffusion component parallel to the director was found faster than the component perpendicular to the director, the anisotropy being $D_{//}/D_{\perp}$=1.7. The anisotropy larger than unity resembles that in the nematic phase, and suggests highly disordered smectic structure. The activation energies were similar for the two components; 40 kJ mol^{-1} for $D_{//}$ and 42 kJ mol^{-1} for $D_{\perp}$. Each of the D components in the S_{A1} phase is smaller than the extrapolation of the data in the S_{Ad} phase. The $D_{//}$ component decreases more significantly, and consequently the anisotropy becomes small. Significant reduction of $D_{//}$ is consistent with our X-ray diffraction result that S_{A1} phase consists of more distinct layer structure than the sinusoidal density wave along the director in S_{Ad}. The slowness of diffusion is also consistent with the high segmental order parameters obtained from deuterium NMR.[1] The mechanism of doubly reentrant phase transition is discussed on the basis of the diffusion coefficient components obtained in this experiment.

Reference

1) S. Miyajima and T. Hosokawa, *Phys. Rev. B*, **52**, 4060 (1995).

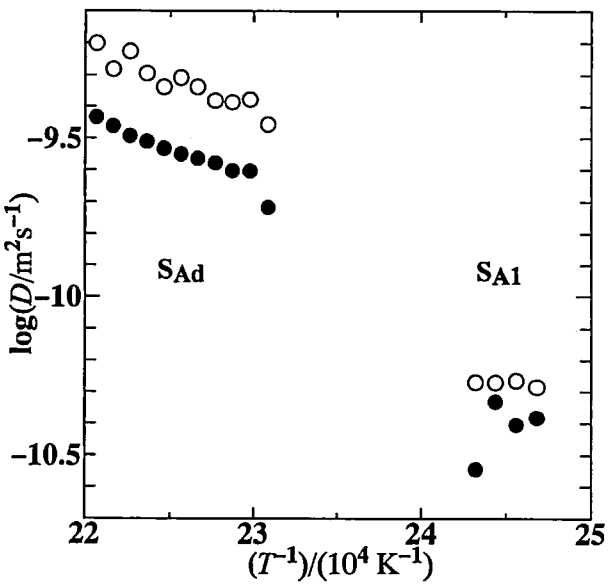


Figure 1. Temperature dependence of the self-diffusion coefficient components, $D_{//}$ (○) and $D_{\perp}$ (●) in the two smectic A (S_{Ad} and S_{A1}) phases of a doubly reentrant liquid crystal 4-cyanobenzoyloxy-[4-octylbenzoyloxy]-*p*-phenylene (CBOBP).

IV-M Phase Transitions and Dynamical Ordering in Liquid Crystals

In 1989 the research group in Tokyo Institute of Technology reported the first discovery of antiferroelectricity in liquid crystal. In an antiferroelectric chiral smectic C phase of the compound, (4-(1-methylheptyloxycarbonyl)phenyl 4-octylbiphenyl-4-carboxylate), abbreviated as MHPOBC, the dielectric polarizations in the adjacent layers order in an antiparallel way. However, the microscopic origin for the coexistence of this dielectric order and dynamic disorder has not been resolved. A number of interaction models have been proposed so far. Among them are an interlayer direct dipole-dipole interaction model, a model of macroscopic electric force acting across the layer, or a model which emphasizes the importance of steric interaction among the chains. To clarify the true origin of the antiferroelectricity in liquid crystal, we are developing extensive NMR studies for the prototypical MHPOBC and related materials.

IV-M-1 Combined Two-Dimensional ^{13}C NMR Spectroscopies for Complete Analysis of the Molecular and Internal Order Parameters in Antiferroelectric Liquid Crystal

Toshihito NAKAI and Seiichi MIYAJIMA

To analyze molecular motion in complex fluids, it is necessary, in principle, to obtain separate information on each

of all the internal degrees of freedom in addition to the information on the molecule as a whole. Such full analysis of molecular dynamics is desirable especially for liquid crystals which exhibit interesting peculiar properties such as ferroelectric/ferrielectric/antiferroelectric transitions, re-entrant transitions, *etc.* because internal degrees of freedom play key roles for these phenomena.

Present two-dimensional (2-D) high resolution NMR experiments enable one to obtain order parameters at each of the carbon sites. First, the complex ^{13}C spectra coming from aromatic core were resolved by tracing the ^{13}C-^{13}C internuclear double quantum coherence transfer with 2-D INADEQUATE spectroscopy in isotropic state (Figure 1). Secondly, each of the ^{13}C chemical shielding tensor components were obtained by local field separated spinning sideband pattern analysis, *i.e.*, 2-D TOSS-DETOSS magic angle sample spinning spectroscopy in solid state (Figure 2). Finally the 1-D ^{13}C NMR experiment was carried out for the field-oriented liquid crystalline sample, and the field-induced shifts were analyzed for each of the carbon sites. Each of the order parameters thus obtained were used for the analysis of molecular motion and phase transitions of MHPOBC.

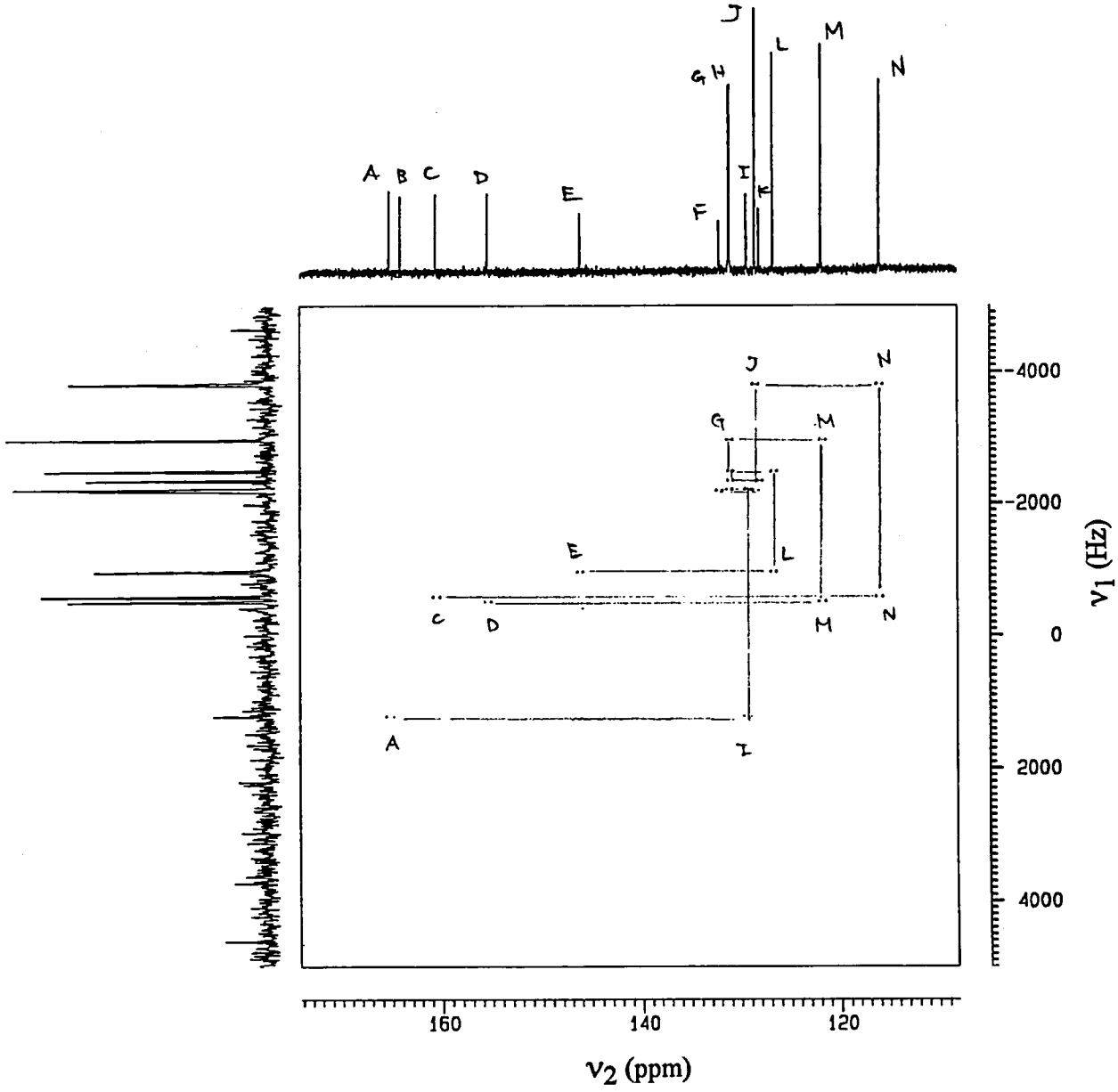


Figure 1. ^{13}C-^{13}C INADEQUATE Spectrum of MHPOBC in the isotropic state.

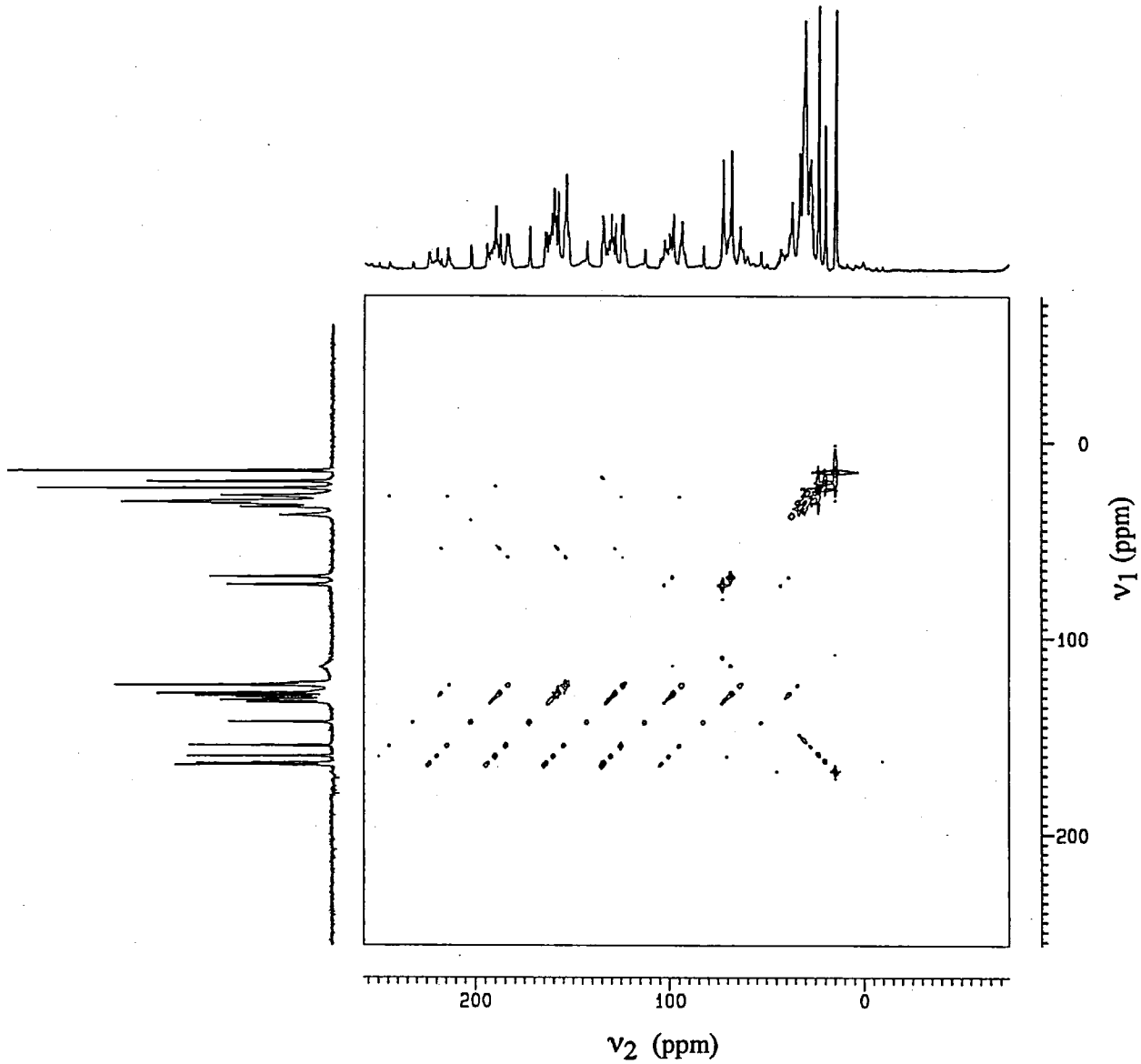


Figure 2. Local field separated spinning sideband pattern (TOSS-DETOSS) ^{13}C spectrum of MHPOBC in the solid state.

IV-M-2 Microscopic Origin of Antiferroelectricity in Liquid Crystal Studied by High Resolution ^{13}C NMR

Toshihito NAKAI, Seiichi MIYAJIMA, Yoichi TAKANISHI*, Shohei YOSHIDA* and Atsuo FUKUDA*
*(*Tokyo Inst. Tech.)*

High resolution ^{13}C NMR study was carried out for the antiferroelectric liquid crystal MHPOBC. Structural and dynamic aspects of chiral and achiral chains were analyzed from the measurements of isotropic shielding, cross polarization efficiency, field induced shift, and spin-lattice relaxation. It was revealed that the chiral chain assumes a bent form, namely, the chain axis makes *ca.* 50 degrees from the molecular long axis, in all the liquid crystalline and isotropic phases studied. The achiral chain axis lies more parallel to the molecular long axis. The bent form of the chiral chain results in a large steric hindrance against rotation, 10-25 kJ mol^{-1}, which is more than twice larger than that for the achiral chain, and therefore the rotational correlation time slows significantly as the temperature is lowered in the smectic A phase, and this situation makes it easier for the dipoles to interact across the layers and become ordered in an antiferroelectric manner.

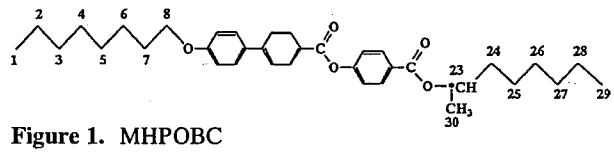


Figure 1. MHPOBC

IV-M-3 Orientational Change of the Trifluoromethyl Group at the Ferroelectric-Antiferroelectric Transition Observed by NMR Spectroscopy

Shohei YOSHIDA*, Bo JIN*, Yoichi TAKANISHI*, Ken ISHIKAWA*, Hideo TAKEZOE*, Atsuo FUKUDA* Toshihito NAKAI and Seiichi MIYAJIMA *(*Tokyo Inst. Tech.)*

[*Mol. Cryst. Liq. Cryst.* in press]

Temperature dependence of the order parameter of the trifluoromethyl group at the chiral part in 4-[(1-trifluoromethylheptyloxy)carbonyl]phenyl 4-[(4-octyloxy)biphenyl] 4-carboxylate (TFMHPOBC) was investigated by ^{13}C and ^{19}F NMR spectroscopies. From the

analysis of the ^{19}F dipolar triplet spectrum in perdeuterated TFMHPOBC, it was concluded that, at the phase transition between the ferroelectric and antiferroelectric phases, discontinuous change takes place for the orientational order parameter of the trifluoromethyl axis with respect to the molecular long axis. This fact shows that conformational change around the chiral center occurs simultaneously with the antiferroelectric phase transition, and suggests an important role of conformational change on dipolar ordering.

IV-N Hydrogen Dynamics in Dielectric Solids with Ferroelectric *vs.* Antiferroelectric Competing Interactions

Dielectric properties caused by hydrogen dynamics in solids were studied. Addition compounds of betaine with inorganic acids have hydrogen-bonded chains in its crystalline states, and exhibit quasi-one-dimensional dielectric properties. Mixed crystals of betaine phosphate (BP) and betaine arsenate (BA) are interesting because each of the pure BP and BA exhibit antiferroelectricity and ferroelectricity, respectively, and so competing interactions exist in BPA mixed crystals. Similar competition is also present in the mixed crystals, RADP, of rubidium dihydrogen phosphate (RDP) and ammonium dihydrogen phosphate (ADP). We studied these mixed crystals by use of low frequency and quasistatic dielectric responses, and revealed peculiar dielectric properties inherent to dimensionality crossover and frustrated interactions.

IV-N-1 Dimensionality Crossover and Nonlinear Dielectric Response in Betaine Phosphate/Arsenate Mixed Crystals

Yong-Hae KIM*, Bog-Gi KIM*, Jong-Jean KIM, Tomoyuki MOCHIDA and Seiichi MIYAJIMA** *(*KAIST, **KAIST and IMS)*

[*J. Phys. Condensed Matter* **8**, 6095 (1996)]

Dielectric properties of quasi one-dimensional hydrogen-bonded chains were studied for mixed crystals of antiferroelectric betaine phosphate and ferroelectric betaine arsenate at three different mixing concentrations, x= 0.1, 0.3, and 0.4 (x being the concentration of arsenate). For mixed crystals with x = 0.3 and 0.4, dielectric study revealed dimensionality crossover at around 82 K, where quasi one-dimensional nature turned into three-dimensional Curie-Weiss behavior on lowering the temperature. The crossover took place well above the antiferroelectric transition point (~75 K). For x=0.1 mixed crystal, on the other hand, the crossover point was almost coincident with the antiferroelectric transition point, showing still too weak interchain coupling and strong one-dimensionality near the antiferroelectric transition. For this system, the electric bias field effect revealed a significant and temperature dependent nonlinearity of the dielectric constant, which may be ascribed to a development of competition between antiferroelectric and ferroelectric interchain couplings, the latter growing with increasing bias field and lowering temperature.

IV-N-2 Anisotropic Dipole-Glass Freezing in Rubidium/Ammonium Dihydrogen Phosphate Mixed Crystal and its Perdeuterated Analogue

Jae-Hyeon KO*, Bog-Gi KIM*, Jong-Jean KIM and Seiichi MIYAJIMA** *(*KAIST, **KAIST and IMS)*

Anisotropic glass freezing phenomenon was studied by dielectric measurements in the dipole glass systems of rubidium/ammonium dihydrogen phosphate, RADP(x), and its perdeuterated analogue, D-RADP(x), where x denotes ammonium concentration. Glass freezing temperatures for a-cut and c-cut single crystals measured at low frequency revealed very small anisotropy (<1 K) in RADP(0.43) but a large anisotropy (7.5 K) in D-RADP(0.40). The higher glass transition temperature as observed along the c-axis than a-axis is in agreement with the cluster model theory of Matsushita and Matsubara.[1)]

Reference

1) E. Matsushita and T. Matsubara, *J. Phys. Soc. Jpn.*, 55, 666 (1986).

IV-O Electronic Properties of Alkali-Hydrogen-Carbon Systems

In alkali-hydrogen-carbon ternary systems, hydrogen or alkali metal elements possibly exhibit a variety of structures and electronic states such as atomic, ionic, molecular, or metallic states when doped or intercalated in the host crystal lattice. Structural and electronic properties were studied for new types of alkali-hydrogen-carbons, *i.e.* sodium-hydrogen-graphite and sodium-hydrogen-C_{60} ternary compounds by means of solid state NMR spectroscopy.

IV-O-1 ^1H and ^{23}Na NMR Studies of Sodium-Hydrogen-Graphite Ternary Intercalation Compound

Hironori OGATA, Seiichi MIYAJIMA, Kazuto MATSUTSUJI* and Toshiaki ENOKI* *(*Tokyo Inst. Tech.)*

^1H and ^{23}Na NMR have been studied for well-characterized stage-4 sodium-hydrogen-graphite ternary intercalation compound (NaH-GIC) prepared from HOPG (highly oriented pyrolytic graphite). By the analysis of the angular dependence of the second moment for ^1H and ^{23}Na spectra on the basis of ^1H-^1H and ^1H-^{23}Na dipole interactions, hydrogen species are suggested to form a two-dimensional sheet of H anions sandwiched by two layers of cationic sodium. The structure and the estimated concentration of hydrogen are similar to those of potassium-hydrogen-graphite ternary compound (KH-GIC). A significant difference from KH-GIC is that the H/Na atomic concentration ratio is close to unity. Consequently the charge transfer is almost completed between Na^+ and H^- and so only small amount of carriers are transferred to the graph-

ite sheets. This result is consistent with the previous reports of ^{13}C NMR[1], Shubnikov-de Haas effect[2] and thermoelectric power[3] experiments.

From the angular and frequency dependences of ^{23}Na shifts at 71.46 MHz and 105.83 MHz, the quadrupole coupling constant tensor at the Na nucleus is evaluated to be e^2Qq/h = 1.79 MHz and η = 0.85, which suggests that ^{23}Na atom exists as non-covalent Na^+ ion and that the in-plane anisotropy of the electric field gradient tensor is small.

References

1) H. Ogata, S. Miyajima, K. Matsutsuji, T. Enoki, *J. Phys. Chem. Solids* 57, 703 (1996).
2) T. Enoki, K. Matsutsuji, K. Suzuki, *J. Alloys and Com pounds* 231, 735 (1995).
3) T. Enoki, N. Sakamoto, K. Nakazawa, K. Suzuki, K. Sugihara, K. Kobayashi, *Phys. Rev.* B 47, 10662 (1993).

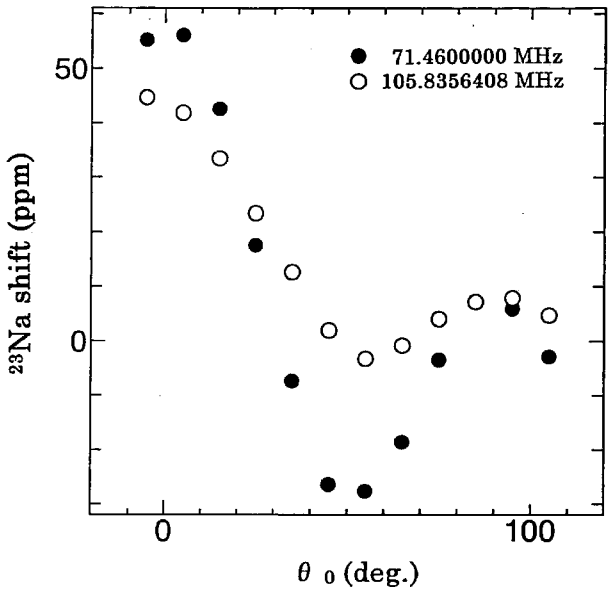


Figure 1. Angular dependence of the ^{23}Na NMR central transition in stage-4 NaH-GIC.

IV-O-2 NMR Study in $Na_xH_yC_{60}$

Hironori OGATA, Seiichi MIYAJIMA, Kenichi IMAEDA, Jonas KRÖBER and Hiroo INOKUCHI

^{23}Na and ^1H NMR studies have been carried out for the new superconductor Na-H-C_{60}. The peak position of the ^{23}Na NMR spectrum is dependent on temperature, and exhibit discontinuous upfield shift of about 20 ppm at 250 K, which is indicating a first order transition. From the line shape of the ^{23}Na spectrum obtained at 56 K, the quadrupole coupling constant tensor is evaluated to be e^2Qq/h =3.3 MHz with the asymmetry parameter close to unity. The ^1H NMR spectrum obtained at room temperature suggests anionic hydrogen state. Temperature dependence of the ^1H spin-lattice relaxation time suggests that hydrogen is in a weakly delocalized electronic state.

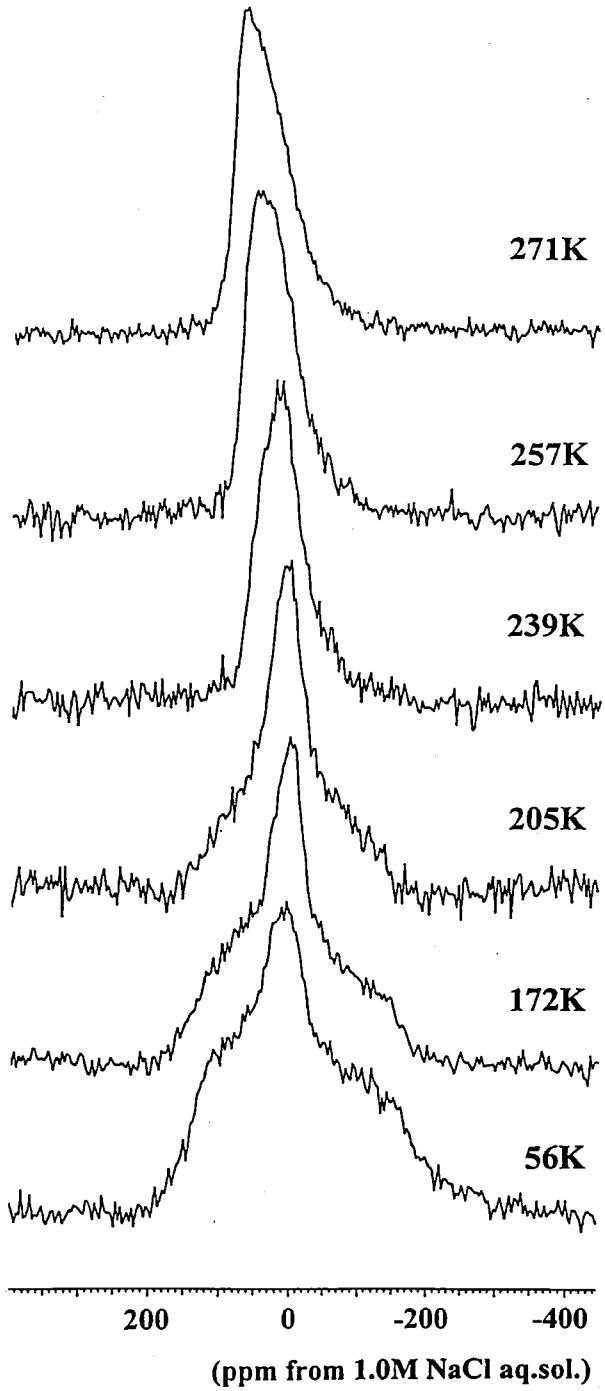


Figure 1. ^{23}Na NMR spectra in $Na_xH_yC_{60}$ superconductor.

IV-P Search for Novel Electronic Systems Based on Organic Charge Transfer Complexes

To search for novel electronic phenomena based on organic donors, we have undertaken systematical investigations into charge transfer complexes based on BEDT-TTF and various TCNQ derivatives. In these two component systems, novel electronic phenomena are to be realized by tuning the sizes and/or electron affinities of acceptors. In this research, in addition to conventional type of charge transfer complexes, some new types were also obtained. We focused further on the correlation between the properties of the acceptor and those of the resultant assemblies to obtain hints for designing novel functional materials.

IV-P-1 Construction of an Organic Spin-Ladder System Based on BEDT-TTF Charge Transfer Complex

Tomoyuki MOCHIDA, Tatsuo HASEGAWA*, Seiichi KAGOSHIMA* and Yoshihiro IWASA** *(*Univ. Tokyo, **JAIST)*

Taking advantage of the side-by-side S...S interaction of the BEDT-TTF molecule, an organic spin ladder system is constructed. Combination of BEDT-TTF with a strongly polar acceptor, 2,3-difluoro-TCNQ, afford a novel type of CT complex, whose donor arrangement is characterized by both a face-to-face interaction through dimerization and a side-by-side S...S interaction. The charge transfer rate is unity, and the enhancement of magnetic susceptibility is observed with increasing temperature above R.T.

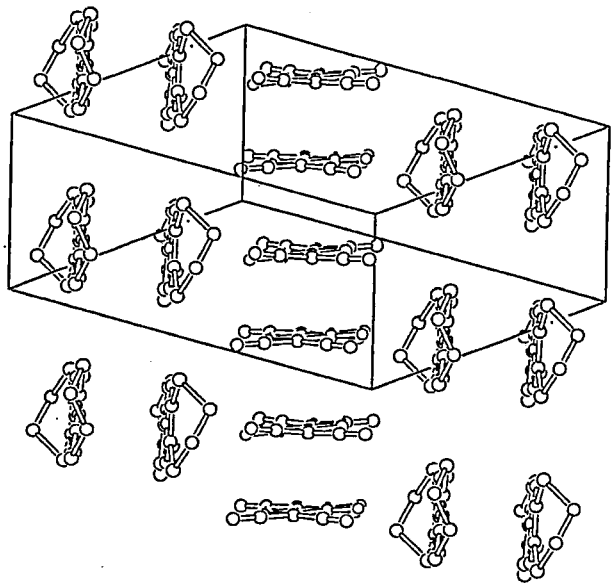


Figure 1. Ladder-like donor arrangement in (BEDT-TTF) (2,3-difluoro-TCNQ) complex viewed along the molecular long axes.

IV-P-2 Organic Antiferromagnets Based on BEDT-TTF and Difluoro-TCNQs with Various Polarity

Tomoyuki MOCHIDA, Tatsuo HASEGAWA*, Seiichi KAGOSHIMA* and Yoshihiro IWASA** *(*Univ. Tokyo, **JAIST)*

In order to search for the tunability of (BEDT-TTF)(F_2-TCNQ) electronic system, charge transfer complexes of three acceptors, 2,5-F_2-TCNQ, 2,6-F_2-TCNQ and 2,3-F_2-TCNQ, with almost the same redox potentials, are compared. Even though the polarities of the acceptors are very different from each other, they afforded isomorphic mixed-stack CT complexes: the crystal structures are not affected by dipole-dipole interactions between the acceptors. The charge transfer rate is unity, and they show antiferromagnetic behavior below T_N=30 K, 26 K, and 23 K, respectively.

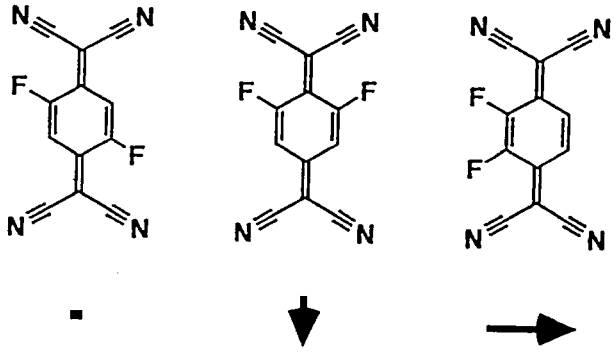


Figure 1. Difluoro-TCNQs. The dipole moments are indicated by arrows.

IV-P-3 Structures and Solid State Properties of (BEDT-TTF)(TCNQ derivatives) : Correlation between the Structure of the Acceptor and the Resultant Complexes

Tomoyuki MOCHIDA, Tatsuo HASEGAWA*, Seiichi KAGOSHIMA*, Sadaki SUGIURA and Yoshihiro IWASA**** *(*Univ. Tokyo, **JAIST)*

Through a systematical investigation into the structures and properties of charge transfer complexes based on BEDT-TTF and various TCNQ derivatives, it was found that the shape of the acceptor molecules play a crucial role in determining the stacking structure and thus physical properties of the resultant charge transfer complexes. The acceptors investigated are F_n-TCNQ (n =1 - 4) and R_1R_2-TCNQ (R_1,R_2 = H, Me, Cl, Br). For the case of fluorinated TCNQ complexes, the molecular long axes of the donor and the acceptor are nearly parallel to each other, leading to a large side-by-side interaction between the donors. On the other hand, when larger substituents (Me-, Cl-. Br-) are introduced into the acceptor, the D-A molecules have twisted configuration due to steric hindrance, resulting in a small side-by-side interaction. These structural differences lead to remarkable differences in their solid state properties.

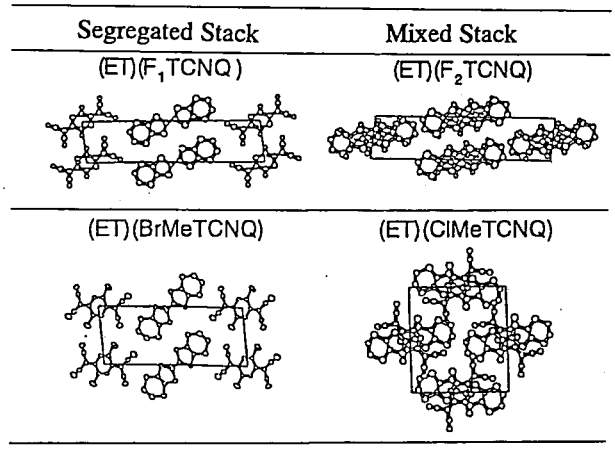


Figure 1. Crystal structures of representative complexes.

IV-Q Strong Correlation Effects in Organic Conductors

A variety of electronic states in organic conductors results from the competition between mutual Coulomb interactions among electrons and electron-lattice coupling. Such a unique feature of organic conductors is enhanced by the existence of larger degrees of freedom in a unit cell than in inorganic crystals in general, i.e. many molecules in a unit cell. This fact has been elucidated by considering the case of $(EX)_2X$ salts. Even though the number of electrons are the same in this family, the electronic states vary in an essential way. It turns out that α-$(ET)_2I_3$ can be basically considered as a band insulator, while κ-$(ET)_2$ is the Mott insulator. Moreover important parameters have been identified which bridge between these two apparently very different states.

IV-Q-1 Phase Diagram of Two-Dimensional Organic Conductors : $(BEDT\text{-}TTF)_2X$

Hiori KINO and Hidetoshi FUKUYAMA *(University of Tokyo)*

[*J. Phys. Soc. Jpn.* **65**, 2158 (1996)]

The effects of on-site Coulomb interaction in two-dimensional organic conductors, κ-$(BEDT\text{-}TTF)_2X$, α-$(BEDT\text{-}TTF)_2I_3$ and $(BEDT\text{-}TTF)_2MHg(SCN)_4$, have been studied within the Hartree-Fock approximation. If the strength of Coulomb interaction exceeds some critical value, various kinds of antiferromagnetic states appear and these phases have been classified on a phase diagram with two key parameters, which leads to a unified view on the ground states of this unique family.

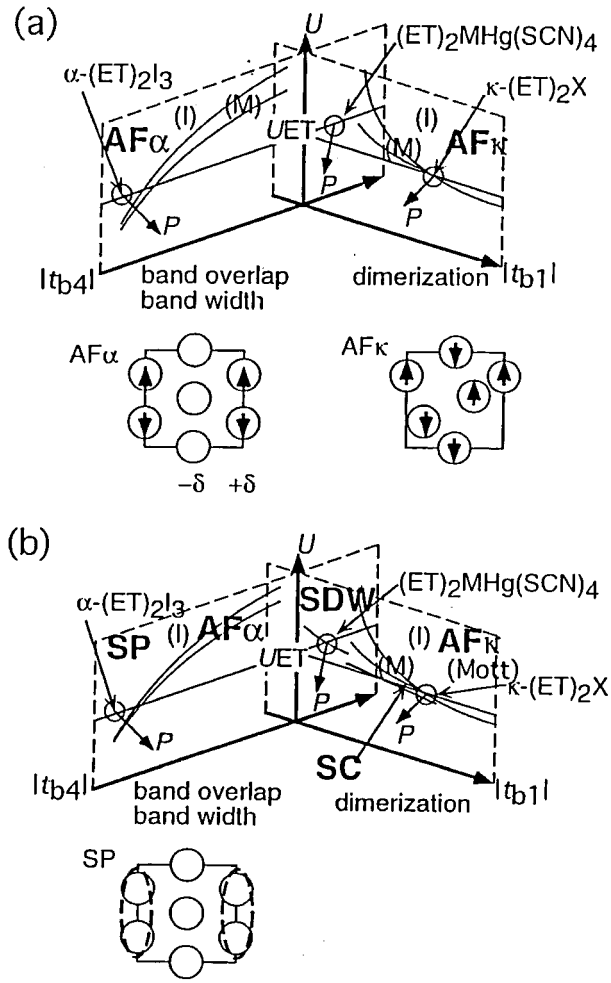


Figure 1. The HF (a) and expected (b) phase diagram for κ-$(ET)_2X$, α-$(ET)_2I_3$ and $(ET)_2MHg(SCN)_4$-types. AFκ, AFα and SP are antiferromagnetic ordered phase for κ and α-type structures and the spin-Peierls phase, respectively. (I) and (M) imply insulating and metallic phases, respectively. Arrows with *P* designate the effects of the applied pressure.

IV-R Spin Gap and Disorder

A remarkable experimental fact observed in the neutron scattering in the disordered spin-Peierls system $CuGe_{1-y}Si_yO_3$, which indicats the coexistence of the two long range orders of the lattice dimerization and the antiferromagnetism, has been explained based on the phase Hamiltonian. This surprising feature because of apparently mutually contradicting nature of the order parameters turns out to be rather universal : spin gap systems of S=1/2 Heisenberg spins, e.g. spin-Peierls, two-leg ladder, Haldane and high T_c cuprates, are very susceptible to disorder, which leads to the true long range order of antiferromagnetism in the ground states once the degree of disorder (e.g. density of impurities) is macroscopic.

IV-R-1 Antiferromagnetic Long Range Order in Disordered Spin-Peierls Systems

Hidetoshi FUKUYAMA, Tetsuhiro TANIMOTO and Masako SAITO *(University of Tokyo)*

[*J. Phys. Soc. Jpn.* **65**, 1182 (1996)]

A theoretical possibility of the existence of disorder-induced antiferromagnetic long range order in spin-Peierls system has been presented, which will be in accordance with the recent experimental indication of the coex-

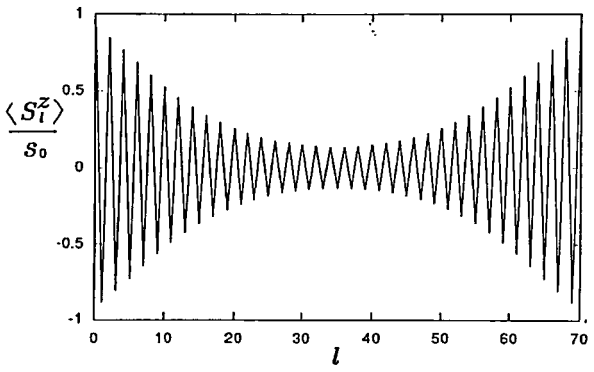
istence of dimerization and antiferromagnetism in $CuGe_{1-y}Si_yO_3$.

IV-R-2 Impurity Induced Antiferromagnetism in Spin-1/2 Heisenberg Two-Leg Ladder Systems

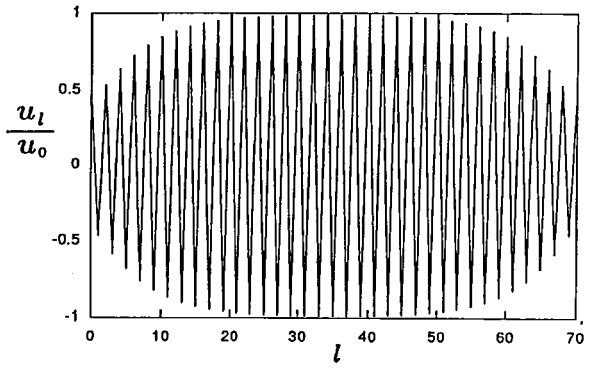
Hidetoshi FUKUYAMA, Naoto NAGAOSA, Masako SAITO and Tetsuhiro TANIMOTO *(University of Tokyo)*

[*J. Phys. Soc. Jpn.* **65**, 2377 (1996)]

Based on the phase Hamiltonian representation of a spin-1/2 Heisenberg two-leg ladder system coupled antiferromagnetically, which has a spin gap if clean, it is shown that a non-magnetic impurity replacing a spin induces a staggered spin modulation. This results in the long range order of antiferromagnetism in the presence of three-dimensional coupling between the ladders. This will be in accordance with a recent experimental observation by Azuma et al. on $Sr(Cu_{1-x}Zn_x)_2O_3$.



(a)



(b)

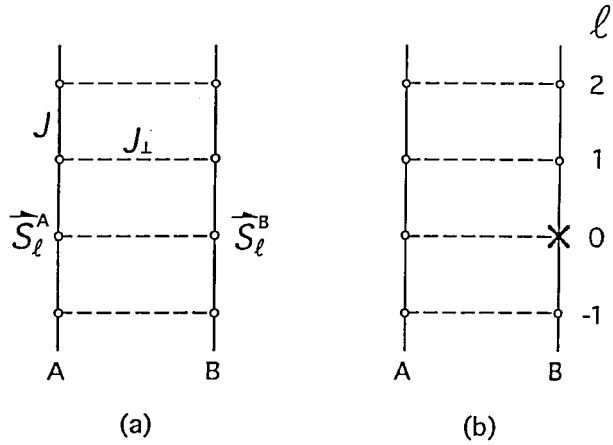
Figure 1. The spacial variation of (a) the magnetic staggered moment, and (b) the lattice distortion u_l / u_0.

IV-R-3 Non-Magnetic Impurities in Spin Gap Systems

Naoto NAGAOSA, Akira FURUSAKI*, Manfred SIGRIST* and Hidetoshi FUKUYAMA *(University of Tokyo) (*University of Kyoto)*

[*To appear in J. Phys. Soc. Jpn.* **65** (1996)]

The effect of non-magnetic impurities is discussed for both the two-leg Heisenberg ladder system and other spin liquids with excitation gap. It is shown that the random depletion of spins introduces a random Berry phase term to the non-linear σ model. The classical nature of the antiferromagnetic correlation is enhanced by the topological decoherence, and the staggered susceptibility shows more singular behavior at low temperatures than in the uniform antiferromagnetic Heisenberg chain.



(a) (b)

Figure 1. (a) A schematic representation of spin-1/2 Heisenberg two-leg ladder system. (b) The depletion of a single from B chain.

IV-S Many-Body Effects and Superconductivity in Organics

IV-S-1 Integrable Chain of Electrons Coupled with Phonons

Valery IVANOV, Michail YE. ZHURAVLEV*, Vladimir V. ACHKASOV* *(*N.S. Kurnakov Institute of the General &Inorganic Chemistry of the Russian Academy of Sciences)*

[*JETP Lett.* **63** (1996) 94-99]

The exact wave function of Schrodinger equation for a chain of electrons interacting with local phonons is constructed. The ground state energy and the gap in the electronic spectrum are calculated.In the limiting case of high electron density the energy gap has an exponential de-

pendence on electron-phonon coupling constant similar to BCS coupling energy.

IV-S-2 Integrable Chain of Electrons Coupled with Squeezed Phonons

Valery IVANOV, Michail Ye. ZHURAVLEV*, Yoshimasa MURAYAMA and Sadao NAKAJIMA***** *(*N.S. Kurnakov Institute of the General &Inorganic Chemistry of the Russian Academy of Sciences, **Hitachi Advanced Research Lab., ***Tokai University)*

[*JETP Lett.* **64** (1996) 148-154]

The exact wave function of Schrodinger equation is constructed for a chain of electrons interacting with squeezed phonons. Based on the Bethe ansatz approach the ground state energy and the gap in the electronic spectrum are calculated. It is found the nonmonotonic dependence of the ground state energy on a number of squeezed phonons.

IV-S-3 Strong Electron Correlations in κ- (BEDT-TTF)$_2$X Salts

Valery IVANOV and Kazushi KANODA

[*Physica C Vol.* **268**, (1996) 205-215]

The κ-ET$_2$X compounds are classified as strongly correlated electron systems. The tight-binding approach for correlated electrons is applied to the κ-ET$_2$X family. It is shown the correlated narrowing of a carrier energy band. The singlet superconducting pairing of different symmetries is studied based on the symmetry of square lattice model of ET$_2$-layer and superconducting coupling comstants are calculated. The comparison of the theoretical speculations with available experimental data is made for normal and superconducting phases in κ-ET$_2$X.

IV-S-4 Superconducting κ-BEDT-TTF Salts as Layered Correlated Electron Systems

Valery IVANOV and Kazushi KANODA

[*Mol. Cryst. Liq. Cryst.* **285** (1996) 211]

For the k-ET$_2$X compounds as strongly correlated electron systems the anisotropic superconducting pairing interaction is constructed based on the symmetry of electronic transfer and superconducting characteristics are calculated. For normal properties, a role of internal degrees of freedom in ET-layers, particularly in the ET$_2$dimers is shown. For study of superconducting condensate it is proposed the anomalous self-energy part which is odd with respect to energy. It has been observed gapless superconductivity with nonBCS critical temperature, specific heat jump etc. It is shown the influence of electron-electron correlations to enhance superconducting condensate. The study is useful for low energy experiments: nonactivated temperature dependence of superconducting specific heat and NMR relaxation rate.

IV-S-5 κ-(BEDT-TTF)$_2$CuX Salts: Electronic Structure, Insulator-Metal Transition, Superconductivity

Valery IVANOV

[*Physica B,* in press]

The κ-(BEDT-TTF)$_2$X salts are classified as strongly correlated electron systems. Therof electronic structure is calculated on the basis of tight-binding approach for correlated electrons mapped on a triangular lattice. It is shown that intradimer electron interactions provide insulating state of system. The insulator-metal phase transition of the Mott-Hubbard kind is derived. Based on the electronic band symmetry in metallic state, the anisotropic superconducting pairing of different symmetries is studied. The obtained results are in agreement with available experimental data and theoretical speculations.

IV-S-6 Insulator-Metal Transition in the κ-ET$_2$X Salts, where "ET" is the bis(ethylenedithio)-tetrathiafulvalane (BEDT-TTF) Molecule

Valery IVANOV

[*Physica C,* **271** (1996) 127-132]

The insulator-metal Mott-Hubbard transition is derived for κ-ET$_2$X salt model. The phase transition has occured due to scattering of electrons on spin and charge fluctuations. The calculated critical magnitude $(t_{er}/U_{ET2})_{crit}$ (ratio of an interdimer carrier hopping to the effective intradimer electron-electron interaction) separates the insulating and metallic κ-ET$_2$X materials at the constructed phase diagram in agreement with noticed empirical regularity.

IV-S-7 κ- BEDT-TTF Organics as It Is Seen for Hubbardist

Valery IVANOV

[*Phil. Mag. B* , in press]

The κ-ET$_2$X family is characterized by high-energy scale of intraET and effective intraET$_2$ Anderson-Hubbard like electron-electron correlations U_{ET}~ 1eV and $U_{ET2} \sim 2t_{ra}$, an intradimer hopping t_{ra} and a weak interdimer hopping t_{er} with emphasized internal degrees of freedom in ET-layers, particularly in the ET$_2$ dimers.The bonding / antibonding branches in the electronic band structure of the ET$_2$X compounds, density of electronic states and semiconducting gap for semimetals are derived. In the frame of the diagrammatic technique for the generalized Okubo-Hubbard operators the insulator-metal transition has been found with phase critical point $(t_{er}/U_{ET})_{crit}$. The anisotropic superconducting pairing interaction is constructed and superconducting features are calculated. Systematics are predicted for metallic and semiconducting κ-ET$_2$X phases in agreement with available experimental data: e. g., the paramagnetic spin susceptibility enhancement due to the dimerization, the negative Knight shift baric derivatives etc.

IV-S-8 Electronic Structure and Origin of κ-ET$_2$X Insulators, where "ET" is the bis(ethylenedithio)-tetrathiafulvalane (BEDT-TTF) Molecule

Valery IVANOV and Kyuya YAKUSHI

[*Physica C,* in press]

The electronic structure of κ-ET_2X salts is studied on the basis of tight-binding approach for correlated electrons in the frame of an effective Hubbard model with two dimer/sites per a unit cell. It is shown that intradimer electron interactions provide an insulating state of the system without any order parameter. The open area of calculated Fermi sutface is provided by projection of upper leaf of antibonding energy dispersion surface. The closed parts of Fermi surface has occured due to projection of lower leaf of energy dispersion surface. The evaluated band gap in the paramagnetic state, density of states and energy dispersion relations are in agreement with available experimental data and theoretical speculations.

IV-S-9 Electron Molecular Vibration Coupling in Organic Charge-Transfer Salts: Application of Spectroscopic and Hubbard Models

Michail E. KOZLOV, Valery IVANOV, Kyuya YAKUSHI and M. TOKUMOTO

[*Synth. Met.,* in press]

Spectroscopic and Hubbard model were utilised for an analysis of vibrational spectra in organic monovalent charge-transfer salts with dimerised structure. It is shown the correlated origin of IR- active electron-vibrational (vibronic) bands.The obtained relation between easy measurable intensitiy and frequency of the vibronic bands gives an opportunity to evaluate coupling constants of materials from the experimentAl spectra. The derived results are in agreement with available data for BEDT-TTF-based and TTF-based charge-transfer complexes.

IV-S-10 Electronic Structure, Insulator-Metal Transition and Superconductivity in κ- BEDT-TTF Salts

Valery IVANOV and Yoshimasa MURAYAMA* *(*Hitachi Advanced Research Lab.)*

[*Proceedings of the 9th Intern. Symposium on Superconductivity,* ISS'96 Springer-Verlag:Tokyo]

The tight-binding approach for correlated electrons is applied to study ET_2X salts with particular attention to their normal and superconducting properties.The electronic band structure, density of carrier states, the enhancement of some magnitudes due to dimerization, semiconducting gap etc. are calculated. The insulator-metal transition is calculated for different types of molecular arrangement in ET-layer with phase transition boundary. It is shown that electron correlations enhance condensation energy. The present treatment may be helpful to discuss comparatively the superconducting properties of cuprates and can be applicable to other superconductors with layer structure.

IV-S-11 The Order of the Band Filling in the Periodical Anderson Model

Anatoly VEDYAYEV*, Valery IVANOV, Michail ZHURAVLEV and Maria MARINARO***** *(* Moscow State University, **N.S. Kurnakov Institute of the General &Inorganic Chemistry of the Russian Academy of Sciences, ***Salerno University, Italy)*

[*Theoret. Math. Phys.* **108** N1(1996) 101-108]

For the periodic Anderson model with contact hybridization it is proposed the procedure of subsequent carrier filling of bands originated due to both Hubbard repulsion and hybridization interaction. In the frame of developed earlier tight-binding method for correlated carriers it is shown that intrasite electron interactions conserves an integer number of electrons in totally filled correlated bands as in atomic limit. For metallic state the dependence chemical potential on electron concentration has been calculated. The obtained results are applicable for systems including correlated localized electrons and noncorrelated itinerant carriers: heavy-fermion systems, p-d materials etc.

IV-S-12 Path-Integral Treatment for Localized Electrons in the Periodic Anderson Model

Valery IVANOV, Renato PUCCI*, Vladimir YARUNIN and Michail ZHURAVLEV***** *(*Catania University, Italy, **Joint Institute for Nuclear Research, Dubna, Russia, ***N.S. Kurnakov Institute of the General &Inorganic Chemistry of the Russian Academy of Sciences)*

[*Physica B (1996),* in press]

It is used the non-pertubative functional integral analysis of localized d-electron subsystem in the Anderson lattice model (periodic Anderson model) based on the assumption that the motion of narrow-band d-electrons is more slow than the motion of broad band s-electrons. The partition function is presented as the path integral over the variables of "slow" and "light" electrons and the adiabatic approximation is applied for d-electrons through the averaging of the thermal distribution over the "light" s-electron Grassman trajectories with antiperiodical boundary conditions. The Lagrangian, temperature dependent electronic spectrum and effective Hamiltonian for d-electrons have been derived. The obtained "Kondo temperature" and temperature dependence of the d-electron density of states can give rise to the thermopower peaks, Schottky-like anomalies in the heat capacity, the increase and saturation of the resistivity, experimental details associated with the magnetic alloy problem, as well as other observed effects in materials with hybridized localized and itinerant electrons.

IV-T Electronic Structures and Physical Properties of Quasi-One-Dimensional Halogen-Bridged Mixed-Valence Metal Complexes (MX-Chains)

Recently quasi-one-dimensional halogen-bridged mixed-valence compounds (MX-chains) have been extensively investigated because they show very interesting properties such as an intense intervalence charge transfer band, an overtone progression in resonance Raman, a luminescence with a Stokes-shift, midgap absorptions attributable to solitons or polarons, large third-order nonlinear optical susceptibilities, one-dimensional model compounds of high Tc copperoxide superconductivities, etc.. These compounds are considered as Peierls-Hubbard system where the electron-phonon interaction (S), the electron transfer (T), the on-site and inter-site Coulomb interactions (U and V) are cooperated or competed with one another. Compared with other inorganic and organic compounds, these MX-chains have charactersitic points as follows; (1)The magnitudes of the physical parameters (S, T, U and V) and/or the band gaps can be tuned by substituting the metal ions, bridging halogens, in-plane ligands, and counteranions; (2) The interchain interactions can can be controlled by using the hydrogen-bonds from one- to three-dimensionally. Therefore we can anticipate the interesting physical properties in these compounds.

IV-T-1 Photoexcitations in MX Chains: Dynamics of Solitons and Polarons in $[Pt(en)_2][Pt(en)_2I_2](ClO_4)_4$

Hiroshi OKAMOTO, Yasuo OKA *(Tohoku Univ.)*, **Tadaoki MITANI***(JAIST)*, **Masahiro YAMASHITA** *(Nagoya Univ. and IMS)* **and Koshiro TORIUMI***(Himeji Inst. of Tech.)*

[*Mol. Cryst. Liq. Cryst.*, **285**, 311(1996)]

Dynamics of photo-induced gap states such as charged-solitons and polarons have been studied in the $[Pt(en)_2][Pt(en)_2I_2](ClO_4)_4$ single crystal using the photo-induced IR absorption (PA) measurements. Annihilation processes of the gap states are well explained by the bimolecular recombination model. The PA intensities and decay characteristics of both charged-solitons and polarons are strongly temperature-dependent. The temperature dependences of the rate constant of recombination for both carriers clearly show a crossover of the transport mechanism from hopping to tunneling with decrease of temperature.

IV-T-2 Subgap Optical Absorption Induced by Quantum Lattice Fluctuations at the Peierls Edge in PtCl-Chain Complexes

Noritaka KURODA, Masato NISHIDA*(Tohoku Univ.)* **and Masahiro YAMASHITA***(Nagoya Univ. and IMS)*

[*Phys. Rev.*, **B54**, 2390(1996)]

The temperature dependence of the low-energy tail of the interband optical absorption band at the Peierls edge has been studied in halogen-bridged linear-chain complexes, $[Pt(en)_2][Pt(en)_2Cl_2]Y_4$ (Y=ClO_4 and BF_4). The absorption spectrum and its temperature dependence are explained well in terms of the subgap density of states of the one-dimensional electronic bands induced by the quantum vibration of Cl ions of the breathing mode. Both substances are found to have a dimensionless electron-phonon coupling-constant of λ~1.2, the zero-temperature gap parameter Δ0~1.45 eV, and the transfer integral of to~0.4 eV. Because of the strong electron-phonon coupling the temperature dependence of the energy gap is dominated by the self-energy effect; even at 0 K the self-energy amounts to 0.07-0.08 eV, being considerably greater than the self-energies in usual semiconductors. The role of the anharmonicity of the chain-like Pt-Cl bonds is discussed in relation to the origin of the large gap parameter.

IV-T-3 Determination of the Electronic Structure in the Strongly Correlated 1-D Electron Systems: X-Ray Photoelectron and Auger Spectroscopy of Halogen-Bridged Nickel Complexes

Hiroshi OKAMOTO, Ashish Chainani, Takashi Takahashi*(Tohoku University)*, **Hiroshi KITAGAWA, Tadaoki MITANI***(JAIST)*, **Toshio MANABE and Masahiro YAMASHITA***(Nagoya Univ. and IMS)*

[*Synth. Met.*, in press]

The electronic structure of the 1-D Ni complexes, $[Ni(chxn)_2X]X_2$ is studied together with the discrete Ni complexes, $[NiX_2([14]aneN_4)]ClO_4$ (X=Cl and Br), using X-ray photoelectron spectroscopy (XPS) and Auger electron spectroscopy (AES). An analysis using a simple X-Ni-X trimer model on the Ni2p XP spectra indicates that the average on-site Coulomb energy U in these Ni complexes is about 5 eV. The obtained results demonstrate that the 1-D Ni complexes are CT insulator.

IV-T-4 Mixed-Valence State in MMX-Chains Complexes, $Pt_2(dta)_4I$

Hiroshi KITAGAWA, Noriaki ONODERA, Jeung-Sun AHN, Tadaoki MITANI*(JAIST)*, **Misa KIM, Yoshiki OZAWA, Koshiro TORIUMI***(Himeji Inst. of Tech.)*, **Kazutomo YASUI, Toshio MANABE and Masahiro YAMASHITA***(Nagoya Univ. and IMS)*

[*Mol. Cryst. Liq. Cryst.*, **285**, 311(1996)]

Physical and structural properties of the MMX-type halogen-bridged mixed-valence complex, $Pt_2(dta)_4I$ (dta=$CH_3CS_2^-$) were investigated. This complex exhibits metallic conduction above room temperature, which is the first observation in halogen-bridged 1D transition-metal complexes. Below 300K, the metal-semiconductor transition was observed. The mixed-valence state of this compound is discussed.

IV-U Organic-Inorganic Hybrid-Type Charge Transfer Complexes

Organic-inorganic hybrid-type charge transfer complexes have been the forcus of much recent reaearch. In these complexes, it is expected that two different electronic states of d and π are coupled to each other, which may provide a unique opportunity for constructing of novel electronic systems.

IV-U-1 Physical Properties of Quasi-One-Dimensional Charge Transfer Metal Complexes; [M(HBQD)$_2$]TCNQ (M=Ni, Pd; H_2BQD=1,2-Benzoquinonedioxime)

Yuka KAGAMI, Fumiyasu IWAHORI, Tachi OHISHI, Tetsuo HAMA, Toshio MANABE, Masahiro YAMASHITA*(Nagoya Univ. and IMS)*, **Hiroshi KITAGAWA, Ken-ichi SAKAI and Tadaoki MITANI***(JAIST)*

[*Synth. Met.*, in press]

We have investigated the physical properties of [M(HBQD)$_2$]TCNQ (M=Ni, Pd; H_2BQD=1,2-benzoquinonedioxime) which consist of alternating -D-A-D-A- type stacking of transition-metal-complex donors and organic TCNQ acceptors. The degree of charge-transfer for each sample was estimated to be ~0.1 from the results of IR, Raman spectra, and bond lengths of TCNQ. From XPS measurements, the valence state of Ni or Pd was found to be transformed at low temperature from +2 to the mixed valency of (+2,+3) or (+2,+4), respectively. This behavior can be considered to be due to the charge transfer from d-orbital of the transition metal to π-antibonding orbital of the HBQD ligands, which was confirmed by the lower-energy shift of IR stretching modes of C=N in HBQD. This temperature-induced charge-transfer between transition metal and ligand is the first observation in the transition-metal-complex assemblies.

IV-V Low-Dimensional Magnetic Systems

Low-dimensional magnetic systems are of current interest because they show peculiar quantum effects. A striking phenomenon is the strong spin-dependent behavior at T=0, of the one-dimensional Heisenberg antiferromagnet (1D-HAF). Haldane predicted that for the integer spin values S 1D-HAF exhibits a singlet ground states separated from the first triplet excited state with an energy gap Eg (Haldane gap), while for the half-integer spin values S the 1D-HAF has a gapless spectrum of the excitation. Although there have been many theoretical works on low-dimensional magnetic systems, only a few systematic works on syntheses and measurements have been carried out.

IV-V-1 Crystal Structure and Magnetic Properties of the S=1 Quasi-One-Dimensional Compound Ni([15]aneN$_4$)N$_3$(PF$_6$)

Yang YU, Zentaro HONDA, Koichi KATSUMATA *(RIKEN)*, **Tachi OHISHI, Toshio MANABE and Masahiro YAMASHITA***(Nagoya Univ. and IMS)*

[*Mol. Cryst. Liq. Cryst.*, **286**, 121(1996)]

A new S=1 quasi-one-dimensional compound Ni([15]aneN$_4$)N$_3$(PF$_6$) has been synthesized. Both crystal structure and magnetic properties of this compound have been characterized using the single crystal samles. The compound crystallizes in the orthorhombic system, with space group P2nn, Z=2 and unit cell parameters a=11.332(5), b=13.861(4) and c=6.173(2) Å, respectively. A superlattice along the c-axis was confirmed by both X-ray Weissenberg film and powder diffraction method. In addition, a disorder of the packing sequence of the ([15]aneN$_4$) in-plane ligands along the c-axis was proposed. The temperature dependence of magnetization of a single crystal was measured using a SQUID magnetometer. We have observed a large difference in zero field cooled and field cooled magnetizations below about 20 K. We have also measured the AC susceptibility of this sample in zero static magnetic field. A cusp is observed at about 22K in the temperature dependence of AC susceptibility.

IV-V-2 Inducing a Magnetic Ordering in the Haldane Materials Ni(C$_5$H$_{14}$N$_2$)$_2$N$_3$(ClO$_4$) by Magnetic Field

Zentaro HONDA, Koichi KATSUMATA, Aruga KATORI*(RIKEN)*, **Tachi OHISHI, Toshio MANABE, Masahiro YAMASHITA***(Nagoya Univ. and IMS)*

[*Phys. Rev. Lett.*, in press]

From a heat capacity measurements in high magnetic field and at low temperature, we have obtained evidence for a magnetic ordering in the S=1 quasi one-dimensional Heisenberg antiferromagnet Ni(C$_5$H$_{14}$N$_2$)$_2$N$_3$(ClO$_4$). The transition temperature is ~0.6 K at 12 T parallel to the chain axis.

IV-W Photoelectron Spectroscopy of Organic Solids in Vacuum Ultraviolet Region

The works of ultraviolet photoelectron spectroscopy (UPS) and also of UPS with synchrotron radiation lightsource (UVSOR-UPS) of organic materials have been proceeded to find their quantitative electronic structures.

IV-W-1 Photoelectron Angular Distribution of Thin Films of Copper Phthalocyanine on MoS$_2$ Surfaces: Quantitative Determination of Molecular Orientation

Koji KAMIYA*, Masahiro MOMOSE*, Yoshiya HARADA*, Nobuo UENO*, Takafumi MIYAZAKI, Shinji HASEGAWA, Hiroo INOKUCHI, Satoru NARIOKA***, **Hisao ISHII and Kazuhiko SEKI*** (**Chiba Univ.*, ***Toyama Univ.*, ****Nagoya Univ.*)

[*Mol. Cryst. Liq. Cryst.* **267**, 211 (1995)]

The angle-resolved ultraviolet photoelectron spectra of ultrathin films of copper phthalocyanine (CuPc) on an MoS_2 substrate were measured using synchrotron radiation. The azimuthal angle dependence of the photoelectron intensity was analyzed using independent-atomic-center approximation combined with molecular orbital calculation. The results indicate that CuPc molecules lie flat on the substrate and that the film grows epitaxially with respect to the three equivalent directions of the MoS_2 surface.

IV-W-2 Angle-resolved Photoemission from Oriented Thin Films of Naphthacene: Comparison with Theoretical Spectra

Shinji HASEGAWA, Hiroo INOKUCHI, Kazuhiko SEKI *(Nagoya Univ.)* **and Nobuo UENO** *(Chiba Univ.)*

[*J. Electron. Spectr. Relat. Phenom.* **78**, 391 (1996)]

The comparison was made between the measured and calculated take-off angle dependencies of the valence-band photoelectron spectra for the thin films of naphthacene on HOPG graphite. A good agreement was obtained between them, and the molecular orientation in the thin films was estimated. In the present calculation, the single-scattering of the outgoing photoelectrons was taken into account. The calculation of the full valence-band spectra is the first example to the organic thin films.

IV-W-3 Angle-resolved UPS of Ultrathin Films of Functional Organic Molecules with Synchrotron Radiation: Determination of Molecular Orientation by Quantitative Analysis of Photoelectron Angular Distribution

Nobuo UENO *(Chiba Univ.)*

[*J. Electron. Spectr. Relat. Phenom.* **78**, 345 (1996)]

This paper describes the determination of the molecular orientation of functional organic molecules in their ultrathin films deposited on crystal surfaces by the quantitative analysis of photoelectron angular distribution observed with synchrotron radiation. The examples of the results are presented for phthalocyanine and bis(1,2,5-thiadiazolo)-p-quinobis(1,3-dithiole), a new type of organic semiconductor. Further, the first theoretical simulation of the valence-band spectrum is also shown for oriented thin films of naphthacene, a conventional organic semiconductor. These analyses were based on the independent-atomic-center approximation (IAC) and single scattering theory (SS) combined with molecular orbital (MO) calculation. It is shown that even the simple IAC/MO model can simulate the photoelectron angular distribution very well for a π band at near flat-lie orientation of planar molecules. Further we found that the SS/MO calculations can give the full valence band spectra of large organic molecules, which are in excellent agreement with observed ones.

IV-X Electrical Conduction and its Related Properties of Organic Solids

Two major categories of organic solids are known to offer the prospect of good electrical conduction. The first group comprises single-component materials; typical examples are polycyclic aromatic compounds and also phthalocyanines. The second group consists of charge-transfer complexes such as the perylene-bromine complexes (donor-acceptor complexes). After the accumulation of large number of works on those charge-transfer complexes, their conductivity ranges from semiconductivity to superconductivity.

To expand the research field of molecular conductors, we always consider to introduce a new category. Recently, with the introduction of gaseous elements such as hydrogen and nitrogen to the charge-transfer complexes, we are finding the third category to produce a new type of molecular conductors.

In this section, therefore, we present the works on the electronic properties of single component organic semiconductors, charge-transfer complexes and also three components organic superconductor based on C_{60}.

IV-X-1 Novel Organic Semiconductor BTQBT with High Conductivity and High Mobility

Hiroo INOKUCHI and Kenichi IMAEDA

[*Acta Physica Polonica A*, **88**, 1161 (1995)]

We have found a novel organic semiconductor, BTQBT, with a high electrical conductivity of about 10^{-3} Scm^{-1} and a high Hall mobility of about 3 $cm^2V^{-1}s^{-1}$ at room temperature. We have also succeeded in measuring the temperature dependence of Hall mobility. It varies with temperature as $T^{-1.6}$, which agrees with the theoretical $T^{-1.5}$ dependence for the mobility determined by lattice scattering. The characteristic transport property of BTQBT results from strong intermolecular interactions in the crystal, which is convinced by the energy dispersion with a bandwidth of about 0.5 eV from the theoretical and experimental band structures.

IV-X-2 Molecular Metals Based on Nonplanar Donor BEDT-ATD: Appearance of Metal-Insulator Transition by Anion or Solvent Replacement

Kenichi IMAEDA, Jonas KRÖBER, Chikako NAKANO, Masaaki TOMURA, Shoji TANAKA, Yoshiro YAMASHITA, Hayao KOBAYASHI, Hiroo INOKUCHI and Akiko KOBAYASHI *(Univ. of Tokyo)*

[*Mol. Cryst. Liq. Cryst.*, in press]

We have prepared the cation radical salts based on a nonplanar donor 4,11-bis(4',5'-ethylenedithio-1',3'-dithiole-2'-ylidene)-4,11-dihydroanthra[2,3-c][1,2,5] thiadiazole (BEDT-ATD), $(BEDT\text{-}ATD)_2X(Solvent)$ ($X=PF_6$, BF_4; Solvent=THF, DHF). The band structure of a stable organic metal $(BEDT\text{-}ATD)_2PF_6(THF)$ is presented. The replacement of an anion or a solvent molecule has induced a metal-insulator transition at 200 K and 150 K for (BEDT-

ATD)$_2$BF$_4$(THF) and (BEDT-ATD)$_2$PF$_6$(DHF), respectively, as shown in the thermoelectric power measurement (Figure 1).

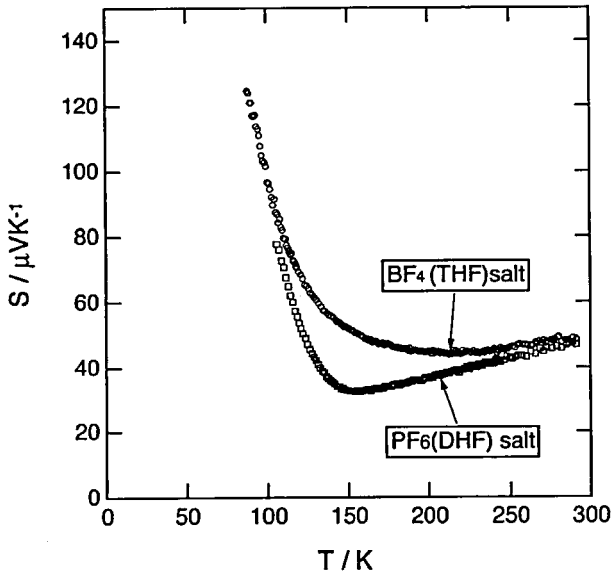


Figure 1. Temperature dependence of the thermoelectric power of (BEDT-ATD)$_2$BF$_4$(THF) and (BEDT-ATD)$_2$PF$_6$(DHF).

IV-X-3 Superconductivity in NaH Intercalated C_{60}

Kenichi IMAEDA, Jonas KRÖBER, Hiroo INOKUCHI, Yukako YONEHARA* and Kenji ICHIMURA*
*(*Kumamoto Univ.)*

[*Solid State Commun.*, **99**, 479 (1996)]

We have found a new superconducting (SC) phase with the nominal composition $(NaH)_4C_{60}$, which was prepared by direct intercalation of sodium hydride (NaH) in C_{60}. In a SQUID magnetization measurement, the SC transition temperature was found to be 15 K, as shown in Figure 1. The SC volume fraction at 2 K was estimated to be 65 %. The large value of the volume fraction suggests the creation of a single phase. This was confirmed by the powder X-ray profile showing a single f.c.c. phase with a lattice constant a=14.356(3) Å. Hydrogen in the SC sample was detected by thermal desorption spectroscopy and seems to exist as fractionally charged hydride ions.

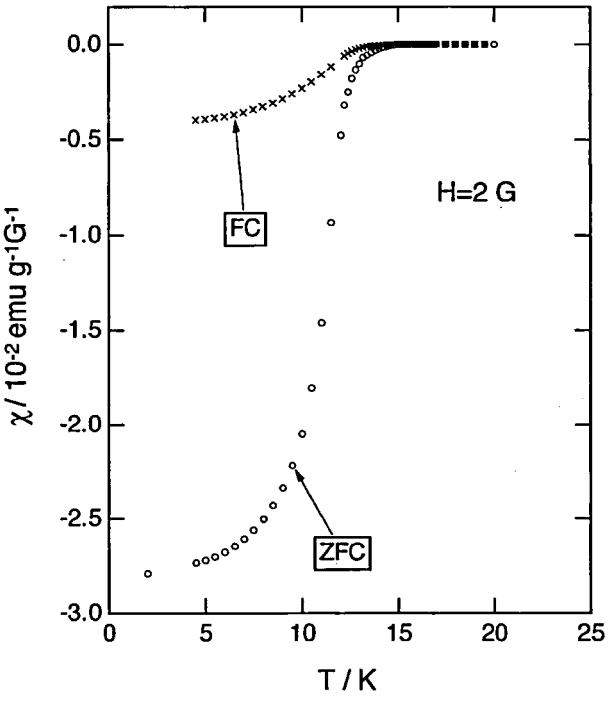


Figure 1. Temperature dependence of the magnetic susceptibility for zero-field cooling (ZFC) and field cooling (FC) runs under a magnetic field of 2 G for the nominal $(NaH)_4C_{60}$ sample.

RESEARCH ACTIVITIES V
Department of Applied Molecular Science

V-A Highly Oxidized Iron Porphyrin and Nonheme Model Complexes

As models for monooxygenases, peroxidases, and heme oxygenases, a series of two electron oxidized iron porphyrin complexes have been prepared. Among them, peroxo-ferric porphyrins and acylperoxo-ferric porphyrins are key intermediates for the catalytic cycles of cytochrome P-450 and heme oxygenase. The major efforts have been concentrated on the elucidation of enzymic oxygen activation mechanisms.

V-A-1 Preparation, Characterization, and Reactivities of O=Fe^{V} Porphyrin Complexes

Tatsuya MURAKAMI,* Isao MORISHIMA *(*Kyoto Univ.)* **and Yoshihito WATANABE**

A new type of high-valent oxo-iron porphyrin, oxo-iron(V) porphyrin (**3b**), has been prepared by the reaction of Fe^{III}TDCPP (**1b**) [TDCPP: 5,10,15,20-tetrakis(2,6-dichlorophenyl)porphyrin] with *p*-nitroperbenzoic acid (*p*NPBA) or pentafluoroiodosylbenzene (F_5-PhIO) in dichloromethane at -90°C *in the presence of methanol*. The UV-vis spectrum of **3b** (λ_{max} at 418 and around 550 nm) is similar to that of O=Fe^{IV}TDCPP (**4b**, λ_{max} 419, 543 nm). However, titration of **3b** by iodide ion indicates the oxidation state of **3b** being two-electron oxidized from the ferric state. Further, **3b** catalyzes epoxidation of olefins such as styrene even at -90°C at the rate constant of 0.11 $M^{-1}s^{-1}$. While UV-vis spectrum of **3b** is completely different from that for the corresponding oxo-iron(IV) porphyrin π-cation radical (**2b**), possible formulation of **3b** as _-cation radical is readily ruled out by deuterium NMR observation. EPR spectrum (g = 4.33, 3.69, 1.99 at 4.2 K) and solution magnetic susceptibility (μ_{eff} = 4.0 ± 0.2 μ_B) of **3b** indicate that **3b** possesses three unpaired electrons. These results indicate the formal description of **3b** to be an oxo-iron(V) porphyrin complex with high spin configuration. The same oxidation of **1b** *in the absence of methanol* gave **2b**. We attribute the ligation of methanol to cause the destabilization of iron d orbitals and it eventually turns upside-down the energy level between the iron d_{xz}, d_{yz} orbitals and porphyrin HOMO orbital (a_{2u}) since the a_{2u} orbital is stabilized by the introduction of electron-withdrawing groups on the porphyrin ring. More importantly, preparation of both **2b** and **3b** allowed us to examine roles of porphyrin π-cation radical on the reactivities.

V-A-2 New Oxidation Reaction of Iron Porphyrin Complex Related to Heme Catabolism

Tatsuya MURAKAMI *(Kyoto Univ.)*, **Isao MORISHIMA** *(Kyoto Univ.)* **and Yoshihito WATANABE**

Heme degradation to biliverdin is carried out by heme oxygenase (HO) under O_2-NADPH-cytochrome P-450 reductase system. It is widely believed that O_2 binding and activation at the heme iron are followed by hydroxylation to form α-hydroxyheme. Further oxidation affords biliverdin IXα through verdoheme with simultaneous elimination of CO derived from α-*meso*-carbon. In order to examine the initial step of heme oxygenase, we have prepared a methylene chloride solution of Fe^{III}BMB*p*CPP-(trifluoroacetate) [**1**, BMB*p*CPP: 5,15-bis(mesityl)-10,20-bis(*p*-chlorophenyl)porphyrin] containing 4 equiv of trifluoroacetic acid in UV-cuvette at -70°C. Reaction of **1** with 1.5 equiv of *p*-nitroperbenzoic acid (*p*NPBA) gave an oxidized complex (**2**). Two intense band in near-IR region for **2** are characteristic of isoporphyrin complexes. The EPR spectrum of **2** exhibits a typical rhombic iron(III) high spin spectrum with g values at 6.18, 5.68, and 1.98, though the spectrum is different from that of the parent iron(III) porphyrin complex (**1**). Different values between g_x and g_y clearly suggest the decrease in symmetry because of the attack of chemical species to the porphyrin ring. From these results, we conclude **2** to be an iron(III) isoporphyrin high spin complex. According to these observations, the following reaction mechanism is proposed.

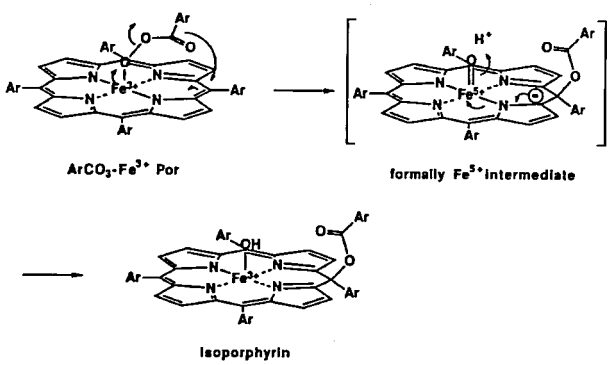
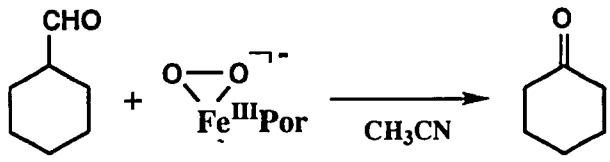


Figure1. A Proposed mechanism for the formation of isoporphyrin

V-A-3 New Carbon-Carbon Bond Cleavage Reactions of Aldehydes by Peroxo(porphinato) iron(III) Complexes

Senji WADA, Yoshio GOTO *(Kyoto Univ., IMS),* **Yoshihito WATANABE and Isao MORISHIMA** *(Kyoto Univ.)*

A peroxo ferric heme complex has been postulated as an intermediate in the catalytic oxygen activation cycle of P-450. At the same time, the direct reactions of the ferric-peroxo species with substrates have been proposed for placental aromatase and NO synthase. Despite the importance of these enzymatic reactions, reactivities of peroxo(porphinato)iron(III) complexes have not been elucidated in detail, though the peroxo complexes have been shown to exhibit nucleophilic character. In this communication, we have investigated reactions of peroxo (porphinato)iron(III) complexes and various aldehydes and found the formation of carbonyl compounds via C-C bond cleavage between the carbonyl carbon and α-carbon of aldehydes. That the oxidation of aldehydes by O=Fe(IV) porphyrin π-cation radicals affords the corresponding carboxylic acids indicates the possible involvement of the peroxo complexes in the aromatase reactions.



V-A-4 A Novel Hydroperoxo-Iron (III) Complex: Synthetic Model for Mono-Nuclear Nonheme Enzymes

Senji WADA, Yoshihito WATANABE, Masakazu IWASE,* Koichiro JITSUKAWA,* Hideki MASUDA* and Hisahiko EINAGA* *(*Nagoya Inst. Tech.)*

Peroxoiron(III) complexes are considered as an intermediates in the oxygen activation processes by nonheme iron centers in biology. As a model complex of the mononuclear nonheme prosthetic group, we have prepared $[Fe^{III}(TNPA)(OH)(PhCO)](ClO_4)$ (**1**, TNPA = tris(6-neopentylamino-2-pyridylmethyl)amine) and determined the crystal structure by X-ray analysis. The reaction of **1** with hydrogen peroxide is under investigation.

V-B Molecular Mechanisms of Oxygen Activation by Heme Enzymes

In order to understand the molecular mechanisms of oxygen activation by a variety of heme enzymes, we have studied roles of amino acid residues around heme vicinities of peroxidases and cytochrome P-450 by alteration of specific amino acid residues to desired ones. The current goal of this project is the preparation of artificial peroxidases and monooxygenases by employing myoglobin as a starting protein.

V-B-1 Preparation and Reactions of Myoglobin Mutants Bearing Both Proximal Cysteine Ligand and Hydrophobic Distal Cavity

Toshitaka MATSUI,* Shingo NAGANO,* Koichiro ISHIMORI* *(*Kyoto Univ.),* **Yoshihito WATANABE and Isao MORISHIMA** *(Kyoto Univ. and IMS)*

[*Biochemistry* in press]

We have reported that H93C human myoglobin (Mb), in which proximal histidine (His93, F8) was replaced by cysteine, gave nearly identical spectroscopic features of P-450.[1] More importantly, the thiolate ligand enhanced its oxygenation activities when H_2O_2 was employed as an oxidant due to the exclusive encouragement of heterolytic O-O bond cleavage of peroxides. However, possible participation of the distal histidine (H64, E7) of H93C Mb in the heterolysis could explain the results, while we have attributed enhanced heterolysis of the O-O bond to the electron donation from the thiolate ligation. In addition, the racemic product formation in the H93C Mb catalyzed oxidation implied that its small distal cavity could prevent substrates from accessing to the heme and the reactions proceed other than P-450 type mechanism (ferryl oxygen transfer). In order to improve accessibility of substrates and to clarify whether the distal histidine is involved in the O-O bond cleavage step, the distal histidine of H93C Mb is replaced by smaller and non-polar residues, glycine (H64G/H93C Mb) and valine (H64V/H93C Mb), by site-directed mutagenesis. Various spectroscopic studies on these double-mutated Mbs revealed the ligation of cysteine to the ferric heme as a thiolate form. In the reaction with cumene hydroperoxide, the anionic nature of the proximal cysteine in the H64G/H93C and H64V/H93C Mbs was found to similarly encourage the heterolytic O-O bond cleavage as observed for H93C Mb. The results clearly demonstrate that the distal histidine of H93C Mb is not involved in the O-O bond cleavage step, and are in good agreement with the role of thiolate ligation for the formation of reactive intermediate, equivalent to compound I, in the catalytic cycle of P-450 reactions. In the oxygenation of methyl *p*-tolyl sulfide, the ratios of ferryl oxygen transfer were increased in H64G/H93C Mb (58%) and H64V/H93C Mb (78%) as compared to H93C Mb (53%). While the increased ratios of ferryl oxygen transfer imply the active site of H64G/H93C and H64V/H93C Mbs being more accessible for substrates, oxygenation of methyl *p*-tolyl sulfide by the ferric mutant Mbs/H_2O_2 system was much slower than that by H93C Mb. The small activities of these mutant Mbs are attributed to large K_m values for H_2O_2 probably due to loss of general base catalyst (His64) in their distal cavity.

Reference

1) S. Adachi, S. Nagano, K. Ishimori, Y. Watanabe, I. Morishima, T. Egawa, T. Kitagawa, and R. Makino, *Biochemistry* **32**, 241-252 (1993).

V-B-2 The Catalytic Roles of the Distal Site Asparagine-Histidine Couple in Peroxidases

Shingo NAGANO,* Motomasa TANAKA,* Koichiro ISHIMORI,* Yoshihito WATANABE and Isao MORISHIMA* *(*Kyoto Univ.)*

[*Biochemistry* in press]

There are highly conserved hydrogen bonds between the distal His and adjacent Asn in many peroxidases. Although the crystal structure of horseradish peroxidase C (HRP) is not available, comparison of the amino acid sequence with cytochrome *c* peroxidase indicates that Asn70 is making the hydrogen bond with the distal His in the active site of HRP. To investigate catalytic roles of the hydrogen bond, Asn70 in HRP was replaced with Val (N70V) or Asp (N70D). Though UV-vis, CD, and ^{1}H-NMR spectra of native (plant enzyme), wild-type (recombinant enzyme), and mutant HRPs suggest that the active site and secondary structure are vary similar even after the mutation, the mutants exhibit low *V*max values for the hydroquinone oxidation (native: 281, wild-type: 283, N70V: 18, N70D: 33 μM·min^{-1}). The rates of compound I formation were decreased to less than 10% of the native enzyme. The reduction rates of compounds I and II by guaiacol also were reduced to less than 10% of the native enzyme. Substituent effects of various phenol derivatives on the reduction of compounds I of native, wild-type, and the mutants were examined. Large negative Hammett ρ-values ($\rho_{N70V:\,fast}$ = -4.0, $\rho_{N70V:\,slow}$ = -3.6, ρ_{N70D} = -3.8, ρ_{native} = -6.9, $\rho_{wild\text{-}type}$ = -6.8) are the indication of electron transfer being the rate determining step in the phenol oxidation. However, these results also indicate that the participation of the deprotonation step in compound I reduction process. The proton abstraction from phenol must be harder for the mutants due to the decrease of basicity of the distal His upon mutation. Contrary to phenol oxidation, ABTS (2,2'-azino-bis-(3-ethylbenzothiazoline-6-sulfonic acid)) oxidation activity was substantially increased by the mutations (native: 73, wild-type: 71, N70V: 217, N70D: 234 μM·sec^{-1}). The redox potentials of N70V and N70D compounds II are 957 and 970 mV (vs. NHE), which are 95 and 108 mV higher than that of native compound II (862 mV), respectively. Therefore, the high ABTS oxidation activities of mutants are attributed to these high redox potentials of compound II.

V-B-3 Conversion of Myoglobin into a Highly Stereospecific Peroxygenase by the L29H/H64L Mutation

Shin-ichi OZAKI, Toshitaka MATSUI and Yoshihito WATANABE

[*J. Am. Chem. Soc.* in press]

The comparison of the X-ray structures of cytochrome *c* peroxidase (*Cc*P) and sperm whale Myoglobin (Mb) suggests that the Leu-29 → His and His-64 → Leu double mutation of Mb would create a heme crevice similar to the active site structure of *Cc*P, and enhance hydrogen peroxide supported monooxygenation activity. We report here that L29H/H64L Mb significantly increases the rate for the oxidation of both thioanisole and styrene, and more importantly the enantioselectivity. The 22-fold rate increase vs. wild type Mb and 97% incorporation of ^{18}O from $H_2{}^{18}O_2$ into the sulfoxide with 97% ee for *R* isomer have been observed for thioanisole oxidation by L29H/H64L Mb. Regardless of the size and electronic properties for *para*-substituents of thioanisle, the L29H/H64L mutant oxidizes sulfides faster than the wild type with high enantioselectivity. However, for sulfoxidation by both the wild type and L29H/H64L mutants, an electron withdrawing group at the *para* position of thioanisole drops the rate, and the electron donating group raises it. A great improvement of enantioselectivity from 9% to 80% is seen for styrene epoxidation by L29H/H64L Mb, and 92% of oxygen atom of epoxide formed is derived from peroxide. The present results clearly indicate that His-29 in the mutant directly plays an important role to improve the ferryl oxygen transfer activity.

V-C Transition Metal Sulfide Clusters

M-S-M' (M and M' = transition metal atoms) groups in high-nuclearity heterometallic sulfide clusters play important roles in the biological systems and in the industrially catalytic processes. We have studied (i) a rational synthesis of heterometallic sulfide clusters with M-S-M' (M and M' = Rh, W, and Cu) groups, (ii) structures and bonding of the M-S-M' groups determined by X-ray crystallographic analysis and IR spectroscopy, and (iii) reactivity of the M-S-M' groups unique to higher-nuclearity heterometallic sulfide clusters toward H_2O and H_2S.

V-C-1 Structures, Bonding, and Reactivity of M-S-M' (M and M' = Rh, W, and Cu) Groups in Higher-Nuclearity Heterometallic Sulfide Clusters

Seiji OGO, Takayoshi SUZUKI *(Osaka Univ.)*, **Yoshiki OZAWA** *(Himeji Inst. Tech.)* **and Kiyoshi ISOBE** *(Osaka City Univ.)*

[*Inorg. Chem.* in press]

A branched-type octanuclear sulfide cluster [{Cp*RhP(OEt)$_3$(μ-WS$_4$)(CuCl)Cu}$_2$(μ-Cl)$_2$] (**4**, Cp* = η^5-C$_5$Me$_5$) was prepared stepwise by the following sequence: [Cp*RhP(OEt)$_3$Cl$_2$] (**1**, mononuclear) → [Cp*RhP(OEt)$_3$WS$_4$] (**2**, dinuclear) → [Cp*RhP(OEt)$_3$(μ-WS$_4$)CuCl] (**3**, linear-type trinuclear) → **4** by a systematic building-block method. A bridging sulfide ligand in the W-S-Cu group of **4** reacts with a water-saturated CH_2Cl_2 solution to convert the terminal O atom of [{Cp*RhP(OEt)$_3$(μ-WOS$_3$)(CuCl)Cu}$_2$(μ-Cl)$_2$] (**5**, linked incomplete cubane-type octanuclear) with a drastic structural change in the cluster framework. The transformation reaction of **4** to **5** includes the first example of the conversion of the bridging S atom in the M-S-M' group into the terminal O atom without releasing the metal atoms, and this reaction is peculiar to the higher-nuclearity heterometallic sulfide cluster **4**. Clusters **4**, **5**, and **6** ([Cp*RhP(OEt)$_3$(μ-WOS$_3$)CuCl], butterfly-type trinuclear) react with H_2S in CH_2Cl_2 to give **3** as a major product. The formation of **3** in these reactions are based on the reactivity of M-S-Cu groups in the sulfide clusters toward H_2S: the (μ_3-S)-Cu bonds are easily broken by H_2S, but not the (μ_2-S)-Cu ones.

V-D New High T_C Molecular Magnets

Construction of molecular based magnetic materials which have well-defined one-, two- or three-dimensional structure is a scientific subject of increasing interest. Heterospin systems consisting of transition metal ions and organic free radicals as ligands constitute one of the mainstreams of such studies. Several of these materials have been established to have finite critical temperatures for undergoing transition to ferro- and/or ferrimagnets. The ligands employed are often organic monoradicals that have two ligating sites, *e. g.*, semiquinones and nitronylnitroxides.

We have introduced a new strategy of employing π-conjugated polynitroxides as ligands in which the spins interact ferromagnetically ($J_{intra} > 0$). The dimensionality of the complex and the sign and magnitude of the exchange coupling between the neighboring spins may be readily tuned by this strategy.

V-D-1 Assemblage of the Electron Spins of the Organic Trinitroxide Radical with a Quartet Ground State by Means of Complexation with Paramagnetic Transition Metal Complexes. A Molecule-Based Magnet with Three-Dimensional Structure and High T_C of 46 K

Katsuya INOUE, Takashi HAYAMIZU,* Hiizu IWAMURA,* Daisuke HASHIZUME and Yuji OHASHI**** *(*Institute for Fundamental Research of Organic Chemistry, Kyushu Univ., **Tokyo Institute of Technology)*

[*J. Am. Chem. Soc.*, **118**, 1803(1996)]

Bis{3-*tert*-butyl-5-(*N*-oxy-*tert*-butylamino) phenyl} nitroxide, a stable triradical with a quartet ground state, formed with bis(hexafluoroacetylacetonato) manganese(II) a 2:3 complex. An X-ray crystal structure analysis of the complex revealed the formation of a parallel crosses-shaped three-dimensional polymeric network in which a linear chain made by ligation of the two terminal nitroxide of the ligand with two different manganese and lying in a *b*/*c* diagonal direction is linked through the middle nitroxide *via* a third manganese to a second linear chain extending in a *b*/-*c* diagonal direction. (Figure 1) The three nitroxide radical centers which are mutually coupled ferromagnetically within the organic radical molecule are coupled antiferromagnetically with the manganese(II) ions. The temperature dependence of the magnetization revealed that the heterospin system behaves as a magnet below 46 K.

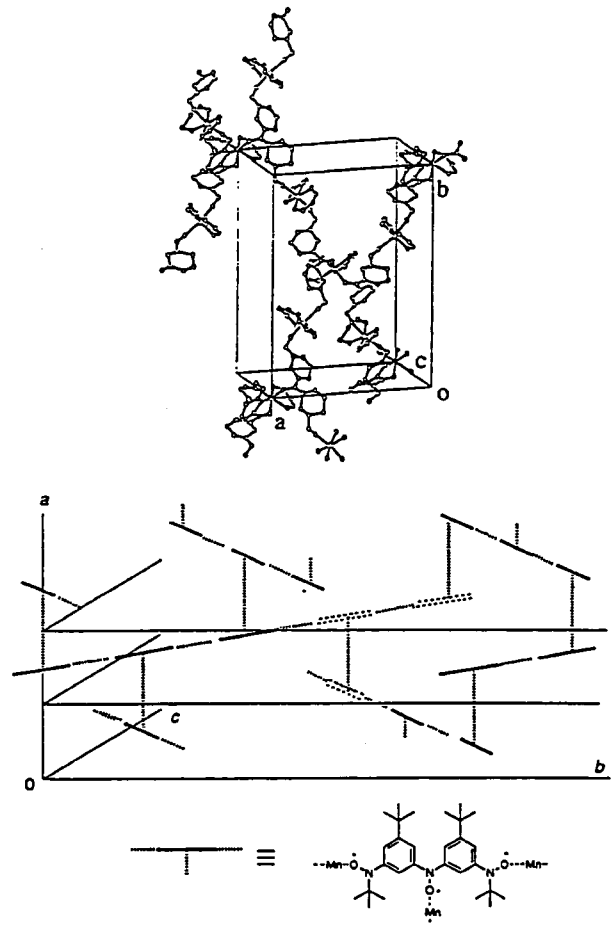


Figure 1. Packing of the polymer complex [{Mn(hfac)$_2$}$_3$ •**1**$_2$] (a. top) projected along [0 0 1] (the CF_3 and *tert*-butyl gloups are not shown for clarity) and (b. bottom) viewed schematically to show the 3-D parallel crosses motif.

V-D-2 Magnetic Characterization of One-Dimensional Molecule-Based Metamagnet Made of Mn(hfac)$_2$ and 1,3-Bis-*N*-oxy-*tert*-butylamino)benzene

Katsuya INOUE, Satoshi MAEKAWA *(Kitasato Univ.)* **and Hiizu IWAMURA** *(Institute for Fundamental Research in Organic Chemistry, Kyushu Univ.)*

[*Mol.Cryst.Liq.Cryst.*, in press]

Manganese bis(hexafluoroacetylacetonate), Mn(hfac)$_2$, reacts with 1,3-bis-(*N*-oxy-*tert*-butylamino) benzene, **1**, to give a 1:1 polymeric complex of formula [Mn(hfac)$_2$•**1**]$_n$. An X-ray crystal structure analysis reveals that the manganese(II) ion and the molecule of **1** makes one-dimensional chains by ligation of the latter serving as a bis(monodentate) ligand to the former. (Fig-

ure 1) A crystalline sample of the complex undergoes transition to a metamagnet at 5.5 K. In the ordered phase, it exhibits a large uniaxial magnetic anisotropy with the uniaxial an-isotropy constant, K_{u1}, of 8.3 × 10^6 J m^{-3} by single crystal magnetic measurements.

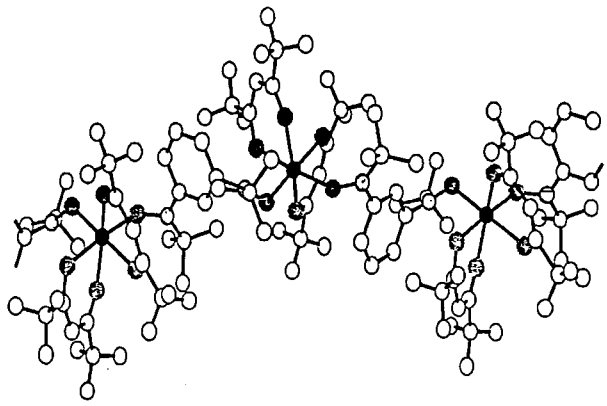


Figure 1. View of a 1-D chain formed by bisnitroxide **1** and Mn(II)$(hfac)_2$.

V-E Synthesis of New High Spin Hydrocarbons

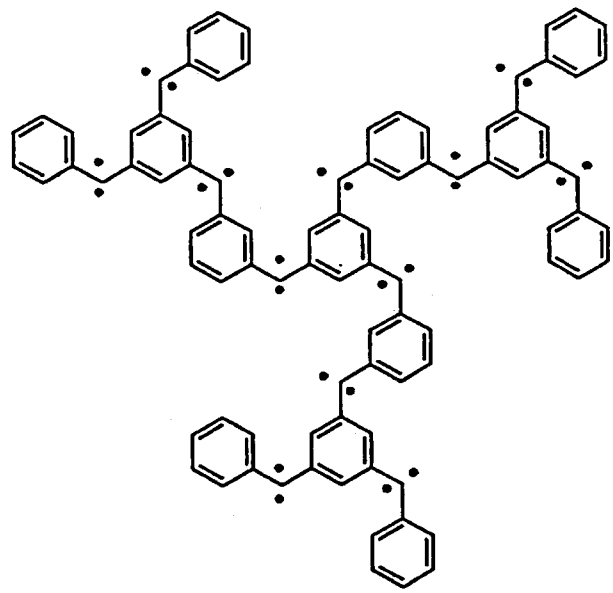
The synthesis and characterization of organic molecules with very high-spin ground states is currently of great interest. In order to make the high spin oragnic molecules, there are two very important factors. First, the spin concentration of the polyradicals must be high. Second, the spin density or the spin polarization on the main chain must be large. It is very difficult to satisfy both the conditions at the same time. We paid attention to the second factor and have studied the high spin molecules having spin centers in the π-conjugated main chain. It has been established that one dimensional polycarbene systems. In order to realize the long-range order at finite temperature, increase of the dimension of the aligned spins is highly necessary. We have now introduced a branched-chain pseudo-two-dimensional structure to make very high-spin hydrocarbones.

V-E-1 Toward Dendritic Two-Dimensional Polycarbenes: Synthesis of 'Starburst'-Type Nona- and Dodecadiazo Compounds and Magnetic Study of Their Phtoproducts

Kenji MATSUDA,* Nobuo NAKAMURA *(Housei Univ.)* **, Katsuya INOUE, Noboru KOGA** *(Kyushu Univ.)* **and Hiizu IWAMURA*** *(*Institute for Fundamental Research of Organic Chemistry, Kyushu Univ.)*

[*Bull. Chem. Soc. Jpn.*, **69**, 1483 (1996)]

'Starburst'-type nona- and dodecadiazo compounds were designed and synthsized by using the cycrotrimerization of ethynyl ketones as a key step. The diazo compounds were phtolyzed in MTHF solid solution at cryogenic temperatures and analyzed by means of Faraday magnetometry and ESR spectroscopy. From the field dependence of the magnetization, the nonacarbene, the phtoproduct of nonadiazo compound, was evidenced to have a nonadecet (S = 9) ground state. This spin multiplicity is the highest value ever reported for purely organic materials. On the other hand, the spin multiplicity was low and antiferromagnetic interaction operated in the phtoproduct of the dodecadiazo compound. This result was interpreted not in terms of the intermolecular antiferromagnetic interaction but of the intramolecular cross-linking between the carbene centers. In the 'Starburst'-type polycarbenes with extended branching, the reactive carbene centers can become mutually too close to each other in space and so appear to recombine readily. This study showed one of the limitations of the extension of the carbene network by way of flexible 'Starburst'-type structures.



Scheme

V-F Pressure Effect on Molecular Magnetism

The study of the pressure effect on molecular magnetism might be important and useful to clarify the nature of magnetic interactions. We have studied the magnetic properties of some organic radicals under pressure and found two examples of the suppression of structural changes by applied pressure.

V-F-1 Pressure Effect on Organic Radicals

Yuko HOSOKOSHI, Masafumi TAMURA *(Toho Univ.)* **and Minoru KINOSHITA** *(Sci. Univ. of Tokyo in Yamaguchi)*

[*Mol.Cryst.Liq.Cryst.*, in press]

It has been found that the phase transition to a diamagnetic state of pure galvinoxyl can be suppressed by applied pressure. As is shown in Figure 1, under 7 kbar, the transition is sufficiently suppressed and the ferromagnetic interactions are preserved down to low temperature. Judging from the pressure dependence of the magnetic properties, we have concluded that the pressurization stabilizes the super-cooled high-temperature phase, *i. e.* pressurization enhances the activation energy of the transition and the thermal equilibrium state cannot be reached in an experimental time scale. The temperature dependence of the paramagnetic susceptibility under 7 kbar obeys the ferromagnetic chain model with $2J/k_B$=25 K. The magnetic order cannot be observed above 1.8 K. As is typically demonstrated by the discrepancy from the linear temperature dependence of χ_p^{-1} below 50 K, one-dimensionality seems to prevent the magnetic ordered state. The extrapolation of χ_p^{-1} to the low temperature region suggests the possibility of the magnetic order below 0.5 K, if it occurs.

The room-temperature crystal structure of F_5PNN involves a uniform chain, while the low-temperature magnetism can be interpreted by the alternating antiferromagnetic chain model with $2J/k_B$=-5.6 K and α=0.4. We found that under 5 kbar, the low-temperature magnetism obeys the uniform antiferromagnetic chain model with $2J/k_B$=-5.6 K, which is consistent with the room-temperature crystal structure. (Figure 2)

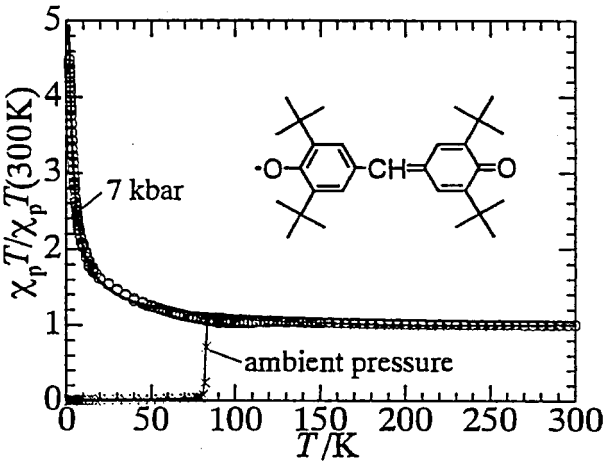


Figure 1. Temperature dependence of $\chi_p T$ of galvinoxyl under 7 kbar compared with that at ambient pressure. Solid curve for the data under 7 kbar is the fit by the ferromagnetic chain model with $2J/k_B$=25 K.

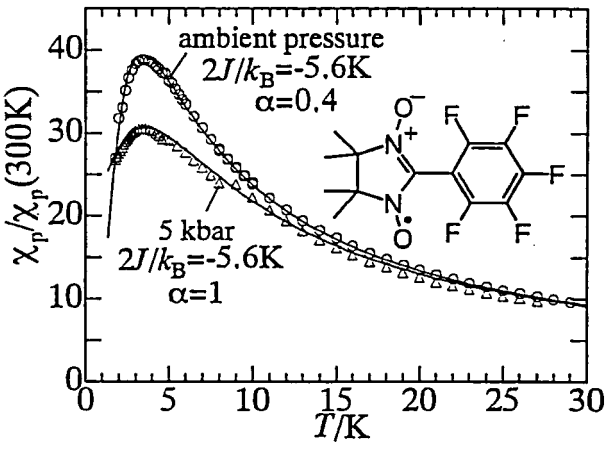


Figure 2. Temperature dependence of χ_p of F_5PNN under 5 kbar compared with that at ambient pressure. Solid curves represent the fitting results on the basis of the antiferromagnetic alternating chain model. When α=1, the system is a uniform chain.

V-G Study of Low-temperature Magnetism of Organic Radicals

One of the remarkable features of organic radicals, compared with transition-metal compounds, is isotropic nature of electron spins as a result of weak spin-orbit coupling in a molecule. Organic radicals are thus suitable for the study of Heisenberg spin systems. We have studied the ground state of some organic radicals using the combination of low temperature and high magnetic field.

V-G-1 Low-temperature Magnetic Properties of Nitronyl Nitroxides

Mitsue TAKAHASHI,* Yuko HOSOKOSHI, Hiroki NAKANO,* Tsuneaki GOTO,* Minoru TAKAHASHI* *(*ISSP, Univ. of Tokyo)* **and Minoru KINOSHITA** *(Sci. Univ. of Tokyo in Yamaguchi)*

[*Mol.Cryst.Liq.Cryst.*, in press]

Magnetic properties of two nitronyl nitroxide radicals which show nearly isotropic S=1/2 alternating chains are investigated down to 0.5 K and up to 9 T.

For F_5PNN, an energy gap above the singlet ground state was clearly observed. It has been confirmed that this material at low temperature is described by a one-dimensional Heisenberg model with alternating antiferromagnetic interactions, despite a uniform-chain structure at room temperature. Moreover, we have found that the interactions in a chain depends on the applied magnetic fields.

We have found that MeNN is a quasi-one-dimensional system of a ferromagnetic and antiferromagnetic alternating chain with weak interchain interactions. Because of the weak interchain interactions, antiferromagnetic order occurs at 1.3 K. The magnetization process

below 1 K shows similar behaviour to the one for the S=1 system except for the low-field region. (Figure 1) This suggests that, in this temperature region, two S=1/2 spins which are ferromagnetically coupled, behave approximately as an S=1 spin.

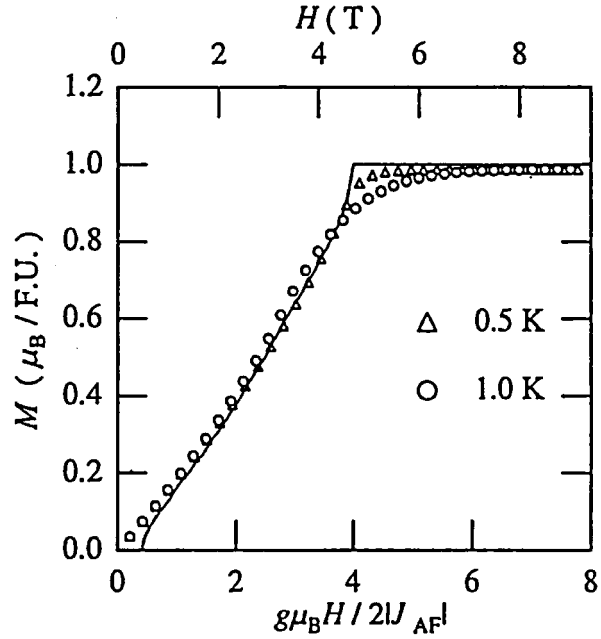


Figure 1. Magnetization curve of MeNN at low temperature as a function of reduced field. The solid curve is normalized and represents an S=1 uniform chain, where $2J_{AF}$ represents the antiferromagnetic interaction in the S=1 chain. Note that J=4J_{AF}. We use g=2.0.

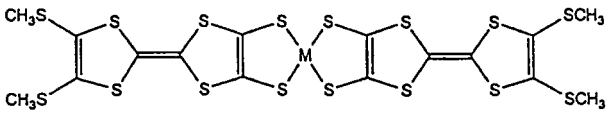
V-H New Charge-Transfer Complexes Exhibiting Novel Magnetic Properties

In 3d transition metals of iron, cobalt and nickel ferromagnetic state can be maintained at extremely high temperature. In contrast, even a highest critical temperature (Tc) of ferromagnetic phase transition is 1.48 K in entirely s/p orbital-based organic ferromagnets, of which the first one has been discovered in a nitronylnitroxide radical crystal and succesively thirteen ones have till now been prepared by using other organic radical crystals and charge-transfer (CT) complexes. In the present study we investigated the synthesis and magnetic properties of new CT complexes with aim at achieving purely organic ferromagnets with high Tc.

V-H-1 Synthesis and Redox Property of Bis(tetrathiafulvalenyldithio)germane

Kazumasa UEDA, Masaru YAMANOHA *(Osaka Pref. Univ.)*, **Toyonari SUGIMOTO** *(Osaka Pref. Univ. and IMS)*, **Akito UGAWA, Kyuya YAKUSHI** *(IMS)* **and Hideo FUJITA** *(Kyoto Univ.)*

New tetrathiafulvalene (TTF) derivatives continue to play an important role as donor molecules in the development of organic conductors and superconductors. We are rather interested in donor molecules such as bis(tetrathiafulvalenyldithio)-methane, -silane and -germane (**1** (M=C, Si, Ge)), where two TTF moieties are arranged perpendicularly by a spiro-bond. In crystals of these donor molecules it is possible that the two perpendicular TTF moieties are two-dimensionally stacked and furthermore ferromagnetic interaction occurs between the perpendicular stacks, giving an unprecedented organic ferromagnetic metal. Now, we succeeded in the synthesis of a germanium compound (**1** (M=Ge)) (a black poweder, mp 126-127 °C) by the reaction of bis (tetramethylammonium) bis(tetrathiafulvalenyldithiolate) zinc complex with an equimolar amount of germanium tetrachloride in DMF at -40 °C. The single crystal suitable for X-ray structure analysis is still not obtained. The redox exhibited two pairs of broad and reversible waves at +0.51 and +0.77 V vs. SCE in benzonitrile at 0°C. These potentials are shifted to a more positive region as compared with those of tetramethylthio-substituted TTF (+0.36 and +0.61 V). The delocalization of an unpaired electron in the radical cation as well as the spin-spin interaction in the dication of **1** (M=Ge) was investigated by ESR.



1 (M = C, Si, Ge)

V-H-2 Ferromagnetic Behavior of a Tetrafluorotetracyanoquinodimethanide Salt at Room Temperature

Toyonari SUGIMOTO *(Osaka Pref. Univ. and IMS)*, **Kazumasa UEDA, Masaya TSUJII** *(Osaka Pref. Univ.)*, **Hideo FUJITA, Nobuyoshi HOSOITO** *(Kyoto Univ.)*, **Nobuko KANEHISA, Yoshiyuki SHIBAMOTO and Yasushi KAI** *(Osaka Univ.)*

[*Chem. Phys. Lett.* **249**, 304-308 (1996)]

Recrystallization of $NMe_4^+ \bullet TCNQF_4^{\bullet -}$ in the presence of $TCNQF_4$ from acetonitrile/ether gave a crystal of $(NMe_4^+ \bullet TCNQF_4^{\bullet -}) \bullet 1/2TCNQF_4$, which very interestingly exhibited ferromagnetism at room temperature. This organic ferromagnet has characteristics of very small saturation monent (1.03×10^{-3} μ_B/molecule) and coercive field (ca. 25 Oe). The origin of this ferromagnetism could be attributed to a unique crystal structure of the radical anion salt: the $TCNQF_4/TCNQF_4^{\bullet -}$ and NMe_4^+ ion layers are alternately stacked and in the $TCNQF_4/TCNQF_4^{\bullet -}$ layer each pair of two $TCNQF_4^{\bullet -}$ molecules is arranged in a completely perpendicular manner to each of one $TCNQF_4$ molecule.

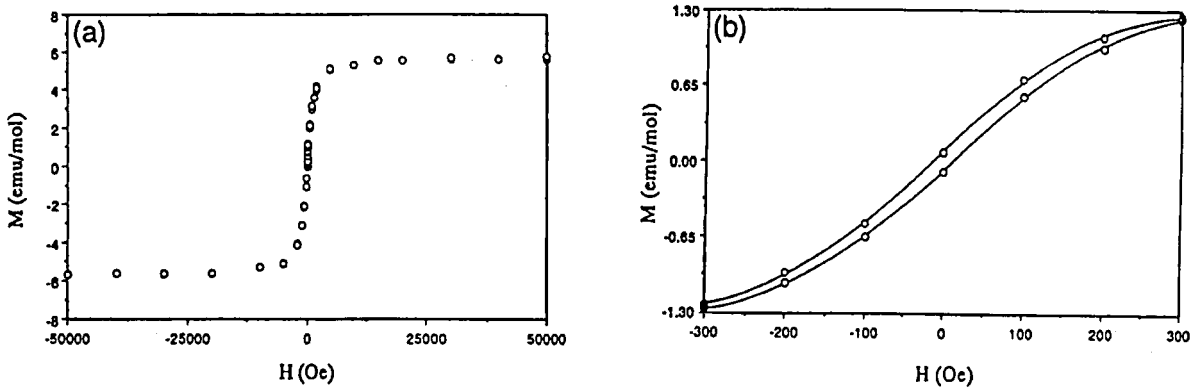


Figure 1. Hysteresis (M versus H) curves of $(NMe_4^+ \bullet TCNQF_4^{\bullet -}) \bullet 1/2TCNQF_4$ at room temperature in the applied field ranges of (a) ±50 kOe and (b) ±300 Oe.

V-H-3 Crystal Structures and Magnetic Properties of Tetrafluorotetracyanoquinodimethanide Salts

Kazumasa UEDA, Hiroshi MORIMOTO *(Osaka Pref. Univ.)*, **Toyonari SUGIMOTO** *(Osaka Pref. Univ. and IMS)*, **Nobuko KANEHISA, Yoshiyuki SHIBAMOTO and Yasushi KAI** *(Osaka Univ.)*

[*Mol. Cryst. Liq. Cryst.* **279**, 123-132 (1996)]

The X-ray structure analyses of tetramethy lammonium and tetraethyl ammonium salts of tetrafluoro tetracyano quino dimethanide ($TCNQF_4^{\bullet -}$) ($NMe_4^+ \bullet TCNQF_4^{\bullet -}$ and $NEt_4^+ \bullet TCNQF_4^{\bullet -}$) were performed. In these crystals the $TCNQF_4^{\bullet -}$ molecules form dimers, which are stacked in a plane-to-plane manner to columns. Recrystallization of $NMe_4^+ \bullet TCNQF_4^{\bullet -}$ in the presence of $TCNQF_4$ or TCNQ gave needle and plate crystals of $(NMe_4^+ \bullet TCNQF_4^{\bullet -}) \bullet 1/2TCNQF_4$ and $(NMe_4^+ \bullet TCNQF_4^{\bullet -}) \bullet 1/2TCNQ$. The needle crystals were not suitable for X-ray structure analysis, while the analysis of plate crystal was successful. The plate crystals are composed of alternating $TCNQF_4$ (or TCNQ)/$TCNQF_4^{\bullet -}$ and NMe_4^+ ion layers, and the $TCNQF_4$ (or TCNQ)/$TCNQF_4^{\bullet -}$ layer adopts a unique packing structure, in which each pair of two $TCNQF_4^{\bullet -}$ molecules is arranged in a completely perpendicular manner to each of one $TCNQF_4$ (or TCNQ) molecule. The similar $TCNQF_4$ (or TCNQ)/$TCNQF_4^{\bullet -}$ mixed salt was not obtained by using $NEt_4^+ \bullet TCNQF_4^{\bullet -}$.

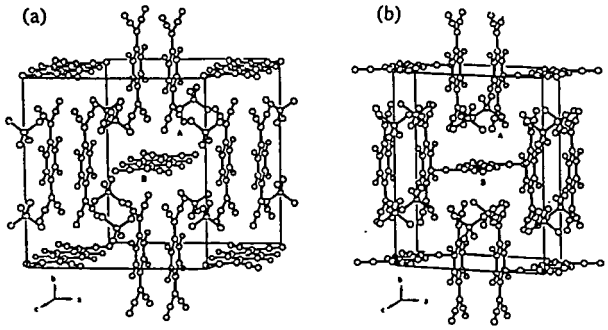


Figure 1. The crystal structures of (a) $(NMe_4^+ \bullet TCNQF_4^{\bullet -}) \cdot 1/2TCNQF_4$ and (b) $(NMe_4^+ \bullet TCNQF_4^{\bullet -}) \bullet 1/2TCNQ$.

V-H-4 Remarkably Strong Antiferromagnetic Interaction through an Intervening Hydrogen Atom in *N*-(*n*-Propyl)pyridinium-substituted Imidazolin-1-oxyl Iodide

Kazumasa UEDA, Masaya TSUJII, Takehito SUGA *(Osaka Pref. Univ.)*, **Toyonari SUGIMOTO** *(Osaka Pref. Univ. and IMS)*, **Nobuko KANEHISA, Yasushi KAI** *(Osaka Univ.)* **and Nobuyoshi HOSOITO** *(Kyoto Univ.)*

[*Chem. Phys. Lett.* **253**, 355-360 (1996)]

For three organic ferromagnets obtained previously it was demonstrated that a hydrogen atom or a methyl group obviously intervenes between ferromagnetically interacting spins. In the course of our success in the synthesis of

the first well-characterized organic ferromagnets based on CT complexes of 2-(4-*N*-alkylpyridinium)-4,4,5,5-tetramethylimidazolin-1-oxyls (**1**(R)$^+$: R = Me, Et, *n*-Pr) with tetrafluorotetracyanoquinodimethanide or hexacyanobutadienide, we have recognized a similar phenomenon in an iodide salt of **1**(*n*-Pr)$^+$ (**1**(*n*-Pr)$^+\cdot$I$^-$), although the spin interaction is antiferromagnetic, but quite strong. In this paper we report on the magnetic properties of the iodide salts of **1**(Me)$^+$ and **1**(Et)$^+$ (**1**(Me)$^+\cdot$I$^-$ and **1**(Et)$^+\cdot$I$^-$) as well as of **1**(*n*-Pr)$^+\cdot$I$^-$, and discuss the origin of spin interaction based on their crystal structures.

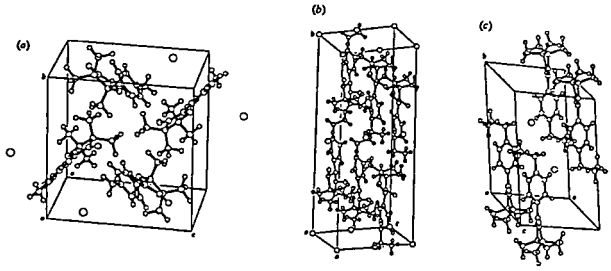


Figure 1. The crystal structures of (a) **1**(Me)$^+\cdot$I$^-$, (b) **1**(Et)$^+\cdot$I$^{-\bullet}$, and (c) **1**(*n*-Pr)$^+$I$^-$.

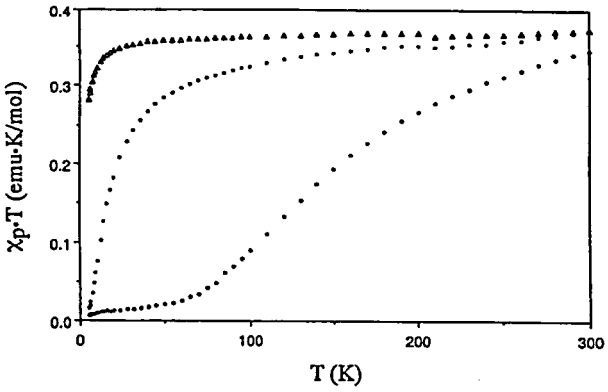


Figure 2. The temperature dependence of χ_p·T for **1**(Me)$^+\cdot$I$^-$ (△), **1**(Et)$^+\cdot$I$^-$ (○), and **1**(*n*-Pr)$^+\cdot$I$^-$ (●).

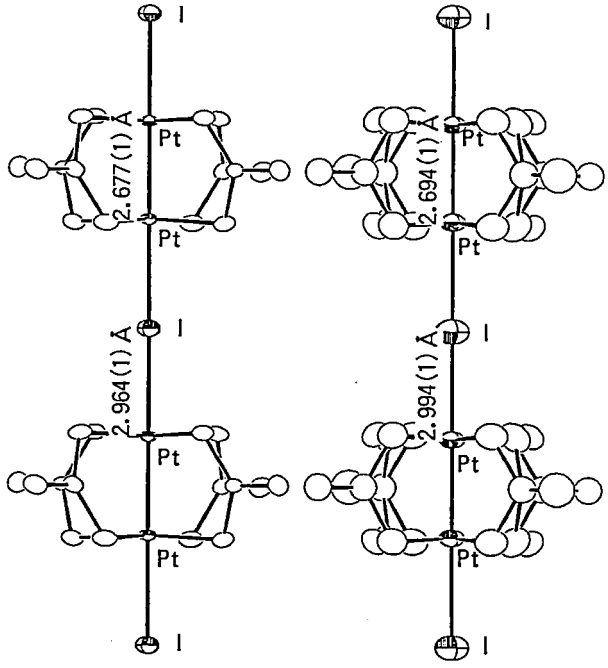
V-I Syntheses, Crystal Structures, and Solid State Properties of Halogen-Bridged Metal Complexes with Linear Chain Structures

Halogen-bridged one-dimensional metal complex consisted from Pt dimer complex, $Pt_2(dta)_4I$ (dta=$CH_3CS_2^-$), is of interest from viewpoint of charge density wave instability, since several electronic states are possible for the many electrons - many atoms system compared to the well-known Pt^{II}-X-Pt^{IV} mixed valence compounds. The electronic conductivity measurement for the single crystal revealed semiconductor → metal → semiconductor transitions at the temperature range 300 – 350K.

V-I-1 X-ray Structural Study of the Phase Transition of Iodo-Bridged One-Dimensional Pt Dimer, $Pt_2(dta)_4I$

K. TORIUMI,[a] M. KIM,[b] Y. OZAWA,[b] K. YASUI,[c] T. MANABE,[c] M.YAMASHITA,[c] H. KITAGAWA,[d] N. ONODERA[d] and T. MITANI[d] *([a]Himeji Inst. Tech. and IMS, [b]Himeji Inst. Tech., [c]Nagoya Univ., [d]JAIST)*

Temperature dependence of the lattice parameters of $Pt_2(dta)_4I$ was measured by single crystal X-ray diffraction method. Anomalous negative hysteresis for the cell volume was observed in the temperature range -20 – 100°C. In order to reveal the transition phenomena, single crystal structure analyses were made at the temperatures below and above the phase transition (-89°C and 130°C). It was revealed that the first order phase transition was occurred from the low-temperature phase with space group C2/c to the high-temperature phase of A2/m, of which the cell volume is half the low-temperature one. Some remarkable structural changes are elucidated by comparison of both the crystal structures. The helical arrangement of the four dta ligand planes around the central Pt–Pt axis is ordered in the low-temperature phase, but it is disordered in the high-temperature phase (Figure 1). It could not be ascertained whether the bridging I atom is ordered at the center between two Pt dimers, which correspond to the electronic structure of –$Ni^{2.5}$–$Ni^{2.5}$–I–$Ni^{2.5}$–$Ni^{2.5}$–, or disordered at two positions around it, corresponding to the mixed-valence state of –Ni^2–Ni^2–I–Ni^3–Ni^3–.



(a) Low Temperature Phase (-89.4 °C) (b) High Temperature Phase (130.0 °C)

Figure 1. ORTEP drawings of the infinite linear chains of $Pt_2(dta)_4I$.

V-J Spectroscopic Studies on Charge Delocalization and Charge Transfer in Molecular Cluster Ions and Pure Liquid.

Charge transfer processes resulting in dynamical charge delocalization such as consecutive proton or electron hopping in molecular clusters and even in pure liquid are highly interesting in relation to the charge transportation in insulating materials. Not only in aromatic molecular liquids but also in pure water itself the electric conductivities are very low when they do not contain impurities of ionic atoms or molecules. We demonstrated that a positive charge in a pure benzene cluster is localized in a dimer unit where the charge resonance (CR) interaction makes the two molecules share an electron forming an intermolecular bond. In fact, aromatic dimer cations show very strong electronic transitions from the bonding states ($\phi_a^+\phi_b + \phi_a\phi_b^+$) to the antibonding states ($\phi_a^+\phi_b - \phi_a\phi_b^+$) in the near IR region, where $\phi_a^+\phi_b$ and $\phi_a\phi_b^+$ are charge localized state on molecule a and molecule b, respectively. Interestingly the upper state has a repulsive potential resulting in the dissociation of the a-b pair. Therefore the electronic excitation by the IR light dissociates the core dimer and generates a new ion pair. Because of energy release through the dissociation, this process also produces a hot molecular group with active intermolecular vibrations. Again the succeeding intermolecular "phonon type" motion may induce the charge transport resonant with the wavy motion. The collaboration with the Yoshihara laboratory has been successfully going on for the measurement of the rise and decay of the dimer cation species in pure liquid benzene. In order to extend this research program, we are now constructing a soft landing matrix isolation system for finding the CR transitions and for observing the ground state vibrational sequences of size selected cluster ions of new systems. On the basis of the low temperature data, photodissociation spectroscopy with an octopole ion trap will be carried out for gas phase ion clusters in a very wide energy region(2,500-48,000 cm^{-1}) with IR, VIS and UV lasers.

V-J-1 Pump-Probe Photodepletion Spectroscopy of Mass-Selected $(C_6H_6)_2^+$

Kazuhiko OHASHI, Yoshiya INOKUCHI(*Kyushu Univ. and IMS*) **and Nobuyuki NISHI**(*IMS and Kyushu Univ.*)

A pump-probe technique has been developed to study mass-selected cluster ions in the gas phase. The technique allows one to address the question of existence of a number of isomeric forms of cluster ions. Photodissociation process is employed as a means to probe as well as to pump. The probe laser is fixed at a certain wavelength. The intensity of the fragment ion signal generated by the probe laser (probe-laser signal) is proportional to the population of the isomer that absorbs a photon at the wavelength. The pump laser, preceding the probe laser in time, reduces the population of the isomer selected by the probe laser. The depopulation is seen as a depletion of the probe-laser signal. Figure 1 shows the photodissociation spectrum of $(C_6H_6)_2^+$ (dotted curve) in the near-infrared region. Both the main band at 920 nm and relatively weak one at 1160 nm are assigned to charge resonance (CR) bands. The issue is whether the two bands are due to two isomers or a single species of $(C_6H_6)_2^+$. The pump-probe experiment is performed by fixing the pump-laser wavelength at 920 nm and changing the probe-laser wavelength from 850 to 1210 nm. In Figure 1, the depletion yield of the probe-laser signal is plotted against the probe-laser wavelength. When the pump laser is introduced, the intensities of the probe-laser signals are reduced by 55-60 % at all wavelengths studied. This finding rules out the possibility that two isomers of $(C_6H_6)_2^+$ are responsible for the appearance of the two CR bands. If the two CR bands were due to different isomers, the depletion yields would be zero at wavelengths in the 1160-nm band region. We therefore conclude that two distinct transitions of a single isomer are responsible for the appearance of the two CR bands. No evidence is found for the existence of other isomers of $(C_6H_6)_2^+$.

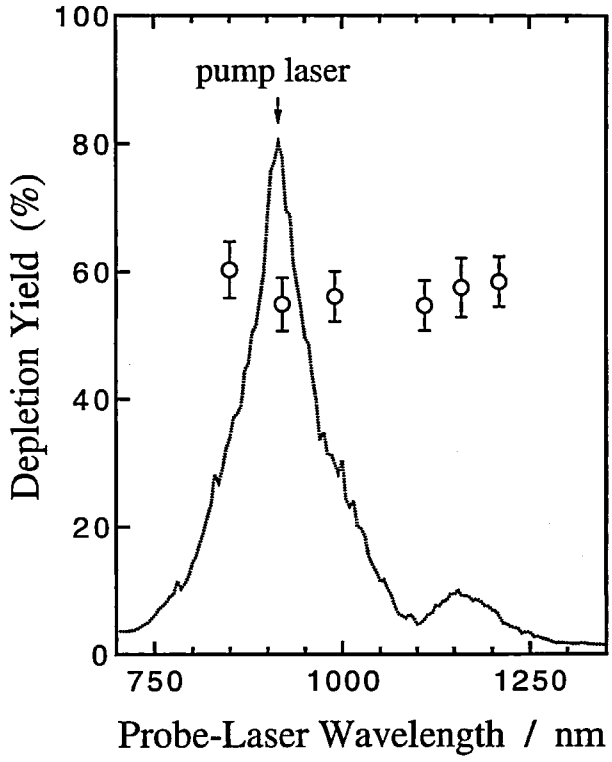


Figure 1. Plots of the depletion yield of the probe-laser signal against the probe-laser wavelength (open circles). The wavelength of the pump laser is fixed at 920 nm. The dotted curve stands for the photodissociation spectrum of $(C_6H_6)_2^+$.

V-J-2 Construction of a Soft Landing Ion Fixation / Matrix Isolation System of Size-selected Molecular Cluster Ions for Direct Absorption Measurements of IR, VIS, and UV Spectra.

Naoto TAKANO(*Kyushu Univ.*) **and Nobuyuki NISHI**(*IMS and Kyushu Univ.*)

In order to carry out ion cluster laser spectroscopy in gas phase, it is necessary to know the energy region of the vibrational or electronic absorption bands of the specific ion clusters. The spectroscopic data of size-selected

ion species isolated in a solid matrix may very much help us to limiting the scan ranges of laser wavelengths to the right region and to estimating minimum laser energies for obtaining photodissociation spectra of isolated cluster ions. We designed energy and mass separation and energy deceleration systems for the soft landing deposition of the selected ions based on the simulation of sion trajectories considering the energy distribution of produced ions. Three kinds of beam sources are planning to be used; a corona discharge continuous beam source, a pulsed electron impact one, and a new cluster beam source with a hot tube collision extension and a liquid droplet-beam nozzle. The last one may be used for variety of cluster systems composed of nonvolatile compounds. Ion beams with appropriate kinetic energies are injected from upside of the ion extraction chamber down to the 10 inch oil-diffusion pump via a static ion lense system and an extraction ion bender. The potential of the quadrupole ion bender coupled with a narrow slit allows us to extract ions with small kinetic energies. After readjustment of the ion beam with a set of static lense plates, interesting ion clusters are mass-selected with a quadrupole mass filter situated in the second chamber evacuated by a diffstak UHV pump and the selected ions are forwarded into a kinetic energy decelerator. The slow positive ions are then deposited very gently with matrix gas atoms on a cold window at 10K. A slow electron source is also placed near the cold window for producing negative ions. The negative ions are attached to the solid surface with matrix gas atoms when the surface positive potential becomes high enough to prevent the deposition of the positive cluster ions. The cold matrix window is situated in a small UHV room evacuated with a turbo molecular pump. This matrix deposition room is placed in a sample box of a commercial UV or FT-IR spectrometer.

This apparatus will be also used for studying ion-molecule reactions on the cold surface. The ion beam technique is expected to make us possible to find novel reaction products which are stable only at very low temperatures. The apparatus can be used not only for the mass analysis but also for the spectroscopy of the reaction productions.

V-K Infrared Laser Spectroscopy of Negatively-Charged Molecular Clusters

While infrared spectroscopy has a long-standing tradition in the studies of vibrational motions of isolated molecules, its applicability to gas-phase clusters have been limited by the lack of an intense infrared radiation source. Our research group, which started in May 1996, has been developing an experimental technique for infrared laser spectroscopy of negatively-charged molecular clusters by combining a single-mode optical parametric oscillator (OPO) with a time-of-flight (TOF) mass spectrometer. By applying this technique, we are planning to identify the coexistence of isomers in cluster anions.

V-K-1 Construction of Apparatus for Infrared Spectroscopy of Cluster Anions

Morihisa SAEKI, Lei ZHU, Tatsuya TSUKUDA *(Univ. of Tokyo)* **and Takashi NAGATA**

We have constructed an apparatus applicable to infrared spectroscopy of molecular cluster anions. Figure 1 shows a schematic of the apparatus. The apparatus consists of an cluster anion source and a tandem TOF mass spectrometer. The ion source chamber is evacuated by a 10" diffusion pump (3700 ls^{-1}). The tandem mass spectrometer is composed of two differentially-pumped regions including several sets of ion optics. The source chamber contains an electron-impact ionized free jet. A high-energy electron beam of ca.250 eV crosses a pulsed supersonic expansion of Ar gas containing sample molecules. The low-energy secondary electrons formed in the free jet rapidly attach to neutral clusters to form negatively-charged clusters. The cluster anions are extracted by applying a pulsed electric field to the repeller and accelerated up to 1500 eV through a stack of electrodes. Mass selection is achieved by a Wiley-McLaren type TOF arrangement. The cluster anions are then intersected at the spatial focus of the mass selector with the pulsed output from an optical parametric oscillator (Continuum Mirage 3000) pumped by an injection-seeded Nd:YAG laser. Absorption of the infrared photons inevitably cause a break of the cluster bonds, resulting in the production of fragment anions and neutrals, both of which can be detected by a microsphere plate located at the end of the flight tube of the second TOF mass spectrometer. Measurements of the fragment intensities as a function of photon energy provides photoabsorption spectra of the cluster anions. The spectral resolution is limited by the band width of the optical parametric oscillator, which is expected to be ca.0.02 cm^{-1} in the wavelength range 2 - 4μm.

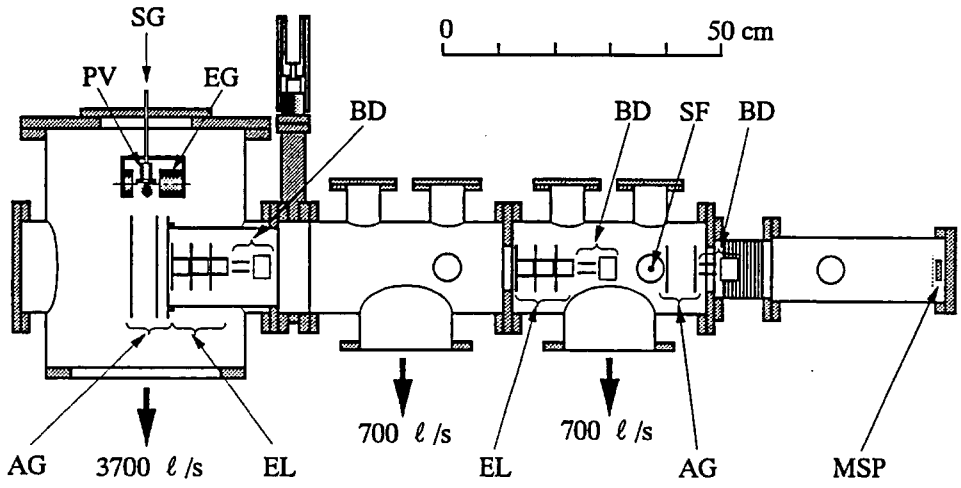


Figure 1. Schematic of experimental apparatus. AG: acceleration grids; BD: beam deflectors; EG: electron gun; EL: Einzel lens; MSP: microsphere plats; PV: pulsed valve; SF: spatial focus; SG: sample gas.

V-K-2 *Ab Initio* Calculations on Geometrical Structures of $[(CO_2)_nH_2O]^-$

Morihisa SAEKI, Tatsuya TSUKUDA *(Univ. of Tokyo)*, **Takashi NAGATA and Suehiro IWATA**

As mentioned above in V-K-1, our interest is focused on the existence of energetically low-lying isomers in molecular cluster anions. As one of the candidates for the infrared-spectroscopic studies, we have investigated the structures and stabilities of $[(CO_2)_nH_2O]^-$ cluster anions by *ab initio* calculations. The calculations at MP2 levels predict the existence of several stable conformers for $[(CO_2)_nH_2O]^-$ with n = 1 and 2. Especially, it is demonstrated that two types of isomers having different electronic structures coexist in $[(CO_2)_2H_2O]^-$, as shown in Figure 1. Vibrational analyses indicate that these species are distinguishable through the measurement of the OH vibrational modes.

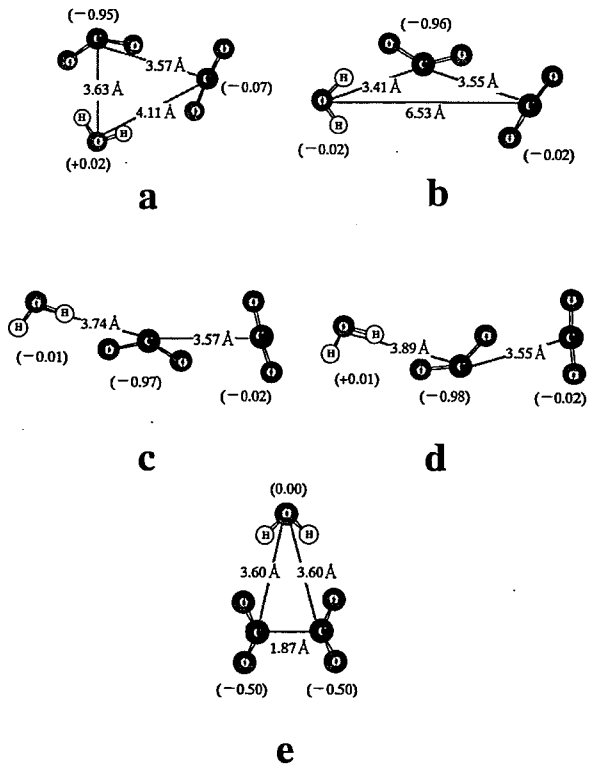


Figure 1. Stable structures of $[(CO_2)_2H_2O]^-$. Structures **a**, **b**, **c** and **d** involve a monomer anionic core CO_2^-, while the excess electron is delocalized over the two CO_2 constituents forming a $C_2O_4^-$ core in structure **e**. Numbers in parentheses indicate the electron populations.

RESEARCH ACTIVITIES VI
Department of Vacuum UV Photoscience

VI-A Electronic Structure and Decay Mechanism of Inner-shell Excited Molecules

This project is being carried out in collaboration with Photon Factory (KEK-PF), Tohoku University, and McMaster University. We have interest in ultrafast ionic fragmentation following the Auger decay upon the molecular inner-shell excitation. Last year we investigated vibronic states in the inner-shell excitation of some polyatomic molecules. We found that the fragmentation takes place on the way of Renner-Teller and Jahn-Teller distortions [See, N. Kosugi, *J. Electron. Spectrosc.* **79**, 351 (1996)]. This year we have extended our approaches to other molecules.

VI-A-1 Angular Distribution of Fragment Ions following the S 1s Photoexcitation of H_2S

Jun-ichi ADACHI, Yasutaka TAKATA, Nobuhiro KOSUGI, Atsunari HIRAYA, Eiji SHIGEMASA*, Akira YAGISHITA* and Yoshinori KITAJIMA* *(*KEK-PF)*

We have measured angle-resolved ion-yield spectra for the S 1s excited states of H_2S using linearly polarized synchrotron radiation. The most intense peak in the ion-yield spectrum observed in the 90° direction to the electric vector of the incident light (I_{90}) is slightly higher in energy (about 0.15 eV) than that in the 0° direction (I_0). This result indicates that the S 1s → $3b_2$ and $6a_1$ excited states can be differentiated in the present spectra and that the $6a_1$ excited state is located at the higher energy side than the $3b_2$ one. The present result also shows that the peak observed around 2476 eV contains the two Rydberg excited states with different symmetries.

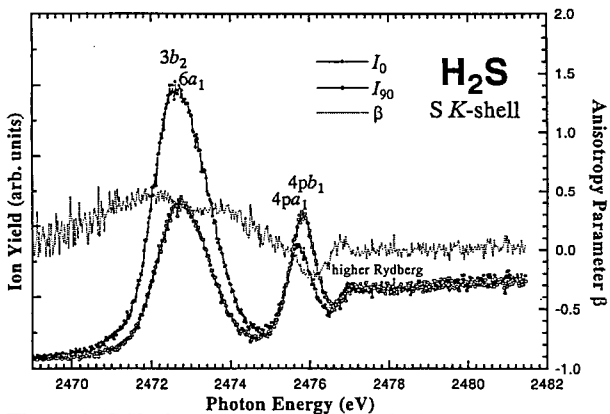


Figure 1. S *K*-edge angle-resolved ion-yield spectra of H_2S. The closed circle shows the ion-yield in the 0° direction to the electric vector of the incident light (I_0) and the open square line shows one in the 90° direction (I_{90}). The broken line shows the experimental anisotropy parameter $\beta = 2(I_0 - I_{90}) / (I_0 + 2 \cdot I_{90})$.

VI-A-2 Jahn-Teller Effect in the S 1s → $6t_{1u}$ excited state of SF_6

Jun-ichi ADACHI, Yasutaka TAKATA, Nobuhiro KOSUGI, Atsunari HIRAYA, Eiji SHIGEMASA*, Akira YAGISHITA* and Yoshinori KITAJIMA* *(*KEK-PF)*

We have measured angle-resolved ion-yield spectra for the S 1s excited SF_6 using linearly polarized synchrotron radiation. The present spectra show the anisotropic fragmentation for the S 1s → $6t_{1u}$ excitation; the ion-yield observed in the 0° direction relative to the electric vector of the incident light is smaller than that in the 90° direction. This anisotropic fragmentation means that the stable geometry is distorted with the Jahn-Teller effect. The Jahn-Teller distortion in the $6t_{1u}$ excited state can occur through the stretching e_g mode or through the bending t_{2g} one. A d-orbital component is mixed with the $6t_{1u}$ one through the distortions; therefore, the transition dipole moment along the distorted axis becomes small. The t_{2g} mode is probably related to the Jahn-Teller distortion. The angular distribution of the fragment ions becomes anisotropic because some S-F bonds are bent relative to the direction of the reduced transition dipole moment.

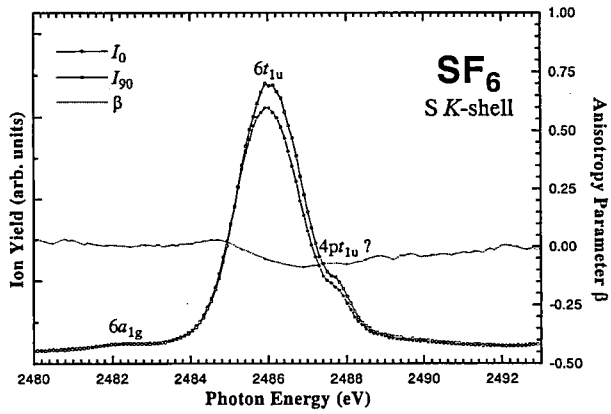


Figure 1. S *K*-edge angle-resolved ion-yield spectra of SF_6. The closed circle shows the ion-yield in the 0° direction to the electric vector of the incident light (I_0) and the open square shows one in the 90° direction (I_{90}). The broken line shows the experimental anisotropy parameter $\beta = 2(I_0 - I_{90}) / (I_0 + 2 \cdot I_{90})$.

VI-A-3 Angular Correlation between Fragment Ions from the Nitrogen *K*-shell Excited and Ionized N_2O

Jun-ichi ADACHI, Nobuhiro KOSUGI, Eiji SHIGEMASA*, Akira YAGISHITA* and Paul A. HATHERLY** *(*KEK-PF, **Univ. of Reading)*

[*J. Electron Spectrosc.* **79**, 491 (1995)]

A newly developed angle-resolved photoion-photoion coincidence (ARPIPICO) measurements for the N 1s ionized and excited N_2O were carried out to obtain the correlation angle dependence of the ARPIPICO rates. The results indicate that the bending motion in the N_c 1s → π* excited state is more strongly excited than that in the N_t 1s → π* one, and is consistent with our calculated results that the Renner-Teller effect in the N_c 1s → π* excited state is stronger than that in the N_t 1s → π* one.

VI-A-4 Rydberg and Valence States in the C 1*s* Photoabsorption and Resonance Auger Spectra of CH_3F

Nobuhiro KOSUGI, Kiyoshi UEDA*, Yuichiro SHIMIZU*, Hiroshi CHIBA*, Misaki OKUNISHI*, Kenji OHMORI* and Yukinori SATO*, Eiji SHIGEMASA**
*(*Tohoku Univ., **KEK-PF)*

[*Chem. Phys. Lett.* **246**, 475 (1996)]

Comparison of the high-resolution C 1*s* electron-yield spectrum of CH_3F with that of CH_4 reveals that the core-to-valence excited state with antibonding character between C and F ($\sigma^*_{C\text{-}F}$) manifests in a broad and strong feature below the 3*s* Rydberg band and all the other features are nearly the same as in CH_4. This is supported by theoretical calculations using the relaxed core-hole potential and avoiding spurious mixing between Rydberg and valence states. In the resonance Auger electron spectra the participant Auger decay rate following the core-to-valence ($1s \rightarrow \sigma^*_{C\text{-}F}$) excitation, ~15 %, is much larger than that of the core-to-Rydberg excitations, 1~5 %.

VI-A-5 Inner-Shell Excitation Spectroscopy of Closo-Carboranes

Adam P. HITCHCOCK*, Stephen G. URQUHART*, Alex T. WEN*, A. L. David KILCOYNE*, Tolek TYLISZCZAK*, Eckart RÜHL, Nobuhiro KOSUGI, John D. BOZEK***, James T. SPENCER****, David N. MCILROY***** and Peter A. DOWBEN*******
*(*McMaster Univ., **Universität Mainz, ***Lawrence-Berkeley Lab., ****Syracuse Univ., *****Univ. Nebraska-Lincoln)*

Oscillator strength spectra in the region of B 1s and C 1s excitation of three isomeric carborane cage compounds [*closo*-1,2-orthocarborane, *closo*-1,7-metacarborane, *closo*-1,12-paracarborane ($C_2B_{10}H_{12}$)] have been derived from inner-shell electron energy loss spectra (ISEELS) recorded under electric dipole scattering conditions. These spectra are compared to total ion yield spectra recorded with synchrotron radiation. The isomeric and core level variations in the discrete core excitations are related to changes in orbital symmetries as well as variations in electron localization in these isomers.

VI-A-6 (LS) versus (jj) Coupling in P 2p Inner-Shell Excited States of PF_3

Nobuhiro KOSUGI, Chris E. BRION, Ronald G. CAVELL and Adam P. HITCHCOCK* *(*Univ. British Columbia, **Univ. Alberta, ***McMaster Univ)*

The total ion yield spectrum of PF_3 in the region of P 2p excitation was recorded at high resolution using synchrotron radiation and time of flight mass spectrometry. We have found that PF_3 has a state at 136.4 eV which is best described as the LS coupled $^1A_1$ state, ignoring spin-orbit splitting. The absence of a spin-orbit partner to this state is confirmed by observation of a single line at 136.4 eV in the PF^{3+} partial ion yield. A theoretical prediction shows that this state has a singlet-triplet splitting of 2.4 eV, much more than that of any other P 2p excited states (0.05-0.5 eV) and much larger than the ion core spin-orbit splitting (0.9eV). In the 2p core level spectroscopy the exchange interaction is as important as the spin-orbit interaction.

VI-B Soft X-ray Photoelectron-Photoabsorption Spectroscopy and Electronic Structure of Transition Metal Compounds

Last year we successfully measured Ni inner-shell photoabsorption and photoelectron spectra by using a high-performance electron energy analyzer connected to the soft X-ray double crystal monochromator of the beamline BL1A at the UVSOR facility. This year we have investigated electronic structures of some molecular Ni complexes with planar structure by measuring both polarized Ni 2p photoabsorption spectra and Ni 3p/3s resonant photoelectron spectra combined with the photoabsorption.

VI-B-1 Polarization Dependence of Ni 2p Photoexcitation of Nickel Dimethylglyoxime

Takaki HATSUI*, Yasutaka TAKATA, Nobuhiro KOSUGI, Kaoru YAMAMOTO, Toshihiko YOKOYAMA* and Toshiaki OHTA*** *(*Grad. Univ. Advanced Studies, **The University of Tokyo)*

The Ni 2p absorption spectra of nickel dimethylglyoxime have been measured to investigate the Ni 3d electronic structure. The polycrystalline nickel dimethylglyoxime sample was prepared by evaporating the powder on a glass substrate and the c axis of each crystal is roughly in the surface plane of the substrate, i. e. the normal axis (z) to the molecular plane (xy) are parallel to the surface. The Ni 2p absorption spectra have been measured at some incident angles as shown in Figure 1. The main peak A was strong at the grazing X-ray incidence, where the electric field vector E was closely in the molecular plane, and it became weaker at the normal incidence, where E was perpendicular to the molecular plane. This indicates that the main peak corresponds to a transition of $2p_x$ or $2p_y$ electrons to the lowest unoccupied $3d_{x2\text{-}y2}$ orbital. On the other hand, the polarization dependence of peak D was opposite to that of peak A. This polarization dependence could be explained by a transition of $2p_x$ or $2p_y$ electrons to a hybrid orbital with ligand π^* and Ni $3d_{xz}/3d_{yz}$ characters.

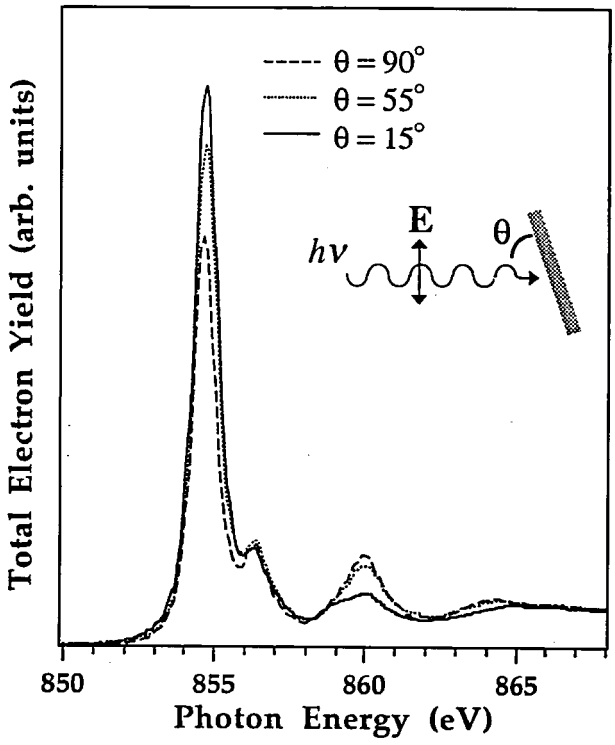


Figure 1. The polarization dependence of Ni 2p photoexcitation. The molecular plane (xy) of nickel dimethylglyoxime is closely parallel to the surface normal.

VI-B-2 Resonant Auger Spectra of Nickel Dimethylglyoxime Following the Ni 2p Excitation

Yasutaka TAKATA, Takaki HATSUI *(Grad. Univ. Advanced Studies)* **and Nobuhiro KOSUGI**

We have measured resonant Auger spectra of nickel dimethylglyoxime [Ni(dmg)$_2$] in the Ni 2p excitation region to investigate the electronic structure. Figure 1 shows resonant Auger spectra measured at the Ni2p$_{3/2}$ → 3d excitations (hv=854.7 eV, and 860.1eV). The normal Auger spectrum is also shown. The Ni 3p and 3s main lines are not enhanced but the satellite lines (a-e) are enhanced by the resonant excitation. The kinetic energies of the enhanced peaks are higher than those of the corresponding normal Auger lines and decrease with increase of the photon energy. Similarly to the case of $K_2Ni(CN)_4$, this indicates that the enhanced peaks originate in the spectator Auger transition, and the spectator Auger electrons behave like a hydrogenic electron. However, the photon energy dependence (kinetic energy vs. photon energy) of this system is -0.25±0.05, different from the value (-0.55±0.05) of $K_2Ni(CN)_4$. Ni(dmg)$_2$ is also a square-planar complex, but has a stacking structure with nickel atoms directly above each other; therefore, the inter-unit interaction is stronger than that of $[Ni(CN)_4]^{2-}$.

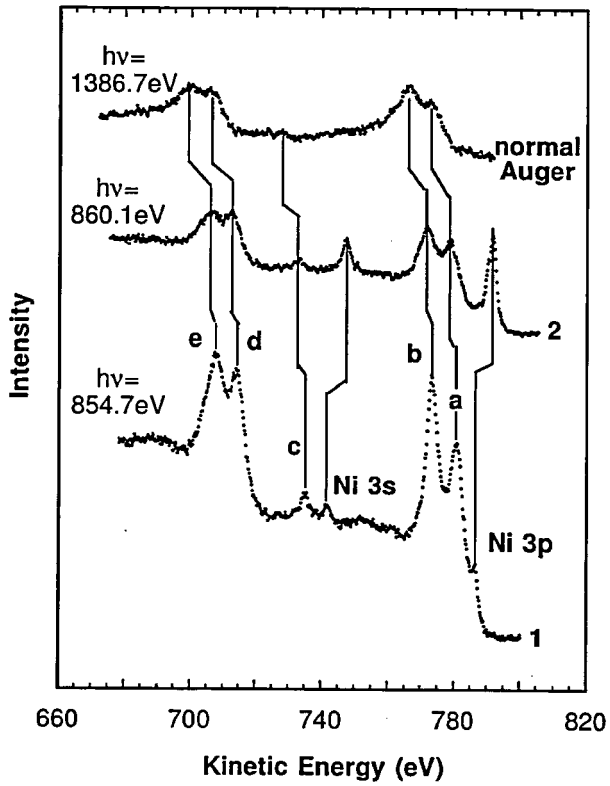


Figure 1. Resonant Auger spectra of Ni(dmg)$_2$ following the Ni 2p$_{3/2}$ → 3d excitation and the normal Auger spectrum.

VI-B-3 Photon Energy Dependence of Ni 2p Resonant Auger Spectra of $K_2Ni(CN)_4$

Yasutaka TAKATA, Motohiko NAKAMURA and Nobuhiro KOSUGI

We have measured photon energy dependence of Ni 2p resonant Auger spectra of $K_2Ni(CN)_4$ involving a square-planar complex ion $[Ni(CN)_4]^{2-}$. Figure 1 shows the kinetic energy shift of the Ni $\underline{2p_{3/2}}X$-$\underline{3p3d}X'$ spectator Auger line relative to the excitation photon energy. The under bar and X (X') denote a hole and a excited electron, respectively. In the $2p_{3/2} \rightarrow 3d$ excitation region, the kinetic energy decreases linearly with the slope of -0.55±0.05. This photon energy dependence can be explained if we assume that the spectator electron behaves like a Wannier exciton and is shaken up ($X \rightarrow X'$) with high probability. This is consistent with the ionic character that the $[Ni(CN)_4]^{2-}$ ion has mainly electrostatic interaction with surrounding ions. In the $2p_{1/2} \rightarrow 3d$ excitation region, the Ni $2p_{3/2}$ Auger line still exists with high intensity in addition to the $\underline{2p_{1/2}}X$-$\underline{3p3d}X'$ spectator Auger line. It is clearly shown in Fig.1 that the kinetic energy of Ni $2p_{3/2}$ Auger line is higher than that of the $\underline{2p_{3/2}}$-$\underline{3p3d}$ normal Auger line even in the $2p_{1/2}$ energy region, and does not depend on the photon energy. This indicates that the $2p_{1/2}$ core-hole created by resonant excitation is converted to the $2p_{3/2}$ hole *via* the fast $\underline{2p_{2/1}}X$-$\underline{2p_{3/2}3d}X''$ Coster-Kronig transition followed by the $\underline{2p_{3/2}3d}X''$-$\underline{3p3d}$ Auger transition, where the $\underline{2p_{3/2}3d}X''$ state is regarded as a $3d \rightarrow X''$ excited state and the final $\underline{3p3d}$ state is the same as the final state of the normal Auger transition.

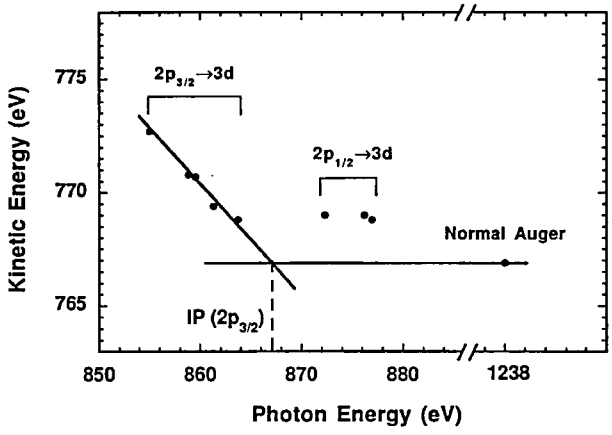


Figure 1. Kinetic Energy shift of the Ni $2p_{3/2}X$-$3p3dX'$ spectator Auger line of $K_2Ni(CN)_4$ relative to the excitation photon energy in the Ni $2p \rightarrow 3d$ excitation region.

VI-C Studies on Photochemical Reactions using Ultrafast Laser and Synchrotron Radiation

Ultrafast lasers have been playing essential roles in the physicochemical studies of photochemical reactions. Thanks to recent advances of the laser technology, we are now able to observe even wavepacket evolution in the course of chemical reactions with femtosecond time-resolution. Synchrotron radiation, on the other hand, affords photons in a very wide energy range from X-ray to far-infrared, which are not obtainable with the present lasers. It has a unique potentiality in time-resolved spectroscopy since the synchrotron radiation is intrinsically given in the form of a picosecond pulse train. In this project, we investigate photochemical reactions, mainly in condensed phase, taking advantage of these two light sources which are complementary to each other. In the past year, we have constructed two time-resolved experimental setups on the basis of a femtosecond mode-locked Ti:sapphire oscillator laser. The first apparatus is a femtosecond time-resolved fluorescence up-conversion spectrometer, which is now used for the studies of several chemical systems relating to *cis-trans* photoisomerization or photo-induced proton transfer. The second apparatus is a femtosecond optical heterodyne detected impulsive stimulated Raman scattering (OHD-ISRS) spectrometer, in which a phase-stabilized complete optical heterodyne detection of the ISRS signal is attained for the first time. In addition, we are now planning picosecond time-resolved measurements in the far-infrared region using synchrotron radiation available at UVSOR.

VI-C-1 Construction of Femtosecond Fluorescence Up-conversion Spectrometer

Satoshi TAKEUCHI and Tahei TAHARA

We have constructed an experimental setup for fluorescence up-conversion (Figure 1) which enables us to measure a temporal evolution of fluorescence intensity in the visible region with a time resolution as good as 150 fs. The light source used in this system is a mode-locked Ti:sapphire laser which generates 50 fs fundamental pulses at 800 nm. The second / third harmonic (SHG : 400 nm, 80 mW; THG : 267 nm, 30 mW) is generated in nonlinear crystals (LBO, BBO), and is used as a pump pulse to photoexcite a sample. The residual fundamental pulse is used as a gate pulse for the up-conversion process. The fluorescence emitted from the sample is collected and focused in a BBO mixing crystal by an aluminum-coated elliptic mirror without any aberration nor dispersion effects. A film polarizer is placed in between the elliptic mirror and the mixing crystal so that the vertically-polarized (i.e. paralell to the gate polarization) component of the fluorescence is selected to be up-converted. The fluorescence detection at the magic angle is achieved by rotating the pump polarization. The fluorescence is up-converted in the mixing crystal via sum-frequency-generation with the gate pulse. The fluorescence wavelength to be up-conveted is selected by changing the phase-matching angle of the mixing crystal, and the spectral bandwidth of the up-conversion process is ± 8 nm for the fluorescence wavelength. The up-converted signal is separated from the other light by an iris, an optical filter, and a 0.32-m monochromator, and is detected by a photon counting equipments. The relative delay time between the fluorescence and the gate pulse is changed by a mechanical stage.

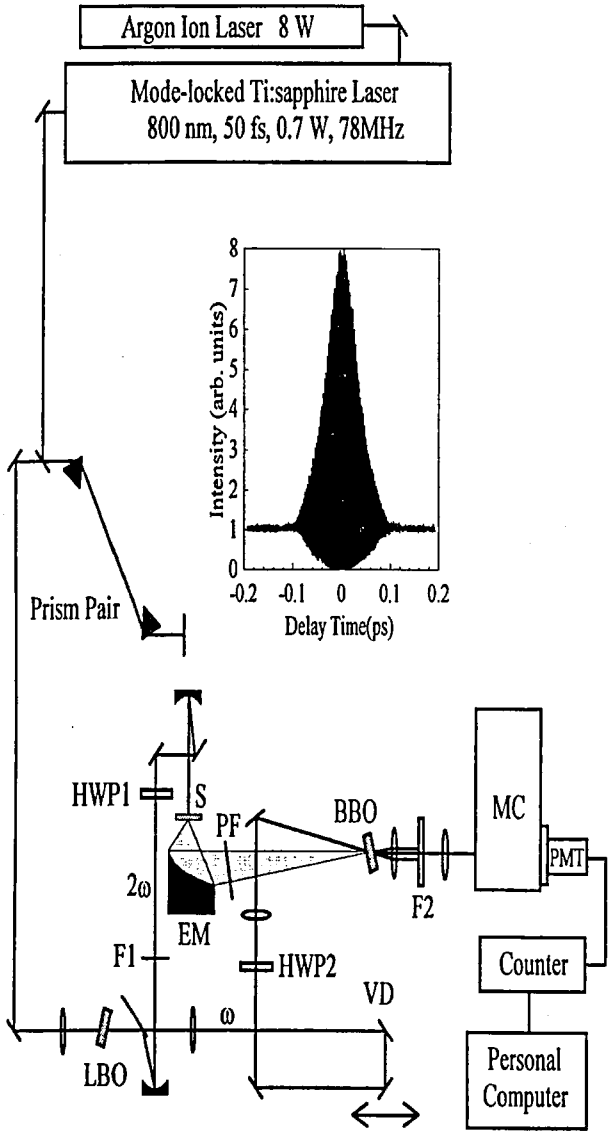


Figure 1. Schematic diagram of the experimental setup used for the fluorescence up-conversion measurements. S : sample, EM : elliptic mirror, PF : polarizing film, F1, 2 : optical filters, HWP1, 2 : half-wave plates for 400 and 800 nm, respectively, VD : variable delay line, MC : monochromator, PMT : photomultiplier. (The optical components for third harmonic generation are not shown.)

VI-C-2 Ultrafast Fluorescence Study on the Excited Singlet State Dynamics of all-*trans* Retinal

Satoshi TAKEUCHI and Tahei TAHARA

[*J. Phys. Chem.*, submitted]

The femtosecond time-resolved fluorescence of all-*trans* retinal in hexane was measured by using fluorescence up-conversion method (Figure 1). It was found that the fluorescence consists of ultrafast ($\tau = 30 \pm 15$ fs, $\lambda_{max} \approx 430$ nm), fast ($\tau = 370 \pm 20$ fs, $\lambda_{max} \approx 440$ nm), and slow ($\tau = 33.5$ ps, $\lambda_{max} \approx 550$ nm) components. These three components were assigned to fluorescences from the ^1B_u, ^1A_g, and $^1n\pi^*$ states, respectively, which are successively populated during the relaxation process in the singlet manifold after photoexcitation. The radiative lifetimes of the three excited singlet states were determined to be 2 ns (^1B_u), 100 ns (^1A_g), and 3 μs ($^1n\pi^*$) based on the obtained time-resolved fluorescence data, and the value for the ^1B_u state was in very good agreement with that calculated from the ground-state absorption spectrum. The state ordering in the singlet manifold as well as quantitative characterization of the three low-lying excited singlet states was discussed.

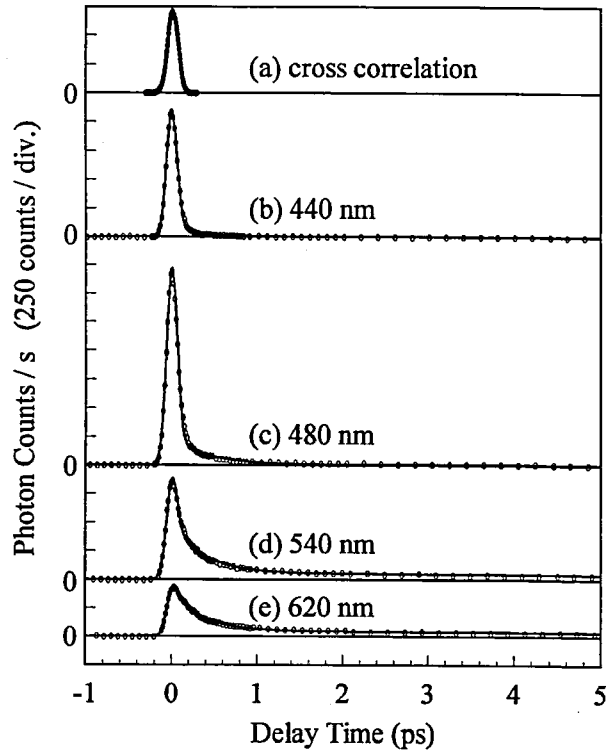


Figure 1. Up-converted fluorescence decay signals obtained from all-*trans* retinal in hexane (1.2×10^{-3} mol dm^{-3}; 400 nm excitation). Cross-correlation trace between the gate pulse and the pump pulse (a), and fluorescence decays of all-*trans* retinal at 440 (b), 480 (c), 540 (d), and 620 nm (e). The open circles are experimental data points, and the solid curves are results of the fitting analysis. The instrumental time-resolution given by the FWHM of the cross-correlation trace is 150 fs.

VI-C-3 Development of an Optical Heterodyne Detected Impulsive Stimulated Raman Scattering Spectrometer with a "phase-stabilizing" Mechanism

Shigeki MATSUO and Tahei TAHARA

[*Chem. Phys. Lett.*, in press]

An apparatus for the measurement of optical heterodyne detected impulsive stimulated Raman scattering (OHD-ISRS) has been developped. The optical setup is schematically shown in Figure 1. The light source (not shown) is a femtosecond mode-locked Ti:sapphire laser. The output of this laser is divided into three; two pump pulses and one probe pulse. The two pump pulses are focused into sample simultaneously, and the probe pulse is focused after a certain time delay. For the optical heterodyne detection, the ISRS signal is interfered with a local oscillator (LO). In the present apparatus, the probe pulse which has passed through the sample is used as a LO. The relative phase between the electric fields of the signal and the LO is controlled by subwavelength adjustment of

optical path length with a piezoelectric transducer. This piezoelectric transducer is also used to suppress undesirable changes in the optical path length which arise from mechanical/optical instabilities. He-Ne laser beams are also introduced to the interferometer as "reference" beams in addition to the signal and the LO, so that the change in path length can be monitored as the intensity change in the interference. Phase drifts were calculated from the temporal change in the OHD-ISRS intensity at the zero time delay, and are shown in the inset (b) of Figure 1. As clearly shown, the phase drift was reduced by the active adjustment of the optical path length, and became negligibly small within typical measurement time of a few minutes. This apparatus enables us to measure the ISRS signal which is linearized to each tensor element of the third order material response.

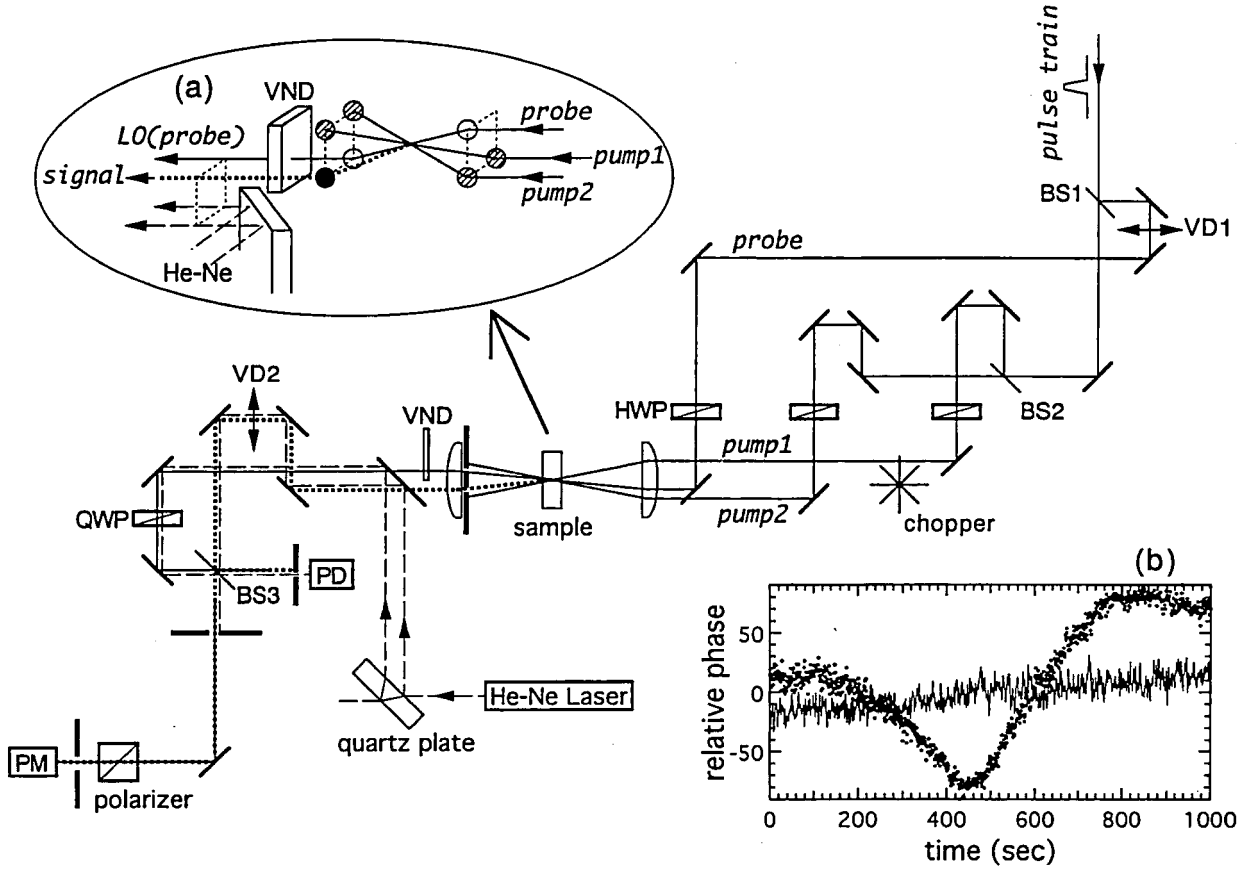


Figure 1. The optical setup for OHD-ISRS. The inset (a) shows the spatial arrangement of laser beams. The inset (b) shows the relative phase drift with (solid line) and without (dots) adjustment of optical path length .

VI-C-4 Polarization Dependence of Optical Heterodyne Detected Impulsive Stimulated Raman Scattering of Liquids

Shigeki MATSUO and Tahei TAHARA

Optical heterodyne detected impulsive stimulated Raman scattering (OHD-ISRS) of CS_2 and CCl_4 has been measured. OHD-ISRS of CS_2 was measured at three polarization conditions: $\chi_{1111}^{(3)}$, $\chi_{1212}^{(3)}$, and $\chi_{1122}^{(3)}$. The semilogarithmic plot of $\chi_{1111}^{(3)}$ component showed an exponential decay with a time constant of 1.65 ± 0.1 ps in the delay time later than 2 ps. This time constant was in good agreement with the diffusive reorientation time constant obtained with OHD-RIKES experiments [1]. This fact implied that the observed ISRS signals were linearized to the third order material response, and that complete phase-stabilized heterodyne detection was achieved in this measurement. The electronic contribution (an instantaneous peak at the time origin) and nuclear contribution (a peak around 0.2 ps followed by a slowly decaying tail) were separately observed in all signals. However, the signal feature differed from each other in the ratio of the electronic to the nuclear contribution. In particular, the electronic and nuclear contributions had opposite sign in the $\chi_{1122}^{(3)}$ signal. These features were interpreted in terms of Raman depolarization ratio. In the OHD-ISRS signal of CCl_4, vibrational signal was clearly observed in addition to an instantaneous peak at the time origin. On the basis of Fourier transform of the signal, it was concluded that the signal was predominantly due to the 218 cm^{-1} and 314 cm^{-1} intramolecular vibrations of CCl_4, and that the contribution from the 458 cm^{-1} vibration was negligibly small because of limited time resolution. The OHD-ISRS signals obtained from CS_2 are shown in Figure 1.

[1] D. McMorrow, W.T. Lotshaw, and G.A. Kenney-Wallace, IEEE J. Quantum Electron. 24 (1988) 443.

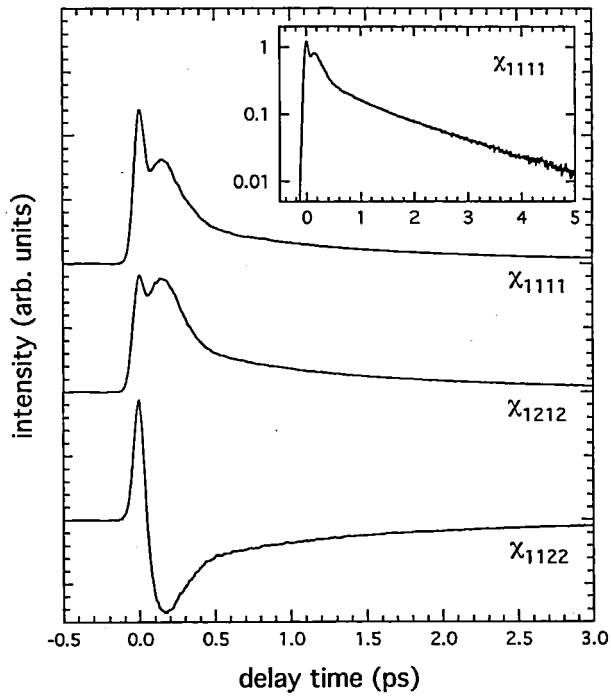


Figure 1. OHD-ISRS signal of CS_2 measured at three polarization conditions: $\chi_{1111}^{(3)}$, $\chi_{1212}^{(3)}$, and $\chi_{1122}^{(3)}$. The inset shows semi-logarithmic plot of $\chi_{1111}^{(3)}$ component.

VI-C-5 Synchronization Between Picosecond Mode-Locked Laser and Synchrotron Radiation

Misa KAYAMA *(Graduate Univ. for Advanced Studies)* **and Tahei TAHARA**

Despite several technical limitations, pump - probe experiments using combination of laser (pump) and synchrotron radiation (probe) are very attractive since they afford unique opportunity of time-resolved measurement in the energy region which is not accessible with the present lasers only. A key technology in the development of this type of spectroscopy is synchronization between picosecond lasers and synchrotron radiation. One of the advantages of the synchrotron radiation in UVSOR is that its repetition rate (90 MHz) matches that of ordinary mode-locked lasers. It allows us to achieve full one-to-one synchronization between laser pulses and synchrotron radiation without reducing the number of the electron bunches in the storage ring. We applied the RF signal given from the storage ring to a cw mode-locked Nd:YAG laser whose cavity length is optimized for the 90-MHz operation, and achieved full synchronization between the laser and synchrotron radiation. The obtained laser pulses were transported to a beamline (BL6B) using single-mode optical fibers, and the timing between the laser pulse and the synchrotron radiation was checked by time-correlated single photon counting technique. As shown in Figure 1, the timing can be controlled by a phase shifter which changes the phase of the RF signal applied to the mode-locker of the laser. In principle, we can now deliver the synchronized picosecond laser pulses to any beamline at UVSOR with use of optical fibers.

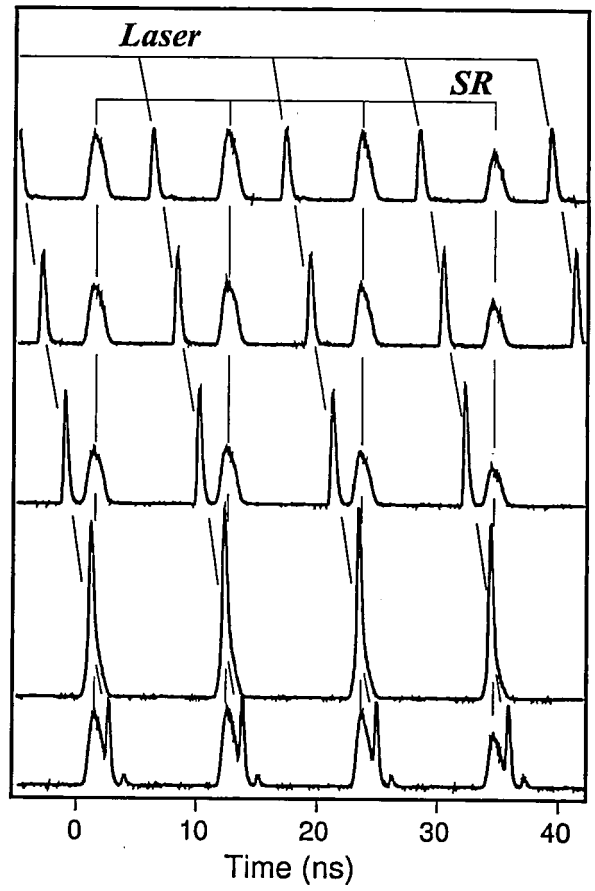


Figure 1. Synchronization between synchrotron radiation and a picosecond mode-locked laser.

VI-C-6 A Proposal of Picosecond Time-resolved Far-Infrared Spectroscopy using Synchrotron Radiation

Tahei TAHARA

It is well known that far-infrared spectra contain much information about low-frequency motions in the materials including intermolecular vibrations in liquids and phonons in the solids. It is highly desirable to develop time-resolved far-infrared (TRFIR) spectroscopy, since it is expected to shed new light on the dynamics from the viewpoint of low-frequency vibrations. However, it is still difficult to carry out TRFIR spectroscopy since (1) short laser pulses in this region can not be generated with the nonlinear optical process owing to the lack of suitable nonlinear crystals, and (2) the responses of ordinary far-infrared detectors (bolometer) are quite slow. Synchrotron radiation affords picosecond optical pulses ranging from X-ray to far-infrared, and it gives us a chance to carry out picosecond TRFIR spectroscopy. In the UVSOR facility, there exist two beamlines (BL6A1 and BL6B) designed for the infrared and/or far-infrared experiments, which are equipped with Fourier-transform-type spectrometers and bolometers. At present, far-infrared spectra of *static* samples are measured with *picosecond synchrotron radiation pulses* which automatically collect spectral information of the sample through a picosecond time window. Therefore, if we can induce a detectable change in the sample using picosecond laser pulses which are synchronized to synchrotron radiation, we can accomplish TRFIR measurement without any change in the detection system

which is already available at UVSOR. The time-resolved measurement in the far-infrared region based on this idea is planned at beamline 6B.

VI-D Synchrotron Radiation Stimulated Surface Reactions

Study of synchrotron radiation (SR) stimulated surface reaction is a promising topic in fundamental science, because dynamical processes induced by the photostimulated core-electron excitations on surfaces are scarcely explored so far. This field is important also in applied science, since the fundamental study is expected to develop the new techniques for semiconductor processing such as SR stimulated etching and SR stimulated epitaxial growth.

VI-D-1 *In Situ* Observation of Silicon Hydrides on Si(100) Surfaces during Synchrotron-Radiation-Stimulated Si_2H_6 Gas Source Molecular Beam Epitaxy

Akitaka YOSHIGOE, Kazuhiko MASE, Yoshiyuki TSUSAKA, Tsuneo URISU, Yoshihiro KOBAYASHI* and Toshio OGINO* *(*NTT, Basic Research Laboratories)*

[*Appl. Phys. Lett.* **67**, 2364 (1995)]

Silicon hydrides (SiH_n) on the Si(100) surface during synchrotron radiation (SR) stimulated Si_2H_6 gas source molecular beam epitaxy has been observed *in situ* at low temperatures (<400 ℃), by means of infrared reflection absorption spectroscopy using $CoSi_2$ buried metal layer substrates. At high temperatures (400 ℃, 370 ℃), SiH is a dominant surface species, while with temperature decrease from 275 to 50 ℃, the number of SiH decreases, and , on the other hand, SiH_2 and SiH_3 increase as shown in Fig. 1. This result explains the change of reflection high-energy diffraction pattern from 2x1 to 1x1. The SiH in the bulk network has not been observed. SR irradiation on the film at 140 ℃ after deposition shows that SiH_2 and SiH_3 are easily decomposed to SiH and that SiH decomposes much more slowly than SiH_2 and SiH_3.

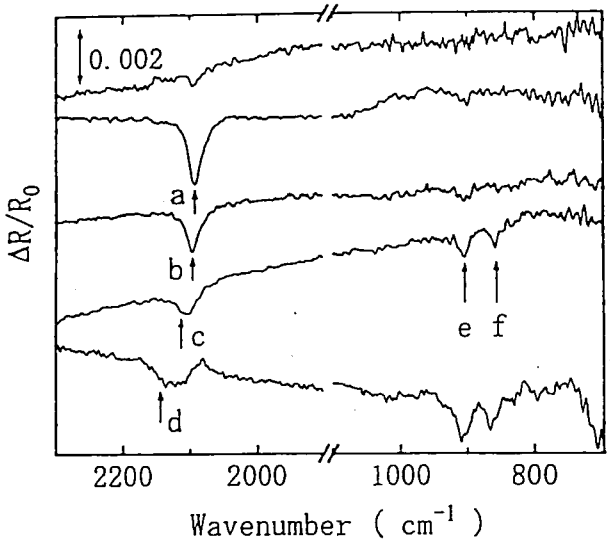


Figure 1. BML-IRAS spectra observed *in situ* during SR-GSMBE deposition of films on the Si(100) BML substrates. The substrate temperature and the dose are from the top to the bottom: 400 ℃-435 mA min; 370 ℃-442 mA min; 275 ℃-335 mA min; 140 ℃-335 mA min; and 50 ℃-300 mA min. The peaks indicated by arrows are assigned as (a) SiH, 2092 cm^{-1}; (b) SiH, 2100 cm^{-1}; (c)SiH_2, 2113 cm^{-1}; (d)SiH_3, 2140 cm^{-1}; (e) SiH_2, 908 cm^{-1} and (f) SiH_3, 860 cm^{-1}.

VI-D-2 Synchrotron Radiation Irradiation Effects for SiH_n on Si(100) Surface in the Synchrotron Radiation Stimulated Si Gas Source Molecular Beam Epitaxy

Akitaka YOSHIGOE, Mitsuru NAGASONO, Kazuhiko MASE and Tsuneo URISU

[*Jpn. J. Appl. Phys.* **34**, 6894 (1995)]

SiH_n on Si(100) surfaces during synchrotron radiation (SR) stimulated gas source molecular beam epitaxy (SR-GSMBE) using Si_2H_6 gas are investigated *in situ* by means of infrared reflection absorption spectroscopy using $CoSi_2$ buried metal layer substrates (BML-IRAS) in the low substrate temperature region (400 ℃-140℃). It has been found that SiH2 and SiH3 on the surface are easily decomposed by SR to SiH and the decom-position rate of SiH is extremely slow. The decomposition reaction cross sections for SiH_2 and SiH_3 for the total irradiating photon flux have been evaluated to be 5.7×10^{-20} cm^2 and 1.7×10^{-19} cm^2, respectively. Experimental results are discussed, considering the model of the localized multihole excitation and its quenching.

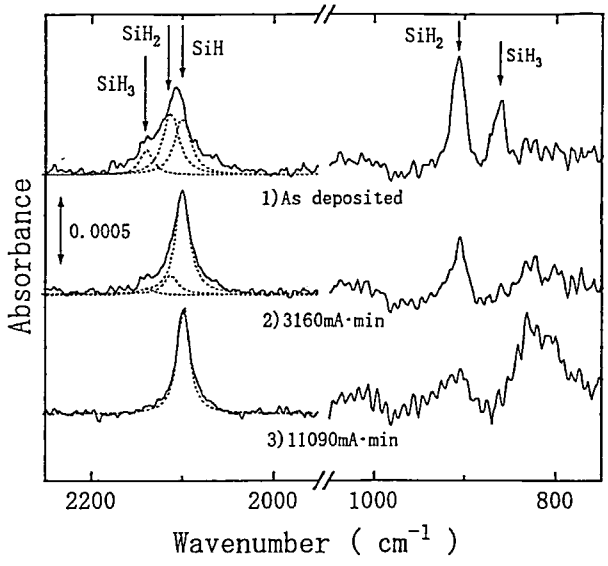


Figure 1. SR irradiation effects on the surface SiH_n.

VI-D-3 IRAS and TDS Study on the Photolytic Decarbonylation of Iron Pentacarbonyl Adsorbed on a SiO_2 Film with a Buried Metal Layer

Shinri SATO, Satoshi MINOURA, Tsuneo URISU and Yoshio TAKASU *(Shinshu Univ.)*

[*Appl. Surf. Science* **90**, 29 (1995)]

IR reflection-absorption spectroscopy (IRAS) is successfully applied to the observation of surface species

formed during the photolytic decarbonylation of $Fe(CO)_5$ adsorbed on a SiO_2 film with a buried Al layer, and thermal desorption spectroscopy (TDS) as well. TDS shows that $Fe(CO)_5$ is molecularly adsorbed on the SiO_2 surface at temperatures lower than 150 K. Irradiation of adsorbed $Fe(CO)_5$ with synchrotron radiation (SR) light (>150 nm) leads to CO photo-evolution due to photo-decarbonylation without the photo-desorption of molecular $Fe(CO)_5$. The average CO/Fe ratio in photo-product obtained from CO evolution during irradiation and subsequent TDS is close to 4, suggestive of formation of $Fe(CO)_4$ intermediate, while the photo-product exhibits broad IRAS band and a broad TDS peak with three maxima, indicative of formation of oligomer species. The photo-product is, however, unlikely to be $Fe_3(CO)_{12}$, a typical product of the photolysis of $Fe(CO)_5$ adsorbed on a SiO_2 powder, since its IRAS band disappears upon heating the substrate up to 200 K even though the product remains unchanged in composition. The disappearance of the band is interpreted in terms of the surface selection rule of IRAS as a change in the geometry of the product.

VI-D-4 Metallization on Piezoelectric Ceramics Surfaces by Synchrotron Radiation Irradiation

Junji OHARA,* Yoshitaka GOTO,* Masao NAGANUBO,* Takashi KURAHASHI,* Tadashi HATTORI,* *(*Nippondenso Co., Ltd)* **and Tsuneo URISU**

[*J. Electron Spectroscopy and Related Phenomena* **80,** 81(1996)]

In order to investigate the potential of applying the synchrotron radiation (SR) process to the micromachine field, the irradiation effects on a piezoceramics PZT $[Pb(Zr_x,Ti_{1-x})O_3]$ were studied. The desorption of O, Ti, Zr atoms from PZT was observed, and the irradiated surface of the sample became lead-rich as shown in Fig. 1. These selective desorptions refer to a modification of the ceramics surface into a metallic one. In fact ohmic conductivity was observed on the irradiated surface, whereas no conductivity was obtained on the unirradiated surface. The results obtained in this study are quite interesting from both aspects of desorption mechanism study and application to electrodes formation on piezoelectric devices.

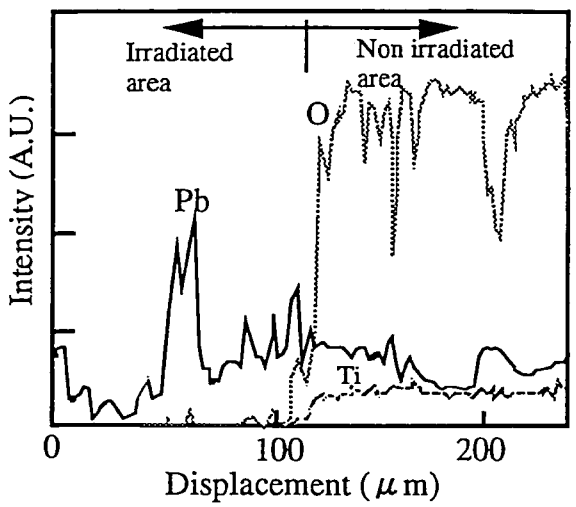


Figure 1. Line profile of AES with SR irradiated and non-irradiated PZT ceramics surface.

VI-D-5 Synchrotron Radiation-Stimulated Semiconductor Process and New Prospects of Core Electron Excitation Photochemistry

Tsuneo URISU, Akitaka YOSHIGOE and Yoshiaki IMAIZUMI

[*Optoelectronics -Devices and Technologies-* **11,** 57 (1996)]

The synchrotron radiation (SR)-stimulated surface processes have been actively studied as a new application field of SR in the last decade. The study of the mechanism of these surface photochemical reactions is necessary to clarify the characteristics unique to the SR-stimulated process and to develop an essentially new process technology. *In situ* observations of SR-stimulated Si gas source molecular beam epitaxy by infrared reflection absorption spectroscopy and SR irradiation effects on the dimethylaluminum hydride condensed layer by X-ray photoelectron spectroscopy suggest the potential importance of the site-specific chemical reaction in the condensed system induced by core electron excitation. A new process technique, selective core electron excitation using a monochromatized SR beam, is proposed.

VI-D-6 Synchrotron Radiation Irradiation Effects on Low-Temperature Condensed Layer of Dimethyl Aluminum Hydride on SiO_2 Surface

Yoshiaki IMAIZUMI, Yoshiyuki TSUSAKA and Tsuneo URISU

[*J. Electron Spectroscopy and Related Phenomena* **80,** 93(1996)]

The synchrotron radiation (SR) irradiation effects on the low temperature condensed layer of dimethyl aluminum hydride (DMAH) were investigated by infrared reflection absorption spectroscopy, quadrupole mass spectroscopy with neutral desorbed species, and x-ray photoelectron spectroscopy (XPS). Both photo-thermal effect and photo-decomposition reaction are induced by SR irradiation. The DMAH dimer forms are changed to trimer by the photo-thermal effects in the condensed layer. The C/Al ratio which is an important parameter of the Al thin film deposition is substantially decreased from the value of the as-deposited layer by SR photo-decomposition but not so much by Mg Kα irradiation decomposition. This indicate that the Al-C bond dissociation occur dominantly by SR irradiations and the C-H bond dissociation occur by Mg Kα irradiations. The SR irradiations may have the potential of less carbon contamination photo chemical vapor deposition.

VI-D-7 Development of Electron-Ion Coincidence Spectroscopy for the Study of Surface Dynamics Combined with Synchrotron Radiation

Kazuhiko MASE, Mitsuru NAGASONO, Shin-ichiro TANAKA, Masao KAMADA, Tsuneo URISU and Yshitada MARATA* *(*The University of Electro-communications)*

[*Rev Sci. Inst.,* submitted]

Energy-selected electron-ion coincidence (EICO) spectroscopy for the study of surface dynamics combined with

synchrotron radiation (SR) has been developed (Figure 1). The equipment consists of an electron gun, a cylindrical mirror analyzer (CMA), and a time-of-flight ion mass spectrometer (TOF-MS). A sample surface was excited by synchrotron radiation, and the energy of the emitted electron was analyzed by the CMA. The TOF spectrum of the desorbed ions was measured taking the energy-analyzed electron signal as the starting trigger. The Ions coincidently desorbed with the electron gave a characteristic peak in the TOF spectrum. The apparatus was evaluated on the basis of photoelectron-photoion coincidence (PEPICO) and Auger electron-photoion coincidence (AEPICO) measurements of H_2O condensed on a gold foil. The results demonstrate that PEPICO and AEPICO combined with SR are most powerful methods for investigating the ion desorption induced by core-level excitations.

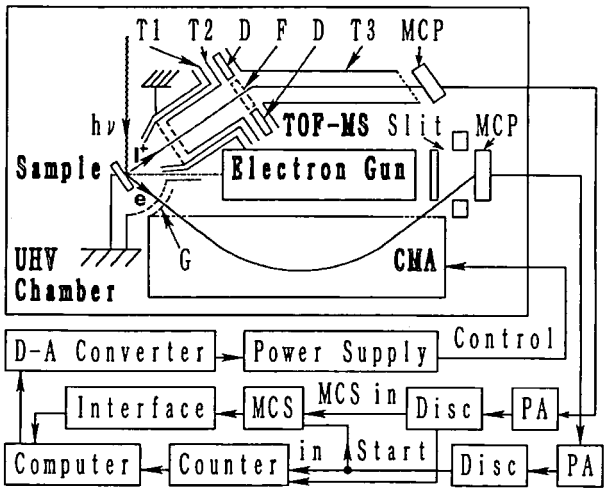


Figure 1. Schematic diagram of the apparatus for energy-selected electron-ion coincidence spectroscopy combined with synchrotron radiation. The abbreviations used are as follows: PA, preamplifier; Disc, discriminator; T1, drift tube with an extraction grid; T2, 95-mm-drift tube; F, focus; D, deflector; G, retarding grids; MCP, micro channel plates; MCS, multichannel scaler.

VI-D-8 Auger-Final-State Selected Ion Desorption Study of Condensed NH_3 and ND_3 by Using Auger Electron-Photoion Coincidence Spectroscopy

Mitsuru NAGASONO, Kazuhiko MASE, Shin-ichiro TANAKA and Tsuneo URISU

[*Surf. Sci.*, in press]

Photostimulated ion desorption induced by core level excitations is studied for condensed NH_3 and ND_3 by using Auger electron-photoion coincidence (AEPICO) spectroscopy with synchrotron radiation. A series of AEPICO spectra for condensed NH_3 and ND_3 are measured as a function of the electron kinetic energy around the N(KVV) Auger electron energy range. Both AEPICO yield of H^+ and D^+ are enhanced at the electron kinetic energies corresponding to N(KVV) Auger transitions (figure 1), which provide a clear evidence of Auger stimulated ion desorption mechanism. We analyzed the fine structure of the AEPICO yield spectra on the basis of the assignment of Auger-final-states, and concluded that Auger-final-states containing two holes in the same valence orbital efficiently lead to the ion desorption. The AEPICO yield of D^+ is found to be one-third to one-half as small as that of H^+. We concluded that the isotope effect is derived from the reneutralization of D^+ on the surface because of the slow desorption velocity of D^+ compared with that of H^+.

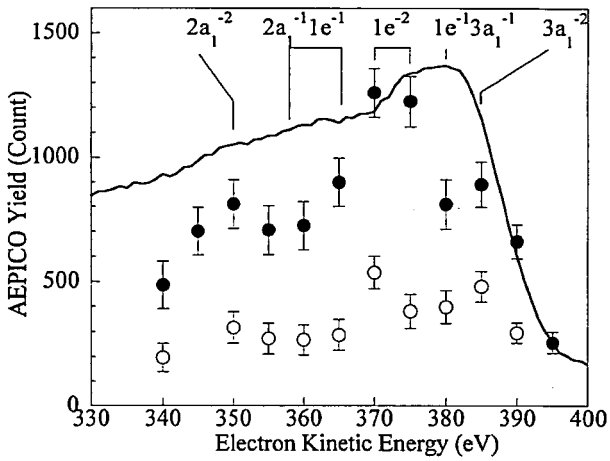


Figure 1. AEPICO yield spectra of H^+ (closed circle) and D^+ (opened circle), and AES (solid line) of NH_3/Au as a function of the electron kinetic energy around N(KVV).

VI-E Photoionization Dynamics Studied by Electron Spectroscopy Combined with a Continuous Synchrotron Radiation Source

Molecular photoionization is a major phenomenon in vacuum UV excitation and provides a large amount of information on fundamental electron-core interactions in molecules. Especially, autoionizing and shape resonances become of main interest, since they often dominate photoabsorption cross sections and lead to various vibronic states which are inaccessible in direct ionization. In order to elucidate dynamical aspects of photoionization, we have developed a versatile machine for photoelectron spectroscopy. Introduction of a new methodology, two-dimensional photoelectron spectroscopy, allows us to investigate autoionization and predissociation of superexcited states of acetylene, nitric oxide, carbonyl sulfide, sulfur dioxide and so on. In this method, the photoelectron yield is measured as a function of both photon energy and electron kinetic energy (binding energy). The spectrum, usually represented as a contour plot, contains rich information on photoionization dynamics.

VI-E-1 Observation of the $(3\sigma_g)^{-1}(3p\sigma_u)^1$ Rydberg State of Acetylene

Hideo HATTORI, Yasumasa HIKOSAKA,* Takumi HIKIDA* and Koichiro MITSUKE *(*Tokyo Inst. of Tech.)*

[*J. Chem. Phys.*, submitted]

Photoelectron spectra of C_2H_2 are measured with a resolution of 30 meV. Panels (a) and (b) of Figure 1 show spectra at photon energies of 13.287 and 14.120 eV, respectively. Panel (a) displays strong excitation of the ν_1 mode in combination with 0 and 1 quantum of the ν_2 mode, which results from autoionization of the valence state $(3\sigma_g)^{-1}(3\sigma_u)^1$. Here, ν_1 and ν_2 correspond mainly to symmetric C-H and C-C stretching vibrations, respectively. Vibrational constants of $C_2H_2^+(X\,^2\Pi_u)$ are estimated by the least-squares fit of the ionization energies of the peaks to the second order anharmonic expansion for these modes. The obtained values are $\omega_1 = 0.410$ eV, $\omega_2 = 0.228$ eV, $x_{11} = -0.007$, $x_{22} = -0.001$, and $x_{12} = -0.002$. On the other hand, a complicated vibrational distribution is observed in Panel (b). A prominent feature is strong excitation of the *trans*-bending vibration (the ν_4 mode), which may reflect the bent geometry of the Rydberg state $(3\sigma_g)^{-1}(3p\pi_u)^1$.

Panel (c) shows a photoelectron spectrum at 13.821 eV; this photon energy falls under the higher energy side of a broad and intense absorption band of the $(3\sigma_g)^{-1}(3\sigma_u)^1$ state. Comparing Panel (c) with the other panels indicates that excitation occurs in the ν_4 mode as well as in the ν_1 and ν_2 modes. This vibrational excitation is attributed to autoionization of an unknown excited state whose potential energy surface is similar to that of the Rydberg state $(3\sigma_g)^{-1}(3p\pi_u)^1$, since only a little difference is observed in the vibrational distribution between Panels (b) and (c). Thus, the excited state lying at ~13.8 eV is concluded to be the Rydberg state $(3\sigma_g)^{-1}(3p\sigma_u)^1$.

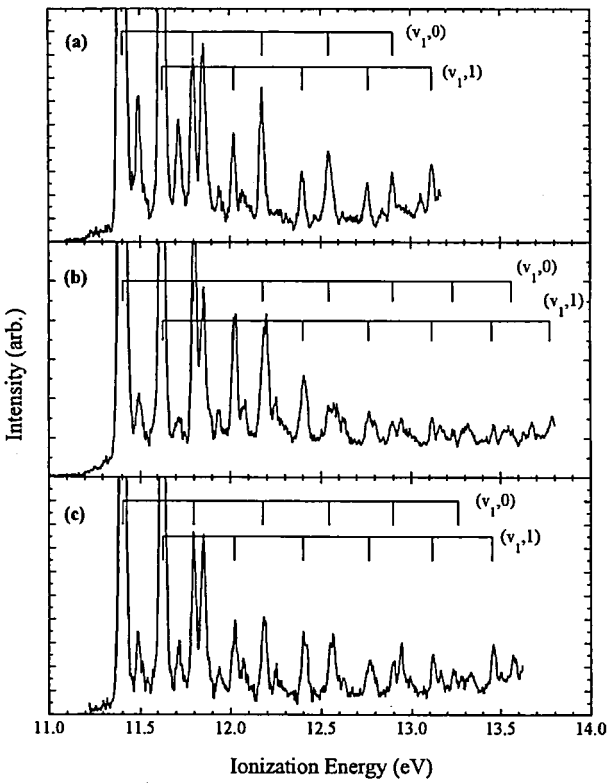


Figure 1. Photoelectron spectra of C_2H_2 taken at photon energies of (a) 13.287, (b) 14.120, and (c) 13.821 eV. The ν_1 progressions in combination with zero and one ν_2 quantum are indicated by bar lines.

VI-E-2 Formation of Autoionizing Atomic Nitrogen from Superexcited States of Nitric Oxide

Yasumasa HIKOSAKA,* Hideo HATTORI, Takumi HIKIDA* and Koichiro MITSUKE *(*Tokyo Inst. of Tech.)*

[*J. Chem. Phys.* **105**, 6367 (1996)]

Photodissociation of NO followed by autoionization of an N atom has been studied by two-dimensional photoelectron spectroscopy using synchrotron radiation. In addition to the bands due to molecular ionization, the two-dimensional spectrum shows several characteristic patterns in the photon energy range of 21.5 - 27 eV which result from autoionization of the Rydberg states converging to $N^+(^1D^e)$ into the ionic ground state $N^+(^3P^e)$. The electronic states of the counter atomic oxygen can be determined from the lower onset energies of these patterns to be $^3P^e$ and/or $^1D^e$. Discussion is made about the transition region for the photodissociation reaction, especially being focused on the nature of the primary molecular states and their dynamical aspects including competitive molecular autoionization.

VI-E-3 Autoionization of Sulfur Atom Produced by Dissociation of Superexcited OCS

Yasumasa HIKOSAKA*, Hideo HATTORI, Takumi HIKIDA* and Koichiro MITSUKE *(*Tokyo Inst. of Tech.)*

Photodissociation of OCS followed by autoionization of an S atom has been studied by two-dimensional photoelectron spectroscopy using synchrotron radiation. Figure 1a) shows a two-dimensional photoelectron spectrum of OCS at the photon energy from 14.2 to 16.8 eV. The vertical axis corresponds to the incident photon energy $E_{h\nu}$ and horizontal axis to the kinetic energy E_k of the ejected electron. Figure 1b) represents the curve obtained by summing electron counts over the whole range of E_k as a function of $E_{h\nu}$. This curve resembles photoabsorption and photoionization spectra very much, and the observed peaks are assignable to the Rydberg states $OCS^*(R_B)$ converging to $OCS^+(\tilde{B}^2\Sigma^+)$ whose vibrational ground state lies at 16.04 eV. Diagonal stripes varying in width from several tens to a few hundreds millielectron volts on Figure 1a) correspond to molecular ionization into vibronic states of OCS^+. If autoionizing transitions of dissociated fragments take place between two particular states, one may expect that emission of electrons with a constant kinetic energy results in a pattern running parallel to the photon energy axis. Actually, several vertical patterns observed at $E_{h\nu}$ = 15-16.8 eV can be interpreted in terms of the two-step mechanism: (1) neutral dissociation of $OCS^*(R_B)$ into a superexcited Rydberg atom, S*[converging to $S^+(^2D^o)$], and $CO(\tilde{X}^1\Sigma^+)$, and (2) delayed autoionization of S* into the ground state $S^+(^4S^o)$. Since electron yields in these patterns are apparently enhanced at photon energies for the $OCS^*(R_B)$ states, a part of autoionizing sulfur atoms are produced by conversion of $OCS^*(R_B)$ to neutral predissociating states.

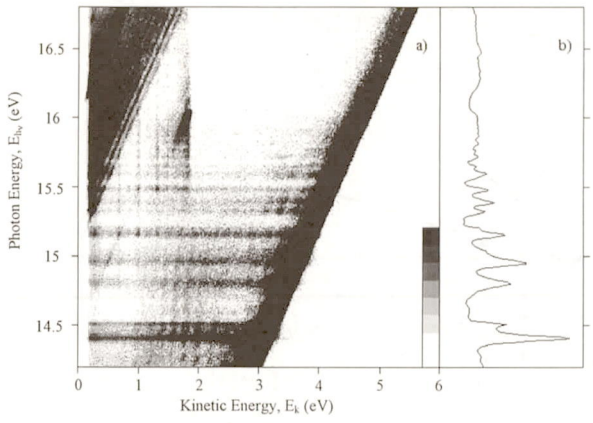


Figure 1. a) Two-dimensional photoelectron spectrum of OCS. The electron counts are plotted on a linear scale and intense structures are truncated. b) The curve obtained by summing electron counts of the two-dimensional spectrum over the whole range of E_k as a function of E_{hv}.

VI-E-4 Autoionization of Superexcited Sulfur Atoms Produced from Doubly Excited Rydberg States of SO_2

Hideo HATTORI, Yasumasa HIKOSAKA* and Koichiro MITSUKE *(*Tokyo Inst. of Tech.)*

Photoelectron spectra of SO_2 are measured at several photon energies between 22 and 32 eV. Three typical spectra are shown in Figure 1. We can identify some peaks whose electron kinetic energy remains constant, independently of the photon energy. In analogy to the N* formation from superexcited states of NO, these peaks are considered to result from autoionizing transitions from superexcited sulfur atoms S* produced by photodissociation of SO_2:

$$SO_2 + h\nu \rightarrow SO_2^* \rightarrow S^* + 2O$$
$$S^* \rightarrow S^+(^4S^o) + e^-.$$

By comparing with the results of proton-impact electron spectroscopy,[1] most of the peaks in Figure 1 are assigned to the Rydberg states converging to $S^+(^2D^o)$, the first excited ionic state. It is probable that SO_2 is primarily excited to doubly excited Rydberg states converging to SO_2^+ satellite states. The S* atoms are then formed by direct dissociation of these primary states.

Reference

1) F. Penent, J. P. Grouard, J. L. Montmagnon and R. I. Hall, *J. Phys. B* **23,** 2105 (1990).

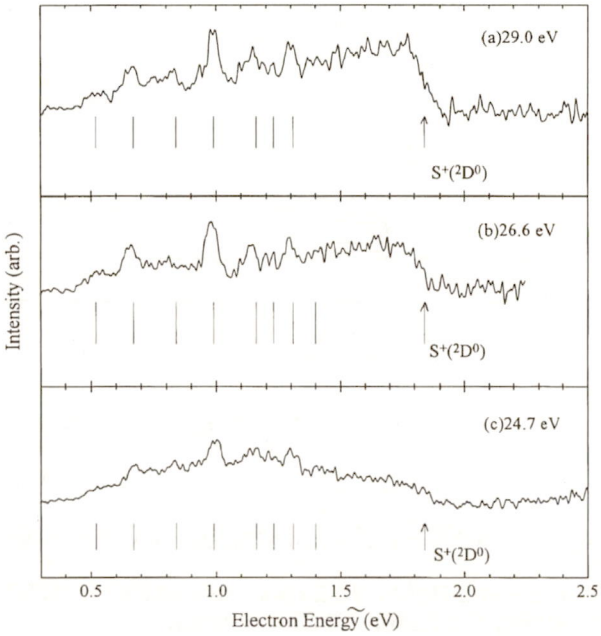


Figure 1. Photoelectron spectra of SO_2 at photon energies of (a) 29.0, (b) 26.6, and (c) 24.7 eV. Bar lines denote the positions of the S* Rydberg states converging to $S^+(^2D^o)$. The ionization energy for S^+ is indicated by the arrows.

VI-F Vacuum UV Spectroscopy Making Use of the Combination of Synchrotron Radiation and Mode-Locked UV Laser

We have developed the ultraviolet laser system synchronizing precisely with the pulses of synchrotron radiation (SR) from the storage ring of the UVSOR facility. A mode-locked Ti:sapphire laser oscillating at 90.115MHz (the frequency for the multibunch operation mode of UVSOR) provides the third harmonic which covers a wavelength range from 243 to 280 nm. The reliability and feasibility of this laser-SR combination technique have been demonstrated by applying pump-probe experiments to several physical systems.

VI-F-1 Detector of the Laser and SR Photon Pulses

Masakazu MIZUTANI, Manabu TOKESHI*, Atsunari HIRAYA and Koichiro MITSUKE** *(*Kyushu Univ., **Hiroshima Univ. and IMS)*

In order to attain perfect synchronization between the laser light and SR, their photon pulses should be simultaneously detected by using an ultrafast photosensitive device. As illustrated in Figure 1, we assembled a photon detector composed of a photomultiplier, a quartz window, a copper block and luminescing substances. The copper block, having a triangular prism shape, is placed in vacuum and connected to the rod of a linear-motion feedthrough so as to be easily put in and out of the path of the photon beams without breaking the system vacuum. The laser light impinges on one of the rectangular sides covered by a thick film of *p*-terphenyl which emits fluorescence at ~ 340 nm by laser excitation. A piece of BaF_2 crystal pasted on the other rectangular side is shined with SR (~ 58 nm) and emits Auger-free luminescence at ~ 220 nm. The two lights from the block pass the quartz window and are simultaneously detected with a metal package photomultiplier. The output signal of the photomultiplier is amplified by a preamplifier and fed into a digital oscilloscope. The duration of the laser and SR pulses are 1.8 and 400 ps, respectively, but a trace of the oscilloscope exhibits peak widths of approximately 2 ns. This broadening may be ascribed to the time constant of the detector and the radiative lifetime of the luminescing substances.

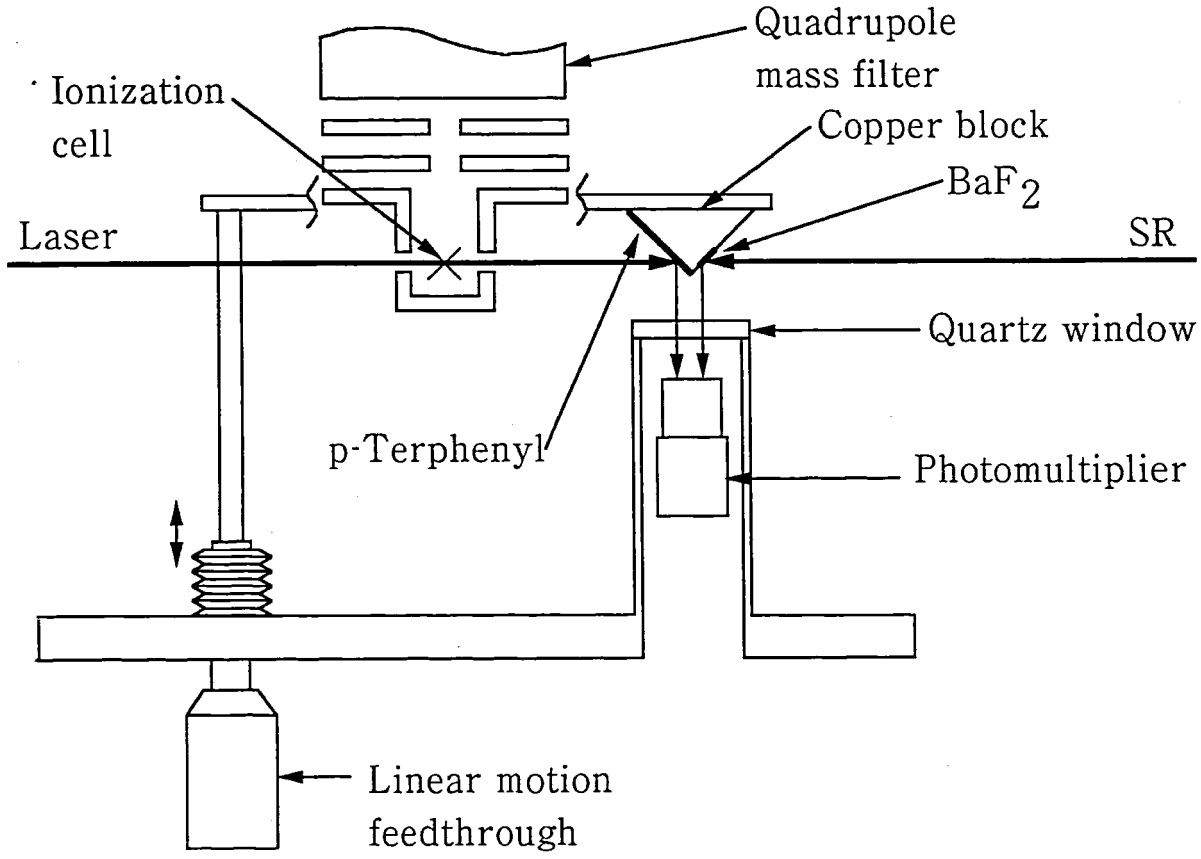


Figure 1. Schematic diagram of the detector of the laser and SR photon pulses.

VI-F-2 Time-Resolved Experiment of $He^*(1s2p\ ^1P)$ by Using the Laser-SR Combination

Masakazu MIZUTANI, Manabu TOKESHI*, Atsunari HIRAYA and Koichiro MITSUKE** *(*Kyushu Univ., **Hiroshima Univ. and IMS)*

[*J. Synchrotron Radiation,* in press]

Combining ultraviolet laser with SR for time-resolved pump-probe spectroscopy has been developed for investigating the dynamics of excited molecules. A mode-locked Ti:sapphire laser is made to oscillate at the frequency of the UVSOR storage ring. The third harmonic of the laser is available at a wavelength range from 243 to 280 nm. Synchrotron radiation from an undulator is monochromatized by a grazing-incidence monochromator and introduced coaxially with the laser beam. A molecular beam, which is discharged from a nozzle made of a multi-channel capillary array, intersects with the two photon beams at 90°. Produced photoions are analyzed by a quadrupole mass filter placed perpendicularly with the photon beams and the molecular beam. The temporal profile of the photon pulses is monitored *in situ* by a luminescing substance/photomultiplier combination. The delay timing between the laser and SR can be changed from 0 to 11 ns with a resolution of 0.1 ns by adjusting an electronic module which provides phase-locked loop stabilization of the laser pulse.

The reliability and feasibility of this method are confirmed by the resonant two-photon ionization. A helium atom is excited with a 21.218 eV photon to the $1s2p\ ^1P$ state whose lifetime is known to be 0.555 ps. This state is subsequently ionized with a 4.8 eV photon of the laser. Figure 1 shows the ratio between He^+ signal counts with and without the laser as a function of the delay of the laser pulse with respect to the SR pulse. The background level is estimated to be ~ 0.95. The He^+ counts are found to be enhanced in a narrow time window from -100 to +400 ps. This enhancement can be accounted for by the signals due to the two-photon ionization by way of He^* ($1s2p\ ^1P$).

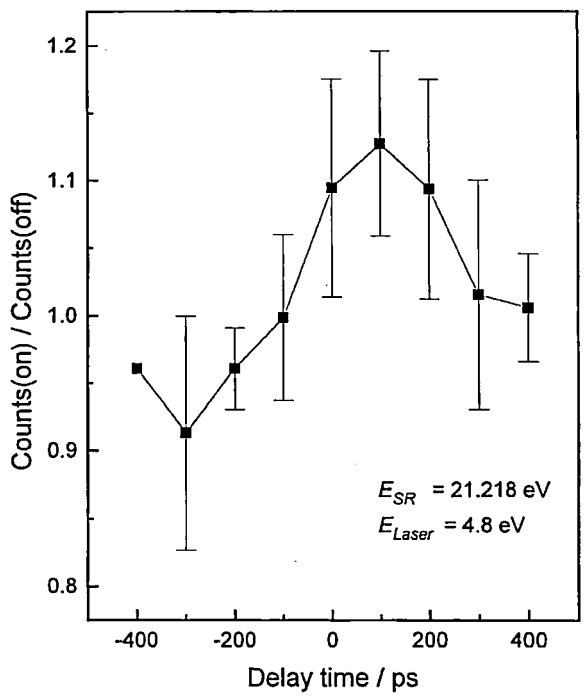


Figure 1. The ratio between the ion counts with and without the laser as a function of the delay of the laser pulse with respect to the SR pulse.

VI-G Rebuilding the Monochromator on the Beamline BL2B2 in UVSOR

On the beamline BL2B2, we are planning to construct a grazing incidence monochromator which supplies photons in the energy region from 20 to 200 eV. This monochromator will bridge the energy gap between the beamlines BL3A2 and BL8B1, thus providing for an accelerating demand for the high-resolution and high-flux photon beam from the research field of photoexcitation of inner-valence electrons or *L*-shell electrons in the second-row atom.

VI-G-1 Main Parameters of the Renewed Beamline

Hiroaki YOSHIDA and Koichiro MITSUKE

An 18m spherical grating monochromator (SGM) with high resolution and high flux is now being manufactured and will be installed in the spring of 1997 on the bending-magnet beamline BL2B2. The schematic layout of the beamline was shown in the Annual Review for 1995 (p. 110). The SGM is designed to cover the energy range of 20 - 200 eV with a resolving power ($E/\Delta E$) of more than 5000 and photon flux of more than 10^{10} photons/s/100mA. Its main parameters are presented in Table 1.

Optical element Mirrors(M) & Gratings(G)		Radii R × ρ (mm)	Material	Coating	Reflective area (mm^2)	Grazing angle (°)
Elliptic cylinder	M0	28914	fuzed quartz	Au	500×20	6.5
Spherical	M1	22580	fuzed quartz	Au	400×30	5.0
Spherical	G1	18000	fuzed quartz	Au	130×20	10.0 (0th order)
	G2	18000	fuzed quartz	Au	130×20	10.0 (0th order)
	G3	9300	fuzed quartz	Au	130×20	20.0 (0th order)
Plane	M2		fuzed quartz	Al	250×20	15.0
Plane	M3		fuzed quartz	Al	600×20	5.0
Troidal	M4	18358×202	fuzed quartz	Au	300×50	5.0

VI-H Absolute Photoabsorption Cross Section and Radiative Dissociation of Polyatomic Molecule Excited at Valence Shell

Determination of total photoabsorption cross section in a wide energy region is the fundamental step for physical and chemical investigation of material. Most of oscillator strengths (photoabsorption cross sections) of molecule are distributed in the energy region up to ≈50 eV, in which the Rydberg, superexcited and ionized states are produced. Absolute photoabsorption cross section and dissociative excitation process of the electronically excited photofragment(s) have been studied in the valence excitation region using synchrotron radiation on the BL2A beamline of UVSOR facility.

VI-H-1 Photoabsorption Cross Section and Radiative Processes of $GeCl_4$ in the Valence Region of 6-31 eV

Toshio IBUKI and Akiko KAMAMOTO*(Kyoto Univ. Educ.)*

[*Chem. Phys. Lett.* **260**, 314 (1996)]

Photoabsorption and emission cross sections of $GeCl_4$ have been measured in the region 6-31 eV. Absolute values obtained by using synchrotron radiation can be subject to serious errors unless higher order light is eliminated. In the present work we used an argon gas filter to suppress the higher order light in the region of 11.3-15.5 eV (110-80 nm), and at $h\nu$<10.8 eV (105 nm) a LiF window was used. The electronic configuration of the valence shell is given by $(2a_1)^2(2t_2)^6(1e)^4(3t_2)^6(1t_1)^6$. The bands observed in the photoabsorption and fluorescence excitation spectra have been assigned as the (4*s*, 4*d*, and n*p*) ← $3t_2$, (4*s* and n*p*) ← 1*e*, and (4*s* and 4*p*) ← $2t_2$ Rydberg transitions where n=4-6. Strong emissions have been observed for the $\tilde{C}^2T_2 \rightarrow \tilde{X}T_1$ *a*nd $\tilde{C}^2T_2 \rightarrow \tilde{A}^2T_2$ transitions of $GeCl_4^+$ molecular ion and the $GeCl_2(^3B_1 \rightarrow \tilde{X}^1A_1)$ triplet radical. Weak fluorescence from the singlet $GeCl_2(\tilde{A}^1B_1 \rightarrow \tilde{X}^1A_1)$ process has also been observed. Absolute total emission cross section has been obtained to be 23.1 ± 0.8 Mb at 21.22 eV. The ionization potential of the $2t_2$ molecular orbital has been determined to be 14.65 ± 0.08 eV.

VI-H-2 Photoabsorption and Fluorescence Excitation Spectra of CF_3CN in the Region of 6-41 eV

Toshio IBUKI and Kazumasa OKADA

[*Chem. Phys. Lett.* in press]

Little spectral information is available on the fluorinated compounds. Total photoabsorption and fluorescence cross sections of gaseous CF_3CN have been measured in the region 6-41 eV. The photoabsorption spectrum observed has little resolvable structure. The bands deconvoluted by using the Gaussian functions have been assigned as the Rydberg transitions to the *ns* (n=3-5), 3*p*, and 3*d* levels of the lone pair electrons on the N and F atoms of CF_3CN. From the analysis of fine structures observed at the 12-15 eV, it has shown that the C≡N and C-F stretching modes and FCF bending frequency are excited in the Rydberg states. Emissions from CN* radical formed are observed for the $A^2\Pi_i \rightarrow X^2\Sigma^+$ and $B^2\Sigma^+ \rightarrow X^2\Sigma^+$ transitions. The fluorescence excitation functions run parallel with the photoabsorption cross section and their intensities suddenly strengthen at 15.44 ± 0.02 eV, in which a repulsive channel to decompose into CF_3 + CN* may open. The emission intensities are increased at = ~ 20 eV by the ionization of the $(2e)^{-1}$ and $(4a_1)^{-1}$ valence electrons which represent the lone pair electrons on the F atoms.

VI-H-3 Photoabsorption and Emission Cross Sections of $SnCl_4$ and $Sn(CH_3)_4$ in the 6-31 eV Region

Ikuo TOKUE *(Niigata Univ.)*, **Kazumasa OKADA and Toshio IBUKI**

The absorption spectrum of $SnCl_4$ showed several peaks in the 6-12 eV range, while that of $Sn(CH_3)_4$ was very broad. Assuming T_d symmetry for $SnCl_4$, the electronic configuration of the valence shell in the ground state is $(2a_1)^2(2t_2)^6(1e)^4(3t_2)^6(1t_1)^6$. The three outermost orbitals are n_{Cl} localized on Cl atoms and the $2t_2$ is σ(Sn-Cl). The absorption peaks observed in the 8.4-11.8 eV range for $SiCl_4$ have been assigned as the Rydberg series converging to the $(1t_1)^{-1}$, $(3t_2)^{-1}$, $(1e)^{-1}$, and $(2t_2)^{-1}$ ionic states. Mean term values obtained for the 4*s*, n*p* (n=4,5), and 4*d* Rydberg transitions are 2.12 ± 0.10, 1.69 ± 0.07, and 0.08 ± 0.04, respectively, which are close to those for Cl atom. The fluorescence excitation spectrum of $SnCl_4$ shows five peaks in the 9-12 eV range and two broad bands around 15.5 and 21.7 eV. The origin of the former peaks is attributed to the $SnCl_2(^3B_1 \rightarrow X)$ transition on the basis of the excitation threshold measured by the use of sharp cutoff filters. The bands observed at 15.5 and 21.7 eV are mainly composed of the $SnCl(A^2\Delta \rightarrow X^2P)$ emission and the Sn I atomic lines, respectively. The fluorescence excitation spectrum of $Sn(CH_3)_4$ shows structure-less bands peaked at 14.5 and 21 eV. The emission cross sections for these bands are about one tenth of those for $SnCl_4$ in the same energy range. The quantum yields for the total fluorescence were measured for both $SnCl_4$ and $Sn(CH_3)_4$ molecules.

VI-H-4 Hydrogen Isotope Effect in the Photodissociative Excitation of CH_3CN, CD_3CN, C_2H_5CN and C_2D_5CN

Toshio IBUKI, Kazumasa OKADA, Mitsuhiko KONO, Atsunari HIRAYA *(Hiroshima Univ.)* **and Kosuke SHOBATAKE** *(Nagoya Univ.)*

In the photodissociative excitation of the titled molecules, emissions from the $B^2\Sigma^+$ and $A^2\Pi_i$ states of CN radical were observed in the region of 8-30 eV. Absolute fluorescence cross sections for the $CN(B^2\Sigma^+)$ radicals were measured for the H- and D-substituted compounds. In acetonitrile the isotopic ratio in the $CN(B^2\Sigma^+)$ emission, $\rho_f(D)/\rho_f(H)$, increases from ≈1 at 10.8 eV to 3.2 at 11.3 eV, and the isotopic ratio decreases again to ≈1 at 21 eV. That is, the hydrogen isotope effect depends strongly on the available excess energy of molecule and negligibly on the electronic state(s) produced primarily. In the wide energy region of 8-30 eV, the total photoabsorption cross sections of the H- and D-acetonitriles agree within a few percent difference. In addition, the study of laser photolyses of the H- and D-acetonitriles at 121.6 nm (10.20 eV) have shown no isotope effect in producing H and D atoms.[1] From these observations we propose a cyclic dark channel which competes with formation of the emitting CN* radical:

$$CX_3CN^* \rightarrow [\text{cyclic complex}]^{\ddagger} \rightarrow CX_2 + XCN,$$
$$CX_3CN^* \rightarrow CX_3 + CN^*, \quad X=H \text{ or } D.$$

In a cyclic activated complex, a H or D atom can make a bridged chemical bond, and thus the tunneling effect effectively works for H-acetonitrile. That is, the larger tunneling effect, the weaker CN* emission intensity in H-acetonitrile. As the primary photon energy is getting higher, the energy eigenstates of the active degrees of freedom for the activated complexes of H- and D-compounds become close, and the $\rho_f(D)/\rho_f(H)$ ratio again decreases to unity. Similar hydrogen isotope effect has been observed in H- and D-propionitriles. The symmetry assignments of the n*p* and 3*d* Rydberg transitions observed in the photoabsorption spectra of CH_3CN and CD_3CN are studied by measuring of the $CN(B \rightarrow X)$ fluorescence anisotropy at the 10.7-11.8 eV (150-105 nm) range.

Reference

1) Private communication from Prof. Honma.

VI-H-5 Photoabsorption Cross Section of C_6F_5X (X=H, F, Cl, Br, I) and Fluorescence Excitation Spectra of $C_6F_5X^{\cdot+}$ Radical Cation in the 30-160 nm Region

Takumi HIKIDA *(Tokyo Inst. Tech.)*, **Kazumasa OKADA and Toshio IBUKI**

Photoabsorption spectra of C_6F_5X (X=H, F, Cl, Br, I) molecules and fluorescence excitation spectra of the photoproducts have been measured in the excitation region 30-160 nm at the BL2A beamline of UVSOR. Nearly the same photoabsorption spectra were observed for these molecules. The main absorption appeared between 120 and 30 nm and two broad peaks around 85 and 60 nm with barely resolved vibrational structures were observed. Similar structured emission excitation spectra were found to start at ≈ 100 up to 35 nm. The ionization energies determined from the threshold wavelengths of the excitation spectra were 12.4, 12.5, 12.1 12.0 and 11.2 eV for X=H, F, Cl, Br and I, respectively. The results indicate that the transitions were between two $(\pi)^{-1}$ ionic states of the photo-products, $C_6F_5X^{\cdot+}$ (X=H, F, Cl, Br, I).

VI-H-6 Photodissociation Spectroscopy of BrCN in the Vacuum Ultraviolet Region

Kazuhiro KANDA *(Iwaki Meisei Univ.)*, **Kosuke SHOBATAKE** *(Nagoya Univ.)*, **Mitsuhiko KONO, Takashi NAGATA and Toshio IBUKI**

Photoabsorption cross section of BrCN and absolute cross section for production of the CN($B^2\Sigma^+ \rightarrow X^2\Sigma^+$) emission were determined in the wavelengths range 40-120 nm. The measurements were performed in window-less experimental configuration, where a gas filter was employed in the wavelengths shorter than LiF cut-off. The quantum yield for the CN($B^2\Sigma^+$) production was obtained from these cross sections. The yield observed increases gradually with the excitation energy from ≅0.05 at 120 nm to ≅0.1 at 105 nm, with a sudden decrease around 104 nm. This decrease corresponds to the opening of the 1st ionization channel of BrCN. In the photoabsorption spectrum, a broad continuum was observed below 91 nm, which corresponds to the 2nd ionization potential. In the wavelength region 91-104 nm, several absorption bands which are ascribed to the transition to the superexcited states, were observed. These states are assigned as the Rydberg series converging to the 2nd ionization potential. On the basis of these measurements, the spectral assignments of the dominant bands in the energy region higher than the 2nd ionization potential are also discussed.

VI-H-7 Photoexcited States of Malononitrile in the VUV Energy Region

Kiyohiko TABAYASHI,* Shinobu UCHIDA,* Koh SAITO, *(*Hiroshima Univ.)*, **Mitsuhiko KONO and Toshio IBUKI**

Photochemistry of simple mono-cyanides, such as HCN, XCN, and CH_3CN has been relatively well studied in the VUV region, since they produce fluorescent CN($B^2\Sigma^+$, $A^2\Pi_i$) fragments from which discussions about photodissociation dynamics are frequently available. Here we extended VUV spectroscopic measurements to dicyano compound, and photoabsorption and fluorescence excitation cross sections for malononitrile, $CH_2(CN)_2$, have been firstly determined in the 105-200 nm energy region.

The observed photoabsorption bands are interpreted in terms of intervalence and the Rydberg transitions of the outer shell electrons. The Rydberg transition $R \leftarrow 2b_1(\pi_{CN})$ was found to be accompanied by vibrational progressions. They are assigned to be the CH_2 scissors and CCC bending frequencies based on *ab initio* MO analysis of the ground and ionic states. In the measurement of dispersed fluorescence spectrum, the CN($A^2\Pi_i \rightarrow X^2\Sigma^+$) and CN($B^2\Sigma^+ \rightarrow X^2\Sigma^+$) emissions have been identified when malononitrile was excited at an intense absorption peak of 124.5 nm. The dissociative excitations, $CH_2(CN)_2 + h\nu \rightarrow CH_2CN + CN(A$ and $B)$, are then confirmed as the prominent fluorescent channels. The emission intensities from the CN(A) and CN(B) radicals were isolated by use of optical filters and the absolute fluorescence cross sections were determined by normalizing with those of CH_3CN molecule. The emission quantum yields for the CN(A and B) radicals show monotonous decrease with decreasing the excitation energy, indicating of no prominent excited state which strongly couples with the dissociative excitation channels.

VI-I Angle-Resolved Photofragmentation of Polyatomic Molecule Excited at *K*-Shell

Reaction dynamics of polyatomic molecule excited at *K*-shell is an unexplored field of research. We have constructed a new experimental apparatus for studying reaction mechanism of the inner core excited polyatomic molecules on the BL8B1 beamline of UVSOR. Photon energy of 30-900 eV is available. The reaction chamber rotates at the angles from -20° to 110° with respect to the direction of the linear polarization of synchrotron radiation. The apparatus has been open to the users who belong to Universities since April 1996. This project started in April 1995 when Prof. Ibuki joined IMS, and Dr. Okada joined to his group recently.

VI-I-1 Reaction Processes of CF_3CN Excited at the *K*-Edge of C, N, and F Atoms

Toshio IBUKI, Kazumasa OKADA, Tatsuo GEJYO, Junichi ADACHI, Atunari HIRAYA *(Hiroshima Univ.)* **and Eiji ISHIGURO** *(Univ. of Ryukyu)*

Breakdown pathways of CF_3CN molecule were studied by exciting *K*-edge of F, N, and C around 690, 400, and 290 eV, respectively, by using TOF mass spectroscopy: Photofragmentation was measured at the energies of excitation from the *K*-shell to the π^* and σ^* levels. Fragment ions observed are C^+, F^+, CN^+, CF^+, CF_2CN^{2+}, CF_2^+, CF_3^+, and CF_2CN^+, neither N^+ nor parent ion. At the right angles, i. e., the photoions formed fly perpendicularly to the direction of the linear polarization of synchrotron radiation, the fragment ions with kinetic energy 0 are dominantly produced at $\pi^* \leftarrow N(1s)$ when compared with those at the $\sigma^* \leftarrow N(1s)$ and the F(1*s*) excitations. At $\sigma^* \leftarrow F(1s)$ large fragment ions such as CF_2CN^+ and CF_3^+ are one order of magnitude more than those at the π^* and $\sigma^* \leftarrow N(1s)$ levels. A large chemical shift of 10.5 eV was observed between the π^* excitations of $C_F(1s)$ and $C_N(1s)$. At the *K*-edge of $C_F(1s)$ the C^+ ion is the most dominant fragment and is about two times larger than that at π^* and $\sigma^* \leftarrow C_N(1s)$, that is, site-selective fragmentation was observed. The difference between the 0° and 90° experiments is not so clear except the data at the $\pi^* \leftarrow N(1s)$ excitation.

VI-J Elucidation of Ion-Solid Chemistry in Ion-Implanted Amorphous SiO_2 and Creation of Novel Materials by Implantation

A variety of structural defects are produced in amorphous SiO_2 and related materials by ion implantation. Characterization of structures, concentrations and depth profiles may provide valuable information on interactions of implanted ions with substrate structure. We consider that some defects may be the origin of new photonic functions such as refractive index gratings and second harmonic generations. In this sense, "defects" may be regarded as "active species" for optoelectronic applications. The purpose of this project is to elucidate chemical interactions of implanted ions with amorphous SiO_2 through structural defects and to create novel photonic materials utilizing activities to photons.

VI-J-1 Proton-Implantation-Induced Nanosized Ge Crystal Formation in SiO_2:GeO_2 Glasses

Ken-ichi KAWAMURA(*Tokyo Inst. Tech.*), **Hideo HOSONO and Hiroshi KAWAZOE**(*Tokyo Inst. Tech.*)

[*J. Appl. Phys.* **80**, 1357-1363(1996)]

Nanometer-sized crystalline Ge colloid particles in $9SiO_2$-$1GeO_2$ glasses were formed by implantation of protons at 1.5 MeV without post-thermal annealing. Although oxygen-deficient type point defects associated with Ge ions were primarily formed to fluences $\lesssim 1\times10^{17}$ cm^{-2}, the formation of Ge fine crystalline particles was observed for fluences $\gtrsim 5\times10^{17}$ cm^{-2}. No formation of Ge colloids and the Ge-related point defects were noted for implantation of 1.5 MeV He^+ to a fluence of 1×10^{18} cm^{-2}. The depth of Ge colloid formation layers was 22-26μm from the implanted surface. This depth region agreed well with the peak region of electronic energy deposition. Ge-OH groups were formed preferentially over Si-OH groups upon implantation of protons and the decay curve upon isochronal annealing was close to that of the optical absorption at ~ 3eV, which was attributed to nanometer-sized Ge. A red photoluminescence peaking at ~ 1.9 eV was observed for all the implanted substrates. A tentative formation mechanism of Ge colloids in these glasses was proposed.

VI-J-2 Probing Interface Properties of Nanocomposites by Third-Order Nonlinear Optics

L. YANG(*Vanderbilt Univ.*), **D. H. OSBORNE**(*Vanderbilt Univ.*), **R.F. HAGLUND, Jr.**(*Vanderbilt Univ.*) , **R. H. MAGRUDER**(*Vanderbilt Univ.*), **C. W. WHITE**(*Oak Ridge Nat. Lab.*), **R. A. ZUHR**(*Oak Ridge Nat. Lab.*) **and Hideo HOSONO**

[*Appl. Phys. A* **62**, 403-415(1996)]

We describe the exploitation of third-order nonlinear optical response — particularly nonlinear absorption and the nonlinear index of refraction — to probe interface dynamics, modifications and relaxation processes in granular materials consisting of metal quantum dots embedded in such dielectrics as fused silica and sapphire. Many features of these materials can be interpreted in terms of the quantum-mechanical model of the "particle-in-a-box". Electronic and thermal relaxation processes in these novel nanocomposites are dominated by interactions of conduction-band electrons at the boundary between the quantum dot and its surrounding host material. Experimental examples presented include measurements of thermal and electronic relaxation rates, dephasing due to electron collisions at the nanocluster surface, effects of local structural order, changes in the saturation parameter due to chemical modification of the substrate, and one-and two-dimensional heat-transfer effects.

VI-K Electronic Structure Design of Wide Gap Conductors and Control of Their Conduction Behavior

Electronic structure of high oxidized p-block metal oxides is of interest from the view point of their variety of the optical and electrical properties. The oxides with band gaps near 3 eV are attractive because they have the specific properties of metallic conduction keeping the transparency to the visible light and have various application such as a transparent electrode of a liquid crystal display, a heat reflector glass, solar cell and so on. In this project , it is aimed to establish a basis of the material design of wide gap semiconductors and to create noble materials. Ongoing study is characterization of the electronic structure of these materials by using synchrotron radiation, control of conduction behavior by ion-implantation and construction of the apparatus of inverse photoemission spectroscopy.

VI-K-1 Working Hypothesis to Explore Novel Wide Band Gap Electrically Conducting Amorphous Oxides and Examples

Hideo HOSONO, Naoto KIKUCHI(*Tokyo Inst. Tech.*), **Naoyuki UEDA and Hiroshi KAWAZOE**(*Tokyo Inst. Tech.*)

[*J. Non-Cryst. Solids* **198-200**, 165-169(1996)]

A working hypothesis for exploring optically transparent and electrically conducting amorphous oxides is proposed on the basis of simple considerations concerning chemical bonding. The hypothesis predicts that amorphous oxides composed of heavy metal cations with an electronic configuration of $(n\text{-}1)d^{10}ns^0$ may be converted into transparent conducting amorphous oxides when doped by Li ion implantation or heating at temperatures below crystallization. Three new materials, amorphous Cd_2GeO_4, $AgSbO_3$ and Cd_2PbO_4, have been prepared as examples.

VI-K-2 Amorphous Transparent Electroconductor $2CdO \cdot GeO_2$: Conversion of Amorphous Insulating Cadmium Germanate by Ion Implantation

Hideo HOSONO, Naoto KIKUCHI(*Tokyo Inst. Tech.*), **Naoyuki UEDA and Hiroshi KAWAZOE**(*Tokyo Inst. Tech.*) **and Ken-ichi SHIMIDZU**(*Keio Univ.*)

[*Appl. Phys. Lett.* **67**, 2663(1995)]

Amorphous $2CdO \cdot GeO_2$ thin films(optical band gap determined by a Tauc plot; 3.4 eV) prepared by rf sputtering were implanted with H^+ or Li^+ ions to a dose of 2×10^{16} cm^{-2}. Direct current conductivities in the specimens at 300 K were increased from 3×10^{-9} S cm^{-1} to ~10 S cm^{-1} after the implantation. The conductivities in these implanted specimens remained almost constant down to 77 K. No deleterious coloring was perceived after implantation. The Hall mobilities (conduction type; *n*) in the implanted specimens at ~300 K were ~5 $cm^2 V^{-1} s^{-1}$, which are larger by several orders of magnitude than those in existing amorphous semiconductors. Such a large mobility indicates that the electronic state near the bottom of the conduction band of this amorphous material is extended.

VI-K-3 New Amorphous Semiconductor: $2CdO \cdot PbO_x$

Hideo HOSONO, Yasuhisa YAMASHITA*(Tokyo Inst. Tech.)*, **Naoyuki UEDA, Hiroshi KAWAZOE***(Tokyo Inst. Tech.)* **and Ken-ichi SHIMIDZU***(Keio Univ.)*

[*Appl. Phys. Lett.* **68**, 661(1996)]

A new amorphous semiconductor, $2CdO \cdot PbO_x$(band gap: 1.58 eV), was found. Thin films of this material were prepared by rf sputtering of a Cd_2PbO_4 target in O_2-Ar. The dc conductivity of the resulting amorphous thin films was ~ 180 S cm^{-1} at 300 K and remained almost constant down to ~ 4 K. The concentration of carrier electrons and the Hall mobility in the as-deposited state were 1×10^{20} cm^{-3} and 9 $cm^2 V^{-1} s^{-1}$, respectively. When the as-deposited specimens were heated to 250℃ , which is far below the crystallization(to Cd_2PbO_4) temperature(460℃), the conductivity and the carrier concentration at 300 K became approximately twice as high. The thermal O_2-desorption measurements demonstrated that carrier electrons are generated via the formation of oxygen vacancies at the initial stage (< 250℃) of thermal desorption of O_2 from the amorphous structure. The effective mass of carrier electrons was estimated as 0.57 m_0.

VI-K-4 Features of Valence Band Structure of $TlAlF_4$

Hiroshi MIZOGUCHI*(Tokyo Inst. Tech.)*, **Takahisa OMATA***(Tokyo Inst. Tech.)*, **Hiroshi KAWAZOE***(Tokyo Inst. Tech.)*, **Satoru FUJITSU***(Shonan Inst. Tech.)* **Hideo HOSONO and Naoyuki UEDA**

[*J. Phys. C* **8**, 303-312 (1996)]

Modulation of the upper edge of valence band of ionic solids by $6s^2$ occupied states of Tl^+ is a primary origin of the changes in optical and electrical properties of host materials containing Tl^+. Semiquantitative estimation of mixing of $6s^2$ states on Tl^+ ions with $2p^6$ on F^- ions in the $TlAlF_4$ crystal was carried out by photoemission, optical absorption, photoluminescence and photocurrent measurements. Photoemission spectra were measured with excitation energies of 60, 130 and 1486.7 eV. The separation between the uppermost two bands was found to be 2.5 eV for $TlAlF_4$ and TlF, which were considerably greater than the corresponding values for TlCl and TlBr. This was interpreted as due to the fact that the energy level of F 2p is deeper than Cl 3p and Br 4p. It was concluded from the excitation energy dependences of the intensities of the respective peaks in the valence band region that the contribution of Tl 6s to the top edge of the valence band of $TlAlF_4$ and TlF was several tens of a per cent. A large Stokes shift of about 2 eV and the long lifetime(1.2μs) of fluorescence suggested that the $6s^2$ levels of Tl^+ ions have a tendency to localize and the top of the valence band did not form such an extended state of TlBr. This conclusion was confirmed by the observation that the photocurrent of $TlAlF_4$ was one fifth of that TlBr.

VI-L UV Photoelectron Spectroscopic Study of Functional Organic Materials and their Interfaces with Metals

Recently, electronically functional organic materials have attracted much attention in relation to their possible applications such as molecular devices, photography, electrophotography, organic electroluminescent (EL) devices and organic solar cells. Often these functions appear at the interfaces of the organic materials with inorganic materials, such as metals. Thus the elucidation of the electronic structures of their bulk and interface is of crucial importance in understanding and improving the devices. We have investigated model interfaces of (i) porphyrin solar cells and (ii) organic EL devices using UV photoelectron spectroscopy (UPS). We also investigated the bulk electronic structure of short oligomer of poly(*p*-phenylene) and examined the translational symmetry in the molecule.

VI-L-1 Electronic Structures of Porphyrins and Their Interfaces with Metals Studies by UV Photoemission

Hisao ISHII, Daisuke YOSHIMURA*, Kiyoshi SUGIYAMA*, Satoru NARIOKA*, Masaki SEI*, Shinji HASEGAWA, Yutaka HARIMA, Kazuo YAMASHITA**, Yukio OUCHI* and Kazuhiko SEKI***
*(*Nagoya Univ. **Hiroshima Univ.)*

[*Mol. Cryst. Liq. Cryst.*, submitted]

The electronic structures of porphyrins and their interfaces with metals were investigated by UV photoemission spectroscopy (UPS). The UPS spectral features of porphine, 5,10,15,20-tetraphenylporphynatozinc(II) (ZnTPP), 5,10,15,20-Tetra(4-pyridyl)porphyrin ($H_2T(4\text{-}Py)P$) and 5,10,15,20-tetra-phenylporphyrin (H_2TPP) could be assigned by comparison with MOPAC PM3 calculations. The electronic structures of the porphyrins can be regarded as the superposition of those of porphine and the substituents. The UPS results for ZnTPP/metal (Mg, Al, Ag, Au) interfaces indicated that the energies of the levels of ZnTPP relative to the Fermi level of substrate metals could be expressed as linear functions of the work function of metals with a shift of the vacuum level at interface. The slope of the linear functions was about unity. This indicates that

the energy levels of ZnTPP are fixed to the vacuum level of substrate metal with constant interfacial dipole. The level positions of ZnTPP at the interface exhibited drastic change by exposure to oxygen. This change could be explained by the change of the work function of metal surface upon oxidization. For $H_2T(4\text{-Py})P$ and H_2TPP/metal (Mg, Ag, Au) interfaces, similar linearity was observed between the energy levels of porphyrin and the work function of metal with the slope of much smaller than unity. This deviation of the slope from unity might be explained by the existence of interface state. These findings require the modification of the traditional concept of a common vacuum level at organic/metal interface. The relation between the observed electronic structures and the conduction type of the porphyrins are also discussed.

VI-L-2 Electronic Structures of Organic Carrier Transporting Material/Metal Interfaces as a Model Interface of Electroluminescent Devices Studied by UV Photomission

Kiyoshi SUGIYAMA*, Daisuke YOSHIMURA*, Eisuke ITO*, Takafumi MIYAZAKI, Yukiko HAMATANI*, Ikuko KAWAMOTO*, Hisao ISHII, Yukio OUCHI* and Kazuhiko SEKI*** *(*Nagoya Univ. **Toyama Univ.)*

[*Synth. Met.* in press]

Electronic structures of N,N'-diphenyl-N,N'-(3-methylphenyl)-1,1'-biphenyl-4,4'-diamine (TPD) / metal and N,N'-dipehyl-1,4,5,8-naphtyltetracarboxylimide (DP-NTCI) / metal interfaces were directly investigated as a model interface of organic electroluminescent (EL) devices using UV photoemission spectroscopy (UPS). At the organic / metal interfaces, abrupt shifts of vacuum level was observed, in contrast to the traditional assumption of common vacuum level at the interfaces. The observed electronic structures were consistent with the carrier-injecting character of the real devices, while the estimated electronic structures by the neglect of vacuum level shift at the interface lead to an incorrect prediction of carrier-injecting nature of the interfaces. These findings strongly suggest the necessity of the direct observation of the interfacial electronic structure by UPS or other techniques for understanding EL devices.

VI-L-3 Angle-Resolved Ultraviolet Photoelectron Spectroscopy of Oriented Film of Model Compound of Poly(*p*-Phenylene): Wave Number(*k*)-Conservation and *k*-Blurring in a System with Small Number of Repeating Units

Hisao ISHII, Satoru NARIOKA*, Kunishige EDAMATSU, Koji KAMIYA***, Shinji HASEGAWA, Toshiaki OHTA****, Nobuo UENO*** and Kazuhiko SEKI*** *(*Nagoya Univ. **Hiroshima Univ. ***Chiba Univ. ****Univ. of Tokyo)*

[*Phys. Rev.* **B52**, 2362-2373(1995)]

The electronic structure of oriented thin films of sexiphenyl (6P) as a short model compound of poly(*p*-phenylene) (PPP) was investigated by angle-resolved ultraviolet photoelectron spectroscopy (ARUPS) using synchrotron radiation. The sample film of 6P was prepared by vacuum evaporation onto a heated Ag substrate. Infrared reflection-absorption spectroscopy, x-ray diffraction, and the observed selection rules for ARUPS indicated that the 6P molecules are highly oriented aligning its molecular axis parallel to the surface normal. In the normal emission spectra of ARUPS, the band intensity of the HOMO and the next HOMO was enhanced at hv=28~40eV. This enhancement can be explained in terms of the wave number(k)-conservation rule in the one-dimensional intramolecular band with some initial state broadening of k (or relaxation of k-conservation rule) due to the small number of repeating units. This indicates that wave number k along the molecular axis serves as a reasonably good quantum number even in a system consisting of only six repeating units.

VI-M Ultraviolet Photoelectron Spectroscopy of Organic and Inorganic Solids

Work of ultraviolet photoelectron spectroscopy (UPS) of organic solids and inorganic compounds has been proceeded. Further, using a photoelectron spectrometer combined with synchrotron radiation light source (UVSOR-UPS) the UPS spectra of several materials were observed.

VI-M-1 Determination of Two-Dimensional Structures of Ultrathin Films of H_2- and Cu-phthalocyanine on MoS_2 by Angle-Resolved Ultraviolet Photoemissn and Low Energy Electron Diffraction

Koji KAMIYA *(Chiba Univ.)*, **Masahiro MOMOSE** *(Chiba Univ.)*, **Akinori KITAMURA** *(Chiba Univ)*, **Yoshiya Harada** *(Chiba Univ.)*, **Nobuo UENO** *(Chiba Univ.)*, **Sinnji HASEGAWA, Takafumi MIYAZAKI** *(Toyama Univ.)*, **Hiroo INOKUCHI, Satoru NARIOKA** *(Nagoya Univ.)*, **Hisao ISHII and Kazuhiko SEKI** *(Nagoya Univ.)*

[*J. Electron Spectr. Relat. Phenom.* **76**, 213 (1995)]

The angle-resolved ultraviolet photoelectron spectra of ultrathin films of metal-free phthalocyanine (H_2Pc) and copper phthalocyanine (CuPc) on MoS_2 single crystal surfaces were measured using synchrotron radiation. The take-off and azimuthal angle dependencies of the photoelectron intensity were analyzed using independent-atomic-center approximation combined with molecular orbital calculation. Further, the low energy electron diffraction was observed for the same ultrathin films. The results indicate that H_2Pc and CuPc molecules form a square lattice with respect to the three equivalent crystal axes of the MoS_2 surface, and at the lattice point lie flat on the substrate with a molecular azimuthal rotation of about 7°.

VI-M-2 Strucure of Ultrathin Films of Chloroalminium Phthalocyanine on MoS_2 Studied by Means of Penning Ionization Electron Spectroscopy, Angle-Resolved UPS and LEED

Masaru AOKI(*Univ. of Tokyo*), **Sigeru MASUDA**(*Univ. of Tokyo*), **Yuichi EINAGA**(*Chiba Univ.*), **Koji KAMIYA**(*Chiba Univ.*), **Akinori KITAMURA**(*Chiba Univ.*), **Masahiro MOMOSE**(*Chiba Univ.*), **Nobuo UENO**(*Chiba Univ.*), **Yoshiya HARADA**(*Chiba Univ.*), **Takafumi MIYAZAKI**(*Toyama Univ.*), **Sinnji HASEGAWA, Hiroo INOKUCHI and Kazuhiko SEKI**(*Nagoya Univ.*)

[*J. Electron Spectr. Relat. Phenom.* **76**, 259 (1995)]

The structure of ultra-thin films (0.5-5 monolayers) of chloroalminium phthalocyanine (ClAlPc) on an MoS_2 substrate was studied by Penning ionization electron spectroscopy (PIES), angle resolved ultraviolet photoelectron spectroscopy (ARUPS) and low-energy electron diffraction (LEED). The change in the molecular orientation was sensitively detected during the variation of the thickness and temperature of the film.

VI-M-3 Photoemission Study on Poly(pyridine-2,5-diyl), Poly(2,2'-bipyridine-5,5'-diyl), and their K-doped States

Takayuki MIYAMAE, Daisuke YOSHIMURA (*Nagoya Univ.*), **Hisao ISHII, Yukio OUCHI**(*Nagoya Univ.*), **Takafumi MIYAZAKI, Tuneaki KOIKE**(*Mitsui Petrochem. Industries LTD*), **Takakazu YAMAMOTO** (*Tokyo Inst. Tech*) **and Kazuhiko SEKI**(*Nagoya Univ.*)

[*J. Electron Spectr. Relat. Phenom.* **78** 399 (1996)]

Ultraviolet photoelectron spectra were measured using synchrotron radiation for two kinds of π-conjugated polymers, poly(pyridine-2,5-diyl) (PPy) and poly(2,2'-bipyridine-5,5'-diyl) (PBPy) which exhibit n-type electrically conducting properties. The two compounds show similar spectra, and they were analyzed with MO calculations. Upon potassium doping of PBPy, two new states appeared in the originally empty energy gap. This finding indicates that bipolaron bands are formed in K-doped PBPy. While K-doped PPy also shows similar gap states, it requires higher dopant concentration to create bipolaron bands than in the case of K-doped PBPy. The difference of the dependence on dopant concentration between K-doped PPy and K-doped PBPy is discussed based on the conformational difference between these polymers.

VI-M-4 Photoemission Spectroscopy of Bi_2CuO_4

Osamu AKAKI(*Tohoku Univg.*), **Ashish CHINANI** (*Tohoku Univ.*), **Takashi TAKAHASHI**(*Tohoku Univ.*) **and Shoichi HOSOYA**(*Yamanashi Univ.*)

We have studied the electronic structure of Bi_2CuO_4 using resonant photoemission spectroscopy. The photoemission spectrum exhibits a small peak about 1 eV away from the Fermi level indicative of a gap opening. This peak is ascribed to the Cu-O hybridized states with the $^1A_{1g}$ symmetry. Since negligible difference in the photoemission-spectral shape is observed in the photon energy range from 20 to 40 eV, the hybridization strength between the Cu 3d and O 2p states is sizably strong. The photoemission spectrum at the Cu3p-3d core threshold (about 74 eV) exhibits a "resonance peak" at about 13 eV binding energy, which has been attributed to the "two-hole-bound state" in the final state. This suggests that the valency of Cu atoms is 2(Cu^{2+}) and the correlation energy between Cu 3d electrons is about 5.5 eV.

VI-M-5 Physical Properties and Electronic Structure of Potassium-Oxygen-Graphite Intercalation Compounds

Tetsuo YAMASHITA(*Tokyo Inst. of Tech.*), **Toshiaki ENOKI** (*Tokyo Inst. of Tech.*),**Kyuya YAKUSHI, Takayuki MIYAMAE and Takafumi MIYAZAKI**

We investigated the Hall, effect, the transverse magnetoresistance, the optical reflectivity and the ultraviolet photoelectron spectra for 1st and 2nd stage of KO_x-GICs ($C_{4n}KO_x$, stage number n=1,2;x~2) in order to clarify the transport properties and the electronic structures. The Hall effect and the magnetoresistance indicate that the electrical conduction in KO_x-GICs is governed by the majority electron carriers with low mobility in graphitic p bands and the minority hole carriers with high mobility in the intercalate bands, the latter of which originates mainly from the oxygen bands as suggested by the incident photon energy dependence of the ultraviolet photoelectron spectra. The optical reflectance spectra give the estimates of the Fermi energies, 1.9 eV and 1.35 eV for 1st and 2nd stage compounds, respectively, on the basis of the Drude-Lorentz model. The contribution of the intercalate hole carriers to the plasma frequency is small in good agreement with the Hall effect indicating the presence of minority hole carriers. These experimental findings suggest the contribution of the intercalate layer to the transport properties and the electronic structure around the Fermi level.

VI-M-6 Ultraviolet Photoelectron Spectra of C_{86} and C_{90}

Shojun HINO (*Chiba Univ.*), **Kazunori UMISHITA** (*Chiba Univ.*), **Kentaro IWASAKI** (*Chiba Univ.*), **Takafumi MIYAZAKI** (*Nagoya Univ. and IMS*), **Koichi KIKUCHI** (*Tokyo Metropol. Univ.*) **and Yohji ACHIBA** (*Tokyo Metropol. Univ.*)

[*Phys. Rev.* **B53**, 7496-7499 (1996)]

Ultraviolet photoelectron spectra (UPS) of higher fullerenes, C_{86} and C_{90}, both of them having C_2 symmetry were measured with a synchrotron radiation light source. The spectral bands above 4.5 eV are characteristic to individual fullerene, while those below 5 eV resemble each other and they are similar to other higher fullerenes. Figure 1 shows the UPS of C_{90}. Its second band envelop can be divided into two parts of which structure has not been observed in other higher fullerenes up to the moment. Upon the incident photon energy change, the intensity of the bands oscillates and their peak positions shift. Figure 2 shows the intensity of the UPS band as a function of the incident photon energy. The bands above 5 eV of both C_2-C_{86} and C_2-C_{90} show a similar incident photon energy dependent intensity oscillation, which suggests that the origin of the intensity oscillation of fullerenes are closely related its molecular nature such as hollow cage structure.

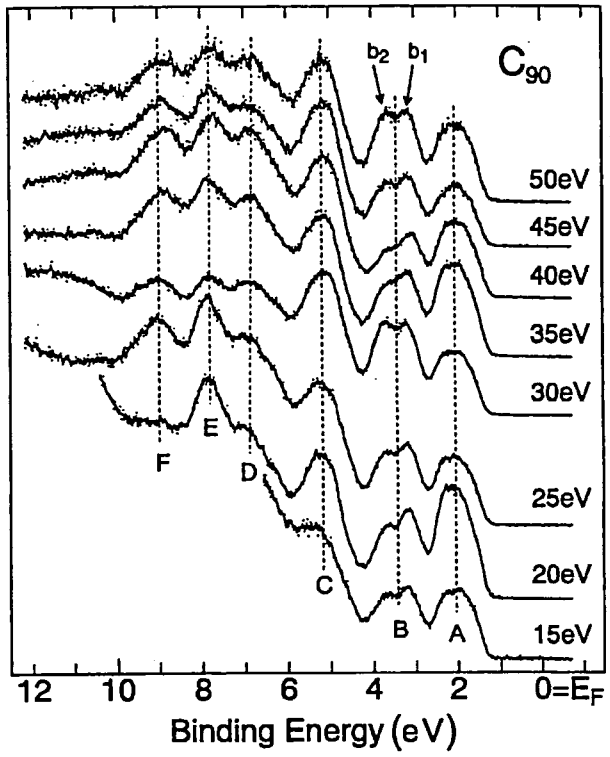


Figure 1. The incident-photon-energy dependence of the UPS of C_2-C_{90}.

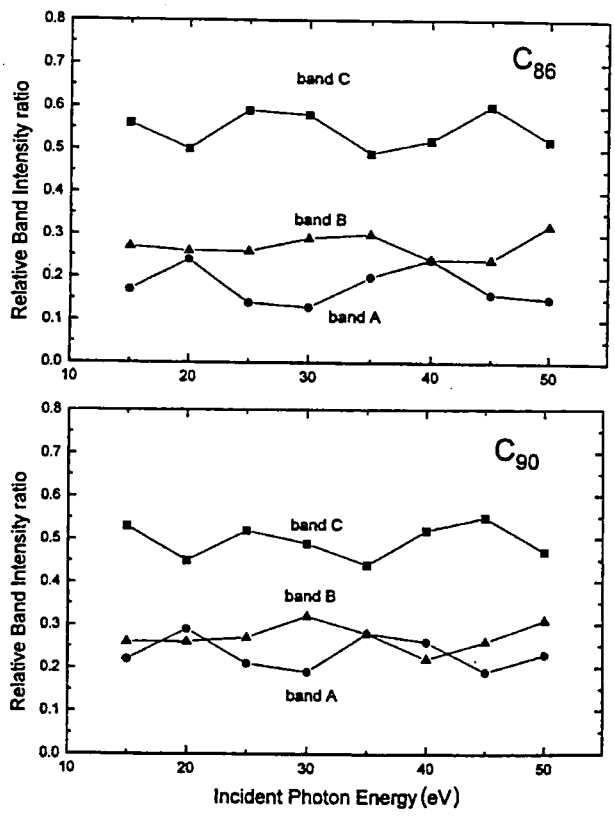


Figure 2. The relative intensity of the bands *A*-*C* of C_2-C_{86} and C_2-C_{96} ploted as a function of the incident-photon energy. The intensity of each band is normalized by the sum of bands *A*-*C*.

VI-M-7 Photoelectron Spectra of Metal Fullerenes: Are Metal Fullerenes Molecular Crystals or Not?

Shojun HINO *(Chiba Univ.)*, **Kentaro IWASAKI** *(Chiba Univ.)*, **Kazunori UMISHITA** *(Chiba Univ.)*, **Takafumi MIYAZAKI** *(IMS)*, **Koichi KIKUCHI** *(Tokyo Metropol. Univ.)* **and Yohji ACHIBA** *(Tokyo Metropol. Univ.)*

[*J. Electron Spectrosc. Relat. Phenom.* **78**, 493-496 (1996)]

Ultraviolet photoelectron spectra (UPS) of GdC_{82} and La_2C_{80} were measured using a synchrotron radiation. The specimens for the measurement were not evaporated films but drying up films obtained from the metal fullerene solutions. Although the effect of the contamination to the specimens remains even after heat treatment, the UPS of the GdC_{82} film (Figure. 1) show several characteristic structures that are essentially identical to those of LaC_{82}. This suggests that the interaction between the GdC_{82} molecules are small and GdC_{82} can be treated as a molecular crystal. The spectrum of La_2C_{80} differs from those of other fullerenes, which indicates either that the interaction among the La_2C_{80} molecules are too large to give a sharp spectrum or that the molecule does not have so-called cage structure.

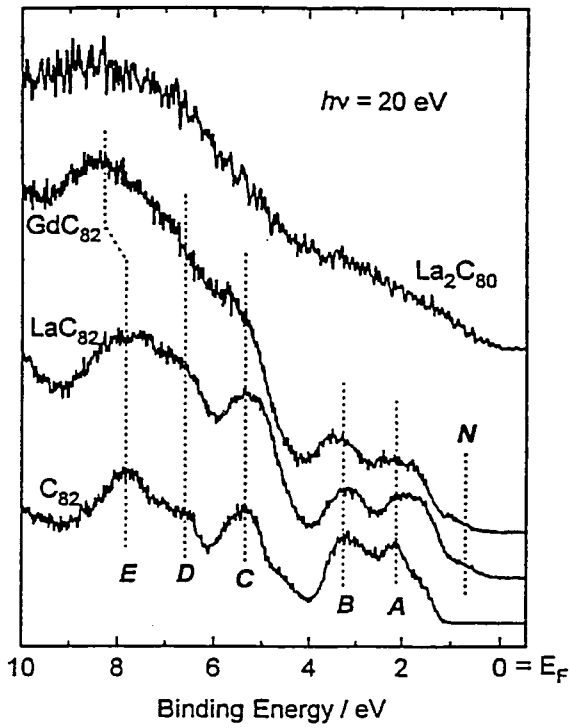


Figure 1. The $h\nu$ = 20 eV spectra of metal fullerenes, LaC_{82}, GdC_{82}, and La_2C_{80}. the spectrum of C_{82} is also shown for comparison.

RESEARCH ACTIVITIES VII
Coordination Chemistry Laboratories

Prof. Yuzo Yoshikawa, Assoc. Prof. Hiroshi Nakazawa, Dr. Yasushige Kuroda, and Dr. Tsutomu Mizuta finished their term in March 1996 in the laboratory of Synthetic Coordination Chemistry, and returned to Okayama University and Hiroshima University. Their contribution to the Coordination Chemistry Laboratories (CCL) during their term is immense and highly acknowledged. Prof. Masa-aki Haga, Prof. Takeshi Sakurai, Dr. Sadamu Takeda, and Dr. Hideaki Monjushiro took the position of Synthetic Coordination Chemistry from April 1996. Dr. Kentaro Tanaka took the position of Assist. Prof. of Laboratory Complex Catalysis. Prof. Yutaka Fukuda (Ochanomizu Women's University) and Assoc. Prof. Kiyoshi Sawada (Niigata University) finished their term as Adjunct Prof. in March 1996 in the Laboratory of Complex Catalysis. Their effort during their term is gratefully appreciated. Prof. Megumu Munakata (Kinki University) and Assoc. Prof. Naohide Matsumoto (Kyushu University) continued their position as Adjunct Prof. of the laboratory of Coordination Bond.

VII-A Proton-induced Molecular Switches Using Supramolecular Metal Complexes

Supramolecular metal complexes as precursors for molecular devices have attracted much attention in recent years. A molecular switching by an external stimulus is one of fundamental functions in the supramolecular complexes. Protonation can act as an external trigger in complexes containing basic sites. We have developed the chemical principle underlying the proton-induced switching in 2-(2-pyridyl)benzimidazole Ru complexes. In order to achieve the proton-induced switching systems, the interlocking between the potential change by protonation/deprotonation and the pKa change by Ru(II) to Ru(III) oxidation is responsible. The judicious molecular design of the Ru complexes containing benzimidazole ligands allows us to synthesize the novel supramolecular metal complexes with bistable property. Our synthetic strategy is the following: (1) The intrinsic properties of monomeric complex are thoroughly examined from the viewpoint of photoactive, electroactive, or proton-responsive building blocks for molecular devices. (2) The monomeric complex modules are organized or integrated for building up the molecular assemblies. Particularly, "complexes-as-ligands" method is useful to synthesize the dendrimer type tri- and tetranuclear complexes. We found that electrospray mass spectra is one of the powerful tools to characterize these polynuclear metal complexes with high positive charge and to check the purity of the complexes.

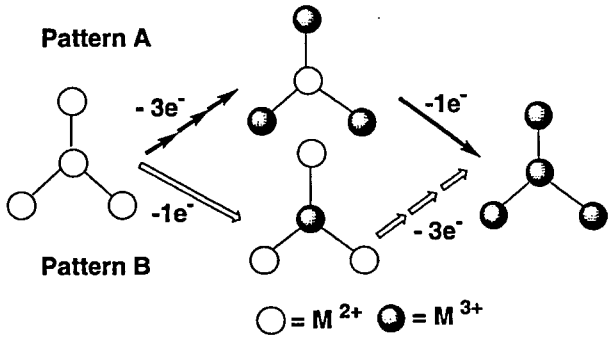
VII-A-1 Proton-induced Switching of Electron Transfer Pathways in Dendrimer-Type Tetranuclear $RuOs_3$ Complexes

Masa-aki HAGA, Md. Meser ALI and Ryuichi ARAKAWA *(Osaka Univ.)*

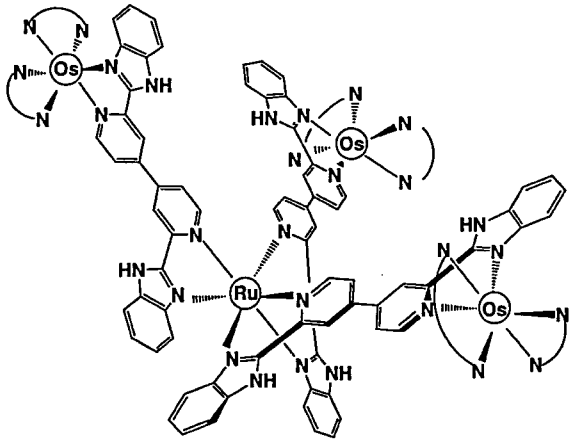
[*Angew. Chem. Int. Ed. Engl*, **35**, 76-78 (1996)]

Reversible protonation of uncoordinated nitrogen site in 2-(2-pyridyl)benzimidazole Ru complexes induces the change of redox potential. This chemical principle has been applied to the dendrimer type tetranuclear $RuOs_3$ complexes. Two oxidation patterns have been reported in ligand-bridged dendrimer tetranuclear complexes: i.e., pattern A consists in simultaneous oxidation of three peripheral metals at almost same potentials prior to one-electron oxidation of the central metal ion and the second pattern B is the reverse(Scheme 1). The two redox patterns A and B can be interchanged by protonation/deprotonation of basic sites in the RuOs mixed metal tetranuclear complex, $[\{Os(bpy)_2(bbbpyH_2)\}_3Ru](ClO_4)_8$(bpy=2,2'-bipyridine, $bbbpyH_2$ = 2,2'-bis(benzimidazol-2-yl)-4,4'-bipyridine) (**1**), represented in Scheme 2.

The cyclic voltammogram of the complex **1** in CH_3CN shows two oxidation waves centered at +0.38 and +0.71 V vs $Fc^{+/0}$, which are assigned to three-electron $Os^{II/III}$ and one-electron $Ru^{II/III}$-based oxidation respectively. In the cyclic voltammogram of the fully deprotonated complex **2**, the order of the two waves is reversed, and they are shifted to -0.34 V and +0.06 V. Thus, deprotonation has switched the site of the first oxidation from peripheral Os centers to central Ru site. This change is accompanied by the negative potential shifts.



Scheme 1



1 Scheme 2

The one-electron oxidized mixed-valence form of the deprotonated complex $2^+(Ru^{III}Os^{II}_3)$ was quantitatively generated by bulk electrolysis at -0.2 V. The deprotonated one-electron oxidized complex did not show any absorption in the near IR region. Protonation induces a drastic change in the near IR spectrum: new bands at 1050, 1900, and 2300 nm appeared. The latter two can be assigned to dπ-dπ transition within Os^{III} part of the complex. This observation indicates that the electron transfer from peripheral Os^{II} to central Ru^{III} moiety has been induced by protonation.

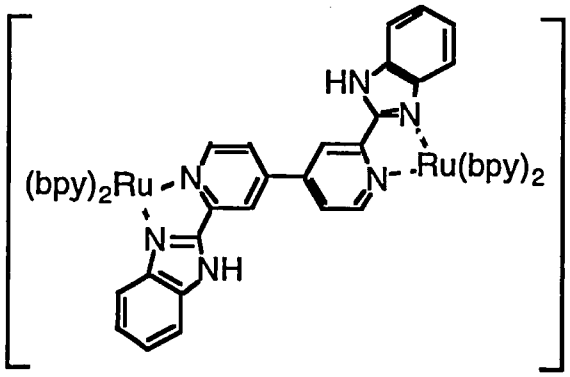
VII-A-2 Proton-induced Tuning of Electrochemical and Photophysical Properties in Mononuclear and Dinuclear Ruthenium Complexes Containing 2,2'-Bis(benzimidazol-2-yl)-4,4'-bipyridine: Synthesis, Molecular Structure, and Mixed-Valence State and Excited-State Properties

Masa-aki HAGA, Md. Meser ALI, Shiro KOSEKI*(Mie Univ.)*, **Kaori FUJIMOTO***(Mie Univ)*, **Akio YOSHIMURA***(Osaka Univ.)*, **Koichi NOZAKI***(Osaka Univ.)*, **Takeshi OHNO***(Osaka Univ)*, **Kiyohiko NAKAJIMA***(Aichi Univ of Educ)* **and Derk J. STUFKENS***(Univ. van Amsterdam)*

[*Inorg. Chem.*, **35**, 3335-3347 (1996)]

A series of mono- and dinuclear $Ru(bpy)_2$ complexes(bpy = 2,2'-bipyridine) containing 2,2'-bis(benzimidazol-2-yl)-4,4'-bipyridine ($bbbpyH_2$) were prepared.

The mononuclear complex $[Ru(bpy)_2(bbbpyH_2)](ClO_4)_2$•



$[(bpy)_2Ru(bbbpyH_2)Ru(bpy)_2]^{5+}$

CH_3OH•$4H_2O$ was characterized by an X-ray structure determination. Crystal data are as follows: triclinic, space group $P\bar{1}$, a = 14.443(4) Å, b = 15.392(4) Å, c = 11.675(2)Å, a = 101.44(2)°, b = 107.85(2)°, g = 96.36(2)°, V = 2380(1) Å^3, Z = 2. The coordination geometry of the ruthenium(II) ion is approximately octahedral as shown in Figure 1. The dihedral angle between the two pyridyl rings in $bbbpyH_2$ is 9.4(3)°, which is close to coplanar, in the complex. Mono- and dinuclear complexes exhibit broad charge-transfer absorption bands at 420-520 nm and emission at 660 - 720 nm in CH_3CN solution with lifetimes of 200-800 ns at room temperature. Transient difference absorption spectra and resonance Raman (rR) spectra were used to assign the charge transfer bands in 420 - 520 nm region and to identify the lowest excited states. Both absorption and emission spectra are sensitive to solvent and solution pH. Deprotonation of the dinuclear complex raises the energies of the π* orbitals of the $bbbpyH_2$ ligand, so that they become closer in energy to the π* orbitals of bpy. The intervalence band of $[(bpy)_2Ru(bbbpyH_2)Ru(bpy)_2]^{5+}$ is observed at 1200 nm (e = 170 $M^{-1}cm^{-1}$) in CH_3CN. The value of the electronic coupling matrix element, H_{AB}, was determined as 120 cm^{-1}. Upon deprotonation, the IT band was not observed. It is therefore concluded that a superexchange pathway occurs predominantly via the Ru(II)dπ-$bbbpyH_2$ π* interaction, since deprotonation decreases the interaction. The role of the intervening fragments in the bridging ligand is discussed from the viewpoint of orbital energies and their orbital mixing with Ru dπ orbitals.

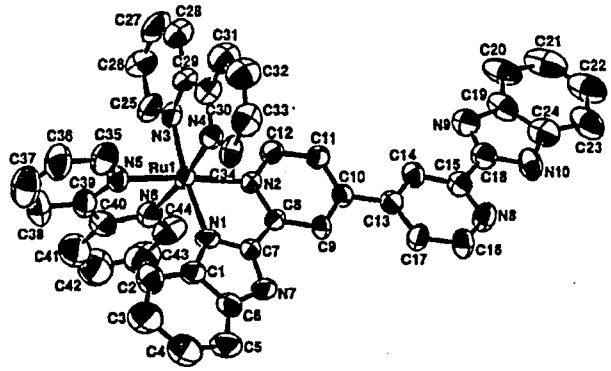


Figure 1. An ORTEP diagram of the structure of the cation $[Ru(bpy)_2(bbbpyH_2)]^{2+}$ with the atomic numbering scheme.

VII-A-3 Electrospray and Collision-induced Dissociation Mass Analysis of Star-burst Type Tetranuclear Complexes

Ryuichi ARAKAWA*(Osaka Univ.)*, **Gen-etsu MATSUBAYASHI***(Osaka Univ.)*, **Noriko OHASHI, Satoshi FURUUCHI***(Tanabe Seiyaku Co.)*, **Takekiyo MATSUO***(Osaka Univ)* **and Md. Meser ALI and Masa-aki HAGA**

[*J. Mass Spectrom*, **31**, 861-866(1996)]

A number of star-burst type tetranuclear complexes denoted by $[M(II)L_2B]_3RuX_8$ (M =Ru, Os) were examined by positive electrospray(ES) mass spectrometry, where L is bpy(2,2'-bipyridine) or btfmb (4,4'-bis(trifluoromethyl)-2,2'-bipyridine), bridging ligand B is 1,1'-dimethyl-2,2'-bis(2'-pyridyl)-6,6'-bibenzimidazole(dmbpbim), 2,2'-bis(benzimidazol-2-yl)-4,4'-bipyridine($bbbpyH_2$) or the related ligand, and X is ClO_4^-. Multiply charged ions with the charge state from 8+ to 3+ were observed in the full-scan ES mass spectra as shown in Figure 1. Different charged ions were generated by the combination of counterion loss and protonation/deprotonation of the bridging ligand B. Collision-induced dissociation(CID) of the multiply charged ion made it clear that loss of one or more HX neutral is a major process for lower charge states, whereas complete fragmentation takes place for higher charge states and the fragments are based on a subunit group of $[M(II)L_2B]^{2+}$. Insertion of formal O_2^- produced from ClO_4^- couterion was observed for the complexes without active protons even if low-energy CID experiments, but not for the complexes with active protons. Advantages of ES mass spectrometry are demonstrated for these multinuclear compounds.

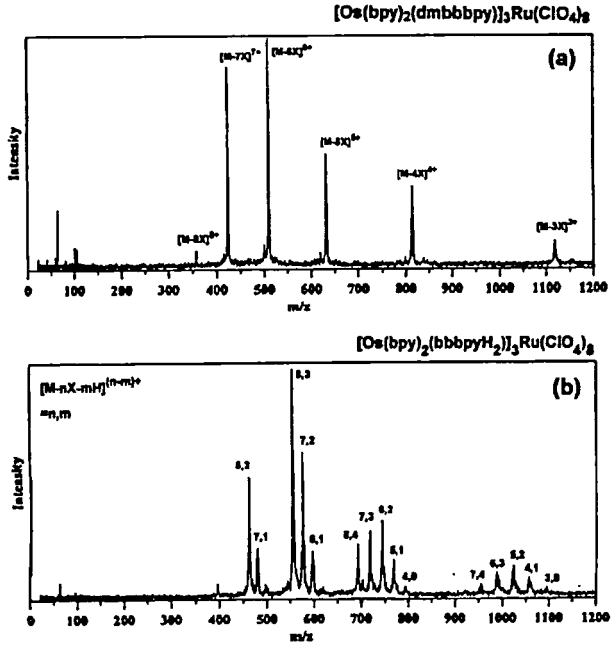


Figure 1. Positive electrospray mass spectra of mixed-metal $RuOs_3$ tetranuclear complexes in acetonitrile(0.1 mM). (a) $\{[Os(bpy)_2(dmbbbpy)]_3Ru\}(ClO_4)_8$; (b) $\{[Os(bpy)_2(bbbpyH_2)]_3Ru\}(ClO_4)_8$. M and X represent the complex and ClO_4^-, respectively.

VII-A-4 Analysis of Multiply Charged Ions of Ruthenium(II) Tetranuclear Complexes by Electrospray Ionization Mass Spectrometry.

Ryuichi ARAKAWA*, Takekiyo MATSUO*, Koichi NOZAKI*, Takeshi OHNO*(*Osaka Univ.) and Masa-aki HAGA

[*Inorg. Chem.*, **34**, 2464-2467 (1995)]

In the electrospray ionization mass spectrometry(ESI-MS) of the Ru(II) tetranuclear complexes, $\{[Ru(bpy)_2(dmbpbim)]_3Ru\}(ClO_4)_8$(molecular weight, mw = 3384) and $\{[Ru(bpy)_2(bbbpyH_2)]_3Ru\}(ClO_4)_8$(mw = 3300), the multiply charged ions ranging from 7+ to 3+ were clearly observed. It was found that these charged ions are resulted from the combination of the dissociation of counterion and the deprotonation of the bridging ligands. Also, the charge distribution shifts to a lower charge state with increase in nuclearity. There seems to be no side reaction in the ESI process such as proton extraction from bpy, the formation of oxidized species, or a variety of ligand dissociation which are usually observed for fast atom bombardment(FAB) spectra. Thus, ESI-MS is a powerful tool for the identification of the Ru(II) complexes with high nuclearity just synthesized and for detecting impurities.

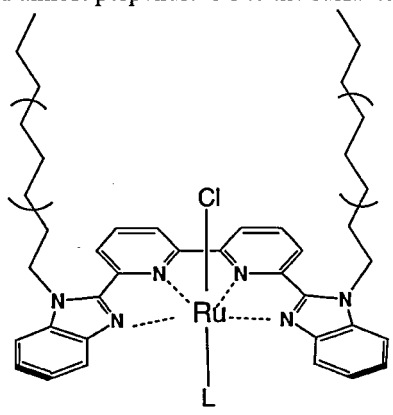
VII-B Synthesis and Characterization of Self-Assembled Organic Ligands and Metal Complexes on Surface Towards Solution-Phase Molecular Epitaxy

Self-assembled organization of metal complexes on surface is an attractive frontier for the coordination chemistry from the viewpoint of molecular electronic devices and biomineralization. In order to synthesize the solid state molecular switches based on metal complexes, the understanding for coordination chemistry on surface is requisite. Novel metal complexes can be constructed on the surface by incorporating covalently bound, self-assembled monolayers of bifunctional ligands as anchors for metal ions. This layered architecture of metal complexes provides the capability of studying the novel properties on nanometer scale. Thus, we examined two methodologies to build up the multilayer films on solid surface; one is the Langmuir-Blodgett(LB) techniques, and the other is self-assembled monolayer(SAM) method on gold or silicon wafer.

VII-B-1 Synthesis and Properties of Surfactant Ruthenium Complexes Containing 6,6'-Bis(benzimidazolyl)-2,2'-bipyridine with Long Alkyl Chains

Miho NAKAURA*(Mie Univ.)*, Kazumasa HARADA, Hideaki MONJUSHIRO, Masa-aki HAGA, Matthew RYAN* and A. B. P. LEVER*(*York Univ)

In order to study the controlled ordering of the metal complex in two dimensions, we have synthesized surfactant ruthenium complexes containing 6,6'-bis(N-octyl- or laurylbenzimidazolyl)-2,2'-bipyridine(R-bpybim)(R= (C_8 or C_{12}) as shown in Scheme 1. Ruthenium complexes, *trans*-$RuCl_2$(R-bpybim)(**1**) and *trans*-[RuCl(DMSO)(R-bpybim)]$^+$ (**2**), were synthesized by the reaction of $[RuCl_2(\eta^6\text{-}p\text{-cymene})]_2$ with R-bpybim in methanol and DMSO respectively and confirmed by nmr and other methods. The complex **1** formed a stable monolayer film on the Langmuir trough air-water interface. A typical π-A isotherm for the complex **1** at 20°C is shown in Figure 1. The isotherm indicates the complex begins to pack into the expanded state at an area/molecule of approximately 110 Å/molecule. As compression continues, a plateau region occurs at 20.5 mNm^{-1}. The isotherm then becomes steeper with a limiting molecular area of about 52 Å/molecule and a collapse pressure of 42 mNm^{-1}. This behavior suggests that at low surface pressure the plane of the complex are lying flat on the surface with the alkyl chains protruding away from the surface. At higher pressure, the complex is packed and oriented almost perpendicular to the surface.



$[Ru(R\text{-}bpybim)Cl(L)]^{n+}$

(R = C_8 or C_{12}; L = Cl (n =0) or DMSO(n =1))

Scheme 1

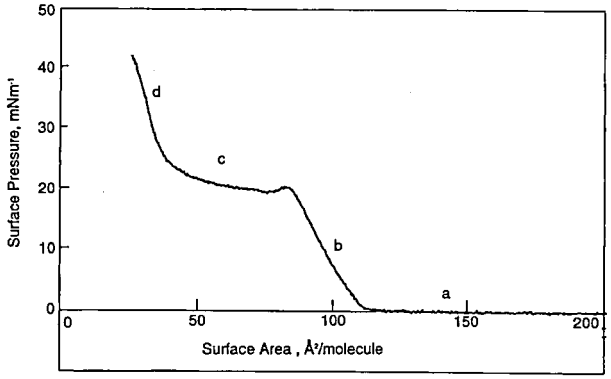


Figure 1. A π-A isotherm for the complex **1**, *trans*-$RuCl_2(C_{12}$-bpybim), at 20°C.

VII-B-2 Characterization of Surface Electronic Structures of Silicon Wafers under Air Atmosphere by Ultraviolet Photoelectron Yield Spectroscopy

Hideaki MONJUSHIRO, Masa-aki HAGA, Tsutomu SASAKI*, Iwao WATANABE* and Hitoshi WATARAI*
*(*Osaka University)*

Ultraviolet photoelectron yield (UPY) spectra of (111) face of silicon wafers with donor or acceptor concentrations of 10^{15} to 10^{20} cm^{-3} were measured in ambient air. Dependence of photoelectron threshold energy E_t and photoelectron yield Y on donor or acceptor concentrations was elucidated. The E_t of heavily doped p-type silicon is *ca.* 0.5 eV smaller than the other samples. This is due to the steep bending of the electron occupied level near the surface. The Y is larger for p-type samples and smaller for n-type samples. These features can also be explained by the surface band structure of doped silicon and the escape depth of low energy photoelectrons in silicon substrate. It is concluded that the surface electronic structure of silicon can be characterized by UPYS under ambient condition.

VII-B-3 Structure of Self-Assembled Layers of Terminally Functionalized Organosilyl Compounds on Silicon Substrates

Hideaki MONJUSHIRO and Masa-aki HAGA

Ultraviolet photoelectron yield spectra(UPYS) and X-ray photoelectron spectra(XPS) were measured for self-assembled layers of four kinds of functionalized organosilyl compounds, trimethoxy-4-aminopropylsilane(**1**), trimethoxy-N-(2-aminoethyl)-4-aminopropylsilane(**2**), trichloro-3-cyanoethylsilane(**3**), and trimethoxy-4-mercaptopropylsilane(**4**). The self-assembled layers were formed on oxidized silicon wafers by immersing the substrate into dilute toluene solution of the compounds. Both UPYS and XPS shows that in the cases of compounds **1**, **2**, and **3**, thick layer was formed on the surface. This is caused by hydrolysis of the organosilyl compounds and their polymerization. Analysis of XPS spectra for these thick layers shows that the molecular orientation in the layer is rather random. On the other hand, thin layer is formed with compound **4** and in this case it is elucidated that mercapto group is present outside of the layer surface. Studies on the capability of the anchored functional groups to the formation of surface metal complexes and characterization of the complexes are now in progress.

VII-B-4 Probing Depth of Ultraviolet Photoelectron Yield Spectroscopy in Hydro-Carbon Films

Hideaki MONJUSHIRO and Iwao WATANABE *(Osaka Univ)*

[*Anal. Sci.*, **11**, 797-800 (1995)]

In order to clarify the probing depth of ultraviolet photoelectron yield spectroscopy, the escape depth(L) of photoelectron with kinetic energy (E_k) lower than 1.5 eV in hydrocarbon films was determined by using self-assembled monolayers of *n-a*lkylmercaptane absorbed on gold. The yield of photoelectron from the gold substance decreased exponentially as the chain length of n-alkylmercaptane increased. As shown in Figure 1, the L was 1.0 ± 0.1 nm for electrons with E_k lower than 0.3 eV, and increased to 3.0 ± 0.9 nm for electrons with the maximum E_k of 1.5 eV.

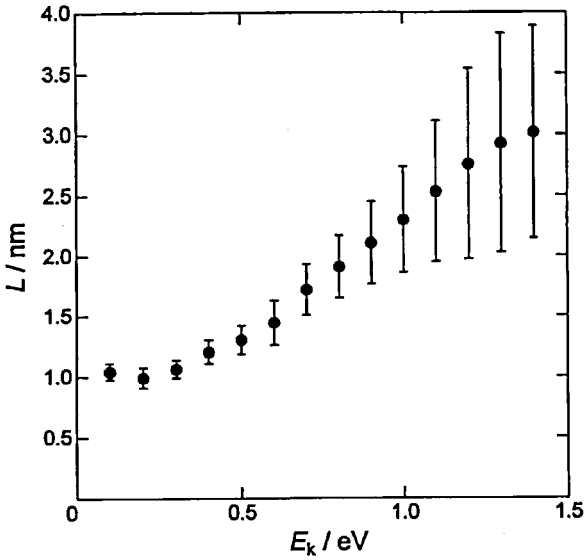


Figure 1. Electron escape depth in hydrocarbon layer L plotted against the maximum kinetic energy E_k of photoelectrons from gold substrate.

VII-B-5 Charge-up Phenomena of Insulated Metals in X-ray Photoelectron Spectroscopy

Takayuki ICHINOSE*(Osaka Univ)*, **Hideaki MONJUSHIRO and Hiroshi WATARAI***(Osaka Univ)*

[*Anal. Sci.*, **12**, 43- 47 (1996)]

The X-ray power dependence of the charge-up shift of a photoelectron line was examined for metal films insulated from a spectrometer. As the X-ray power increased, the observed line position shifted to a higher binding energy, and approached an asymptotic value. This charge-up behavior was treated based on the balance between the photoelectron emission from the sample surface and electron injection from an aluminum window of the X-ray source and from other electron sources. It was concluded that, for insulated metals, the vacuum level of the sample is aligned to that of the spectrometer when

the X-ray power is extrapolated to zero, i.e., the magnitude of the charge-up is equal to zero. The work function of the spectrometer was successfully determined with samples having a known work function. A new method to obtain the binding energy relative to the vacuum level for insulators is proposed.

VII-C Metal Ions in Biological Systems

In order to reveal the biological roles of transition metal ions, structures and reactions of blue copper proteins and multicopper oxidases, whose intrinsic roles are electron-transfer and oxidation of substrate utilizing dioxygen as the final electron acceptor, respectively, have been studied by absorption, CD, and EPR spectroscopies, and electrochemistry.

VII-C-1 Restrained Reduction of Type 3 Copper in Laccase and Ascorbate Oxidase by Azide

Takeshi SAKURAI

[*Biochem (Life Sci. Adv.)* **14**, 17(1995)]

The inhibitory effect of azide on laccase and ascorbate oxidase has been investigated by absorption, CD, and ESR spectroscopies. When laccase and ascorbate oxidase previously treated with excess azide were anaerobically reacted with pyrocatechol and L-ascorbate, respectively, the ESR signal due to the type 3 copper was obtained. The inhibitory effect of azide appears not only to compete with dioxygen for the trinuclear site composed by the types 2 and 3 Cu, but also to slow down the reduction of the type 3 copper.

VII-C-2 EPR Spectra of Type 3 Copper Centers in *Rhus vernicifera* Laccase and *Cucumis sativus* Ascorbate Oxidase

Takeshi SAKURAI and Junya TAKAHASHI

[*Biochim. Biophys. Acta* **1248**, 143(1995)]

In order to reveal the detailed structure of the trinuclear center composed by the type 2 copper and a pair of the type 3 coppers in multicopper oxidases, the action of inhibitors such as azide, thiocyanate, and fluoride on laccase and ascorbate oxidase has been investigated by absorption, CD, and EPR spectroscopies. Anaerobic reaction of inhibitor-treated laccase and ascorbate oxidase with a reducing agent gave ESR signals originating from the inhibitor-bound type 3 copper except for the case of fluoride-laccase. The hyperfine splittings of these ESR signals ($|Az| = 10 \times 10^{-3} - 18 \times 10^{-3}$ cm^{-1}) were smaller than those of the type 2 copper centers (ca. 20×10^{-3} cm^{-1}), indicating that the type 3 copper has a tetragonal geometry with a significant tetrahedral distortion. The facile detection of a series of the inhibitor-bound type 3 copper centers indicates that the action of the exogenous anionic inhibitors is not only to interfere the access of dioxygen to the trinuclear site, but also to restrain the reduction of the type 3 copper by lowering its reduction potential.

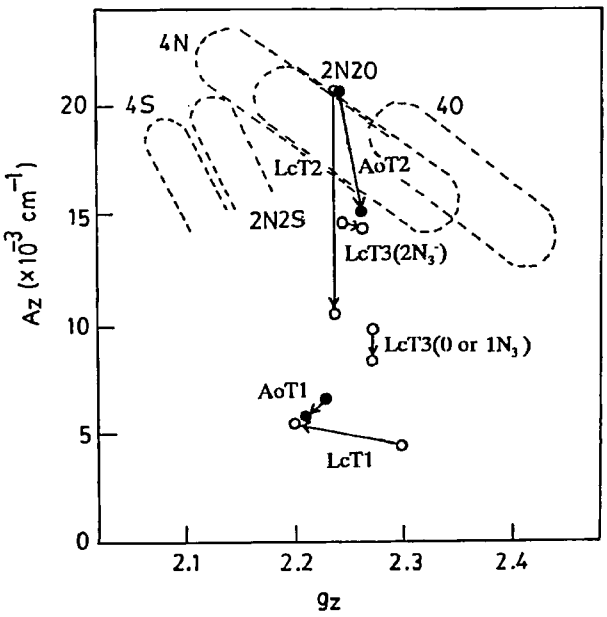


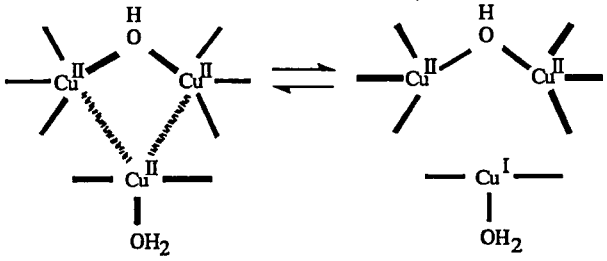
Figure 1. The relation between gz and Az of the Type 1, 2 and 3 coppers .

VII-C-3 Room Temperature ESR Spectra of *Rhus vernicifera* Laccase and Derivatives

Takeshi SAKURAI and Junya TAKAHASHI

[*Biochem. Biophys. Res. Commun.* **215**, 235(1995)]

Although both the type 1 and type 2 coppers of *Rhus vernicifera* laccase are fully ESR detectable at 77K, only 30% of the type 2 copper are in the cupric form at room temperature. The residual 70% of the type 2 copper were easily transferred into the ESR detectable form by irradiating the resting enzyme with high-powered microwave, indicating that the type 2 copper can be in both the ESR detectable and ESR undetectable forms in solution. The room temperature ESR spectra of the type 2 copper-depleted laccase and of the azide-bound type 3 copper signals were also measured at room temperature and compared with those at 77K.

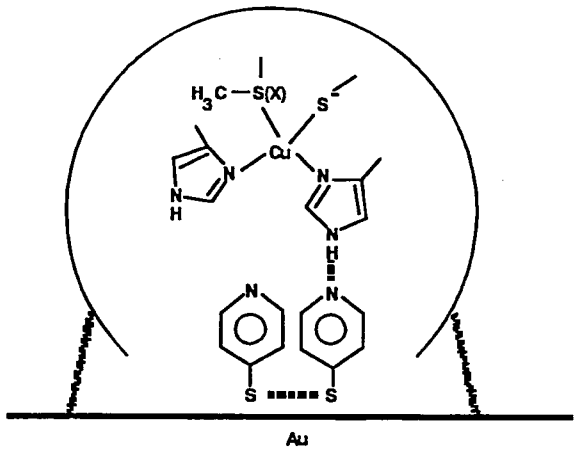


VII-C-4 Direct Electrochemistry of Blue Copper Proteins at Au Electrodes Modified with Promoters

Takeshi SAKURAI and Fumitaka NOSE

[*Chem. Lett.* 1075(1995)]

Cyclic voltammetry of six blue copper proteins, plastocyanin, azurin, umecyanin, plantacyanin, pseudoazurin, and stellacyanin was performed at Au electrodes modified with five promoters. A proper combination of non-covalent interactions such as hydrophobic interaction, hydrogen bonding, and electrostatic interaction realizes the access of the northern area of the protein molecules towards the electrode surface.

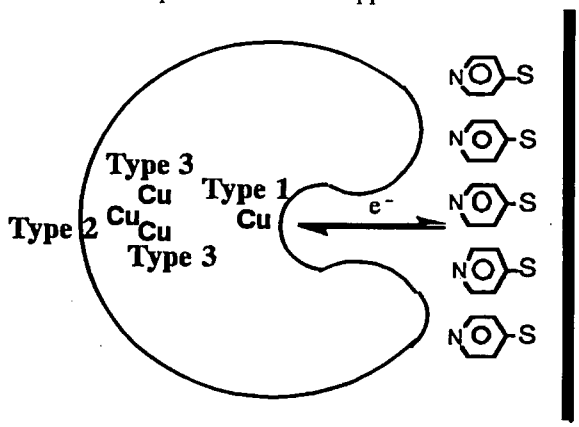


VII-C-5 Cyclic Voltammetry of Cucumber Ascorbate Oxidase

Takeshi SAKURAI

[*Chem. Lett.* 481(1996)]

Direct electrochemistry of cucumber ascorbate oxidase at Au electrode modified with promoters gave redox waves originating from the type 1 copper, not only extending the limit of electrochemistry for macromolecules but also giving a clue in studying the electron-transfer process of multicopper oxidase.

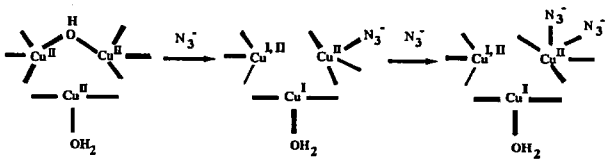


VII-C-6 FT-IR Spectra of the Azide-Type 3 Copper in Laccase and Ascorbate Oxidase

Takeshi SAKURAI, Junya TAKAHASHI and Hong-wei HUANG

[*Chem. Lett.* 651(1996)]

The biphasic binding constants of azide with a type 3 cooper in laccase and ascorbate oxidase were determined at room temperature and 77K based on the absorption and EPR spectra. The azide-treated laccase and ascorbate oxidase gave asymmetric stretching bands (ν_a) at 2056 and 2054 cm^{-1} in the FT-IR spectra, respectively. The coordination mode was suggested to be the end-on fashion.



VII-C-7 Dinuclear Nickel Complexes Containing a Dinucleating Ligand *N,N,N',N'*-Tetrakis-[(1-ethyl-2-benzimidazolyl)methyl]-2-hyrdoxy-1,3-diaminopropane and an Acetate Ion

Yasuo NAKAO*(* *Okayama Univ.*), Chikako MORI,* Wasuke MORI(*Kanagawa Univ.*), Takeshi SAKURAI, Kenji MATSUMOTO(*Osaka City Univ.*) and Hiroshi KIMOTO(*Ind. Res. Inst. Nagoya*)

[*Chem. Lett.* 641(1996)]

The dinuclear nickel(II) complexes $[Ni_2(L^1)(OAc)(MeOH)_2](ClO_4)_2 \cdot H_2O \cdot MeOH$ **1** and $[Ni_2(L^1)(OAc)(H_2O)_2](ClO_4)_2$ **2** (HL^1 = *N,N,N',N'*-Tetrakis-[(1-ethyl-2-benzimidazolyl)methyl]-2-hyrdoxy-1,3-diaminopropane) were prepared as a model for urease. The complex **1** turns to **2** upon exposure to air. The crystal structure of **1** and the magnetic (J = 21.6 cm^{-1}) and spectroscopic properties of **2** were determined.

VII-C-8 Crystal Structures and Hydrogen Bonding in One-Dimensional Chains of 4,5-Dicyanoimidazole and 4,5-Dichloroimidazole

Shigenori NAGATOMO, Sadamu TAKEDA, Hatsue TAMURA and Nobuo NAKAMURA

[*Bull. Chem. Soc. Jpn.* **68**, 2783(1995)]

The crystal structure of 4,5-dicyanoimidazole ($(CN)_2Imd$) was determined by an X-ray diffraction at room temperature; monoclinic, $P2_1/a$, a = 7.529(2), b = 7.529(1), c = 10.0972(9) Å, β = 102.74(1)°, V = 538.2(2) Å^3, Z = 4, R = 0.043, and R_w = 0.066 for 1090 observed reflections. Crystal structure of 4,5-dichloroimidazole (Cl_2Imd) was redetermined: tetragonal, $P4_12_12$, a = 6.843(4), c = 24.236(7) Å, V = 1134(1) Å^3, Z = 8, R = 0.043, and R_w = 0.058 for 427 observed reflections. Molecules in Cl_2Imd and CN_2Imd are linked by intermolecular N-H···N hydrogen bonds to form one-dimensional chains. The hydrogen bonds in Cl_2Imd are formed between the ring nitrogen atoms, while those in CN_2Imd are between the ring and the cyano nitrogens. The hydrogen bond distance (3.051(2)Å) of N···N in CN_2Imd is long, compared with that (2800(6) Å) in Cl_2Imd. The weak hydrogen bond in CN_2Imd was also indicated by IR an ^{15}N CP/MAS NMR spectra.

VII-C-9 EPR Study on the Charge Transfer Complexes of *N*-salicylideneanilines Containing NHO Hydrogen Bond as a Dynamic Function

Sadamu TAKEDA, Tamotsu INABE *(Hokkaido Univ.)*, Tadaoki MITANI *(Jpn. Adv. Inst. Sci. Tech.)*, Yusei MARUYAMA and Kizashi YAMAGUCHI

[*Syn. Met.* **70**, 1211(1995)]

Temperature dependence of EPR line shape was measured for the charge transfer complexes of *N*-salicylideneaniline derivatives with particular reference to the delocalization or mobility of proton in their intramolecular NHO hydrogen bound. Concentration of paramagnetic centers depends on the various complexes and was in the region between 10^{-1} and 10^{-4} spins per unit formula. Spin susceptibility almost obeyed Curie law. It was found that the EPR line narrows as temperature increased for the complexes with delocalized proton and the line shape deviated the simple Lorenzian. The result suggests one dimensional motion of unpaied spins in the low temperature region.

VII-C-10 Characterization of Poly-CuPc Sheet Polymers Synthesized under High Pressure

Kyuya YAKUSHI, Ichimin SHIROTANI *(Muroran Inst. Tech.)*, I. I. KHAIRULLIN, Yashuhiro NAKAZAWA, Kazushi KANODA, Nobuhiro KOSUGI and Sadamu TAKEDA

[*Syn. Met.* **71**, 2287(1995)]

We have characterized the material which has been prepared by the heat treatment of the mixture of 1,2,4,5-tetracyanobenzene and Cu powder at 5 Gpz and 500 °C. Dark gray material which incorporates Cu showed high conductivity (σ_{RT} = 1 Scm^{-1}) at room temperature. Although X-ray diffraction and ^{13}C NMR indicate the inhomogeneous structure, EXAFS and EPR suggest the local structure which is expected in the Poly-CuPc sheet polymer.

VII-C-11 New Cation-Diffusing Phase of $(CH_3NH_3)Bi_2Cl_{11}$

Shigenori NAGATOMO, Sadamu TAKEDA, Kizashi YAMAGUCHI, Makoto IWATA* *(Nagoya Univ.)* and Yoshiro ISHIBASHI*

[*J. Phys. Soc. Jpn.* **64**, 391(1995)]

A new phase transition of $(CH_3NH_3)Bi_2Cl_{11}$ was found at 520 K by proton NMR and differential thermal analysis. By the phase transition, the activation energy of transitional diffusion of $CH_3NH_3^+$ cation was reduced from 83 kJ/mol to 9 kJ/mol. Rotational motion of the cation in the low-temperature phase is also discussed.

VII-C-12 Charge-Transfer Effects in a Strongly Hydrogen-Bonded System: Potassium Salt of Acetylenedicarboxylic Acid

Taro SEKIKAWA, Keisuke MIYAKUUBO *(Osaka Univ.)*, Sadamu TAKEDA and Takayoshi KOBAYASHI *(TiokyoUniv.)*

[*J. Phys. Chem.* **100**, 5844(1996)]

A potassium salt of acetylenedicarboxylic acid with a strong ionic hydrogen bound between the two carboxyl groups was investigated by IR spectroscopy from the mid- to far-IR region. In such a strongly hydrogen-bonded system, the effects of the charge transfer in the hydrogen bounds were observed in the IR absorption spectrum under hydrostatic pressure at various temperatures. The absorption coefficient of a C=O stretching vibration increases with decreasing hydrogen-bond length. Broadening of the absorption-line width was observed at higher temperatures. The former and latter effects are attributed to the enhancement of the transition-dipole moment due to the charge transfer and the anharmonic coupling between the vibrational modes induced by the charge transfer, respectively.

VII-D Stereochemical and Kinetic Studies of Coordination Compounds

VII-D-1 New Triamine-type Platinum(II) Complexes of Phenyl-subsituted Ethylenediamine : Reactivity with 5'-GMP

Koji YUTOH, Masaaki KOJIMA* and Yuzo YOSHIKAWA(**Okayama University)*

[*J. Coord. Chem.*, in press]

New triamine-type platinum(II) complexes, $[PtCl(amine)(diamine)]^+$ (amine = 2-aminoethanol (ae-OH) or 2-methoxyethylamine (ae-OMe), diamine = $(NH_3)_2$, ethylenediamine (en), *N,N'*- dibenzylethylenediamine (dibenzylen) or 1,2-diphenylethylenediamine (stien)) were synthesized and their reactions with 5'-guanosine monophosphate (5'-GMP) were studied through the ^1H NMR measurements. The rate constants of stien complexes are half those of the en complexes. The dibenzylen complex has lower reactivity because of the bulky benzyl groups. The resulting order of their reactivities is en > stien > $(NH_3)_2$ ≧ dibenzylen. In the comparison of monoamine ligands, the complexes of 2-methoxyethylamine have clearly higher reactivities than those of 2-aminoethanol.

VII-D-2 Thermodynamic and Kinetic Studies of Zinc(II)-Triamine Complexes as Models of CA and AP

Toyofumi ITOH,* Yuki FUJII,* Toshiji TADA,** Yuzo YOSHIKAWA and Hiroyuki HISADA* *(*Ibaraki University, **Osaka Prefecture University)*

[*Bull. Chem. Soc. Jpn.*, **69**, 1265(1996)]

The formation constant(K_{ZnL}), enthalpy and entropy changes (ΔH and ΔS), and deprotonation constant (K_a) of coordinated water for hydrated zinc(II)-triamine (1:1) complexes(N_3-Zn-$(OH_2)_n$ (N_3 = diethylenetriamine(dien),

N-(2-aminoethyl)-1, 3-propanediamine(epd), dipropylenetriamine(dpt), *cis*, *cis*-1,3,5-triaminocyclohexane(tach), and 1,5,9-triazacyclododecane([12]aneN$_3$)) were determined by potentiometry. The pK_a linearly increased along with an increase in ΔH, and was explained in terms of a ligand-ligand interaction through the N_3-Zn-O bond on the bases of a thermodynamic analysis and strain-energy calculation(MM2). The zinc(II) complex-promoted hydrolysis of 2,4-dinitrophenyl diethylphosphate was investigated in 1% (v/v) methanol-water; the rate constants linearly increased along with dereases of pK_a and $-\Delta H$. This fact indicates that the hydrolysis proceeds via a concerted direct nucleophilic attacking mechanism of the coordinated hydroxide ion, in which the phosphate ester coordinates to the zinc(II) ion. X-ray structure analyses for synthesized model complexes, $[Zn(OAc)(dien)](ClO_4)$, $[\{Zn(dpt)\}_3(CO_3)](ClO_4)_4 \cdot NaClO_4$ and $[Zn(OAc)(tach)](ClO_4)$, are also reported.

VII-D-3 Photochemical Desulfurization of a Sulfinato-*S*-Cobalt(III) Complex. Formation of an Organic Peroxide Complex

Farooque MD. AKHTER,* Masaaki KOJIMA,* Kiyohiko NAKAJIMA and Yuzo YOSHIKAWA** *(*Okayama University, **Aichi University of Education)*

[*Chem. Lett.*, **1996**, 81]

The photolysis of *trans*(*t*- N,S)-$[Co\{S(O)_2CH(CH_3)COO\text{-}S,O\}(tren)]^+$ (*t*- N = tertiary amine nitrogen; tren = tris(2-aminoethyl)amine) was carried out in the same way as for *trans*(*t*- N,S)-$[Co\{S(O)CH_2COO\text{-}S,O\}(tren)]ClO_4$. An aqueous solution (200 cm^3) of *trans*(*t*-N,S)-$[Co\{S(O)_2CH(CH_3)COO\text{-}S,O\}(tren)]ClO_4$ (0.10g) was irradiated at ca. 5°C for 25 min using a 400 W high-pressure mercury lamp (internal irradiation type) equipped with a Pyrex glass filter. Isosbestic points were retained throughout the reaction. The irradiated solution was passed through a recycling chromatographic column (ϕ1.5 cm x 70 cm) of SE-Toyopearl. After three recyclings at 5°C (eluent: 0.05 M sodium (+)-tartrate), three bands, pink, yellow, and red, were separately eluted in this order, and the eluates containing the two faster eluted bands were separately collected. The remaining red band was further recycled seven times and the band was separated into red-1 and red-2. The formation ratio, pink : yellow : red-1 : red-2 was about 3:6:5:5. the yellow complex was the unreacted starting complex. the red-1 and red-2 complexes can be assigned as linkage isomerized sulfinato-*O* complexes on the basis of the UV- Vis spectra. The red-2 complex is thermally stable, while the red-1 complex thermally reverts to the starting complex. All these properties have been also observed in the two photoproducts of *trans*(*t*-N,S)-$[Co\{S(O)_2CH_2COO\text{-}S,O\}(tren)]^+$. Thus, the red-1 and red-2 complexes can be assigned to *trans*(*t*-N,O(S))- and *cis*(*t*- N,O(S))-$[Co\{OS(O)\text{-}CH(CH_3)COO\text{-}O,O\}(tren)]^+$, respectively. The X-ray struture analysis showed that in the pink complex, the sulfur atom of 2-sulfinatopropionate is lost and 2-peroxidopropionate coordinates to cobalt with the carboxylate and peroxide oxygen atoms. The tren ligand occupies the remaining four coordiation sites. As far as we know, this is the first peroxide complex formed by photodesulfurization. It is noted that not only desulfurization but also geometrical isomerization took place upon photolysis.

VII-D-4 Syntheses, Characterization, and Molecular Mechanics Calculations of Optically Active Silatrane Derivatives

Motoyuki TASAKA,* Masakazu HIROTSU,* Masaaki KOJIMA,* Shunji UTSUNO and Yuzo YOSHIKAWA** *(*Okayama University, **Shizuoka University)*

[*Inorg. Chem.*, submitted]

A series of optically active silatrane derivatives, $[Si\{N(CHRCH_2O)(CH_2CH_2O)_2\}X]$ (R = Me, *i*- Pr, X = Ph, OMe) has been synthesized by the reaction of optically active triethanolamine derivatives with $XSi(OMe)_3$, and charaterized by ^{1}H NMR, ^{13}C NMR, ^{29}Si NMR, mass spectroscopy, and the structure of six compounds have been determined by X-ray analysis. Molecular mechanics methods have also been employed to obtain the energy-minimized structures. The ^{29}Si NMR chemical shifts and the lengths of Si-N determined by X-ray analysis are sensitive to the bulkiness of the substituent(R). The Si-X bond length(X: trans position to nitrogen) do not appreciably differ from one another. The MM2 calculations indicated that the substituent exists in the equatorial position and the results are in agreement with those of X-ray analysis and ^{1}H NMR spectroscopy. Crystallographic data : [R = H, X = OMe], $C_7H_{15}NO_4Si$, orthorhombic, $Pna2_1$, $a = 13.407(1)$, $b = 8.761(2)$, $c = 8.191(1)$ Å, $Z = 4$; [R = Me, X = OMe], $C_8H_{17}NO_4Si$, orthorhombic, $P2_12_12_1$, $a = 10.110(3)$, $b = 11.083(2)$, $c = 9.474(2)$ Å, $Z = 4$; [R = *i*- Pr, X = OMe], $C_{10}H_{21}NO_4Si$, monoclinic, $P2_1$, $a = 8.481(1)$, $b = 7.805(1)$, $c = 10.218(2)$ Å, $\beta = 11.31(1)°$, $Z = 2$; [R = Me, X = Ph], $C_{13}H_{19}NO_3Si$, orthorhombic, $P2_12_12_1$, $a = 8.813(1)$, $b = 11.137(2)$, $c = 13.757(1)$ Å, $Z = 4$; [R = *i*- Pr, X = Ph], $C_{15}H_{23}NO_3Si$, orthorhombic, $P2_12_12_1$, $a = 8.365(1)$, $b = 13.538(2)$, $c = 13.841(2)$ Å, $Z = 4$.

VII-D-5 Preparation of a Stable Sulfonato-Cobalt(III) Complex by Oxidation of a Sulfinato-*O* Complex

Mayumi MURATA,* Masaaki KOJIMA,* Masakazu KITA, Setsuo KASHINO* and Yuzo YOSHIKAWA** *(*Okayama University, **Naruto University of Education)*

[*Chem.Lett.*, **1996**, 675]

A stable sulfonato complex, $[Co\{OS(O)_2CH_2CH_2NH_2\text{-}O,N\}(en)_2]^{2+}$, was prepared upon oxidation of $[Co\{OS(O)CH_2CH_2NH_2\text{-}O,N\}(en)_2]^{2+}$ in acid media. This sulfonato complex was resolved by SP-Sephadex column chromatography (eluent: 0.1 mol dm^{-3} $Na_2[Sb_2\{(+)\text{-tartrate}\}_2]$). The absolute configuration of the slower eluted $(-)_{589}$-isomer was determined to be Δ by the X-ray method.

The hydrolysis of *cis*- $[Co(NH_2CH_2CH_2SO_3\text{-}N)Cl(en)_2]Cl$(the complex contains the same ligand but the oxygen atom is not bound), in an alkaline solution was reported to yield only *cis*- $[Co(NH_2CH_2CH_2SO_3\text{-}N)(OH)(en)_2]^+$, which shows the low coordinating ability of an oxygen atom of the sulfonate ligand. However, the absorption and CD spetra of the present complex remained unchanged for 4 days at room temperature. To our knowledge, this is the first stable sulfonato cobalt(III) complex. The stability of the *O,N*- chelate is interesting when compared with the above

VII-D-6 Stereochemistry of (*R*)-2-Methylaziridine Complexes of Cobalt(III) and Dimerization of the Ligand

Masaaki KOJIMA,* Akiko SAKURAI,* Mayumi MURATA,* Kiyohiko NAKAJIMA, Setsuo KASHINO* and Yuzo YOSHIKAWA** *(*Okayama University, **Aichi University of Education)*

[*J. Coord. Chem.*, submitted]

A cobalt(III) complex containing (*R*)-2-methylaziridine (*R*- meaz), $[Co(R\text{-meaz})(NH_3)_5]^{3+}$, was prepared and the two diastereomers arising from the presence of the chiral nitrogen atom (N(*R*) and N(*S*)) were separated by the column chromatographic method. Molecular mechanics calculations estimated the N(*R*)-isomer to be more stable. This result was supported by the X-ray structure determination of the more abundant (*ca.* 94%) isomer, N(*R*)-$[Co(R\text{-meaz})(NH_3)_5]Br_3 \cdot H_2O$. Crystal data: monoclinic, $P2_1$, $a = 7.357(1)$, $b = 9.780(1)$, $c = 10.426(1)$ Å, $\beta = 93.58(1)°$, $V = 748.7(3)$ Å^3, $Z = 2$. Kinetic studies of isomerization (epimerization) between the two isomers revealed that the inversion at the nitrogen center was very slow (5×10^{-2} M^{-1} s^{-1} at 25 °C). The small rate constant seems to be related to the strained three-membered structure of the meaz ligand. The reaction of $Na_3[Co(NO_2)_6]$ and *R*-meaz yielded a complex containing two dimerized *R*- meaz chelates, *trans*-$[Co(NO_2)_2(di\text{-}R\text{-meaz})_2]^+$ (di-*R*- meaz = (*RR*)-α,2-dimethyl-1-aziridineethanamine). The crystal structure of *trans*-$[Co(NO_2)_2(di\text{-}R\text{-meaz})_2]ClO_4 \cdot H_2O$ was established by the X-ray method. Crystal data: orthorhombic, $P2_12_12_1$, $a = 11.784(6)$, $b = 21.023(9)$, $c = 8.608(7)$ Å, $V = 2133(2)$ Å^3, $Z = 4$.

VII-D-7 Photolysis of Cobalt(III) Complexes Containing Sulfinate-*S* Ligands. Formation of Organic Peroxide Complexes through Desulfurization

Masaaki KOJIMA,* Farooque MD. AKHTER,* Kiyohiko NAKAJIMA and Yuzo YOSHIKAWA** *(*Okayama University, **Aichi University of Education)*

[*Bull. Chem. Soc. Jpn.*, **69**, 2889 (1996)]

The photolysis of *trans*(*t*- N,S)-$[Co\{S(O)_2CH(CH_3)COO\text{-}S,O\}(tren)]^+$ (*t*- N = tertiary amine nitrogen; tren = tris(2-aminoethyl)amine) with visible light yielded three complexes: pink, red-1, and red-2. The molecular structure of the pink complex tetraphenylborate was determined by the X-ray method to be *trans*(*t*- N,O(C))-$[Co\{OOCH(CH_3)COO\text{-}O,O\}(tren)][B(C_6H_5)_4]CH_3OH \cdot H_2O$ (O(C) = oxygen of carboxylate group); irradiation induced desulfurization and yielded an organic peroxide complex. Crystal data: $C_{34}H_{48}BCoN_4O_6$, FW 678.52, triclinic, *P* 1(No. 2), $a = 19.583(3)$, $b = 19.838(4)$, $c = 9.996(1)$ Å, $\alpha = 103.60(1)$, $\beta = 102.13(1)$, $\gamma = 70.29(1)°$, $V = 3517(1)$ Å^3, $Z = 4$, $Dx = 1.29$ g cm^{-3}, $\mu = 0.533$ mm^{-1} for Mo *K*α radiation ($\lambda = 0.71073$ Å). The red-2 complex is thermally stable, while the red-1 one thermally reverts to the starting complex. The red-1 and red-2 complexes were assigned as linkage isomerized sulfinato-*O* complexes, *trans*(*t*- N,O(S))- and *cis*(*t*- N,O(S))-$[Co\{OS(O)CH(CH_3)COO\text{-}O,O\}(tren)]^+$ (O(S) = oxygen of sulfinate group), respectively, on the basis of the UV-vis and IR spectra and thermal stability. The irradiation of *trans*(*t*- N,S)-$[Co\{S(O)_2CH_2COO\text{-}S,O\}(tren)]^+$ and $[Co\{S(O)_2CH(CH_3)COO\text{-}S,O\}(en)_2]^+$ also yielded both peroxide complexes and linkage isomerized sulfinato-*O* complexes.

VII-D-8 Photochemistry of Cobalt(III) Complexes Containing a Sulfinate-*S* Ligand. Linkage and Geometrical Isomerization

Farooque MD. AKHTER,* Masakazu HIROTSU,* Isamu SUGIMOTO,* Masaaki KOJIMA,* Setsuo KASHINO* and Yuzo YOSHIKAWA *(*Okayama University)*

[*Bull. Chem. Soc. Jpn.*, **69**, 643(1996)]

The Photolysis of *trans*(*t*-N,S)-$[Co\{S(O)_2CH_2COO\text{-}S,O\}(tren)]^+$ (**1**, *t*-N = tertiary amine nitrogen; tren = tris(2-aminoethyl)amine) with visible light yielded two complexes, orange and red. The molecular structure of the orange complex perchlorate was determined by the X-ray method to be *cis*(*t*-N,O(S))-$[Co\{OS(O)CH_2COO\text{-}O,O\}(tren)]ClO_4 \cdot H_2O$ (**2**, O(S) = oxygen of sulfinate group); geometrical isomerization as well as linkage isomerization took place upon photolysis. A mechanism for the geometrical isomerization was proposed. The red complex, which was assigned as *trans*(*t*-N,O(S))-$[Co\{OS(O)CH_2COO\text{-}O,O\}(tren)]^+$ (**3**), was thermally unstable and reverts to the starting complex. This observation is in accord with molecular mechanics calculations, which estimate the starting complex to be more stable. The kinetic studies were performed using the HPLC method in the temperature range 28-70 °C, giving $\Delta H^{\ddagger} = 100$ kJ mol^{-1} and $\Delta S^{\ddagger} = -23$ J K^{-1} mol^{-1}. Photolysis of a cobalt(III) complex containing the L- cysteinesulfinate-*S*,*N* ligand, *cis*(*t*- N,S)-$[Co\{S(O)_2CH_2CH(COOH)NH_2\text{-}S,N\}(tren)]^{2+}$ (**4**) with visible light provided two types of linkage isomers, *cis*(*t*- N,O(C))-$[Co\{NH_2CH(CH_2SO_2^-)COO\text{-}N,O\}(tren)]^+$ (**4b**, O(C) = oxygen of carboxylate group) with an uncoordinated sulfinate group, and a pair of diastereomers of *cis*(*t*-N,O(S))-$[Co\{OS(O)CH_2CH(COOH)NH_2\text{-}O,N\}(tren)]^{2+}$ (**4a**). The molecular structures of the perchlorate of **4b** and the bromide of **4a** with the (*S*)-sulfur atom have been determined by X-ray diffraction. Isomerization (epimerization) from **4a**-*R* to **4a**-*S* was studied in the temperature range 55-75 °C, giving $\Delta H^{\ddagger} = 105$ kJ mol^{-1} and $\Delta S^{\ddagger} = -20$ J K^{-1} mol^{-1}. Photolysis of *trans*(*t*- N,S)-$[Co\{S(O)_2CH_2CH(COOH)NH_2\text{-}S,N\}(tren)]^{2+}$ (**5**) yielded six products. Three of them were the same as those obtained by the photolysis of **4**, indicating that geometrical isomerization took place.

VII-E Creation of Complexes Containing New Types of Bonds between a Transition Metal and a Phosphorus

The most typical bond fashion between a transition metal and a phosphorus is a dative bond, where the lone-pair electrons on a phosphorus atom are donated to a vacant d orbital of a transition metal. We focus on rather new types of bond fashion between a transition metal and a phosphorus, such as a covalent bond, a multiple bond, and a hypervalent

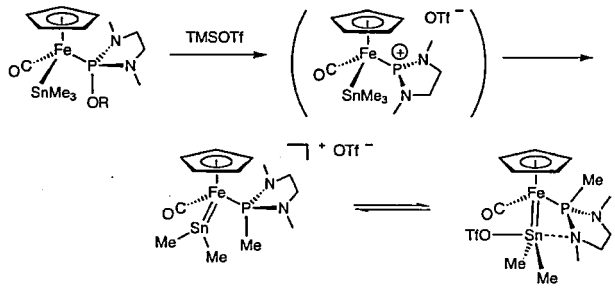
bond. New preparative methods of complexes containing such bonds have been developed and the reactivities of these complexes have been examined.

VII-E-1 Conversion of Transition-Metal Complexes with Stannyl and Phosphenium Ligands into Those with Stannylene and Phosphine Ligands by Alkyl Migration from Sn to P

Hiroshi NAKAZAWA *(Hiroshima Univ. and IMS)*, **Yoshitaka YAMAGUCHI and Katsuhiko MIYOSHI** *(Hiroshima Univ.)*

[*Organometallics*, **15**, 1337 (1996)]

Treatment of $Cp(CO)(SnMe_3)Fe\{PN(Me)CH_2CH_2NMe(OR)\}$(R=Me,Et) with $Me_3SiOSO_2CF_3$(TMSOTf) at -78°C yields $[Cp(CO)(SnMe_2)Fe\{PN(Me)CH_2CH_2NMe(Me)\}]OTf$, showing that P-OR bond cleavage and Me migration from Sn to P take place. The X-ray analysis of the product reveals that this is a stannylene complex of iron stabilized by both an OTf and N atom in the phosphorus ligand. In solution, there is an equilibrium between a base-stabilized stannylene form as shown in a solid state and a base-free form.



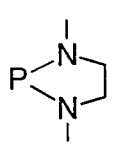
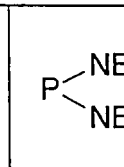
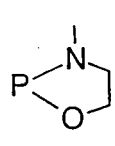
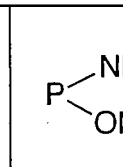
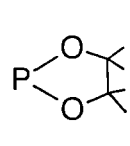
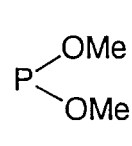
VII-E-2 Cationic Phosphenium Complexes of Group 6 Transition Metals. Systematic Approach to Elucidation of Influence of Substituents of the Phosphenium Phosphorus on the Stability of the Complexes

Yoshitaka YAMAGUCHI, Hiroshi NAKAZAWA *(Hiroshima Univ. and IMS)*, **Tomonori ITOH** *(Hiroshima Univ.)* **and Katsuhiko MIYOSHI** *(Hiroshima Univ.)*

[*Bull. Chem. Soc. Jpn.*, **69**, 983 (1996)]

Group 6 transition-metal phosphite complexes, *fac*-$[(bpy)(CO)_3M\{PXY(OMe)\}]$ (M = Cr, Mo, and W: XY = $(NEt_2)_2$,**1a**; $N(Me)CH_2CH_2O$, **2a**; $(NEt_2)(OMe)$, **3a**; $OCMe_2CMe_2O$, **4a**; $(OMe)_2$, **5a**) have been prepared and subjected to the reaction with $BF_3{\cdot}OEt_2$. In these reactions, cationic phosphenium complexes $[(bpy)(CO)_3M\{PXY\}]^+$ are formed by an OMe abstraction as an anion from the phosphorus ligand for **1a**, **2a**, and **3a** (M=Mo, W). The reaction of **3a**(M=Cr) yields *fac*-$[(bpy)(CO)_3Cr\{P(OMe)_2F\}]$(**Cr-5c**) and $[(bpy)(CO)_3Cr\{P(NEt_2)F_2\}]$ (**Cr-7d**). In the reaction of **4a** and **5a** for all group 6 congeners, an OMe/F substitution reaction takes place to give *fac*-$[(bpy)(CO)_3M\{POCMe_2CMe_2O(F)\}]$ and *fac*-$[(bpy)(CO)_3M\{P(OMe)_2F\}]$. These results reveal that the stability of cationic phosphenium complexes increases with (i) going to a heavier congener, (ii) increasing the number of amino substituents on the phosphenium phosphorus, and (iii) adding an ethylene bridge between X and Y when at least one of X and Y is an amino substituent.

Stability of cationic phosphenium complexes formulated as $[(bpy)(CO)_3M\{PXY\}]^+$

M \ PXY						
Cr	◎	○	○	F	F	F
Mo	◎	◎	◎	○	F	F
W	◎	◎	◎	○	F	F

◎ Stable, both the *fac* and *mer* isomers are observed.

◎ Stable, but only the *mer* isomer is observed.

○ A phosphenium complex is observed with by-products.

F A phosphenium complex in not detected but a fluorinated complex is formed.

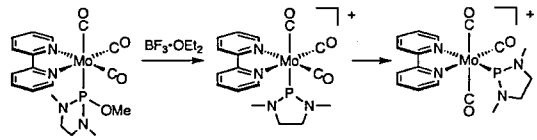
VII-E-3 ^{95}Mo NMR Studies on Cationic Phosphenium Complexes of Molybdenum

Hiroshi NAKAZAWA *(Hiroshima Univ. and IMS)*, **Yoshitaka YAMAGUCHI, Katsuhiko MIYOSHI** *(Hiroshima Univ.)* **and Akira NAGASAWA** *(Saitama Univ.)*

[*Organometallics*, **15**, 2517 (1996)]

The ^{95}Mo NMR spectra of cationic molybdenum phosphenium complexes have been measured. Going from

fac-[(bpy)(CO)$_3$Mo{PN(Me)CH$_2$CH$_2$NMe(OMe)}] (**1a**) to *fac*-[(bpy)(CO)$_3$Mo{PN(Me)CH$_2$CH$_2$NMe}]$^+$ (*fac*-**1b**) to *mer*-[(bpy)(CO)$_3$Mo{PN(Me)CH$_2$CH$_2$NMe}]$^+$ (*mer*-**1b**) causes deshielding to the ^{95}Mo doublet resonance (δ -1081 (**1a**), -1049 (*fac*-**1b**), -1015 (*mer*-**1b**)), an increase in the Mo-P coupling constant (193 Hz (**1a**), 264 Hz (*fac*-**1b**), 337 Hz (*mer*-**1b**)), and an increase in the line width (35 Hz (**1a**), 90 Hz (*fac*-**1b**), 300 Hz (*mer*-**1b**)). The conversion of *fac*-[(bpy)(CO)$_3$Mo {PN(Me)CH$_2$CH$_2$O(OMe)}] (*fac*-**2a**) into *mer*-[(bpy)(CO)$_3$Mo{PN(Me)CH$_2$CH$_2$O}]$^+$ (*mer*-**2b**) showed a similar trend in ^{95}Mo NMR data, though *fac*-[(bpy)(CO)$_3$Mo{PN(Me)CH$_2$CH$_2$O}]$^+$ was not detected in this case. *mer*-**2b** exhibits the largest Mo-P coupling constant (343 Hz) among those reported so far. These changes can be reasonably attributed to a dominant contribution from the imbalance of electron density at the Mo in the Ramsey equation due to a significant double-bond character between the molybdenum and the phosphenium phosphorus. Comparison of coupling constants between M and a phosphenium P in [(bpy)(CO)$_3$Mo{PN(Me)CH$_2$CH$_2$NMe]$^+$ (M = Mo, W) revealed that the ratio $^1J_{W\text{-}P}/^1J_{Mo\text{-}P}$ is 1.67, which is very close to the ration (1.76) reported for many series of M-phosphine (or phosphite) complexes (M = Mo, W). The ^{95}Mo NMR spectra of *cis* and *trans*-[(bpy)(CO)$_2$Mo{PN(Me)CH$_2$CH$_2$X(OMe)}{PN(Me)CH$_2$CH$_2$X}]$^+$ (X = NMe, O) have also been measured; the chemical shifts are understood similarly in terms of the imbalance of electron density at Mo.



^{95}Mo NMR Data	**1a**	*fac*-**1b**	*mer*-**1b**
δ (ppm)	-1081 (d)	-1049 (d)	-1015 (d)
$^1J_{Mo\text{-}P}$ (Hz)	193	264	337
$W_{1/2}$ (Hz)	35	90	300

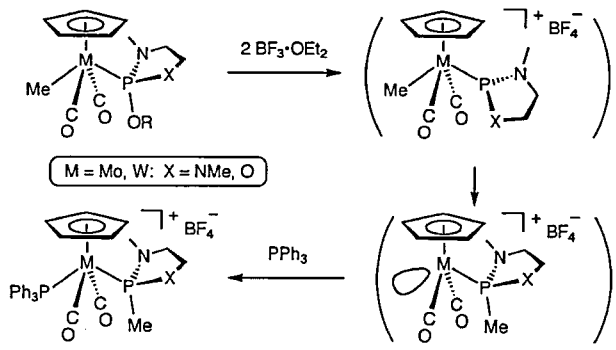
VII-E-4 Migratory Insertion Reaction of a Phosphenium Ligand into Mo- and W-alkyl Bonds

Hiroshi NAKAZAWA *(Hiroshima Univ, and IMS)*, **Mitsuru KISHISHITA, Shizuyo YOSHINAGA** *(Hiroshima Univ.)*, **Yoshitaka YAMAGUCHI, Tsutomu MIZUTA** *(Hiroshima Univ. and IMS)* **and Katsuhiko MIYOSHI** *(Hiroshima Univ.)*

[*J. Organomet. Chem.* in press]

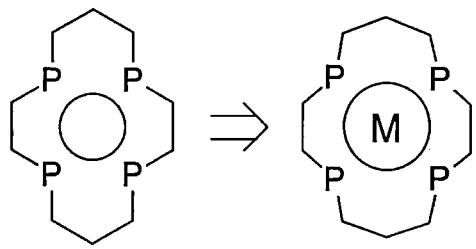
Treatment of Cp(CO)$_2$MeM{PN(Me)CH$_2$CH$_2$X(OR)} (M = Mo, W; X = NMe, O) with BF$_3$•OEt$_2$ and then PPh$_3$ yields *trans*-[Cp(CO)$_2$(PPh$_3$)M{PN(Me)CH$_2$CH$_2$X(Me)}]BF$_4$. Reaction of Cp(CO)$_2$MeM{P(OMe)$_3$} (M = Mo, W) with BF$_3$•OEt$_2$ and then with PPh$_3$ gives a mixture of [Cp(CO)$_2$(PPh$_3$)M{P(OMe)$_2$Me}]BF$_4$ and [Cp(CO)$_2$(PPh$_3$)M{P(OMe)$_3$}]BF$_4$. These reactions reveal that migratory insertion of a phosphenium ligand into an M-alkyl bond (M = Mo, W) takes place. The structures of *trans*-[Cp(CO)$_2$(PPh$_3$)Mo{PN(Me)CH$_2$CH$_2$NMe(Me)}]OTf and [Cp(CO)$_2$(PPh$_3$)W{P(OMe)$_3$}]BF$_4$ were determined by single X-ray diffraction studies.

VII-E-5 Palladium (II) and Platinum(II) Complexes of Tetraphosphamacrocycle. X-Ray Crystal Structures of Phosphorus Analogs of a (Tetramethylcyclam)metal Complex



Tsutomu MIZUTA *(Hiroshima Univ. and IMS)*, **Akihiro OKANO** *(Hiroshima Univ.)*, **Hiroshi NAKAZAWA** *(Hiroshima Univ. and IMS)* **and Katsuhiko MIYOSHI** *(Hiroshima Univ.)*

The palladium(II) and platinum(II) complexes with 1,4,8,11-tetramethyl-1,4,8,11-tetraphosphacyclotetradecane (Me$_4$[14]aneP$_4$) were prepared by a template reaction in which [M(MeHPCH$_2$CH$_2$PHMe)$_2$]Cl$_2$ (M = Pd, Pt) reacts with 1,3-dibromopropane in the presence of K$_2$HPO$_4$ as a base. The bromide salts of the Pd^{2+} (**1a**) and Pt^{2+} (**1b**) products were isolated as crystals. Their molecular structures were determined by X-ray crystallography. Both compounds have a square-planar geometry around the transition metals in which the stereochemical arrangement of the four asymmetric phosphorus atoms is the transIII (RRSS) type. The M-P bond distances for **1a** and **1b** are 2.268(1) and 2.277(2) Å, respectively, which are slightly shorter than those of the complexes with non-cyclic phosphines, suggesting that the Pd^{2+} and Pt^{2+} are larger in size than to be incorporated cozily into the hole of the macrocycle. It is noteworthy that the macrocycle distorts considerably its bond angles on the maclocyclic framework so as to incorporates too large metal ion into its hole.

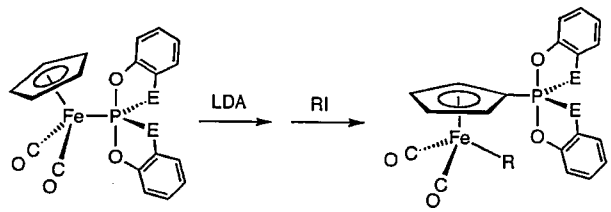


VII-E-6 Migration Reactions of a Phosphorane Fragment to the Cyclopentadienyl Ring in Ru-Phosphorane Complexes

Hiroshi NAKAZAWA *(Hiroshima Univ. and IMS)*, **Kazumori KAWAMURA** *(Hiroshima Univ. and IMS)* **and Katsuhiko MIYOSHI** *(Hiroshima Univ.)*

Treatment of [Cp(CO)$_2$Ru{P(OC$_6$H$_4$NMe)$_2$}] with lithium diisopropylamide (LDA) at -78°C in THF and then with an excess of alkyl iodide (RI: R = Me, CH$_2$Ph) gives [(η^5-C$_5$H$_4${P(OC$_6$H$_4$NMe)$_2$})(CO)$_2$RuR] (R = Me; **1**, CH$_2$Ph; **2**) which is assigned by the ^{1}H, ^{13}C, ^{31}P NMR data and the IR spectrum. [Cp(CO)$_2$Ru{P(OC$_6$H$_4$O)$_2$}] shows the similar reactivity in the reaction with LDA and then MeI to give [(η^5-C$_5$H$_4${P(OC$_6$H$_4$O)$_2$})(CO)$_2$RuMe]. These reactions show that a phosphorane fragment migrates from the Ru to the Cp ring. The structure of **2** was determined by the X-ray analysis. The geometry around the phosphorus

atom is almost trigonal-bipyramidal with two oxygens occupying the apical positions.



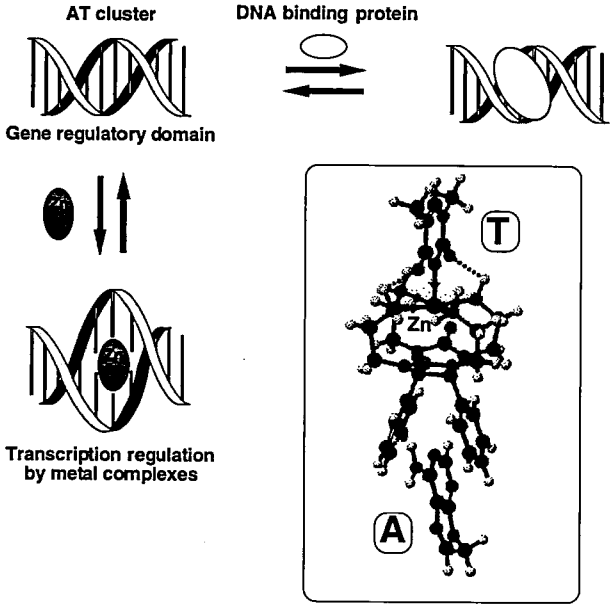
VII-F Targeting of Nucleic Acids and Related Biomolecules by Metal Complexes

Enzymes that catalyze the chemical transformation of nucleotides or nucleic acids, DNA and RNA, invariably require metal ions; in addition, metal ions or their complexes affect the stability of the confirmational states and three-dimensional structures of DNA and RNA. The research in our group focuses on the supramolecular chemistry of nucleic acids, peptides, and synthetic metal complexes. Central to this work is the design and synthesis of new metal complexes which can recognize and/or convert the structures of specific DNA sequences, with the goal of understanding of molecular basis of noncovalent complexes formed cooperatively and of making artificial activators or repressors for gene expression. A second project the group is working on is the study of interactions of metallopeptides with DNA. A goal of the research is to discover catalytic functions of DNA and understand how its structure gives rise to catalysis.

VII-F-1 Design and Synthesis of a Novel Zn(II) Complex for the Structural and Functional Conversion of AT-Rich Sequences in the Transcriptional Regulatory Domain of DNA

Akio OJIDA, Motoyuki TASAKA* and Mitsuhiko SHIONOYA *(*Graduate Univ. for Advanced Studies)*

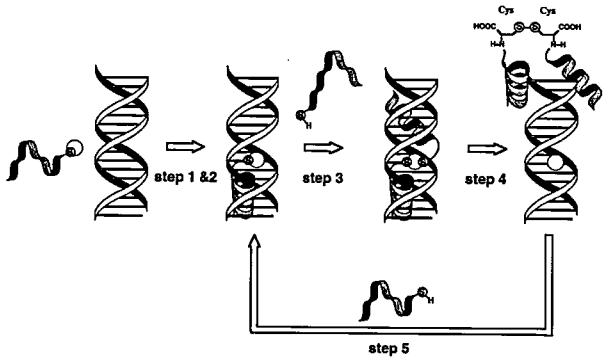
Zinc is critical in gene expression and plays structural and catalytical roles in proteins, enzymes, and transcription factors. Taking these special features of zinc into consideration, we have designed and synthesized a novel zinc complex by using a rigid and concave shape of glycouril as a building block. This zinc complex is expected to convert the structure and function of AT-rich sequences such as TATA box in the transcriptional regulatory domain of a specific gene by binding to both thymine and adenine bases. The ligand moiety was synthesized from benzil and urea in seven steps. The solution behaviors of the metal complexes is now underway.



VII-F-2 Catalytic DNA with a Metallic Reaction Center

Kentaro TANAKA and Mitsuhiko SHIONOYA

Although it is well known that DNA controls heredity in the principle of life, only a part of whole DNA has genetical codes especially in higher lives and roles of the other parts have been little elucidated. In this study, we demonstrate the possibility that DNA has an enzymatic character with the aid of a metallic reaction center. Our strategy consists of the following key steps. 1) A metallopeptide, in which a platinum(II) ion is coordinated by a C-terminus Cys attached extensively to DNA binding domain of estrogen responsive factor, binds to DNA specifically (Point delivery of a metal ion onto DNA). 2) The secondary structure of the peptide is induced upon binding to a specific DNA groove (Structural transition from coil to α-helix). 3) Another peptide, which has also a C-terminal Cys, binds to the opposite side of the palindromic DNA. 4) The central platinum ion is oxidized to tetravalence by weak oxidant such as molecular dioxygen and Cys' on each peptide to produce a dimeric cystine derivative (Reaction step on the catalytic DNA). 5) Next substrate peptides bind to the metallic reaction center of DNA and are catalyzed (Catalytic step).



VII-F-3 Novel Redox-Active Metallopeptides for Structural Control of DNA

Michito SHIOTSUKA and Mitsuhiko SHIONOYA

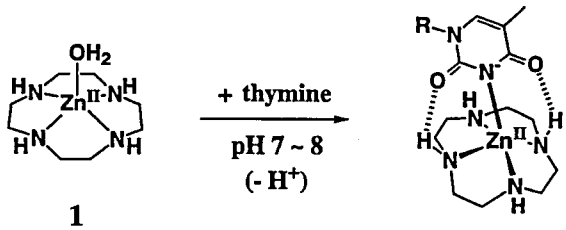
Regulation of transcriptional processes of DNA depends on the site-specificity of DNA-binding proteins. Distortion and/or bending of DNA which are induced by proteins are important factors to control the initiation of transcription. We have designed and synthesized a novel peptide, a cystine bearing two MetGlyGlyMetGly chains, as a building block for DNA-binding metallopeptides. This ligand is capable to donate metal ions with four sulfur atoms on methionyl residues to form possibly tetrahedral or square-pyramidal metal (Zn, Cu, Ni, etc.) complexes. Redox-active metal complexes of this ligand would give rise to changes of coordination geometries of the metal ions and subsequently conformations of the peptide moieties, and would be a promising element for DNA-binding metallopeptides with recognition sites. Studies on metal binding properties of this peptide are underway.

VII-F-4 Macrocyclic Metal Complexes for Selective Recognition of Nucleic Acid Bases and Manipulation of Gene Expression

Eiichi KIMURA*, Takuya IKEDA* and Mitsuhiko SHIONOYA *(*Hiroshima Univ.)*

[*Pure & Appl. Chem.*, in press]

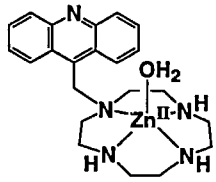
Interaction of Zn(II)-cyclen complexes **1**-**4** with uracil and thymine bases in double-stranded poly(A)·poly(U) and poly(dA)·poly(dT) has been investigated. These zinc(II) complexes lowered the melting temperatures (T_m) of poly(A)·poly(U) and poly(dA)·poly(dT) in 5 mM Tris-HCl buffer (pH 7.6) containing 10 mM NaCl as their concentrations increased, indicating that they destabilized the duplex structures of polynucleotides. The comparison of CD spectra of poly(A)·poly(U), poly(A), and poly(U) in the presence of zinc(II) complex **2** led us to conclude that their spectral changes of poly(A)·poly(U) were due to the structural change from double to single-strand, which was caused by zinc(II) complex **2** binding exclusively to uracils in poly(U). On the other hand, destabilization effect of the zinc(II) complexes was not observed on poly(dG)·poly(dC) in the thermal denaturation experiments in 50 % formamide aqueous solution containing 2.5 mM Tris-HCl buffer (pH 7.6) and 5 mM NaCl. However, the acridine-pendant cyclen complex **2**, which associates with guanine at N7 and O6, and through π-π stacking, interacted with poly(dG) in the double helix and greatly stabilized the poly(dG)·poly(dC) double-strand, as was indicated by the higher T_m than those with reference intercalating agents. Poly(A)·poly(U) double-strand was most effectively broken with a bis(Zn^{II}-cyclen) bridged by para-xylyl group **3** that was designed as a host molecule to bind to two succeeding uracils in a 1:2 complex. Zn(II)-cyclen complexes thus may become a new prototype of small molecules that can affect the biological properties of nucleic acids at the molecular level.



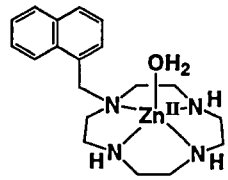
1

Zn^{II}-cyclen

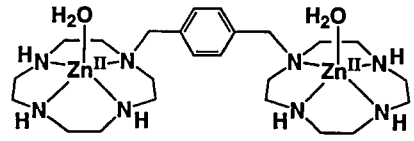
a ternary complex with thymine



2



4



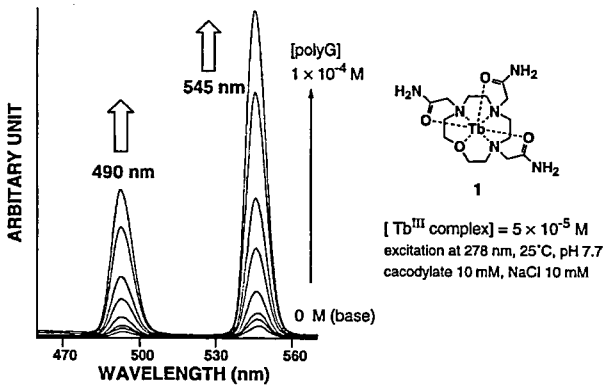
3

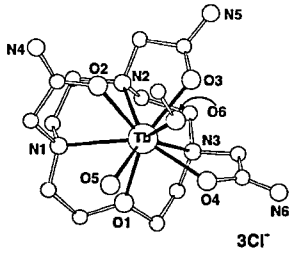
VII-F-5 Recognition and Transformation of Biomolecules by Macrocyclic Polyamine Rare Earth Complexes

Mitsuhiko SHIONOYA, Yuko HATA*, Tohru KOIKE*, Eiichi KIMURA*, Kimiko KOBAYASHI** and Sei TSUBOYAMA** *(*Hiroshima Univ., **RIKEN)*

We have been developing novel functionalized rare earth metal complexes of macrocyclic polyamines. These ligands can form stable rare earth metal complexes at physiological pH and control their coordination environments. Tb(III) ion is known to exhibit a low level of intrinsic fluorescence, which is enhanced many-fold upon interaction with nucleotides and single-stranded nucleic acids. This behavior is consistent with findings that there is general enhancement of the fluorescence of rare earth cations by energy transfer from excited ligands chelating the ion. The intensity of the fluorescence enhancement is dependent upon the base of the ligand moiety, in the order G > C ~ T > A. In the hope of applying the fluorescent characters with Tb(III) to probing nucleic acid constituents, we have synthesized a new macrocyclic complex **1**. We have synthesized a new Tb(III) complex **1** and found by a potentiometric pH titration method that this complex is stable in aqueous solution at physiological pH. The X-ray crystal analysis of **1** has disclosed that three nitrogen atoms and one oxygen atom of the macrocyclic ligand and three carbonyl oxygen atoms of the pendant groups are coordinated to the Tb(III) ion. Fluorescence of **1** and other four Tb(III) complexes were measured with or without homopolynucleotides. Among the complexes tested, **1** exhibited most significant fluorescence enhancement as a consequence of the interaction with poly G while it showed almost no

fluorescence enhancement with poly U, poly A, or poly C. Excitation spectra of **1** in the presence of poly G displayed evidence for enhancement of the fluorescence of **1** by energy transfer from guanine bases in poly G.





X-ray crystal structure of 1

VII-F-6 DNA Cleavage by a Novel Nickel(II) Complex of Pyridyl-pendant Dioxocyclam

Eiichi KIMURA*, Masatoshi SASADA*, Mitsuhiko SHIONOYA, Tohru KOIKE*, Hiromasa KUROSAKI and Motoo SHIRO***** *(*Hiroshima Univ., **Kumamoto Univ., ***Rigaku Corp.)*

[*J. Bioinorg. Chem.*, in press]

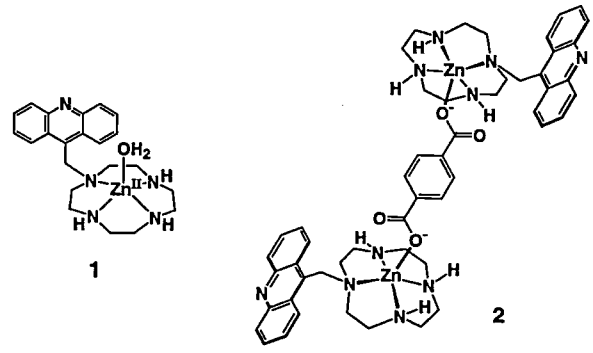
Novel potentially five-coordinate pyridyl-pendant dioxocyclam and its homologues have been synthesized to study nickel(II) complexation. A purple nickel(II) complex with a deprotonated amide and a yellow nickel(II) complex with two deprotonated amides were isolated and the structure of the latter complex was determined by X-ray analysis. It was concluded from the visible absorption and NMR studies of this complex in aqueous solution that the four-coordinate nickel(II) complex is in equibrium with a five-coordinate square-pyramidal nickel(II) complex with the apical coordination of the pyridyl-pendant. A voltammetric study disclosed a low nickel(II/III) redox potential of +0.29 V*vs* SCE for this complex at pH 9.5 and 25°C. The nickel(II) complex absorbed an equimolar amount of O_2 at pH and 25°C, and the O_2 was activated to cleave plasmid DNA.

VII-F-7 Molecular Recognition of Terephthalic Acid by Supramolecular Self-Assembly of an Acridine-pendant Cyclen-Zn^{II} Complex

Eiichi KIMURA*, Takuya IKEDA*, Mitsuhiko SHIONOYA and Motoo SHIRO** *(*Hiroshima Univ., **Rigaku Corp.)*

[*Angew. Chem. Int. Ed. Engl.*, **34**, 663 (1995)]

In the context of our work on zinc(II) complexes of cyclen and its acridine-pendant derivative **1**, which were initially designed for selective recognition of thymine and its derivatives, we have found that **1** has a fairly strong affinity for benzoate anions. Complex **1** interacts with terephthalic acid in aqueous solution to form a crystalline precipitate of **2** immediately in 90% yield. The isolated complex **2** comprises two zinc(II) complexes **1** and one terephthalic dianion. It was characterized by ^{1}H NMR and IR spectroscopies and elemental analysis. We initially suspected this 2:1 complex of having pronounced intramolecular π(guest)-π(host) stacking interactions. However, the X-ray crystal structure analysis of **2** showed more complex interactions. The zinc(II) ion resides in a distorted square-pyramidal environment, coordinated by four nitrogen atoms of the cyclen subunit and an oxygen atom of the terephthalate carboxylate anion. Furthermore, the intermolecular interactions between the two acridine groups and between an acridine group and the ethylene unit of a cyclen ring form a well-organized chainlike aggregate **3**. The tendency of **2** to self-assemble into **7** permitted terephthalate to be separated efficiently from its isomers, phthalate and isophthalate. Metal complexes with aromatic pendants should be useful for the molecular recognition of other anionic molecules in aqueous media.



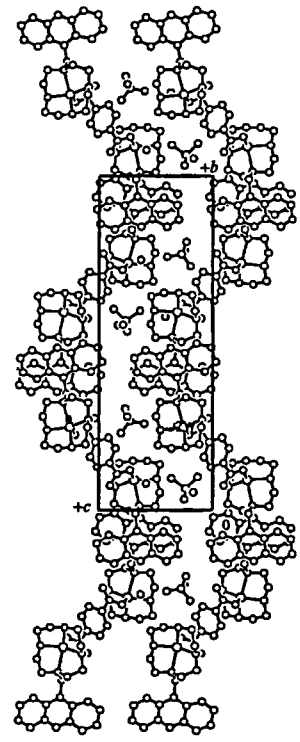


Figure 1. Arrangement of the complex **3** in the crystal along the crystallographic *a* axis.

VII-F-8 A Zinc(II)-Cyclen Complex Attached to an Anthraquinone Moiety that Acts as a Redox-Active Nucleobase Receptor in Aqueous Solution

James H. TUCKER*, Mitsuhiko SHIONOYA, Tohru KOIKE* and Eiichi KIMURA* *(*Hiroshima Univ.)*

[*Bull. Chem. Soc. Jpn.*, **68**, 2465 (1995)]

Recently, we demonstrated that a zinc(II) macrocyclic tetraamine complex, Zn^{II}-cyclen, could bind to thymidine (dT) and uridine (U) selectively among the DNA/RNA bases in aqueous solution at physiological pH. This paper describes the design and synthesis of the zinc(II) complex of an anthraquinone-pendant cyclen. The interaction of this complex with a variety of nucleosides has been studied by potentiometric pH titration, ^1H NMR, and a polarographic technique. The effect of the anthraquinone functionality in this complex is an enhanced 1:1 association with N(3)-deprotonated dT ($\log K = 6.6 \pm 0.1$ against 5.6 for Zn^{II}-cyclen system at 25°C with $I = 0.10$ ($NaNO_3$)) and its congeners, implying an additional anthraquinone-thymine aromatic stacking π-π interaction. This complex, moreover, can electrochemically recognize thymidine and other related organic substrates in aqueous solution, and is therefore a new prototype for electrochemical oligonucleotide recognition.

VII-F-9 Differential Contribution of Metal Complexation and Dimerization to the Chemotherapeutic Potential of Bicyclen-Zn^{II}_2 Complex against Human Immunodeficiency Virus

Yoshio INOUYE*, Tatsuyuki KANAMORI*, Tetsuya YOSHIDA*, Tohru KOIKE*, Mitsuhiko SHIONOYA, Haruto FUJIOKA** and Eiichi KIMURA* *(*Hiroshima Univ., **Fukuyama Univ.)*

[*Biol. Pharm. Bull.*, **19**(3), 456 (1996)]

m-Xylenediyl-biscyclen-Zn^{II}_2 complex, a potent inhibitor of human immunodeficiency virus (HIV), was obtained from cyclen by a combination of dimerization and metal complexation. The ratio of median cytotoxic concentration against host cells (CC_{50}) and median effective concentration against HIV cytopathogenicity (EC_{50}), referred to as the selectivity index (SI), was regarded to be a measure of anti-HIV activity. These two chemical modifications contributed to a potent, *in vitro* anti-HIV activity of *m*-xylenediyl-bicyclen-Zn^{II}_2 by respectively increasing the CC_{50} and decreasing the CC_{50} in comparison with those of cyclen.

VII-G Activation of Carbon Dioxide on Metal Complexes

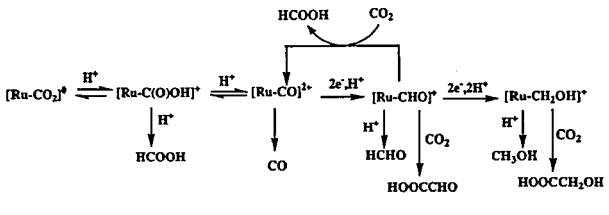
Smooth generation of coordinatively unsaturated metal centers is required for catalytic reduction of CO_2 under mild conditions. Site opening of the metal centers is usually achieved by two-electron reduction of 18-electron metal complexes. An M-η^1-CO_2 complex formed by an electrophilic attack of CO_2 to a reduced metal center is a reasonable precursor to M-CO, but it is not suitable for fixation of CO_2 directed toward C-C bond formation with the CO_2 moiety. Fission of a C-O bond of CO_2 is not completely inhibited in case CO_2 is bonded to an μ_3-S ligand in metal-sulfur clusters. A metal-metal bond in metal-sulfur clusters with μ_3-S ligands is subject to fission upon two-electron reduction . As a result, two-electron reduction of metal-sulfur clusters provides two reaction sites for an electrophilic attack of CO_2; one is μ_3-S and the other is coordinatively unsaturated metals. Oxalate is selectively produced by a coupling reaction of two molecules of CO_2 activated on the adjacent sulfur and metal sites. Besides a metal-metal bond cleavage in metal-sulfur clusters, a dynamic equilibrium of chelation and dechelation of ligands with a little energy barrier is of interest in the viewpoint of site opening and closing of the reaction centers, since such a system would be preferable for stabilization of the catalysts, inhibition of side reactions, and promotion of eliminating the products from a reaction center. Along this line, dynamic behavior of napy (naphtyl) on $[Ru(bpy)_2(\eta^1\text{-napy})(solvent)]^{n+}$ and $[Ru(bpy)_2(\eta^2\text{-napy})]^{n+}$ (n = 1 and 2; bpy = 2, 2' - bipyridine) in solutions was examined to control of the η^1- and η^2-modes of napy directed toward effective site-opening and -closing system in homogeneous catalysts.

VII-G-1 Ruthenium Formyl Complexes as the Branch Point in Two- and Multi-Electron Reduction of CO_2

Kiyotsuna TOYOHARA, Hirotaka NAGAO, Tetsunori MIZUKAWA and Koji TANAKA

[*Inorg. Chem.*, 5399(1995)]

A formyl complex, $[Ru(bpy)(trpy)(CHO)]^+$ (bpy=2,2'-bipyridine; trpy= terpyridine) formed through two-electron reduction of $[Ru(bpy)(trpy)(CO)]^{2+}$ in $EtOH/H_2O$ at -20°C functions as precursors not only for HCHO, CH_3OH, HOOCCHO, and $HOOCCH_2OH$ but also for $HCOO^-$ in electrochemical CO_2 reduction. Scheme 1 represents multi-electron reduction of CO_2 *via* formyl and hydroxycarbonyl intermediates in protic media. The finding of formyl intermediate (Scheme 1) as the branch point for two- and multi-electron reduction of CO_2 reasonably explaines why most of the reduction products have been limited to CO and/or HCOOH in electro- and photochemical CO_2 reductions catalyzed by metal complexes reported so far.



Sheme 1. Function of formyl intermediate in multi-electron reduction of CO_2.

VII-G-2 Multi-Step CO_2 Reduction Catalyzed by $[Ru(bpy)_2(qu)(CO)]^{2+}$ (bpy = 2,2'-bipyridine, qu = quinoline). Double Methylation of Carbonyl Moiety Resulting from Reductive Disproportionation of CO_2

Hiroshi NAKAJIMA, Yoshinori KUSHI, Hirotaka NAGAO and Koji TANAKA

[*Organometallics* 5093(1995)]

A well characterized η^1-CO_2 complex, $[Ru(bpy)_2(CO)(\eta^1\text{-}CO_2)]$ shows no reactivity toward CO_2. On the other hand, replacement of the CO group by an electron donating quinoline ligand greatly enhanced the reactivity of $[Ru(bpy)_2(qu)(\eta^1\text{-}CO_2)]$ (qu = quinoline). Since $[Ru(bpy)_2(qu)(\eta^1\text{-}CO_2)]$ smoothly reacts with CO_2 to produce $[Ru(bpy)_2(qu)(CO)]^{2+}$ and CO_3^{2-}. Furthermore, $[Ru(bpy)_2(qu)(CO)]^{2+}$ catalyzes reductive disproportionation of CO_2 forming CO and CO_3^{2-} in the electrochemical CO_2 reduction in the presence of $LiBF_4$. The same reduction in the presence of $(CH_3)_4NBF_4$ instead of $LiBF_4$ produces $CH_3C(O)CH_3$ and $CH_3C(O)CH_2COO^-$ in addition to CO and $HCOO^-$ in DMSO/CH_3CN (1:1 v/v). In this reaction, $(CH_3)_4N^+$ functions as the methylation agent of the carbonyl moiety resulting from reductive disproportionation of CO_2. The produced $CH_3C(O)CH_3$ undergoes the abstraction of its α-position and subsequent carboxylation to afford $CH_3C(O)CH_2COO^-$. The first catalytic formation of ketones by double methylation of metal-carbonyl resulting from reductive disproportionation of CO_2 is expresed by eq 1 and 2.

$$2(CH_3)_4N^+ + 2CO_2 + 4e^- \longrightarrow CH_3C(O)CH_3 + 2(CH_3)_3N + CO_3^{2-} \quad (1)$$

$$CH_3C(O)CH_3 + 2CO_2 + 2e^- \longrightarrow CH_3C(O)CH_2COO^- + HCOO^- \quad (2)$$

VII-G-3 Comparison of Ru-C Bond Characters Involved in Successive Reduction of Ru-CO_2 to Ru-CH_2OH

Kiyotsuna TOYOHARA, Kiyoshi TSUGE and Koji TANAKA

[*Organometallics*, 5099(1995)]

Smooth reduction from CO_2 to highly reduced organic compounds under mild conditions is highly desired in the viewpoint of utilization of CO_2 as C1 resources. Electrochemical CO_2 reduction by $[Ru(bpy)(trpy)(CO)]^{2+}$ in EtOH/H_2O at -20°C produces HCOOH, CO, HCHO, CH_2OH, HOOCCHO, and $HOOCCH_2OH$ via Ru-CO_2, Ru-C(O)OH, Ru-CO, Ru-CHO, and Ru-CH_2OH species. The distinct changes in the Ru-C bond chracters (sp_2, sp, and sp_3) were examined Raman specta. The fact that multi-electron reduction of CO_2 is more favorable than two-electron reduction in a thermodynamic sense may correlate with the bond character involved in multi-electron reduction of CO_2 affording HCOOH, CO, HCHO, CH_3OH, and CH_4. Comparisons of Raman spectra of a series of $[Ru(bpy)_2(CO)X]^{n+}$ (X = CO, C(O)OH, $C(O)OCH_3$, CO_2, CHO, and CH_2OH; n = 0, 1, 2) and their ^{18}O or deuterium isotope analogs permit reasonable assignments of ν(Ru-X) and ν(Ru-CO) bands around 520 and 470 cm^{-1}, respectively. The ν(Ru-X) bands shift to higher wavenumbers with lengthening the Ru-X bond distances (d(Ru-X)). Such unusual dependence of ν(Ru-X) upon d(Ru-X) may be associated with multi-bond characters of the C≡O, C=O, and C-O bonds in the Ru-X moieties.

VII-G-4 Crystal Structure of $[Ru(bpy)_2(CO)(\eta^1\text{-}C(O)OH)]^+$ as a Key Intermediate in CO_2/CO Conversion

Kiyotsuna TOYOHARA, Hirotaka NAGAO and Koji TANAKA

[*Chem Lett.*, 27(1996)]

The CO_2/CO conversion under protic conditions is explained by an acid-base equilibrium among η^1-CO_2, -COOH and -CO metal complexes (eq 1). The molecular structures of both $[Ru(bpy)_2(CO)_2]^{2+}$ and

$$[M\text{-}CO_2]^{n+} \underset{OH^-}{\overset{H^+}{\rightleftharpoons}} [M\text{-}C(O)OH]^{(n+1)+} \underset{OH^-}{\overset{H^+}{\rightleftharpoons}} [M\text{-}CO]^{(n+2)+} \quad (1)$$

$[Ru(bpy)_2(CO)(CO_2)]$ were already demomstrated by X-ray analysis. The molecular structure of the remaining $[Ru(bpy)_2(CO)((COOH)]^+$ is specially of interest, since the amphoteric reactivity of $[Ru(bpy)_2(CO)((COOH)]^+$ plays the key role in the CO_2/CO conversion in both CO_2 reduction and water gas shift reaction. X-ray analysis of $[Ru(bpy)_2(CO)(C(O)OH)](PF_6)$ revealed that the Ru-COOH bond distance of $[Ru(bpy)_2(CO)(C(O)OH)]^+$ (2.003 Å) is much shorter than the Ru-CO_2 one of $[Ru(bpy)_2(CO)(CO_2)]$ (2.064 Å). The shortening of the former is ascribed to an increase in a π-acceptor ability of the COOH moiety, since the Ru-N bond (*trans* to Ru-C) also show the similar behavior (Figure 1). The smooth conversion of eq. 1 in H_2O, therfore, is assited by synergic σ-donor and π-acceptor chracteristics of bpy ligands.

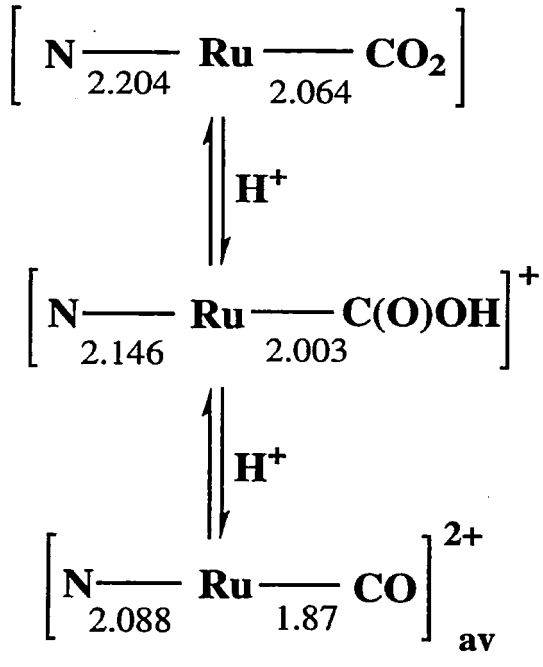


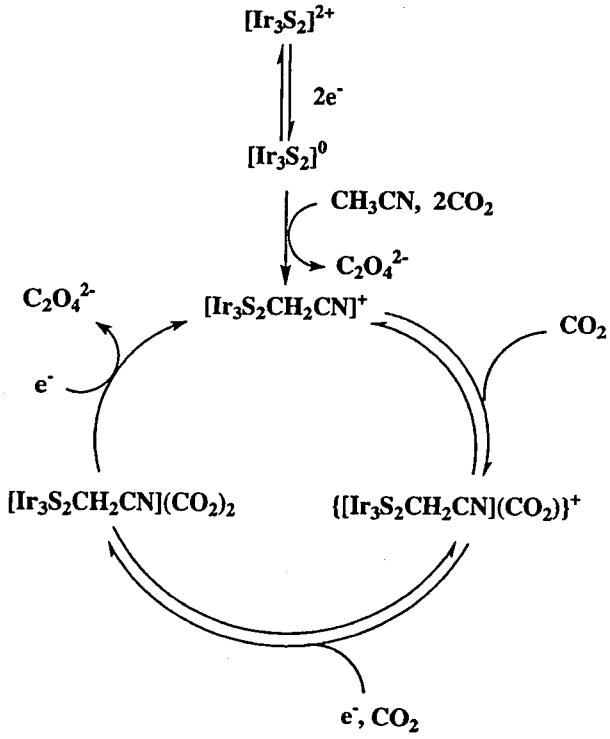
Figure 1. Bond distances of the N-Ru-C moiety in $[Ru(bpy)_2(CO)X]^{n+}$ (X = CO_2, C(O)OH, CO; n = 0, 1, 2).

VII-G-5 Catalytic Generation of Oxalate through Activation of Two CO_2 Molecules on $[(IrCp^*)_2(Ir\text{-}\eta^4\text{-}Cp^*CH_2CN)(\mu_3\text{-}S)_2]$

Koji TANAKA, Yoshinori KUSHI, Kiyoshi TSUGE,

Kiyotsuna TOYOHARA, Takanori NISHIOKA *(Osaka city University)* **and Kiyoshi ISOBE** *(Osaka city University)*

Electrochemical reduction of CO_2 in the presence of $[(IrC_p^*)_3(\mu_3\text{-}S)_2](BPh_4)_2$ ($[Ir_3S_2](BPh_4)_2$) in CH_3CN at -1.30 V (*vs.* Ag/AgCl) produced $C_2O_4^{2-}$ with a current efficiency of 60%, and $[(IrC_p^*)_2(Ir\text{-}\eta^4\text{-}C_p^*CH_2CN)(\mu_3\text{-}S)_2]^+$ ($[Ir_3S_2CH_2CN]^+$) was isolated from the electrolyte solution. The crystal structure of $[Ir_3S_2CH_2CN](BPh_4)$ by X-ray analysis revealed that a linear CH_2CN group is linked at the exo-position of a C_p^* ligand, and the $C_p^*CH_2CN$ group coordinates to an Ir atom with an η^4-mode. The cyclic voltammogram of $[Ir_3S_2CH_2CN]^+$ in CH_3CN under CO_2 exhibited a strong catalytic current due to the reduction of CO_2, while that of $[Ir_3S_2]^{2+}$ did not show an interaction with CO_2 in the same solvent. Thus, the reduced form of $[Ir_3S_2CH_2CN]^+$ works as the active species in the reduction of CO_2. The IR spectra of $[Ir_3S_2CH_2CN]^+$ in CD_3CN showed a reversible adduct formation with CO_2. The controlled potential electrolysis of $[Ir_3S_2CH_2CN]^+$ at -1.50 V under CO_2 evidenced the generation of $C_2O_4^{2-}$ through a 1: 2 adduct between $[Ir_3S_2CH_2CN]^0$ and CO_2. A coupling reaction of two CO_2 molecules activated on adjacent μ_3-S and Ir in $[Ir_3S_2CH_2CN]^0$ is proposed for the first selective generation of $C_2O_4^{2-}$.



Scheme 1. Oxalate formation in electrochemical reduction of CO_2 catalyzed by $[Ir_3S_2CH_2CN]^+$.

VII-G-6 Structural and Electrochemical Comparison of Copper(II) Complexes with Tripodal Ligands

Hirotaka NAGAO *(Sophia University)* **, Nobutoshi KOMEDA, Masao MUKAIDA** *(Sophia University)* **, Masatatsu SUZUKI** *(Kanazawa University)* **and Koji TANAKA**

[*Inorg. Chem.*, in press]

A series of copper(II) complexes with tripodal polypyridylmethylamine ligands, such as tris(2-pyridylmethyl)amine (tpa), (6-methyl-2-pyridylmethyl)bis(2-pyridylmethyl)amine (Me_1tpa), bis(6-methyl-2-pyridylmethyl)(2-pyridylmethyl)amine (Me_2tpa), and tris(6-methyl-2-pyridylmethyl)amine (Me_3tpa), have been synthesized and characterized by X-ray crystallography: $[Cu(H_2O)(tpa)](ClO_4)_2$ (**1**) crystallized in the monoclinic system, space group $P2_1/a$, with a = 15.029(7) Å, b = 9.268(2) Å, c = 17.948(5) Å, β = 113.80(3)°, and Z = 4 . $[CuCl(Me_1tpa)]ClO_4$ (**2**) crystallized in the triclinic system, space group P, with a = 13.617(4) Å, b = 14.532(4) Å, c = 12.357(4) Å, α = 106.01(3)°, β = 111.96(2)°, γ= 71.61(2)°, and Z = 4. $[CuCl(Me_2tpa)]ClO_4$ (**3**) crystallized in the monoclinic system, space group $P2_1/n$, with a = 19.650(4) Å, b = 13.528(4) Å, c = 8.55(1) Å, β = 101.51(5)°, and Z = 4 (R = 0.071, Rw = 0.050). $[CuCl(Me_3tpa)]$-$[CuCl_2(Me_3tpa)]ClO_4$ (**4**) crystallized in the monoclinic system, space group $P2_1/a$, with a = 15.698(6) Å, b = 14.687(7) Å, c = 19.475(4) Å, β = 97.13(2)°, and Z = 4 . **1**- **4** are penta-coordinate geometries with three pyridyl and one tertiary amino nitrogen atoms, and a chloride or aqua oxygen atom. Nitrite ion coordinated to the Cu(II) center of Me_1tpa, Me_2tpa, and Me_3tpa complexes with only oxygen atom to form nitrito adducts, and the catalytic activity for the reduction of NO_2^- increases in the order of Me_3tpa << Me_2tpa << Me_1tpa < tpa complexes.

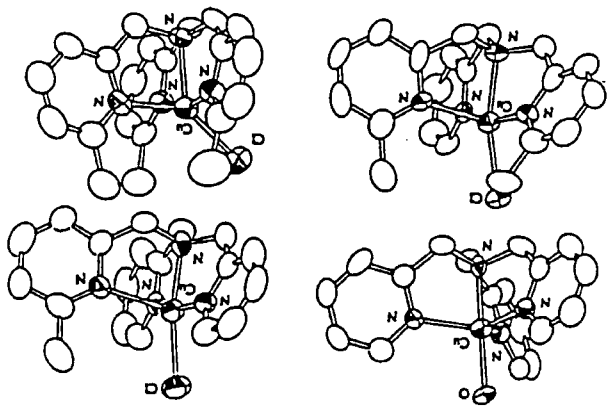


Figure 1. Molecular structures of Cu complexes with tripodal polypyridylmethylamine ligands.

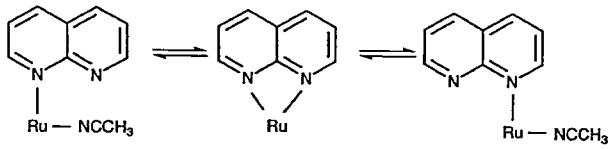
VII-G-7 Control of Coordination Mode of η^1- and η^2-1,8-Naphthyridine Ligated to Ru(II)-bis(bipyridine) Complexes

Hiroshi NAKAJIMA, Hirotaka NAGAO and Koji TANAKA

[*J. Chem. Soc. Dalton Trans.*, 1405(1996)]

Both $[Ru(bpy)_2(\eta^1\text{-}napy)(CH_3CN)](PF_6)_2$ ($[\mathbf{1}](PF_6)_2$) and $[Ru(bpy)_2(\eta^2\text{-}napy)](PF_6)_2$ ($[\mathbf{2}](PF_6)_2$) (bpy = 2,2'-bipyridine, napy = 1,8-naphthyridine) were prepared, and thier crystal structures were determined by X-ray analysis. Crystal data for $[\mathbf{1}](PF_6)_2$: triclinic, space group P1 with Z = 2 in a unit of dimension, a = 13.389(5), b = 13.590(2) and c = 10.577(2) Å, a = 104.19(2), b = 109.47(2) and c = 76.48(2)°; for $[\mathbf{2}](PF_6)_2$: orthorhombic, space group Pbcn with Z = 2 in a unit of dimension, a = 12.497, b = 15.085 and c = 17.594 Å The crystal structure of $[\mathbf{1}]^{2+}$ displays an octahedral

coordination with monodentate napy, acetonitrile and two chelating bpys. Despite the inequivalency of two nitrogens of napy of $[1]^{2+}$ in the solid state, ^{1}H-NMR spectra of $[1]^{2+}$ in aromatic region resembles that of $[2]^{2+}$ in a wide-range of -90 to 60 °C, which implies dynamic behavior of napy in $[1]^{2+}$ in solutions (Scheme 1). Both $[1]^{2+}$ and $[2]^{2+}$ undergo an irreversible reduction at -0.98 V (*vs.* Ag|AgCl) in DMF, and the process gradually becomes a reversible redox reaction on raising temperature up to 30 °C. EPR spectra of $[1]^{+}$ revealed that one-electron reduction of $[1]^{2+}$ takes place in the napy localized orbital without an appreciable increase in the electron density on one of the nitrogen of napy. The distinct inequivalence in the charge density between two nitrogen atoms of singly reduced napy results in stabilization of the N rather than N, N' co-ordination mode.



Sheme 1. Dynamic equilibrium of Ru-η^1- and -η^2-napy complexes.

VII-G-8 Synthesis and Characterization of Ruthenium-dioxolene-terpyridine Complexes

Masato KURIHARA, Stephane DANIELE *(Universite de Nice-Sophia Antipolis)*, **Kiyoshi TSUGE and Koji TANAKA**

A series of ruthenium complexes with terpyridine and substituted dioxolene ligands were prepared. The molecular structure of [Ru(terpy)(dbcat)Cl] was determined by X-ray crystallography, where terpy and dbcat denote terpyridine and 3,5-di-*t*-butylcatecholato, respectively. Crystal data: monoclinic, space group $P2_1/c$, Z = 8, a = 11.548(1) Å, b = 18.224(5) Å, c = 30. 002(8) Å, β = 96.51(2)°, and R = 0.077 (Rw = 0.068). The carbon-oxygen bond lengths of the dbcat moiety are situated between those of catecholato and semiquinonato ligands and are strongly affected by the terpyridine ligand. Ruthenium(III)-catecholato complexes were readily oxidized by Ag^+ to form Ru(II)-quinone complexes rather than Ru(III)-semiquinonato ones based on the ν(C=O) bands. Abnormal high-field shifts of a-protons (H^6 and $H^{6''}$) of the terpyridine in the ^{1}H-NMR spectra of Ru(II)(terpy)(quinone) complexes are attributed to a larger π-back donation to the terpy ligand from the Ru(dioxolene) moiety. ESR spectra of a series of Ru(III)-catecholato complexes revealed electron delocalization over the catecholato ligands at low temperature.

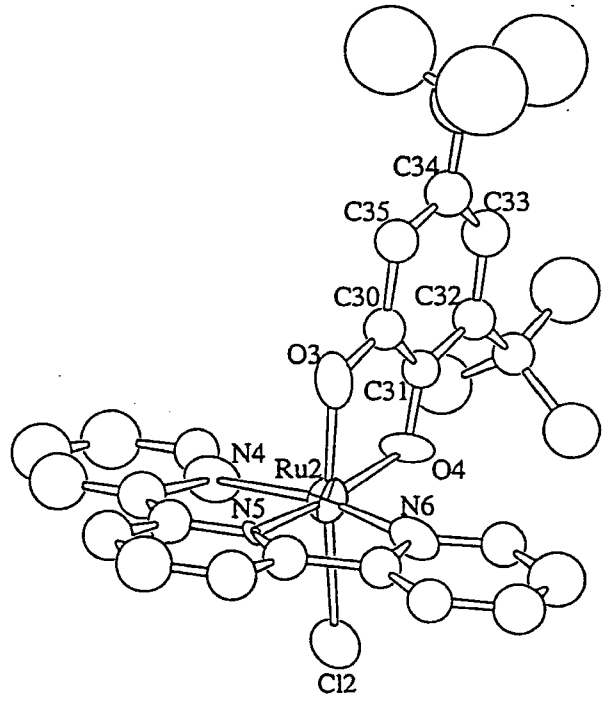


Figure 1. Molecular structure of [Ru(terpy)(dbcat)Cl].

VII-G-9 Interconversion among CO, CO_2 and CO_3^{2-} using Ruthenium Complex in Aprotic Media

Hiroshi NAKAJIMA, Kiyotsuna TOYOHARA, Kiyoshi TSUGE, Koji TANAKA

Much attention is being devoted to metal-η^1-CO_2 complexes which are the key intermediate for CO_2/CO conversion. In protic media, CO_2/CO conversion on metals takes place through acid-base equilibria among [M-η^1-CO_2]$^{n+}$, [M-η^1-C(O)OH]$^{(n+1)+}$ and [M-CO]$^{(n+2)+}$ (eq 1). In the absence of proton donors, CO_2/CO conversion is achieved by oxide transfer between metal-CO_2 and CO_2 (eq 2), which may be more useful that that in H_2O (eq 1)

$$[M\text{-}\eta^1\text{-}CO_2]^{n+} \overset{H^+}{\rightleftharpoons} [M\text{-}\eta^1\text{-}C(O)OH]^{(n+1)+} \overset{H^+}{\rightleftharpoons} [M\text{-}CO]^{(n+2)+} \quad (1)$$

$$[M\text{-}CO_2]^{n+} + CO_2 \rightleftharpoons [M\text{-}CO]^{(n+2)+} + CO_3^{2-} \quad (2)$$

from the viewpoint of utilization of CO_2 as C1 resources. Reversible oxide transfer reactions from CO_3^{2-} to $[Ru(bpy)_2(CO)_2]^{2+}$ and from $Ru(bpy)_2(CO)(\eta^1\text{-}CO_2)$ to CO_2 are established (Scheme 1). The oxide transfer reaction from CO_3^{2-} to $[Ru(bpy)_2(CO)_2]^{2+}$ producing $Ru(bpy)_2(CO)(\eta^1\text{-}CO_2)$ and CO_2 in CH_3CN is ascribed to the less basicity of the Ru-η^1-CO_2 group compared with that of CO_3^{2-}. The reverse oxide transfer from $Ru(bpy)_2(CO)(\eta^1\text{-}CO_2)$ to CO_2 affording $[Ru(bpy)_2(CO)_2]^{2+}$ is assisted by Li^+ due to low solubility of Li_2CO_3 in CH_3CN.

$$[Ru(bpy)_2(CO)_2]^{2+} \overset{CO_3^{2-}}{\rightleftharpoons} (bpy)_2Ru(CO)(C(=O)OC(=O)O) \overset{CO_2}{\rightleftharpoons} [Ru(bpy)_2(CO)(\eta^1\text{-}CO_2)]$$

Scheme 1. Rversible CO and CO_2 conversion on Ru.

VII-H Multidimensional Crystal Engineering of Supramolecular Metal Complexes

A global persistent searching for new materials with improved properties has led to an extensive investigation into inorganic and organic polymers. The reasoning behind this strategy is that if these new materials possess some properties unique to either organic polymers or inorganic polymers, they may produce revolutionary development in fundamental science and technology. Thus, attention is being focused increasingly on supramolecular metal complexes which possess both properties of inorganic and organic compounds. In order to find new materials we have attempted to synthesize one-, two- and three-dimensional copper and silver complexes with donor organic compounds.

VII-H-1 Construction of Three-dimensional Supramolecular Coordination Copper(I) Compounds with Channel Structures Hosting a Variety of Anions by Changing the Hydrogen-Bonding Mode and Distances

Megumu MUNAKATA *([a]Kinki Univ. and IMS)*, **Ling Ping WU[a], Mikiko YAMAMOTO[a], Takayoshi KURODA-SOWA[a] and Masahiko MAEKAWA[a]**

[*J. Am. Chem. Soc.*, **118**, 3117-3124 (1996)]

This paper describes four novel hydrogen-bonded copper(I) supramolecules with channel structures. The structures of all four compounds $[Cu(Hcmp)_4]X$, where Hcmp = 3-cyano-6-methyl-2(1H)-pyridinone; X = ClO_4^- (**1**), BF_4^- (**2**), PF_6^- (**3**) and $CF_3SO_3^-$ (**4**) contain a three-dimensional framework of tetrahedral CuN_4 centers linked by intermolecular hydrogen bonds through pyridinone N and O atoms in a head-to-tail mode. The very special structural features of the four compounds are related to the two types of hydrogen bonding. Complexes **1** and **2** with smaller counter anions involve each Hcmp group hydrogen-bonded to two adjacent others, which generates an open square channel filled with aligned ClO_4^- or BF_4^- ions (Figure 1), whereas **3** and **4** involve 1:1 pairwise hydrogen-bonding of Hcmp which results in a four independent interpenetrating diamond-like framework with big cavities to accommodate larger anions of PF_6^- and $CF_3SO_3^-$.

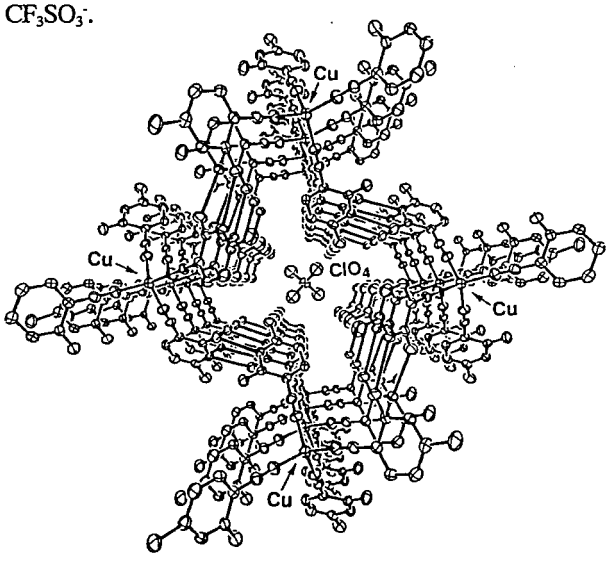


Figure 1. Molecular packing of $[Cu(Hcmp)_4]\ ClO_4^-$ with open channels.

VII-H-2 Self-assembly of Copper(I) Complexes into Three-Dimensional Coordination Polymers with Channel Networks by Hydrogen Bonding or Tridentate Ligands

Ling Ping WU[a], Mikiko YAMAMOTO[a], Takayoshi KURODA-SOWA[a], Masahiko MAEKAWA[a] and Megumu MUNAKATA *([a]Kinki Univ. and IMS)*

[*J. Chem. Soc. Dalton Trans.*, 2179-2180 (1996)]

Reaction of the appropriate copper(I) salt with 3-cyano-6-methylpyridinone-2(1*H*)-one(Hcmp) gave two polymeric co-ordination compounds, $[Cu(cmp)(Hcmp)_3]\cdot C_5H_{12}$ (**1**) and $[Cu_5(cmp)_4]ClO_4$ (**2**). Complex **1** contains a three-dimensional supramolecular framework of tetrahedral CuN_4 centres linked by intermolecular hydrogen bonds through the pyridone N and O atoms. The open square microchannels created enclathrate *n*-pentane as the guest molecule. The unique structural feature of complex **2** is that it does not involve hydrogen bonding as in **1** , instead each cmp^- monoanion employs all its three functional groups bridging three copper atoms forming a supramolecular channel architecture containing a Cu_4 cluster (Figure 1).

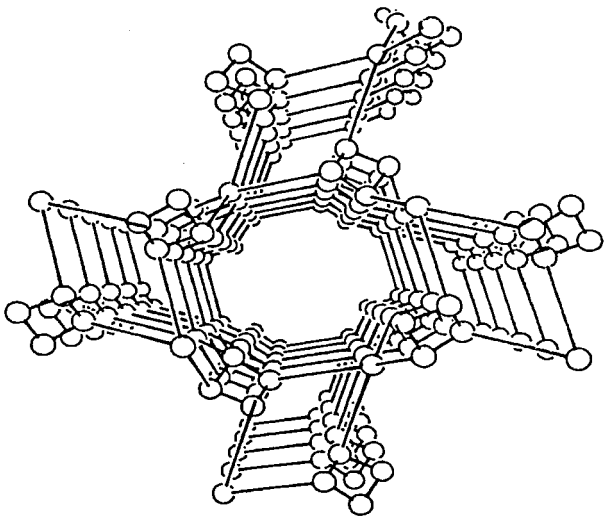


Figure 1. Perspective view of the supramolecular channel framework in $[Cu_5(cmp)_4]^+$. Only copper centers are shown.

VII-H-3 One-, Two- and Three-Dimensional Copper(I), and Silver(I) Complexes of 2,11-Dithia[3,3]paracyclophane

Megumu MUNAKATA *([a]Kinki Univ. and IMS)*, **Ling Ping WU[a], Takayoshi KURODA-SOWA[a], Masahiko MAEKAWA[a] and Yusaku SUENAGA[a]**

[*J. Chem. Soc. Dalton Trans.*, 1525-1530(1996)]

All three structures of two copper(I) and one silver(I) complex of 2, 11-dithia[3, 3]paracyclophane (dtpcp), $[Cu_2Br_2(dtpcp)(MeCN)_2]$ (**1**), $[Cu_2I_2(dtpcp)_2]\cdot$thf

(2) and [Ag(dtpcp)(NO_3)] (3), contain an infinite network comprising metal cations linked *via* dithia-bridged paracyclophane and the counter anions. The repeating dinuclear units [Cu_2Br_2(dtpcp)($MeCN)_2$] joined by dtpcp in **1** generate a one-dimensional polymeric chain. Complex **2** is a two-dimensional sheet structure in which a large ring containing six copper atoms includes a tetrahydrofuran molecule as guest inside the open cavity. The one-nitrate oxygen bridging two metal centres in complex **3** yields a unique three-dimensional channel framework of silver(I) ions (Figure 1). The iodine-doped black products of compounds **1-3** at room temperature exhibited conductivities of $10^{-5.9}$, $10^{-5.1}$ and $10^{-4.7}$ Scm^{-1}, respectively.

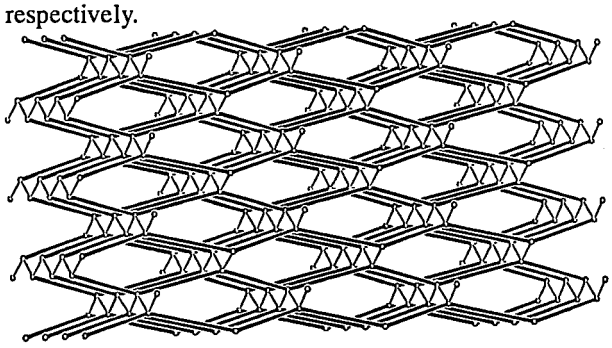


Figure 1. A view of the three-dimensional channel framework of silver ions (open circles) interconnected by dtpcp (bold lines) and NO_3^- (thin lines) in [Ag(dtpcp)(NO_3)].

VII-H-4 Synthesis, Structures and Polymeric Silver(I) Complex of Tetrakis-(methylthio)tetrathiafulvalene: The First Example of the Silver(I) Ion Coordinated Directly to TTF-Derivatives

Megumu MUNAKATA (*[a]Kinki Univ. and IMS*), **Ling Ping WU[a], Xinmin GAN[a], Takayoshi KURODA-SOWA[a] and Yusaku SUENAGA[a]**

[*Mol. Cryst. Liq. Cryst.*, **284**, 319-327 (1996)]

Reaction of silver(I) trifluoromethanesulfonate with tetrakis(methylthio)tetrathiafulvalene (TMT-TTF) yielded polynuclear silver(I)complex [Ag(TMT-TTF)(O_3SCF_3)]. It is a neutral 1:1 metal/ligand complex in which each Ag(I) ion is six-coordinated by four sulfur atoms from the bridging TMT-TTF and two oxygen atoms from the bidentate O_3SCF_3 anion, which results in a two interwoven polymeric chain structure (Figure 1).

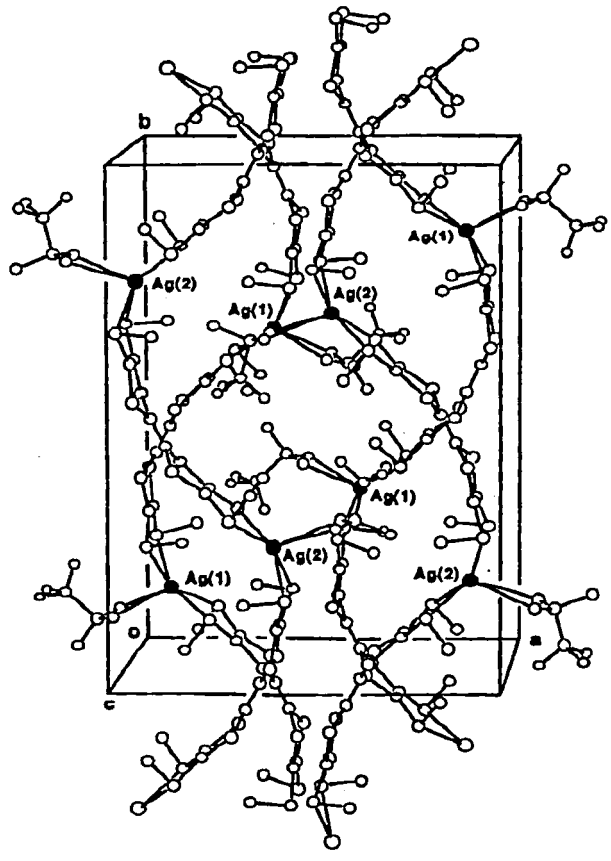


Figure 1. Packing diagram of [Ag(TMT-TTF)(O_3SCF_3)] showing two independent polymeric chains of Ag(1) and Ag(2) interwoven.

VII-H-5 Three-fold Interpenetrating Diamond Frameworks with π-π Stacking of Alternate Coordinated and Uncoordinated Ligands: Crystal Structures of Copper(I) Coordination Compounds, [Cu(DMTPN)$_2$]$_2$X(DMTPN)(thf) (DMTPN=2,5-Dimethylterephthalonitrile; X=BF_4, ClO_4)

Takayoshi KURODA-SOWA[a], Mikiko YAMAMOTO[a], Megumu MUNAKATA (*[a]Kinki Univ. and IMS*), **Makiko SETO[a] and Masahiko MAEKAWA[a]**

[*Chem. Lett.*, 349-250 (1996)]

Two novel coordination polymer compounds, [Cu(DMTPN)$_2$]X(DMTPN)(thf) (DMTPN = 2, 5-dimethylterephthalonitrile, X = BF_4 and ClO_4 are prepared and characterized by single crystal X-ray analysis; both are isostructural and have three-fold interpenetrated diamondoid structure with π-π stacking column of alternate coordinated and uncoordinated DMTPN molecules (Figure 1).

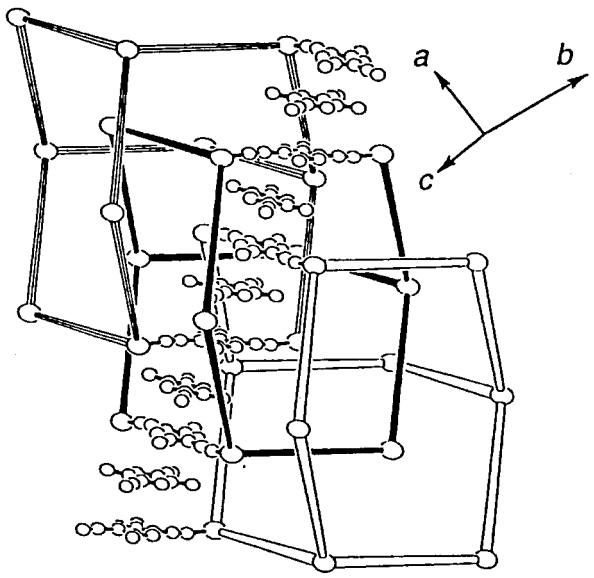


Figure 1. Three-independent diamondoid framework of copper atoms (large circles) connected by DMTPN (rods) in $[Cu(DMTPN)_2]X(DMTPN)(thf)$.

VII-H-6 Synthesis and Characterization and X-Ray Crystal Structures of Tetrakis(ethylthio)-tetrathiafulvalenium Hexachlorodicopper(II) and Hexabromodicopper(II)

Xinmin GAN[a], Ling Ping WU[a], Megumu MUNAKATA *([a]Kinki Univ. and IMS)*, **Takayoshi KURODA-SOWA[a] and Yusaku SUENAGA[a]**

[*Mol. Cryst. Liq. Cryst.*, **285**, 75-82 (1996)]

Oxidation of tetrakis(ethylthio)tetrathiafulvalene (TTC_2-TTF) with $CuCl_2$ and $CuBr_2$ in acetonitrile yielded the organic radical cation salts, (TTC_2-TTF)$[Cu_2Cl_6]$ (**1**) and (TTC_2-TTF)$[Cu_2Br_6]$ (**2**). Both structures consist of two segregated stacks of TTC_2-TTF^+ donors and $Cu_2X_6^{2-}$ acceptors associated via short S•••X contacts (Figure 1). Consistent with the structural results, the two compounds exhibit low electrical conductivities with $\sigma_{25°C}$ being 4×10^{-8} and 8×10^{-8} Scm^{-1} for **1** and **2**, respectively.

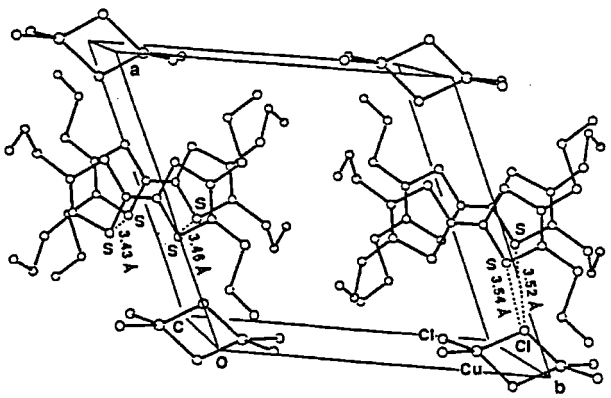


Figure 1. Packing diagram of (TTC_2-TTF)$[Cu_2Cl_6]$. The dashed lines show the close S···S and S···Cl contacts.

VII-H-7 A Unique Coordination Polymer Consisting of Two Parallel $C_5H_4S_5$ Molecules Bridging Two Silver(I) Ions ($C_5H_4S_5$=4,5-ethylenedithio-1,3-dithiole-2-thione)

Jie DAI[a], Megumu MUNAKATA *([a]Kinki Univ. and IMS)*, **Takayoshi KURODA-SOWA[a], Ling Ping WU[a] and Mikiko YAMAMOTO[a]**

[*Inorg. Chim. Acta,* in press]

The silver(I) complex with 4,5-ethylenedithio-1,3-dithiole-2-thione ($C_5H_4S_5$), $[Ag(C_5H_4S_5)_2NO_3]$, was synthesized and the molecular structure and packing was characterized crystallographically. The Ag atom is coordinated with four ligands through two thiocabonyl sulfur atoms (C=S) and two thioether sulfur atoms (-S-) of six-membered ring (-S-) respectively, forming a extremely distorted tetrahedral geometry. Two parallel $C_5H_4S_5$ molecules are connected by two Ag(I) ions to give a unique infinite chain. The S···S contacts of 3.41 Å between two nearby chains along the *b* axis generate two dimensional network (Figure 1).

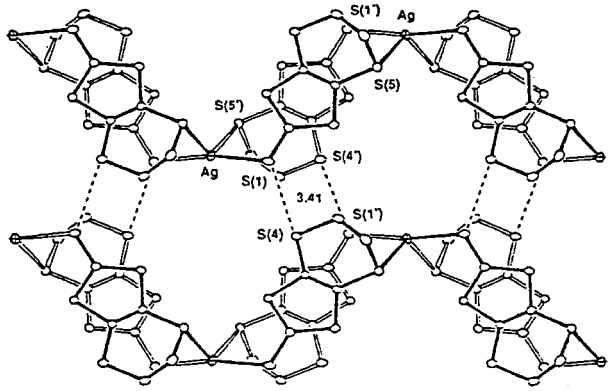


Figure 1. Packing diagram of $[Ag(C_5H_4S_5)_2]^+$. The dashed lines show the close S···S contacts.

VII-H-8 Reversible Photochromism of a Crystalline Dithienylethene Copper(I) Polymer

Megumu MUNAKATA *([a]Kinki Univ. and IMS)*, **Ling Ping WU[a], Takayoshi KURODA-SOWA[a], Masahiko MAEKAWA[a] and Yusaku SUENAGA[a] and Koichi FURUICHI[a]**

[*J. Am. Chem. Soc.*, **118**, 3305-3306 (1996)]

We synthesized the first photochromic copper(I) compound with cis-1,2-dicyano-1,2-bis(2,4,5-trimethyl-3-thienyl)ethene (*cis*--L), $[Cu(cis\text{-}L)_2]ClO_4$ (**1**). Two copper(I) ions in **1** are in turn bridged by two *cis*-L molecules to form an infinite chain. On irradiation of the orange fine crystals of ring-open form, **1** with 405 nm light for 1 hour at room temperature, the color of the crystals turned red ring-closed form. The ring-closed form reverts to the orange ring-open form on irradiation with 550 nm light. This cycle can be repeated many times. The photochromic interconversion between the twisted ring-open form and coplanar ring-closed form accompanied by bond order change of the ethene backbone of the *cis*-L indicates crystal oscillation in the copper(I) coordination polymer in crystalline state (Figure 1).

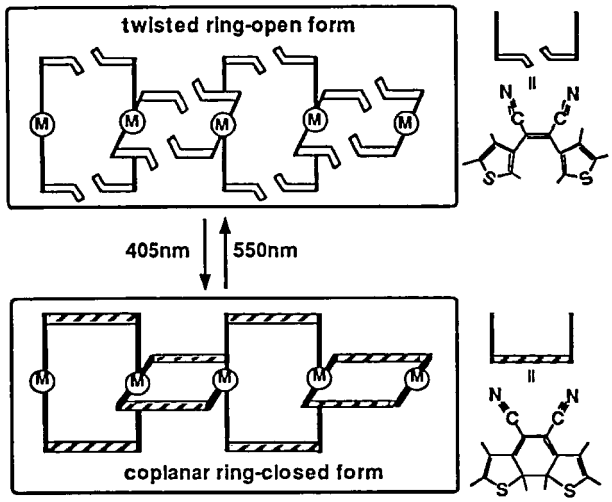


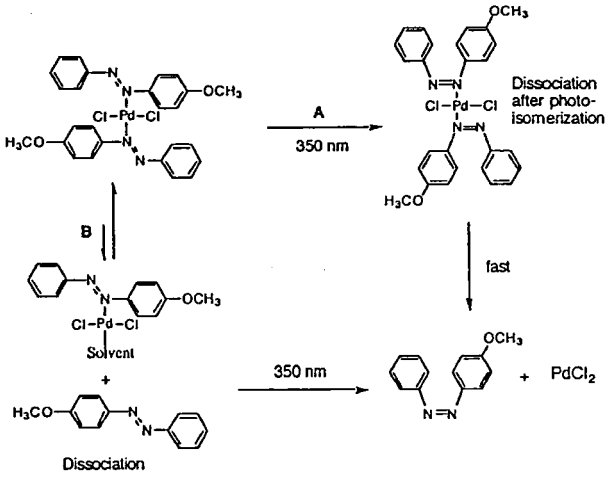
Figure 1. Schematic figure of light-induced crystal oscillation of $[Cu(cis\text{-}L)_2]ClO_4$.

VII-H-9 Synthesis, Structures and Properties of Palladium(II) Complexes with Photochromic 4-Methoxyazobenzene

Megumu MUNAKATA *([a]Kinki Univ. and IMS)*, **Ling Ping WU[a], Takayoshi KURODA-SOWA[a] Masahiko MAEKAWA[a] and Yusaku SUENAGA[a] and Koichi FURUICHI[a]**

[*Inorg. Chim. Acta,* **248**, 147-152 (1996)]

The molecular structure of palladium(II) complex with photochromic ligand 4-methoxyazobenzene (Moaz), $[Pd(Moaz)(PhCN)(H_2O)](ClO_4)$ (**1**) shows a distorted square planar coordination around the Pd atom and the Moaz group forms a five-membered chelate ring with the metal ion by means of σ-bond at an *ortho*-carbon atom and the lone pair of the further nitrogen. In $[Pd(Moaz)_2Cl_2]$ (**2**) the palladium atom lies on an inversion center and surrounded ion an essentially square planar fashion by the symmetry related two Moaz ligands and two chloride ions. Moaz in **2** acts as a monodentate ligand to bind the metal center via a Pd-N σ-bond. It was found that the monodentate-coordinated Moaz in **2** shows a *trans-cis* photoisomerization (Scheme 1), while rigidity imparted to the Moaz linkage by palladium in **1** inhibits its photochromic reaction,



Scheme 1. A *trans-cis* photoisomerization of Moaz molecules in $[Pd(Moaz)_2Cl_2]$.

VII-H-10 An Unusual Tetranuclear Copper(I) Acetate Structure with an Open Cubane Cu_4O_4 Framework

Ling Ping WU[a], Takayoshi KURODA-SOWA[a], Masahiko MAEKAWA[a], Yusaku SUENAGA[a] and Megumu MUNAKATA *([a]Kinki Univ. and IMS)*

[*J. Chem. Soc. Dalton Trans.*, 2031-2037 (1996)]

The tetranuclear copper(II) $[\{Cu(O_2CMe)(OMe)\}_4]$ has been found to contain as unusual open cubane Cu_4O_4 framework defined by two interpenetrating copper and oxygen planes rather than two tetrahedra (Figure 1) and to show strong antiferromagnetic coupling.

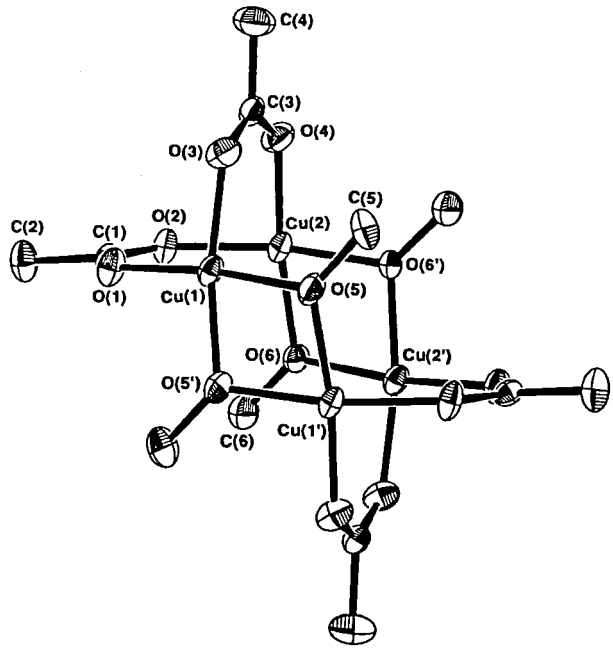


Figure 1. Molecular structure of $[\{Cu(O_2CMe)(OMe)\}_4]$ showing strong antiferromagnetic coupling.

VII-I Metal-Complex Based Magnetic Materials Constructed by Building Block Method

The field of molecular magnetism has shown quite spectacular advances in the last decade and several different approaches are currently used. The molecular engineering and the crystal engineering are necessary to design the magnetic material. We have focused on a building block method by the use of two kinds of building blocks, one of them containing a potential bridging ligand and other of them potential coordination sites. This method is very effective to control the multi-dimensional extended structure and the magnetic property by choosing proper building blocks. The reaction of two building components, $[MnL(H_2O)]ClO_4$ and $[Fe(CN)_6]^{3-}$, produces a variety of extended structures including one-dimensional, two-dimensional and three-diemnsional structures as well as polynuclear structures and they show a variety of magnetic properties.

Reference

1) H. Miyasaka, N. Matsumoto, H. Okawa, N. Re, E. Gallo, and C. Floriani, J. Am. Chem. Soc., **1996**, 118, 981-994.)
2) H. Miyasaka, N. Matsumoto, H. Okawa, N. Re, E. Gallo, and C. Floriani, Angew. Chem. Int. Ed. Engl. 1995, 34, 1446-1448.

VII-I-1 Synthesis, Crystal Structure, and Magnetic Property of a One-Dimensional Ferromagnet with a Mn(III)-NC-Fe(III) Linkage $[NEt_4]_2[Mn(acen)][Fe(CN)_6]$ (NEt_4 = Tetraethylammonium, acen = N, N'-Ethylenebis(acetylacetonylideneiminato))

Nazzareno RE, Emma GALLO, Carlo FLORIANI *(Lausanne Univ.)*, **Hitoshi MIYASAKA and Naohide MATSUMOTO***(Kyushu Univ. and IMS)*

A one-dimensional compound with a Mn(III)-NC-Fe(III) linkage of the formula of $[NEt_4]_2[Mn(acen)][Fe(CN)_6]$ (NEt_4=tetraethylammonium, acen=N,N'-ethylenebis(acetylacetonylideneiminato)) has been prepared by the assembly reaction of [Mn(acen)Cl] and $[NEt_4]_3[Fe(CN)_6]$ in ethanol/2-propanol. The compound crystallizes in the orthorhombic space group *Pnma* with the cell dimensions of a=17.415(5) Å, b=19.79(1) Å, c=11.471(4) Å, V=3952(2) Å^3 with Z=4 to converge the final values of R=0.042 and Rw=0.043. The compound assumes a one-dimensional snaky-chain structure consisting of $(-Mn-NC-Fe-CN-)_n$ as the repeating unit with the dimensions of Fe-C=1.952(4) Å, Mn-N=2.316(4) Å, Mn-N-C=152.6(3)°, Fe-C-N=177.1(4)°, in which the Fe ion is positioned at the inversion center, the [Mn(acen)] moiety lies on a mirror plane, and the adjacent one-dimensional chains run like a snake along the b-axis with the same phase. On lowering the temperature, the effective magnetic moment per FeMn increases gradually from 5.05 μ_B at room temperature and then abruptly below ca. 20 K to 15.5 μ_B at 1.9 K, indicating that the one-dimenional chain is a ferromagnetic chain due to an intrachain ferromagnetic coupling between Mn(III) and Fe(III) ions through the bridging CN^- group. The FCM curve (field-cooled magnetization) under 1 Oe showed a spontaneous magnetization below 2.5 K. The magnetization vs H upto 55 kOe at 1.9 K showed an extremely large zero-filed susceptibility, indicating that the compound is a ferromagnet due to a weak interchain ferromagnetic couplung.

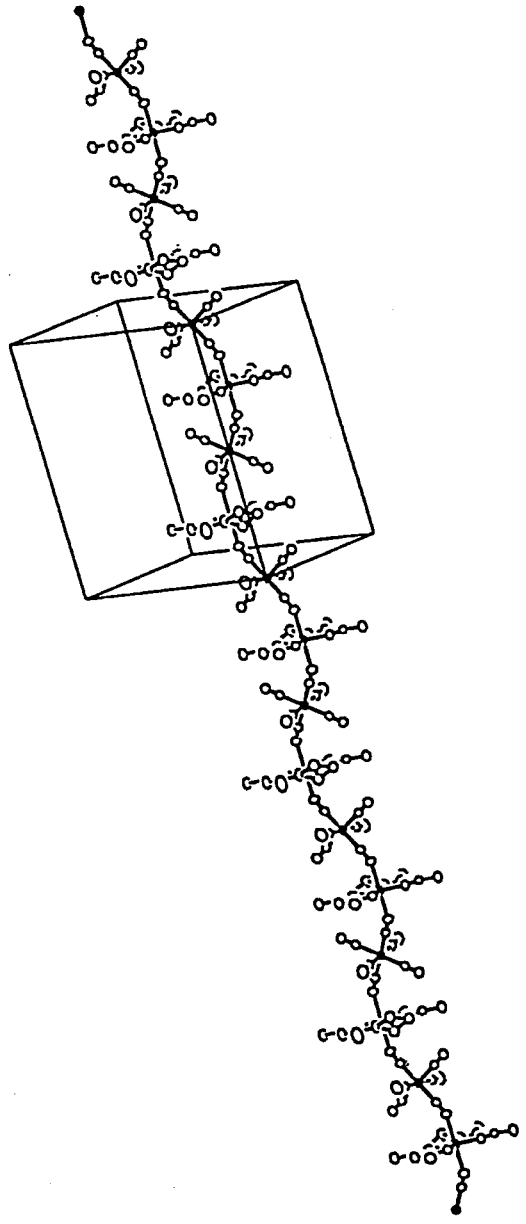


Figure 1. One-dimensional structure consisting of a $(-Mn-NC-Fe-CN-)_n$ as a repeating unit

VII-I-2 Synthesis, Crystal Structure, and Magnetic Property of a Ferrimagnetic Layer Compound, $[NEt_4][Mn(5\text{-}ClSalen)]_2[Fe(CN)_6]$ (NEt_4 = Tetraethylammonium, 5-ClSalen = N, N'-Ethylenebis(5-chlorosalicylideneiminato))

Hitoshi MIYASAKA, Naohide MATSUMOTO(*Kyushu Univ. and IMS*) **Nazzareno RE, Emma GALLO and Carlo FLORIANI**(*Lausanne Univ.*)

A two-dimensional hetero-metal assembly with the formula of $[NEt_4][Mn(5\text{-}Clsalen)]_2[Fe(CN)_6]$ (NEt_4=tetraethylammonium, 5-Clsalen=N,N'-ethylenebis(5-chlorosalicylideneiminato)) has been prepared and the crystal structure and the magnetic properties have been characterized. The compound crystallizes in the monoclinic space group $P2_1/c$ with the cell dimensions of a=13.104(3) Å, b=12.861(3) Å, c=15.526(2) Å, b=105.98(1) °, V=2515.3(8) Å^3, and that is isostructural to a metamagnet K[Mn(3-MeOsalen)][Fe(CN)$_6$]·2DMF, composing of an intralayer ferromagnetic interaction and an interlayer antiferromagnetic interaction, in the space group, the cell dimensions, and the atomic parameters. The structure assumes a two-dimensional network structure consisting of cyclic octanuclear (-Mn-NC-Fe-CN-)$_4$ as a net unit with the dimensions of Fe-C1=1.947(8) Å, Fe-C2=1.951(8) Å, Mn-N1 = 2.286(7) Å, Mn-N2 = 2.266(7) Å, Mn-N-C = 154.4(7)°, Mn-N-C=146.1(7)°. The magnetic measurements(magnetic susceptibility vs T, field-cooled magnetization, remnant magnetization, and zero-filed cooled magnetization vs T, and saturation magnetization vs H upto 55 kOe) demonstrated that the compound is a ferrimagnetic layer compound with the magnetic phase transition temperature, T_N = 10.9 K, in which intralayer interaction operating between Mn(III) and Fe(III) ions through bridging CN$^-$ group is antiferromagnetic and interlayer interaction is antiferromagnetic. The structural similarity and the distinct different magnetic properties of the two compounds are discussed.

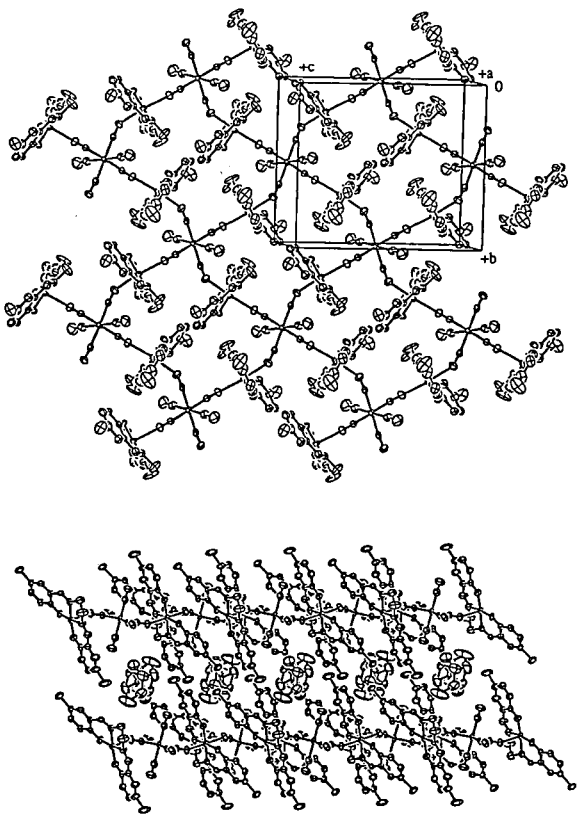


Figure 1. (a) Projection along the a-axis, showing a two-dimensional network structure, in which a net unit is composed of a cyclic octanuclear structure (–Mn–NC–Fe–CN–)$_4$. (b) Projection perpendicular to the a-axis, showing a stacking of the layers.

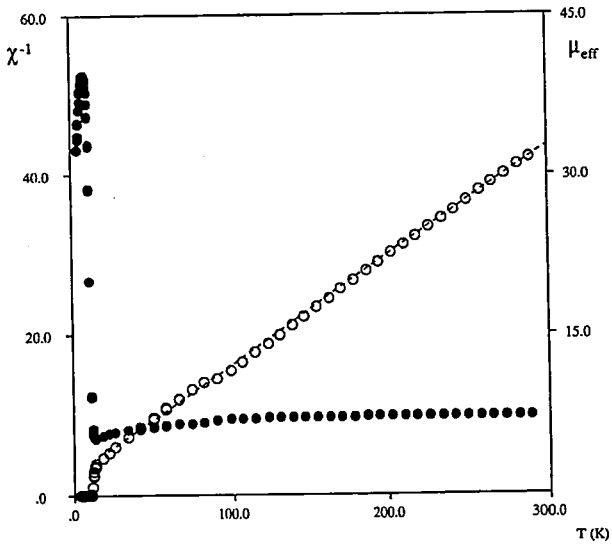


Figure 2. Temperature dependence of the effective magnetic moment and the reciprocal magnetic susceptibility, showing a negative Weiss constant

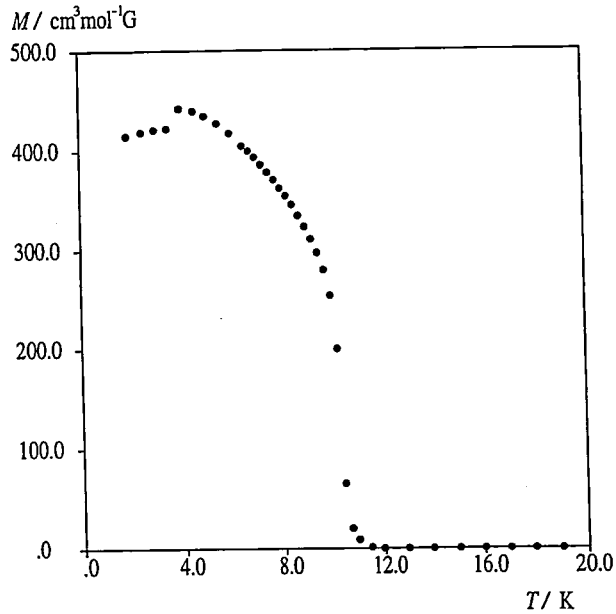


Figure 3. FCM (field-cooled magnetization vs. T) curve under magnetic field 3 Oe.

VII-I-3 Syntheses, Structures, and Magnetic Properties of Discrete Bi-, Tri-, and Penta-nuclear Complexes derived from Manganese(III) Salen-like Schiff Base Complexes and Tetraethylammonium Hexacyanoferrate and Spontaneous Magnetization Behavior of their Desolvated Compounds

Hitoshi MIYASAKA, Hidenori IEDA, Naohide MATSUMOTO(*Kyushu Univ. and IMS*), **Nazzareno RE, Emma GALLO, Carlo FLORIANI**(*Lausanne Univ.*)

The assembly reaction between $[Mn(BS)(H_2O)]ClO_4$ and $[NEt_4]_3[Fe(CN)_6]$ in methanol or ethanol gave a binuclear $[NEt_4]_2[\{Mn(BS)(S)\}\{Fe(CN)_6\}]$ **1**, three trinuclear, $[NEt_4][\{Mn(BS)(S)\}_2\{Fe(CN)_6\}]$ **2, 3, 4**, and a pentanuclear $[Mn(BS)(S)]_4[Fe(CN)_6]ClO_4$ **5**, hetero-metal complexes, depending on the nature of the quadridentate Schiff base

ligands and regardless of the reaction ratio of the precursor components. Complexes **1** and **2** have been characterized by the single-crystal X-ray analyses. **1** crystallizes in the monoclinic space group $P2_1/m$ and the structure consists of a discrete cyano-bridged Mn(III)-Fe(III) binuclear unit $[(H_2O)Mn(saldmen)Fe(CN)_6]^{2-}$ and the binuclear units are hydrogen-bonded between the coordinated water molecule and the methanol of the crystal solvent and between the methanol and the CN group of the adjacent unit to form a one-dimensional chain structure (-NC-Fe-CN-Mn-H_2O-MeOH-)n. **2** crystallizes in the orthorhombic space group *P*bcn and the structure consists of a discrete centrosymmetric trinuclear unit $[(MeOH)Mn(salmen)Fe(CN)_6Mn(salmen)(MeOH)]^-$ and the trinuclear units are weekly hydrogen-bonded between the methanol and the CN group of the adjacent unit to form a two-diemnsional network structure having a cyclic octanuclear $(-NC-Fe-CN-Mn-MeOH-)_4$ as a net unit. The temperature dependence of the magnetic susceptibilities of **1-5** were well reproduced on the basis of the corresponding discrete polynuclear structures. The desolvated compounds of **1-5**, **1'-5'**, were prepared by evaporating the solvent molecules through the procedure of the thermogravimetric analyses. **1'**, **2'**, and **3'** showed a spontaneous magnetization, indicating the formation of the extended multi-dimensional structures, whereas **4'** and **5'** did not. The route from the discrete isolated structure to the extended structure was discussed.

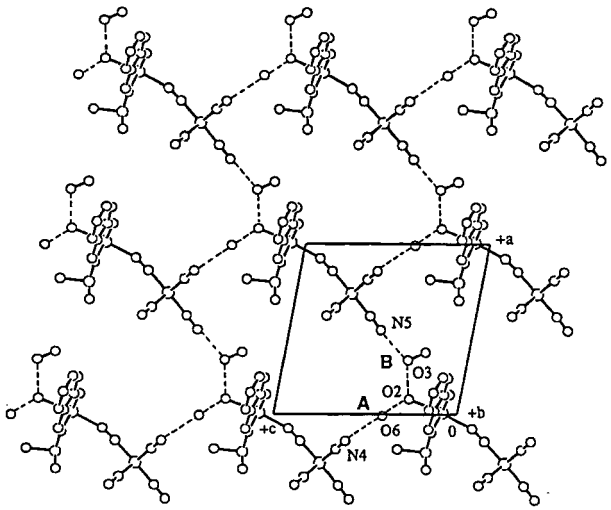


Figure 1. Projection along the *b* axis for **1**, showing a one-dimensional chain structure formed by hydrogen bonds.

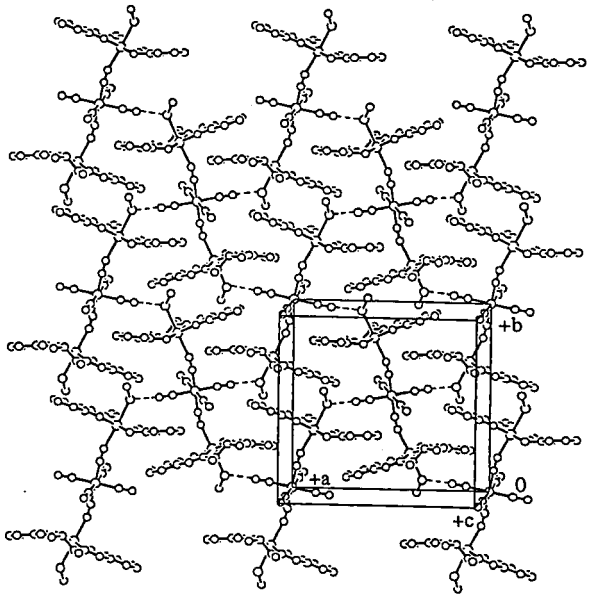


Figure 2. (a) Projection along the *c*-axis of **2**, showing a two-dimensional network structure formed by hydrogen bonds.

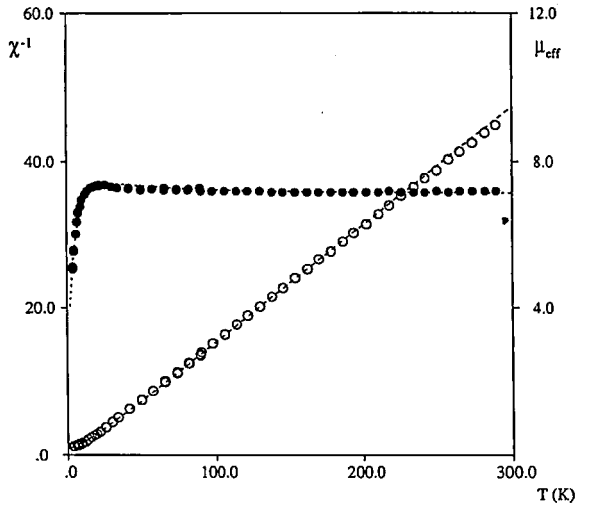


Figure 3. Temperature dependence of the effective magnetic moment and the reciprocal magnetic susceptibility of a solvated compound **2**

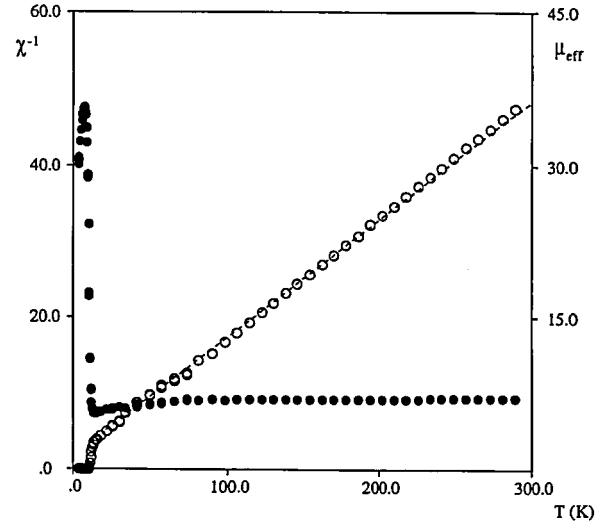


Figure 4. Temperature dependence of the effective magnetic moment and the reciprocal magnetic susceptibility of a desolvated compound **2**, indicating a spontaneous magnetization and suggesting a formation of the extended structure.

RESEARCH ACTIVITIES VIII
Computer Center

VIII-A Theoretical Studies of Highly Excited Vibrational States in Polyatomic Molecules

Research activities of this year include: (a) semiclassical study of nonintegrable systems, and (b) electronic structure and dynamics of small polyatomic molecules.

VIII-A-1 Semiclassical Study of Nonintegrable Systems

Toshiya TAKAMI

We study nonadiabatic process in classically nonintegrable systems such as 2D billiards and kicked rotators to reveal essence of the dynamical characters in the highly excited states of molecules. One of the typical character in the nonintegrable systems is avoided crossings between adiabatic levels. Nonadiabatic transition between adjacent states, which was described first by Landau and Zener, etc., is one of the well-known quantum processes in molecular systems. In the highly excited states of nonintegrable systems, however, it is difficult to predict the final state semiclassically, because each eigenlevels around the initial state can be a final state of the transition.

Our approach to this problem is twofold: (1) to study statistical properties of the transition by quantum mechanical calculations; (2) to analyze the interaction between adiabatic states by classical information such as periodic-orbit scars.

VIII-A-2 Theoretical Study of the Potential Energy Surfaces and Dynamics of CaNC/CaCN

Shinkoh NANBU, Satoshi MINAMINO and Mutsumi AOYAGI

Potential energy surfaces for electronic ground and two low-lying excited states of CaNC/CaCN, were obtained by the ab initio molecular orbital (MO) configuration interaction (CI) calculations. On the obtained potential energy surfaces the wave packet dynamics for the nuclear motion were carried out to estimate the theoretical absorption and emission spectra.

We found that the stational structures of the $1^2\Sigma^+$ and $1^2\Pi$ states are linear conformation of calcium isocyanide (CaNC). And also these two states are characterized by ionic bonding and especially the potential energy along the bending coordinate are isotropic. In this study by using the wave packet propagation, we demonstrate the possibility of the large amplitude motion related to pseudorotational motion which could be seen as Ca^+ rotating around CN^- in the bending vibration. The estimated theoretical spectra reproduce the feature of experimental ones.

VIII-A-3 Theoretical Calculation of Reaction Rate Constant of Hydrofluorocarbon

Satoshi MINAMINO, Kouichi MOGI and Mutsumi AOYAGI

Hydrofluorocarbon(HFC) is recently the focus of the attention of the world as one of the substitute for Chlorofluorocarbon(CFC). The study of the reaction of HFC with OH radical is very important in atmospheric chemistry because it can estimate the life time of HFC in atmosphere.

The activation energy and rate constant of the H-abstraction reactions of fluoroethanes and ethane by OH radical are determined by using ab initio methods and transition state theory. The transition state structures of these reactions were fully optimized at MP2 method by using 6-311++G** basis sets. The activation energies were determined by MP4(SDTQ)/6-311++G**. As shown in the Table 1, the order of activation energy for these reactions were determined as $CH_3CH_2F < CH_3CH_3 < CH_3CHF_2 < CH_2FCF_3 < CHF_2CF_3 < CH_3CF_3$, which are in good agreement with experiment[1]. The calculated rate constants are underestimated, compared with experimental values. As shown in the Figure 1, It is found that with the effect of CF_3 group, the rate constant becomes smaller. This is explained by the fact that the effect of CH_3 group makes C-H bond weaker, while the effect of CF_3 group makes C-H bond stronger.

1) R. Atkinson, *Chem. Rev.* **86**, 69 (1986).

Reaction	Ea (kcal/mol)	log k(298) calc.	log k(298) exp.[1]
CH3CH3 + OH	3.52	-13.06	-12.56
CH3CH2F + OH	2.58	-13.01	-12.64
CH3CHF2 + OH	3.40	-13.63	-13.47
CH3CF3 + OH	6.52	-15.40	-14.70
CH2FCF3 + OH	5.59	-14.77	-14.07
CHF2CF3 + OH	6.24	-15.04	-14.60

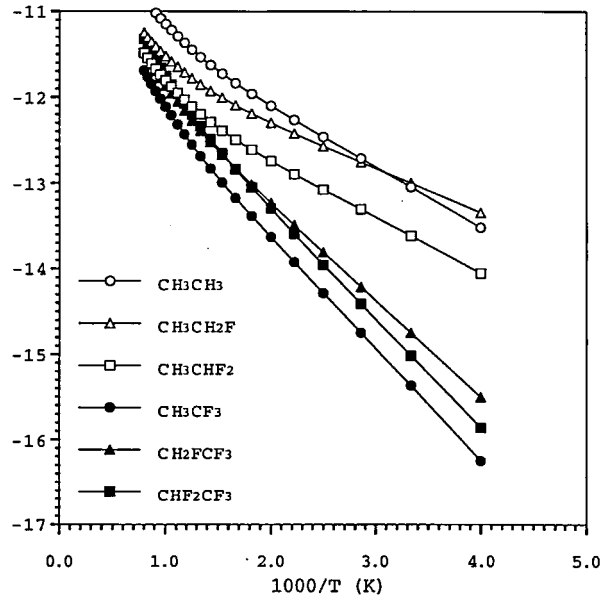


Figure 1. Arrhenius plot of fluoroethanes and ethane with OH radical.

VIII-A-4 Theoretical Analysis of the Jahn-Teller Distortions of C_{60}^-

Kouichi MOGI and Mutsumi AOYAGI

Recently, T. Kodama and T. Kato (IMS) observed the angular dependent ESR spectra of single crystal C_{60}^- salts and they determined the anisotropic components of the g factor of C_{60}^-. They suggested that the molecular structure of C_{60}^- should be distorted to the lower symmetry of C_{2h} or C_i from the analysis of their experimental data. Koga and Morokuma[1] suggested from their *ab initio* calculations at the UHF/3-21G level of calculations that the geometries of the negative ion of C_{60} could be characterized as the Jahn-Teller distortion toward D_{5d}, D_{3d}, and D_{2h} symmetry, which lie almost isoenergetically.

In order to understand the detailed structure of C_{60}^-, we carried out the geometry optimization of C_{60}^- by using UHF/3-21G and UHF/6-31G methods and performed the vibrational analysis of C_{60}^- in D_{2h}, C_{2h}, and C_i symmetry. The energy levels of D_{2h}, C_{2h}, and C_i species of C_{60}^- were found to be very close. We found that the ^2A_u electronic state of C_{2h} structure has one imaginary frequency mode with b_g symmetry, which can lead to the C_i symmetric structure with lower energy level. From the geometry optimization, we finally obtained the C_i structure in which all the calculated vibrational frequency has the real values. These results are consistent with the experimental analysis of the anisotropic components of the g factor.

1) N. Koga and K. Morokuma, *Chem. Phys. Lett.* **196**, 191 (1992)

Chemical Materials Center

VIII-B Preparation and Properties of Novel Heterocyclic Compounds for Advanced Materials

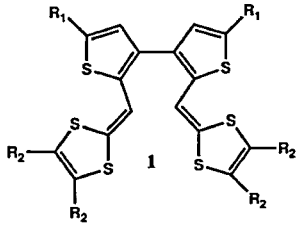
Heterocycles containing chalcogen atoms are useful as components of organic conductors since heteroatoms in their rings are helpful to stabilize ions or ion-radical species, and extended π-conjugation decreases Coulombic repulsion. In addition intermolecular interactions caused by heteroatom contacts can be expected to form unique molecular assemblies. In this project novel electron acceptors and donors based on heterocycles such as 1,2,5-thiadiazole and 1,3-dithiole were synthesized and their properties including those of the charge-transfer complexes or ion-radical salts were investigated. Thiophene derivatives with fused heterocycles were also synthesized and led to new types of oligomers and polymers having narrow bandgaps.

VIII-B-1 Oxidative Intramolecular Cyclization of 2,2'-Bis(1,4-dithiafulven-6-yl)-3,3'-bithienyls Affording Bis(1,3-dithiole) Electron Donors

Akira OHTA *(Graduate Univ. for Advanced Studies)* **and Yoshiro YAMASHITA**

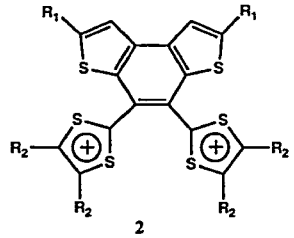
[*J. Chem. Soc., Chem. Commun.*, 1761 (1995)]

Although 1,4-dithiafulvene derivatives are known to undergo oxidative intermolecular coupling reactions to give TTF vinylogues, the corresponding intramolecular cyclization is unknown. The title bis(1,3-dithiole) compounds **1** were expected to undergo the cyclization reaction by oxidation to give a novel type of electron donors **3**. The compounds **1a-e** actually afforded the oxidation products **2** by chemical oxidation with $(4\text{-}BrC_6H_4)_3N^+SbCl_6^-$ in high yields. Reduction of **2** with zinc gave the corresponding neutral donors **3** in high yields. The donors **3** showed reversible one-stage two-electron oxidation waves and the oxidation potentials were fairly low compared with that of TTF (0.18 - 0.41 V vs. SCE). The X-ray structure analyses of **2d** and **3d** reveal that in the neutral state the two 1,3-dithiole rings deviate largely from the plane of the tricyclic ring, while in the dication the dithiole rings are almost orthogonal to the benzodithiophene moiety.

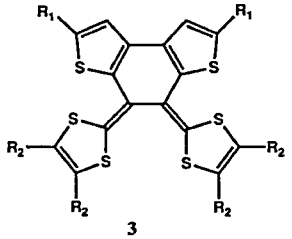


a; R_1 = H, R_2 = SMe
b; R_1 = H, R_2 = benzo
c; R_1 = Me, R_2 = H
d; R_1 = Me, R_2 = SMe
e; R_1 = Me, R_2 = benzo

1



2

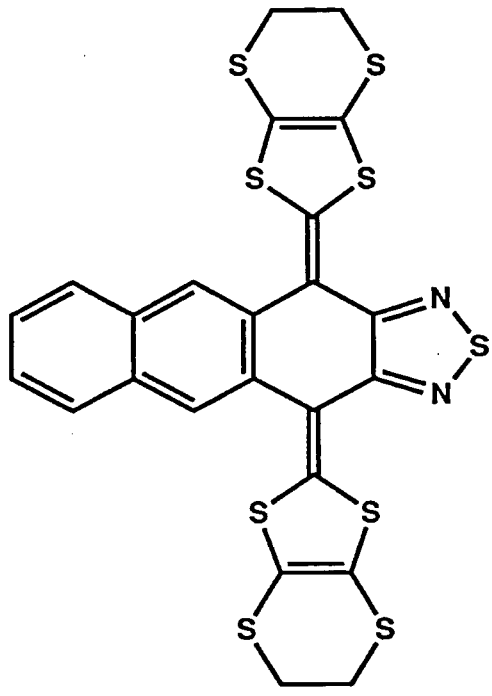


3

VIII-B-2 Metallic Cation Radical Salts of BEDT-ATD Incorporating Solvent Molecules

Yoshiro YAMASHITA, Masaaki TOMURA and Kenichi IMAEDA

We have recently prepared BEDT-ATD **1** which is a new type of electron donor with a butterfly-shaped structure. This donor molecule afforded cation radical salts whose composition is 2:1:1 (donor:cation:THF) when electrochemically oxidized in THF. In an extension of this work, we have now prepared the cation radical salts incorporating 2,5-dihydrofuran (DHF) and 1,3-dioxolane (DO). They were obtained as single crystals by electrochemical oxidation in those solvents. In order to examine the difference in structures, the X-ray analyses were carried out. The crystal structures are very similar to that of the THF incorporated one. There is no distinctive difference except solvent molecules which are located in a disordered manner. However, the physical properties were strongly dependent on the incorporated solvent molecules. The electrical conductivities of $\mathbf{1}_2(PF_6)$(DHF) and $\mathbf{1}_2(PF_6)$(DO) at room temperature were both 25 Scm^{-1}, which are comparable to that of the THF incorporated one. In contrast to the THF salt showing metallic behavior down to low temperature, the DHF and DO salts showed metal-insulator transition at 150 K and 100 K, respectively. This difference seems related to the ordering of the solvent molecules.



1, BEDT-ATD

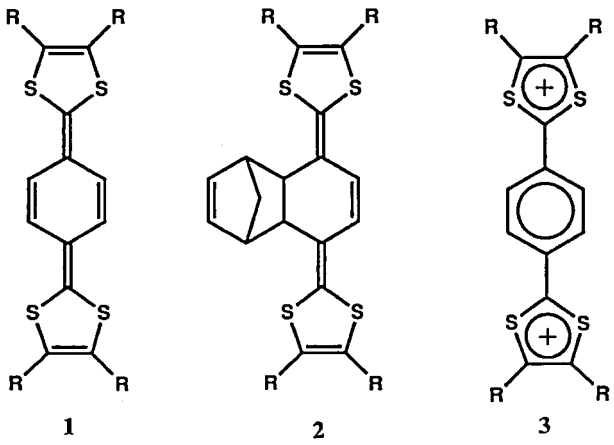
VIII-B-3 Synthesis and Properties of Dication Salts of TTF Analogues Containing Quinoid Structures

Yoshiro YAMASHITA

TTF analogues **1** which can be prepared by a retro-Diels-Alder reaction of **2** are very strong electron donors.[1] The dications **3** have now been prepared by reaction of **2** with $NOBF_4$ in THF in 70-90% yields. The reaction smoothly proceeded at room temperature, while the reaction to give **1** occurred above 180 °C. The dications are soluble in acetonitrile and stable in solution in contrast to the neutral compounds **1** which have low solubilities in common organic solvents and are unstable in solution. The absorption maxima are **3a**; 385 nm (log ε = 4.46), **3b**; 416 (4.52), **3c**; 539 (4.35), **3d**; 566 (4.23), **3e**; 422 (4.26). This result indicates that alkythio groups make the absorptions much red-shifted. This reaction was applied to prepare the dication salts of TTF analogues containing various quinoid structures.

Reference

1) Y. Yamashita, Y. Kobayashi, and T. Miyashi, *Angew. Chem., Int. Ed. Engl.*, **28**, 1052 (1989).



1 **2** **3**

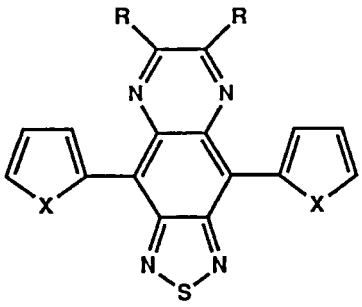
R = H, Me, SMe, SCH_2CH_2S, benzo

VIII-B-4 New Narrow-Bandgap Polymers Composed of [1,2,5]Thiadiaolo[3,4-g]quinoxaline and Aromatic Heterocycles

Chitoshi KITAMURA *(Graduate Univ. for Advanced Studies)*, **Shoji TANAKA and Yoshiro YAMASHITA**

[*Chem. Lett.*, 63 (1996)]

We have now succeeded in the synthesis of heterocyclic compounds **1** consisting of a new class of *o*-quinoid acceptor unit, [1,2,5]thiadiazolo[3,4-b]quinoxaline (**TDQ**), and various aromatic donor units. Alkyl substituents were introduced to improve the solubilities. The compounds **1** have small HOMO-LUMO gaps and showed high amphoteric redox properties. Electrochemical oxidation of **1** afforded the corresponding polymers as green-black films. They were stable to air, and insoluble in organic solvents even in the presence of the long alkyl groups. All the polymers exhibited both p- and n-doping processes. The absorption spectra of neutral polymers on ITO glasses showed bandgaps of ca. 0.7 eV. Furthermore, the N-methyl derivatives **2** were synthesized and led to the polymers by electrochemical oxidation. Although pyrrole has a higher HOMO level than thiophen, the bandgaps of the polymers of **2** were almost the same with those of the polymers of **1**. This is attributable to the nonplanar conformation of **2** due to the steric repulsion between **TDQ** and the N-methyl group.



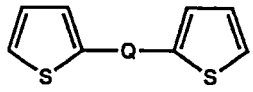
1; X = S
a; R = H
b; R = CH_3
c; R = C_6H_{13}
2; X = NMe
a; R = CH_3
b; R = C_6H_{13}

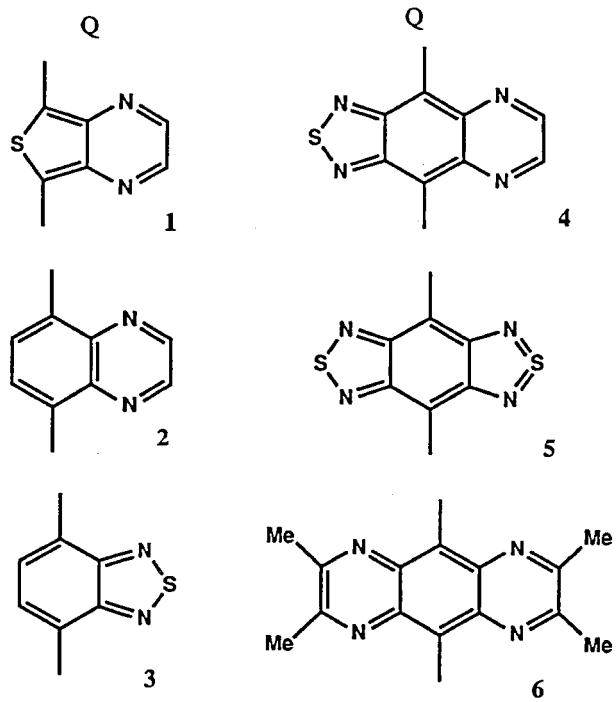
VIII-B-5 Design of Narrow-Bandgap Polymers. Syntheses and Properties of Monomers and Polymers Containing Aromatic-Donor and *o*-Quinoid-Acceptor Units

Chitoshi KITAMURA *(Graduate Univ. for Advanced Studies)*, **Shoji TANAKA and Yoshiro YAMASHITA**

[*Chem. Mater.*, **8**, 570 (1996)]

A series of novel monomers and polymers containing aromatic-donor and *o*-quinoid-acceptor units was prepared and the relationship between their spectral and electrochemical properties was investigated. We have actually synthesized various new monomers **1-6** which consist of thiophene as aromatic-donor and 10π or 14π-electron heterocycles as *o*-quinoid acceptor. The X-ray analyses revealed that the molecules have almost planar conformations. The electronic spectra and the electrochemical behavior of monomers were greatly affected by the properties of the *o*-quinoid acceptor heterocycles. The polymers were prepared using a successive potential scan technique. They exhibited redox waves in both p- and n-doping regions. The p-doping process was broad and irreversible, while the n-doping process was sharp and quasi-reversible. The bandgaps determined from the absorption spectra of polymers **1-6** on ITO-coated glass electrodes were 1.0, 1.4, 1.2 0.7, 0.5, and 0.9 eV, respectively. This result shows that the bandgap is widely tunable by the polymer structure. In this case, the bandgaps are dependent on the electron-accepting properties of the *o*-quinoid-acceptor segments.



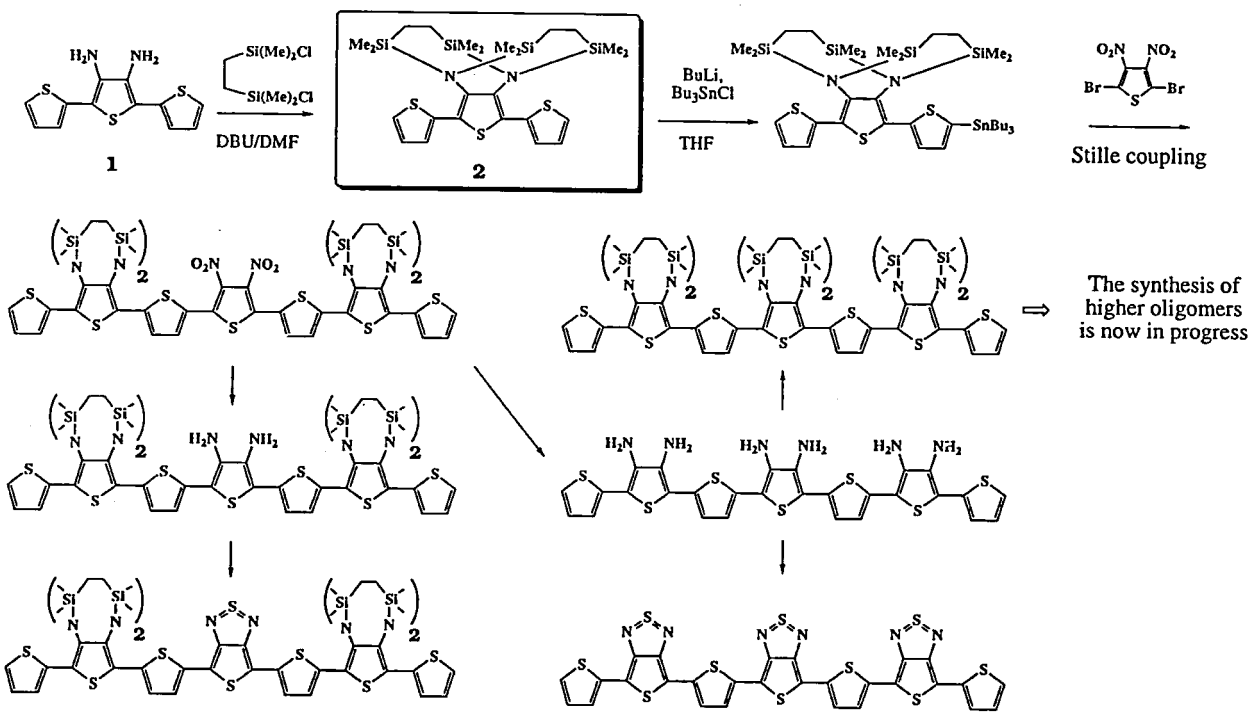


VIII-B-6 Synthesis and Properties of N-Silylated Diaminothiophene Derivatives: A Novel Building Block for Precisely Defined Conjugated Macromolecules

Shoji TANAKA, Masaaki TOMURA and Yoshiro YAMASHITA

Conjugated macromolecules of precisely controlled "length", "composition", and "sequence" have generated a great deal of interest, because such systems will be the main components to construct electronic or photonic devices operating at the molecule level. We have developed a new synthetic approach to precisely-defined conjugated oligomers containing various types of thiophene units as shown in Scheme 1. The key synthetic precursor here is compound **2**: the protection of the NH_2 groups by the silyl substituent makes the amino moieties inert during the course of the subsequent reactions and increases the solubility in organic solvents.

Compound **2** has bulky groups at the β-positions of the central thiophene ring. In general such bulky substituents tend to induce blue-shifts of absorption bands due to the lack of coplanarity. However, the UV-vis spectrum shows that the lowest energy absorption maximum of **2** is quite comparable to those of **1** and unsubstituted α-terthienyl (**2**: λ_{max}=363 nm; **1**: λ_{max}=359 nm; α-terthienyl: λ_{max}=355 nm in CH_2Cl_2). This finding indicates a high degree of π-conjugation over the whole molecule of **2** as in the case of unsubstituted thiophene trimer. In consistent with this, the X-ray structural analysis of **2** exhibits nearly coplanar conformation of the skeleton (the twisted angle is 20°) as shown in Figure 1. MM2 calculations suggest that the methyl carbons of the protecting groups of **2** claw the adjacent thiophene rings and stabilize the coplanar conformation.



Sheme 1

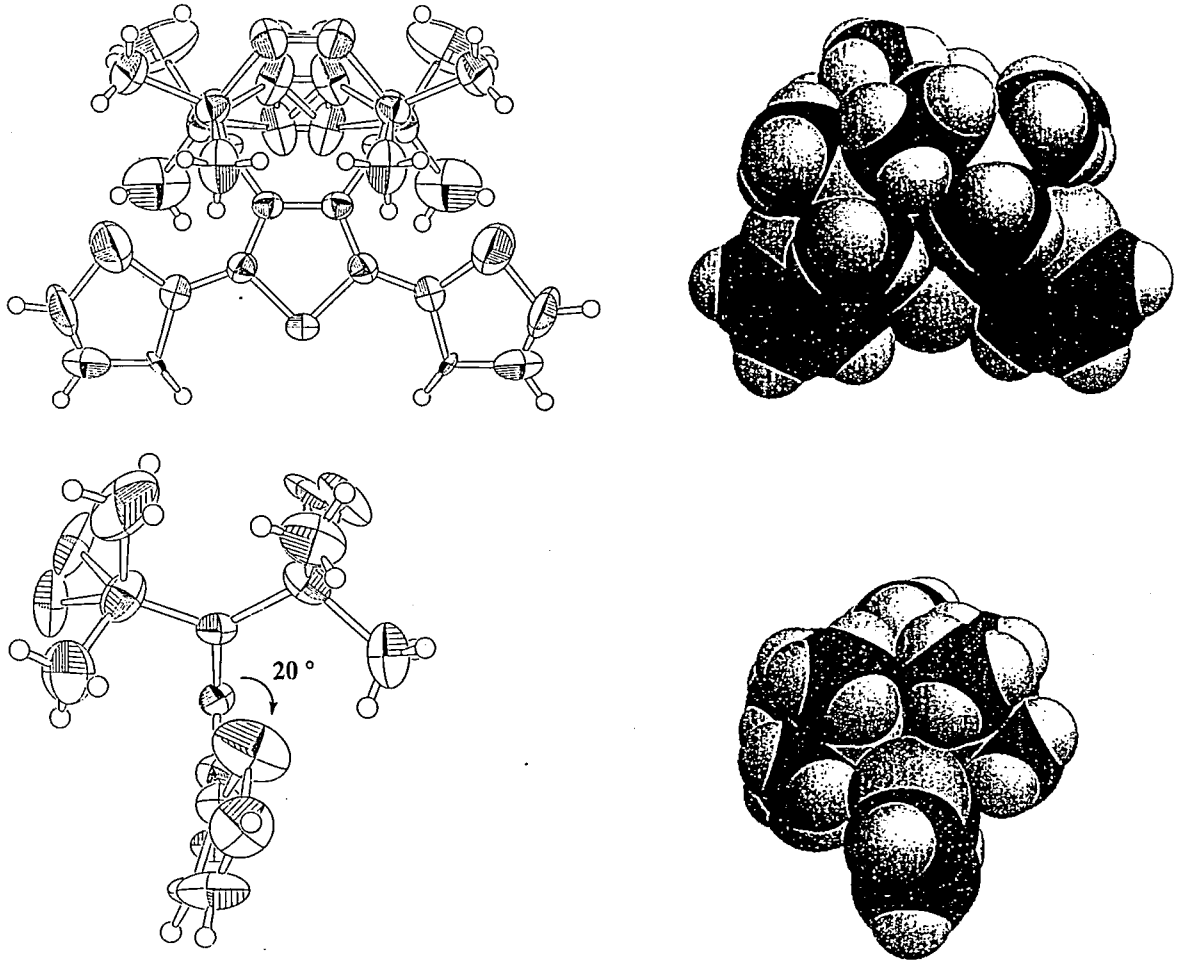
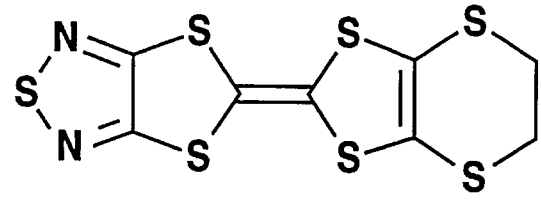


Figure 1. Molecular structure of compound 2

VIII-B-7 Crystal Structure and Physical Properties of (EDTTDA-TTF)SbF_6 Salt

Masaaki TOMURA, Shoji TANAKA and Yoshiro YAMASHITA

Black single crystals of the title radical cation salt were prepared by electrochemical oxidation of an unsymmetrical tetrathiafulvalene derivative with a fused 1,2,5-thiadiazole ring, EDTTDA-TTF, in the presence of n-Bu_4NSbF_6 in tetrahydrofuran or dichloromethane at room temperature. The composition of the resulting salt was determined to be 1:1 based on elemental analysis. However, the salt exhibited a high conductivity (σ_{rt} = 2.0×10^{-1} S cm^{-1}, E_a = 0.09 eV). The X-ray crystallographic analysis of the salt shows that the two crystallographically independent donor molecules form a dimer with an overlap of the two 1,2,5-thiadiazole rings as shown in Figure 1. The donor molecules are connected by many short intermolecular S···N (2.87 - 3.46 Å) and S···S (3.51 - 3.76 Å) contacts. Calculations of the overlap integrals of the conduction orbitals also suggest a two-dimensional property of the salt. Crystal data for (EDTTDA-TTF)SbF_6: M = 588.29, triclinic, $P\bar{1}$, a = 8.788(1) Å, b = 23.934(3) Å, c = 8.285(2) Å, α = 97.97(1)°, β = 102.00(1)°, γ = 94.71(1)°, V = 1677.2(5) Å^3, Z = 4, and R = 0.055 for 4731 reflections with $I > 3\sigma(I)$.



EDTTDA-TTF

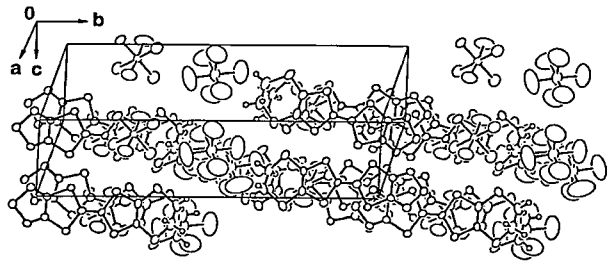


Figure 1. Crystal structure of (EDTTDA-TTF)SbF_6 viewed perpendicular to the donor molecule.

Instrument Center

VIII-C Developments and Researches of New Laser Materials

Although development of lasers is remarkable, there are no lasers which lase in ultraviolet and far infrared regions. However, it is expected that these kinds of lasers break out a great revolution in not only the molecular science but also in the industrial world.

In this project we research characters of new materials for ultraviolet and far infrared lasers, and develop new lasers by using these laser materials.

VIII-C-1 Broad-Band Tunable, Compact, Low-Threshold, Ti:Sapphire Laser Using a Single Set of Extremely Broad-Band Optics

Nobuhiko SARUKURA, Zhenlin LIU, Shinji IZUMIDA, Takao IZAWA, Shigenori MATSUI, Masaharu MAEDA, Norihiko YAMAMURA, Ryuji UCHIMURA, Teruo YAKUOH *(Showa Optronics Co., LTD)*

We developed an extremely broad-band, low-loss coating and applied this to a compact, low-threshold, broad-band tunable Ti:sapphire laser which can be pumped by modest all-solid-state green-light sources of around a few watts. The low-loss, broad-band coatings were deposited on a high-reflection mirror and a Brewster-cut Ti:sapphire crystal using an electron beam deposition. The high-reflection coatings consist of 10 stacks and each stack has 6 to 12 layers (99 layers in total). Optics losses as low as 500 to 1500 ppm (R=99.85 to 99.95) were attributed mainly to optical scattering. This loss level in the 650-1020 nm region , which completely covers the Ti:sapphire gain curve, is comparable with that of narrow-band output coupler. A wide-range, finely tunable birefringent filter consisted of 6 plates. The free spectral span is well over 500 nm. A three-mirror cavity was designed. Instead of a laser-diode-pumped, intra-cavity frequency-doubled Nd:YAG laser, we used an all-line Ar laser as a pumping source. As shown in Figure 1, tuning from 716 to 951 nm was demonstrated for 885 mW absorbed pumping. Output power was 85 mW at 773 nm, and the line width was less than 0.2 nm. [1]

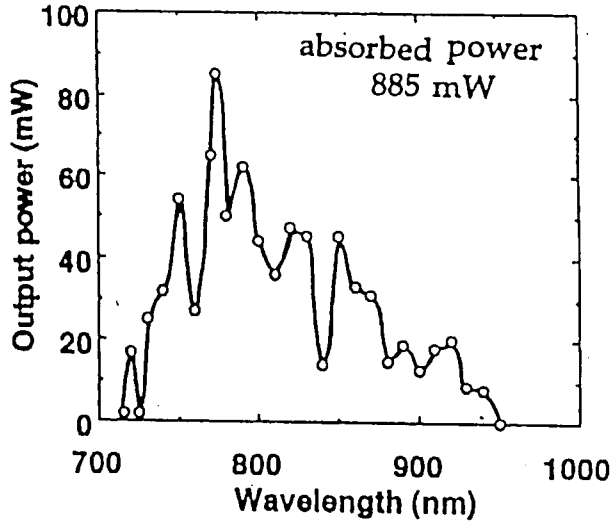


Figure 1. Tuning curves of the Ti:sapphire laser for 885 mW absorbed power.

Reference

1) T. Izawa, S. Matsui, M. Maeda, N. Yamamura, R. Uchimura, T. Yakuoh, N. Sarukura, Z. Liu, S. Izumida, and Y. Segawa, *Conference on Lasers and Electro-Optics '96*, (Optical Society of America, Washington, D.C., 1996), paper CTuL27.

VIII-C-2 1-GHz Repetition-Rate Mode-Locked Ti:Sapphire Laser Using a Saturable Bragg Reflector

Zhenlin LIU, Shinji IZUMIDA, Nobuhiko SARUKURA, Taro ITATANI, Takeyoshi SUGAYA, Tadashi NAKAGAWA, Yoshinobu SUGIYAMA *(Electrotechnical Lab., Tsukuba)*

Saturable Bragg reflectors (SBR) can mode-lock laser-diode-pumped solid-state lasers robustly and stably. We investigated high-repetition rate mode-locked operation of a Ti:sapphire laser with SBR. The saturable Bragg reflector was grown on a (100)-oriented semi-insulating GaAs substrate by molecular beam epitaxy. After a 500-nm-thick buffer layer was grown on the substrate, a Bragg reflector including a single quantum well was formed. The Bragg reflector consists of 24 pairs of $Al_{0.33}Ga_{0.67}As$/AlAs quarter-wave layers and a top quarter-wave layer of AlGaAs including a single quantum well of 10 nm. The AlAs layer thickness is 72.6 nm, and that of the AlGaAs layer is 63.2 nm.

The mode-locked laser setup using a saturable Bragg reflector as a saturable absorber is shown in Figure 1. The laser cavity consists of a Brewster cut crystal with high reflection coating on one side, a folding mirror with 5-cm concave curvature, a 1.0% transmittance 2.5-cm focal-length concave output coupler, and a saturable Bragg reflector at the focus of the lens. We obtained self-starting 10.3 psec pulses at a 1.02-GHz repetition rate with 640-mW output power. A pulsewidth as short as 1.6 psec has been obtained after external dispersion compensation. [1]

Reference
1) Z. Liu, S. Izumida, C. Liu, N. Sarukura, T. Hikida, Y. Segawa, T. Itatani, T. Sugaya, T. Nakagawa, Y. Sugiyama, *Conference on Lasers and Electro-Optics '96*, (Optical Society of America, Washington, D.C., 1996), paper CME4.

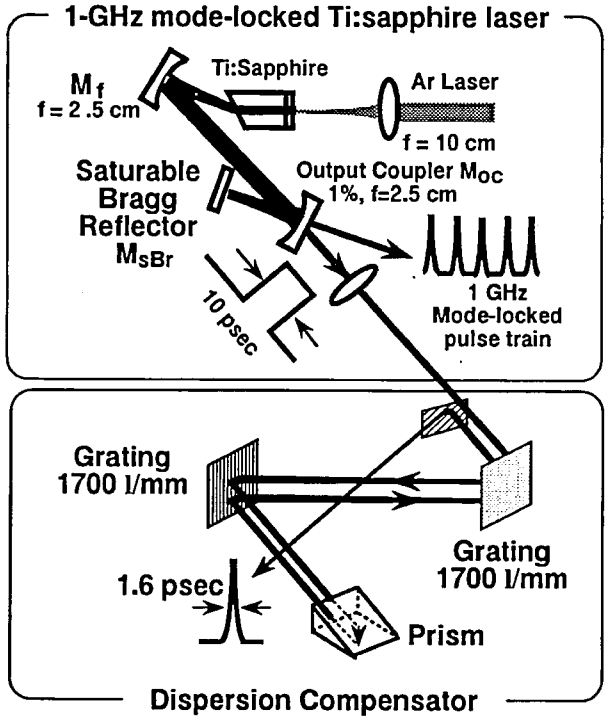


Figure 1. Experimental setup of 1-GHz repetition rate Ti:sapphire laser with an external dispersion compensator.

VIII-C-3 Ultraviolet Picosecond Pulses from an All-Solid-State Ce:LiSAF/Ce:LiCAF Master Oscillator and Power Amplifier System

Zhenlin LIU, Nobuhiko SARUKURA, Shinji IZUMIDA, Hideyuki OHTAKE, Mark A. DUBINSKII *(Howard Univ., USA)*, **Vadim V. SEMASHKO, A. K. NAUMOV, Stella L. KORABLEVA and Ravil Yu. ABDULSABIROV** *(Kazan State Univ., Russia)*

UV picosecond pulse generation and amplification in a all-solid-state master oscillator and power amplifier (MOPA) system was demonstrated. Solid-state tunable UV-laser materials such as Ce^{3+} ion activated $LuLiF_4$ (LLF), $LiCaAlF_6$ (LiCAF), and $LiSrAlF_6$ (LiSAF) have been developed. With their broad gain-width, they are attractive for ultrashort pulse applications. [1)]

Ce:LiCAF is the first known all-solid-state tunable UV laser directly pumped by the fourth harmonic of a Nd:YAG laser. Ce:LiSAF is an isomer of Ce:LiCAF with similar properties. The experimental setup of the Ce:LiSAF/Ce:LiCAF MOPA system is shown in Figure 1. The low-Q, short-cavity Ce:LiSAF master oscillator was formed by a flat high-reflection mirror and a 70% transmission output coupler. A single 590-psec, 3-mJ pulse at 290-nm was obtained. Ce:LiCAF was employed as the power amplifier stage. The amplifier was designed with a confocal 4-pass configuration. The input 3-mJ pulse was amplified up to 300-mJ. The duration of the amplified pulse observed by a streak camera was still 590 psec. [2)]

Reference
1) N. Sarukura, M. A. Dubinskii, Z. Liu, V. V. Semashko, A. K. Naumov, S. L. Korableva, R. Yu. Abdulsabirov, K. Edamatsu, Y. Suzuki, T. ITOH, and Y. Segawa, *IEEE J. of Selected Topics in Quantum Electronics*, 1,792 (1995).
2) Z. Liu, N. Sarukura, S. Izumida, Y. Segawa, M. A. Dubinskii, V. V. Semashko, A. K. Naumov, S. L. Korableva, and R. Y. Abdulsabirov, *OSA Trends in Optics and Photonics on Advanced Solid-State Lasers*, (Optical Society of America, Washington, D.C., 1996), 1, 66.

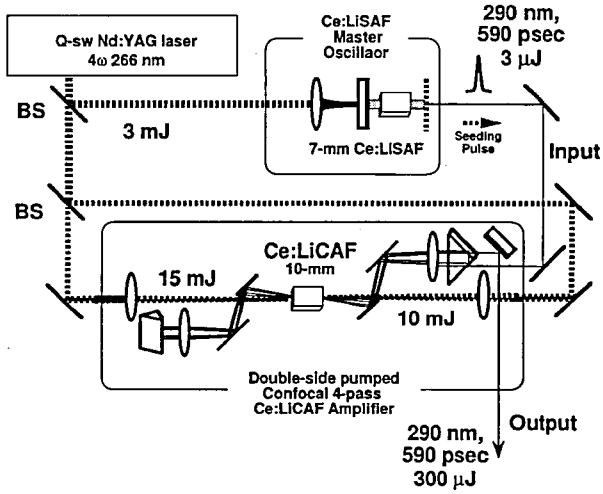


Figure 1. Experimental setup of the Ce:LiSAF/Ce:LiCAF MOPA system.

VIII-C-4 Lithium Tetraborate ($Li_2B_4O_7$) Crystals for the High-Energy Fifth Harmonic Generation of Nd:YAG Lasers

Nobuhiko SARUKURA, Zhenlin LIU, Shinji IZUMIDA, Ryuichi KOMATSU, Tamotsu SUGAWARA, Koichi SASSA *(Mitsubishi Materials Corporation)*, **Satoshi UDA, Tsuguo FUKUDA, Kazuhiko YAMANOUCHI** *(Tohoku Univ.)*

Efficient nonlinear crystals are key devices for developing ultraviolet light sources. we report an application of Lithium tetraborate ($Li_2B_4O_7$) crystals for ultraviolet frequency-conversion including the fifth harmonic generation of a Nd:YAG laser.

$Li_2B_4O_7$ single crystals of 2 to 2.5 inch diameter were grown in air by the Czochralski (CZ) technique. To evaluate these crystals, we used an optical parameteric oscillator (440-1800 nm). $Li_2B_4O_7$ is known as a uniaxial negative crystal, and the phase-matching condition was type I. The shortest SHG wavelength was 243.8 nm for $\theta_m = 90$, and the SHG wavelength was 348.7 nm for $\theta_m = 45$. As shown in Figure 1, we demonstrated wide-range second harmonic generation for the fundamental light from 487.6 nm up to 1265 nm, using a single 1-cm, 45 degree cut crystal. Fifth harmonic generation was also demonstrated using a 4.2-cm, 70 degree cut crystal in Type I SFG configuration. We obtained 69-mJ, 213-nm (the fifth harmonic of Nd:YAG laser) pulses for ~110 mJ, 266 nm and ~400 mJ, 1064 nm input pulses with a ~1-cm beam diameter from a Q-sw Nd:YAG laser. The shortest SFG wavelength with a 266 nm pulse mixed with an idler pulse of OPO was 209.3nm for $\theta_m = 90$. [1)]

Reference

1) R. Komatsu, T. Sugawara, K. Sassa, N. Sarukura, Z. Liu, S. Izumida, Y. Segawa, S. Uda, T. Fukuda, and K. Yamanouchi, *OSA Trends in Optics and Photonics on Advanced Solid-State Lasers*, (Optical Society of America, Washington, D.C., 1996), 1, 346.

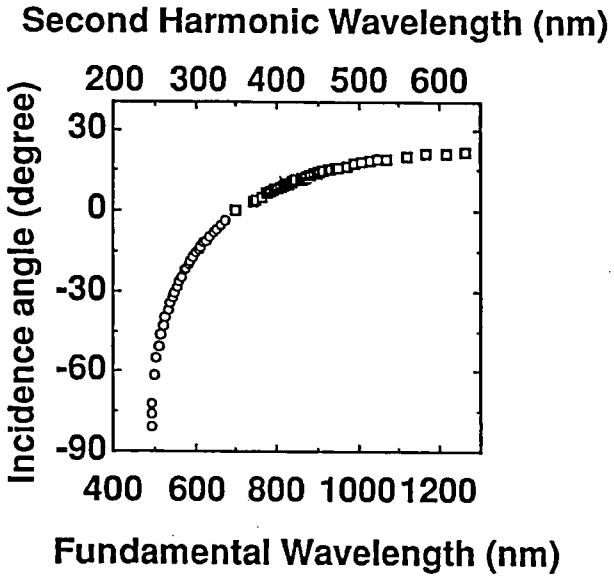


Figure 1. Wide range second harmonic generation using a 45-degree cut crystal.

VIII-C-5 Characterization of Far Infrared Radiation from InAs and GaAs Excited by Femtosecond Optical Pulses

Hideyuki OHTAKE, Zhenlin LIU, Takaya YAMANAKA, Nobuhiko SARUKURA, Tohru SUEMOTO *(ISSP, Tokyo Univ.)*

We have measured far infrared radiation originating from photoexcited carriers in InAs and GaAs crystals at RT when stimulated by 1.58-eV femtosecond optical pulses. The polarization configuration of the incident light was parallel to the <010> axis of the crystal and the radiated light. The incident laser was chopped by an optical chopper. The beam was softly focused onto the sample with the diameter about 10 mm. The far infrared radiation was collimated to parallel beam by an off-axis parabolic mirror. The collimated beam went through an interferometer and was detected by a liquid-helium cooled-Ge-bolometer.

Figure 1 shows the excitation power dependence of far infrared radiation intensity from InAs (closed circles) and GaAs crystals (opened circles). We did not observe any changes of spectral shape when varying excitation power, however, their power dependence represent non-linear power dependence. From fitting to the data, one can see the integrated intensity of InAs has a P^2 dependence, and that of GaAs has a $P^{1.5}$ dependence. This will be ascribed to the band structure difference.

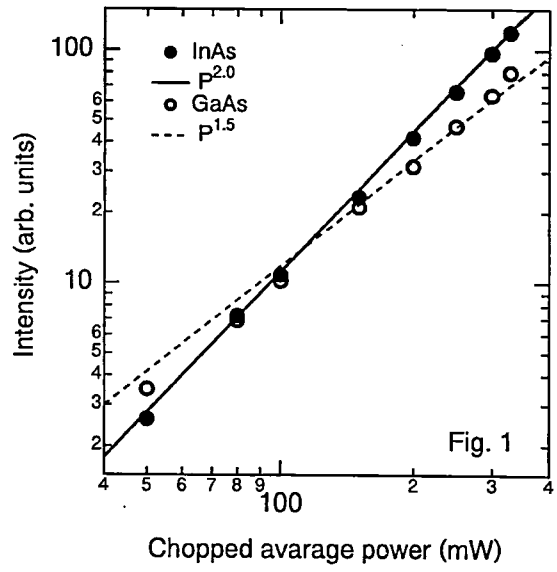


Figure 1. Excitation power dependence of the far infrared radiation intensity in InAs (closed circle) and GaAs (opened circle). Solid and dashed lines show P^2 and $P^{1.5}$ dependence. Expected error in the intensity is same size of opened and closed circles.

VIII-C-6 All-Solid-State, Short Pulse, Far-Infrared Source Using a Saturable Bragg Reflector in a Femtosecond Mode-Locked Laser

Nobuhiko SARUKURA, Zhenlin LIU, Hideyuki OHTAKE, Shinji IZUMIDA and Takaya YAMANAKA, Taro ITATANI, Takeyoshi SUGAYA, Tadashi NAKAGAWA and Yoshinobu SUGIYAMA *(Electro-technical Laboratory ETL)*

In this paper, we describe direct generation of THz radiation using SBR as the THz-radiation emitter placed inside the cavity of mode-locked Ti:sapphire laser. The SBR consists of a dielectric multilayer made of semiconductor with a single quantum well inside. The dielectric coating exhibits very high reflectivity, and the quantum well produces the nonlinear polarization required to generate THz radiation. The mode-locked Ti:sapphire laser with SBR as an intracavity THz emitter is shown in Figure 1. The SBR is placed at a shallow incidence angle to match the high reflectivity region of the SBR. 180-fsec pulses assuming a $sech^2$ shape were obtained with 3.9-nm spectral width at 768 nm. The average and peak output powers inside the cavity were 5.4 W and 375 kW (80 MHz repetition rate). The peak power of the optical pulse irradiating SBR exceeded 8.3 MW/cm^2, assuming ~1 mm beam diameter and considering the 80 degree incidence angle. The THz radiation was emitted in the transmitted direction and reflection direction. The transmitted THz radiation was picked off by a flat Al-mirror and detected by a liquid-helium-temperature cooled InSb bolometer (QMC model QFI/2) with submircowatt sensitivity using lock-in detection technique. The spectra of the THz radiation were obtained by the Fourier transformation of autocorrelation of the radiation from a Polarizing Michelson interferometer (Graseby Specac) as shown in Fig. 1. The interferometer was evacuated to avoid water-vapor absorption. The peak positions of radiation were 0.66 THz. In conclusion, we have proposed a new THz-radiation generation scheme using an intra-cavity SBR.

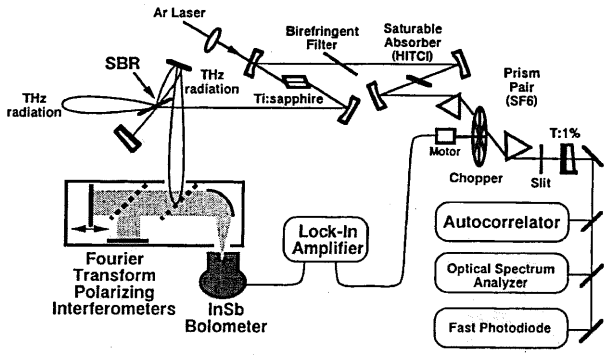


Figure 1. Schematic diagram of a femtosecond cw passively mode-locked Ti:sapphire laser system with SBR as THz-radiation emitter.

VIII-D Studies of Nanoscale Carbons

The structure of carbon nanotubes can be visualized by rolling up a graphene sheet to form seamless tubule. Graphene itself is a zero-gap semiconductor. However, when the flat sheet rolled up and formed seamless tubule, it presents either semiconducting or metallic feature depending on the cyclic boundary condition around the tube wall or, simply, on the tube diameter. Single- and multi-wall carbon nanotubes can be synthesized, respectively, via metal catalyzed carbon arc plasma and carbon arc deposition. However, at the same time, numerous number of sp^2 carbon nanospheres and carbon nanoballs would be produced with the nanotubes. We effectively separate the carbon nanotubes from these coexisting carbons by centrifugalization and microfiltration.

VIII-D-1 Removal of sp^2 Carbon Nanospheres from Single-Wall Carbon Nanotubes by using Microfiltration Method

Shunji BANDOW

The starting sample used for this study was produced by condensation of a laser-vaporized carbon-nickel-cobalt mixture by Smalley's group at Rice University.[1] This sample has already included more than 70 % of single-wall tubules. We first removed the fullerenes and polyaromatic carbons from the sample by soaking in CS_2. Insoluble component was then dried up and sonicated in 0.1 % of aqueous solution of surfactant (benzalkonium chloride) for 3 hours. The suspension liquid were put into a filtration cell with a 0.3 micrometer pore size filter and pressurized at 2 kg/cm^2 for the filtration. The suspension materials passed through filter were almost the carbon nanospheres and small metal particles (Fig. 1 **a** and **c**). The solid caught on filter was the single-wall carbon nanotubes (Fig. 1 **b** and **d**) with a concentration approximate to 85 %.

Reference

1) A. Thess, R. Lee, P. Nikolaev, H. Dai, P. Petit, J. Robert, C. Xu, Y.-H. Lee, S.-G. Kim. A. G. Rinzler, D. T. Colbert, G. E. Scuseria, D. Tom‡nek, J. E. Fischer and R. E. Smalley, *Science* **273**, 483 (1996).

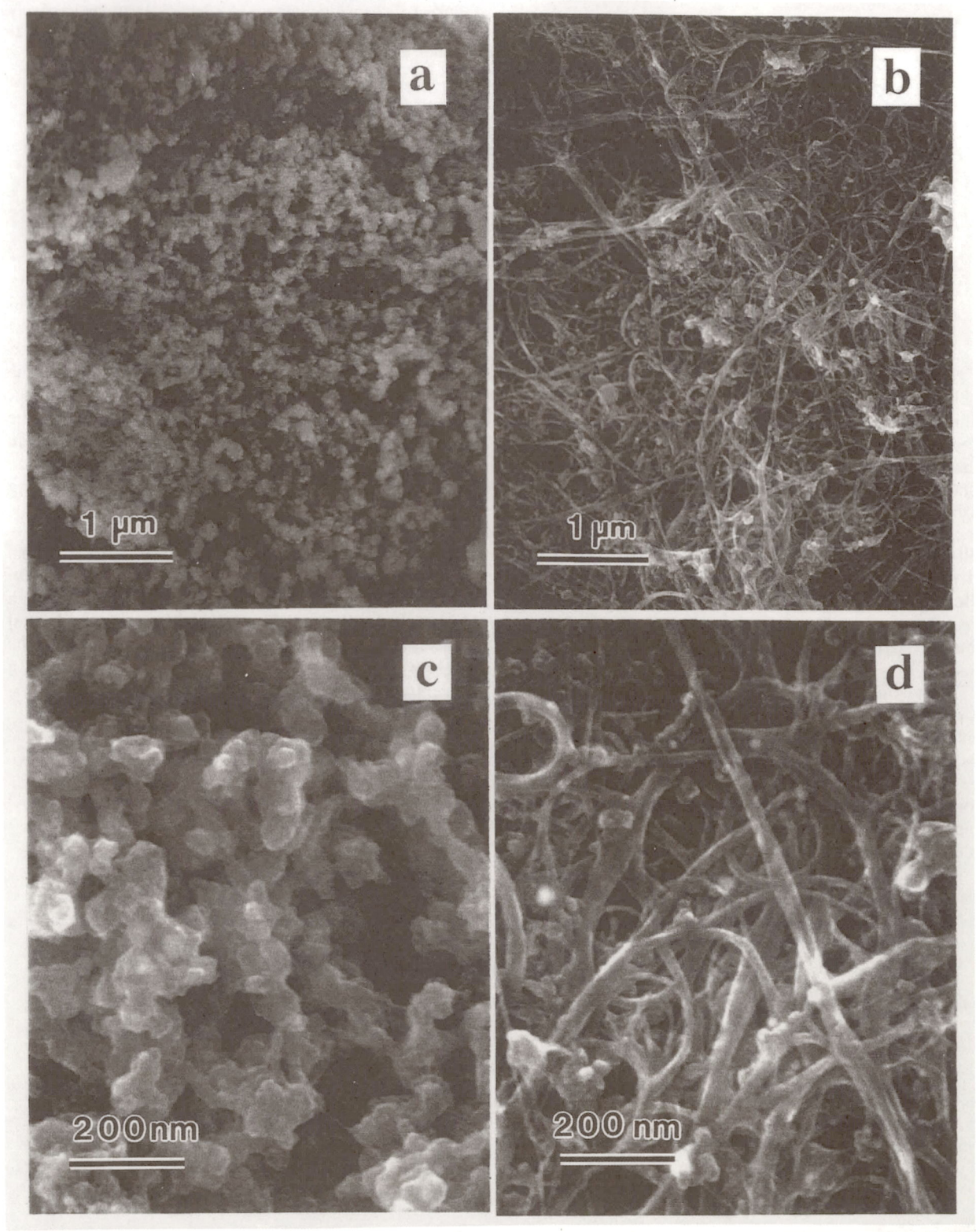


Figure 1. Scanning electron micrographs of filtered (a and c) and unfiltered (b and d) components. Only the spherical particles can be seen in a and c.

VIII-D-2 Tube Diameter Analysis of Triangular Packed Single-Wall Nanotubes by Electron Diffraction

Shunji BANDOW, Keith A. WILLIAMS* and Peter C. EKLUND* *(*Department of Physics and Astronomy, and Center for Applied Energy Research, University of Kentucky)*

It was found by the transmission electron microscopy that the single-wall carbon nanotubes arranged in triangular structure and organized into crystalline ropes. Side view of crystalline ropes are shown in top panel of Fig. 1. Electron diffraction from these ropes showed clear spots corresponding to 11 reflection from triangular lattice, which give the plane spacing d_{11} of 1.35 nm, as shown in bottom panel of Fig. 1. When we assume intertubular distance to be the van der Waals distance 0.34 nm, tube diameter can

be calculated by d_{11}/cos30 - 0.34 and will be 1.22 nm. We have taken 50 or more electron diffraction patterns from different ropes to make a size distribution of the tube diameter. As a result, the size distribution can be represented by a Gaussian function with a frequent diameter of 1.24 nm and a 2-sigma of 0.12 nm.

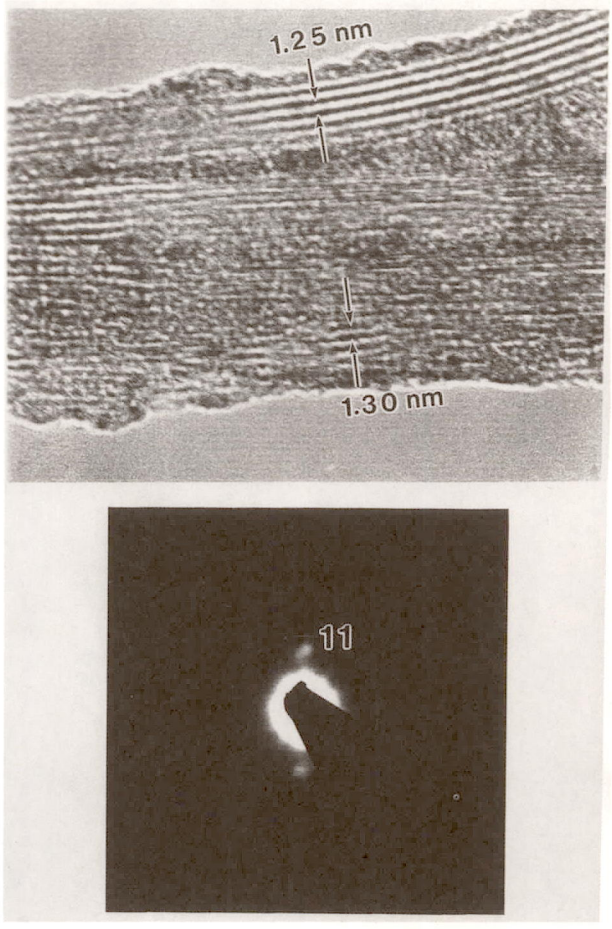


Figure 1. Transmission electron microscopy image of crystalline ropes of single-wall carbon nanotubes (top panel) and electron diffraction pattern from these ropes (bottom panel).

VIII-D-3 Infrared and Raman Spectroscopic Studies of Single-Wall Carbon Nanotubes

A. M. RAO[a], E. RICHTER[a], S. BANDOW, P. C. EKLUND[a], K. A. WILLIAMS[a], M. MENON[a], K. R. SUBBASWAMY[a], A. THESS[b], R. E. SMALLEY[b], G. DRESSELHAUS[c] and M. S. DRESSELHAUS[c] *([a] Univ. of Kentucky, [b] Rice Univ. and [c] MIT)*

Recently it has been demonstrated that a laser-assisted process can convert a carbon target into a carbonaceous sample containing a high fraction (70-90 %) of single-wall nanotubes (SWNTs); the remaining fraction is primarily carbon nanospheres (CNS). We present theoretical and experimental results on the infrared and Raman-active vibrational modes of SWNTs. Interfering spectral contribution from the coexisting CNS is identified by separating the SWNTs and CNS into two separate fractions. TEM and high resolution SEM was used to characterize the samples at various stage of purification process. The Raman spectrum of the SWNTs is particularly rich, with structure at 115, 185*, 220, 376*, 475, 754, 780, 857, 961, 1075, 1347*, 1368, 1396, 1566*, 1592*, 1736* and 1762 cm^{-1}, where the strong lines are marked by the asterisks. The infrared spectrum, on the other hand, reveals only one sharp line (1384 cm^{-1}) which can be assigned to SWNTs.

VIII-D-4 Magnetic Properties of Nested Carbon Nanostructures Studied by Electron Spin Resonance and Magnetic Susceptibility Measurements

Shunji BANDOW

[*J. Appl. Phys.* **80**, 1020 (1996)]

Nested carbon nanostructures, *e.g.*, nanotubes and nanoballs, are separated from the coexisting materials of carbon flakes and needle-like fragments by sonication, centrifugalization and low temperature combustion. Content of nanotubes at the final stage separation is in excess of 85% by weight. The nested carbon nanostructures (> 85 weight % tubules) are studied by electron spin resonance (ESR) and magnetic susceptibility measurements. The temperature dependence of the conduction-ESR intensity for the nested carbons is similar to that for graphite. On the other hand, the g-value is almost constant (g = 2.0096 +/- 0.0004 at room temperature) between 40 and 300 K, in contrast to that of graphite. These ESR features are discussed in terms of the electronic structure of carbon nanotubes predicted by theoretical calculation. The magnetic field dependence of differential magnetic susceptibility (χ_{diff}) indicates a logarithmic divergence in the magnetic field H < ~2 kG and the χ_{diff} comes to be a positive value at H approximate to 0.8 kG, which consist qualitatively with the magnetic properties of metallic carbon nanotube enunciated by Ajiki and Ando.

VIII-E The Applications of a Magic-Angle Turning Technique for Half-Integer Quadrupolar Nuclei

VIII-E-1 Spinning Sideband Summation for Quadrupole MAS NMR Spectra Using a Magic-Angle Turning Technique

Toshihito NAKAI and Daisuke KUWAHARA

[*Chem. Phys. Lett.*, **249** (1996) 205-209]

Two-dimensional(2D) magic-angle spinning(MAS) NMR measurements for unravelling the overlapping spinning sidebands(SSBs) for quadrupolar nuclei having half-integer spins were reported; the method utilizes a magic-angle turning technique recently exploited for chemical-shift spectra. The projection of the resultant 2D spectrum reconstructs the inherent MAS lineshapes without SSBs, which can be straightforwardly analyzed to yield quadrupolar parameters. The SSB-free ^{23}Na MAS spectrum for Na_2SO_4, which would otherwise be observed under an infinite spinning speed, was obtained.

VIII-E-2 Spinning-Sideband Suppression in DOR NMR Spectra Using a Magic-Angle Turning Technique

Daisuke KUWAHARA and Toshihito NAKAI

[*Chem. Phys. Lett.*, in press]

Spinning sidebands(SSBs) in double rotation(DOR) NMR spectra for quadrupolar nuclei having half-odd-integer spins were suppressed using a two-dimensional(2D) NMR method based on a magic-angle-turning technique. The resultant 2D spectrum showed substantially no SSBs along one frequency axis whereas, along the other axis, conventional SSBs exhibited themselves.

Equipment Development Center

VIII-F Activities of Division of "IMS Machines"

A group of the staff in the Equipment Development Center works on planning, researching, designing and constructing "IMS machines". This machine, crowned with the acronym of the Institute for Molecular Science, is a high-tech experimental instrument, with emphasis on new technical idea and co-operative work with people inside and outside the Institute including those in industries. We collect suggestions of instruments once every year.

In this fiscal year, 1995, one project theme (1 in the list below) was adopted as an IMS Machine. IMS machines (2 and 3) adopted in 1994 are under construction.

1. **Ultrashort Pulse Molecular Beam Valve**
   (Proposed by Nobuaki YONEKURA)
2. **High Precision Slit Driver for Ultra-High-Vacuum Monochromator**
   (Masao KAMADA and Nobuaki MIZUTANI)
3. **Electron-Stimulated-Desorption-Ion-Angular-Distribution Detector with Time-of-Flight Type Mass Separator**
   (Kyoichi SAWABE, Tatsuharu TORII, Koichi UCHIYAMA and Shuji ASAKA)

Application of patents is promoted in this division. For fiscal year of 1995, the following was applied for an international patent.

1. **Optical Window and its Fabrication Method** (applied in collaboration with Sumitomo Electron Industry)

A brief report of the project 3 is presented in the following.

VIII-F-1 ESDIAD Detector with Time-of-Flight Type Mass Separator

Kyoichi SAWABE, Tatsuharu TORII, Koichi UCHIYAMA and Shuji ASAKA

The angular distribution of desorbing ions produced by electron stimulated desorption is closely connected to the bonding directions of molecules on crystal surfaces. The imaging technique of this distribution is called as Electron Stimulated Desorption Ion Angular Distribution (ESDIAD). The present project is aimed at developing an ESDIAD detector with time-resolved detection, which will enable us to obtain ion angular distribution of mass specified molecules . As a first step we are now constructing an ESDIAD detector without time-resolving feature.

The schematic diagram of the instrument is shown in Figure 1. The electron beam from gun (2) irradiates the sample (1), and the desorbing ions are accelerated toward micro channel plate (MCP) (5) through three hemispherical grids (for collection) and two planar grids (for acceleration). MCP converts ions into electron flux, and then the amplified flux is converted into visible image on the phosphorescent plate attached to MCP. The image is observed with a CCD camera (6) through a glass window (7). We made the grids with molybdenum (ϕ0.03 wire, #80 mesh), considering its low out-gassing, good electrical conductivity, and no magnetism. Because of lack of space for a conventional cone-flat flange [1] for the window (7) in the present design, we adopted a clamp-chain coupling flange (KF flange). A soft aluminum alloy gasket bakable up to 150 °C was used for vacuum sealing. In order to ease sample exchange, we made a mechanism to move the inner flange (9) off the sample. When the handle (8), and simultaneously an angle screw (male), is rotated, a linear translation table (10) is moved by way of a female screw (11) attached to it. Adoption of a slide bearing (LM guide, THK company) ensures a precise translation of the table. The inner flange is supported by three supporting stays (12). The adjustable stoppers (13) are for repositioning the inner flange for measurement after sample exchange. The whole mechanism of the ESDIAD is mounted on a single vacuum flange (UFC203) enabling its portability to any types of vacuum chambers for measurement.

Most of assembly and tests have been finished. Remaining tests are operation of MCP and acquisition of image from desorbing dummy ions.

Reference

1) N. OKADA, T. URISU, S. ASAKA, and T. HORIGOME, **IMS Annual Review 1995**, VIII-H-1.

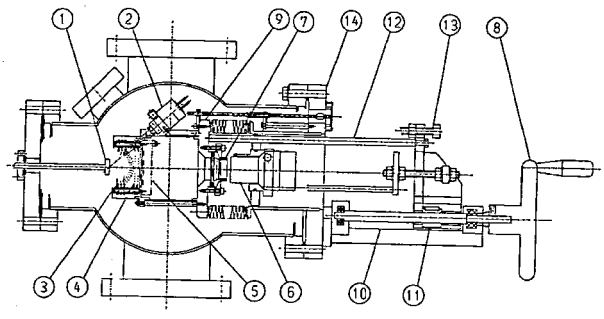


Figure 1. Design of ESDIAD detector.

VIII-G Development of Experimental Devices

VIII-G-1 Design and Construction of SGM-TRAIN* Monochromator

Nobuo MIZUTANI, Toshio HORIGOME and Masami HASUMOTO

We have newly developed a monochromator which is to be established to renew BL5A in UVSOR facility. The planned goals of the renewal of beam line BL5A are: 1) improved energy resolution in photoelectron measurement: 150 meV before, 20 meV after, 2) improved resolution in monochromator: 500 to 1000 before, 1000 to 2000 after, 3) utilization of circular polarization, 4) ability of photoelectron spectroscopy with spin angular resolution, 5) spectroscopic system available of undulater light as light source. The specifications of the monochromator necessary for these goals are: 1) mounting method: CL-SGM+NIM, which works in Rowland geometry in high energy region, and normal incidence in low energy region, 2) energy region to cover: 5 to 250 eV, 3) rejection of higher order diffraction utilizinag combination of mirrors, 4) resolution: 3000 to 10000, 5) driving method: computer-controlled drive, connection of rotational and translational motion: CL-SGM method, rotation: DRAGON type, ability to adjust exit slit position, distance between entrance and exit slits: 3500 mm. The designed optical geometry and the outline of the monochromator are shown in Figures 1 and 2, respectively. The main chamber, which has a mirror and grating exchange mechanism, a sine bar mechanism, and vacuum pumps, can be translated up to 1400 mm in light axis along a rail, the inclination of which can be varied up to 5 degrees. The exit slit chamber can also be translated up to ±25 mm. Welded bellows connect each other of entrance slit chamber, main chamber, and exit slit chamber. All of the movable parts are computer-controlled: the translational chambers, the sine bar, six mirror exchange mounts, four grating exchange mounts, and the variable width slit. We have obtained a resolution of 5000 as a tentative performance result of the constructed monochromator. Since conventional monochromators show values of resolution about 1000, our new machine has already a better performance. We hope an optimized adjustment of optical components will lead us to the design goal of resolution 10000.

* SGM-TRAIN is acronym of Spherical Grating Monochromator with Translational and Rotational Assembly Including Normal-incidence mount.

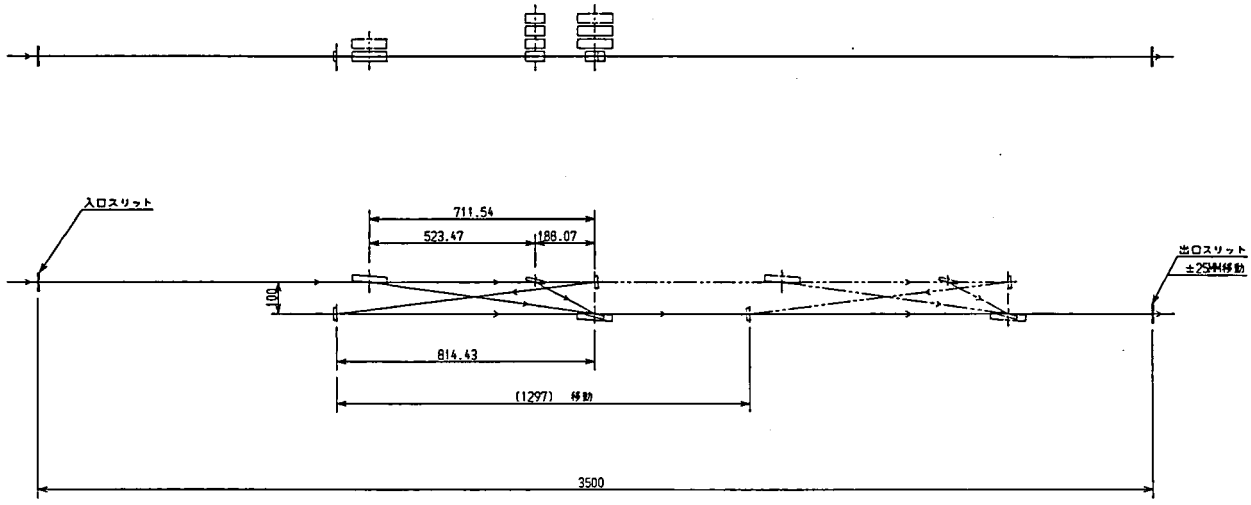


Figure 1. Optical design of SGM-TRAIN Monochromator.

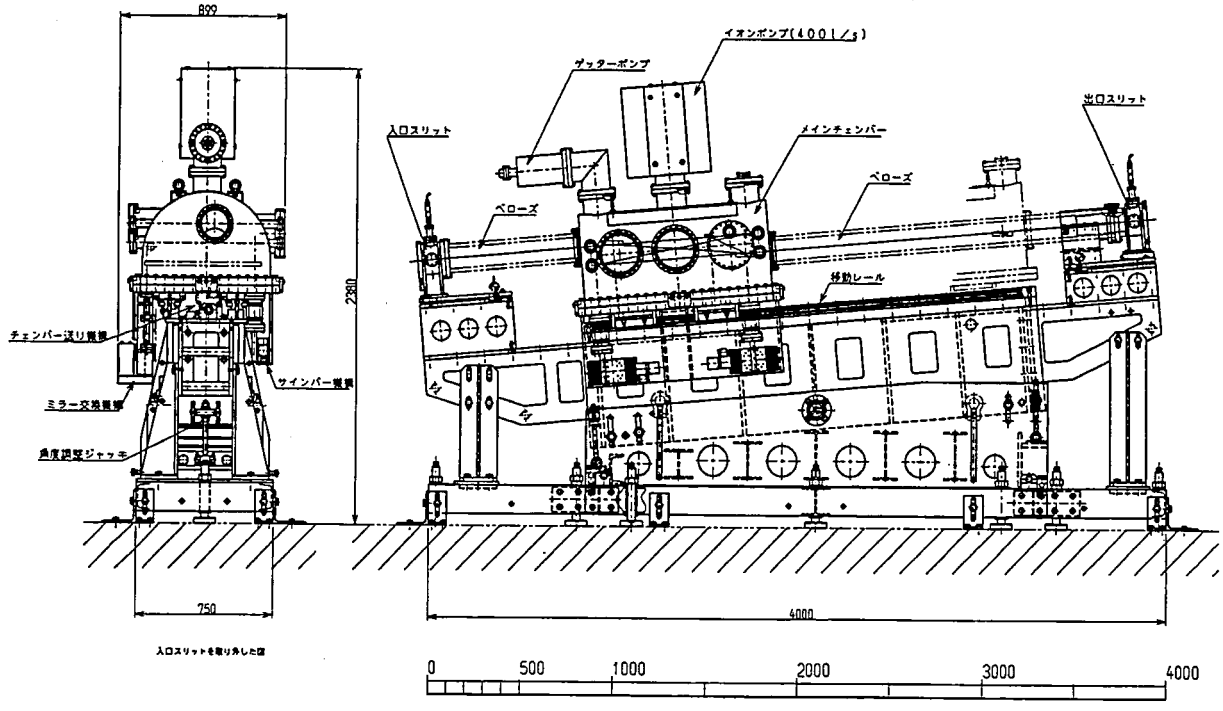


Figure 2. Newly constructed SGM-TRAIN Monochromator.

Ultraviolet Synchrotron Orbital Radiation Facility

VIII-H Development of the UVSOR Light Source

VIII-H-1 A Helical Optical Klystron for UV Storage Ring Free Electron Lasers

Hiroyuki HAMA, Kazuhiko KIMURA, Masahito HOSAKA, Jun-ichiro YAMAZAKI and Toshio KINOSHITA

A new helical optical klystron (HOK) was installed and commissioned on the UVSOR storage ring lately. Advantages for storage ring free electron laser (SRFEL) of HOK has been already evaluated[1]. There are less higher harmonics on the axis which is quite favorable to avoid mirror degradation, and the FEL gain is estimated to be higher than that of conventional OK. Moreover circular polarized FEL with both direction is able to be obtained.

Effects of the HOK for the storage ring as an insertion device have been measured and compared with the theoretical estimation. Because the tune shift in betatron oscillation is caused in both vertical and horizontal planes, an operation point of the storage ring should be chosen carefully and local correction of beta functions is absolutely necessary. The most important fact is that the spontaneous radiation from the HOK is very sensitive to the beam orbit in the HOK because the region of uniform magnetic field is quite narrow. Alignment of the HOK had been carefully done and the positioning error of less than several tens μm for the center of quadrupoles was obtained.

By adjusting the beam orbit to the center of the HOK, a preliminary measured spectrum of the spontaneous radiation with the electron energy of 600 MeV became fairly good. However optimization of the storage ring for the HOK has been not finished yet, and a beam based alignment is still continued. In test experiments of FEL oscillation, lasings at wavelengths at 470, 270 and 240 nm were successfully obtained. The 240 nm FEL is one of the most shortest wavelength of FELs in the world.

The HOK was initially designed by consideration of the mirror degradation. Namely low on-axis photon density of higher harmonics from the helical undulator would reduce the degradation rate. To demonstrate the reduction of the mirror degradation rate, the mirrors in the optical cavity were irradiated by the radiation from the HOK of a planar mode magnet configuration with a same set-up of the lasing experiment. Consequently lasing was not obtained because the degradation rate was pretty fast. It is quite impressive result that the degradation rate with the planar mode was more than 50 times faster than that with the helical mode. Although we have not analyzed the relation between the degradation rate and the photon number at higher harmonics quantitatively, it is clearly recognized that absorption of the high energy on-axis photon in the multilayer deprives the mirror reflectivity.

We have not measured the polarization of the FEL precisely. Observed degree of the polarization of the 270 nm laser was $P \sim 0.05$, where the polarization is defined as $P = \left| I_{\perp} - I_{=} \right| / \left| I_{\perp} + I_{=} \right|$ and I denotes an intensity of respective azimuthal angle, and then $P = 0$ for the complete circular polarization (the helicity has not been measured yet). First of all, to obtain the complete circular polarization, both phase and strength of the vertical and the horizontal magnetic field should be precisely adjusted. Although further investigation is required on the circular polarization, we can conclude the helical SRFEL is a possible tool to develop a new aspect of photoelectron spectroscopy and other fields.

References

1) Hiroyuki Hama, Nucl. Instr. and Meth, A **375**, 57- 61 (1996).

VIII-I Development of Beam Lines and Equipment for UVSOR

VIII-I-1 Construction of New Monochromator (SGM-TRAIN) at BL5A

Masao KAMADA, Kusuo SAKAI, Masami HASUMOTO, Nobuo MIZUTANI, Toshio HORIGOME, Shin-ichi KIMURA, Sayumi HIROSE, Kazutoshi FUKUI* and 5A-WORKING GROUP *(*Fukui Univ.)*

[*Rev. Sci. Instrm* **66**, 1537 (1995)]

A new monochromator called SGM-TRAIN (Spherical Grating Monochromator with Tranlational and Rotational Assemblies Including Normal-incident-mount) has been constructed at beam line 5A. This SGM-TRAIN is an improved version of the constant deviation and constant length monochromator (CDCL-SGM) designed by UVSOR at BL3A2. Figure 1 shows the drawing of SGM-TRAIN, which has a constant length of 3500mm between entrance and exit slits. The length can be changed by 40 mm. A grating-and-mirror chamber translates with rotating a grating in order to get a good focus by following the Rowland condition approximately. The stable and precise motion of the chamber is required in order to get high resolution. Our new driving system using a computer control system did a big job to translate the chamber and rotate gratings independently, resulting in high resolving power. The SGM-TRAIN is now tentatively aligned along a beam line with 152° in horizontal direction and will move to a new line, where circularly polarized lights from a new helical undulator are available.

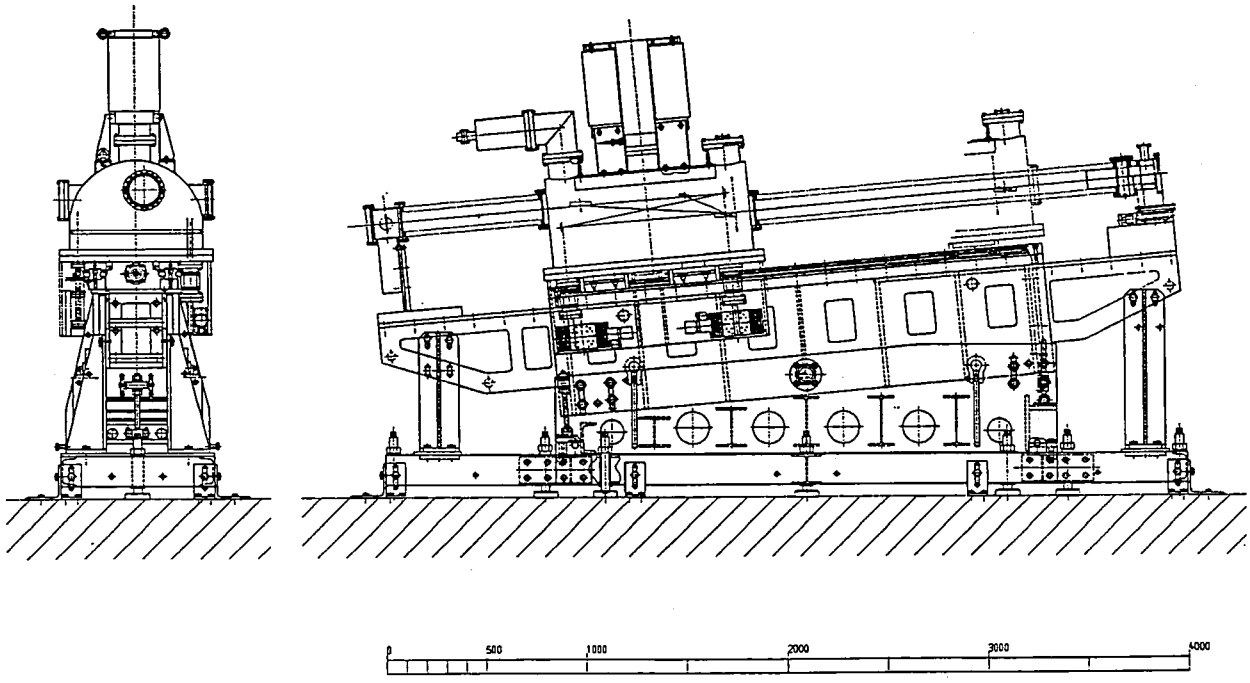
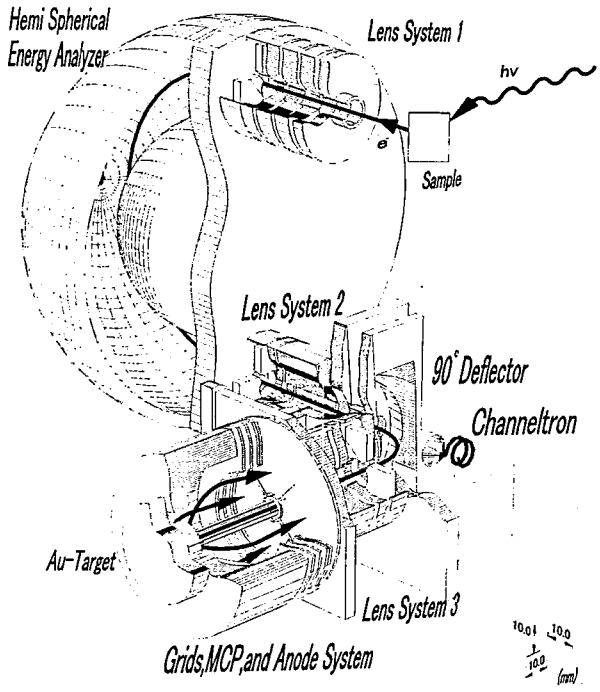


Figure 1. Drawing of SGM-TRAIN

VIII-I-2 Construction of Spin- and Angle-resolved Photoelectron Spectrometer

Naoshi TAKAHASHI, Masatake ICHIKAWA, Koichi NAKANISHI*, Yasuo FUJII*, Shigeo OHARA, Shin-ichiro TANAKA and Masao KAMADA** *(*Osaka City Univ., **Nagoya Inst. Tech.)*

Spin-resolved photoelectron spectroscopy is a powerful method to investigate the electronic structures of solids and surfaces completely (energy, momentum, and spin). The most popular spin detector is of a Mott type, which is based on the high energy electron scattering. This detector needs a very high voltage for accelaration and a large space for isolation, and thus is not applicable to the angle-resolved photoelectron spectroscopy. We have therefore constructed a new compact spin- and angle-resolved photoelectron spectrometer. Figure 1 shows a three dimensional drawing of the spectrometer, which consists of an electron-energy analyzer, lens systems, and a spin detector of low energy electron diffraction type.



VIII-I-3 Design of a Helical Undulator for UVSOR

Shin-ichi KIMURA, Masao KAMADA, Hiroyuki HAMA, X. MARECHAL*, Takashi TANAKA and Hideo KITAMURA*** *(*SPring-8, **Kyoto Univ.)*

[*J. Electron Spectroscopy and Related Phenomena* **80**, 437(1996)]

The design concept and the expected performance of a helical undulator which we plan to install in the UVSOR 0.75 GeV storage ring is reported. It is expected that the perfectly circularly polarized undulator light is made up in the energy range 2 - 45 eV and the elliptically and linerly polarized light is obtained up to 300 eV.

VIII-I-4 Reconstruction of BL7B for UV, VIS and IR Spectroscopy with a 3m Normal Incidence Monochromator

Hideyuki NAKAGAWA*, Kazutoshi FUKUI*, Kazumichi NAKAGAWA, Takao NANBA** and Toyohiko KINOSHITA** *(*Fukui Univ., **Kobe Univ.)*

The beamline BL7B is now under reconstruction. The 1m Seya-Namioka type monochromator is replaced to the 3m normal incidence monochromator (3m NIM; McPHERSON upgrade model of 2253) for the extended researches of the highest level with the higher resolution and intensity, the wider wave-length region available and so on. It will be also possible to utilize the linear and circular polarization inherent in synchrotron radiation (SR) and to realize some combined experimental systems, for example, with the synchronized laser to SR pulse or with the extended field. The outline of the new beamline is shown in Figure 1.

The main parts of the system are a pre-mirror focusing system, a 3-m NIM and a post-mirror focusing system. The light from 50 to 1000 nm wavelength region is covered by changing three gratings *in situ*. Each spherical grating is original laminar type fabricated on SiO_2 and has effective grooved area of 120x40mm^2. The specifications of the gratings are listed in Table 1. At the position between G and H in Figure 1, LiF or MgF2 window valve is installed. Therefore, the measurements for the organic materials, liquid and biochemical ones are possible at the 2nd focal position H.

After the final adjustment and test run, this beamline will be used for absorption, reflection and fluorescence measurements on various materials with higher performance (high energy resolution, high intensity, well-polarized light, short repetitive pulse light) not only in the VUV region but also in the near UV, VIS and near IR region.

	Coverage (nm)	Grooves (/mm)	Dispersion (nm/mm)	Duty factor	Groove depth(nm)	Coat(thickness,nm)
G1	50~150	1200	0.2	0.497	16.4	Au (75)
G2	100~300	600	0.5	0.497	32.9	Al (52)
G3	250~1000	300	1.0	0.497	73.3	Al (40)

Table 1. Specifications of the gratings of the new BL7B.

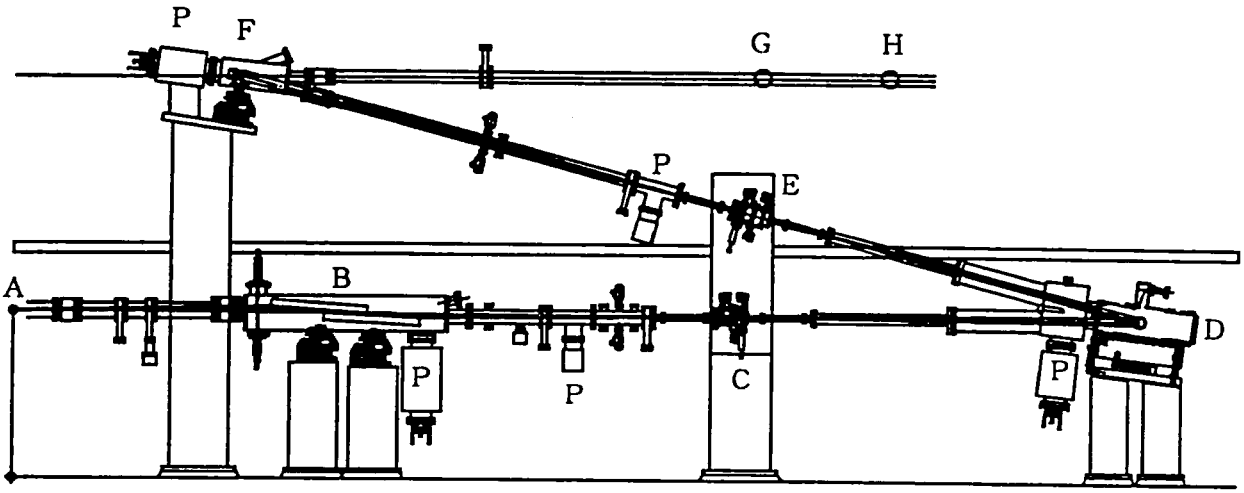


Figure 1. The outline of the side view of the new beamline BL7B.

VIII-I-5 Performance of YB66 Soft X-ray Monochromator Crystal at the Wiggler Beamline

Toyohiko KINOSHITA, Yasutaka TAKATA, Tokuo MATSUKAWA*, Hirofumi ARITANI, Shigehiro MATSUO**, Takashi YAMAMOTO**, Masao TAKAHASHI***, Hisao YOSHIDA****, Tomoko YOSHIDA**** and Yoshinori KITAJIMA******* *(*Naruto Univ. Education, **Kyoto Univ., ***Osaka Univ., ****Nagoya Univ., *****KEK-PF)*

We have succeeded to measure soft X-ray spectra by using YB66 monochromator crystal at the double crystal monochromator beamline BL7A of the UVSOR facility, where the 4T wiggler radiation is provided. The YB66 is known to be one of the best monochromator crystals which cover soft X-ray region from 1.1 to 2keV with higher performance[1]. So far only the SSRL (Stanford synchrotron radiation laboratory) group employed the YB66 crystal[2], since the crystal is easily deformed by higher heat load from synchrotron radiation from higher energy storage ring. The storage ring of the UVSOR facility is operated at rather lower energy (750 MeV) which produce rather lower heat

load. Further, the 4T wiggler to provide higher photon flux in the region of soft X-ray is installed at the UVSOR. These are the motivations why we tried to make a performance check of the YB66 monochromator crystal at the UVSOR facility.

Figure 1 shows the throughput of the monochromator with the use of YB66 (400). We have also measured the XAFS spectra for Mg and Al compounds (not shown here). The deviation originated from deformation effect by heat load to the crystal is less than 0.01 degree which corresponds to the energy shifts of about 0.1eV. These results show that the YB66 crystal can be enough to use as the monochromator crystal. In Fig. 1, two positive glitches at 1385.6 and 1438 eV are observed. These two glitches are known to be due to the 600 reflection light corresponding to the Y $L_{2,3}$ absorption edges whose original (400 reflection light) peaks are also shown in Figure 1 at 2080 and 2156 eV, respectively[3]. In order to take more precise XAFS data especially for the Mg compounds, the reduction of the higher energy component of the light is necessary for the next step of the improvement of the beamline.

The use of the YB66 crystal might be very powerful and valuable for the future studies of the soft X-ray spectroscopy at the UVSOR.

References

1) J. Wong, G. Shimkaveg, W. Goldstein, M. Eckart, T. Tanaka, Z. U. Rek and H. Tompkins, *Nucl. Instr. and Meth.* **A195**, 243 (1990).
2) M. Rowen, Z. U. Rek, J. Wong, T. Tanaka, G. N. George, I. J. Pickering, G. H. Via and G. E. Brown Jr., *Synchrotron Radiation News* **6**, 25 (1993).
3) T. Tanaka, T. Aizawa, M. Rowen, Z. U. Rek, Y. Kitajima, I. Higashi, J. Wong and Y. Ishizawa, submitted to *J. Appl. Crystallography*

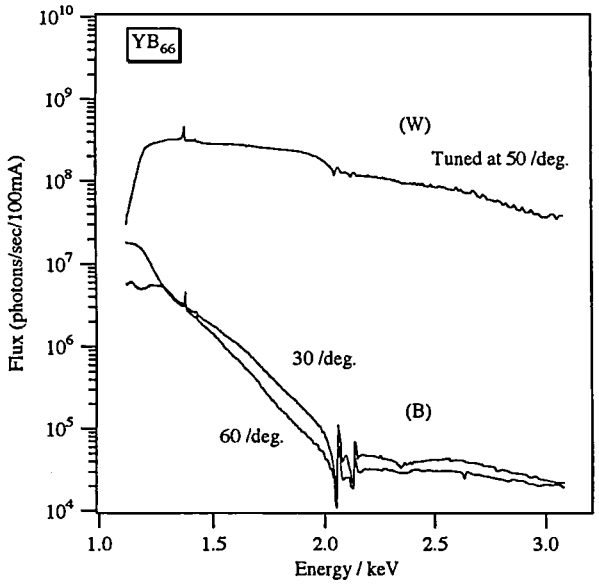


Figure 1. Throughput from the double crystal monochromator with YB66(400). Radiations from the 4T wiggler (W) and the bending magnet (B) are used respectively. The position of the 2nd crystal of the monochromator was tuned at 50, 30 and 60 degrees, respectively.

VIII-J Researches by the USE of UVSOR

VIII-J-1 Photoelectron and Luminescence Spectra of BaFCl, BaFBr, and $CsTaF_6$

Masao KAMADA, Naoshi TAKAHASHI, Sayumi HIROSE, Shigeo OHARA*, M. A. TEREKHIN, S. S. GALAKTIONOV*** and S. S. GALAKTIONOV******
*(*Nagoya Ins. Tech., **Russian Research Center, Russia, ***Mendeleev Univ., Russia, ****NPO "Simplex", Russia)*

[*J. J. Elec.Spec.*, **80**, 143 (1996)]

The photoelectron spectra as well as the excitation spectra of the optical luminescence have been investigated in BaFCl, BaFBr, and $CsTaF_6$. It was found that the valence bands of BaFCl and $CsTaF_6$ consist of mixing states of constituents, while that of BaFBr is separated into two branches. It was also found that the luminescence intensity of BaFBr is much enhanced around the excitation energy of the Ba-4d holes, while the enhancements in BaFCl and $CsTaF_6$ due to the decay of the 4d holes are very small.

VIII-J-2 Photon-Stimulated Desorption of Excited-State Sodium Atom from NaF and NaCl under Valence-Band and Core-Level Excitations

Sayumi HIROSE and Masao KAMADA

[*J. Phys. Soc. Jpn*, **65**, 1849 (1996)]

The excitation energy dependence of excited-state Na desorption from NaF and NaCl has been investigated in the energy range of 20-47 eV with synchrotron radiation. The excited-state Na desorption from NaF was observed with valence-band excitation as well as core-level excitation. The excitation spectra of excited-state Na desorption from NaF and NaCl showed a peak corresponding to the Na L2,3 core-exciton band. Contributions of core-level and valence-band excitations to the Na desorption at the Na L2,3 core-exciton band were estimated by using the absorption and excitation spectra. The present results indicate that the Knotek-Feibelman mechanism based on the core-level excitation is not valid to explain the excited-state alkali desorption. The desorption with valence-band and core-level excitations showed the similar time response having two components, indicating the two PSD models which correspond to the instability induced by electronic excitations in the surface layer and the thermal instability of surface defects, respectively.

VIII-J-3 Surface Core Exciton of Alkali Chloride Film on Si(100)

Shin-ichiro TANAKA, Naoshi TAKAHASHI, K-P. LEE* and Masao KAMADA(**Kyungpook National Univ. Korea)*

[*J. Elec. Spectros. Related Phenom.* **80 205** (1996)]

Surface core exciton has been observed in the partial-photoelectron-yield spectra in the Cl-$L_{2,3}$ region of alkali chloride (KCl and NaCl) film deposited on the Si(100) surface. Compared to the bulk core exciton peaks, the surface core exciton peaks were shifted by 0.7 eV towards lower photon energy. This may be to the change in Madelung potential at the surface. The photoelectron spectra was measured with various photon energies near the Cl-$L_{2,3}$ edge for NaCl/Si(100), and it was found that the Auger spectra drastically change in shape at the excitation energies corresponding to the bulk and surface core excitons.

VIII-J-4 Magnetic Circular Dichroism at $M_{2,3}$ edges of Ni(110) Surface

Shinya YAGI and Toyohiko KINOSHITA

We have measured magnetic circular dichroism (MCD) for the well-established Ni(110) surface at $M_{2,3}$ edges in order to investigate surface magnetic properties. The experiments was done at the beamline BL6A2. In order to obtain circularly polarized light, we used the upper part light above the beam orbit by using the diaphragm which was set in front of the first mirror. The sample shaped into a picture frame was magnetized in remanence before the measurements. One side of the picture frame was wrapped by a coil. To magnetize the sample without stray magnetic field, a pulse current was supplied to the coil. Angle between the incident light and the sample was fixed at 10° . The polarization degree of the circularly polarized light was estimated to be about 20%.

Figure 1 shows the total photoelectron yield (PY) spectra of Ni $M_{2,3}$ edges for two opposite magnetization directions. Inset of the figure shows the MCD spectrum derived from the PY spectra. It is shown that the present MCD intensity of negative contribution in the lower energy region (pre-threshold energy) is nearly equal to that of positive contribution in the higher energy region (post-threshold energy). The result was quite different from those reported by Koide et al.[1] and Muto et al.[2], in which they measured the bulk sensitive MCD and magnetized the sample perpendicular to the surface.When we measure an absorption spectra, it has been known that surface sensitivity is enhanced by using total PY and grazing light incidence. Thus, it seems that our MCD result reflects the surface electronic structure of Ni. According to sum rule, the shape of the MCD spectrum depends upon the ratio between orbital magnetic moment and spin one. If the orbital magnetic moment is absent, the intensity of the positive region for the MCD signal is equal to the negative one at $M_{2,3}$ region[3]. Our MCD result shows nearly equal ratio between positive and negative contribution. This means that the in-plane component of the 3d orbital magnetic moment in the Ni(110) surface is almost absent whereas the perpendicular one exists.

References

1) T. Koide, T. Shidara, H. Fukutani, K. Yamaguchi, A. Fujimori and S. Kimura, *Phys. Rev.* B44, 4697 (1991).
2) S. Muto, Y. Kagoshima and T. Miyahara, *Rev. Sci. Instrum.* **63**, 1470 (1992).
3) A. Yoshida and T. Jo, *J. Phys. Soc. Jpn.* **60**, 2098 (1991).

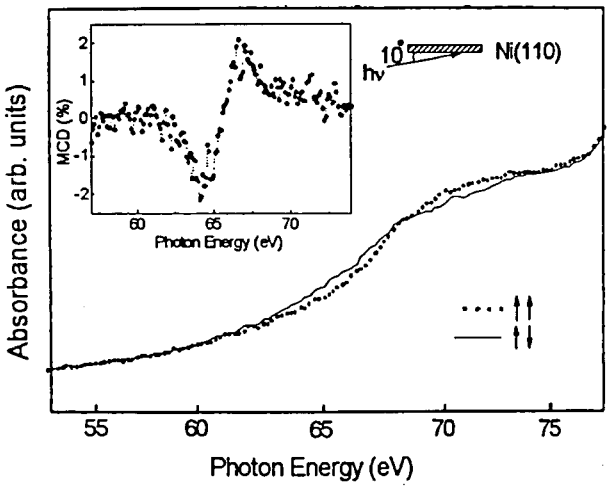


Figure 1. Photoelectron yield spectra of Ni $M_{2,3}$ edges excited by circularly polarized light for two opposite magnetization directions. The experimental geometry is also shown. MCD spectrum derived from the yield spectra is shown inset.

VIII-J-5 Photoelectron Spectro-Microscopy Studies at the UVSOR

Toyohiko KINOSHITA, Masamitsu WATANABE, Krishna G. NATH, Shinya YAGI, Shinichi KIMURA and Andreas FANELSA* *(*Düsseldorf Univ.)*

In order to investigate the surfaces and interfaces of solids, we have started the photoelectron spectro-microscopy studies at the UVSOR facility. The outline and the performance of the apparatus have been described previously[1]. Our system (FISONS instruments, ESCALAB 220i-XL) consists of a hemispherical electron analyzer with 150 mm radius, an electrostatic lens system, a magnetic lens system for further magnification of the photoelectron image, an X-ray tube (Mg Kα, Al Kα) for photoexcitation, a sputtering gun, and so on. It is expected that spatial resolution of 2 μm for the imaging mode and 20 μ m for the spectroscopic mode respectively, can be achieved. In conjunction with monochromatized (and polarized) synchrotron radiation light from UVSOR storage ring, we plan to undertake some experiments with this apparatus. In 1996, the experiments have been performed at the beamlines BL7A and BL5B[2], which cover the photon energy range from 5 eV to 5 keV. The studies with X-ray tube have also been performed.

As a first demonstration of our apparatus, we show the magnetic domain image with new type of magnetic linear dichroism; MLDAD[3] (Magnetic Linear Dichroism in Angular Distribution). Figure 1 shows magnetic domain image taken with MLDAD effect of Fe 2p 3/2 at BL7A. The contrast between up magnetized area and down one is apparent. Since the unpolarized X-ray light can be considered as the incoherent superposition of s- and p-polarized lights, it is also possible to observe the MLDAD effect by using conventional X-ray tube[4]. The example of the MLDAD effect by unpolarized light is shown in Figure 2, where the small area (50 μm) Fe 2p photoemission spectra from two different regions were measured.

References

1) T. Kinoshita, S. Yagi and S. Kimura, *Annual review of IMS*, 1995, p.158.
2) *UVSOR activity report*, 1995.
3) Ch. Roth, F. U. Hillebrecht, H. B. Rose and E. Kisker, *Phys. Rev. Lett.* **70**, 3479 (1993).
4) A. Fanelsa, PhD thesis (**Düsseldorf Univ.*), 1996: F. U. Hillebrecht and W. D. Herberg, *Z. Phys.* B**93**, 299 (1994).

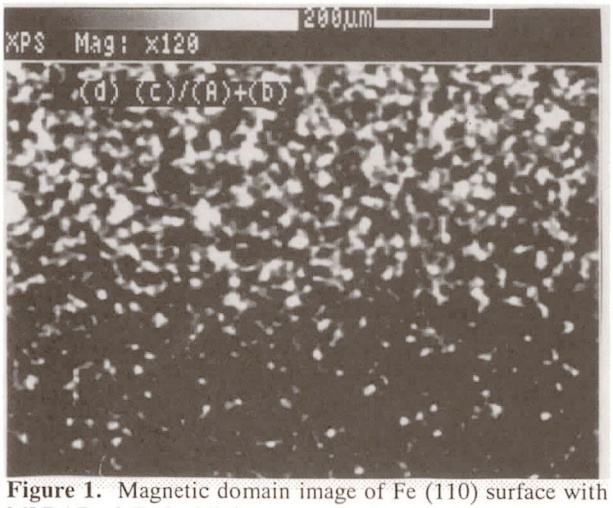


Figure 1. Magnetic domain image of Fe (110) surface with MLDAD of Fe 2p 3/2 (hν = 1758eV).

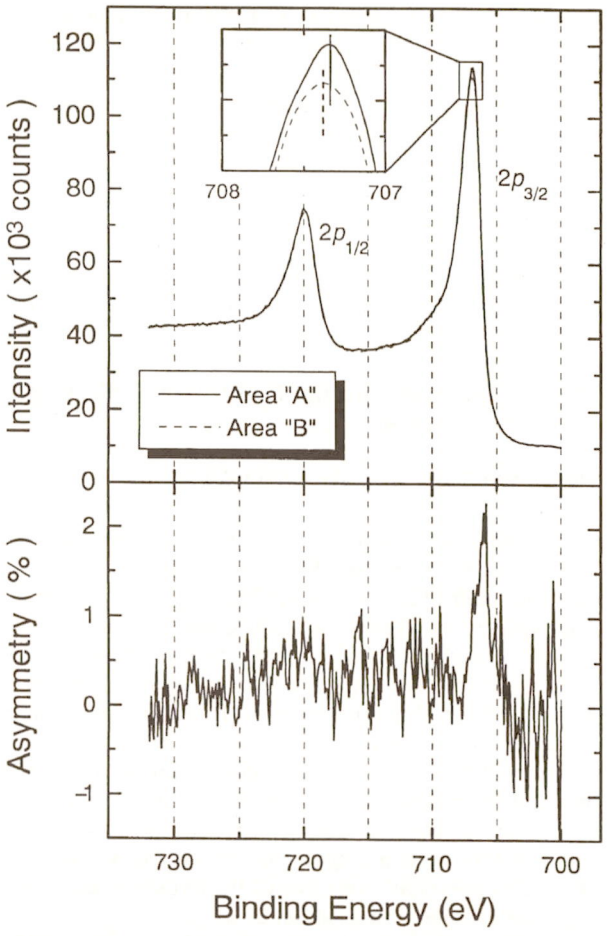


Figure 2. Small area (50 µm) photoemission spectra from two different regions of the Fe (110) surface excited by Al Kα line. The MLDAD signal can be observed reflecting the magnetic domain information.

RESEARCH FACILITIES

For the sake of brevity the present issuue iniludes only the newly installed facilities and activities since September 1995. Concerning the activities and facilities before September 1995, please refer to older IMS Annual Review issues (1978~1995).

Computer Center

The main computers at the Center are a super-computer NEC SX-3/34R, NEC HSP (High-Speed Scalar Processor) and IBM SP2. The computers are linked to international networks through Science Information Network (SINET). About 30% of the computer time is used by the research staffs at IMS, and the remaining 70% is given out as research grants to scientists outside the institute in molecular science and related field. As of March 1996, the number of project group was 205, consisting of 719 users.
In September, 1996, the NEC High Performance Computing (HPC) Server was installed. The library programs of the Center amount to 805. Among them, more than 200 programs can be executed immediately. Recent additions include GAUSSIAN 94-Linda and Molpro electronic structure codes for IBM SP2. The Quantum Chemistry Literature Database (QCLDB) has been developed by the Center in collaboration with the QCLDB group.

Chemical Materials Center

The Chemical Materials Center plays an important role in the synthesis and purification of chemical substances in IMS. The scientists and technical associates of this facility support other people in IMS to carry out the above works. Upon request, technicians carry out elemental and mass spectrometric analyses of new compounds prepared at IMS. They also carry out their own researches on synthesis of new interesting compounds, developments of new selective chemical transformations, elucidation of reaction mechanism, and application of new methodologies developed in IMS to the analysis of chemical substances and reactions.

Instrument Center

Catching to the world trends in the laser spectroscopy, the Instrument Center have newly equipped profitable all solid state light sources in various temporal and spectral regions, including femtosecond and nanosecond Optical Parametric Oscillators (OPO). The synchronously femtosecond OPO (OPAL; SPECTRA PHYSICS) is tunable from 1.1 μm up to 1.6 μm. The nanosecond OPO has extraordinary tuning range form 420 nm down to 2.2 μm. The Instrument Center also replaced the old spectro-fluorometer to new one (FLUOROLOG; SPEX) which is composed of a xenon lamp house, a double monochromator which makes lamp beam monochromatic, and a single monochromator for spectroscopy. The detector is changable by rotating a mirror (CCD and PM). Using these instrument, one can carry out various experiments in not only the ultrafast temporal region but also steady state photon counting region.

Low-Temperature Center

The main task of Low-Temperature Center is a steady supply of liquid helium and liquid nitrogen to the users in the Institute. The total amounts of liquid helium and liquid nitrogen supplied in 1995 were 43,995*l* and 74,467*l*, respectively. A dilution refrigerator (KELVINOX 36115, Oxford Instruments) and a SQUID magnetometer (MPMS 2, Quantum Design) are now available for general users. A high-resolution solid state NMR spectrometer (DSX-400, Bruker Analytical Instrument) equipped in 1995 is working well and now available for general users as well.

Equipment Development Center

A number of research instruments have been designed and constructed by making use of the mechanical, electronic and glass-blowing technologies at this Facility. Representative instruments developed during this fiscal year of 1995 are listed below.

- High-pressure pulse valve
- Light pipe assembly for infra-red light
- Wobbler for far-infra-red spectroscopy
- Centrifugal separator for large sample
- Micro current source for crystal growth
- Data processor for acousto-optical spectrometer
- Thermo-controller for baking of vacuum chamber
- Platinum electrode for crystal growth
- Quartz Cells

Division of IMS Machines

Equipment Development Center has the division of IMS Machines. Activitiy of this division is described in detail in section "RESEARCH ACTIVITIES".

Ultraviolet Synchrotron Orbital Radiation Facility

From February to May in 1995, the UVSOR had a shutdown to install the gate valve into a 750 MeV storage ring in order to separate the beam pipe into four sections for easy maintenance and upgrade. The first Front-end manual valve was replaced by new one at beam lines 3B, 5A, 5B, 6B, 7A, 8A, and 8B. The gratings and mirrors of the plane-grating

monochromator at beam lines 5B and 8B2, and of the Seya-Namioka monochromator at BL1B were replaced. The FT-IR interferometer was purchased from a Brucker Co. Ldt, and the combinational use of the new FT-IR and the existing FT-FIR systems provided the experiments in the wide wavelength region. The time-resolved spectroscopy is ready to use at the present stage.

After spring shutdown, the UVSOR light source was operated at an electron energy of 750 MeV with an initial current of 240 mA, up to May, 1996. The UVSOR systems have been operated for 36 weeks. Among them, two weeks were used for machine studies, besides every Monday and Saturday, and 34 weeks were abailable for users. Four weeks were operated under a single bunch mode, while 4-T wiggler was used for 7 weeks to provide hard and soft x-rays to experiments at BL 7A. A new monochromator named SGM-TRAIN has been constructed at a beam line 5A and was adjusted to get high-resolution spectra.

In the spring shutdown in March, 1996, a long beam pipe with a NEG pump and a new type of helical undulator were installed into the section No. 3 of the storage ring. The power systems of RF cavity for the storage ring and the booster synchrotron were replaced by the solid-state type. The beam line 7B was scrupped to replace by new monochromator. The pre-mirror chamber for the multi-layer monochromator was also constructed at beam line 4A. The monitoring system of radiation from the accelerator complex (750 MeV storage ring, 600 MeV synchrotron, and 15MeV linac) and the enrty system into the experimental hall were replaced by new ones.

SPECIAL RESEARCH PROJECTS

IMS has special research projects supported by national funds. Three projects in progress are:
(1) Development of microscopic environments with functionality and quantum steering for reactions (1995-)
(2) Study of molecular solid toward molecular electronics (1995-)
(3) Material control in multi-reaction centers (1993-)
These three projects are being carried out with close collaboration between research divisions and facilities. Collaborations from outside also make important contributions. Research fellows join these projects.

(1) Development of Microscopic Environments with Functionality and Quantum Steering for Reactions

Structures, Reactions and Spectroscopies of Molecules and Molecular Clusters

Suehiro IWATA, Seiichiro TEN-NO, Tsutomu IKEGAMI, Takeshi TSURUSAWA, Toshio ASADA, Toshiaki FUJII *(GUAS)*, **Hidekazu WATANABE** *(GUAS)*, **Chang-Guo ZHAN** *(Central China Normal Univ. and IMS)*, **Jong K. PARK, Yumin LI, Fernando R. ORNELLAS** *(São Paulo Univ. and IMS)*, **Pradipta BANDYOPADHYAY** *(GUAS)*, **Jan HRUSAK** *(J.Heyrovsky Institute of Physical Chemistry and IMS)*, **Andreas FIEDLER and Patrizio SEVERINO**

Ab initio molecular orbital methods were applied to various chemical and physical problems. The works were carried out under close collaboration with several experimental groups. Besides, new theoretical techniques in molecular electronic calculations were developed. Followings are the systems we have been working on.

1. Complexes of water clusters with atoms, atomic ions, and organic acids.
2. Binary element molecules and clusters.
3. The reaction intermediates, and unstable molecules and clusters.
4. Potential energy surfaces of low-lying states of simple molecules.
5. Basic molecules containing the transition metal atoms.
6. Rare gas atomic cluster cations.
7. Novel molecular systems with symmetry-breaking.

For most of cases, in addition to electronic structure calculations, the nuclear motions of the systems were studied either quantum mechanically, semi-classically or classically. For these studies, the computer codes have been developed.

Prediction of Protein Tertiary Structures by Multicanonical Algorithms

Yuko OKAMOTO, Ulrich H.E. HANSMANN, Masato MASUYA and Ayori MITSUTAKE *(Nara Women's Univ.)*

Proteins are the most complicated molecules that exist in nature. Since protein structures are closely related to their biological functions, the prediction of their three-dimensional stuructures from the first principles (by minimizing their energy functions) is not only very challenging but also very important a problem in theoretical molecular science. To be more specific, it is widely believed that three-dimensional structure of proteins is determined by their amino-acid sequences. However, nobody has succeeded in predicting it solely from the amino-acid-sequence information (prediction from the first principles). This is because there exist huge number of local minima in the energy function, and conventional simulation techniques will necessarily get trapped in one of the local minima without ever finding the energy global minimum. Multicanonical algorithms are new Monte Carlo algorithms that are known in other research fields (such as a spinglass problem in condensed matter physics) to alleviate this difficulty. We proposed to apply this method to the protein folding problem.[1] The goal of the present project is to further test the effectiveness of the multicanonical algorithms in the protein folding problem and to succeed eventually in the prediction of tertiary structures of proteins from the first principles.

Reference

1) U.H.E. Hansmann and Y. Okamoto, *J. Comp. Chem.* **14**, 1333 (1993).

Quantum Mechanical and Semiclassical Studies of Chemical Reaction Dynamics

Hiroki NAKAMURA, Chaoyuan ZHU, Katsuyuki NOBUSADA, Miyabi HIYAMA *(Graduated Univ. for Advanced Studies)* **and Yoshiaki TERANISHI** *(Graduate Univ. for Advanced Studies)*

Dynamics of triatomic chemical reactions can now be clarified accurately with use of the hyperspherical coordinate approach. A couple of reaction systems are now being studied. One of the intriguing results obtained recently is the effects of reagent rotational excitation on the reaction dynamics in the $O(^3P)$+HCl system. Because of the non-linear transition state the rotational excitation strongly enhances the reaction.

Based on our recent achievements in the theory of nonadiabatic transitions due to curve crossing, we have further extended our theoretical studies to multi-channel curve crossing problems and time-dependent problems. The two-state theory can be usefully applied to multi-channel problems. Time-dependent crossing and non-crossing problems can also be treated nicely by the newly developed two-state theory. Some exponential potential models are solved exactly either quantum mechanically or semiclassically. This would enable us to formulate a general semiclassical theory for general exponential potential models, which represent an important third class of nonadiabatic transitions in addition to the Landau-Zener-Stueckelberg and the Rosen-Zener-Demkov problems.

A general theoretical procedure has been developed to reveal the characteristics and dynamics of superexcited states of diatomic molecules, and has been applied to CO. The electronic couplings for the $s\sigma$ and $d\sigma$ symmetries are calculated and the resonant preionization

problem is evaluated.

Based on the intriguing phenomenon of complete reflection in the nonadiabtic tunneling type transition, we have proposed a new mechanism of molecular switching. Complete switching is demonstrated by numerical evaluations of wave packet propagation.

Gaussian-Markovian Multi-State Quantum Fokker-Planck Equation Approach to Nonlinear Spectroscopy of Displaced Morse Oscillators System

Yoshitaka TANIMURA and Yutaka MARUYAMA

Quantum coherence and its dephasing by coupling to a dissipative environment plays an important role in time-resolved nonlinear optical response as well as nonadiabatic transitionsvand tunneling processes in condensed phases. We discuss nonlinear optical processes on multistate one-dimensional system with Morse potential surfaces. This is based on numerical study using multi-state quantum Fokker-Planck equation for a colored Gaussian-Markovian noise bath, which is expressed as a hierarchy of kinetic equations introduced by Tanimura and Kubo. This equation can treat strong system-bath interactions as well as a low temperature heat bath, where the correlated effects of noise play an important role, without using a white noise approximation and a rotating wave approximation for the system-bath interaction. The approach applies to coherent Raman measurements as well as any other four-wave mixing including pump-probe spectroscopy. Model calculations are made using potential surfaces of Cs_2. We calculated nuclear wave packets in Wigner representation and their monitoring by femtosecond pump-probe spectroscopy. Change of line shapes for various displacements of potentials and heat-bath parameters are discussed.

Constructing Molecular Theory of Chemical Processes in Solution

Fumio HIRATA, Hirofumi SATO, Sarah A. MAW*(Univ. Manchester)*, **Masahiro KINOSHITA***(Kyoto Univ.)*, **Masayuki IRISA***(Kyushu Inst. Tech.)*, **Song-Ho CHONG***(Kyoto Univ.)*, **Tateki ISHIDA***(Kyoto Univ.)* **and Shigeki KATO***(Kyoto Univ.)*

Chemical processes taking place in the liquid phase have been of great interest in many aspects in chemistry including organic reactions and the stability of biomolecules. However, the theoretical description of the phenomena is far from complete, especially, in the molecular level. The difficulty lies in the coupling of complicated intramolecular process including the electronic structure and the many body nature of the liquid state, each of which by itself is a non-trivial theoretical problem. Particulary, the description of chemical specificity exhibited in molecualr liquids, represented by the hydrogen-bonding in water, was the main obstacle faced by the liquid state theory. The major break through toward the liquid state theory in chemistry has been made by D. Chandler and H.C. Andersen in 1972 with their theory for the reference interaction site model (RISM).[D. Chandler and H. C. Andersen, J. Chem. Phys., 57, 1930 (1972)] The theory is a natural extension of the Ornstein-Zernike equation of simple liquids to a mixture of atoms but with strong intramolecular correlation which represents chemical bonds. The theory takes account for one of the two important chemical aspects of molecules, geometry, in terms of the site-site interactions between atoms. However, it does not handle the other chemical aspect of molecules, electrostatics, in its original forms. The charge distribution in a molecule, which is a classical manifestation of the electronic structure, plays a dominant role in determining the chemical specificity of the molecule. Therefore, without including the charge distribution in molecules, the description is incomplete in terms of chemical specificity. A complete chemical characterization of molecular liquids became possible in 1981 due to the appearence of the extended RISM theory which takes the charge distribution as well as the molecular geometry into account.[F. Hirata and P. J. Rossky, Chem. Phys. Lett., 83, 329 (1981)] Applications of the theory to a variety of liquids and solutions have demonstrated its capability of describing the chemical specificity, such as hydrogen-bonding, of liquids in a molecular detail.[F. Hirata, Kikan Kagaku Sosetsu No.26, Molecular Picture of Solution, (in Japanese), pp. 148 (1995)]

Our current research interests and activities are concentrated upon three important problems in the chemical physics, in each of which the extended RISM theory plays a key role: 1. the electronic structure of a molecule in solution, 2. solvation thermodynamics of protein and related molecules, 3. characterization of spatial and temporal density fluctuation in molecular liquids. In each of the three problems, we have recently proposed new method. The work along the three lines are now in progress.

Development of High-Sensitivity Submillimeter-wave to Far Infrared Spectrometer Systems for the Study of Transient Molecules

Hiroyuki OZEKI and Shuji SAITO

Spectroscopy in the submillimeter-wave to far infrared region has been less exploited, compared with that in other electro-magnetic wave regions, because high spectral purity and tunable radiation sources have not been available. We developed a frequency tunable far infrared sideband spectrometer suitable for the study of transient molecules. We installed a stable high-power CO_2 laser and an optically pumped far-infrared laser, and constructed a mixer mounting with a non-linear element of Ga-As Schottky diode, which is mounted in a Martin-Puplett diplexer separating a tunable sideband radiation from the fundamental laser radiation as given in previous Annual Reviews.

Currently we have obtained a power of 0.1 micro watts for both sidebands in the frequency range of 2522 +/-26.5 GHz. The system noise is dominated by detector noise whose typical value is approximately $2.5\mu V/(Hz)^{1/2}$. The minimum detection sensitivity is 3×10^{-5} at the condition of 1 s time constant, when a perfect separation of the sideband is achieved. We tested the frequency accuracy of our spectrometer by measuring the frequency of the J=22-21 transition of CO, which is known to be 2528172.067 MHz,[1)] and found that our measured frequency is 2528172.119 MHz, which differs by about 50 kHz from the reported value. This indicates that a frequency accuracy of less than 100kHz can be attained if we can oscillate the far infrared laser under optimum conditions.

Reference

1)T. D. Varberg and K. M. Evenson, *IEEE, Inst. and Meas.* **42**, 412(1993).

(1) Studies on Laser Cooling and Trapping of Neutral Atoms
(2) Laser Spectroscopic Studies of Ions in Liquid Helium

Norio MORITA, Mitsutaka KUMAKURA and Yoshiki MORIWAKI

For studies on laser cooling and trapping of neutral atoms, we have continued the work on a magneto-optical trap of helium atoms. Especially, the laser control of ultracold collisions in the trap has been studied. To perform this study, we need another independent near-infrared laser to control the collision processes, and the laser should provide tunable wavelengths around 1.083μm, which is nearly resonant with the $2s^3S$-$2p^3P$ transition of the helium atom. For this use, we have employed a tunable diode laser, and have developed a frequency-stabilization system for the laser. With this new laser system as well as the laser trapping apparatus so far developed in our research group, we have clearly observed a manifestation of laser control effects on ultracold collision processes in the helium trap. In particular, as a result of suppression of the ultracold collisions through the collision-control laser, considerable enhancement in the number of trapped atoms has been observed (see II-D-1).

On the other hand, for laser spectroscopic studies of ions in liquid helium, we have developed a special cryostat system suitable to this experiment, which is equipped with a mechanism for making ions through laser-ablation of a metal piece in liquid helium, many optical windows for laser incidence and fluorescence detection, and many electrodes for repelling ions away from the metal piece and also for convenience of future experiments on ion-trapping inside the cryostat. With this apparatus, we have performed a preliminary experiment, and observed many spectra of atoms and ions produced in liquid helium, though behaviors of those spectra are not clearly understandable yet. (see II-E-1).

Mechanism of Oxygen Activation by Heme-Copper Terminal Oxidase Superfamily

Teizo KITAGAWA, Takashi OGURA, Jörg MATYSIK, Shun HIROTA, Denis A. PROSHLYAKOV*(Graduate Univ. for Advanced Studies)*, Shinya YOSHIKAWA *(Himeji Inst. Tech.)*, Tatsushi MOGI*(Univ. of Tokyo)*

The terminal oxidase in respiratory chains is cytochrome *c* oxidase for aerobic organisms and quinol oxidase for *E. Coli*. Both have two heme groups; one works for electron transfers and the other provides the catalytic site for dioxygen reduction. The heme iron at the catalytic site is antiferromagnetically coupled with a copper ion in the oxidized state. The dioxygen reduction is coupled with proton translocation through membrane, generating electrochemical potential which could be used for ATP synthesis. The final goal of this study is to elucidate the coupling mechanism between the electron- and proton transfers, but currently a mechanism of dioxygen reduction at the catalytic site is of spectroscopic concern. This year we treated *bd* -type cytochrome oxidase and assigned the axial ligand-related Raman bands. For bovine cytochrome *c* oxidase, we investigated reaction intermediates present in the time range between 0.1 and 11 ms following initiation of the reaction by using time-resolved resonance Raman spectroscopy combined with our original "artificial cardiovascular system for pursuit of enzymic reaction". The first intermediate gave the oxygen isotope sensitive band at 571 cm^{-1} for $^{16}O_2$. Since the corresponding band for $^{16}O^{18}O$ split into two bands. it became confident that the binding of O_2 is of an end-on type. In subsequent steps, we observed three oxygen isotope sensitive bands at 804/769, 785/750 and 355/340 cm^{-1} for $^{16}O_2/^{18}O_2$ derivatives. Experiments at lower temperatures clarified that the 804 cm^{-1} species appears prior to the 785 cm^{-1} species, while the 355 cm^{-1} band was seen together with the 804 cm^{-1} band. Raman excitation of the intermediates at 607nm provided only the 804/769 cm^{-1} bands for $^{16}O_2/^{18}O_2$ derivatives while that at 580nm gave only the 785/750 cm^{-1} bands. Therefore, the electronic characters of hemes of the two intermediates are distinct. Although the 804 cm^{-1} band appeared with a similar rate in H_2O and D_2O, the appearance of the 788 cm^{-1} band was significantly delayed in D_2O, suggesting that the generation of 788 cm^{-1} species from the 804 cm^{-1} species is coupled with the proton translocation. The experiments with $^{16}O^{18}O$ demonstrated that both bands should arise from the Fe^{IV}=O stretching but not from the O-O stretching. The reaction of oxidized enzyme with hydrogen peroxide also gave the three sets of the oxygen-isotope-sensitive bands at the same frequencies as those of dioxygen reduction. It is likely that the 804 and 788 cm^{-1} bands arise from the Fe^{V}=O and Fe^{IV}=O stretching modes, respectively, while the 355 cm^{-1} band is associated with the His-Fe=O bending mode.

Laser Raman Beat Detection of Magnetic Resonance

Tatsuhisa KATO and Michio MATSUSHITA

Laser Raman beat detection is a coherent optical-RF double resonance technique where the optical and RF field induce coherence within a three level system and a resultant Raman beat signal is detected using heterodyne detection. This technique can be applied to the study of electron paramagnetic resonance and nuclear magnetic resonance not only in the ground state of a molecule but also in the electronic excited state.

There are some causes to hide the Raman beat signal, that is, the inhomogeneity of the circumstance of the molecule, the fluctuation of the applied field, and the interference by the crystal phonon. It is the key to success in the Raman beat detection to eliminate these cause of the incoherence. Then it is needed to prepare the sophisticated single crystal sample, the highly stabilized magnetic field, and a cryostat of liquid helium. It has been completed to set up the apparatus, and the Raman beat detection was applied to the study on the zero-field NMR transitions of Pr^{3+} in LaF_3 crystal, as reported in Section II-I-1.

Liquid Dynamics Studied by New Ultrafast Higher-Order Nonlinear Spectroscopy

Keitaro YOSHIHARA, Keisuke TOMINAGA, Janseok MA and Yuuichi FUJIMURA *(Tohoku Univ.)*

Understanding of microscopic dynamics and structures of liquids is quite important in chemistry because many chemical reactions and various relaxation phenomena in condensed phase such as vibrational dephasing or energy relaxation are strongly affected by microscopic details of liquid molecules. In this research project we have developed techniques to observe higher order (fifth

and seventh order) nonlinear optical response from liquids. The experiments include vibrational echo-type measurement for low-frequency modes and temporally one- and two-dimensional overtone dephasing measurement for high-frequency modes. The vibrational echo-type experiments are temporally two-dimensional spectroscopy and can determine the relative importance of inhomogeneity of the spectral broadening. The one-dimensional overtone dephasing experiments allow us to investigate the vibrational quantum number dependencies of the dephasing mechanisms. By analyzing the two-dimensional overtone dephasing signal we can study correlation of the fluctuations of transition frequencies between different vibrational modes.

Ultrafast Chemical Reactions in Condensed Phase

Keitaro YOSHIHARA, Keisuke TOMINAGA, Yukito NAITOH, Shigeichi KUMAZAKI, Isamu IKEGAMI*(Teikyo Univ.)*, **Sigeru ITOH***(NIBB)*, **Masayo IWAKI***(NIBB)*, **Haridas PAL, Igor V. RUBTSOV, Nobuyuki NISHI** *(Kyusyu Univ. and IMS)* **and Kazuhiko OHASHI***(Kyusyu Univ. and IMS)*.

The femtosecond solid state lasers such as Ti:Sapphire laser and Cr:Fosterite laser are stable light sources with high energy, high repetition rate and high tunability. Using these lasers, we investigated the chemical reactions in the condensed phase as follows. 1) The elementary processes of photoexcited simple molecules in solution such as photodissociation of CH_2I_2, isomerization of linear polyene, chemical reaction in neat CH_3I, and ionization of neat benzene to form the dimer cation. 2) The deuterium isotope effects and the substituent effects in the ultrafast intermolecular electron transfer. The examination of the vibrational modes playing an important role in electron transfer reactions. 3) Energy and electron transfers in photosynthetic reaction centers, and the their dependence on excited chlorophyll spectral forms and on temperature.

Studies of Laser-Induced Photochemistry on Solid Surfaces

Yoshiyasu MATSUMOTO, Kyoichi SAWABE, Kazuo WATANABE, Hiroyuki KATO *(Graduate Univ. for Advanced Studies)*, **M.C. LIN***(Emory University and IMS)*, **Ikuo KINOSHITA***(Yokohama City Univ.)* **and Toshihisa ANAZAWA**

Light sources such as lasers and synchrotron radiation can be useful for the various processes in the fabrication of microelectronics, including etching, chemical vapor deposition, atomic layer epitaxy. On the other hand, it has also been well recognized that there is an important class of catalytic reactions with the aid of photon irradiation. Although those applications of light are practically useful and important, fundamental understanding of these processes is still lacking. Therefore, this project is mainly aimed for investigating how the interaction of light and adsorbates and /or substrates promotes chemical reactions from the fundamental point of view.

We have continuously performed the studies on surface photochemistry particularly of nitrous oxide adsorbed on semiconductor surfaces and methane on Pt(111) in this year. A UHV apparatus used is equipped with a retractable LEED/Auger electron spectrometer, a differentially pumped quadrupole mass spectrometer, a X-ray source, a photoelectron analyzer, an ion gun, a high precision sample manipulator, a closed cycle He refrigerator, and a gas doser. The main chamber was evacuated to a base pressure of 1×10^{-10} Torr by cascaded turbo-molecular pumps. With this apparatus, we can perform not only conventional analytical measurements in surface science including LEED, AES, temperature-programmed desorption, XPS, and work function measurements, but also measurements providing information on nuclei dynamics including angular-resolved time-of-flight spectroscopy of neutral species desorbed from the surface with sub-monolayer coverage.

In additon, we have newly developed an apparatus for multiphoton photoelectron spectroscopy that enables us to obtain electronically excited states of surface states of clean surfaces and those of adsorbates. The information of energetic positions and widths of the excited states is vital to understanding of excitation mechanisms in surface photochemistry. The apparatus is composed of light sources and a magnetically shielded UHV chamber. We have used two kinds of light sources: a tunable dye laser pumped by a Nd:YAG laser at a repetition rate of 10 Hz and a mode-locked Ti:Sapphire-seeded regenerative amplifier system (Spectra Physics, Spittfire) at a repetition rate of 50 kHz. Using this apparatus, we have investigated surface states at a clean Pt(111) surface.

Light Sensitivity of the Self-Organizing Chemical Systems

Ichiro HANAZAKI, Akiko KAMINAGA, Noriaki OKAZAKI* and Gyula RÁBAI** *(*IMS fellow, ** Inst. Phys. Chem., Kossuth Lajos Univ., Debrecen, Hungary)*

The self-organizing process in chemical systems is known to occur as a result of nonlinear chemical events. The temporal (oscillatory) behavior and the possibility of spatial pattern formation in such systems have been interested in relation to the understanding of living systems and also to their possible application to sensing and memory-storage devices. The response of such systems to light illumination has been studied many times but not in a systematic manner. We have established the method by which the response of these systems to light illumination and applied it to determine the state diagram and photo-induced bifurcation structure for the Belousov-Zhabotinsky system, the minimal bromate oscillator, the $Fe(CN)_6^{4-}$ / H_2O_2 system, and the Briggs-Rauscher system. We have established the photoresponse of the BrO_3^--SO_3^{2-}-ferrocyanide system, which can be divided into two subsystems, namely, the BrO_3^--SO_3^{2-}-H^+ system and the BrO_3^--ferrocyanide-H^+ system. We have studied the photoresponse of the latter subsystem and found that the protonated ferrocyanide, $HFe(CN)_6^{3-}$, is responsible for the photoresponse, while ferricyanide, which has a more intense absorption band in the visible region, is not effective. A related system, BrO_3^--H_2O_2-marble, was found to exhibit the chemical chaos. We have proposed a new exact reaction scheme for this system which can reproduce the chaotic and other oscillatory behaviors quite well. The photoresponse of the Briggs-Rauscher reaction has also been established, in which we found the photo-induced tristability among an oscillatory and two steady states and the bistability between two oscillatory states. A new photo-assisted autocatalytic mechanism was also pro-

posed to explain these observed phenomena.

Laser Investigation of Elementary Reactions in the Gas Phase

Toshinori SUZUKI, Michael C. Heaven, Kenichi TONOKURA, Hiroshi KOHGUCHI, Yang SHI and Hideki KATAYANAGI

Complex reactions in combustion, plasma, and atmospheric chemistry are essentially governed by the dynamics of atomic and molecular collisions. The most detailed knowledge on such microscopic dynamics are learned from scattering experiments, as has been demonstrated by Ernest Rutherford. In chemical dynamics, however, internal excitations of atoms and molecules play crucial role, so that these internal degrees of freedom must be resolved in scattering experiment. Such requirement can only be fulfilled by the extensive use of state-of-the-art laser spectroscopic techniques that provide ultimate state resolution and capability of analyzing directional properties of atoms and molecules. We have developed imaging method to visualize the scattering distribution of photofragments with quantum state selection. A new crossed molecular beam machine equipped with the ion imaging apparatus has been constructed to measure state-resolved differential cross sections for inelastic and reactive scattering.

Spectroscopic Studies of Intermolecular Interaction in Molecular Dimer Cations

Nobuyuki NISHI*(IMS and Kyushu Univ.)*, **Kazuhiko OHASHI and Yoshiya INOKUCHI***(Kyushu Univ. and IMS)*

In molecular clusters and pure molecular liquids with positive charges, singly occupied orbitals of cation molecules produce intermolecular bonds coupled with highest occupied orbitals of adjacent neutral molecules. In such a system, strong intermolecular interaction is limited to the area of two molecules (a cation + a neutral). This situation is in contrast with negatively charged molecular culusters like $(H_2O)_n^-$, or $(CO_2)_n^-$ where an electron moves over numbers of molecules. An excess electron in a negative ion travels over Rydberg orbitals, while the electron in a caion cluster moves on highest occupied valence orbitals of neutral species. This is just the reason why the charge in a cation cluster is localized in a dimer unit.

Intermolecular interaction in a dimer cation is therefore originated in charge resonance interactions between a hole and an electron in the higherst occupied valence orbitals of the two molecules. Close location of a cation and a neutral molecules always produces a lower bonding state and an upper untibonding state. By observing the electronic transition from the bonding state to the untibonding state, one can estimate the lowest limit of the interaction energy. As we demonstrated, the half of the transition energy coincides with the binding energy in the case of a pair of a benzene cation and a neutral benzene. This kind of transition is sometimes called an intervalence or charge resonance transition and can be observed in most of cation and neutral pairs of molecules. This special research project is based on this situation proposing the direct measurement of intermolecular binding energies of various dimer cations. We apply photodissociation spectroscopy for this measurement, since the excitation to the untibonding state results in the dissociation of the dimer. The interaction energy of a naphthalene cation and a neutral benzene was obtained to be 0.38 eV that is smaller than those of benzene-benzene$^+$ (0.67 eV) and naphthalene-naphthalene$^+$ (0.52 eV). In a benzene-naphthalene dimer cation, 10% of the charge is found tobe delocalized on a benzene molecule.

Reactions of Gas-Phase Cluster Anions Studied by Photoelectron Spectroscopy

Morihisa SAEKI, Tatsuya TSUKUDA *(Univ. of Tokyo)* **and Takashi NAGATA**

Although negatively-charged clusters are often thought as being gas-phase analogue to anionic species in the condensed phase, it is not always the case; e.g., there is a striking difference in the electronic structures between $(CO_2)_N^-$ and a $\cdot CO_2^-$ anion in solution. In $(CO_2)_N^-$ the excess electron is delocalized over the two CO_2 constituents to form $C_2O_4^-$. Our interest is focused on a fundamental question regarding the chemical properties of negatively-charged molecular clusters: whether or not the reactivities of gas-phase cluster anions differ from those of corresponding anions in solution. Recently, we have examined the reactions of $(CO_2)_N^-$ with CH_3I by using photoelectron spectroscopy combined with mass spectrometry. The photoelectron spectroscopic study of the reaction products revealed that the reactions of $(CO_2)_N^-$ with CH_3I lead to the formation of a novel molecular anion with the formula $[CH_3CO_2\cdots I]^-$, which has never been observed in the corresponding condensed-phase reaction. In solution the dominant reaction process is electron transfer, $\cdot CO_2^- + M \rightarrow CO_2 + \cdot M^-$. The present study has demonstrated clearly the difference in reactivities between gas-phase clusters and their counterparts in solution.

Time-resolved Spectroscopic Studies on Chemical Reactions using Ultrafast Laser and Synchrotron Radiation

Tahei TAHARA, Satoshi TAKEUCHI, Shigeki MATSUO, Atsuhiko SHIMOJIMA and Misa KAYAMA

One of the goals of the researches in chemistry is to elucidate the mechanism and dynamics of chemical reactions and to design and control them. Since chemical reactions generally consist of a series of elementary processes in which a variety of intermediates appear and disappear, it is indispensable to examine the details of each process for full understanding of a whole chemical reaction. Time-resolved spectroscopy is one of the most powerful tools and has been widely utilized for the studies on chemical reactions since it enables us to directly observe the temporal changes in the course of chemical reactions. Recent progress of time-resolved spectroscopy relies on the drastic advances of the laser technology, and we are now able to examine the dynamics of primary processes of chemical reactions with pico/femtosecond time-resolution. Time-resolved spectroscopy based on ultrafast lasers is, and will continue, playing crucial roles in physicochemical studies on chemical reactions. Synchrotron radiation, on the other hand, has unique potentiality to be alternative light source in time-resolved spectroscopy since it is intrinsically given in the form of a picosecond pulse train from a storage ring. The potential of synchrotron radiation in time-resolved spectroscopy lies on the fact that it

affords picosecond optical pulses in a very wide energy range from X-ray to far-infrared. Thus, synchrotron radiation may open up new possibility of time-resolved spectroscopy in the energy region which is not accessible with the present lasers only. The aims of this project are the development of new time-resolved spectroscopic methods and their application to the studies on chemical reactions, taking advantage of these two light sources which are complementary to each other. In the past year, we have constructed a femtosecond time-resolved fluorescence upconversion spectrometer and a femtosecond optical heterodyne detected impulsive stimulated Raman scattering (OHD-ISRS) spectrometer, based on a mode-locked Ti:sapphire oscillator laser. We are now planning picosecond time-resolved measurements in the far-infrared region using synchrotron radiation available at UVSOR.

Study of Ion Desorption Induced by Core-Level Excitations of Condensed $Si(CH_3)_4$ by Using Photoelectron-Photoion Coincidence Spectroscopy (PEPICO) Combined with Synchrotron Radiation

Kazuhiko MASE, Mitsuru NAGASONO, Shin-ichiro TANAKA, Tsuneo URISU and Shin-ichi NAGAOKA*
*(*Ehime University)*

[*Surf. Sci.*, in press]

Photoelectron-photoion coincidence (PEPICO) spectra of condensed $Si(CH_3)_4$ are measured with C 1*s* and Si 2*p* photoelectron by using synchrotron radiation (Figure 1). H^+ is found to be the only species desorbed in both the cases. Furthermore, the H^+ yield in coincidence with C 1*s* photoemission is found to be three times as large as that with Si 2*p* photoemission. These results indicate that Auger stimulated ion desorption mechanism is responsible for the H^+ desorption, that the neutralization probability of the polyatomic ions is much larger than that of H^+, and that C 1*s* photoemission leads more efficiently to H^+ desorption than Si 2*p* photoemission.

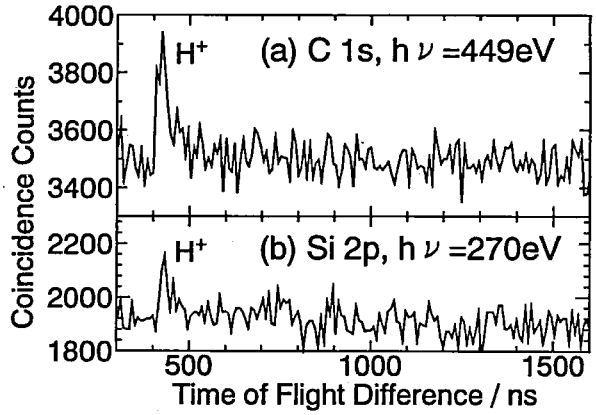


Figure 1. PEPICO spectra of condensed $Si(CH_3)_4$ obtained with (a) C 1*s* photoelectron at hv= 449 eV, and (b) Si 2*p* photoelectron at hv= 270 eV. The accumulation time was 3600 s in both the cases.

Pump-Probe Spectroscopy of Atoms and Molecules with a Combination of Ultraviolet Laser and Synchrotron Radiation

Koichiro MITSUKE, Masakazu MIZUTANI, Manabu TOKESHI *(Kyushu Univ.)* **and Atsunari HIRAYA** *(Hiroshima Univ. and IMS)*

A mode-locked Ti:sapphire laser is made to oscillate at the frequency of the UVSOR storage ring, 90.115 MHz, in a multibunch operation mode. The third harmonic of the laser is available at a wavelength range from 243 to 280 nm. The synchrotron radiation (SR) from an undulator is monochromatized by a grazing-incidence monochromator and introduced coaxially with the laser. The temporal profile of the photon pulses is monitored *in situ* by a luminescing substance/photomultiplier combination. The delay timing between the laser and SR can be changed from 0 to 11 ns by adjusting an electronic module which provides phase-locked loop stabilization of the laser pulse. The reliability and feasibility of this laser-SR combination technique are demonstrated by applying pump-probe experiments to two physical systems. The first example is photodissociation of iodomethane (CH_3I) with a laser photon, followed by photoionization of an iodine fragment with SR. Second, two-photon ionization of helium atoms is studied as the prototype of the time-resolved experiment. The He^+ signal counts as a function of the laser-SR delay are found to be enhanced in a narrow time window, which can be interpreted in terms of a short lifetime of the resonant state, $He^*(1s2p\ ^1P)$, produced by primary SR excitation.

New Apparatus for Studying Reaction Dynamics of the Inner Core Excited Polyatomic Molecule

Toshio IBUKI, Kazumasa OKADA, Tatsuo GEJYO and Atsunari HIRAYA *(Hiroshima Univ. and IMS)*

A new experimental setup for studying reaction dynamics of the inner core excited polyatomic molecule has been constructed on the BL8B1 beamline of UVSOR facility (Figure 1). The main chamber can be rotated at the angles from -20° to 110° with respect to the direction of linear polarization of synchrotron radiation in order to measure the angle-resolved photofragment ions. The base pressure of the chamber is better than 2 x 10^{-9} Torr. Photon energy of 30-900 eV is available from a constant-deviation constant-length spherical grating monochromator (CDCL-SGM) by using three gratings, and thus the *K*-shells of C, N, O and F atoms in a molecule can be excited. This apparatus is also usable for studying the valence shell excitation. A reflectron type TOF mass spectrometer is installed to the main chamber. The mass resolution is better than 100 for the fragment ions with the kinetic energy of 20 eV. A quadrupole mass spectrometer with a energy analyzer is also installed in order to measure the kinetic energy distribution of the fragment ion produced. This apparatus has been open to the users of UVSOR facility.

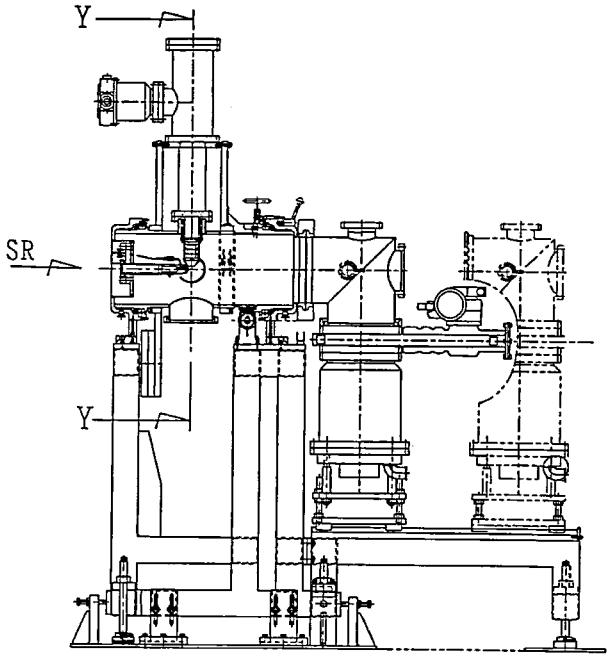


Figure 1. Side view of a newly constructed experimental apparatus to study the inner core excited polyatomic molecule on the BL8B1 beamline of UVSOR facility. The main chamber ratates at the angles from -20° to 110° on the Y-Y plane.

Rotation Induced Vibrational Mixing in Highly Excited Vibrational States of Formaldehyde II

Mutsumi AOYAGI

The effects of both anharmonic and Coriolis interactions on the intramolecular dynamics in Formaldehyde are investigated quantum mechanically. Variational calculations including all of the vibrational modes, and the rotational modes are performed using the ab initio SDCI potential energy surface. Both time-dependent and time-independent analyses are made on the calculated eigenstates (up to 12000 cm-1) to elucidate the role of Coriolis interaction in highly excited vibrational states. We also carried out the analyses of curvature distribution with respect to Hamiltonian parameters both on H_2CO and model Hamiltonian systems; the stadium billiard and the kicked rotator systems. We found that the anharmonic couplings assisted by b- and c-type Coriolis interactions and extensive K-mixings play a crucial role in the intramolecular dynamics at high energy region (E>7500 cm-1). We also found that curvature distribution obtained from the H_2CO results shows similar characteristics with one from the stadium billiard system. Based on these results, we developed effective Hamiltonian of H_2CO system with a reduced dimensionality approximation.

Development of the New Lasers for Molecular Science

Nobuhiko SARUKURA, Zhenlin LIU, Hideyuki OHTAKE and Shinji IZUMIDA

The history of science shows that the advance and breakthrough in laser science and technology have open up new directions in physics and chemistry. Here in this laboratory, we are trying to develop to new laser system and technology specially for molecular science. The targets of our laser research are the new tunable ultraviolet ultrashort-pulse laser based on new laser materials and nonlinear crystals, ultrashort-pulse far-infrared laser based on new nonlinear process, and compact all-solid state lasers.

Ultra-High-Vacuum Friction Test Apparatus

Michio WATANABE and Shuji ASAKA

Actuators that can operate in ultra-high-vacuum are useful for experimental apparatus in many fields of molecular science. Such actuators consist of many moving parts which require no seizing and no degassing. In order to develop such actuators, we have newly designed an apparatus to test frictions under UHV shown in Figure 1. The apparatus consists of a thrust-bearing assembly mounted in an UHV vacuum chamber, a drive system, and a friction force measuring system. Its construction is now under way. By using this apparatus, as the first step we will develop a coating that reduces seizing and degassing on metal surface .

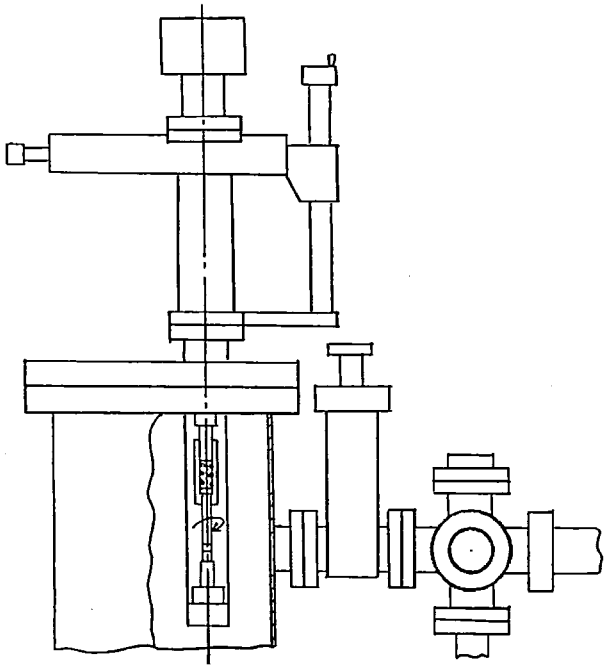


Figure 1. Outline design of the ultra-high vacuum friction test apparatus.

Investigation of Electronic Structures of New Materials by Using Synchrotron Radiation

Masao KAMADA and Shin-ichiro TANAKA

Insulator surface is one of the interesting targets for surface science, but usual techniques such as UPS, Auger, and LEED are not available because of the charging of the samples. Therefore, we have grown the thin crystalline insulator films on semiconductor surfaces and investigated their electronic structures by using synchrotron radiation. For examples, we found clear peaks due to the surface core-excitons in NaCl/Si(100). We have also investigated the coadsorbed states of alkali atoms and oxygen atoms on GaAs(100), which is useful to achieve photo-sensitive surfaces with negative electron affinity. Moreover, we have investigated the reflection, luminescence, and desorption of new materials such as CsTaF6, C60F48, and high-temperature superconductors in collabo-

ration with foreign scientists. New experimental systems and methods with synchrotron radiation were constructed. For examples, new beamline consisting of the helical undulator, monochromator covering the energy range of 5-250 eV with high resolving power, and a spin- and angle-resolved photoelectron spectrometer has been constructed. By using this beamline we will carry out the complete experiment of the electronic structures of non-magnetic materials and also investigate the dynamics of the spin memory in the excited-states in insulators/semiconductor surfaces.

Study for High Brilliant Radiation Using the UVSOR Electron Storage Ring

Hiroyuki HAMA and Shiro TAKANO *(SPring-8)*

[*Nucl. Instr. and Meth., A357,* 32 (1996)]

Since, on the storage ring free electron laser (FEL), the FEL photons are produced by the interaction with the *same* electron bunch turn-by-turn, the beam quality such as the energy spread becomes no longer same as an initial condition. It is generally so called "bunch-heating". However the longitudinal motion of the electrons in a bunch recovers their quality after taking the time longer than the synchrotron damping time without the FEL interaction. To undertand the bunch-heating process during laser macropulse evolution in the G-switching mode, we analyzed the gain variation with a simple empirical formura, and then we draw a simple picture of that an ability of the electron bunch for photon production is diminished as the photons are emitted, which is analogous to the population inversion in conventional lasers. The result essentially agrees with a theoretical consideration by Dattoli et al.

Taking account the bunch-cooling due to the synchrotron damping, we analytically obtained the growth rate of the energy spread for one beam bunch and deduced the relative saturation energy for the equilibrated state of the FEL power. For the current UVSOR FEL, the saturation energy of one electron with the energy of 500 MeV has been expected to be approximately 700 keV from Renieri's limit. On the other hand the experimentally derived value of 160 keV was found to be much smaller than the calculation. We do not have an answer for the discrepancy at the moment. It may be difficult to experimentally find out whether the saturation energy is reduced by other factors of the ring such as growth of beam emittance. However to gather experimental data at various lasing conditions including different beam energies will be worth.

Studies of Solid Surfaces by Photoelectron Spectroscopy

Toyohiko KINOSHITA

We are studying the electronic structures of solid surfaces, interfaces and adsorbates by using photoelectron spectroscopy, especially with synchrotron radiation from the UVSOR storage ring.In 1995, we have started the construction of the new equipment for photoelectron spectro-microscopy measurements (see, annual review of IMS, 1995, p.158). The apparatus has been connected to the 2 beamlines (BL5B and BL7A) and we have obtained the preliminary data for the ferromagnetic iron crystal in 1996. We have also measured the magnetic circular dichroism (MCD) for the ferromagnetic materials. It has been observed that MCD of the photoelectron yield spectra from Ni(110) surface is affected by the surface component of the local magnetic moment.

The details of these studies are appeared in this issue (Research activities at ultraviolet synchrotron orbital radiation facility; UVSOR).

(2) Study of Molecular Solid toward Molecular Electronics

Theory of Electronic Phases in Molecular Conductors and Insulators: Electron Correlation and Electron-Phonon Effects in Quasi-One-Dimensional Systems

Kenji YONEMITSU and Masatoshi IMADA *(Univ. of Tokyo)*

To understand various electronic phases in novel organic materials like the κ-phase family of BEDT-TTF charge transfer salts and the DCNQI metal complexes, electron correlation must be properly taken into account. Since the electronic motions are constrained in low dimensions, electron-electron interactions drastically change the physical properties from conventional ones in both metallic and insulating cases. In the related fields of high-temperature superconductivity and strongly correlated electron systems, separation of spin and charge degrees of freedom in low-energy excitations, a spin gap, and a possibility of non-Fermi liquid states are intensively investigated. In the materials mentioned above, electron-phonon interaction and/or a multi-band structure also play an important role in addition to electron-electron interactions. Here we focus our study on the interplay between an electronic Umklapp scattering process and electron-phonon interaction at and near commensurate electron fillings, using a renormalization-group method suitable to asymptotic, long-distance and low-energy behaviors of excitation spectra and correlation functions. Due to spin-charge coupling via electron-phonon interaction, the spin correlation varies with electron filling as well as the charge correlation. Various phases appear depending on the relation between cut-off energy scales of the Umklapp process and of the electron-phonon interaction. The former energy scale is controlled by the electron filling. In one-dimensional systems, we found a metallic phase with a spin gap and a dominant charge-density-wave correlation near half filling between a gapless density-wave phase and a superconductor phase with a spin gap. It is shown how the formation of a spin gap depends upon interference of phonon-assisted backward scatterings with the Umklapp process. The finding is consistent with the fact that conducting polymers have a spin gap but never show superconductivity. In the $(DCNQI)_2Ag$ complexes, the bands are quarter filled. Then a coupling between electrons and $4k_F$ phonons becomes important as well as the coupling with $2k_F$ phonons since the former localizes charge via Umklapp processes associated with $4k_F$ charge-density-wave fluctuations. Meanwhile, a spin gap opens when the coupling with $2k_F$ phonons is strong enough. Effects of three-dimensionality are found essential and explain the qualitative differences between $(DMe\text{-}DCNQI)_2Ag$ and (DI-

$DCNQI)_2Ag$, i.e., the spin-Peierls ground state in the former and the Neel state in the latter, the difference in their metal-insulator transition temperatures, etc.

Materials Science on Molecular Devices π-d Interaction in Molecular Metals

Kyuya YAKUSHI, Toshihiro HIEJIMA and Mkhitar SIMONYAN

We have undertaken a systematic study on the solid molecular systems in which transition metals are embedded in a π-conjugated system from the viewpoint of the future design of the superconducting material. The highly conductive phthalocyanine salts such as $CoPc(AsF_6)_{0.5}$ and $NiPc(AsF_6)_{0.5}$ are the prototype of the one-dimensional conductors in which the d- and π-orbitals form a double-chain (two-bands) system.

A comparative study has been done on the solid state properties of metallic $NiPc(AsF_6)_{0.5}$ and nonmetallic $CoPc(AsF_6)_{0.5}$. The crystal structure, polarized reflection spectrum, microwave resistivity, thermoelectric power, and magnetic susceptibility of these two compounds were compared. All these data indicate that the correlation effect is much larger in $CoPc(AsF_6)_{0.5}$ than in $NiPc(AsF_6)_{0.5}$. To elucidate the origin of these differences, further study is going on. (*see IV-A-1*)

The effect of the magnetic moment on CoPc is the most possible origin of this strong correlation. The anisotropy of the magnetic susceptibility was examined using aligned single crystals of $CoPc(AsF_6)_{0.5}$. (*see IV-A-3*) The anisotropy of the susceptibility is much larger than the anisotropy of the g-factor of CoPc, which means that the exchange interaction has an anisotropy as well.

Subsequently to the finding of the pressure-induced mtal-ligand charge transfer, we examined the pressure-dependent lattice constants of $NiPc(AsF_6)_{0.5}$ and $CoPc(AsF_6)_{0.5}$.(*see IV-A-2*) Compared with organic conductors such as TTF-TCNQ, the compressibility of $CoPc(AsF_6)_{0.5}$ along the stacking axis is rather small, but that of $NiPc(AsF_6)_{0.5}$ is unusually large below 0.5 GPa. The Ni-Ni distance of $NiPc(AsF_6)_{0.5}$ is shortened from 3.24 Å at ambient pressure to 2.91 Å at 4.1 GPa.

The analysis of the plasmon absorption of $NiPc(AsF_6)_{0.5}$ suggests that the pressure-induced metal-ligand charge transfer causes a nonmtallic phase in $NiPc(AsF_6)_{0.5}$. To confirm this phase change more directly, the electrical resistivity measurement was done under high pressure. (*see IV-A-2*) A resistivity enhancement was observed in three samples at the same pressure where the metal-ligand charge transfer occurred. The temperature dependence of the resistivity below and above this critical pressure supports the metal-nonmetal phase change.

Search for Negative-*U* Materials in Molecular Solid

Kyuya YAKUSHI, Mikio URUICHI, Yoshiro YAMASHITA and Jingui QIN

The negative-*U* material comprises the molecule which has a negative on-site Coulomb energy or, in other words, an attractive force between two electrons within the molecule. A strong electron-phonon interaction is the characteristics of organic conductors, so in some molecules, a strong interaction may overcome the repulsive force within the molecule and stabilize a on-site bipolaron state. The similar state has been found in the insulating compound, Cs_2SbCl_6, superconducting compound, $BaPb_{1-x}Bi_xO_3$, and conducting polymer, polypyrrole, but never been in a organic charge-transfer compound. To look for such molecules, multi-step-oxidation properties of electron donors are one of the key parameters. Generally, the difference (ΔE) between the first and second oxidation potentials is thought to be a measure of the on-site Coulomb energy in the organic conductor. BDNT shows an unusual property that the first and second oxidation potentials are not resolved. From the analysis of the width of the oxidation wave, ΔE is estimated to be 0.024 eV.

Subsequently to the characterization of *m*-BDNT-PF_6 in the last two years, we examined the charge-transfer salts of BDNT with $M(mnt)_2^-$ (M=Co, Ni, Cu, Au, Pd, and Pt) as counter anions. (*see IV-B-3*) We prepared new conductive charge-transfer salts of $[Au(mnt)_2]_2$-BDNT-I, $[Au(mnt)_2]_2$-BDNT-II, $Au(mnt)_2$-BDNT, $Ni(mnt)_2$-BDNT, $Pd(mnt)_2$-BDNT, $Pt(mnt)_2$-BDNT, but we have not succeeded yet to grow single crystals except low-conductive $[Au(mnt)_2]_2$-BDNT-I. The most interesting finding is the ferromagnetic interaction in conductive $Ni(mnt)_2$-BDNT. This compound is not well characterized, since the single crystal is not obtained. The relation between the conductivity and ferromagnetic property is an interesting subject.

Toward Comprehensive Understanding of Various Electronic Phases in Molecular Conductors; Superconductivity in $(BEDT\text{-}TTF)_2X$ Family

Kazushi KANODA, Yasuhiro NAKAZAWA, Kazuya MIYAGAWA, Hiromi TANIGUCHI, Ko-ichi HIRAKI and Atsushi KAWAMOTO *(Ochanomizu Univ.)*

Organic charge transfer salts exhibit various kinds of electronic phases. Even if we focus our attention to the family of $(BEDT\text{-}TTF)_2X$ layered systems with hole concentration of one half per molecule, metallic, superconducting and insulating states appear, depending on the molecular arrangement within the conducting layer or the kind of anion. In this special research project, we aim at clarifying the origin of the variety of the electronic phases. Last year we found that the effect of the electron correlation is responsible for the metal-to-insulator transition in this family. In this year's program, we have pursued interrelation between the electron correlation and the superconductivity in α-$(BEDT\text{-}TTF)_2NH_4Hg(SCN)_4$, β_L-$(BEDT\text{-}TTF)_2I_3$ and κ-$(BEDT\text{-}TTF)_2X$ [X=$Cu(NCS)_2$, $Cu[N(CN)_2]Br$] in order to get insight into the origin and nature of the superconductivity. In BCS theory, the transition temperature is expected to correlate with the electronic density of states. Surprisingly the electronic specific heat coefficients of the above materials are nearly the same, while the transition temperatures are varied by one order of magnitude. One of the important findings is that the transition temperature is correlated with the low-temperature values of $(T_1T)^{-1}$, which is a measure of the magnitude of the correlation effect. This implies that the Coulomb repulsion works in favor of occurrence of superconductivity.

Development and General Phase Diagram of Two-Dimensional Organic Superconductors

Hayao KOBAYASHI, Hiroki AKUTSU, Emiko ARAI, Hisashi TANAKA*(The University of Tokyo)* **and Akiko KOBAYASHI** *(The University of Tokyo)*

The improvement of the molecular design of two-dimensional (2D) π metals in 1980s has clarified the way to remove the metal instability from molecular conductors and hence various types of stable π metals and superconductors with 2D electronic structures have been discovered. However there is no reliable theory of the superconducting mechanism in molecular conducting systems, which prevents to establish the guiding principle to develop new organic superconductors. If the mechanism of the formation of Cooper pair can be described in terms of the structures and arrangements of constituent molecules and their electronic structures, the designability of molecular systems will promise the large progress in the development of new molecular superconductors. The most intensively studied organic superconductor is κ-type BEDT-TTF compound whose phase diagram is characterized by the high-temperature non-metallic state and antiferromagnetic ground state bordering on the superconducting phase. The superconducting phase which neighbors antiferromagnetic insulating phase is also observed in the first organic superconductor, Bechgaard salt with 1D electronic structure. But Bechgaard salt does not have high-temperature non-metallic region. Contrary, we have recently noticed that the resistivity behavior of λ-type BETS superconductor (BETS=bis(ethylenedithio) tetraselenafulvalene) having 2D electronic structure closely resembles that of κ-type BEDT-TTF superconductor. This indicates the existence of the general phase diagram in the 2D π metal systems, which will be verified by the precise examination of a series of new organic superconductors, λ-$BETS_2GaCl_{4-x}Y_x$ (Y=Br, F; 0<x<4). Systematic studies on the preparation, resistivities, magnetic susceptibilities and the crystal structure analyses of λ-$BETS_2GaCl_{4-x}Y_x$, whose superconducting behavior can be controlled continuously by changing the x-value, are now in progress.

Development of Magnetic Molecular Metals

Hayao KOBAYASHI, Hideki FUJIWARA, Hiroki AKUTU Akane SATO *(Graduate Univ. for Advanced Studies)* **and Akiko KOBAYASHI** *(The University of Tokyo)*

The development of new materials is most important for the progress of solid state chemistry of molecular crystals. Since the highest superconducting transition temperature (T_c) still remains less than only 15 K, a new molecular superconductor with enhanced T_c will be highly desirable. However owing to the lack of the knowledge on the superconducting mechanism in molecular crystals, the control of T_c is beyond the scope of the present molecular design. On the other hand, the organic ferromagnetic metals and single component molecular metals or superconductors seem to be possible targets for the future studies. With the aim of the developing magnetic molecular metals, we are now trying to prepare various molecular metals incorporated magnetic moments. BETS metals with magnetic anion $FeCl_4^-$ is one of them. ESR and susceptibility measurements revealed the antiferromagnetic Fe^{3+}···Fe^{3+} interaction in the metallic states of κ- and λ-$BETS_2FeCl_4$. The cooperative metal-insulator (MI) and antiferromagnetic transitions at 8.5 K indicates the important role of π-d interaction in this system. The mixed anion system λ-$BETS_2(Ga_{1-x}Fe_x)Cl_4$ takes (antifferromagnetic) insulating ground state at 0.5<x<1 and superconducting ground state (T_c>4 K) at 0<x<0.5. T_{MI} decreases with increasing x (0.5<x<1). At the same time Weiss temperature indicating the magnitude of antiferromagnetic Fe···Fe interaction becomes small with increasing x. It is quite surprising that the system with 50 % of Fe^{3+} ions undergoes superconducting transition around 4.5 K, above which Fe^{3+} ions are interacting antiferromagnetically with each other. This system suggests a new possibility of the development of magnetic molecular superconductors.

NMR Studies on the Dynamical Properties of Condensed Matter Systems

Seiichi MIYAJIMA, Hironori OGATA, Tomoyuki MOCHIDA, Osamu OISHI, Toshihito NAKAI and Jong-Jean KIM

We studied the dynamics-related properties of condensed matter systems by means of nuclear magnetic resonance (NMR) spectroscopy. The following five subprojects are reported.

(1) Development of pulsed field gradient (PFG) NMR spectroscopy to the strongly dipole-coupled spin systems. To this goal we designed and constructed a new PFG-NMR spectrometer. Combining the line-narrowing technique with sharp and intense pulsing of two-dimensional field gradient, we obtained anisotropic diffusion coefficient tensors in smectic A liquid crystals. This method is being applied to study the molecular dynamics related to dielectric order/disorder phenomena in liquid crystals, and the ionic transport in solids.

(2) One- and two-dimensional high resolution NMR of antiferroelectric liquid crystals. How the antiferroelectricity and dynamic disorder can coexist in chiral smectic liquid crystals is an interesting problem. To reveal the key to interlayer correlation of electric dipoles, we developed extensive high resolution NMR studies for MHPOBC and related materials.

(3) Hydrogen dynamics in dielectric solids.
Hydrogen dynamics were studied in solids where forroelectric *vs.* antiferroelectric competing interactions exist.

(4) Electronic states of alkali-hydrogen-carbon ternary systems.
Hydrogen or alkaline metal elements can, when incorporated into carbon hosts, exhibit various electronic states depending on charge transfer, electron-electron, and electron-phonon interactions. ^{13}C, ^{23}Na, and ^{1}H NMR studies were conducted for ternary materials of Na-H-graphite intercalation compounds and a new superconductor, Na-H-C_{60}.

(5) Search for novel electronic systems based on organic charge transfer complexes. Novel organic charge transfer complexes were synthesized based on BEDT-TTF and various TCNQ derivatives.

Pressure Effect on Molecule-Based Magnetism

Yuko HOSOKOSHI and Katsuya INOUE

The magnetic measurement under high pressure might be useful and important for the study of molecule-based magnetism. We have made a high pressure clamp cell made of Cu-Ti alloy which can be equipped to a Quantum Design MPMS SQUID magnetometer. A cross-sectional view of the cell is given in Figure 1. The cell enables an internal pressure to be maintained up to 7 kbar. The sensitivity is so high that we can measure paramagnetism and antiferromagnetism in addition to ferromagnetism.

Observation of the large pressure effect on some organic radicals is described in V-F.

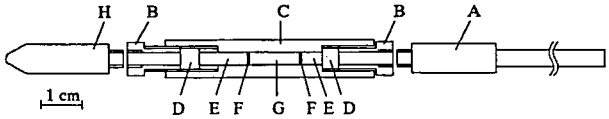


Figure 1. Cross-sectional view of the pressure clamp cell. A: Dummy cell (connected to a sample lod), B: Locking nut, C: Cylinder, D:Backing plate (ZrO_2), E: Piston (ZrO_2), F: Cu seal, G: Teflon backet, H: Dummy cell.

Construction of the Ultraviolet Inverse Photoemission Spectrometer

Naoyuki UEDA, Hideo HOSONO and Hiroshi KAWAZOE *(Tokyo Inst. Tech.)*

Our group has created a novel class of inorganic semiconductor, i.e., transparent and conducting crystalline and amorphous oxides. These materials have a band gap of > 3 eV and electrically insulating in as-prepared state. However, these materials can be converted into almost metallic conductors without almost loss of transparency to visible radiation. Example are $MgIn_2O_4$, $ZnGa_2O_4$ and $2CdOGeO_2$. Experimental evaluation of conduction band is a key step to obtain a fundamental understanding of these materials. This is the motivation we decided to start this special project.

The spectrometer is composed of a low speed electron gun, an ellipsoidal mirror and a photon detector. The detector is a band pass type which consists of an electron multiplier tube with a Cu-BeO first dynode (Hamamatsu Photonics R595) and a CaF_2 window deposited with the KCl thin film. The thickness of the thin film and the substrate was considered from a viewpoint of sensitivity and energy resolution. Bandpass characteristics of the detector with the various windows were measured at the BL7B beamline of the UVSOR facility. As a result, we adopted the window of 10.5 nm KCl film on 1.0 mm CaF_2 substrate. The performance is a FWHM 0.58 eV with a maximum response at 9.96 eV. The sensitivity is twice as much as that of the case of using a SrF_2 window.

Photoelectron Spectroscopic Study of Organic / Metal Interfaces

Hisao ISHII, Daisuke YOSHIMURA*, Takayuki MIYAMAE, Shinji HASEGAWA and Kazuhiko SEKI*
*(*Nagoya Univ.)*

Recently organic devices such as transistors, photovoltaic cells, and electroluminescent (EL) devices fabricated from organic semiconductors have been extensively studied. The elucidation of the electronic structures of organic-semiconductor/metal interfaces is indispensable for understanding and refining the performance of such devices. So far it has mostly been estimated by lining up separately observed electronic energy levels of the two components, assuming a common vacuum level at the interface. However, the validity of the assumption has not yet been examined for organic-semiconductor/metal interfaces. In order to clarify this point, we have investigated the electronic structures of the interfaces between metals (Au, Ag, Al, Mg) and various organic materials such as porphyrins, phthalocyanines, n-alkanes, and, donor-type and acceptor-type materials used in organic EL devices, using ultraviolet photoemission spectroscopy (UPS) at BL8B2 of UVSOR. In all the measured systems, abrupt shifts of vacuum level were observed at the interfaces, clearly indicating the invalidity of the concept of a common vacuum level.

For a deeper insight for understanding the electronic structure of organic / metal interfaces, it is important to clarify the origin of the shift of vacuum level. UV and X-ray photoelectron spectroscopic study of well-defined interface is highly desired for investigating this point. In order to perform such studies, we have reconstructed our UPS spectrometer. The cleaning system for metal single crystal including LEED/AES optics and an Ar+ ion gun, evaporation gun with liquid nitrogen shroud, retarding field analyzer, and an X-ray source were added to the old system as shown in figure 1. We could prepare clean Cu(001) surface and well-ordered perylene film on it which exhibited c(8x4) LEED pattern. Now experiments for monolayer perylene / Cu(001) interface using UPS and X-ray photoelectron spectroscopy is underway.

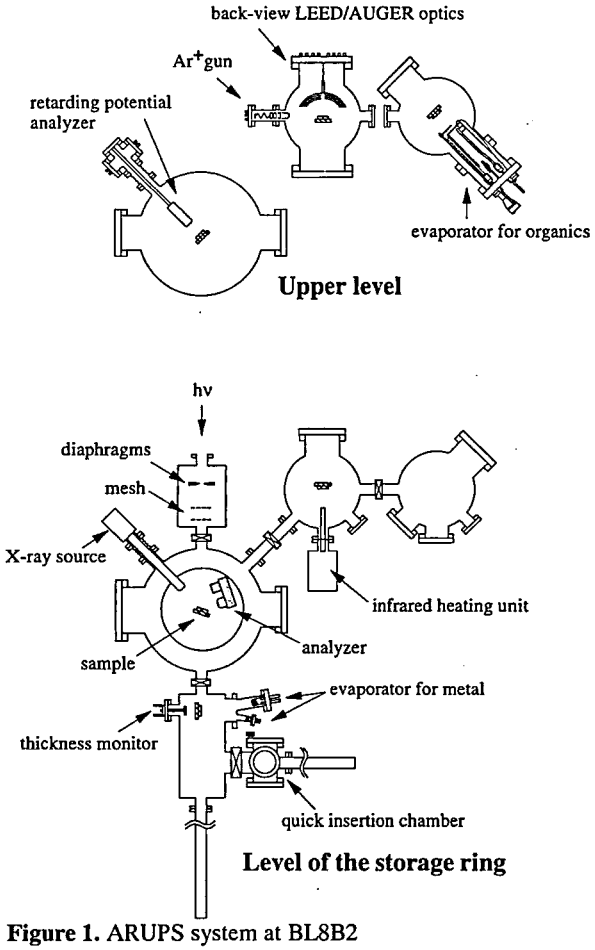


Figure 1. ARUPS system at BL8B2

Organic Conductors Based on Novel Heterocyclic Compounds

Yoshiro YAMASHITA, Shoji TANAKA and Masaaki TOMURA

We have succeeded in preparing new electron donors giving organic conductors. For example, π-extended tetrathiafulvalene analogues containing a benzobisthiophene moiety were prepared by oxidative intramolecular cyclization. They are strong electron donors which show one-stage two-electron oxidation. The dications of TTF analogues containing quinoid structures were prepared in

high yields using an oxidation reaction with $NOBF_4$ involving a concomitant retro-Diels-Alder reaction. Butterfly-shaped bis(1,3-dithiole) donors containing a fused naphthalene and a thiadiazole ring gave metallic cation radical salts incorporating various solvent molecules. Their properties were strikingly dependent on the incorporated solvent molecules although there was no distinctive difference in crystal structures. Furthermore, a series of novel monomers and polymers containing aromatic-donor and *o*-quinoid-acceptor units was prepared and the relationship between their spectral and electrochemical properties was investigated. The bandgaps were found to be widely tunable by the polymer structures. One polymer exhibited a very small bandgap. Details of those works are described in VIII-B section.

(3) Material Control in Multi-Reaction Centers

Catalytic Intermediates of Polyethylene Glycoled Horseradish Peroxidase (PEG-HRP) in Benzene

Shin-ichi OZAKI and Yoshihito WATANABE

Horseradish peroxidase (HRP) was solubilized in benzene homogeneously by the covalent modification of lysine residues on the protein's surface with poly(ethylene glycol) (PEG). The addition of a stoichiometric amount of hydrogen peroxide to PEG-HRP in benzene gave the compound I chromophore (Figure 1). In the presence of a large excess of guaiacol, compound I was first reduced to compound II, then to the ferric enzyme. Thus, catalytic intermediates in benzene were the ferryl species as established in aqueous buffer. The slower compound I reduction with guaiacol in benzene than in buffer suggested that the accessibility of the active site for the substrates decreases in the organic solvent.

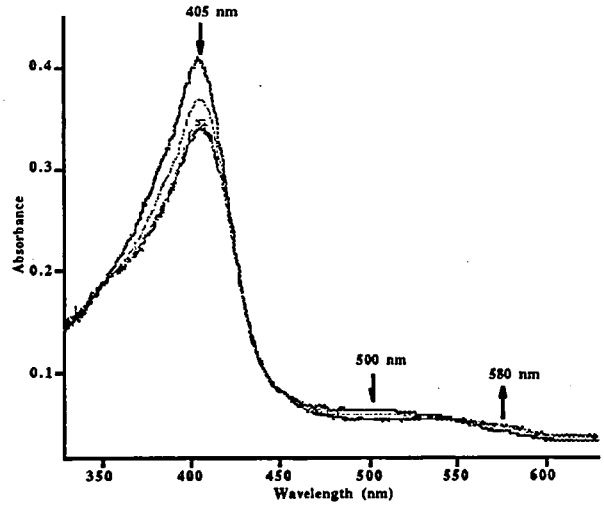


Figure 1. Time dependent spectral changes of HRP-PEG due to the formation of compound I

Coordination Chemistry on Surface Towards Solution-phase Molecular Epitaxy

Masa-aki HAGA, Hideaki MONJUSHIRO, Kazumasa HARADA, M. Delower HOSSAIN, Itsuko MURATA and Noriaki KATO

Self-assembled organization of metal complexes on surface is an attractive frontier for the coordination chemistry from the viewpoint of molecular electronic devices and biomineralization. We have studied the molecular switching of metal complexes based on ruthenium-2,2'-bipyridine unit by the external stimuli such as light or proton in solution. We have observed a large pKa shift on N-H group in Ru-benzimidazole complexes when the Ru(II) complexes were oxidized to Ru(III) state. Furthermore, protonation can induce the electron transfer in Ru-Os mixed-valence tri- and tetranuclear complexes. Thus, the interlocking between proton transfer and electron transfer inspired us to make a proton-pump system based on metal complexes. Multilayered structure is prerequisite for making such proton-pump system to generate the potential gradient and proton gradient at the same time through layers. We have started to prepare self-assembled solid state multilayer films based on the metal complexes. The stepwise layer-by-layer formation on surface can be achieved by anchoring the ligand on the surface at first and then coordination of the metal ion, and again incorporation of the bifunctional ligand to the first metal ion and so on. Since these processes in solution are almost identical to the gas-phase molecular beam epitaxy, this process can be regarded as solution-phase molecular epitaxy, which will be more versatile than the gas-phase one. For making the self-assembled multilayer films on gold, we used the terpyridine phosphonate as a ligand. Incorporation of Ru-terpyridine complex with zirconium phosphonate layer is under way.

The multilayer films can also be produced by the Langmuir-Blodgett(LB) techniques. Bis(benzimidazolyl)-pyridine or -bipyridine with long alkyl chain(L) was used as a ligand for LB method. We found that the complex, $Ru(L)Cl_2$, formed a stable monolayer film on the Langmuir trough air-water interface and transferred to solid surface. Further investigation to synthesize surfactant dinuclear Ru complexes which can respond to the external stimuli such as protonation is now in progress.

Assembled Metal Centers in Enzymes

Takeshi SAKURAI, Sadamu TAKEDA, Nobuhiko SAKURAI, Hong-wei HUANG, Isao HARA and Hiroki MATSUMOTO

Metal centers as the active site in metalloproteins and metalloenzymes do not exist as isolated centers but as functionally related centers or as metal clusters to exert integrated functions such as electron-transfer, activation of small molecules like dioxygen, NOx, SOx, etc. Laccase, ascorbate oxidase, ceruloplasmin, and bilirubin oxidase, which belong to a super family of multicopper oxidase are such the enzymes. The active site of these enzymes is composed of the three types of coppers, the type 1 Cu(blue Cu) the type 2 Cu(non-blue Cu), and a pair of the type 3 Cu's (EPR non-detectable Cu at the resting state). The latter two types of copper form the unique trinucelar site, at which electrons transferred from the type 1 Cu site by the intramolecular long range process are pooled and a

dioxygen is reduced to two water molecules. Such the four-electron reduction of dioxygen is performed only by multicopper oxidases and the Cu-Fe center in terminal oxidases in the respiration process. Our goal of the study is to reveal the unique steric structure and magnetic property of the Cu trinuclear center and the reaction mechanism by using absorption, CD, MCD, EPR, SQUID, electrochemistry, etc. Another target of our study is NO reductase from denitrifying bacteria. Although special attention has been paid for NO for these years, many studies have been focused on to forming and detecting this inorganic hormone. We have almost finished to establish the purification method of this membrane protein and started the biophysical characterization of it. NO reductase is apparently a complex of *b* type and *c* type cytochromes. The aim is not only to reveal the structure of each active site but also to reveal the integrated function of them.

Construction of Metal Complexes for Artificial Gene Control

Mitsuhiko SHIONOYA, Kentaro TANAKA, Akio OJIDA, Michito SHIOTSUKA and Motoyuki TASAKA

Small molecules that bind to specific sites of DNA or RNA *in aqueous media* are of much interest for synthetic gene-targeted drugs. Compounds that give rise to the structural and functional perturbation of regulatory domain of specific genes would be applicable to the treatment of gene disorders. Transition metal complexes are quite advantageous for this purpose and are currently attracting great interest. We previously demonstrated that Zn^{II} macrocyclic polyamine complexes bind selectively and reversibly to thymine (or uracil) base in aqueous solution at physiological pH. These Zn^{II} complexes also lower the melting temperatures of double-stranded poly(A)·poly(U) and poly(dA)·poly(dT), indicating that the double helical structures of the polynucleotides are destabilized by the strong interaction between these complexes and thymine (or uracil) bases. Based on these findings, we designed and synthesized a new type of Zn^{II} complex that would break A-T base pairs by interacting with both thymine and adenine bases. Further investigation on new dynamic functions of this complex such as unwinding or melting of TATA box (AT-rich region) in the transcriptional regulatory domain of DNA is now in progress. In this connection, we also have been synthesizing metallointercalators bearing two oligopeptide chains that are expected to bind to a specific palindromic sequence of DNA with a structural change of the peptide moieties from coil to α-helix.

Stereochemistry and Electrochemistry of Cobalt(II) and Cobalt(III) Complexes Containing Optically Active Tetradentate Schiff Base Ligands

Masakazu HIROTSU,* Masaaki KOJIMA,* Kiyohiko NAKAJIMA, Setsuo KASHINO* and Yuzo YOSHIKAWA** *(*Okayama University, **Aichi University of Education)*

[*Bull. Chem. Soc. Jpn.*, **69**, 2549 (1996)]

Cobalt(II) complexes containing tetradentate Schiff base ligands with phenyl substituents, [Co(Schiff base)], have been prepared and the electrochemical properties are reported. The crystal structure of [Co{7-Phsal-(*rac*)-stien}], where the Schiff base ligand was derived from 2-hydroxybenzophenone and (*rac*)-1,2-diphenylethylenediamine, has been determined by X-ray structure analysis. Crystal data: monoclinic, $P2_1/n$, a = 13.956(2), b = 14.703(2), c = 17.808(3) Å, β = 112.21(1)°, V = 3383.0(9) Å^3, Z = 4, and R = 0.052 and R_w = 0.039 for 3976 unique reflections with $I > 3\sigma(I)$. The two phenyl groups in the N-N chelate moiety are in the axial positions and block the apical sites. In this complex, the redox potential of the Co(III)/Co(II) couple is 0.20 V vs. Ag/Ag^+ in acetonitrile and becomes more positive by *ca.* 300 mV than that for [Co(salen)]. This large positive shift is attributed to the steric effect of the two axially disposed phenyl groups. The redox potentials of the analogous cobalt(II) Schiff base complexes, where (*meso*)-1,2-diphenylethylenediamine and (*R*)-1-phenylethylenediamine were used as a diamine, are also explained in terms of the steric effect of the phenyl substituents. The corresponding cobalt(III) Schiff base complexes with two additional axial ligands, [Co(Schiff base)$(L)_2$]ClO_4 (L = imidazole (im), 1-methylimidazole (Meim)), have been prepared. The steric interaction between the phenyl groups on the N-N chelate moiety and the axial ligands is discussed based on the X-ray structure, the circular dichroism (CD) spectra, and the ^1H NMR spectra. The crystal structure determination of [Co{sal-(*meso*)-stien}$(Meim)_2$]ClO_4 has been performed. Crystal data: monoclinic, $P2_1/c$, a = 10.789(2), b = 20.512(3), c = 15.330(2) Å, β = 99.88(1)°, V = 3342.3(8) Å^3, Z = 4, and R = 0.051 and R_w = 0.049 for 3414 unique reflections with $I > 3\sigma(I)$. In order to study the steric effect of the phenyl substituents, the [Co(Schiff base)$(L)_2$]ClO_4 complexes have been prepared using (*R*)-1,2-propanediamine as a diamine. The different behavior shows that the interaction between the phenyl groups is sensitive to the orientation.

1,3-Migration of a Substituent on a Phosphorus in a Transition Metal Coordination Sphere

Hiroshi NAKAZAWA *(Hiroshima Univ. and IMS)*, **Yoshitaka YAMAGUCHI, Mitsuru KISHISHITA and Katsuhiko MIYOSHI** *(Hiroshima Univ.)*

A cationic phosphenium complex of Mo, *mer*-$[(bpy)(CO)_3Mo\{PN(Me)CH_2CH_2O\}]^+$ was prepared from *fac*-$[(bpy)(CO)_3Mo\{PN(Me)CH_2CH_2O(NEt_2)\}]$ and $HOSO_2CF_3$ by NEt_2 abstraction as an anion. A CH_2Cl_2 solution of the phosphenium complex thus prepared was treated with $PN(Me)CH_2CH_2NMe(Y)$ (Y = OMe, OEt, SEt and $N(CH_2)_3CH_2$) to give *cis*- and *trans*-$[(bpy)(CO)_2\{PN(Me)CH_2CH_2O(Y)\}Mo\{PN(Me)CH_2CH_2NMe\}]^+$. The product shows that 1,3-migration of Y from P to P is involved during the reaction sequence. The following reaction pathway is proposed. The starting phosphenium complex reacts with $PN(Me)CH_2CH_2NMe(Y)$ to give *cis*-$[(bpy)(CO)_2\{PN(Me)CH_2CH_2NMe(Y)\}$-$Mo\{PN(Me)CH_2CH_2O\}]^+$. Since the complex has phosphenium and phosphite ligands in mutually *cis* position, the Y group may donate its lone pair electrons to the vacant p orbital of the phosphenium phosphorus, then the cleavage of the original P-Y bond with the concomitant formation of the new P-Y bond results in the 1,3-migration of Y. The complex thus produced isomerizes to more stable geometrical isomers to give the final products.

Activation of Carbon Dioxide on Metal Complexes Directed Toward Carbon-Carbon Bond Formation

Koji TANAKA, Kiyoshi TSUGE, Masato KURIHARA and Tetsunori MIZUKAWA

Direct electrochemical reduction of CO_2 is not thermodynamically favorable process because of the large negative redox potential of $E°(CO_2/CO_2^-)$ at -2.21 V (*vs.* SCE). On the other hand, carbon dioxide bonded to metals is subject to a C-O bond cleavage reaction to form metal-CO complex since the electron density of the CO_2 moiety is highly enhanced by π-back donation from occupied d orbital to empty π^* orbital of CO_2. Along this line, a variety of metal complexes have been used as catalysts precursors for the reduction of CO_2, though the active species have hardly been confirmed in those reactions. Highly reduced products such as HCHO, CH_2OH, HOOCCHO and $HOOCCH_2OH$ have been obtained in electrochemical CO_2 reduction catalyzed by Ru-polypyridyl complexes at low temperature, and the reaction mechanism is established by successive reduction of CO_2 to CH_2OH on Ru. To construct more efficient catalytic system that can reduce CO_2 at ambient temperature, site opening and closing would be preferable for stabilization of the reaction centers, inhibition of side reactions, and promotion of eliminating the products from a reaction center. An equilibrium of chelation and dechelation of ligands with a little configuration barrier may be utilized as the construction of homogeneous catalysts. The purpose of this project is to develop new catalytic systems directed toward the activation of not only CO_2 but also small molecules.

OKAZAKI CONFERENCES

The Fifty-Third Okazaki Conference

New Trends in Spin Chemistry *(October 19-21, 1995)*

Organizers: H. HAYASHI *(Inst. Phys. Chem. Research)*, **N. HIROTA** *(Kyoto Univ.)*, **H. SATO** *(Mie Iniv. & IMS)*, **and I. HANAZAKI** *(IMS)*
Invited Overseas Speakers: K. A. MCLAUCHLAN *(Oxford Univ., UK)*, **G. J. FERRAUDI** *(Univ. of Notre Dame, USA)*, **J. B. PEDERSEN** *(Odense Univ., Denmark)*, **C. K. OTTINGER** *(MPI Stromungsforsvhung, Gottingen, Germany)*, **K. P. DINSE** *(TH-Darmstat, Germany)*, **H. LEVANON** *(Hebrew Univ., Jerusalem, Israel)*

Magnetic field effects (MFEs) on dynamic behavior of excited molecules such as energy transfers and chemical reactions have been studied extensively . The progress of such investigations has brought about the advent of a new research branch which may be called "spin chemistry".

Recent developments of spin chemistry have achieved innovations in various aspects: (1) New types of MFEs on chemical reactions have been found in solution under higher fields than 10 T; (2) MFEs and magnetic isotope effects (MIEs) on reactions of heavy atom-centered radicals have been found for many radicals such as Si-, P-, S-, and Ge-radicals, although the spin-orbit interaction of such heavy atoms have hitherto been believed to reduce greatly their MFEs and MIEs; (3) In magnetodynamics of excited molecules in the gas phase, measurements have been extended to higher fields up to 10 T, super high-resolution (sub-Doppler) spectroscopies have been applied, and detailed studies of excess energy dependence have been carried out; (4) Combined effects of different phenomena have been tried to be investigated : magnetic fields + microwave and ESR + NMR, for example; (5)Studies of MFEs have also been extended to new areas such as chemical equilibrium of ferromagnetic systems, balance of gravitational and magnetic fields, and various biological reactions and phenomena; (6) The above-mentioned new trends in MFEs and MIEs have stimulated theoretical studies.

The conference consisted of 26 oral and 19 poster representations, and was attended by 66 scientists including 12 overseas ones. It was organized to discuss the above-mentioned new trends in spin chemistry from various points of view, i.e., MFEs vs. magnetic resonance, chemical reactions vs. biological ones, behavior in the gas phase vs. that in the condensed phases, theories vs. experiments, etc. From such discussions, future prospects in spin chemistry were obtained.



The Fifty-Fourth Okazaki Conference

Dynamic Studies on Hydrogen Atom Transfer Reactions
(*January 23-25*)

Organizers: H. SHIZUKA (*Gunma Univ.*), **K. FUKE** (*Kobe Univ.*) **and S. IWATA** (*IMS*)
Invited Overseas Speakers: J. C. (Tito) SCAIANO (*Univ. of Ottawa, Canada*) **and S. J. FORMOSINHO** (*Univ. de Coimbra, Portugal*), **J. A. SYAGE** (*Aerospace Co., Los Angeles, U. S. A.*), **T. S. ZWIER** (*Purdue Univ., U. S. A.*) **and M. T. H. LIU** (*Univ. of Prince Edward Island, Canada*)

Hydrogen atom transfer, proton transfer and electron transfer reactions are elementary processes both in chemistry and biochemistry. Relatively little attention has been paid to the studies of the hydrogen atom transfer reaction compared to those of proton transfer and electron transfer ones, except for hydrogen abstraction of triplet aromatic ketones.

Hydrogen atom has the wave-particle duality of matter, since it is an extremely light atom compared with others. Therefore, the tunnelling effect on the hydrogen atom transfer is expected. The reaction mechanisms for inter- and intra-hydrogen atom (or proton) transfer reactions should be revealed from the quantum mechanical viewpoints.

The main subjects of the conference are (1) the new types of hydrogen atom transfer reactions including environmental effects, (2) dynamic analyses of hydrogen atom (or proton) transfer reactions both in the ground and excited states, and (3) the tunnelling effects on hydrogen atom (or proton) transfer reactions.

The conference consisted of nineteen oral presentation and also nineteen posters. The above topics were discussed well experimentally and theoretically by about fifty audience (mainly physical chemists). The mechanistic studies on hydrogen atom (or proton) transfer reactions involving the tunnelling effects will be expanded in future.



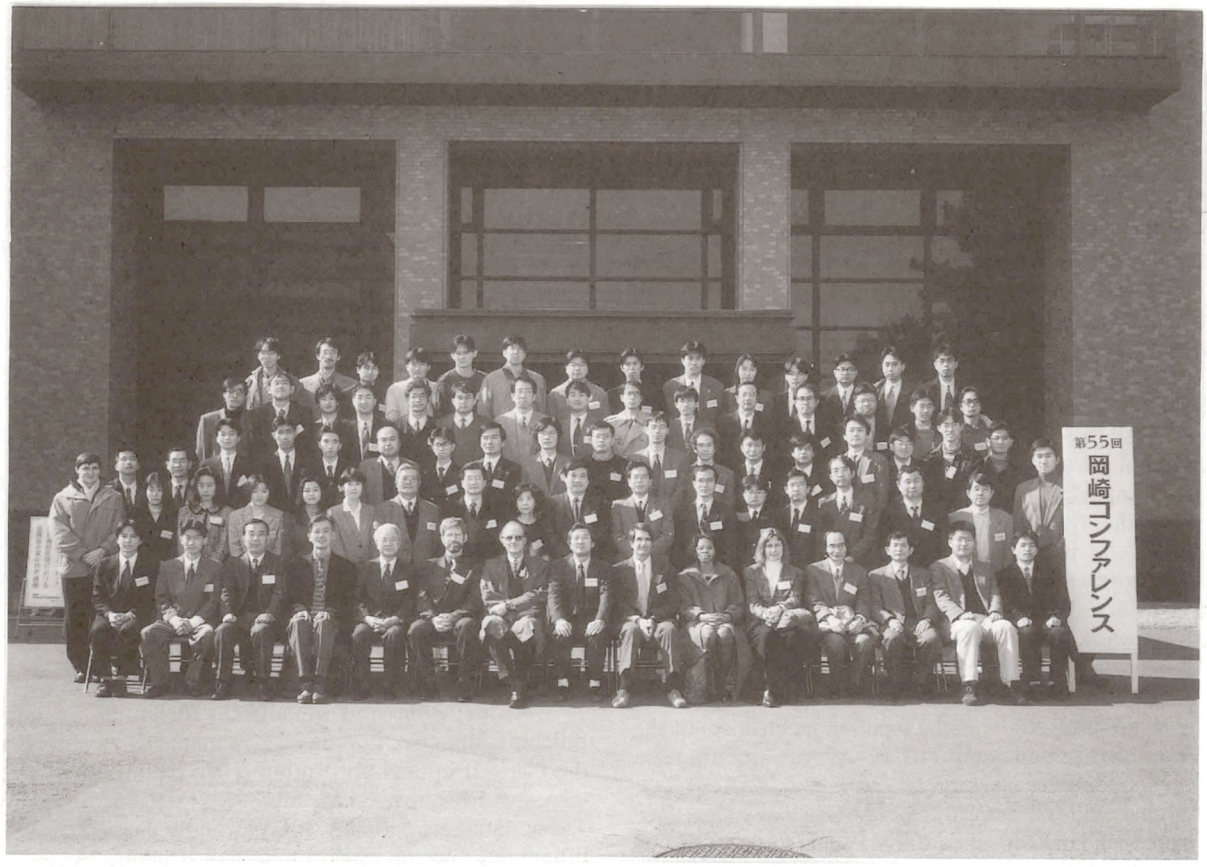
The Fifty-Fifth Okazaki Conference

Molecular Mechanisms on the Metalloproteins in Biological Functions*(February 5 - 7, 1996)*

Organizers: M. HIDAI *(Tokyo Univ.)* **and Y. WATANABE** *(IMS)*
Invited Overseas Speakers: L. QUE, Jr. *(Univ. of Minnesota, U.S.A.)*, **D. SELLMANN** *(Univ. Erlangen-Nürnberg, Germany)*, **P. F. KNOWLES** *(Univ. of Leeds, U.K.)*, **R. STEVENS-TRUSS** *(Univ. of Michigan, U.S.A.)*, **A. M. PYLE** *(Columbia Univ. U.S.A.)*, **T. L. POULOS** *(Univ. California at Irvin, U.S.A.)*

Metal ions play very important roles in biological systems. For instance, iron and copper ions serve as molecular oxygen carriers. In addition, these metals are crucial for reductive activation of molecular oxygen to form superoxide, peroxide, oxo-metals, and so on. Thus, the 55th Okazaki Conference concentrated on the molecular mechanisms of "the metalloproteins in biological functions." In addition, unique feature of the 55th Conference was that the most of participants were under 45 years old scientists who are frontiers in the above fields.

The conference consists of four major topics: (1) electron transfer and energy transduction, (2) metalloenzymes catalyzing oxidations, (3) roles of metal ions in synthesis and functionalization of nucleic acids, and (4) signal transduction in biological systems. Among those topics, a variety roles of heme enzymes including nitric oxide synthase and cytochrome c oxidase, roles of metal ions in ribozymes catalyzed hydrolysis, site specific binding of metal complexes to DNA and RNA, and structures and molecular mechanisms of iron and copper containing nonheme proteins were extensively discussed.



JOINT STUDIES PROGRAMS

As one of the important functions of an inter-university research institution, IMS undertakes joint studies programs for which funds are available to cover reseach expenses as well as travel and living expenses of individuals. The proposals from domestic scientists are reviewed and controlled by inter-university commitee. The programs are carried out under one of five categories:

1) Joint Studies on special projects (a special project of significant relevance to the advancement of molecular science can be carried out by ateam of several groups of scientists).
2) Research Symposia (on timely topics in collaboration with both outside and IMS scientists).
3) Cooperative Research (carried out in collaboration with both outside and IMS scientists).
4) Use of Facilities (the Computer Center, Instrument Center and other research facilities at IMS are open to all researchers throughout the country).
5) Joint studies programs using UVSOR facilities.

a) Special Projects, b) Cooperative Research Projects, c) Invited Research Projects, d) Use-of-UVSOR Projects.

In the fiscal year 1995, numbers of joint studies programs accepted amounted to 3,7,95 and 261 for categories 1)-4), respectively 4, 23, 4 and 133 for 5a)-5d), respectively.

1) Special Projects

Synthesis and Catalysis of Oxide Clusters

Contributors: **Koji TANAKA, Kiyoshi ISOBE***(Osaka City Univ.)*, **Masaaki ABE, Masaru ICHIKAWA***(Hokkaido Univ.)*, **Satoshi Takara***(Osaka City Univ.)*, **Yusuke IZUMI** *(Nagoya Univ.)*

This research project aims at synthesis of new types of oxide clusters that have active sites for chemical reactions, and at development of unique catalytic reactions for hydrocarbon transformation by using newly prepared oxide clusters

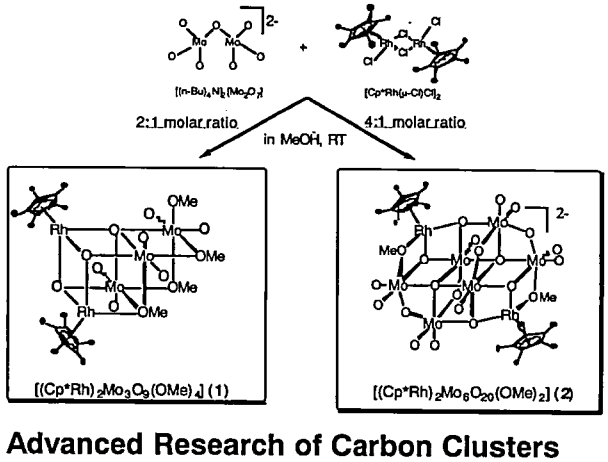
(1) Synthesis and Reactivity of Organometallic Oxide Clusters with Multi Active Sites

We have been preparing new oxide clusters with unique frameworks and constracting new heterogeneous catalysts of the oxide-supported new cluster since this research project started in 1994. Recently, we found that the SiO_2-supported cubane-type molybdenum oxide cluster, $[RhCp^*MoO_4]_4$, promotes propene metathesis reaction. $[(RhCp^*)_4V_6O_{19}]$ grafted on silica was also investigated by EXAFS and IR. The gas-phase oxidation and hydration of acetonitrile proceeds on this silica-grafted Rh-VO cluster at 300-423 K. Furthermore we clarified the planar cluster of $[\{\eta^3\text{-}C_4H_7)_2Rh\}_2V_4O_{12}]$ grafted on SiO_2 exhibits higher activities and selectivities in ethene hydroformylation to C_2H_5CHO and propene oxidation toward acetone at 300-423 K.

In these catalitic reactions the coordinatively unsaturated metal sites and vally sites in the supported clusters play an important role to activate substrates. Hence we develop the synthesis of oxide clusters which have incomplete cubane-frameworks and vally sites.

The triple cubane-type cluster, $[(RhCp^*)_4Mo_4O_{16}]$ ($Cp^* = \eta^5\text{-}C_5Me_5$), shows a novel fragmentation of cube size in the framework to form an incomplete doublecubane-type methoxide cluster $[(RhCp^*)_2Mo_3O_9(OMe)_4]$ (**1**). The yield of **1** from this fragmentation is quite low, which was the difficult point to studying the reaction mechanism of the fragmentation and reactivities of the incomplete doublecubane-type cluster.

Another oxide cluster, $[(RhCp^*)_4V_6O_{19}]$, has valley sites. We have found that the sites are able to interact with CH_3CN through the CH···O-V hydrogen bonds. This suggests that inactive C-H bonds in organic molecules are activated by the valley sites in $[(RhCp^*)_4V_6O_{19}]$. We are now developing a new reaction by using the incomplete cubic structure and valley sites in $[(RhCp^*)_2Mo_3O_9(OMe)_4]$ and $[(RhCp^*)_4V_6O_{19}]$.



Advanced Research of Carbon Clusters

Contributors: **Yusei MARUYAMA** *(Housei Univ.)*, **Kyuya YAKUSHI, Tadaoki MITANI** *(JAIST)*, **Hirotsugu ACHIBA** *(Tokyo Metropolitan Univ.)*, **Tatsuhisa KATO, Hidetoshi FUKUYAMA** *(Univ, of Tokyo)*, **Hiroyoshi SUEMATSU** *(Univ. of Tokyo)*, **Toshiyasu SUZUKI** *(NEC)*, **Seiichi MIYAJIMA and Keiichirou NASU** *(KEK)*

The aim of this research is to search for new families of fullerene materials and to obtain a comprehensive understanding of various unique featuers of fullerene materials. The research was carried out in a wide range covering physical chemistry of fullerene synthesis, solid state properties of fullerenes, and structural and electronic propertiesof carbon nanotubes. To accelarate our collaborative project, we have held a workshop on 24 and 25 December, 1995.

(1) Chemistry of Higher Fullerenes

Electronic and gemetrical structure of large fullerenes upto C_{120} have been systematically examined on the basis of optical absorption (UV/visible), photoelectron spectroscopy, STM, and ^{13}C NMR spectroscopy. These data accumulated so far strongly suggest that the fullerene grows up toward tube-like structure by adding hexagons between two caps consisting of six pentagons

each. Several kinds of tube-like structures with different helicity and/or diameter have been suggested to be formed. In order to understand fullerene growth processes in detail, a laser-furnace method was carried out combined with a high performance liquid chromatography. The resulting temperature dependence of fullerene ismoer production indicates the presence of several important precursors which play a role on the selective ismoer formation.

(2) Superconductivity of Multinary Complex Fullerides

We succeeded to synthesize two kinds of new superconducting multinary fullerides, which are expressed as $(NH_3)_xNaA_2C_{60}$ (x=0.5-1.0 and A=K and Rb) and $K_3Ba_3C_{60}$. The former compounds are new derivertives of A_3C_{60}-type superconductors, involving neutral ammonia molecules. This class of compounds show an anomalous trend in T_c vs. lattice parameter: In sharp contrast with the conventional superconducting fullerides, Tc decreases with increasing the lattice parameter. (Fig. 1) The second superconductor was synthesized by intercalation of potassium into Ba_3C_{60}. A simple electron counting indicates that $K_3Ba_3C_{60}$ is the first materila which has a half-filled state of the next LUMO (t_{1g} level) derived bands. These two examples indicates that multinary complex fullerides are useful for controlling the band-filling and lattice parameter, independently.

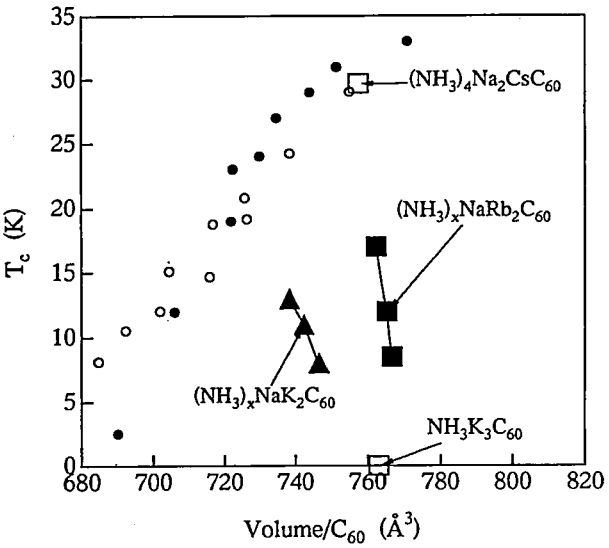


Figure 1. Relation between T_c and the volume per C_{60} for various A_3C_{60}-type superconductors.

(3) Electronic Properties of a Carbon Nanotube

We have measured electrical resistance of a multiwall carbon nanotube from 300 K to 2 K under magnetic field up to 7 T. For measurement, electrical contacts were made by means of micro-lithography method with scanning electron microscopy. At room temperature, the applied current, I, vs. voltage, V, curve shows an ohmic response and the V is proportional to the distance between contacts on a carbon nanotube. The conductance decreases with decreasing temperature and exhibits a ln(T) dependence from 200 K down to 15 K. The resistivity is estimated to be about $1x10^{-2}$ and $3x10^{-2}$ ohm.cm at 300 K and 2 K, respectively. A negative magnetoresistace has been observed up to 200 K. Observation of a ln(T) dependence in conductance and of a negative magnetoresistace suggest that the carbon nanotube is in the two-dimensional weak localization regime. In addition, an oscillation of resistance with magnetic field superposed on the negative magnetoresistace has been observed below 40 K. The amplitude of oscillation shows $T^{-1/2}$ dependence above 15 K. This behavior can be described in terms of the universal conductance fluctuation.

From these results, we have concluded that the carbon nanotube shows quantum interference in the two-dimensional weak localization regime with the temperature range between 15 K and 200 K. On the other hand, temperature dependence of conductance shows a kink at ca. 15 K and the temperature at this kink (T*) depends slightly on magnetic field. Below T*, the behavior of magnetoresistance also differs from that above T*. This feature is attributable to a dimensional crossover of electronic state or a size effect in a carbon nanotube.

Oxygen Molecular Conversion with Chemical Models of Metalloenzymes

Contributors: **Yoshinori NARUTA** *(Kyushu Univ.)*, **Yoshito WATANABE, Fumito TANI** *(Kyushu Univ.)*, **Alain KOSSANYI** *(Kyushu Univ.)*, **Kanako ICHIHARA** *(Kyushu Univ.)*, **Takao SASAKI** *(Kyushu Univ.)*

This research project aims at the molecular-level understanding of the reaction mechanism of metalloenzymes paticipating the molecular conversion of oxygen, i. e., cytochrome P-450, cytochrome *c* oxidase, and oxygen-evolving complex in plant PSII by use of artificial chemical models and the developing new reaction systems with these catalysts.

(1) Modeling of Cytochrome P-450 Active Center with New Chiral Porphyrins bearing Hydroxyl Groups at the O_2-binding Site

Cytochrome P-450 has an array of polar peptide residues around its O_2-binding/activation site. These groups are assumed to play a key role in proton relay and the acceleration of O-O bond cleavage. As a model compound, we prepared a chiral binaphthalene-linked porphyrin which bears hydroxyl groups at the proximal position of the Fe ion inside its cavity. Under the aprotic conditions, the Fe(II) complex showed irreversible binding of O_2 and high affinity of O_2 than CO. This indicates that the strong hydrogen bonding stabilizes the coordinated O_2 and overcomes the strong affinity of CO to the Fe(II) complex. This is the first example which a heme has strong affinity to O_2 than CO. This allows the new design of O_2 complex which is capable of O-O-bond cleavage by successive reduction.

(2) New Modeling System of Cu_B-heme a_3 Center in Cytochrome *c* Oxidase

In cytochrome *c* oxidase (CCO), the Cu_B-heme a_3 center performs four-electron reduction of O_2 and promotes the resulting proton flow through membrane. Tris(pyridylmethyl)amino group (TPA)-linked porphyrin derivatives were prepared as its active-center model compounds. In the preparation of Cu-Fe complex, we found a new transmetallation reaction from Fe(II) to Cu(I) at the TPA site. The reaction of the reduced form with O_2 was monitored by spectroscopic methods. At lower tempera-

ture (-20°C). it formed the corresponding intermediary O_2 complex, which was ESR silent and was capable of oxidation in further two electrons. By means of resonance Raman spectroscopy, the assignment of the detailed structure is under way.

(3) Formation and Characterization of Convergent High-Valent Mn Oxo Porphyrins as the Model Reaction of Oxygen-Evolution in PSII

Manganese porphyrin dimers having appropriate Mn-Mn separation cause catalytic water oxidation through four-electron oxidation. This is considered to be a good functional model of water oxidation in plant photosystemII. In this reaction the Mn(V) oxo complex and the resulting m-peroxo Mn complexes are supposed to be possible intermediates. Thus, we prepared the Mn(V) oxo complex of *o*-phenylene-linked TPP-type porphyries dimers with use of an external oxidizing reagent and observed the resulting product by spectroscopic methods. In the applied porphyrins, the metal-metal separation is tunable by incorporation of suitable groups and a linker molecule. When the porphyrin having ca. 40 Å Mn-Mn separation, we observed the transient formation of the Mn(V) complex and its quick recovery to the starting Mn(III) dimer at -60°C. ESI MS also showed the formation of the corresponding Mn_2O_2 complex. The dimers having lager metal separation showed stable formation of their Mn(IV) complex under the same conditions.

2) Research Symposia

1. Present Status and Future of Photo-Electron Spectroscopy - SOR and Molecular Science
   (November 13th-14th, 1995)
   Organizer: K. Seki
2. Molecular Science of Liquid Crystals
   (November 30th-December 2nd, 1995)
   Organizer: S. Miyajima
3. Molecular Science of Polymers and Biological Systems
   (May 9th-11th, 1996)
   Organizer: Y. Okamoto
4. Symposium on Physical Chemistry for Young Researchers of Molecular Science
   (May 24th, 1996)
   Organizer: I. Koyano
5. Elemental Reaction Processes in Atomospheric Chemistry
   (May 27th-28th, 1996)
   Organizer: M. Kawasaki
6. Molecular Design of New π-Electron Systems for Advanced Organic Materials
   (June 7th-8th, 1996)
   Organizer: T. Otsubo
7. Excitons - recent progress and future prospect -
   (June 20th-22nd, 1996)
   Organizer: T. Hayashi (Kyoto Univ.) and M. Kamada (IMS)

3) Cooperative Research

This is the most important programs which IMS undertakes for conducting its own research that interests both outside and IMS scientists, by using the facilities at IMS. During the first half of the fiscal year 1995 ending on September 30, 39 outside scientists joined this program and during the second half, 56 outside scientists did. The names and affiliations of those collaborators are found in Research Activities.

4) Use of Facilities

The number of projects accepted for the Use-of-Facility Program of the Computer Center during the fiscal year 1995 amounted to 205 (719 users) and computer time spent for these projects is 25909 hours (converted to the HITAC M-680H time), and amounted to 70% of the total annual CPU time used. The number of projects accepted for the Use-of-Facility Program of the Instrument Center during the fiscal year 1995 amounted to 56 (159 users).

5) UVSOR

In the UVSOR Facility with the 750 MeV electron storage ring, there are nineteen beam lines available for synchrotron radiation research (see "UVSOR ACTIVITY REPORT 1996"). The Experimental Facility of each beam line is described in the introductory pamphlet "OUTLINE of UVSOR". The Japanese and English versions are available through the UVSOR Facility. Under the following programs, a number of SR studies have been carried out by many users outside and inside IMS: a) the UVSOR Special Projects, b) the UVSOR Cooperative Research Projects, c) the UVSOR Invited Research Projects, and d) the Use-of-UVSOR Projects.

5-a) UVSOR Special Project

In fiscal year of 1995, following UVSOR special projects have been carried out.

i) Title: Development of the spin-resolved photoelectron spectrometer system
   Beam Line: 5A
   Representative of project: **Masao KAMADA** (IMS)
ii) Title: Construction of multilayer monochromator system for photochemical reactions
   Beam Line: 4A
   Representative of project: **Tsuneo URISU** (IMS)
iii) Title: Construction of glancing incident monochromator at BL2B2
   Beam Line: 2B2
   Representative of project: **Koichiro MITSUKE** (IMS)
iv) Title: Upgrade of VUV beam line with installation of new monochromator
   Beam Line: 7B
   Representative of project: **Hideyuki NAKAGAWA** (*Fukui Univ.*)

5-b) UVSOR Cooperative Research Projects

Under this joint-study program, many synchrotron radiation experiments have been carried out at the beam lines of in-house staff in cooperation with scientists who were invited from other institutions. The total number of the projects in this category was 23 in the fiscal year of 1995.

5-c) The UVSOR Invited Research Projects

Under this joint-study program, several scientists were invited from other institutions of help for construction of

new beam lines and improvement of the UVSOR storage ring and others. The total number of the projects in this category was 4 in the fiscal year of 1995.

5-d) The Use-of-UVSOR Projects

Ten out of the total of nineteen UVSOR beam lines are available for general users outside and inside IMS for their synchrotron radiation studies in the field of molecular science. The total number of the projects in this category was 133 in the fiscal year of 1995.

FOREIGN SCHOLARS

Visitors from abroad play an important role in research activities and always welcome at IMS. The following is the list of foreign scientist who visited IMS in the past year (Aug. 1995 - Jul. 1996). The sign *1 indicates an attendant to an Okazaki Conference, *2 an IMS or Japan Society for the Promotion of Science Invited Foreign Scholar, *3 an IMS councillor, *4 an IMS visiting scientst, and *5 an IMS adjunct professor or associate professor from abroad (period of stay from 9 to 12 months). Scientists who wish to visit IMS under program *2 and *5 are invited to make contact with an IMS faculty in a related field.

Prof. Chang-Guo Zhan*2	Central China Normal Univ.	(China)	-Aug. 1995,Jun1996-
Prof. D. Lee*2	Sogang Univ.	(Korea)	-Aug./Dec.1995-Feb.1996
Prof. A. Ben-Reuven*2	Tel-Aviv Univ.	(Israel)	Aug.-Oct.1995
Dr. C. Granier*2	Hiroshima Univ.	(Japan)	Aug.-Sep.1995
Prof. Jong-Jean Kim*2	KAIST	(Korea)	Aug.-Sep.1995/Dec.1995-Feb.1996
Prof. O. N. Ulenikov*2	Tomsk State University	(Russia)	Aug.1995
Dr. L. Nahon*2	Univ. Paris-Sud	(France)	Aug.1995
Mr. D. Spanke*2	Heinrich-Heine Univ. Dusseldorf	(Germany)	Aug.1995
Prof. S. Mathieu*4	Univ. Paul Sabatier	(France)	Aug.1995-Feb.1996
Prof. F. R. Ornellas*5	Inst. of Chem, Univ. Sao Paulo	(Brazil)	Aug.1995-Jul.1996
Prof. F. O. Goodman*5*4	Univ. of Waterloo	(Canada)	-Sep.1995,Jul.1996
Prof. D. Chandler*2	Univ. of California, Barkely	(U.S.A.)	Sep.1995
Prof. A. Harriman*2	Utah State University	(U.S.A.)	Sep.1995
Prof. I. H. Munro*2	Deresbury Lab.	(U.K.)	Sep.1995
Prof. D. Norman*2	Deresbury Lab.	(U.K.)	Sep.1995
Dr. G. van der Lean*2	Deresbury Lab.	(U.K.)	Sep.1995
Prof. S. S. Hasnain*2	Deresbury Lab.	(U.K.)	Sep.1995
Dr. J. B. West*2	Deresbury Lab.	(U.K.)	Sep.1995
Dr. L. Federico*2	Instiuto di Struttura Della Materia Center	(Itary)	Sep.1995
Prof. E. Kisker*2	Heinrich-Heine Univ. Dusseldorf	(Germany)	Sep.1995
Prof. Se-Jung Oh*2	Seoul Natl. Univ.	(Korea)	Sep.1995
Mr. U. Flechsig*2	BESSY	(Germany)	Sep.1995
Dr. C. Jung*2	BESSY	(Germany)	Sep.1995
Mr. Han Zhengfu*2	NSRL	(China)	Sep.1995
Mr. Sheng Liusi*2	NSRL	(China)	Sep.1995
Prof. Shi Chaoshu*2	Univ. of Sci. and Tech. of China	(China)	Sep.1995
Mr. Lu Gdong*2	NSRL	(China)	Sep.1995
Dr. Ping Wang*2	Univ. of Alabama	(U.S.A.)	Sep.1995-Jan.1996
Prof. V. Stankevitch*2	Kurchatov Inst.	(Russia)	Sept.1995
Dr. K. Kaznacheev*2	Kurchatov Inst.	(Russia)	Sept.1995
Prof. G. Lodha*2	CAT	(India)	Sept.1995
Dr. L. Mishra*2	Banaras Hindu Univ.	(India)	Sept.1995
Prof. Jingui Qin*2	Wuhan Univ.	(China)	-Oct.1995
Prof. M. Shapiro*2	Weizman Inst.	(Israel)	Oct.1995
Prof. S. Singh*2	Indian Inst. of Tech. Madras	(India)	Oct.1995
Prof. Y. Demkov*2	St. Petersburg Univ.	(Russia)	Oct.1995
Prof. P. C. Eklund*2	Kentuky Univ.	(U.S.A.)	Oct.1995
Prof. M.Diehl*1	RIKEN	(Japan)	Oct.1995
Prof. V.F.Tarasov*1	Tohoku Univ.	(Japan)	Oct.1995
Prof. K.P. Dinse*1	Tohoku Univ.	(Japan)	Oct.1995
Prof. L. Haim*1	Rikaken	(Japan)	Oct.1995
Prof. P. J. Boiden*1	Odense Univ.	(Denmark)	Oct.1995
Prof. O. C. Karl-Heinrich*1	Max-Planck Inst.	(Germany)	Oct.1995
Prof. M. K. Alan*1	Oxford Univ.	(U.K.)	Oct.1995
Prof. F. G. Jorge*1	Univ. of Notre Dame	(Argentina)	Oct.1995
Mr. O. Dippel*2	Fritz-Haber-Inst. der Max-Plank -Gesellschaft	(Germany)	Oct.1995
Prof. A. B. Myers*2	Univ. of Rocherster	(U.S.A.)	Oct.1995
Dr. Dongho Kim*2	Korea Res. Inst. of Standards and Sci.	(Korea)	Oct.1995
Dr. G. Singh*2	CAT	(India)	Oct.1995
Prof. C. A. Brau*2	Vandelbilt Univ.	(U.S.A.)	Oct.1995
Prof. B. Bagchi*2	Indian Inst. of Sci.	(India)	Oct.1995/Feb.1996
Prof. H. Szichman*5	Soreq Nuclear Res. Center	(Israel)	Oct.1995-
Prof. W. T. Borden*2	Univ. of Washington	(U.S.A).	Nov.1995

Prof. R. Carbo*2	Univ. of Girona	(Spain)	Nov.1995
Dr. J. Vogt*2	Ciba-Gegy AG Fosschungszerntrum	(Switzerland)	Nov.1995
Dr. M.E. Bartram*2	Sandia Natl. Lab.	(U.S.A.)	Nov.1995
Prof. J. Gorecki*5	Polish Acad. of Sci.	(Poland)	Nov.1995
Prof. E. I. Solomon*2	Stanford Univ.	(U.S.A.)	Nov.1995
Ms. V. Olga*2	Louisiana State Univ.	(U.S.A.)	Nov.1995
Prof. P. Lablanquie*2	Univ. Paris-Sud	(France)	Nov.1995
Prof. J. L. Sessler*2	Univ. of Taxas at Austin	(U.S.A.)	Nov.1995
Prof. V. A. Ivanov*2	Russian Acad. of Sci.	(Russia)	Nov.1995-
Dr. A.A. Zakhidov*2	Uzbekistan Acad. of Sci.	(Uzbek)	Nov.1995-Feb.1996
Prof. V. Mckoy*2	California Inst. Tech.	(U.S.A.)	Dec.1995
Prof. K. Morokuma*2	Emory Univ.	(U.S.A.)	Dec.1995
Dr. J. N. Moore*1*4	Univ. of York	(U.K.)	Dec.1995
Dr. W.Wang*2	Fudan Univ.	(China)	Dec.1995-Feb.1996
Prof. Park Yong-Kwang*2	Kanguwan Natl. Univ.	(Korea)	Dec.1995-Feb.1996
Prof. V. L. Osherov*2	Inst. of Chem. Phys.	(Russia)	Dec.1995-Jun1996
Mr. P. Kapusta*2	Tech. Univ. of Prague	(Czech)	Jan.-Mar.1996
Dr. D. A. Padmavathi*2		(India)	Jan.-May1996
Dr. M. Naphcha*2		(Israel)	Jan.-May1996
Dr. U. Hansmann*2	ETH Zürich	(Switzerland)	Jan.1996/Feb.-Mar.1996
Dr. Yang Shi*2	Chinese Acad. of Sci.	(China)	Jan.1996-
Prof. M. C. Heaven*5	Emory Univ.	(U.S.A.)	Jan.1996-
Dr. M. V. Simonyan*2	Armenian Natl. Acad. of Sci.	(Armenia)	Jan.1996-
Prof. L. Que, Jr.*1	Univ. of Minnesota	(U.S.A.)	Feb. 1996
Prof. D. Sellmann*1	Univ. Erlagen-Nürnberg	(Germany)	Feb. 1996
Prof. P. F. Knowles*1	Univ. of Leed	(U.K.)	Feb. 1996
Dr. R.Stevens-Truss*1	Univ. of Michigan	(U.S.A.)	Feb. 1996
Prof. A. M. Pyle*1	Columbia Univ.	(U.S.A.)	Feb. 1996
Prof. T. L. Poulos*1	Univ. of California at Irvin	(U.S.A.)	Feb. 1996
Mr. G. Goodno*2	Univ. of Rochester	(U.S.A.)	Feb.-Mar.1996
Dr. A. Fanelsa*2	Heinrich-Heine Univ. Dusseldorf	(Germany)	Feb.-Mar.1996
Dr. E. J. J. Groenen*2	Leiden Univ.	(Netherlands)	Feb.1996
Prof. K. Duppen*2	Univ. of Groningen	(Netherlands)	Feb.1996
Prof. D. Miller*2	Univ. of Toronto	(Canada)	Feb.1996
Prof. J. Fourkas*2	Boston College	(U.S.A.)	Feb.1996
Mr. W. Nessler*2	Fritz-Harber Inst.	(Germany)	Feb.1996
Prof. M. Berg*2	Univ. of South Carolina	(U.S.A.)	Feb.1996
Mr. Kim K. Hoe*2	Sung Kyum Kwan Univ.	(Korea)	Feb.1996
Prof. Y. S. Kwon *2	Sung Kyum Kwan Univ.	(Korea)	Feb.1996
Prof. M. E. Couprie*2	LURE, Univ. of Paris Sud	(France)	Feb.1996
Dr. D. Robin*2	ALS, Lawrenie Berkeley Lob.	(U.S.A.)	Feb.1996
Prof. He Duohui*2	Univ. of Sci. and Tech. China	(China)	Feb.1996
Prof. D. H. Kim*2	Pohang Univ. of Sci. and Tech.	(Korea)	Feb.1996
Ms. Jung, M. Hwa*2	Sung Kyun Kwan Univ.	(Korea)	Feb.1996/Apr.1996
Prof. G. Rabai*2	Kossuth Laios Univ.	(Hungary)	Feb.1996-
Dr. H. Pal*2	Bhabha Atomic Res. Inst.	(India)	-Mar. 1996
Prof. G. Balint-Kurti*2	Bristol Univ.	(U.K.)	Mar.-Apr.1996
Prof. M. R. Wills*2	Nottingham Univ.	(U.K.)	Mar.-Apr.1996
Prof. Y.S. Kwon*2	Sung-Kyung-Kwan Univ.	(Korea)	Mar.-Apr.1996
Dr. S. Daniele*2	Nice-Sophia-Antipolis Univ.	(France)	Mar.-Jun1996
Dr. N. Sarkar*2	Indian Assoc. for Cultivation of Sci.	(India)	Mar.-May1996
Prof. S. R. Meech*2	Univ. of East Anglia	(U.K.)	Mar.-May1996
Prof. M. A. El-Sayed*3	Georgia Inst. of Tech.	(U.S.A.)	Mar.1996
Prof. E. W. Schlag*3	Munchen Tech. Univ.	(Germany)	Mar.1996
Prof. N. M. Plakida*2	Joint Inst. for Nuclear Res.	(Russia)	Mar.1996
Prof. J. Eichler*2	Hahn-Meitner Inst.	(Germany)	Mar.1996
Prof. G. Schatz*2	North Western Univ.	(U.S.A.)	Mar.1996
Prof. N. Makri*2	Univ. of Illinois at Urbana	(U.S.A.)	Mar.1996
Dr. M. Newton*2	Brookheaven Natl. Lab.	(U.S.A.)	Mar.1996
Prof. L. S. Cederbaum*2	Univ. Heidelberg	(Germany)	Mar.1996
Prof. R. R. Cunl, Jr.*2	Rice Univ.	(U.S.A.)	Mar.1996
Dr. A. I. Jaman*2	Saha Inst. of Nuclear Phys.	(India)	Mar.1996
Prof. J. P. Shermann*2	Univ. of Paris-North	(France)	Mar.1996
Prof. R. Bersohn*2	Columbia Univ.	(U.S.A.)	Mar.1996
Prof. Kopin Liu*2	Inst. of Atomic and Mol. Sci.	(Taiwan)	Mar.1996
Prof. Jyhpyng Wang*2	Inst. of Atomic and Mol. Sci.	(Taiwan)	Mar.1996
Prof. R. N. Lyubovskaya*2	Russian Acad. of Sci.	(Russia)	Mar.1996

Prof. E. Silinsh*2	Latvian Acad. of Sci.	(Latvian)	Mar.1996
Prof. J. S. Miller*2	Univ. of Utah	(U.S.A.)	Mar.1996
Prof. O. Kahn*2	Bordeaux Univ.	(France)	Mar.1996
Prof. J. Chin*2	McGill Univ.	(Canada)	Mar.1996
Prof. A. E. Underhill*2	Univ. of Wales, Bangor	(U.K.)	Mar.1996
Dr. J. Hrusak*2	J. Heyrousky Inst. of Phys. Chem. Academy of Sci.	(Czech)	Mar.1996-
Dr. I. K. Ahmad*2	Lodon Univ.	(U.K.)	Mar.1996-
Dr. J. K. Park*2		(Korea)	-Apr.1996
Mr. K. A. Williams*2	Kentuky Univ.	(U.S.A.)	Apr.-May1996
Prof. F. G. Mertens*2	Univ. of Bayreuth	(Germany)	Apr.1996
Prof. R. M. Levy*2	Rutgers Univ.	(U.S.A.)	Apr.1996
Mr. P. Hinnen*2	Vrÿe Universiteit Amsterdam	(Netherlands)	Apr.1996
Dr. M. Kozlov*2	Natl. Inst. of Mate. and Chem. Res.	(Japan)	Apr.1996
Prof. Nguyen Van Hung*2	Hanoi Univ.	(Vietnam)	Apr.1996
Dr. S. A. Pande*2	Center for Advanced Tech.	(India)	Apr.1996
Dr. D. Nolle*2	DELTA, Dortmund Univ.	(Germany)	Apr.1996
Ms. Jung M. Hwa*2	Sungkyunkwan Univ.	(Korea)	Apr.1996
Prof. R. B. Martin*2	Univ. of Virginia	(U.S.A.)	Apr.1996
Dr. I. V. Rubtsov*4	Russian Acad. of Sci. .	(Russia)	Apr.1996-
Dr. P. de Forcrand*2	ETH Zürich	(Switzerland)	May.1996
Prof. D. Nesbitt*2	Colorado Univ.	(U.S.A.)	May.1996
Prof. R. Gadonas*2	Vilnius Univ.	(Lithuania)	May.1996
Dr. A. Orr-Ewing*2	Bristol Univ.	(U.K.)	May.1996
Prof. D.M. Neumark*2	Univ. of California, Berkeley	(U.S.A.)	May.1996
Dr. R. Pierre*2	CNRS	(France)	May.1996
Dr. J. Fluegge*2	Natl. Inst. for Acad. Interdisciplinary Res.	(Japan)	May.1996
Dr. Yumin Li*2		(China)	May1995-
Prof. C. Meanes*2	Univ. of California	(U.S.A.)	May1996.
Dr. P. Severino*2		(Itary)	May1996-
Dr. A. Fiedler*2		(Germany)	May1996-
Prof. Ahn Kwang-Hyun*2	Kyung Hee Univ.	(Korea)	Jun.1996-
Prof. Tai Jong Kang*2	Taegu Univ.	(Korea)	Jun1996-
Dr. H. Heitele*2	Tech. Univ. Muenchen	(Germany)	Jun.1996
Dr. J. Kröber*2*4	Paris XI Univ.	(Germany)	-Jul.1996
Ms. S. Maw*2	Manchester Univ.	(U.K.)	Jul.1996
Dr. P. Kolandoivel*2	Bharathiar Univ.	(India)	Jul.1996
Prof. V. E. Fedorov*2	Russian Acad. of Sci.	(Russia)	Jul.1996
Prof. K. Bhattacharrya*1*4	Indian Acad. for the Caltivation of Sci.	(India)	Jul.1996
Prof. Kim Gyu-Shik*2	Kangwon Natl. Univ.	(Korea)	Jul.1996
Dr. I. O. Tolstikhin*2	Univ. of Electro Communications	(Japan)	Jul.1996-
Prof. W. C. Lineberger*2	Univ. of Colorado	(U.S.A.)	Jul.1996-

AWARDS

Professor Yoshihara's Scientific Achievements

Prof. Keitaro Yoshihara of Department of Electronic Structure received the Chemical Society of Japan Award in 1996 for his contributions to "Studies on Excited Molecules by Ulrtafast Laser Spectroscopy". His scientific contributions are summarized in the following.

1. Dynamical aspects on intermolecular electron transfer. He has studied the intermolecular electron transfer occurring much faster than the solvation process in a system of a dye molecule and electron-donating solvent, and investigated the contribution of intramolecular vibrational modes to electron transfer. He has also clarified the dynamical features of various electron transfer processes such as the electron transfer between dye molecules adsorbed on the surface and substrate and the primary processes in photosynthetic reaction centers.
2. Reaction mechanisms of the cis-trans photoisomerization. He has studied reaction mechanisms of cis-trans photoisomerization of molecules with C-C double bonds such as stilbene, simple linear polyenes, and retinal protein. Especially, he has observed the transition state of photoisomerization of simple polyenes for the first time.
3. Excited state of benzene. He has explored a new excited state of benzene and cooling process of highly excited vibrational state by the flash photolysis method.
4. Developments of ultrafast laser spectroscopy and its application to molecular science. He has pioneered various new laser spectroscopies for molecular science such as optical parametric amplification and higher order nonlinear spectroscopy.

Professor Kitagawa's Scientific Achievements

Professor Teizo Kitagawa of Department of Molecular Structure received the Scientific Award of the Spectroscopical Society of Japan for 1996 for his contribution to "Structural Study of Biomolecules by Vibrational Spectroscopy". This award is given to a scientist who made an outstanding contribution in the field of spectroscopy in Japan. He has devoted himself to interpreting enzymatic reactions on the basis of microstructure of proteins. Among a number of Professor Kitagawa's prominent achievements, the followings are regarded to have the highest impacts.

1. Establishment of the vibrational assignments of resonance Raman spectra of Ni-octaethylporphyrin as a model of catalytic site of heme proteins both through isotopic labeling experiments and normal coordinate calculations.
2. Elucidation of the allosteric mechanism in cooperative oxygen binding to hemoglobin through observation of the Fe-histidine stretching resonance Raman band.
3. Clarification of the interaction mode of flavin and the substrate in flavoproteins through observation of charge-transfer resonance Raman spectra.
4. Resonance Raman identification of the Fe=O heme in the reaction intermediate of peroxidases as the key structure for the enzymatic activity.
5. Studies of protein dynamics of hemoglobins and myoglobins with ultraviolet resonance Raman spectroscopy
6. Establishment of the mechanism of four-electron dioxygen reduction catalyzed by cytochrome *c* oxidase

Associate Professor Tahara's Scientific Achievements

Associate Professor Tahei Tahara of Department of Vacuum UV Photoscience received the 1995 Award of Research Foundation for Opt-Science and Technology for his contribution to "Development and Application of Two-dimensional Picosecond Time-resolved Spectroscopy". This award is given to young scientists (under 35 years old) who published remarkable papers in the last two years in the fields of opt-science and opt-technology. Prof. Tahara developed a new method of picosecond time-resolved spontaneous/coherent Raman spectroscopy, making use of pico/femtosecond lasers, nanosecond lasers, and a streak camera. This method enables us to obtain spectral and temporal information of samples as a two-dimensional image which is taken with a single short measurement. He applied this new method to the study of photochemical reactions in the condensed phase, and clarified the dynamics and the mechanism of photoisomerization of retinals.

Dr. Hirota's Scientific Achievements

Inoue Research Award for Young Scientists in 1996 was given to Dr. Shun Hirota, who is now a research associate in Faculty of Science, Nagoya University. This award is given to 30 young scientists (under 35 years old) who obtained remarkable results during their Ph. D. work in the fields of basic science, engineering, medicine, pharmacy and agriculture. Dr. Hirota was awarded this prize for his Ph. D. study, "Resonance Raman Studies of Fe-Ligand Vibrations of Oxygen Binding Heme Proteins and Structure-Function Relationship of Terminal Oxidases," which was carried out in Department of Functional Molecular Science, The Graduate University for Advanced Studies under supervision of Prof. Teizo Kitagawa.

LIST OF PUBLICATIONS

R. KISHI, M. GOMIE, A. NAKAJIMA, S. IWATA, and K. KAYA, "Theoretical Studies of Carbon Doped Small Silicon Clusters: Electron Affinities of Si_nC (n=2 - 5)," *J.Chem.Phys.* **104,** 8593 (1996).

F. R. ORNELLAS and S. IWATA, "Ab initio Studies of Silicon and Nitrogen Clusters: Cyclic or Linear Si_2N?," *J. Phys. Chem.* **100,** 10919 (1996).

H. WATANABE and S. IWATA, "Theoretical Studies of Geometric Structures of Phenol-Water Clusters and their Infra-Red Absorption Spectra in the O-H Stretching Region," *J.Chem.Phys.* **105,** 420 (1996).

H. WATANABE and S. IWATA, "Theoretical Studies of Boron - Water Cluster Ions $B^+(H_2O)_N$ and Aluminium - Water Clusters $Al^+(H_2O)_N$: Isomers and Intra-Cluster Reactions," *J.Phys.Chem.* **100,** 3377 (1996).

Y. SONODA and S. IWATA, "Theoretical Studies of the Chemical Processes of Producing Methylamine and Methanol in the Interstellar Space," *Bull.Chem.Soc.Jpn.* **69,** 575 (1996).

T. S. FUJII and S. IWATA, "Theoretical Studies of the Ground and Low-Lying Excited Electronic States of the Early Transition Metal Dihydrides with State Averaged MC SCF Method," *Chem. Phys. Letters* **251,** 150 (1996).

C. G. ZHAN and S. IWATA, "Ab initio Studies on the Structures, Vertical Electron Detachment Energies and Fragmentation Energies of CN_n^- Clusters," *J.Chem.Phys.* **104,** 9058 (1996).

R. KISHII, A. NAKAJIMA, S. IWATA and K. KAYA, "Electron-Correlation Effects on Geometrical and Electronic Structures of Si_nNa Clusters," *Surface Review and Letters* **3,** 365 (1996).

A. NAKAJIMA, T. TAGUWA, K. NAKAO, K. HOSHINO, S. IWATA and K. KAYA, "Photoelectron Spectroscopy of Binary Metal Cluster Anion Containung Sulfur Atom," *Surface Review and Letters* **3,** 417 (1996).

A. NAKAJIMA, T. TAGUWA, K. NAKAO, M. GOMEI, R. KISHII, S. IWATA and K. KAYA, "Photoelectron Spectroscopy of Silicon-Carbon Cluster Anions," *Surface Review and Letters* **3,** 411 (1996).

C. G. ZHAN and S. IWATA, "Ab initio Studies on Structures of the Hexa-Coordinate Phosphorus Intermediate for the Phosphoryl Ester Exchange and N→Omigration Reactions of Dimethyloxyphosphoryl-Threonine," *Chem.Phys.Letters* **247,** 401 (1995).

A. NAKAJIMA, T. TAGUWA, K. NAKAO, M. GOMEI, R. KISHII, S. IWATA and K. KAYA, "Photoelectron Spectroscopy of Silicon-Carbon Cluster Anions ($Si_nC_m^-$)," *J. Chem. Phys.* **103,** 2050 (1995).

A. MITSUTAKE, T. IITAKA and Y. OKAMOTO, "A Method for Calculating the Eigenvalues of Large Hermitian Matrices by Second-Order Recursion Formulae," *Comp. Phys. Comm.* **96,** 217 (1996).

U. H. E. HANSMANN, Y. OKAMOTO and F. EISENMENGER, "Molecular Dynamics, Langevin, and Hybrid Monte Carlo Simulations in Multicanonical Ensemble," *Chem. Phys. Lett.* **259,** 321 (1996).

A. SHUDO and K. S. IKEDA, "Stokes Phenomenon in Chaotic Systems: Pruning Trees of Complex Paths with Principle of Exponential Dominance " *Phys. Rev. Lett.* **76,** 4151 (1996).

K. TSUDA, K. MORIBAYASHI and H. NAKAMURA, "Quantum Dynamics of the Mu+H_2 (HD, D_2) and H+MuH(MuD) Reactions," *J. Chem. Phys.* **103,** 5512 (1995).

K. MORIBAYASHI and H. NAKAMURA, "Accurate Quantum Dynamics of the Light Atom Transfer Chemical Reaction O+HCl→OH+Cl," *J. Phys. Chem.* **99,** 15410 (1995).

F. O. GOODMAN and H. NAKAMURA, "On the Multiple Peaks in Charge-Transfer Probability vs. Laser Frequency in the Theory of Laser Assisted Surface Ion Neutralization," *Prog. in Surface Science* **50,** 389 (1995).

M. HIYAMA and H. NAKAMURA, "Superexcited States of CO Near the First Ionization Threshold," *Chem. Phys. Lett.* **248,** 316 (1996).

C. ZHU, E. E. NIKITIN and H. NAKAMURA, "Semiclassical Analysis of Resonance States Induced by a Conical Intersection," *J. Chem. Phys.* **104,** 7059 (1996).

V. I. OSHEROV and H. NAKAMURA, "Quantum Mechanically Exact Analytical Solutions of a Two-State Exponential Model," *J. Chem. Phys.* **105,** 2770 (1996).

C. ZHU and H. NAKAMURA, "Two-by-two Diabatic Approach for Multi-Channel Curve Crossing Problems," *Chem. Phys. Lett.* **258,** 342 (1996).

K. OKUMURA and Y. TANIMURA, "Unified Time-Path Approach to the Generating Functional of the Brownian Oscillator System: The Bilinearly Corrected Feynman Rule for Nonequilibrium Processes," *Phys. Rev. E* **53,** 214 (1996).

M. SASAI, "Conformation, Energy and Folding Ability of Selected Amino Acid Segunces", *Proc Natl. Acad. Sci.* USA, **92,** 8438 (1995).

E. SHIRATANI and M. SASAI, " Growth and Collapse of Structural Patterns in the Hydrogen Bond Network in Liquid Water ," *J. Chem. Phys.* **104,** 7671 (1996).

H. FRIEDMAN, F. RAINERI, F. HIRATA, B. PERN, "Surrogate Hamiltonian Description of Solvation Dynamics. Site-number Density and Polarization Charge Density Formulations," *J. Stat. phys.*, **78,** 239 (1995).

M. KAWATA, S. TENNO, S. KATO, F. HIRATA, "Irregular Order in Basicities of Methylamines in Aqueous Solution: A RISM-SCF Study," *J. Am. Chem. Soc.*, **117,** 1638 (1995).

S. CHONG, S. MIURA, G. BASU, F. HIRATA, "Molecular Theory for the Non- Equilibrium Free Energy Profile in Electron Transfer Reaction," *J. Phys. Chem.* **99,** 10526 (1995).

M. KAWATA, S. TENNO, S. KATO, F. HIRATA, "The Solvation Effect on the Acidities of Haloacetic Acids in Aqueous Solution: A RISM-SCF Study," *Chem. Phys. Letters* **240,** 199 (1995).

M. IRISA, T.TAKAHASHI, K. NAGAYAMA, F. HIRATA, "Solvation Free Energies of Non-Polar and Polar Solutes Reproduced by a Combination of Extended Scaled Particle Theory and the Poisson-Boltzmann Equation," *Mol. Phys.* **85,** 1227 (1995).

F. HIRATA, T. MUNAKATA, F. RAINERI and H. L. FRIEDMAN, "An Interaction-Site Representation of the Dynamic

Structure Factor of Liquid and the Solvation Dynamics," *J. Mol. Liquids* **65/66,** 15 (1995).
S. CHONG, F. HIRATA, "Non-linear Effects in the Free Energy Profile of Electron Transfer Reaction: an Integral Equation Approach," *J. Mol. Liquids* **65/66,** 345 (1995).
M. IRISA, T. TAKAHASHI, F. HIRATA and T. YANAGIDA, "Solvation Free Energy of Protein Reproduced by the Combination of the Extended Scaled Particle Theory and the Poisson-Boltzmann Equation," *J. Mol. Liquids* **65/66,** 381 (1995).
S. CHONG and F. HIRATA, "The Free Energy Profiles for the Electron Transfer Reactions Calculated from the Integral Equation Method of Liquids," Molecular Simulation **16,** 3 (1996).
M. KAWATA, S. TEN-NO, S. KATO and F. HIRATA, "Solvent Effect on Acidity: A Hybrid Approach Based on the RISM and the Hartree-Fock Equations," *J. Phys. Chem.* **100,** 1111 (1996).
M. KAWATA, S. TEN-NO, S. KATO and F. HIRATA, "Theoretical Study for the Basicities of Methylamines in Aqueous Solution: A RISM-SCF Calculation of Solvation Theromodynamics," *Chem. Phys.* **203,** 53 (1996).
M. KINOSHITA and F. HIRATA, "Application of the Reference Interaction Site Model Theory to Analysis on Surface-Induced Structure of Water," *J. Chem. Phys.* **104,** 8807 (1966).
R. UEOKA, Y. MATSUMOTO, K. GOTO, T. ITO, S. MORI, Y. MATSUMOTO, A. SAKOGUCHI, Y. IHARA and F. HIRATA, "A Remarkably Enhanced Diastereoselectivity for the Hydrolysis of Dipeptide Esters Responding to pH and Temperature in Buffer Solutions," *Tetrahedron letters* **37,** 3461 (1996).
H. SATO, F. HIRATA and S. KATO, "Analytical Energy Gradient for the Reference Interaction Site Model Multiconfigurational Self-Consistent-Field Method: Application to 1,2-difluoroethylene in Aqueous Solution," *J. Chem. Phys.* **105,** 1546 (1996).
K. YONEMITSU and M. IMADA, "Electron-Phonon Interaction and Spin Gap in Nearly-Half-Filled Correlated Electron Systems," *Physica C* **263,** 82 (1995).
K. YONEMITSU and M. IMADA, "Spin-Gap Phase in Nearly-Half-Filled One-Dimensional Conductors Coupled with Phonons," *Phys. Rev. B* **54,** 2410 (1996).
M. GOTO, K. NAMIKI and S. SAITO, "Microwave Spectra of the ZnH and ZnD Radicals in the $X\,^2\Sigma^+$ State," *J. Mol. Spectrosc.* **173,** 585 (1995).
A. H. SALECK, H. OZEKI and S. SAITO, "Isotopic NS Rotational Spectra: $^{14}N^{33}S$ and $^{15}N^{32}S$," *Chem. Phys. Lett.* **244,** 199 (1995).
J. TANG and S. SAITO, "Microwave Spectra of Isotomers of HCS^+ and its Substitution Structure," *Astrophys. J.* **451,** L93(1995).
H. OZEKI and S. SAITO, "Laboratory Submillimeter-Wave Spectroscopy of the $CH_2(^3B_1)$ Radical," *Astrophys. J.* **451,** L97 (1995).
M. GOTO and S. SAITO, "Laboratory Measurement of the J=1-0 Transition of AlH near 387 GHz," *Astrophys. J.* **452,** L147(1995).
M. KANADA, S.YAMAMOTO, S. SAITO and Y. OSAMURA, "Molecular Structure of the Linear C_3H Radical: Microwave Spectrum of the ^{13}C Substituted Species," *J. Chem. Phys.* **104,** 2192 (1996).
H. OZEKI and S. SAITO, "The Microwave Spectrum of the CD_2 Radical," *J. Chem. Phys.* **104,** 2167 (1996).
J. TANG and S. SAITO, "Microwave Spectrum of the FS_2 Radical in the Ground Electronic $X\,^2A'$ State," *J. Chem. Phys.* **104,** 7437 (1996).
K. NAMIKI and S. SAITO, "Microwave Spectrum of the NiO Radical in the $X\,^3\Sigma^-$ State," *Chem. Phys. Lett.* **253,** 343 (1996).
K. KOBAYASHI, M. GOTO, S. YAMAMOTO and S. SAITO, "The Microwave Spectrum of the NCl Radical in the Electronically Excited ($a\,^1\Delta$)State," *J. Chem. Phys.* **104,** 8865 (1996).
T. HIRAO, S. SAITO and H. OZEKI, "Microwave Spectrum and Molecular Structure of the Dihydrophosphoryl Radical H_2PO in the $X\,^2A'$ Ground Electronic State," *J. Chem. Phys.* **105,** 3450 (1996).
M. IZUHA, S. YAMAMOTO and S. SAITO, "Microwave Spectrum of Silylidene, H_2CSi," *J. Chem. Phys.* **105,** 4923 (1996).
Y. SEKIMOTO, H. YOSHIDA, T. HIROTA, Y. TAKANO, E. FURUYAMA, S. YAMAMOTO, S. SAITO, H. OZEKI, J. INATANI, M. OHSHI, A. G. CARDIASMENOS and S. L. HENSEL, "Measurements of 220 GHz Atmospheric Opacity on Mt. Fuji with a Radiometer/Radome System," *Internat. J. Infrared and MM Wave*, **17,** 1263 (1996).
B. KETZER, F. J. HARTMANN, H. DANIEL, T. VON EGIDY, A. NIESTROJ, S. SCHMID, W. SCHMID, T. YAMAZAKI, I. SUGAI, K. NAKAYOSHI, R. S. HAYANO, F. E. MAAS, H. A. TORII, T. ISHIKAWA, H. TAMURA, N. MORITA, D. HORVATH, J. EADES and E. WIDMANN, "Isotope Effects on Delayed Annihilation Time Spectra of Antiprotonic Helium Atoms in a Low-Temperature Gas" *Phys. Rev. A* **53,** 2108 (1996).
E. WIDMANN, I. SUGAI, T. YAMAZAKI, R. S. HAYANO, M. IWASAKI, S. N. NAKAMURA, H. TAMURA, T.M. ITO, A. KAWACHI, N. NISHIDA, W. HIGEMOTO, Y. ITO, N. MORITA, F. J. HARTMANN, H. DANIEL, T. von EGIDY, W. SCHMID, J. HOFFMANN and J. EADES, "Effects of Impurity Atoms and Molecules on the Lifetime of Antiprotonic Helium Atoms" *Phys. Rev. A* **53,** 3129 (1996).
H. A. TORII, M. HORI, T. ISHIKAWA, F. E. MAAS, R. S. HAYANO, N. MORITA, M. KUMAKURA, I. SUGAI, B. KETZER, H. DANIEL, F. J. HARTMANN, R. POHL, R. SCHMIDT, T. VON EGIDY, D. HORVATH, E. WIDMANN, J. EADES and T. YAMAZAKI, "Laser-Induced Resonant Transitions in the v=n-l-1=2 and 3 Metastable Cascades of Antiprotonic ^{3}He Atoms" *Phys. Rev. A* **53,** R1931 (1996).
M. ASANO-SOMEDA, S. SATO, K. AOYAGI and T. KITAGAWA, "Time-Resolved Resonance Raman Spectra of Meso-Substituted Copper Porphyrins in the T_1 State: Implication for the Solvent Dependent Red-Shift of Emission Spectra," *J. Phys. Chem.* **99,** 13800 (1995).
P. JEWSBURY, S. YAMAMOTO, T. MINATO, M. SAITO and T. KITAGAWA, "The Proximal Residue Largely Determines the CO Distortion in Carbon Monoxy Globin Proteins. An *ab initio* Study of a Heme Prosthetic Unit," *J. Phys. Chem.* **99,** 12677 (1995).
M. NAGAMI, K. IMAI, S. KAMINAKA, Y. MIZUTANI and T. KITAGAWA, "UV Resonance Raman Studies of Quaternary

Structure Changes of Human Hemoglobin Using a Tyrosine α42 Mutant," *J. Inorg. Chem.* **59,** 347 (1995).
T. KITAGAWA, T. OGURA, S. HIROTA, D. A. PROSHLYAOV, K. SHINZAWA-ITOH, S. YOSHIKAWA and E. H. APPELMAN, "Mechanism of Dioxygen Reduction at the Iron-Copper Binuclear Center of Cytochrome *c* Oxidase; Time-Resolved Resonance Raman Study.," *J. Inorg. Chem.* **59,** 284 (1995).
J. S. AHN, T. KITAGAWA, Y. KANEMATSU, Y. NISHIKAWA and T. KUSHIDA, "Glass Transition of Zn-Substituted Myoglobin Probed by Absorption and Site-Selective Fluorescence Spectroscopies," *J. Lumin.* **64,** 81 (1995).
S. MASATOKI, M. TAKAMURA, M. MATSUURA, K. KAMOGAWA and T. KITAGAWA, "Raman Spectroscopic Observations of Anomalous Conformational Behavior of Short Poly(oxyethylene) Chains in Water," *Chem. Lett.* 991 (1995).
T. KOHZUMA, C. DENNISON, W. MCFARLANE, S. NAKASHIMA, T. KITAGAWA, T. INOUE, Y. KAI, N. NISHIO, S. SHIDARA, S. SUZUKI and A. G. SYKES, "Spectroscopic and Electrochemical Studies on Active-Site Transitions of the Type 1 Copper Protein Pseudoazurin from *Achromobacter Cycloclastes*," *J. Biol. Chem.* **270,** 25733 (1995).
Y. HAYASHI, T. KAYATANI, H. SUGIMOTO, M. SUZUKI, A. UEHARA, Y. MIZUTANI, T. KITAGAWA and Y. MAEDA, "Synthesis, Characterization, and Reversible Oxygenation of μ-alkoxo-diiron(II) Complexes with a Dinucleating Ligand, N, N, N', N'-tetrakis{2-(6-methylpyridyl)methyl}-1,3-diaminopropan-2-olate," *J. Am. Chem. Soc.* **117,** 11220 (1995).
S. HIROTA, T. MOGI, Y. ANRAKU, R. B. GENNIS and T. KITAGAWA, "Resonance Raman Study on Axial Ligands of Heme Irons in Cytochrome *bd*-type Ubiquinol Oxidase from *Escherichia coli*.," *Biospectroscopy* **1,** 305 (1995).
P. JEWSBURY and T. KITAGAWA, "The Distal-CO Interaction in Carbonmnooxy Myoglobins: the Molecular Dynamics of 3 Distal Mutants," *Biophys. J.* **68,** 1283 (1995).
S. NAKASHIMA, T. KITAGAWA and J. S. OLSON, "Time-Resolved Resonance Raman Study of the Recombination Dynamics Photodissociated Carbon Monoxide to Sperm Whale Myoglobin and its Mutants," *J. Mol. Liquids* **65/66,** 317 (1995).
D. A. PROSHLYAKOV, T. OGURA, K. SHINZAWA-ITOH, S. YOSHIKAWA and T. KITAGAWA, "Microcirculating System for Simultaneous Determination of Raman and Absorption Spectra of Enzymatic Reaction Intermediates and its Application to the Reaction of Cytochrome *c* Oxidase with Hydrogen Peroxide," *Biochemistry* **35,** 76 (1996).
T. OGURA, S. HIROTA, D. A. PROSHLYAKOV, K. SHINZAWA-ITOH, S. YOSHIKAWA and T. KITAGAWA, "Reduction Mechanism of Respiratory Dioxygen and its Coupling with Proton Pumping Revealed by Time-Resolved Resonance Raman Spectroscopy," *J. Am. Chem. Soc.* **118,** 5443 (1996).
I. FREBORT, P. PEC, L. LUHOVA, H. TOYAMA, K. MATSUSHITA, S. HIROTA, T. KITAGAWA, T. UENO, Y. ASANO, Y. KATO and O. ADACHI, "Two Amine Oxidases from *Aspergillus niger* AKU 3302 Contain Topa Quinone as the Cofactor. Unusual Cofactor Link to the Glutamyl Residue Occurs Only at One of the Enzymes," *Biochim. Biophys. Acta* **1295,** 59 (1996).
M. NAGAI, K. IMAI, S. KAMINAKAA, Y. MIZUTANI and T. KITAGAWA, "Ultraviolet Resonance Raman Studies of Hemoglobin Quaternary Structure Using a Tyrosine α42 Mutant: Changes of $\alpha_1\beta_2$ Subunit Interface upon the T → R Transition," *J. Mol. Struct.* **379,** 65 (1996).
D. A. PROSHLYAKOV, T. OGURA, K. SHINZAWA-ITOH, S. YOSHIKAWA and T. KITAGAWA, "Resonance Raman/ Absorption Characterization of the Oxo-Intermediates of Cytochrome *c* Oxidase Generated in its Reaction with Hydrogen Peroxide: pH and H_2O_2 Concentration Dependence," *Biochemistry* **35,** 8580 (1996).
T. SUZUKI, Y. MARUYAMA, T. KATO, T. AKASAKA, K. YAMAMOTO, H. FUNASAKA and T. TAKAHASHI, "Chemical Reactivities of the Metallofullerene: EPR Study of Diphenylmethano-La@C_{82} Radicals," *J. Am. Chem. Soc,* **117,** 9606 (1995).
T. AKASAKA, S. NAGASE, K. KOBAYASHI, T. SUZUKI, T. KATO, K. KIKUCHI, Y. ACHIBA, K. YAMAMOTO, H. FUNASAKA and T. TAKAHASHI, "Synthesis of the First Adducts of the Dimetallofullerenes $La_2@C_{80}$ and $Sc_2@C_{84}$ by Addition of a Disilirane," *Angew. Chem. Int. Ed. Engl,* **34,** 2139 (1995).
T. SUZUKI, Y. MARUYAMA, T. KATO, K. KIKUCHI, Y. NAKAO, Y. ACHIBA, K. KOBAYASHI and S. NAGASE, "Electrochemistry and Ab Initio Study of the Dimetallofullerene $La_2@C_{80}$," *Angew. Chem. Int. Ed. Engl,* **34,** 1094 (1995).
T. AKASAKA, T. KATO, S. NAGASE, K. KOBAYASHI, K. YAMAMOTO, H. FUNASAKA and T. TAKAHASHI, "Chemical Derivatization of Endohedral Metallofullerene La@C_{82} with Digermirane," *Tetrahedron* **52,** 5015 (1996).
T. S. KIM, Y. S. CHOI and K. YOSHIHARA, "Fluorescence Lifetimes of the van der Waals Clusters of Octatetraene (S_1)-Rare-Gas Atoms:External Heavy Atom Effect," *Chem. Phys. Lett.* **247,** 541 (1995).
K. TOMINAGA, G. P. KEOGH and K. YOSHIHARA, "Liquid Dynamics Studied by Higher Order Non-Linear Optical Spectroscopy ," *J. Mol. Liq.* **65/66,** 398 (1995).
K. YOSHIHARA, Y. NAGASAWA, A. YARTZEV, A. E. JOHNSON and K. TOMINAGA, "Solvent and Nuclear Dynamic Effects on Intermolecular Electron Transfer," *J. Mol. Liq.* **65/66,** 59 (1995).
E. V. SLOBODCHIKOV, J. MA and K. YOSHIHARA, "High-Power and High-Repetition Rate Femtosecond Chromium-Doped Forsterite Laser," *Rev. Laser Engin.* **23,** 1090 (1995).
E. V. SLOBODCHIKOV, J. MA, V. KAMALOV, K. TOMINAGA and K. YOSHIHARA, "Cavity-Dumped Femtosecond Kerr-Lens Mode Locking in a Chromium Forsterite Laser," *Opt. Lett.* **21,** 354 (1996).
M. J. E. MORGENTHALER, K. YOSHIHARA and S. R. MEECH, "Red-Edge Excitation Fluorescence Study of the Inhomogeneous Broadening of Electronic Transitions in Solution," *J. Chem. Soc. Faraday Trans.* **93,** 629 (1996).
K. TOMINAGA and K. YOSHIHARA, "Temporally Two-Dimensional Femtosecond Spectroscopy of Binary Mixture of CS_2," *J. Chem. Phys.* **104,** 1159 (1996).
K. TOMINAGA and K. YOSHIHARA, "Fifth-Order Nonlinear Spectroscopy on the Low-Frequency Modes of Liquid CS_2," *J. Chem. Phys.* **104,** 4419 (1996).
H. PAL, Y. NAGASAWA, K. TOMINAGA and K. YOSHIHARA, "Deuterium Isotope Effect on Ultrafast Intermolecular Electron Transfer," *J. Phys. Chem.* **100,** 11964 (1996).
M. IWAKI, S. KUMAZAKI, K. YOSHIHARA, T. ERABI and S. ITOH, "ΔG_0 Dependence of the Electron Transfer Rate in Photosynthetic Reaction Center of Plant Photosystem I: Natural Optimization of Reaction between Chlorophyll *a* (A_0)

and Quinone," *J. Phys. Chem.* **100,** 10802 (1996).
V. F. KAMALOV, I. A. STRUGANOVA and K. YOSHIHARA, "Temperature Dependent Radiative Lifetime of J-Aggregates," *J. Phys. Chem.* **100,** 8640 (1996).
J. M. REHM, G. L. McLENDON, Y. NAGASAWA, K. YOSHIHARA, J. MOSER and M. GRAETZEL, "Femtosecond Electron-Transfer Dynamics at a Sensitizing Dye-Semiconductorn(TiO_2) Interface," *J. Phys. Chem.* **100,** 9577 (1996).
S. A. P. MERRY, S. KUMAZAKI, Y. TACHIBANA, D. M. JOSEPH, G. PORTER, K. YOSHIHARA, J. R. DURRANT and D. KLUG, "Sub-picosecond Equilibration of Excitation Energy in Isolated Photosystem II Reaction Centers Revisited: Time-Dependent Anisotropy," *J. Phys. Chem.* **100,** 10469 (1996).
K. OHTA, Y. NAITOH, K. SAITOW, K. TOMINAGA, N. HIROTA, and K. YOSHIHARA, "Ultrafast Dynamics of the Photoexcited trans-1,3,5-Hexatriene in Solution by Femtosecond Transient Absorption Spectroscopy," *Chem. Phys. Lett.* **256,** 629 (1996).
K. TOMINAGA and K. YOSHIHARA, "Overtone Vibrational Dephasing in Liquids Studied by Femtosecond Fifth-Order Nonlinear Spectroscopy," *Phys. Rev. Lett.* **76,** 987 (1996).
T. HAYASHI, T. MIYAHARA, S. KUMAZAKI, H. OGOSHI and K. YOSHIHARA, "Intermolecular Photoinduced Electron Transfer between Multifunctional Porphyrin and Ubiquinone Analogues Linked by Multi-Hydrogen Bonding Interaction," *Angew. Chem.* **35,** 1964 (1996).
S. KUMAZAKI, D. M. JOSEPH, B. CRYSTALL, Y. TACHIBANA, J. R. DURRANT, J. BARBER, G. PORTER, K. YOSHIHARA and D. R. KLUG, "Experimantal Observation of Multiple Trapping/charge Separation Steps in the Isolated PS2 Reaction Centre," in *Photosynthsis:from Light to Biosphere*, Vol. *1*, P. Mathis Ed., Kluwer Acdemic Publ. Dordrecht, p.883 (1995).
M. IWAKI, S. KUMAZAKI, K. YOSHIHARA, T. ERABI and S. ITOH, "ΔG Dependence of the Rate Constant of $P700^+A_0^-$ -- $P700^+Q^-$ Reaction in the Quinone-Reconstracted PSI Reaction Center," in *Photosynthsis:from Light to Biosphere*, Vol. *2*, P. Mathis Ed., Kluwer Acdemic Publ. Dordrecht, p.147 (1995).
K. YOSHIHARA, H. PAL, H. SHIROTA, Y. NAGASAWA and K. TOMINAGA, "Femtosecond Intermolecular Electron Transfer: Towards Better Understanding of the Role of Vibrational Motions," in *Femtochemistry: Chemistry and Physics of Ultrafast Processes in Molecular Media*, M. Chergui Ed., World Scientific, p. 540 (1996).
K. SAITOW, Y. NAITOH, K. TOMINAGA and K. YOSHIHARA, "Photoinduced Reactions of CH_2I_2 in Solution Studied by the Ultrafast Transient Absorption Spectrocopy," *Chem. Phys. Lett.* **266,** 621 (1996).
K. TOMINAGA, "Temporally One- and Two-Dimensional Spectroscopies on Overtone Vibrational Dephasing of Liquids," in "Ultrafast Phenomena X," P. F. Barbara, J. G. Fujimoto, W. H. Knox and W. Zinth Eds, Springer-Verlag, p.298 (1996).
K. OHTA, Y. NAITOH, K. TOMINAGA, N. HIROTA and K. YOSHIHARA, "The Photochemical Dynamics of trans -1, 3, 5 - Hexatriene in Solution Investigated by the Ultrafast Transient Absorption Spectroscopy," in "Ultrafast Phenomena X," P. F. Barbara, J. G. Fujimoto, W. H. Knox and W. Zinth Eds, Springer-Verlag, p.262 (1996).
K. YOSHIHARA, H. PAL, H. SHIROTA, Y. NAGASAWA and K. TOMINAGA, "Ultrafst Dynamics in Intermolecular Electron Transfer," in "Ultrafast Phenomena X," P. F. Barbara, J. G. Fujimoto, W. H. Knox and W. Zinth Eds, Springer-Verlag, p.227 (1996).
D. R. KING, J. R. DURRANT, D. M. JOSEPH, S. KUMAZAKI, S. MERRY, L. BARTER, K. YOSHIHARA, J. BARBER and G. PORTER, "Observation of an Intermediate Step During Primary Charge Separation bt Photosystem Two," in "Ultrafast Phenomena X," P. F. Barbara, J. G. Fujimoto, W. H. Knox and W. Zinth Eds, Springer-Verlag, p.342 (1996).
H. KATO, K. SAWABE and Y. MATSUMOTO, "Adsorbed States and Thermal Reactions of N_2O on Si(100) below Room Temperature: Desorption Induced by Dissociation," *Surf. Sci.* **351,** 43 (1996).
Y. A. GRUZDKOV, K. WATANABE, K. SAWABE and Y. MATSUMOTO, "Photochemistry of Methane on a Deuterium Covered Pt(111) Surface," *Surf. Sci.* **363,** 195 (1996).
K. WATANABE, M. C. LIN, Y. A. GRUZDKOV and Y. MATSUMOTO, "Mechanism for the Desorption of Molecularly and Dissociatively Adsorbed Methane on Pt(111) Probed by Pulse-Laser Heating," *J. Chem. Phys.* **104,** 5974 (1996).
K. WATANABE, K. SAWABE and Y. MATSUMOTO, "Adsorbate-Localized Excitation in Surface Photochemistry: Methane on Pt(111)," *Phys. Rev. Lett.* **76,** 1751 (1996).
Y. MATSUMOTO, Y. A. GRUZDKOV, K. WATANABE and K. SAWABE, "Laser-Induced Photochemistry of Methane on Pt(111) : Excitation Mechanism and Dissociation Dynamics," *J. Chem. Phys.* **105,** 4775 (1996).
I. KINOSHITA, T. ANAZAWA and Y. MATSUMOTO, "Surface and Image-Potential States on Pt(111) Probed by Two- and Three-Photon Photoemission," *Chem. Phys. Lett.* **259,** 445 (1996).
V. K. VANAG and I. HANAZAKI, "The pH Dependence of the Belousov-Zhabotinsky Reaction in Water-in-Oil Reverse Microemulsion of AOT in Octane," *J. Phys. Chem.*, **100,** 10609 (1996).
N. TANAKA, M. TAKAYANAGI and I. HANAZAKI, "Nascent Rotational and Vibrational Distribution in ^{16}OH and ^{18}OH produced in the Reaction of $O(^1D)$ with $H_2{}^{18}O$," *Chem. Phys. Letters*, **254,** 40 (1996).
M. TAKAYANAGI and I. HANAZAKI, "Internal Rotation of the Methyl Group in the *m*-Tolunitrile·Rare Gas Complexes," *J. Phys. Chem.*, **100,** 10037 (1996).
A. KAMINAGA, G. RÁBAI, Y. MORI and I. HANAZAKI, "Photo-Response of the Ferrocyanide-Bromate-Sulfite Chemical Oscillator under the Flow Condition," *J. Phys. Chem.* **100,** 9389 (1996).
G. RÁBAI and I. HANAZAKI, "pH Oscillations in the Bromate-Sulfite-Marble Semibatch and Flow Systems," *J. Phys. Chem.* **100,** 10615 (1996).
N. OKAZAKI, Y. MORI and I. HANAZAKI, "Photoinduced Bifurcation and Multistability in the Oscillating Briggs-Rauscher Reaction," *J. Phys. Chem.* **100,** 14941 (1996).
G. RÁBAI and I. HANAZAKI, "Chaotic pH Oscillations in the Sulfur(IV)-Hydrogen Peroxide-Marble Flow System," *J. Phys. Chem.* **100,** 15454 (1996).

I. HANAZAKI and G. RÁBAI, "Origin of Chemical Instability in the Bromate-Sulfite Flow System," *J. Chem. Phys.* **105,** 9912 (1996).
G. RÁBAI, A. KAMINAGA and I. HANAZAKI, "Chaotic pH Oscillations in the Hydrogen Peroxide-Sulfite-Ferrocyanide-Hydrogen Carbonate Flow System," *Chem. Commun.* 2181 (1996).
G. RÁBAI, A. KAMINAGA and I. HANAZAKI, "Mechanism of the Oscillatory Bromate Oxidation of Sulfite and Ferrocyanide in a CSTR. A Comment," *J. Phys. Chem.* **100,** 16441 (1996).
Y. MO, H. KATAYANAGI and T. SUZUKI, "223 nm Photodissociation of OCS: Two Components in $S(^1D_2$ and $^3P_2)$ Channels," *Chem. Phys. Lett.* **247,** 571 (1995).
N. HASHIMOTO and T. SUZUKI, "Energy and State Dependence in the Quenching and Predissociation of C_2H_2," *J. Chem. Phys.* **104,** 6070 (1996).
S. W. NORTH, T. J. SEARS, G. E. HALLA and T. SUZUKI, "Comment on "Energy Partitioning in Photodissociation of methyl. ethyl, and *n*-propyl iodides at 304 nm," *Chem. Phys.* 211, 515 (1996).
Y. MO. H. KATAYANAGI, M. C. HEAVEN and T. SUZUKI, "Simultaneous Measurement of Recoil Velocity and Alignment of $S(^1D_2)$ Atoms in Photodissociation of OCS," *Phys. Rev. Lett.* **77,** 830 (1996).
T. SUZUKI, H. KATAYANAGI, Y. MO and K. TONOKURA, "Evidence for Multiple Dissociation Components and Orbital Alignment in 205 nm Photodissociation of N_2O," *Chem. Phys. Lett.* **256,** 90 (1996).
T. SHIBATA and T. SUZUKI, "Photofragment Ion Imaging with Femtosecond Laser Pulses," *Chem. Phys. Lett.* **262,** 115 (1996).
M. FUKUSHIMA and K. OBI, "Laser Induced Fluorescence Spectra of Jet Cooled *p*-Chlorobenzyl Radical," *Chem. Phys. Lett.* **248,** 264 (1996).
T. SEKIGUCHI, H. IKEURA, K. TANAKA and K. OBI, "Kinetic Energy Released Distributions of Ions Desorbed from H_2O/Si (100) Adsorbtion System by O1s Excitaion," *J. Electron Spect.* **80,** 65 (1996).
A. KAWAI, A. AOKI, Y. KOBORI and K. OBI, "Time-Resolved ESR Studies on Ketyl Type Radical-Amine Complexes," *J. Phys. Chem.* **100,** 10021 (1996).
Y. KOBORI, M. MITSUI, A. KAWAI and K. OBI, "Absolute Magnitude of Spin Polarization in the Radical-Triplet Pair Mechanism: CIDEP Generation by Level Crossings in a Triplet-Doublet Interaction," *Chem. Phys. Lett.* **252,** 355 (1996).
M. FUKUSHIMA, K. SAITO and K. OBI, "Jet Spectroscopy of the $D_1\,2^2B_1$ - $D_0 1^2B_1$ Transition of the *p*-Cyanobenzyl Radical," *J. Mol Spectrosc.* **248,** 264 (1996).
H. SATO, Y. HORIKI and O. ITO, "Laser Ablation-Molecular Beam (LAMB) Method: Coordination (Solvation) Chemistry of Monopositive Metal Ions in the Gas Phase," *J. Photochem. Photobiol., A Chem.* **92,** 17 (1995).
S. NISHIO, T. CHIBA, A. MATSUZAKI and H. SATO, "Control of Structures of Deposited Polymer Films by Ablation Laser Wavelength: Polyacrylonitrile at 308, 248, and 193 nm," *J. Appl. Phys.* **79,** 7198 (1996).
H. SHINOHARA, M. TANSHO, M. INAKUMA, Y. SAITO, H. SATO, N. HAYASHI, T. KATO, T. HASHIZUME and T. SAKURAI, "Structures and Dynamics of Endohedral Scandium Metallofullerenes," *Surf. Rev. Lett.* **3,** 799 (1996).
H. SATO, A. MATSUZAKI, S. NISHIO, Y. HORIKI and O. ITO, "Reactions of Monovalent Metal Ions (M^+) with Mixed Molecular Clusters like $(NH_3)_m(H_2O)_n$ As Studied by Laser Ablation-Molecular Beam (LAMB) Method. Preferred or Nonspecific Coordination," *Surf. Rev. Lett.* **3,** 671 (1996).
H. SATO, A. MATSUZAKI, S. NISHIO, M. YOSHIMI, K. YAMAMOTO and H. TOMIOKA, "A Raman Spectroscopic Study of Merocyanine Aggregates of a ^{15}N-Isotopomer of 6-Nitro-1',3',3'-trimethylspiro[2H-1-benzopyran-2,2'-indoline]. A Direct Evidence for the Association through the NO_2-Bridges," *Chem. Lett.* 715 (1996).
Y. TEKI, Y. TAJIMA, K. ITOH, S. UENO, Y. KITAGISHI and Y. MIURA, "Ferro- and Antiferromagnetic Behaviors of Stable Free Radical Crystals of *N*-(Arylthio)-2,4,6-triarylphenylaminyls," *Mol. Cryst. Liq. Cryst.*, **278,** 301 (1996).
Y. MIURA, M. MOMOKI, T. FUCHIKAMI, Y. TEKI, K. ITOH and H. MIZUTANI, "Exceptionally Persistent Nitrogen-Centered Free Radicals. Syntheses, ESR Spectra, Isolation, and X-ray Crystallographic Structures of *N*-(Arylthio)-2-*tert*-butyl-4,6-diarylphenylaminyl and *N*-(Arylthio)-4-*tert*-butyl-2,6-diarylphenylaminyl Radicals," *J. Org. Chem.*, **61,** 4300 (1996).
H. ARAKI, A. A. ZAKHIDOV, J. SAIKI, N. YAMAZAKI, K. YAKUSHI and K. YOSHINO, "Superconductivity in Conducting Polymer-Fullerene Composite Doped by Alkali Metal," *J. J. Appl. Phys.*, **34,** L1041 (1995).
A. A. ZAKHIDOV, H. ARAKI, K. TADA, K. YAKUSHI and K. YOSHINO, "Granular Superconductivity in "Conducting Polymer-Fullerene-Alkali Metal" Composite," *Physics Lett. A*, **205,** 317-326 (1995).
J. DONG, K. YAKUSHI, Y. YAMASHITA, "Spectroscopic Study of BDNT and its Monocation and Dication Salts," *J. Mater. Chem.*, **5,** 1735 (1995).
J. DONG, K. YAKUSHI, Y. YAMASHITA, K. IMAEDA and H. INOKUCHI, "Electronic and Vibronic Structure of Organic Charge-Transfer Salt, *m*-BDNT-PF_6," *phys. stat. sol. (b)* **195,** 611 (1996).
V. N. DENISOV, A. N. IVLEV, B. N. MAVRIN, K. YAKUSHI, J. DONG and Y. YAMASHITA, "Resonant Raman Scattering in Single Crystals of BDNT, $BDNT^+$, and $BDNT^{2+}$," *Chem. Phys. Lett.*, **246,** 176 (1995).
K. YAKUSHI, J. DONG, M. URUICHI and Y. YAMASHITA, "Spectroscopic Studies on BDNT Having a Property of One-Step Two-Electron Oxidation: $BDNT^0$, $BDNT^{1+}$, and $BDNT^{2+}$," *Mol. Cryst. Liq. Cryst.*, **284,** 223 (1996).
K. YAKUSHI, T. HIEJIMA and H. YAMAKADO, "π-d Interaction in Phthalocyanine Conductors," "*Materials and Measurements in Molecular Eelectronics*" ed. by K. Kajimura and S. Kuroda, Springer Proceedings in Physics 81, p.203 (1996).
E. FRANKEVICH, A. A. ZAKHIDOV, K. YOSHINO, Y. MARUYAMA and K. YAKUSHI, "Photoconductivity of Poly(2,5-diheptyloxy-p-phenylene vinylene) in the Air Atmosphere. Magnetic Field Effect and mechanism of Generation and Recombination of Charge Carriers," *Phys. Rev B* **53,** 4498 (1996-II).
M. E. KOZLOV, V. A. IVANOV and K. YAKUSHI, "A Key to the Understanding of Electron-Molecular Vibration Coupling in Organic Charge-Transfer Salts: Application of the Two-Side Hubbard Model," *J. Phys.: Condens. Matter* **8,** 1011(1996).

N. YAMASAKI, H. ARAKI, A. A. ZAKHIDOV, H. MISOBUCHI, K. YAKUSHI and K. YOSHINO, "A New Metastable Superconductor $Li_2Na_2N_yC_{60}$ Prepared from Azides," *Physica C*, **259,** 265 (1996).
H. ARAKI, A. A. ZAKHIDOV, K. TADA, K. YAKUSHI, K. YOSHINO, "Alkali-Metal Doping of Fullerene-Conducting Polymer Composite: Evolution of Conductivity and ESR," *Synthetic Metals*, **77,** 291 (1996).
K. YOSHINO, A. A. ZAKHIDOV, H. KAJII, H. ARAKI, K. TADA, T. NOGUCHI, T. OHNISHI, K. YAKUSHI, "Multiphase Superconductivity in OO-PPV/C60 Composite Doped by Alkali Metals. Low-Field Microwave Absorption and SQUID Study," *Physica C*, **264,** 161 (1996).
A. OTSUKA, G. SAITO, T. TERAMOTO, Y. SUGITA, T. BAN, A. A. ZAKHIDOV and K. YAKUSHI, "A Search for New Ionic C_{60} Charge Transfer Complexes," *Mol. Cryst. Liq. Cryst.*, **284,** 345 (1996).
T. YOKOYAMA, K. KOBAYASHI, T. OHTA and A. UGAWA, "Anharmonic Interatomic Potentials of Diatomic and Linear Triatomic Molecules Studied by Extended X-ray-Absorption Fine Structure," *Phys. Rev.* **B53,** 6111 (1996).
T. YOKOYAMA, Y. YONAMOTO, T. OHTA and A. UGAWA, "Anharmonic Interatomic Potentials of Octaheadral Pt-halogen Complexes Studied by Extended X-ray-Absorption Fine Structure," *Phys. Rev.* **B54,** 6921 (1996).
I. SHIROTANI, K. TACHI, K. TAKEDA, S. TODO, T. YAGI and K. KANODA, "Superconductivity of ZrRuSi Prepared at High Pressure," *Phys. Rev.* **B52,** 6197 (1995).
Y. NAKAZAWA, A. KAWAMOTO and K. KANODA, "Characterization of Low-Temperature Electronic States of Organic Conductors, α-(BEDT-TTF)$_2$MHg(SCN)$_4$ [M=K, Rb and NH_4], by Specific Heat Measurements," *Phys, Rev.* **B52,** 12890 (1995).
A. KAWAMOTO, K. MIYAGAWA, Y. NAKAZAWA and K. KANODA, "Electron Correlation in κ-Phase Family of BEDT-TTF Compounds Studied by ^{13}C-NMR," *Phys. Rev.* **B52,** 15522 (1995).
Y. NAKAZAWA and K. KANODA, "Electronic Structure of Insulating Salts of κ-(BEDT-TTF)$_2$X Family Studied by Low-Temperature Specific Heat Measurements," *Phys. Rev.* **B53,** R8876 (1996).
H. TANIGUCHI, H. SATO, Y. NAKAZAWA and K. KANODA, "Highly Anisotropic Superconductivity in the Layered Organic Conductor, α-(BEDT-TTF)$_2$NH$_4$Hg(SCN)$_4$," *Phys. Rev.* **B53,** R8879 (1996).
K. KANODA, K. MIYAGAWA, A. KAWAMOTO and Y. NAKAZAWA, "NMR Relaxation Rate in the Superconducting State of the Organic Conductor, κ-(BEDT-TTF)$_2$Cu[N(CN)$_2$]Br," *Phys. Rev.* **B54,** 76 (1996).
V. IVANOV and Y. MARUYAMA, "Disorder and Phonon Windows for Superconductivity in Doped Fullerides," *Physica C* **247,** 147 (1995).
S. BANDOW, Y. MARUYAMA, X. -X. BI, R. OCHOA, J. M. HOLDEN, W. T. LEE and P. C. EKLUND, "Electronic and Vibrational Properties of Rb-intercalated MoS_2 Nanoparticles," *Mat. Sci. Eng.* **A204,** 222 (1995).
T. PASINSZKI, M. AOKI, S. MASUDA, Y. HARADA, N. UENO, H. HOSHI and Y. MARUYAMA, "Characterization of Ultrathin Films of Chloroaluminium Phthalocyanine during Layer-by-Layer Preparation on Graphite: PIES and UPS Study". *J. Phys. Chem.* **99,** 12858 (1995).
T. SUZUKI, Y. MARUYAMA, T. KATO, T. AKASAKA, K. KOBAYASHI and S. NAGASE, "Chemical Reactivity of a Metallofullerene: EPR Study of Diphenylmethano-La@C_{82} Radicals," *J. Am. Chem. Soc.* **117,** 9606 (1995).
K. AWAGA, T. OKUNO, A. YAMAGUCHI, M. HASEGAWA, T. INABE, Y. MARUYAMA and N. WADA, "Crystal Structures and Magnetic Properties of (*m*-Pyridinium Nitronyl Nitroxide) + X-: Possible Spin-1 Kagome Antiferromagnet," *Synth. Met.* **71,** 1807 (1995).
H. MORI, I. HIRABASHI, S. TANAKA, T. MORI and Y. MARUYAMA, "Organic Conductors with Three-Component System Containing Co, Zn, and Cd Based Upon BEDT-TTF," *Synth. Met.* **70,** 789 (1995).
H. MORI, I. HIRABAYASHI, S. TANAKA, T. MORI and Y. MARUYAMA, "Physical and Chemical Properties of MDSe-TTF and EDSe-TTF Salts," *Synth. Met.* **70,** 877 (1995).
H. MORI, I. HIRABAYASHI, S. TANAKA, T. MORI and Y. MARUYAMA, "Preparation, Properties, and Structures of Planar Anion Complexes," *Synth. Met.* **70,** 1177 (1995).
H. MORI, S. TANAKA, T. MORI and Y. MARUYAMA, "Crystal Structures and Electrical Resistivities of Three-Component Organic Conductors : (BEDT-TTF)$_2$ MM' (SCN)$_4$ [M = K, Rb, Cs ; M' = Co, Zu, Cd]," *Bull. Chem. Soc. Jpn.* **68,** 1136 (1995).
H. GOTO, H. ASAHI, T. INABE, H. OGATA, S. MIYAJIMA and Y. MARUYAMA, "High-Resistance Phase and Low-Resistance Phase in 1,6-Diaminopyrene-*p*-Chloranil (DAP-CHL)," *Synth. Met.* **70,** 1237 (1995).
H. GOTO, T. FUJINAWA, H. ASAHI, T. INABE, H. OGATA, S. MIYAJIMA and Y. MARUYAMA, "Crystal Structures and Physical Properties of 1,6-Diaminopyrene-*p*-Chloranil (DAP-CHL) Charge-Transfer Complex. Two Polymorphs and Their Unusual Electrical Properties," *Bull. Chem. Soc. Jpn.* **69,** 85 (1996).
E. FRANKEVICH, Y. MARUYAMA and H. OGATA, "Laser Pulse Induced Transient Photoconductivity of C_{70} Single Crystal," *J. phys. Chem. Solid* **57,** 483 (1996).
S. L. FANG. H. HOSHI, K. KOHAMA, and Y. MARUYAMA, "Non-Linear Optical Characteristics of Vanadyl Phthalocyanine Thin Film Grown by Molecular-Beam-Epitaxial Method," *J. Phys. Chem.* **100,** 4104 (1996).
E. FRANKEVICH, A. ZAKHIDOV, K. YOSHINO, Y. MARUYAMA and K. YAKUSHI, "Photoconductivity of Poly (2,5-Diheptyloxy-*p*-Phenylene Vinylene) in the Air Atmosphere : Magnetic-Field Effect and Mechanism of Generation and Recombination of Charge Carriers," *Phys. Rev. B***53,** 4498 (1996).
A. KOBAYASHI, A. SATO, K. KAWANO, T. NAITO, H. KOBAYASHI and T. WATANABE, "Origin of the Resistivity Anomalies of (EDT-TTF)[M(dmit)$_2$]," *J. Mater. Chem.* **5,** 1671 (1995).
H. KOBAYASHI, H. TOMITA, T. NAITO, A. KOBAYASHI, F. SAKAI, T. WATANABE and P. CASSOUX, "New BETS Conductors with Magnetic Anions," *J. Am. Chem. Soc.* **118,** 368 (1996).
M. INOKUCHI, H. TAJIMA, T. OHTA, H. KURODA, A. KOBAYASHI, A. SATO, T. NAITO and H. KOBAYASHI, "Electrical Resistivity under High Pressure and Upper Critical Magnetic Field of the Molecular Superconductor α-(EDT-TTF)[Ni(dmit)$_2$]," *J. Phys. Soc. Jpn.* **65,** 538 (1966).
H. TAJIMA, A. KOBAYASHI, Y. OHTA, A. SATO, T. NAITO and H. KOBAYASHI, "Meissner and Diamagnetic Shield-

ing Efect of α-(EDT-TTF)[Ni(dmit)$_2$]," *Syn. Met.* **79,** 141 (1996).
H. TAJIMA, A. KOBAYASHI, T. NAITO and H. KOBAYASHI, "Shubnikov-de Haas EffecAngular-Dependent Magnetoresistance Oscillation of κ-(BETS)$_2$GaCl$_4$," *Solid State Commun.* **48,** 755 (1996).
T. NAITO, H. KOBAYASHI, A. KOBAYASHI and A. E. UNDERHILL, "New Synthetic Metals Based on a Thiadiazole Network," *J. C. S. Chem. Commun.*, 521 (1996).
H. KOBAYASHI, A. KOBAYASHI, H. TANAKA, T. SAITO, M. TOKUMOTO, L. BROSSARD and P. CASSOUX, "New BETS Superconductors and Metals with Tetrahedral Non- Magnetic and Magnetic anions," *Mol. Cryst. Liq. Cryst.* **284,** 61 (1996).
N. KUSH, C. FAULMANN, P. CASSOUX, L. VALADE, I. MALFANT, J. -P. LEGROS, C. BOWLAS, A. ERRAMI, A. KOBAYASHI and H. KOBAYASHI, "Molecular Compounds ExhibitingCcoupled Conducting and Magnetic Properties and Based on (Cation)$_n$[M(dmit)$_2$]$_2$ and (BETS)$_2$(anion) Salts," *Mol. Cryst, Liq. Cryst.* **284,** 247 (1996).
H. OGATA, S. MIYAJIMA, K. MATSUTSUJI and T. ENOKI, "NMR Study of Sodium-Hydrogen-Graphite Ternary Intercalation Compound" *J. Phys. Chem. Solids* **57,** 703 (1996).
H. GOTO, T. FUJINAWA, H. ASAHI, T. INABE, H. OGATA, S. MIYAJIMA and Y. MARUYAMA, "Crystal Structures and Physical Properties of 1,6-Diaminopyrene-*p*-Chloranil (DAP-CHL) Charge Transfer Complex. Two Polymorphs and their Unusual Electrical Properties" *Bull. Chem. Soc. Jpn.* **69,** 85 (1996).
Y. -H. KIM, B. -G. KIM, T. MOCHIDA and S. MIYAJIMA, "Dimensionality Crossover and Nonlinear Dielectric Response in Betaine Phosphate/Arsenate Mixed Crystals" *J. Phys. Condens. Matter*, **8,** 6095 (1996).
Y. -S. CHOI, J. -J. KIM and S. MIYAJIMA, "Diffusive Loss of Surface Adatoms and Surface Enhanced Raman Scattering Intensity" *Chem. Phys. Lett.* **255,** 45 (1996).
T. NAKAI and D. KUWAHARA, "Spinning Sideband Summation for Quadrupole MAS NMR Spectra Using Magic-Angle Turning Technique" *Chem. Phys. Lett.* **249,** 205 (1996).
K. NISHI, H. SEKIYA, H. HAMABE, Y. NISHIMURA, T. MOCHIDA and T. SUGAWARA, "Fluorescence Excitation Spectra of Jet-Cooled 9-Hydroxyphenalenone Derivatives. Effects of Symmetrical Substitution on Deuterium Atom Tunneling" *Chem. Phys. Lett.* **257,** 499 (1996).
K. KAMIYA, M. MOMOSE, Y. HARADA, N. UENO, T. MIYAZAKI, S. HASEGAWA, H. INOKUCHI, S. NARIOKA, H. ISHI and K. SEKI, "Photoelectron Angular Distribution of Thin Films of Copper Phthalocyanine on MoS_2 Surfaces: Quantitative Determination of Molecular Orientation," *Mol. Cryst. Liq. Cryst.* **267,** 211 (1995).
T. MIYAZAKI, H. FUJIMOTO, K. ICHIMURA, K. P. LEE, S. HASEGAWA and H. INOKUCHI, "UPS Study of $NiPS_3$ and $FePS_3$ Crystals Using Synchrotron Radiation," *Chem. Phys.* **201,** 539 (1995).
A. TANAKA, A. CHAINANI, T. YOKOTA, T. TAKAHASHI, T. MIYAZAKI, S. HASEGAWA and T. MORI, "Electronic Structure of the Quasi-one-dimensional Organic Conductors DCNQI (N,N'-dicyanoquinonediimine)-Cu Salts," *Phys. Rev.* **B52,** 7951 (1995).
S. ZHOU, K. ICHIMURA and H. INOKUCHI, "X-ray Photoelectron Spectroscopy Characteristics of a Novel Organic Semiconductor BTQBT and Its Derivatives," *J. Mater. Chem.* **5,** 1725 (1995).
K. IMAEDA, K. YAKUSHI and H. INOKUCHI, "Preparation and Properties of Lithium-doped C_{60} by Lithium Azide," *Fullerene Sci. Tech.* **3,** 545 (1995).
S. HASEGAWA, H. INOKUCHI, K. SEKI and N. UENO, "Angle-resolved Photoemission from Oriented Thin Films of Naphthacene: Comparison with Theoretical Spectra," *J. Electron Spectr. Relat. Phenom.* **78,** 391 (1996).
N. UENO, "Angle-resolved UPS of Ultrathin Films of Functional Organic Molecules with Synchrotron Radiation: Determination of Molecular Orientation by Quantitative Analysis of Photoelectron Angular Distribution," *J. Electron Spectr. Relat. Phenom.* **78,** 345 (1996).
H. INOKUCHI and K. IMAEDA, "Novel Organic Semiconductor BTQBT with High Conductivity and High Mobility," *Acta Physica Polonica A* **88,** 1161 (1996).
K. IMAEDA, J. KRÖBER, H. INOKUCHI, Y. YONEHARA and K. ICHIMURA, "Superconductivity in NaH Intercalated C_{60}," *Solid State Commun.* **99,** 479 (1996).
Y. LI, K. IMAEDA and H. INOKUCHI, "Conductivity Characteristics and Vis-NIR Absorption Spectra of Polypyrrole Films at Higher Temperatures," *Polymer J.* **28,** 559 (1996).
S. OZAWA, E. SAKAMOTO, T. ICHIKAWA, Y. WATANABE and I. MORISHIMA, "Model Studies of Nitrosyl Intermediates in the Catalytic Cycle of Dissimilatory Nitrite Reductases," *Inorg. Chem.* **34,** 6362 (1996).
K. INOUE, T. HAYAMIZU, H. IWAMURA, D. HASHIZUME and Y. OHASHI, "Assemblage of the Electron Spins of the Organic Trinitroxide Radical with a Quartet Ground State by Means of Complexation with Paramagnetic Transition Metal Complexes. A Molecule-Based Magnet with Three-Dimensional Structure and High T_C of 46 K," *J. Am. Chem. Soc.* **118,** 1803 (1996).
K. MATSUDA, N. NAKAMURA, K. INOUE, N. KOGA and H. IWAMURA, "Design and Synthesis of a "Starburst"-Type Nonadiazo Compound and Magnetic Characterization of Its Photoproduct," *Chem. Euro. J.* **2,** 259-264 (1996).
K. MATSUDA, N. NAKAMURA, K. INOUE, N. KOGA and H. IWAMURA, "Toward Dendritic Two-Dimensonal Polycarbenes: Synthesis of 'Starburst'-Type Nona- and Dodecadiazo Compounds and Magnetic Study of their Photoproducts," *Bull. Chem. Soc. Jpn.*, **69,** 1483 (1996).
T. SUGIMOTO, K. UEDA, M. TSUJII, H. FUJITA, N. HOSOITO, N. KANEDA, Y. SHIBAMOTO and Y. KAI, "Ferromagnetic Behavior of a Tetrafluorotetracyanoquinodimethanide Salt at Room Temperature," *Chem. Phys. Lett.* **249,** 304 (1996).
K. UEDA, H. MORIMOTO, T. SUGUMOTO, N. KANEHISA, Y. SHIBAMOTO and Y. KAI, "Crystal Structure and Magnetic Properties of Tetrafluorotetracyanoquinodimethanide Salts," *Mol. Cryst. Liq. Cryst.* **279** , 123 (1996).
K. UEDA, M. TSUJII, T. SUGA, T. SUGIMOTO, N. KANEHISA, Y. KAI and N. HOSOITO, "Remarkably Strong Antiferromagnetic Interaction through an Intervening Hydrogen Atom in *N*-(*n*-Propyl)Pyridinium-substituted Imidazolin-1-oxyl Iodide," *Chem. Phys. Lett.* **253,** 355 (1996).

Y. OZAWA, T. IKUNO, S. AMANO, T. IDA, A. IBARAKI, K. KIMURA and K. TORIUMI, "Electrocrystallization, Crystal Structure, and Solid State Properties of Halogen-Bridged One-Dimensional Compound, $\{[Ni(en)_2Br](ClO_4)_2\}_\infty$, Having an Elongated Ni•••Ni Distance," *Mol. Cryst. Liq. Cryst.* **278,** 189 (1996).
S. HOSOKAWA, T. KOUCHI, I. ONO, M. TANIGUCHI, Y. TAKATA and N. KOSUGI, "A Soft-X-Ray Core Absorption Study on the Electronic States in Ag- and Cu-Photodissolved Amorphous $GeSe_2$ Using Synchrotron Radiation," *J. Phys.: Condens. Matter* **8,** 1607 (1996).
M. NAKAMURA, Y. TAKATA and N. KOSUGI, "Resonant Ni 3p and 3s Photoemission for the Ni 2p Core-Excitation in NiO," *J. Electron Spectrosc. Relat. Phenom.* **78,** 115 (1996).
K. UEDA, Y. SHIMIZU, H. CHIDA, M. OKUNISHI, K. OHMORI, Y. SATO, E. SHIGEMASA and N. KOSUGI, "C1s and F 1s Photoabsorption and Subsequent Electronic Decay of CH_4, CH_3F, CH_2F_2, CHF_3, and CF_4," *J. Electron Spectrosc. Relat. Phenom.* **79,** 441 (1996).
N. KOSUGI, "Molecular Symmetries and Vibrations in High-Resolution Inner-Shell Spectroscopy," *J. Electron Spectrosc. Relat. Phenom.* **79,** 351 (1996).
S. NAOE, K. FUKUI, H. ABE, M. WATANABE, A. HIRAYA, N. KOSUGI, Y. TAKAKTA, "L_3 Absorption Spectrum of Germanium Single Crystal", *J. Electron Spectrosc. Relat. Phenom.* **79,** 5 (1996).
H. OJI, R. MITSUMOTO, E. ITO, H. ISHII, Y. OUCHI, K. SEKI and N. KOSUGI, "Core Hole Effect in NEXAFS Spectroscopy of Aromatic Hydrocarbons: Chrysene, Perylene and Coronene," *J. Electron Spectrosc. Rel. Phenom.* **78,** 383 (1996).
T. YOKOYAMA, S. TERADA, A. IMANISHI, Y. KITAJIMA, N. KOSUGI and T. OHTA, "Adsorption of SO_2 on Ni(100) and Ni(111) Surfaces", *J. Electron Spectrosc. Relat. Phenom.* **80,** 161 (1996).
J. ADACHI, N. KOSUGI, E. SHIGEMASA, A. YAGISHITA and P. A. HATHERLY, "Angular Correlation between Fragment Ions from the Nitrogen *K*-shell Excited and Ionized N_2O," *J. Electron Spectrosc. Relat. Phenom.* **79,** 491 (1996).
N. KOSUGI, K. UEDA, Y. SHIMIZU, H. CHIDA, M. OKUNISHI, Y. SATO, E. SHIGEMASA, "Rydberg and Valence States in the C 1s Photoabsorption and Resonance Auger Spectra of CH_3F," *Chem. Phys. Letts.* **246,** 475 (1995).
J. T. FRANCIS, C. C. TURCI, T. TYLISZCZAK, G. G. B. DE SOUZA, N. KOSUGI and A. P. HITCHCOCK, "Electron-Impact Core Excitation of SF_6. I. S 2*p*, S 2*s*, and F 1*s* Spectroscopy," *Phys. Rev. A* **52,** 4665 (1995).
A. YOSHIGOE, K. MASE, Y. TSUSAKA, T. URISU, Y. KOBAYASHI and T. OGINO, "*In Situ* Observation of Silicon Hydrides on Si(100) Surfaces During Synchrotron-Radiation-Stimulated Si_2H_6 Gas Source Molecular Beam Epitaxy, "*Appl. Phys. Lett.* **67,** 2364 (1995).
A. YOSHIGOE, M. NAGASONO, K. MASE and T. URISU, "Synchrotron Radiation Irradiation Effects for SiH_n on Si(100) Surface in the Synchrotron Radiation Stimulated Si Gas Source Molecular Beam Epitaxy, "*Jpn. J. Appl. Phys.* **34,** 6894 (1995).
Y. PARK, S. RHEE, Y. IMAIZUMI and T. URISU, "Effect of SR Irradiation on SiO_2 Thin Film, "*J. Korean Vac. Soci.* **4,** 156 (1995).
S. SATO, S. MINOURA, T. URISU and Y. TAKASU, "IRAS and TDS Study on the Photolytic Decarbonylation of Iron Pentacarbonyl Adsorbed on a SiO_2 Film with a Buried Metal Layer," *Appl. Surf. Science* **90,** 29 (1995).
S. I. GHEYAS, T. OGATA, M. NISHIO, T. URISU and H. OGAWA, "Synchrotron Radiation Assisted Surface Processes of Diethylzinc on GaAs(100)," *Jpn. J. Appl. Phys.* **34,** 6886 (1995).
Y. IMAIZUMI, Y. TSUSAKA and T. URISU, "Synchrotron Radiation Irradiation Effects on Low-temperature Condensed Layer of Dimethyl Aluminum Hidride on SiO_2," *J. Electron Spectroscopy and Related Phenomena* **80,** 93 (1996).
J. OHARA, Y. GOTO, M. NAGASONO, T. KURAHASHI, T. HATTORI and T. URISU, "Metallization on Piezoelectric Ceramics Surfaces by Synchrotron Radiation Irradiation," *J. Electron Spectroscopy and Related Phenomena* **80,** 81 (1996).
K. MASE, M. NAGASONO, T. URISU and Y. MURATA, "Development of Electron-Ion Coincidence Spectroscopy for the Study of Surface Dynamics," *Bull. Chem. Soc. Jpn.* **69,** 1829 (1996).
M. NAGASONO, K. MASE and T. URISU, "Auger Electron-Ion Coincidence Study for H_2O Adsorbed on SiO_2/Si(100) at 80 K," *Surface Sci.* **363,** 342 (1996).
T. URISU, A. YOSHIGOE and Y. IMAIZUMI, "Synchrotron Radiation-Stimulated Semiconductor Process and New Prospects of Core Electron Excitation Photochemistry," *Optoelectronics -Devices and Technologies-* **11,** 57 (1996).
K. MITSUKE, Y. HIKOSAKA, T. HIKIDA and H. HATTORI, "Autoionization of NO in an Excited Valence State Affected by Perturbations from Valence-Rydberg Mixing," *J. Electron Spectrosc. Rel. Phenom.* **79,** 395 (1996).
H. YOSHIDA and K. MITSUKE, "Positive Ion-Negative Ion Coincidence Spectroscopy of CO_2 for Observation of Doubly Excited Rydberg States," *J. Electron Spectrosc. Rel. Phenom.* **79,** 487 (1996).
H. HATTORI and K. MITSUKE, "Autoionization of Acetylene Studied by Two-Dimensional Photoelectron Spectroscopy," *J. Electron Spectrosc. Rel. Phenom.* **80,** 1 (1996).
T. HIRAYAMA, T. NAGAI, M. ABO, I. ARAKAWA, K. MITSUKE and M. SAKURAI, "Excitonic Energy Transfer Process in Ne-Kr Alloy Studied by Photon Stimulated Desorption of Metastable Atoms," *J. Electron Spectrosc. Rel. Phenom.* **80,** 101(1996).
T. N. OLNEY, C. E. BRION and T. IBUKI, "Absolute Photoabsorption of BrCN in the Valence Shell and the Bromine M, Carbon K and Nitrogen K Shell Regions (5-450 eV)," *Chem. Phys.* **201,** 505 (1995).
T. IBUKI, A. HIRAYA, T. N. OLNEY and C. E. BRION, "Ionic Photofragmentation (11.5-160 eV) and PIPICO Spectroscopy (40-130 eV) of BrCN in the Valence Shell and Bromine 3*d* Regions," *Chem. Phys.* **203,** 359 (1996).
H. HOSONO, H. UN'NO, N. UEDA, H. KAWAZOE, N. MATSUNAMI and H. TANOUE, "Conversion of insulating thin films of $MgIn_2O_4$ into transparent conductors by ion implantation," *Nuclear Instruments and Methods in Physics Research B* **106,** 517 (1995).

H. MIZOGUCHI, H. KAWAZOE, T. UEDA, S. HAYASHI, H. HOSONO and N. UEDA, "Formation and Optical Absorption Spectra of Mixed Valence State of Tl in $Tl_2Nb_2O_{6+x}$ with Pyrochlore Structure," *Bull. Chem. Soc. Jpn.* **69,** 111 (1996).

K. KAWAMURA, H. HOSONO, H. KAWAZOE, N. MATSUNAMI and Y. ABE, "Large Enhancement of Electrical Conductivity in Magnesium Phosphate Glasses by Ion Implantation of Proton," *J. Ceram. Soc. Jpn.* **104,** 688 (1996).

H. HOSONO, M. MIZUGUCHI, H. KAWAZOE and J. NISHII, "Correlation between Ge E' Centers and Optical Absorption Bands in SiO_2:GeO_2 Glasses," *Jpn. J. Appl. Phys.* **35,** 234 (1996).

H. HOSONO, H. TANOUE, S. HISHITA and A. NAKAMURA, "Formation and Optical Properties of Nanometer-Sized Amorphous Arsenic Clusters Embedded in Amorphous SiO_2 by Ion Implantation," *Nuclear Instruments and Methods in Physics Research,* **116,** 178 (1996).

H. HOSONO, H. KAWAZOE and J. NISHII, "Defect Formation in SiO_2:GeO_2 Glasses Studied by Irradiation with Excimer Laser Light," *Phys. Rev. B* **53,** R11921 (1996).

H. HOSONO, K. KAWAMURA, H. KAWAZOE and J. NISHII, "Nanometer-Scale Heterogeneity in SiO_2-GeO_2 Glass Preforms and Fibers Prepared by Vapor Phase Axial Deposition Method," *J. Appl. Phys.* **80,** 1463 (1996).

T. OMATA, H. IKAWA, S. FUJITSU, N. UEDA, H. HOSONO and H. KAWAZOE, " Optical Absorption Spectra and the Nature of Conduction Carriers of Hole-Doped $Sr_{1+x}La_{1-x}FeO_4$," *Solid Sate Commun.* **97,** 411 (1996).

T. OMATA, T. KAWANO, H. IKAWA, T. SASAMOTO, H. HOSONO, H. MIZOGUCHI and H. KAWAZOE, "Electronic Transport Properties of Hole-Doped $Sr_{1+x}La_{1-x}Cr_{4+\delta}$," *J. Ceram. Soc. Jpn,* **103,** 1112 (1995).

H. MIZOGUCHI, H. HOSONO, N. UEDA and H. KAWAZOE, "Preparation and Electrical Properties of Bi_2S_3 Whiskers," *J. Appl. Phys.*, **78,** 1376 (1996).

M. HAGA, M. M. ALI and R. ARAKAWA, "Proton-Induced Switching of Electron Transfer Pathways in Dendrimer-Type Tetranuclear $RuOs_3$ Complexes," *Angew. Chem. Int. Ed. Engl.* **35,** 76 (1996).

M. HAGA, M. M. ALI, S. KOSEKI, K. FUJIMOTO, A. YOSHIMURA, K. NOZAKI, T. OHNO, K. NAKAJIMA and D. J. STUFKENS, "Proton-Induced Tuning of Electrochemical and Photophysical Properties in Mononuclear and Dinuclear Ruthenium Complexes Containing 2,2'-Bis(benzimidazol-2-yl)-4,4'-bipyridine: Synthesis, Molecular Structure, and Mixed-Valence State and Excited-State Properties," *Inorg. Chem.* **35,** 3335 (1996).

R. ARAKAWA, G. MATSUBAYASHI, N. OHASHI, S. FURUUCHI, T. MATSUO and M. M. ALI and M. HAGA, "Electrospray and Collision-Induced Dissociation Mass Analysis of Star-burst Type Tetranuclear Complexes," *J. Mass Spectrom.* **31,** 861 (1996).

R. ARAKAWA, T. MATSUO, K. NOZAKI, T. OHNO and M. HAGA, "Analysis of Multiply Charged Ions of Ruthenium(II) Tetranuclear Complexes by Electrospray Ionization Mass Spectrometry", *Inorg. Chem.* **34,** 2464 (1995).

H. MONJUSHIRO and I. WATANABE, "Probing Depth of Ultraviolet Photoelectron Yield Spectroscopy in Hydrocarbon Films," *Anal. Sci.* **11,** 797 (1995).

T. ICINOSE, H. MONJUSHIRO and H. WATARAI, "Charge-up Phenomena of Insulated Metals in X-ray Photoelectron Spectroscopy," *Anal. Sci.* **12,** 43 (1996).

H. MONJUSHIRO, K. MIZUGUCHI and Y. YOKOYAMA, "Measurement of Photoacoustic Spectra with Improved Resolution and Its Application to Uranyl Complexes," *Anal. Sci.* **11,** 841-842 (1995).

M. HAGA, K. HIRATSUKA, M. KATO, H. KUROSAKI, M. GOTO, R. ARAKAWA and S. YANO, "Self-assembled Dinuclear Platinum(II) Complexes with 6,6'-Bis(1-methylbenzimidazol-2-yl)-2,2'-bipyridine:Synthesis, X-ray Structure, and Solution Behaviors," *Chem. Lett.* 1143 (1995).

H. NAGASHIMA, M. SAITO, Y. KATO, H. GOTO, E. OSAWA, M. HAGA and K. ITOH, "Electronic Structures and Redox Properties of Silylmethylated C_{60}," *Tetrahedron,* **52,** 5053 (1996).

T. SAKURAI, "Restrained Reduction of Type 3 Copper in Laccase and Ascorbate Oxidase by Azide", *Biochem. (Life Sci. Adv.)* **14,** 17(1995).

T. SAKURAI and J. TAKAHASHI, "EPR Spectra of Type 3 Copper Centers in *Rhus vernicifera* Laccase and *Cucumis sativus* Ascorbate Oxidase," *Biochim. Biophys. Acta* **143,** 1248 (1995).

T. SAKURAI and J. TAKAHASHI, "Room Temperature EPR Spectra of *Rhus vernicifera* Laccase and Derivatives," *Biochem. Biophys. Res. Commun.* **215,** 235 (1995).

T. SAKURAI and F. NOSE, "Direct Electrochemistry of Blue Copper Proteins at Au Electrodes Modified with Promoters," *Chem. Lett.* 1075 (1995).

T. SAKURAI, "Cyclic Voltammetry of Cucumber Ascorbate Oxidase," *Chem. Lett.* 481(1996).

T. SAKURAI, J. TAKAHASHI and H. HUANG, "FT-IR Spectra of the Azide-Type 3 Copper in Laccase and Ascorbate Oxidase," *Chem. Lett.* 651 (1996).

Y. NAKAO, C. MORI, W. MORI, T. SAKURAI, K. MATSUMOTO and H. KIMOTO, "Dinuclear Nickel(II) Complexes Containing a Dinucleating Ligand *N,N,N',N'*-Tetrakis-[(1-ethyl-2-benzimidazolyl)methyl]-2-hydroxy-1,3-diaminopropane and an Acetate Ion," *Chem. Lett.* 641 (1996).

S. NAGATOMO, S. TAKEDA, H. TAMURA and N. NAKAMURA, "Crystal Structures and Hydrogen Bonding in One-Dimensional Chains of 4,5-Dicyanoimidazole and 4,5-Dicholoroimidazole," *Bull. Chem. Soc. Jpn.* **68,** 2783 (1995).

S. TAKEDA, I. INABE, T. MITANI, Y. MARUYAMA and K. YAMAGUCHI, "ESR Study on the Charge Transfer Complexes on *N*-Salicylideneanilines Containing NHO Hydrogen Bond as a Dynamic Function," *Syn. Met.* **70,** 1211(1995).

K. YAKUSHI, I. SHROTANI, I. I. KHAIRUILLIN, Y. NAKAZAWA, K. KANODA, N. KOSUGI and S. TAKEDA, "Characterization of Poly-CuPc Sheet Polymers Synthesized under High Pressure," *Syn. Met.* **71,** 2287 (1995).

S. NAGATOMO, S. TAKEDA, K. YAMAGUCHI, M. IWATA and Y. ISHIBASHI, "New Cation-Diffusion Phase of $(CH_3NH_3)_5Bi_2Cl_{11}$," *J. Phy. Soc. Jpn.* **64,** 391(1995).

T. SEKIKAWA, K. MIYAKUBO, S. TAKEDA and T. KOBAYASHI, "Charge-Transfer Effects in a Strongly Hydrogen-Bonded System: Potassium Salt of Acetylenedicarboxylic Acid," *J. Phys. Chem.* **100,** 5844 (1996).

Y. KURODA, Y. YOSHIKAWA and M. NAGAO, "Desorption Phenomenon of Adsorbed Water on a Homogeneous SrF_2 Surface at Lower Temperatures," *Lungmuir,* **11,** 4031 (1995).

M. HIROTSU, K. NAKAJIMA, M. KOJIMA and Y. YOSHIKAWA, "Maganese(III) Complexes Containing Optically Active Tetradentate Schiff Base Ligands. Effect of Phenyl Substituents," *Inorg. Chem.* **34,** 6173 (1995).

T. YOSHII, M. KOJIMA and Y. YOSHIKAWA, "Force Field Calculations of Antitumor Platinum Complex Systems," *J. Coord. Chem.* **37,** 305 (1995).

F. MD. AKHTER, M. KOJIMA, K. NAKAJIMA and Y. YOSHIKAWA, "Photochemical Desulfurization of a Sulfinato-*S* Cobalt(III) Complex. Formation of an Organic Peroxide Complex," *Chem. Lett.* 81 (1996).

F. MD. AKHTER, M. HIROTSU, I. SUGIMOTO, M. KOJIMA, S. KASHINO and Y. YOSHIKAWA, "Photochemistry of Cobalt(III) Complexes Containing a Sulfinate-*S* Ligand. Linkage and Geometrical Isomerization," *Bull. Chem. Soc. Jpn.* **69,** 643 (1996).

S. UTSUNO, A. SUGANUMA and Y. YOSHIKAWA, "Solid-State Circular Dichroism Specta of *Trans*-diamminetetranitrocobaltate(III) Salts and *Mer*-triamminetrinitrocobalt(III)," *Inorg. Chim. Acta,* **244,** 1 (1996).

Y. KURODA, Y. YOSHIKAWA, H. HAMANO and M. NAGANO, "Dielectric Behavior in the Y_2O_3-H_2O System at Lower Temperature with Desorption Phenomenon of Adsorbed H_2O in the SrF_2-H_2O System," *Langmuir,* **12,** 399 (1996).

T. ITOH, Y. FUJII, T. TADA, Y. YOSHIKAWA and H. HISADA, "Thermodynamic and Kinetic Studies of Zinc(II)-Triamine Complexes as Models of CA and AP," *Bull. Chem. Soc. Jpn.* **69,**1265 (1996).

M. HIROTSU, M. KOJIMA, K. NAKAJIMA, S. KASHINO and Y. YOSHIKAWA, "Sterochemistry and Electrochemistry of Cobalt(II) and Cobalt(III) Complexes Containing Optically Active Tetradentate Schiff Base Ligands," *Bull. Chem. Soc. Jpn.* **69,** 2549 (1996).

M. MURATA, M. KOJIMA, M. KITA, S. KASHINO and Y. YOSHIKAWA, "Preparation of a Stable Sulfonato-Cobalt(III) Complex by Oxidation of a Sulfinato-*O* Complex," *Chem. Lett.* 675 (1996).

M. KOJIMA, F. MD. AKHTER, K. NAKAJIMA and Y. YOSHIKAWA, "Photolysis of Cobalt(III) Complexes Containing Sulfinate-*S* Ligands. Formation of Organic Peroxide Complexes through Desulfurization," *Bull. Chem. Soc. Jpn.* **69,** 2889 (1996).

H. NAKAZAWA, Y. YAMAGUCHI, T. MIZUTA and K. MIYOSHI, "Cationic Phosphenium Complexes of Group 6 Transition Metals. The Reactivity, Isomerization, and the X-ray Structures," *Organometallics,* **14,** 4173 (1995).

H. NAKAZAWA, Y. YAMAGUCHI, T. MIZUTA, S. ICHIMURA and K. MIYOSHI, "Migratory Insertion of a Phosphorus Ligand into a Transition Metal-Alkyl Bond," *Organometallics,* **14,** 4635 (1995).

T. MIZUTA T. YAMASAKI, H. NAKAZAWA and K. MIYOSHI, "P-C Bond Cleavage of Phosphorus-Bridged [1]Ferrocenophane Coordinated to the $[Cp(CO)_2Fe]^+$ Fragment," *Organometallics,* **15,** 1093 (1996).

H. NAKAZAWA, Y. YAMAGUCHI and K. MIYOSHI, "Conversion of Transition-Metal Complexes with Stannyl and Phosphenium Ligands into Those with Stannylene and Phosphine Ligands by Alkyl Migration from Sn to P," *Organometallics,* **15,** 1337 (1996).

Y. YAMAGUCHI, H. NAKAZAWA, T. ITOH and K. MIYOSHI, "Cationic Phosphenium Complexes of Group 6 Transition Metals. Systematic Approach to Elucidation of Influence of Substituents of the Phosphenium Phosphorus on the Stability of the Complexes," *Bull. Chem. Soc. Jpn.* **69,** 983 (1996).

H. NAKAZAWA, Y. YAMAGUCHI and K. MIYOSHI, "Reactivity of Cationic Transition-Metal Phosphenium Complexes," *Phosphorus, Sulfur and Silicon,* **109,** 129 (1996).

H. NAKAZAWA, Y. YAMAGUCHI, K. MIYOSHI and A. NAGASAWA, "^{95}Mo NMR Studies on Cationic Phosphenium Complexes of Molybdenum," *Organometallics,* **15,** 2517 (1996).

E. KIMURA, T. IKEDA, M. SHIONOYA and M. SHIRO, "Molecular Recognition of Terephthalic Acids by Supramolecular Self-Assembly of Acridine-Pendant Zn(II)-cyclen Complex," *Angew. Chem., Int. Engl.* **34,** 663 (1995).

X. H. BU, D. L. AN, Y. T. CHEN, M. SHIONOYA and E. KIMURA, "New 1,4,7,10-Tetraazacyclotridecane-11,13-dione Ligands Appended with Additional Donor(s) 8-Methylquinoline(s): Crystal Structures and Characterization of Their Copper(II) Complexes," *J. Chem. Soc. Dalton Trans.* 2289 (1995).

J. H. R. TUCKER, M. SHIONOYA, T. KOIKE and E. KIMURA, "A Zinc(II)-Cyclen Complex Attached to an Anthraquinone Moiety that Acts as a Redox-Active Nucleobase Receptor in Aqueous Solution," *Bull. Chem. Soc. Jpn.* **68,** 2465 (1995).

Y. INOUYE, T. KANAMORI, M. SUGIYAMA, T. YOSHIDA, T. KOIKE, M. SHIONOYA, K. ENOMOTO, K. SUEHIRO and E. KIMURA, "Dimeric Macrocyclic Polyamines with Potent Inhibitory Activity against Human Immunodeficiency Virus," *Antiviral Chem. Chemother.* **6,** 337 (1995).

K. KOBAYASHI, M. SHIONOYA, E. KIMURA, K. TSUBOYAMA and S. TSUBOYAMA, "Molecular Structure of Chloro-[(2*S*, 5*S*, 8*S*, 11*S*)-2,5,8,11-tetraethyl-1,4,7,10-tetraazacyclododecane] zinc(II) Perchlorate," *Anal. Science.* **11,** 1029 (1995).

X. H. BU, D. L. AN, X. C. CAO, Y. T. CHEN, M. SHIONOYA and E. KIMURA, "Stabilization of Ni(III) Ion by Novel Macrocyclic Dioxotetraamines Bearing Functional Pendant," *Polyhedron* , **15,** 161 (1996).

Y. INOUYA, T. KANAMORI, M. SUGIYAMA, T. YOSHIDA, T. KOIKE, M. SHIONOYA, H. FUJIOKA and E. KIMURA, "Differential Contribution of Metal Complexation and Dimerization to the Chemotherapeutic Potential of Bicyclen-Zn_2^{II} Complex against Human Immunodeficiency Virus," *Biol. Pharm. Bull.* **19**(3), 456 (1996).

X. H. BU, X. C. CAO, Z. H. ZHANG, Z. A. ZHU, Y. T. CHEN, M. SHIONOYA and E. KIMURA, "Novel Structure of an Unusual *cis* Nickel(II) Complex of a New Dioxocyclam bearing 2-Methylfuran Pendants," *Polyhedron* , **15,** 1203 (1996).

E. KIMURA, Y. KODAMA, M. SHIONOYA and T. KOIKE, "A New Cyclam with a Triphenylphosphine-pendant and Its Metal Complexes," *Inorg. Chim. Acta* **246,** 151 (1996).

K. TOYOHARA, H. NAGAO, T. MIZUKAWA and K. TANAKA, "Ruthenium Formyl complexes as the Branch point in Two- and Multi-Electron Reduction of CO_2," *Inorg. Chem.* **34,** 5399 (1995).

H. NAKAJIMA, Y. KUSHI, H. NAGAO and K. TANAKA, "Multi-Step CO_2 Reduction Catalyzed by $[Ru(bpy)_2(qu)(CO)]^{2+}$ (bpy = 2,2'-bipyridine, qu = quinoline). Double Methylation of Carbonyl Moiety Resulting from Reductive Disproportionation of CO_2," *Organometallics,* **14,** 5093 (1995).

K. TOYOHARA, K. TSUGE and K. TANAKA, "Comparative of Ru-C Bond Characters Involved in Successive Reduction of Ru-CO_2 to Ru-CH_2OH," *Organometallics,* **14,** 5099 (1995).

H. NAKAJIMA, T. MIZUKAWA, H. NAGAO and K. TANAKA, "Catalytic Formation of Ketones *via* Double Alkylation of Carbon Monoxide Resulting from Reductive Disproportionation of Carbon Dioxide by $[Ru(bpy)_2(qu)(CO)]^{2+}$ (bpy = 2,2'-bipyridine, qu=quinoline)," *Chem. Lett.* 251 (1995).

N. KOMEDA, H. NAGAO, Y. KUSHI, G. ADACHI, M. SUZUKI, A. UEHARA and K. TANAKA, "Molecular Structure of Nitro- and Nitrito-Copper Complexes as Reaction Intermediates in Electrochemical Reduction of Nitrite to Dinitrogen Oxide," *Bull. Chem. Soc. Jpn.* **68,** 581 (1995).

D. OOYAMA, N. NAGAO, F. S. HOWELL, M. MUKAIDA, H. NAGAO and K. TANAKA, "Successive Chemical Reactions Accompanying a One-Electron Oxidation of a $\{MNO\}^6$-Type Nitrosyl Complex, Pentachloro(nitrosyl)ruthenium(2-), and a Chracterization of the Product Species," *Bull. Chem. Soc. Jpn.* **68** 2897 (1995).

H. NAKAJIMA and K. TANAKA, "Novel Reversible Metallacyclization in $[Ru(bpy)_2(h^1\text{-napy})(CO)]^{2+}$ (bpy = 2,2'-bipyridine, napy = 1,8-naphtyridine) by Intramolecular Attack of Non-Bonded Nitrogen of napy to Carbonyl Carbon," *Chem. Lett.* 891(1995).

T. DANIEL, N. SUZUKI, K. TANAKA and A. NAKAMURA, "Fluxional Behavior of *tert*-butyl-substituted 2,2':6'2"-terpyridylmolybdenum(0) and 2,2'-bipyridylmolybdenum(II) Complexes: Enhanced Solubility and Ease in NMR Study Caused by the *tert*-Butyl Group," *J. Organometallic Chem.* **505,** 109 (1955).

T. DANIELE, H. NAGAO, K. TANAKA and A. NAKAMURA, "Norbonadiene(bipyridyl)molybdenum(II) Complexes: Synthesis, Structure and Reactivity of $[Mo(CO)(C_7H_8)(C_{10}H_6R_2N_2)X_2]$ (X = I, Br)," *Chem. Ber.* **128,** 1007 (1995).

K. TOYOHARA, H. NAGAO, T. ADACHI, T. YOSHIDA and K. TANAKA, "Crystal Structure of $[Ru(bpy)_2(CO)(h^1\text{-}C(O)OH)]^+$ (bpy =2,2'-bipyridine) as a Key Intermediate in CO_2/CO Conversion," *Chem. Lett.* 27 (1996).

H. NAKAJIMA, H. NAGAO and K. TANAKA, "Control of the Co-ordination Mode of 1,5-Naphthylidine Ligated to Ruthenium(II) Bipyridine Complexes," *J. Chem. Soc. Dalton Trans.* 1405 (1996).

T. OOKUBO, H. SUGIMOTO, T. NAGAYAMA, H. MASUDA, T. SATO, K. TANAKA, Y. MAEDA, H. OKAWA, Y. HAYASHI, A. UEHARA and M. SUZUKI, "*cis*-μ-1,2-Peroxo Diiron Complex: Structure and Reversible Oxygenation," *J. Am. Chem. Soc.* **118,** 701 (1996).

T. DANIELE, H. NAGAO, H. NAKAJIMA, K. TANAKA and A. NAKAMURA, "Seven-coordinated 2,2':6'2"-terpyridinemolybdenum(II) Complexes: Synthesis, Structure and Reactivity of $[Mo(CO)(C_7H_8)(4,4',4''\text{-}R_3terpy)X]X'$ (R = H or ^{t}Bu)," *J. Organometallic Chem.* **509,** 225 (1996).

H. MIYASAKA, N. MATSUMOTO, H. OKAWA, N. RE, E. GALLO and C. FLORIANI, "Complexes Derived from the Reaction of Manganese(III) Schiff Base Complexes and Hexacyanoferrate: Syntheses, Multidimensional Network Structures, and Magnetic Properties, " *J. Am. Chem. Soc.* **118,** 981 (1996)."

Y. SATO, H. MIYASAKA, N. MATSUMOTO and H. OKAWA, "Syntheses, Structures and Magnetic Properties of the Tricyanoethanolate Adducts of Quadridentate Schiff Base Manganese(III) Complexes," *Inorg. Chimica Acta* **247,** 57 (1996).

S. EGUCHI, T. NOZAKI, H. MIYASAKA, N. MATSUMOTO, H. OKAWA, S. KOHATA and N. HOSHINO-MIYAJIMA, "Synthesis and Characterization of Alkoxo-Oxygen Bridged Copper(II) Complexes Having Disc- and Rod-Like Shapes, " *J. Chem. Soc. Dalton Trans.* 1761 (1996).

A. OHTA and Y. YAMASHITA, "Oxidative Intramolecular Cyclization of 2,2'-Bis(1,4-dithiafulven-6-yl)-3,3'-bithienyls affording Novel Bis(1,3-dithiole) Electron Donors," *J. Chem. Soc. Chem. Commun.* 1761 (1995).

M. HIRAYAMA, T. TERASAKA, M. ITASAKA, T. SUZUKI, Y. YAMASHITA and T. MIYASHI, "ESR of the Trianion and Anion Radicals of Benzo[g][1,2,5]thiadiazolo[3,4-b]quinoxaline-5,10-dione and Its Selenium Analogue," *Chem. Lett.* 837 (1995).

E. HASEGAWA, H. KATAGIRI, D. NAKAGAWA, T. HORAGUCHI, S. TANAKA and Y. YAMASHITA, "Electron Transfer Induced Stereoselective Cyclization of 2,2'-Disubstituted Dibenzoylmethane to anti-Cyclopropane-1,2-diol," *Tetrahedron Lett.* **36,** 6915 (1995).

M. TOMURA and Y. YAMASHITA, "Syntheses and Properties of Novel Conducting Dithiolato-Metal Complexes Having Peripheral Heteroatoms and Extended π-Conjugated Systems," *J. Mater. Chem.* **5,** 1753 (1995).

M. HIRAYAMA, T. TERASAKA, Y. MORITA, T. SUZUKI, Y. YAMASHITA and T. MIYASHI, "ESR of the π-Radical Formed by Photoreduction of Bis(1,2,5-selenadiazolo)tetracyano-quinodimethane in Methanol. Observation of a Large ^{77}Se Hfs," *Chem. Lett.* 1021 (1995).

M. HIRAYAMA, T. TERASAKA, Y. YAMASHITA, T. SUZUKI, T. MIYASHI and Y. USUI, "ESR of the Anion Radical of 2,6-Dithioxobenzo[1,2-d:4,5-d']bis[1,3]dithole-4,8-dione. Observation of the Satellites of ^{17}O, ^{13}C, and ^{33}S and the Second-Generation Satellites due to Both ^{13}C and ^{33}S in Natural Abundance," *Bull. Chem. Soc. Jpn.* **68,** 3337 (1995).

C. KITAMURA, S. TANAKA and Y. YAMASHITA, "New Narrow-Bandgap Polymers Composed of [1,2,5]Thiadiazolo[3,4-g]quinoxaline and Aromatic Heterocycles," *Chem. Lett.* 63 (1996).

C. KITAMURA, S. TANAKA and Y. YAMASHITA, "Design of Narrow-Bandgap Polymers. Syntheses and Properties of Monomers and Polymers Containing Aromatic-Donor and *o*-Quinoid-Acceptor Units," *Chem. Materials* **8,** 570 (1996).

S. BANDOW, Y. MARUYAMA, X.-X. BI, R. OCHOA, J. M. HOLDEN, W.-T. LEE and P. C. EKLUND, "Electronic and Vibrational Properties of Rb-Intercalated MoS_2 Nanoparticles," *Mater. Sci. & Engin.*, **A204,** 222 (1995).

S. BANDOW, "Magnetic Properties of Nested Carbon Nanostructures Studied by Electron Spin Resonance and Magnetic Susceptibility Measurements," *J. Appl. Phys.*, **80,** 1020 (1996).

T. NAKAI and D. KUWAHARA, "Spinning sideband Summation for Quadrupole MAS NMR Spectra Using a Magic-Angle Turning Technique," *Chem. Phys. Lett.* **249,** 205 (1996).

M. KAMADA, N. TAKAHASHI, S. HIROSE, S. OHARA, M. A. TEREKHIN, S. S. GALAKTINOV and S. S. GALAKTINOV, "Photoelectron and Luminescence Spectra of BaFCl, BaFBr, and CsTaF6," *J. Electron Spectroscopy and Related Phenomena* **79,** 143 (1996).

S. HIROSE and M. KAMADA, "Photon-Energy Dependence of Excited-State Na Desorption from Na Halides by Synchrotron Radiation," *J. Electron Spectroscopy and Related Phenomena* **80,** 113 (1996).

S. HIROSE and M. KAMADA, "Photon-Stimulated Desorption of Excited-State Sodium Atom from NaF and NaCl under Valence-Band and Core-Level Excitations," *J. Phys. Soc. Jpn.* Vol.**65,** 1849 (1996).
S. HIROSE and M. KAMADA, "Dynamics of Photon-Stimulated Desorption of Excited-State Alkali Atoms from Alkali Halides," *J. Phys. Soc. Jpn.* **64,** 4434 (1995).
M. ITOH, N. OHNO, H. YOSHIDA, S. HASHIMOTO, K. KAN'NO and M. KAMADA, "Auger-Free Luminescence in Mixed Alkali Halides" *J. Electron Spectroscopy and Related Phenomena* **79,** 117 (1996).
N. SHINO, S. SUGA, S. IMADA, Y. SAITOH, H. YAMADA, T. NANBA, S. KIMURA and S. KUNII, "Photoemission, Inverse Photoemission and Optical Studies of Rare-Earth Hexaborides," *J. Phys. Soc. Jpn.* **64,** 2980 (1995).
S. KIMURA, Y. SATO, F. ARAI, M. IKEZAWA, M. KAMADA, K. KATO and M. KASAYA, "Optical and Photoelectrical Studies of Electronic Structure of $R_3Au_3Sb_4$ (R=La, Ce and Pr)," *J. Phys. Soc. Jpn* **64,** 4278 (1995).
S. KIMURA, F. ARAI and M. IKEZAWA, "Mixed Valence of Praseodymium Oxides," *J. Electron Spectroscopy and Related Phenomena* **78,** 135 (1996).
M. MATSUMOTO, K. SODA, K. ICHIKAWA, T. TAGUCHI, K. JOUDA, M. KAGEYAMA, S. TANAKA, N. SATA, Y. TEZUKA, S. SHIN, S. KIMURA and O. AITA, "Photoemission Study of CeO_2 and $SrCeO_3$," *J. Electron Spectroscopy and Related Phenomena* **78,** 179 (1996).
S. KIMURA, H. HAMA, M. KAMADA, X. MARECHAL, T. TANAKA and H. KITAMURA, "Design of a Helical Undulator for UVSOR," *J. Electron Spectroscopy and Related Phenomena* **80,** 437 (1996).
S. TANAKA, N. TAKAHASHI, K-P. LEE and M. KAMADA, "Surface Core Exciton of Alkali Chloride Film on Si(100)" *J. Elec. Spectros. Related Phenom.* **80,** 205 (1996).
I. OUCHI, I. NAKAI, M. KAMADA and S. TANAKA, "Polarized Abosrption Spectra of Polyethylene Terephthalate and Polyethylene Naphthalate Films in Soft X-Ray Region" *J. Electron Spectros.* **78,** 363 (1996).
T. YAMANAKA, T. MATSUSHIMA, S. TANAKA and M. KAMADA, "Orientation and Desorption of Oxygen Admolecules on a Pt(113) Stepped Surface" *J. Electron Spectroscopy and Related Phenomena* **80,** 105 (1996).
T. YAMANAKA, T. MATSUSGIMA, S. TANAKA and M. KAMADA, "Orientation of Oxygen Admolecules on a Stepped Platinum (113) Surface" *Surface Science* **349,** 119 (1996).
T. KINOSHITA, H. B. ROSE, C. ROTH, D. SPANKE, F. U. HILLEBRECHT and E. KISKER, "A New Type of Magnetic Linear Dichroism at Fe and Co $M_{2,3}$ edges"; *J. Electron Spectrosc. Relat. Phenom.* **78,** 237 (1996).
T. KINOSHITA, H. B. ROSE, C. ROTH. F. U. HILLEBRECHT and E. KISKER, "Magnetic Linear Dichroism in Spin-Resolved Gd 4f Photoemission"; *J. Electron Spectrosc. Relat. Phenom.* **78,** 333 (1996).
D. SPANKE, J. DRESSELHAUSE, T. KINOSHITA, Ch. ROTH, H. B. ROSE, F. U. HILLEBRECHT and E. KISKER, "Element-Specific Magnetic Domain Imaging Based on Linear and Circular Magnetic Dichroism in Photoabsorption"; *J. Electron Spectrosc. Relat. Phenom.* **78,** 299 (1996).
H. B. ROSE, A. FANELSA, T. KINOSHITA, Ch. ROTH, F. U. HILLEBRECHT and E. KISKER, "Spin-Orbit-Induced Spin-Polarization in W 4f Photoemission;" *Phys. Rev. B***53** 1630 (1996).

REVIEW ARTICLES AND TEXTBOOKS

R. KISHI, A. NAKAJIMA, S. IWATA, and K. KAYA, Electronic and Geometric Structures of Silicon-M Binary Clusters (M= C and Na) "Structures and Dynamics of Clusters", Ed. by T.Kondow, K. Kaya, A. Terasaki, p.209-218 (1996).
S. IWATA and H. WATANABE, Theoretical Studies of Molecular Spectroscopies of Some Small Clusters "Structures and Dynamics of Clusters", Ed. by T.Kondow, K.Kaya, A.Terasaki, p. 209-218 (1996).
Y. OKAMOTO, "Predicting Protein Tertiary Structures from the First Principles," *Association of Asia Pacific Physical Societies Bulletin*, Vol. 5, No. 3&4, December, 4 (1995).
Y. OKAMOTO, "Towards the *ab initio* Prediction of 3-Dimensional Structure of Proteins," *Butsuri* (in Japanese) **51**, 279 (1996).
A. SHUDO, "Tunneling Phenomena in Chaotic Systems" Parity (in Japanese), Vol.10, No.11, 30 (1995).
H. NAKAMURA, "Nonadiabatic Transitions : Beyond Born-Oppenheimer," In "Dynamics of Molecules and Chemical Reactions" edited by R. E. Wyatt and J. Z. H. Zhang, (Marcel Dekker Inc., 1996) p.473-529.
H. NAKAMURA and C. ZHU, Landau, Zener, Stueckelberg, and All That Now Completely Solved, Comments on Atomic and Molecular Physics **32**, p.249-266 (1996).
H. NAKAMURA, Theory for Nonadiabatic Transitions Governing Chemical Phenomena,--Complete Solutions in Sixty Years, Chemistry Today No.305, p.36-42 (1996) (in Japanese).
R. FUKUDA, M. KOMACHIYA, S. YOKOJIMA, Y. SUZUKI, K. OKUMURA and T. INAGAKI, "Novel Use of Legendre Transformation in Field Theory and Many Particle Systems—On-Shell Expansion and Inversion Method," *Prog. Theor. Phys. Suppl.* **121** (1995).
S. SAITO and H. OZEKI, "High-Sensitivity and High-Resolution Submillimeter-Wave and Far-Infrared Spectroscopy," *Solid State Physics* (in Japanese) **31**, 343(1996).
S. SAITO, "Letters from Space," *Kagaku to Kogyo* (in Japanese), **49**, 643(1996).
T. KITAGAWA and K. SEKI, "Polymer Effects," in "Functionality of Molecular Systems," Chapter 5.3, S. Nagakura Ed., *Springer Verlag,* Tokyo (1996).
T. KITAGAWA, "Raman Spectroscopy," in "Guide to Instrumental Analyses," Vol. 3, *Kagaku Dojin* (in Japanese), p.140-158(1996).
T. KITAGWA, "Time-Resolved Resonace Raman Spectroscopy," in "New Applied Protein Engineering," M. Hatano Ed., *Fujitechno System*, p.102-109 (1996).
K. YOSHIHARA, "Rising Research Activities in Asia," *JPA NEWSLETTER* **34**, 1 (1995).
K. YOSHIHARA, "Femtosecond Higher Order Non-Linear Vibrational and Rotational Spectroscopy of Molecules: CARS and Raman Echo," *Ultra Precision* **5**, 8 (1995).
K. YOSHIHARA, "Solvent and Nuclear Dynamics of Ultrafast Intermolecular Electron Transfer," in *Ultrafast Processes in Chemistry and Biology*, International Union of Pure and Applied Chemistry monograph series on "Chemistry for the 21 st Century," M.A. El-Sayed, I. Tanaka, and Yu. Molin Eds., Blackwell Science Publisher, p.105 (1995).
K. YOSHIHARA, K. TOMINAGA and Y. NAGASAWA, "Effects of the Solvent Dynamics and Vibrational Motions in Electron Transfer," *Bull. Chem. Soc. Jpn.* **68**, 696 (1995).
K. YOSHIHARA, "Prospects for Ultrafast Phenomena in Chemistry," *Kagaku to Kogyo* (in Japanese) **49**, 905 (1996).
K. YOSHIHARA and K. TOMINAGA, "Development and Application of High-Order Nonlinear Vibrational Spectroscopy," *Opt News* (in Japanese) **92**, 16 (1996).
K. SAWABE and Y. MATSUMOTO, "Photoinduced Reaction of Surface Adsorbates," *Hyomen* (in Japanese) **27**, 273 (1996).
T. SUZUKI, "Studies on Chemical Reaction Dynamics by Photoion Imaging," *J. Spectrosc. Soc. Jpn.* (in Japanese) **45**, 3 (1996).
T. SUZUKI, "Visualization of the Scattering Distribution of Reaction Products and Full Characterization of Their Quantum State Distribution," *Surface* (in Japanese) **34**, 323 (1996).
H. KOBAYASHI and A. KOBAYASHI, "Development of Low-Temperature X-Ray Imaging Plate system and Its Applications to Metallic Molecular Crystals," *Solid State Phys.*(in Japanese) **31**, 35 (1996).
H. KOBAYASHI, A. KOBAYASHI and M. TOKUMOTO, "Organic Metal with Magnetic Counter Ions-λ-$BETS_2FeCl_4$," *Solid State Phys.* (in Japanese) **31**, 653 (1996).
Y. WATANABE, "Metal Ions in Enzymes," *Kagaku* (in Japanese) **50**, 500 (1995).
K. INOUE, "Construction of Transition Metal Complex with High-spin Polynitroxides- Approach to High T_C Moecule-based Magnets -," *Kagaku to kogyo* (in Japanese) **49**, 119 (1996).
K. TORIUMI, "A Guidebook to Measure Intensities of Reflections," *J. Cryst. Soc. Jpn.* (in Japanese) **38**, 189 (1996).
N. KOSUGI, Theory and Analysys "X-Ray Absorption Fine Structure for Catalysts and Surfaces," Y. Iwasawa Ed., World Scientific Publishing, p.60-76 (1996).
N. KOSUGI, "*Ab Initio* Bound-State Calculations for Inner-Shell Ionized Excited States of Simple Molecules" in "Atomic and Molecular Photoionization", A. Yagishita and T. Sasaki Eds., Universal Academy Press, p.89-98 (1996).
E. SHIGEMASA, J. ADACHI, M. OURA, N. WATANABE, K. SOEJIMA and A. YAGISHITA, "Molecular Shape Resonances Studies by Angle-Resolved PEPICO" in "Atomic and Molecular Photoionization," A. Yagishita and T. Sasaki Eds., Universal Academy Press, p.69-78 (1996).
K. MITSUKE, "Ion-Pair Formation from Superexcited Molecules," in "Atomic and Molecular Photoionization," A. Yagishita and T. Sasaki Eds., Universal Academy Press, p.187-196 (1996).
T. IBUKI, "Application of Synchrotron Radiation to Molecular Science" in "Atomic, Molecular and Cluster Physics" S.

A. Ahmad Ed., Narosa Pub. House, India, p.266-271 (1996).
H.HOSONO, "Structure of Oxide and Database," in "Report on Oxide Electronics," Vol.1, Japan Electronic Industry Promotion Association, p.1-8(1996).
J. NISHII and H.HOSONO, "Formation and Mechanism of Photo-induced Bragg Gratings," Optronics, [8] p.57-63 (1996).
T. SAKURAI, "EPR of Photosynthetic System in Plant," in "Bioscience EPR," Vol. *2*, H. Sakurai Ed., Hirokawa Pub. Co., p.443-455(1996).
M. SHIONOYA and E. KIMURA, "Zinc Complexes and Nucleic Acids," *Pharmacia* (in Japanese) **31**, 598 (1995).
E. KIMURA and M. SHIONOYA, "Zinc Complexes as Targeting Agents for Nucleic Acids," in "Metal Ions in Biological Systems: Probing of Nucleic Acids by Metal Ion Complexes of Small Molecules," Vol. *33*, H. Sigel and A. Sigel Ed., Marcel Dekker Inc., p.29-52 (1996).
K. TANAKA, "Carbon Dioxide Fixation by Catalysed by Metal Complexes", *Adv. of Inorg. Chem.* **43**, 409 (1995).
H. B. ROSE, T. KINOSHITA, Ch. ROTH and F. U. HILLEBRECHT, "Photoelectron Diffraction in Spin-Resolved Photoemission and Magnetic Linear Dichroism;" *Proceedings of the International Workshop on Spin-Orbit Influenced Spectroscopies of Magnetic Solids, Herrsching, Germany, April 1995, in Lecture Notes of Physics, edited by H. Ebert and G. Schütz, Springer Verlag, Berlin*, p.105-124 (1995).

AUTHOR INDEX RESEARCH ACTIVITIES AND SPECIAL RESEARCH PROJECT

A

Abdulsabirov, Ravil Yu 183
Achiba, Yohji 149, 150
Achkasov, Vladimir V. 111
Adachi, Junichi 130, 145
Adachi, Osao 47
Adachi, Takafumi 87
Ahmad, Imtiaz 40
Ahn, Jeung-Sun 114
Akaki, Osamu 149
Akasaka, Takeshi 51
Akhter, Farooque MD. 158, 159
Akutsu, Hiroki 96, 98, 99, 207, 208
Ali, Md, Meser 151, 152
Amaya, Kiichi 85
Anazawa, Toshihisa 66, 202
Aoki, Atsushi 82
Aoki, Masaru 149
Aonuma, Shuji 99
Aoyagi, Katsuhiro 50
Aoyagi, Mutsumi 77, 176, 177, 205
Arai, Emiko 96, 98, 100, 207
Arakawa, Ryuichi 151, 152, 153
Aritani, Hirofumi 193
Asada, Toshio 16, 17, 199
Asaka, Shuji 189, 205
Asano, Yasuhisa 47
Asano-Someda, Motoko 50

B

Baer, Michael 27
Bandow, Shunji 185, 186, 187
Bandyopandhyay Pradipta 199
Basu, Gautam 36
Bozek, John D. 131
Brion, Chris E. 131
Brossard, L. 98

C

Cardiasmenos, Apostle G. 42
Carter, C. C. 16
Cassoux, P. 98, 99
Cavell, Ronald G. 131
Chainani, Ashish 114
Chiba, Hiroshi 131
Chiba, Tomonori 83
Chinani, Ashish 149
Cho, S-H. 42
Chong, Song-Ho 34, 36, 200

D

Dai, Jie 171
Daniel, H. 43, 44
Daniele, Stephane 168
Daniels, Lizla B. 78
Dong, Jian 88, 89
Dowben, Peter A. 131
Dresselhaus, G. 187
Dresselhaus, M. S. 187
Dubinskii, Mark A. 183

E

Eades, J. 43, 44
Ebisawa, Hiromichi 38
Edamatsu, Kunishige 148
Egidy, T. von 43, 44
Einaga, Hisahiko 119
Einaga, Yuichi 149
Eisenmenger, Frank 25
Eklund, Peter C. 186, 187
Enoki, Toshiaki 107, 149
Erabi, Tatsuo 61

F

Fanelsa, Andreas 195
Fiedler, Andreas 23, 199
Floriani, Carlo 173, 174
Frfbort, Ivo 47
Friedman, Harold L. 35, 36
Fuchikami, Tomohiro 85
Fujii, T.Shunmei 23
Fujii, Toshiaki 199
Fujii, Yasuo 192
Fujii, Yuki 157
Fujimoto, Kaori 152
Fujimura, Yuuichi 201
Fujioka, Haruto 165
Fujita, Hideo 90, 124, 125
Fujita, Y. 44
Fujitsu, Satoru 147
Fujiwara, Hideki 100, 208
Fujiwara, Hideo 41, 42, 43
Fukuda, Atsuo 106
Fukuda, Tsuguo 183
Fukui, Kazutoshi 191, 193
Fukushima, Masaru 82
Fukutome, Hideo 30
Fukuyama, Eri 42
Fukuyama, Hidetoshi 110, 111
Furuichi, Koichi 171, 172
Furukawa, Koji 83
Furusaki, Akira 111
Furuuchi, Satoshi 152

G

Galaktinov, S. S. 194
Galaktinov, S. S. 194
Gallo, Emma 173, 174
Gan, Xinmin 170, 171
Gandai, Suketu R. 69
Gejyo, Tatsuo 77, 145, 204
Gomei, Motoki 19
Goodman, Frank O. 29
Goto, Tsuneaki 123
Goto, Yoshio 119
Goto, Yoshitaka 138
Graetzel, Michael 62
Gruzdkov, Yuri A. 64

H

Haga, Masa-aki 151, 152, 153, 154, 210
Haglund, Jr. R. F. 146
Hama, Hiroyuki 191, 192, 206
Hama, Tetsuo 115
Hamatani, Yukiko 148
Hanazaki, Ichiro 66, 67, 68, 69, 70, 71,72, 73, 74, 75, 76, 202
Hansmann, Ulrich H. E. 25, 199
Hanzawa, Hiromasa 51
Hara, Isao 211
Harada, Kazumasa 153, 210
Harada, Yoshiya 115, 148, 149

Harayama, Takahisa 26
Harima, Yutaka 147
Hartmann, F. J. 43, 44
Hasegawa, Shinji 115, 116, 147, 148, 149, 209
Hasegawa, Tatsuo 109
Hashimoto, Nobuhisa 78
Hashizume, Daisuke 121
Hasinoff, M. 44
Hasumi, Ryouji 16
Hasumoto, Masami 189, 191
Hata, Yuko 163
Hatherly, Paul A. 130
Hatsui, Takaki 131, 132
Hattori, Hideo 139, 140, 141
Hattri, Tadashi 138
Hayamizu, Takashi 121
Hayano, R. S. 43, 44
Hayashi, Michiro 40
Hayashi, Naoki 52
Heaven, Michael C. 76, 79, 81, 203
Hensel, Samuel L. 42
Hiejima, Toshihiro 87, 207
Hikida, Takumi 139, 140, 144
Hikosaka, Yasumasa 139, 140, 141
Hino, Shojun 149, 150
Hiraki, Ko-ichi 95, 207
Hirano, M. 16
Hirao, Tsuyoshi 39, 40
Hirata, Fumio 31, 32, 33, 34, 35, 36, 200
Hiraya, Atsunari 130, 141, 142, 144, 145, 204
Hirose, Sayumi 191, 194
Hirota, Noboru 59
Hirota, Shun 46, 47, 201
Hirota, Tomoya 42
Hirotsu, Masakazu 158, 159, 211
Hisada, Hiroyuki 157
Hitchcock, Adam P. 131
Hiyama, Miyabi 28, 199
Honda, Zentaro 115
Hori, M. 44
Horigome, Toshio 43, 189, 191
Horiki, Yasuhiro 83
Horvath, D. 43, 44
Hosaka, Masahito 191
Hosoito, Nobuyoshi 125
Hosokoshi, Yuko 123, 208
Hosono, Hideo 146, 147, 209
Hosoya, Shoichi 149
Hossain, M. Delower 210
Hrušák, Jan 23, 24, 199
Huang, Hong-wei 156, 211

I

Ibuki, Toshio 143, 144, 145, 204
Ichikawa, Masatake 192
Ichimura, Kenji 89, 117
Ichinose, Takayuki 154
Ieda, Hidenori 174
Iitaka, Toshiaki 25
Ikawa, Akira 30
Ikeda, Takuya 163, 164
Ikeda, Kensuke S. 26
Ikegami, Isamu 60, 202
Ikegami, Tsutomu 24, 199
Imada, Masatoshi 37, 206
Imaeda, Ken-ichi 87, 108, 116, 117, 178
Imahori, Hiroshi 48
Imai, Yoshio 49
Imaizumi, Yoshiaki 138
Imamori, Hiroshi 48
Inabe, Tamotsu 100, 157
Inada, Naomi 40
Inatani Junji 42
Inokuchi, Hiroo 87, 108, 115, 116, 117, 148, 149
Inokuchi, Yoshiya 127, 203
Inoue, Katsuya 121, 122, 208
Inouye, Yoshio 165
Irisa, Masayuki 34, 200
Ishibashi, Yoshiro 157
Ishida, Tateki 200
Ishiguro, Eiji 145
Ishii, Hisao 115, 147, 148, 149, 209
Ishikawa, Ken 106
Ishikawa, T. 43, 44
Ishimori, Koichiro 48, 119
Isobe, Kiyoshi 120, 167
Itatani, Taro 182, 184
Ito, Eisuke 148
Ito, Osamu 83
Itoh, Koichi 84, 85
Itoh, Shigeru 61, 202
Itoh, Tomonori 160
Itoh, Toyofumi 157
Ivanov, Valery A. 89, 111, 112, 113
Iwahashi, Makio 52
Iwahori, Fumiyasu 115
Iwaki, Masayo 61, 202
Iwamura, Hiizu 121, 122
Iwasa, Yoshihiro 109
Iwasaki Kentaro 149, 150
Iwase, Masakazu 119
Iwata, Makoto 157
Iwata, Suehiro 15, 16, 17, 18, 19, 20, 21, 22, 23, 24, 48, 129, 199
Izawa, Takao 182
Izumida, Shinji 182, 183, 184, 205

J

Jaman, A. 41
Jewsbury, Philip 46
Jin, Bo 106
Jitsukawa, Koichiro 119

K

Kagami, Yuka 115
Kagoshima, Seiichi 109
Kai, Yasushi 125
Kaifu, Norio 42
Kajita, Koji 99, 100
Kamada, Masao 138, 191, 192, 194, 205
Kamalov, Valey K. 62
Kamamoto, Akiko 143
Kaminaga, Akiko 71, 72, 73, 74, 75, 202
Kamiya, Koji 115, 148, 149
Kanamori, Tatsuyuki 165
Kanda, Kazuhiro 145
Kanehisa, Nobuko 125
Kanoda, Kazushi 91, 92, 93, 94, 95, 112, 157, 207
Kartsovnik, M. V. 99
Kashino, Setsuo 158, 159, 211
Katayama, Norihisa 52
Katayanagi, Hideki 76, 77, 78, 81, 203
Kato, Hiroyuki 65
Kato, Masako 51
Kato, Noriaki 210
Kato, Reizo 99, 101
Kato, Shigeki 31, 32, 200

Kato, Shinobu 83, 84
Kato, Tatsuhisa 51, 52, 201
Kato, Yasuo 47
Katori, Aruga 115
Katsumata, Koichi 115
Kawai, Akio 82
Kawamata, Hiroshi 19
Kawamoto, Atsushi 91, 92, 207
Kawamoto, Ikuko 148
Kawamura, Kazumori 161
Kawamura, Ken-ichi 146
Kawano, Koichi 103
Kawata, Masaaki 31, 32
Kawazoe, Hiroshi 146, 147, 209
Kaya, Koji 16, 19
Kayama, Misa 136, 203
Ketzer, B. 43, 44
Khairullin, I. I. 157
Kidera, Akinori 34
Kikuchi, Koichi 149, 150
Kikuchi, Naoto 146, 147
Kilcoyne, A.L. David 131
Kim, Bog-Gi 107
Kim, Hong Lae 67
Kim, Jong-Jean 107
Kim, Misa 114, 126
Kim, Yong-Hae 107
Kim, Jong-Jean 208
Kimito, Hiroshi 156
Kimura, Eiichi 163, 164, 165
Kimura, Kazuhiko 191
Kimura, Shin-ichi 191, 192, 195
Kino, Hiori 110
Kinoshita, Hajime 83
Kinoshita, Ikuo 66, 202
Kinoshita, Masahiro 33, 34, 200
Kinoshita, Minoru 123
Kinoshita, Takamasa 85
Kinoshita, Toshio 191
Kinoshita, Toyohiko 193, 195, 206
Kishi, Reiko 19
Kishishita, Mitsuru 161, 211
Kita, Masakazu 158
Kitagawa, Hiroshi 114, 115, 126
Kitagawa, Teizo 46, 47, 48, 49, 50, 201
Kitagishi, Yuichi 84
Kitajima, Yoshinori 130, 193
Kitamura, Akinori 148, 149
Kitamura, Chitoshi 179
Kitamura, Hideo 192
Ko, Jae-Hyeon 107
Kobayashi, Akiko 96, 97, 98, 99, 100, 101, 102, 103, 116, 207, 208
Kobayashi, Hayao 96, 98, 99, 100, 101, 102, 103, 116, 207, 208
Kobayashi, Kaori 40, 41
Kobayashi, Kaoru 51
Kobayashi, Kimiko 163
Kobayashi, Takayoshi 157
Kobayashi, Tatsuo 85
Kobayashi, Yoshihiro 137
Kobori, Yasuhiro 82
Kodama, Takeshi 51
Koga, Noboru 122
Kohguchi, Hiroshi 80, 203
Koike, Tohru 163, 164, 165
Kojima, Masaaki 157, 158, 159, 211
Komatsu, Ryuichi 183
Komeda, Nobutoshi 167
Kono, Mitsuhiko 144, 145
Korableva, Stella L. 183
Koseki, Shiro 152
Kosugi, Nobuhiro 130, 131, 132, 157
Kozlov, Michail E. 89, 113
Kröber, Jonas 108, 116, 117
Kumakura, Mitsutaka 44, 45, 201
Kumazaki, Shigeichi 60, 61, 202
Kurahashi, Takashi 138
Kurihara, Masato 168, 212
Kuroda, Noritaka 114
Kuroda-Sowa, Takayoshi 169, 170, 171, 172
Kurokawa, Sinya 85
Kurosaki, Hiromasa 164
Kushch, N. D. 99
Kushi, Yoshinori 166, 167
Kuwahara, Daisuke 188

L

Lee, K-P. 194
Lever, A. B. P. 153
Li, Tiansheng 47
Li, Yumin 20, 22, 199
Lin, M. C. 64
Liu, Zhenlin 182, 183, 184, 205
Lubovskii, R. B. 99
Luhova, Lenka 47

M

Ma, Jangseok 57, 201
Maas, F. E. 43, 44
Maeda, Masaharu 182
Maekawa, Masahiko 169, 170, 171, 172
Maekawa, Satoshi 121
Magruder, R. H. 146
Manabe, Toshio 114, 115, 126
Marata, Yshitada 138
Marechal, X. 192
Marie, C. 44
Marinaro, Maria 113
Marumo, Kenji 84
Maruyama, Yusei 157
Maruyama, Yutaka 200
Mase, Kazuhiko 137, 138, 139, 204
Masuda, Hideki 119
Masuda, Sigeru 149
Masuya, Masato 199
Matsubayashi, Gen-etsu 152
Matsuda, Kenji 122
Matsui, Shigenori 182
Matsui, Toshitaka 119, 120
Matsukawa, Tokuo 193
Matsumoto, Hiroki 211
Matsumoto, Kenji 156
Matsumoto, Naohide 173, 174
Matsumoto, Yoshiyasu 63, 64, 65, 66, 202
Matsuo, Shigehiro 193
Matsuo, Shigeki 134, 135
Matsuo, Takekiyo 152, 153
Matsushita, Kazunobu 47
Matsushita, Michio 51, 201
Matsutsuji, Kazuto 107
Matsuzaki, Akiyoshi 83, 84
Matysik, Jörg 49, 201
Maw, Sarah A. 200
Mcilroy, David N. 131
Mclendon, George L. 62
Menon, M. 187
Miller, Terry A. 16

Minamino, Satoshi 176
Minato, Tsutomu 46
Minoura, Satoshi 137
Miskovic, Zoran. L. 29
Mitani, Tadaoki 114, 115, 126, 157
Mitsui, Masaaki 82
Mitsuke, Koichiro 139, 140, 141, 142, 143, 204
Mitsuo, Shigeki 203
Mitsutake, Ayori 25, 199
Miura, Shin-ichi 36
Miura, Yozo 84, 85
Miyagawa, Kazuya 91, 92, 207
Miyajima, Seiichi 103, 104, 106, 107, 108, 208
Miyakuubo, Keisuke 157
Miyamae, Takayuki 149, 209
Miyasaka, Hitoshi 173, 174
Miyazaki, Takafumi 115, 148, 149, 150
Miyoshi, Katsuhiko 160, 161, 211
Mizoguchi, Hiroshi 147
Mizukawa, Tetsunori 165, 212
Mizuta, Tsutomu 161
Mizutani, Hisashi 85
Mizutani, Manabu 142
Mizutani, Masakazu 141,142, 204
Mizutani, Nobuo 189, 191
Mizutani, Yasuhisa 48, 50
Mo, Yuxiang 76, 78
Mochida, Tomoyuki 107, 109, 208
Mogi, Kouichi 176, 177
Mogi, Tatsushi 201
Momoki, Masayoshi 85
Momose, Masahiro 115, 148, 149
Monjushiro, Hideaki 153, 154, 210
Mori, Chikako 156
Mori, Wasuke 156
Mori, Yoshihito 73, 74, 75
Moribayashi, Kengo 26
Morimoto, Hiroshi 125
Morishima, Isao 48, 118, 119
Morita, Norio 43, 44, 45, 201
Moriwaki, Yoshiki 45, 201
Moriyama, Hiroshi 102
Moser, Jacques 62
Mukai, Masahiro 47, 48
Mukaida, Masao 167
Munakata, Megumu 169, 170, 171, 172
Munakata, Toyonori 36
Murakami, Tatsuya 118
Murata, Itsuko 210
Murata, Mayumi 158,159
Murayama, Yoshimasa 112, 113

N

Nagano, Shingo 48, 119
Naganubo, Masao 138
Nagao, Hirotaka 165, 166, 167
Nagaoka, Shin-ichi 204
Nagaosa, Naoto 111
Nagasawa, Akira 160
Nagasawa, Yutaka 53, 62
Nagase, Shigeru 51
Nagashima, Umpei 67
Nagasono, Mitsuru 137, 138, 139, 204
Nagata, Takashi 21, 128, 129, 145, 203
Nagatomo, Shigenori 156, 157
Nagayama, Kuniaki 34
Naito, Toshio 96, 97, 98, 99, 100, 101, 103
Naitoh, Yukito 58, 59, 202
Nakagawa, Hideyuki 193
Nakagawa, Kazumichi 193
Nakagawa, Tadashi 182, 184
Nakai, Toshihito 104, 106, 188, 208
Nakajima, Atsushi 16, 19
Nakajima, Hiroshi 166, 167, 168
Nakajima, Kiyohiko 152, 158, 159, 211
Nakajima, Sadao 112
Nakamura, Haruki 34
Nakamura, Hiroki 26, 27, 28, 29, 199
Nakamura, Motohiko 132
Nakamura, Nobuo 122, 156
Nakanishi, Koichi 192
Nakano, Chikako 116
Nakano, Hiroki 123
Nakao, Yasuo 156
Nakaura, Miho 153
Nakayoshi, K. 43
Nakazawa, Hiroshi 160, 161, 211
Nakazawa, Yasuhiro 89, 93, 94, 95, 157, 207
Namiki, Kei-ichi 41
Nanba, Takao 193
Nanbu, Shinkoh 29, 77, 176
Narioka, Satoru 115, 147, 148
Nath, Krishna G. 195
Naumov, A. K. 183
Negishi, Yuichi 19
Niestroj, A. 43
Nikitin, Evgueni E. 27
Nishi, Nobuyuki 127, 202, 203
Nishida, Masato 114
Nishida, Yoshio 51
Nishio, Satoru 83, 84
Nishio, Takayuki 38
Nishio, Yutaka 99
Nishioka, Takanori 167
Nobusada, Katsuyuki 26, 199
Nose, Fumitaka 156
Nozaki, Koichi 152, 153

O

Obi, Kinichi 82
Ogata, Hironori 108, 208
Ogino, Toshio 137
Ogo, Seiji 120
Ogura, Takashi 46, 48, 49, 201
Ohara, Junji 138
Ohara, Shigeo 192, 194
Ohashi Yuji 121
Ohashi, Kazuhiko 127, 202, 203
Ohashi, Noriko 152
Ohishi, Masatoshi 42
Ohishi, Tachi 115
Ohmori, Kenji 131
Ohmura, Yoshimasa 85
Ohno, Takeshi 152, 153
Ohta, Akira 178
Ohta, Kaoru 59
Ohta, Toshiaki 131, 148
Ohtake, Hideyuki 183, 184, 205
Oishi, Osamu 103, 104, 208
Ojida, Akio 162, 211

Oka, Yasuo 114
Okada, Atsuhiko 85
Okada, Kazumasa 144, 145, 204
Okamoto, Hiroshi 114
Okamoto, Yuko 25, 34, 199
Okamura, Melvin 49
Okano, Akihiro 161
Okazaki, Noriaki 75, 202
Okumura, Ko 29, 30
Okunishi, Misaki 131
Olson, John S. 47
Omata, Takahisa 147
Onodera, Noriaki 114, 126
Ootuka, Y. 97
Ornellas, Fernando R. 17, 22, 23, 199
Osborne, D. H. 146
Osherov, Vladimir I. 27, 28
Otsibo, Tetsuo 88
Ouchi, Yukio 147, 148, 149
Ozaki, Shin-ichi 120, 210
Ozawa, Y. 126
Ozawa, Yoshiki 114, 120
Ozeki, Hiroyuki 39, 40, 41, 42, 43, 200

P

Paeng, Ki-Jung 47
Paeng, Insook R. 47
Pal, Haridas 53, 55, 57, 202
Park, Jong K. 21, 199
Pec, Pavel 47
Perng, Baw-Ching 35
Phillips, George N. Jr. 47
Pohl, R. 44
Proshlyakov, Denis A. 46, 47, 210
Pucci, Renato 113

Q

Qin, Jingui 89, 207

R

Rábai, Gyula 70, 71, 72, 73, 74, 202
Raineri, Fernando O. 35, 36
Rao, A. M. 187
Re, Nazzareno 173, 174
Rehm, Julie M. 62
Richter, E. 187
Rubtsov, Igor V. 57, 202
Rühl, Eckart 131
Ryan, Matthew 153

S

Saeki, Morihisa 21, 128, 129, 203
Saito, Ko 40
Saito, Koh 145
Saito, Masako 110
Saito, Minoru 46
Saito, Seiji 31
Saito, Shuji 39, 40, 41, 42, 43, 200
Saito, Taro 96, 100
Saitow, Ken-ichi 59
Sakai, F. 98
Sakai, Ken-ichi 115
Sakai, Kusuo 191
Sakata, Yoshiteru 48
Sakurai, Akiko 159
Sakurai, Nobuhiko 211
Sakurai, Takeshi 155, 156, 211
Saleck, Axel H. 42
Sarukura, Nobuhiko 182, 183, 184, 205
Sasada, Masatoshi 164
Sasai, Masaki 30, 31
Sasaki, Tsutomu 154
Sassa, Koichi 183
Sato, Akane 97, 99, 101, 102, 103, 208
Sato, Hirofumi 32, 200
Sato, Hirohiko 93
Sato, Hiroyasu 83, 84
Sato, Shinri 137
Sato, Yukinori 131
Sawa, Hiroshi 99
Sawabe, Kyoichi 63, 64, 65, 189, 202
Schmid, S. 43
Schmid, W. 43
Schmidt, R. 44
Sei, Masaki 147
Seki, Kazuhiko 115, 116, 147, 148, 149, 209
Seki, Takahiro 52
Sekikawa, Taro 157
Sekimoto, Yutaro 42
Semashko, Vadim V. 183
Seto, Makiko 170
Severino, Patrizio 199
Shi, Yang 79, 203
Shibamoto, Yoshiyuki 125
Shibata, Takeshi 79
Shigemasa, Eiji 130, 131
Shimidzu, Ken-ichi 146, 147
Shimizu, Yuichiro 131
Shimojima, Atsuhiko 203
Shimomura, Osamu 87
Shinzawa-Itoh, Kyoko 46, 49
Shionoya, Mitsuhiko 162, 163, 164, 165, 211
Shiotsuka, Michito 162, 211
Shiratani, Eli 30
Shiro, Motoo 164
Shirota, Hideaki 53, 55, 57
Shirotani, Ichimin 87, 157
Shobatake, Kosuke 144, 145
Shudo, Akira 26
Sigrist, Manfred 111
Simonyan, Mkhitar 87, 207
Smalley, R. E. 187
Sonoda, Yoko 20
Spencer, James T. 131
Steimle, Timothy C. 41
Struganova, Irina A. 62
Stufkens, Derk J. 152
Subbaswamy, K. R. 187
Suemoto, Tohru 184
Suenaga, Yusaku 169, 170, 171, 172
Suga, Takehito 125
Sugai, I. 43, 44
Sugawara, Tamotsu 183
Sugaya, Takeyoshi 182, 184
Sugimoto, Isamu 159
Sugimoto, Toyonari 90, 124, 125
Sugiura, Sadaki 109
Sugiyama, Kiyoshi 147, 148
Sugiyama, Yoshinobu 182, 184
Suzuki, Masatatsu 167
Suzuki, Takayoshi 120
Suzuki, Toshinori 76, 77, 78, 79, 80, 81, 203
Szichman, Henrik 27

T

Tabayashi, Kiyohiko 145
Tada, Toshiji 157
Tahara, Tahei 133, 134, 135, 136, 203
Tajima, Hiroyuki 97
Tajima, Yuko 84
Takada, Shoji 27
Takada, Yasutaka 193
Takahashi, Junya 155, 156
Takahashi, Masao 193
Takahashi, Minoru 123
Takahashi, Mitsue 123
Takahashi, Naoshi 192, 194
Takahashi, Takashi 114, 149
Takahashi, Takuya 34
Takami, Toshiya 176
Takanishi, Yoichi 106
Takano, Naoto 127
Takano, Shiro 206
Takano, Yasushi 42
Takasu, Yoshio 137
Takata, Yasutaka 130, 131, 132, 193
Takayanagi, Masao 66, 67, 68
Takeda, Sadamu 156, 157, 211
Takeuchi, Satoshi 133, 134, 203
Takezoe, Hideo 106
Takimiya, K. 88
Takui, Takeji 85
Tamura, H. 43, 44
Tamura, Hatsue 156
Tamura, Masafumi 99, 100, 123
Tanaka, Hisashi 96, 100, 207
Tanaka, Kazuyoshi 83
Tanaka, Kentaro 162, 211
Tanaka, Koji 165, 166, 167, 168, 212
Tanaka, Motomasa 48, 119
Tanaka, Nobuaki 66, 67
Tanaka, Shin-ichiro 138, 139, 192, 194, 204, 205
Tanaka, Shoji 116, 179, 180, 181, 209
Tanaka, Takashi 192
Tang, Jiang 39
Taniguchi, Hiromi 93, 207
Tanimoto, Tetsuhiro 110
Tanimura, Yoshitaka 29, 30, 200
Tasaka, Motoyuki 158, 162, 211
Tasaki, Shuichi 26
Teki, Yoshio 84, 85
Ten-no, Seiichiro 15, 23, 30, 31, 32, 199
Teranishi, Yoshiaki 28, 199
Terekhin, M. A. 194
Thess, A. 187
Tokeshi, Manabu 141, 204
Tokue, Ikuo 144
Tokumoto, Madoka 98, 113
Tominaga, Keisuke 53, 55, 56, 59, 201, 202
Tomioka, Hideo 84
Tomita, Hideto 98
Tomita, Norikazu 30
Tomita, Takeshi 49
Tomura, Masaaki 116, 178, 180, 181, 209
Tonokura, Kenichi 78, 203
Torii, H. A. 43, 44
Torii, Tatsuharu 189
Toriumi, Koshiro 114, 126
Toyama, Hirohide 47
Toyohara, Kiyotsuna 165, 166, 167, 168
Tsuboyama, Sei 163
Tsuge, Kiyoshi 166, 167, 168, 212
Tsujii, Masaya 125
Tsukuda, Tatsuya 21, 128, 129, 203
Tsurusawa, Takeshi 15, 199
Tsusaka, Yoshiyuki 137, 138
Tsuyama, Shingo 49
Tucker, James H. 165
Tyliszczak, Tolek 131

U

Uchida, Shinobu 145
Uchimura, Ryuji 182
Uchiyama, Koichi 189
Uda, Satoshi 183
Ueda, Kazumasa 90, 124, 125
Ueda, Kiyoshi 131
Ueda, Naoyuki 146, 147, 209
Ueno, Nobuo 115, 116, 148, 149
Ueno, Sadaharu 84, 85
Ueno, Tamio 47
Ueno, Leonardo T. 17
Uesugi, Yuki 50
Ugawa, Akito 90, 124, 90
Umishita, Kazunori 149, 150
Underhill, A. E. 100
Urisu, Tsuneo 137, 138, 139, 204
Urquhart, Stephen G. 131
Uruichi, Mikio 89, 207
Utsuno, Shunji 158

V

Vanag, Vladimir K. G. 75
Vedyatev, Anatoly 113

W

Wada, Senji 119
Wang, Wenning 19
Watanabe, Hidekazu 15, 16, 17, 199
Watanabe, Iwao 154
Watanabe, Kazuo 63, 64, 202
Watanabe, Masamitsu 195
Watanabe, Michio 205
Watanabe, Tokuko 98, 102, 103
Watanabe, Yoshihito 48, 118, 119, 120, 210
Watarai, Hiroshi 154
Watarai, Hitoshi 154
Wen, Alex T. 131
White, C. W. 146
Widmann, E. 43, 44
Williams, Keith A. 186, 187
Williamson, J. M. 16
Wu, Ling Ping 169, 170, 171, 172

Y

Yagi, Shinya 195
Yagishita, Akira 130
Yakuoh, Teruo 182
Yakushi, Kyuya 87, 88, 89, 90, 112, 113, 124, 149, 157, 207
Yamabe, Tokio 83
Yamaguchi, Kizashi 157
Yamaguchi, Yoshitaka 160, 161, 211
Yamakado, Hideo 87
Yamakage, Hirokazu 85
Yamamoto, Kaoru 131

Yamamoto, Katsutoshi 84
Yamamoto, Kazunori 51
Yamamoto, Mikiko 169, 170, 171
Yamamoto, Satoshi 42
Yamamoto, Shigeyoshi 46
Yamamoto, Takakazu 149
Yamamoto, Takashi 193
Yamamura, Norihiko 182
Yamanaka, Takaya 184
Yamanoha, Masaru 124
Yamanouchi, Kazuhiko 183
Yamashita, Kazuo 147
Yamashita, Masahiro 114, 115, 126
Yamashita, Tetsuo 149
Yamashita, Yasuhisa 147
Yamashita, Yoshiro 89, 116, 178, 179, 180, 181, 207, 209
Yamazaki, Jun-ichiro 191
Yamazaki, T. 43, 44
Yamguchi, Yoshitaka 160
Yanagida, Toshio 34
Yang, Chuluo 89
Yang, L. 146
Yarunin, Vladimir 113
Yasui, Kazutomo 114, 126
Yata, Shizukuni 83
Yokoyama, Toshihiko 131
Yomo, Tetsuya 31
Yonehara, Yukako 117
Yonekura, Nobuaki 80
Yonemitsu, Kenji 37, 38, 206
Yoshida, Hiroaki 143
Yoshida, Hiroshige 42
Yoshida, Hisao 193
Yoshida, Hisashi 43
Yoshida, Ryo 84
Yoshida, Shohei 106
Yoshida, Shuhei 36
Yoshida, Tetsuya 165
Yoshida, Tomoko 193
Yoshigoe, Akitaka 137, 138
Yoshihara, Keitaro 53, 55, 56, 57, 58, 59, 60, 61, 62, 201, 202
Yoshikawa, Shinya 46, 49, 201
Yoshikawa, Yuzo 157, 158, 211
Yoshimi, Motohiro 84
Yoshimura, Akio 152
Yoshimura, Daisuke 147, 148, 149, 209
Yoshinaga, Shizuyo 161
Yoshizawa, Yuzo 158, 159
Yu, Yang 115
Yutoh, Koji 157

Z

Zhan, Chang-Guo 18, 20, 48, 199
Zhao, Xiaojie 48, 49
Zhu, Chaoyuan 27, 28, 199
Zhu, Lei 128
Zhuravlev, Michail Ye 111, 112, 113
Zuhr, R. A. 146

Institute for Molecular Science, Myodaiji, Okazaki 444, Japan